Volume 57
No. 1/2
2008

Eiszeitalter und Gegenwart

E & G

Quaternary Science Journal

Special issue:

Recent progress in Quaternary dating methods

Guest editors: Frank Preusser, Irka Hajdas and Susan Ivy-Ochs

E. Schweizerbart´sche Verlagsbuchhandlung
(Nägele u. Obermiller) – Stuttgart

www.deuqua.de

Deutsche Quartärvereinigung e.V.
German Quaternary Association

Founded 1948

Office:

D-30655 Hannover, Stilleweg 2, P.O. 510153

E-Mail: deuqua@lbeg.niedersachsen.de

Web: www.deuqua.de

Bank accounts:

Postbank Hannover: Konto 45303 308, BLZ 250 100 30, BIC: PBNKDEFF, IBAN: DE84 2501 0030 0045 3033 08

Sparkasse Hannover: Konto 2000 806 311, BLZ 250 501 80, BIC: HANSDE2HXXX, IBAN: DE10 2505 0180 2000 8063 11

Executive board

(2006-2010)

The subscription rates for DEUQUA mempership are as follows:

Ordinary Members	45,- €
Student, retired and unwaged members	20,- €
Institutions	55,- €

In Germany subscription rates are paid by standing order. For all other members, subscription rates should be paid by bank transfer into one of the two accounts listed above prior to 1st March each year. If you would like to join DEUQUA or have questions regarding missing or past volumes of Eiszeitalter und Gegenwart – Quaternary Science Journal, please contact the DEUQUA office.

Manuscript Submission: Manuscripts for E&G – Quaternary Science Journal must be submitted to the editor: PD Dr. Holger Freund, ICBM – Marine Laboratory, Schleusenstr. 1, D-26382 Wilhelmshaven; E-Mail: holger.freund@icbm.terramare.de

Front cover picture: (top left) Erratic boulder from Kaçkar Mountains, Turkey, sampled for dating by cosmogenic nuclides (photo: Naki Akçar); (top right) AMS facilities at ETH Zürich (photo: Susan Ivy-Ochs); (bottom left) sampling of loess for palaeomagnetic measurements (photo: Ulrich Hambach); (bottom right) fluvial deposits at Solenberg, Switzerland, sampled for luminescence dating (photo: Frank Preusser).

Titelbild: (oben links) Dieser erratischer Block aus dem Kaçkar Gebirge, Türkei, wurde für die Datierung mittels kosmogener Nukliden beprobt (Foto: Naki Akçar); (oben rechts) AMS Anlage an der ETH Zürich (Foto: Susan Ivy-Ochs); (unten links) Beprobung eines Lösses für paläomagnetische Messungen (Foto: Ulrich Hambach); (unten rechts) Fluviale Ablagerungen bei Solenberg, Schweiz, die für die Datierung mittels Lumineszenz beprobt worden sind (Foto: Frank Preusser).

Forthcoming Volume of Eiszeitalter & Gegenwart

E&G
Quaternary Science Journal

Special issue 57/3-4 (printed in December 2008)

The Heidelberg Basin Drilling Project

Special issue editors: Gerald Gabriel, Dietrich Ellwanger,
Christian Hoselmann & Michael Weidenfeller

Including:

and others…

E&G – Quaternary Science Journal is printed by Papierflieger Offsetdruck GmbH,
38678 Clausthal-Zellerfeld – E-Mail: papierflieger_offsetdruck@web.de

Eiszeitalter und Gegenwart

E & G

Quaternary Science Journal

Volume 57 Number 1/2

252 pages, 116 f gures and 13 tables

Editor and publishing: Deutsche Quartärvereinigung e. V. Hannover

Editor: H O L G E R F R E U N D

Distribution: E. Schweizerbart´sche Verlagsbuchhandlung (Nägele u. Obermiller) – Stuttgart

2008

Eiszeitalter und Gegenwart

Volume 57 Number 1/2
August 2008

E&G

Quaternary Science Journal

Published for Deutsche Quartärvereinigung e. V.

Editor: Holger Freund

Contents

E. Schweizerbart´sche Verlagsbuchhandlung
(Nägele u. Obermiller) – Stuttgart

Preface

This volume of *Quaternary Science Journal* (*Eiszeitalter und Gegenwart*) comprises a number of articles reviewing the present status of physical dating methods in Quaternary research, with a special focus on continental deposits and archaeological materials.
During the past two decades there has been an increased need for establishing independent timeframes in the context of, in particular, archaeological and palaeoclimate research. Over the same time period, enormous methodological improvements have been achieved with regard to Quaternary dating methods. These have had a similar pace as the developments in computer and information technology.
The ten articles in the present volume aim to provide the non-specialist with an overview on the physical basis of different dating approaches, which kind of procedures are applied from sampling to age calculation, which problems may interfere with proper age calculation and how these problems can be identified and corrected for. The articles should fill the gap between text books, usually only scratching the surface of particular methods, and pure methodological reviews, mostly inaccessible for the non-specialist who lacks the necessary background. We are aware that not all methods for dating Quaternary materials are included but the present volume should cover the most common approaches used in Quaternary research.

Frank Preusser (Bern), Irka Hajdas (Zürich) and Susan Ivy-Ochs (Zürich)

Vorwort

Diese Ausgabe von *Quaternary Science Journal* (*Eiszeitalter und Gegenwart*) umfasst eine Anzahl an Artikeln, die den gegenwärtigen Stand physikalischer Datierungsmethoden in der Quartärforschung zusammenfassen, wobei ein spezieller Fokus auf kontinentale Ablagerungen und archäologische Materialien gerichtet ist.
Während der letzten beiden Jahrzehnte hat die Notwendigkeit unabhängige Zeitskalen zu etablieren, vor allem im Zusammenhang mit archäologischer und paläoklimatologischer Forschung, stark zugenommen. Im selben Zeitraum wurden enorme methodische Verbesserungen im Bereich quartärer Datierungsmethoden erzielt, die sich zusammen und mit derselben Rasanz wie die Computer- die Informationstechnologie entwickelt haben.
Die zehn Artikel der vorliegenden Ausgabe verschaffen dem Nichtspezialisten einen Überblick über die physikalischen Grundlagen der verschiedenen Datierungsansätze, welche Prozeduren von der Probennahme bis zur Altersberechnung angewendet werden, welche Probleme eine korrekte Altersberechnung erschweren können und wie diese Probleme erkannt und behoben werden können. Die Artikel sollen helfen die Lücke zu schließen, zwischen Lehrbüchern, die üblicherweise bestimmte Methoden nur oberflächlich behandeln, und reinen methodischen Übersichtsarbeiten, die für den Nichtspezialisten wegen des fehlenden Hintergrundwissens meist kaum zugänglich sind. Es ist uns bewusst, dass nicht alle Methoden zur Datierung quartärer Materialien im vorliegenden Band enthalten sind, die wichtigsten Ansätze, die in der Quartärforschung benutzt werden sollten aber berücksichtigt sein.

Frank Preusser (Bern), Irka Hajdas (Zürich) und Susan Ivy-Ochs (Zürich)

Eiszeitalter und Gegenwart Quaternary Science Journal	57/1–2	2–24	Hannover 2008

Radiocarbon dating and its applications in Quaternary studies

Irka Hajdas*)

Abstract: This paper gives an overview of the origin of ^{14}C, the global carbon cycle, anthropogenic impacts on the atmospheric ^{14}C content and the background of the radiocarbon dating method. For radiocarbon dating, important aspects are sample preparation and measurement of the ^{14}C content. Recent advances in sample preparation allow better understanding of long-standing problems (e.g., contamination of bones), which helps to improve chronologies. In this review, various preparation techniques applied to typical sample types are described. Calibration of radiocarbon ages is the final step in establishing chronologies. The present tree ring chronology-based calibration curve is being constantly pushed back in time beyond the Holocene and the Late Glacial. A reliable calibration curve covering the last 50,000-55,000 yr is of great importance for both archaeology as well as geosciences. In recent years, numerous studies have focused on the extension of the radiocarbon calibration curve (INTCAL working group) and on the reconstruction of palaeo-reservoir ages for marine records.

[Die Radiokohlenstoffmethode und ihre Anwendung in der Quartärforschung]

Kurzfassung: Dieser Beitrag gibt einen Überblick über die Herkunft von Radiokohlenstoff, den globalen Kohlenstoffkreislauf, anthropogene Einflüsse auf das atmosphärische ^{14}C und die Grundlagen der Radiokohlenstoffmethode. Probenaufbereitung und das Messen der ^{14}C Konzentration sind wichtige Aspekte im Zusammenhang mit der Radiokohlenstoffdatierung. Gegenwärtige Fortschritte in der Probenaufbereitung erlauben ein besseres Verstehen lang bekannter Probleme (z.B. die Kontamination von Knochen) und haben zu verbesserten Chronologien geführt. In diesem Überblick werden verschiedene Aufbereitungstechniken für typische Probengattungen beschrieben. Der letzte Schritt beim Erstellen einer Chronologie ist die Kalibration der Radiokohlenstoffalter. Die gegenwärtige auf Baumringzeitreihen basierende Kalibrationskurve wird stetig über das Holozän und Spätglazial hinaus erweitert. Eine zuverlässige Kalibrationkurve für die letzten 50.000–55.000 Jahre ist von herausragender Bedeutung sowohl für die Archäologie als auch die Geowissenschaften. In den letzten Jahren haben zahlreiche Studien an der Erweiterung der Radiokohlenstoff-Kalibrationskurve (INTCAL working group) und an der Rekonstruktion des Paläo-Reservoireffekts in marinen Archiven gearbeitet.

Keywords: Radiocarbon dating, sample preparation, calibration, Quaternary

*Address of author: I. Hajdas, Ion Beam Physics, ETH/PSI Zürich, Schafmattstrasse 20, 8093 Zürich, Switzerland. E-Mail: hajdas@phys.ethz.ch

1 Introduction

The cosmogenic (produced by cosmic rays) isotope of carbon ^{14}C, also called radiocarbon, is the heaviest of the three isotopes of this element occurring in nature. The two stable isotopes ^{12}C and ^{13}C (representing 99.9% and 0.1%, respectively, of all natural carbon) originate from the primordial composition of the planet. Although ^{14}C takes up only a minute fraction of the carbon content (10^{-12}), its presence in carbon-bearing materials and the half-life ($T_{1/2}$) of 5730 ± 40 yr (Godwin 1962) form the basis for important geochronological and environmental applications.

Cosmic rays hitting the Earth's atmosphere produce cascades of secondary particles. Thermal neutrons, which are products of cosmic ray interaction, react with nitrogen of the atmosphere (Fig. 1). On average, 2 atoms cm^{-2} of ^{14}C are produced in the atmosphere every second. Oxidised to CO and CO_2 molecules, which takes weeks and weeks to months, respectively (Rom et al. 2000), ^{14}C is then quickly mixed within the atmosphere. Monitoring of the atmospheric ^{14}C levels of the nuclear tests in the 1960s has shown that inter-hemispheric mixing occurs in one to two years. For the purpose of radiocarbon dating, the difference between various regions is marginal. However, the difference between the hemispheres (ca. 5 ‰) might be reconsidered through regional calibration (McCormac et al. 2004).

Age measurements are possible because ^{14}C becomes a part of all organic and inorganic carbon compounds and a steady state between the uptake (photosynthesis or food) and the decay of ^{14}C exists as long as the organism is alive (Libby et al. 1949). After death, the only remaining process is decay (beta decay in which ^{14}C decays to nitrogen). Measurement of the beta-decay rate (conventional method) or counting the remaining ^{14}C atoms (AMS method) gives a measure of the time that elapsed since the steady state was broken. The half-life of 5730 ± 40 yr (Godwin 1962) allows the application of this method for the last 50,000-55,000 yr.

The main processes of the carbon cycle also control the ^{14}C exchange of the atmosphere with other main reservoirs: the ocean, the biosphere and the sediments (Fig. 2). The very fast exchange rate between the atmosphere and the biosphere assures equal ^{14}C concentration in contemporary living organisms, which is important for the use of radiocarbon as a dating tool. The ocean, which is the largest carbon reservoir, has a long residence time of ^{14}C and in consequence, the surface water and the deep-water

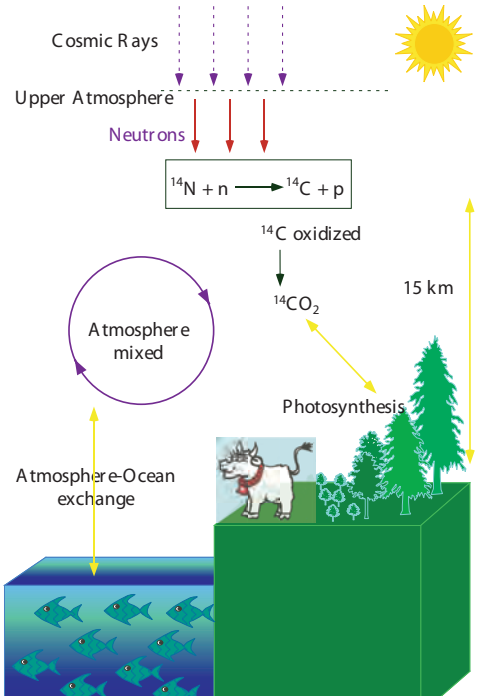

Fig. 1: Production and distribution of cosmogenic ^{14}C. Produced mainly in the upper atmosphere due to interaction of thermal neutrons with nitrogen, ^{14}C is relatively quickly oxidised and mixed in the atmosphere. Through photosynthesis, it enters the biosphere and through gas exchange, the oceans.

Abb. 1: Produktion und Verbreitung von kosmogenem ^{14}C. Das hauptsächlich in der oberen Atmosphäre durch Interaktion von thermischen Neutronen mit Stickstoff produzierte ^{14}C wird relativ schnell oxidiert und in der Atmosphäre vermischt. Durch Photosynthese gelangt es in die Biosphäre und durch Gasaustausch in die Ozeane.

masses have ages relative to the atmosphere, giving rise to the so-called reservoir age.
Due to various mechanisms such as changes in production rate and/or in the exchange rate between the carbon reservoirs, the atmospheric ^{14}C content fluctuates over time. These variations affect radiocarbon dating and often limit precision of age estimates.

2 Production rate and global carbon cycle.

In general, the cosmic rays flux remains constant (VOGT et al. 1990) and observed fluctuations in production rate of atmospheric ^{14}C are controlled by geomagnetic field strength as well as solar activity. In effect, a correlation exists between the number of solar spots (active sun) and the production rate of cosmogenic isotopes. The influence of solar and geomagnetic shielding on the production rate of cosmogenic isotopes can be simulated (MASARIK & BEER 1999). Based on these simulations, the globally averaged production rate calculated for ^{14}C is 2.02 atoms cm^{-2} s^{-1}.

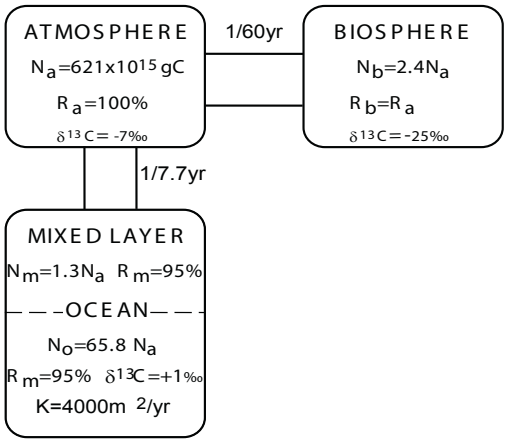

Fig. 2: The global carbon cycle (parameters used by SIEGENTHALER et al. 1980). N_i = amount of carbon in reservoir i; R_i = $^{14}C/^{12}C$ ratio; $\delta^{13}C$ = isotopic fractionation

Abb. 2: Der globale Kohlenstoffkreislauf (mit den Kenngrößen verwendet von SIEGENTHALER et al. 1980). N_i = Menge Kohlenstoff im Reservoir i; R_i = $^{14}C/^{12}C$ Verhältnis; $\delta^{13}C$ = isotopische Fraktionierung.

Various natural archives of cosmogenic isotopes have documented variability of production rate with time. For example, higher production rates of the cosmogenic isotopes ^{10}Be and ^{14}C are observed in ice cores and tree rings from the most pronounced periods of low solar activity: the Maunder, Wolf and Spörer minima, when the shielding was weaker (BEER et al. 1988). Variations in the strength of the geomagnetic dipole are also reconstructed using records of relative palaeointensity of the deep-sea sediments (CHANNELL et al. 2000; LAJ et al. 2000). A comparison of production rates derived from geomagnetic strength with the ice core record of ^{10}Be shows a striking correlation (LAJ et al. 2002). Relatively short changes (events) have been observed during the last 50 ka. Higher production rates of the cosmogenic isotopes ^{10}Be, ^{36}Cl and ^{14}C characterised periods/intervals of the Laschamp (41 ka) and Mono Lake (32 ka) geomagnetic excursions when the intensity of the geomagnetic field was low (Fig. 3) (HUGHEN et al. 2004a; LAJ et al. 2002; VOELKER et al. 2000; WAGNER et al. 2000).
Distribution of ^{14}C within and between reservoirs of carbon affects atmospheric ^{14}C content. The main mechanism of these changes is climatic variability because the ocean, which is the largest C reservoir (Fig. 2), is also an important component of the Earth's climate system. For example, changes of deep ocean ventilation during the glaciations had an impact on the atmosphere-ocean exchange of ^{14}C. Models have been developed to reconstruct the effect of such changes in the ocean ventilation on the ^{14}C inventory of both reservoirs. The simple box model of the ocean-atmosphere showed that reduced ventilation rates result in an increase, whereas the vigorous ocean ventilation results in a decrease of atmospheric ^{14}C content (SIEGENTHALER et al. 1980).

3 Anthropogenic impact on atmospheric ^{14}C

3.1 Suess effect

The industrial revolution of the late 19th century changed the ^{14}C content of the atmosphere. The

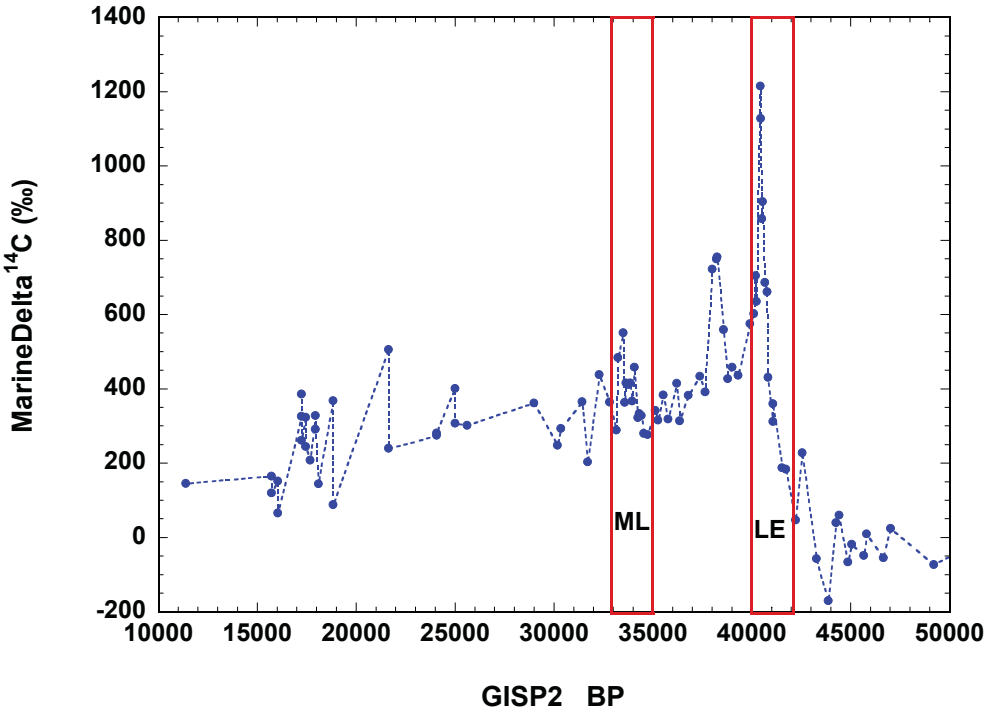

Fig. 3: Variations in ^{14}C concentration in foraminifera shells from Late Pleistocene Icelandic Sea sediments (Voelker et al. 2000). The increases in marine $\Delta^{14}C$, the measure of difference from the 'present day, i.e. 1950 AD ^{14}C level (Stuiver & Polach 1977), observed at 40-42 ka and 33-35 ka BP, coincide with low relative magnetic field intensity (Laj et al. 2002), i.e. weak geomagnetic shielding of the Laschamp Event (LE) and Mono Lake (ML) event, respectively.

Abb. 3: Variationen in der ^{14}C Konzentration in Foraminiferenschalen aus spätpleistozänen Sedimenten aus dem Isländischen Meer (Voelker et al. 2000). Der Anstieg des marinen $\Delta^{14}C$, als Maß des Unterschiedes zu heutigen, d.h. 1950 AD ^{14}C Niveau (Stuiver & Polach 1977), der bei 40-42 ka und 33-35 ka auftritt, fällt mit einer niedrigen Intensität des magnetischen Feld zusammen (Laj et al. 2002), d.h. mit einer schwachen geomagnetischen Abschirmung während des Laschamp Exkursions (LE) und des Mono Lake (ML) Exkursions.

increased burning of fossil fuels, which are free of ^{14}C (virtually all of the ^{14}C fixed in organic matter from millions of years ago has already decayed), added a significant part of ^{14}C free carbon dioxide to the atmosphere. In effect, the atmospheric $^{14}C/^{12}C$ ratio was lowered and thus, radiocarbon ages measured in post-industrial times will overestimate the real age of the sample. The effect was named after Hans Suess who first described it in the 1950s (Suess 1955). The observed effect of fossil fuel burning is most pronounced in the air from urban areas (Levin et al. 2008; Pawelczyk & Pazdur 2004).

3.2 The ^{14}C 'bomb peak'

The nuclear tests in the 1950s caused an increased stream of thermal neutrons into the stratosphere, which produced additional ^{14}C atoms and created an excess ^{14}C activity in the atmosphere (Fig. 4). Bomb produced ^{14}C was identified soon after the tests started and continuous monitoring has been carried out (Nydal et al. 1984; Nydal & Lovseth 1965, 1983). The peak (ca. 100% above the normal levels) reached its maximum in 1963 in the northern hemisphere, where most of the tests took place. In the southern hemisphere, the bomb peak

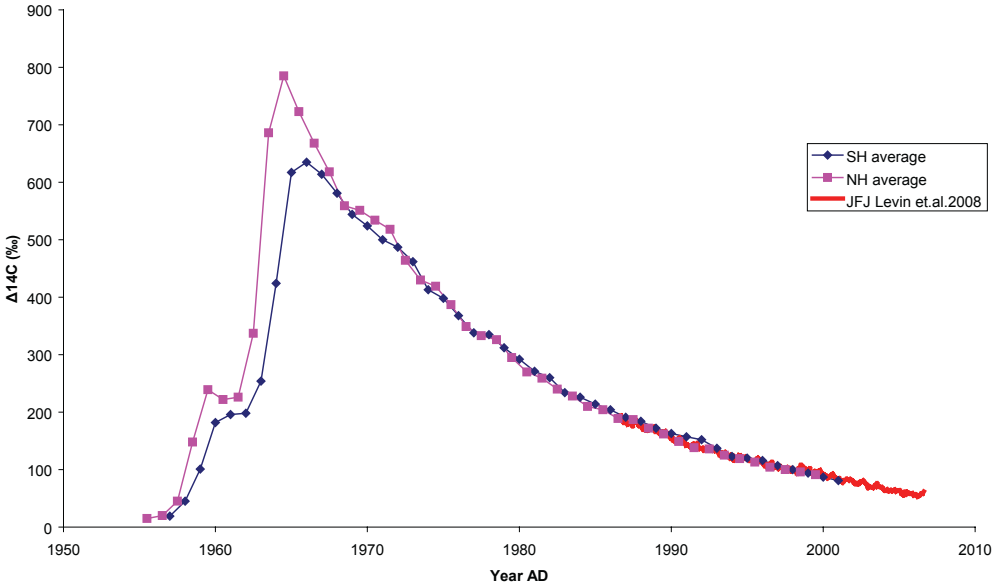

Fig. 4: The ^{14}C 'bomb peak'. Measurements of post 1950 AD atmospheric ^{14}C concentration for both the Northern (NH) and Sothern Hemispheres (SH) compiled by HUA & BARBETTI (2004). The monthly atmospheric ^{14}C data sets from measurements at the High Alpine Research Station Jungfraujoch (JFJ) show the present level of atmospheric $\Delta^{14}C$ (LEVIN et al. 2008).

Abb. 4: Der ^{14}C „Bomben-Peak". Die nach 1950 AD durchgeführten Messungen der ^{14}C Konzentration für sowohl die Nördliche (NH) als die Südliche Hemisphäre (SH) wurden von HUA & BARBETTI (2004) kompiliert. Der monatliche ^{14}C-Datensatz von Messungen an der Hochalpinen Forschungsstation Jungfraujoch (JFJ) zeigt das gegenwärtige Nivea des atmosphärischen $\Delta^{14}C$ (LEVIN et al. 2008).

reached lower values (ca. 80 % of normal level) and was delayed by ca. two years. After the ban on above-ground nuclear tests in 1963, the atmospheric ^{14}C content began to decrease mainly due to uptake by the ocean and the biosphere (NYDAL et al. 1980). During the last decade, the decline has been caused mostly by dilution of the atmospheric CO_2 with ^{14}C-free fossil fuel CO_2 (ca. 2-3 per mil yr^{-1}) (LEVIN et al. 2008). Continuous monitoring of the atmospheric $^{14}C/^{12}C$ ratio during the years following the nuclear tests provided the basis for environmental studies (LEVIN & KROMER 2004; ROZANSKI et al. 1995). Applications range from studies of the ocean circulation, CO_2 uptake, and carbon storage in soils to medical and forensic studies as well as detection of forgeries (LEVIN & HESSHAIMER 2000; SPALDING et al. 2005a,b; TAYLOR et al. 1992).

4 Radiocarbon dating

The method as established by Libby and coworkers in late 1940s assumed a constant atmospheric ^{14}C content. For the reasons discussed above, such an assumption is invalid, as shown by more precise measurements of tree rings performed in early 1950s. Moreover, the half-life $T_{1/2}$ = 5568 yrs used by ARNOLD & LIBBY (1949) was later found to be off by 3 % from its real value. However, an agreement has been reached that conventional radiocarbon ages (Libby ages) are calculated using the Libby half-life and then later calibrated (where a calibration curve is available) to obtain calendar ages that correspond to the measured ^{14}C concentration (age).

4.1 Conventional radiocarbon ages (Libby radiocarbon ages)

The ^{14}C concentration measured either by counting (Kromer & Münnich 1992; Hogg et al. 2006 and references therein) or AMS techniques (Finkel & Suter 1993; Jull & Burr 2006 and references therein) provides information about the time elapsed since the time of deposition or death.

The activity of ^{14}C can be measured by counting of beta particles emitted by decaying ^{14}C or by measuring the ^{14}C /^{12}C ratio using accelerator mass spectrometry (AMS). Both methods allow the dating of natural carbon-bearing material. After death or deposition, the equilibrium between uptake from the environment (atmosphere, ocean, lake) and ^{14}C decay is broken. When the, new ^{14}C atoms cannot be incorporated by the organism, the activity begins to decrease with a half-life of 5730 yr. Application of the decay law for radiocarbon dating requires that the activity of the organic matter after the death of the organism changes only due to radioactive decay (i.e. the dated matter was a closed system). Radiocarbon age (conventional or Libby radiocarbon age) T can be calculated thusly:

$$T = 8033 \ln (A/A_0)$$

A = ^{14}C activity at the time of dating
A_0 = initial ^{14}C activity at time t_0 (deposition, death)
$T_{1/2}/\ln 2 = 8033$ yr, where
$T_{1/2}$ = 5568 yr half-life used by Libby

In order to calculate ages, the initial activity A_0 at time t_0 must be known. As already discussed, A_0 is not constant over time and therefore an activity of pre-industrial wood grown in 1890 AD was chosen as reference. Although the half-life $T_{1/2}$ of 5568 yr (Libby half-life) is underestimated, it was accepted for use in the calculation of conventional radiocarbon ages (Olson et al. 1966; Stuiver & Polach 1977). Conventional radiocarbon age can then be corrected and expressed in radiocarbon ages for the half-life of 5730 years ($t_{5730} = 1.03\ t_{Libby}$).

In addition, small variations in the initial activity of the sample are related to the mass dependent fractionation of carbon isotopes by chemical and physical reactions that occur in nature, e.g. photosynthesis in the case of plants (which is then passed to animal tissue via the food chain) or precipitation processes of carbonates. The degree of fractionation in a dated sample, defined as a depletion or enrichment of the isotope relative to the standard material (Craig 1953), is different for various materials (Craig 1954; Stuiver & Polach 1977). Counting techniques use mass spectrometry measurements of gas split of CO_2 in order to obtain the correction value and some of AMS facilities measure the $^{14}C/^{13}C$ as well as $^{13}C/^{12}C$ ratios, which then can be applied to correct for fractionation.

Because the ^{14}C fractionation effect is approximately twice as much for ^{13}C, the correction applied to the ^{14}C content measured in the dated material is two times $\delta^{13}C$. Recently Mook & Van Der Plicht (1999), Reimer et al. (2004c) and Van der Plicht & Hogg (2006) summarised the conventions used for age calculation. The nomenclature used by these authors is summarised below. The ^{14}C concentration or ^{14}C activity of a sample is described as a fraction of reference material:

$$^{14}a = {}^{14}A\ (\text{sample})/{}^{14}A\ (\text{reference})$$

^{14}A (reference) or standard activity corresponds to 95% of the activity of a specific batch of the Oxalic Acid standard HOx1 in the year 1950 AD. The secondary standard HOx2 used presently by most laboratories has a defined activity ratio of 1.2933 in relation to the original HOx1 (Mann 1983).

$$^{14}A^0_{RN} = 0.95\ {}^{14}A^0_{OX1N} = 0.7459\ {}^{14}A^0_{OX2N} = 13.56 \pm 0.07 \text{ dpm gC}^{-1}$$

dpm gC^{-1} = disintegrations per minute and per gram of carbon

$^{14}A_{RN}$ is the specific activity of the standard corrected for isotopic fractionation to

$\delta^{13}C$ = -25‰ for HOx2 and $\delta^{13}C$ = -19.0 ‰ for HOx1

The activity ratio of the measured sample or concentration is defined as:

$$^{14}a = {}^{14}A/{}^{14}A_{RN}$$

This value is independent of when the measurement was carried out because it is relative to the standard of 1950 AD. The relative activity is expressed in per mil and defined as

$$^{14}\delta = {}^{14}a\text{-}1$$

The measured isotopic ratio has to be corrected for mass fractionation, which occurs during chemical and physical processes in nature (see above). The ^{14}C activity and the relative content are normalised to $^{13}\delta$= -25 ‰ (wood):

$$^{14}a_N = {}^{14}a\left[\frac{1+{}^{13}\delta_N}{1+{}^{13}\delta}\right]^2 = {}^{14}a\left[\frac{0.975}{1+{}^{13}\delta}\right]^2$$

Another symbol for the activity ratio has been proposed by REIMER et al. (2004c) and is frequently used in publications:

$$F^{14}C = {}^{14}a_N$$

This expression stands for the activity ratio of the measured sample to the standard corrected for the fractionation (as defined above) and for the background activity (blank values for AMS samples). Similar to the convention discussed above and published by STUIVER & POLACH (1977), the radiocarbon age T is calculated using the measured and normalised values of $^{14}a_N$ or $F^{14}C$:

$$T = -8033\ln(F^{14}C) \text{ or } T = -8033\ln({}^{14}a_N)$$

Conventional radiocarbon ages are reported as Before Present (BP), where 0 BP = year 1950 AD.

VAN DER PLICHT & HOGG (2006) define the frequently used value of $\Delta^{14}C$ (STUIVER & POLACH 1977), which illustrates the variations of ^{14}C in the atmosphere. The original ^{14}C content of the measured sample can be reconstructed for samples of known calendar age (tree rings, varves, U/Th dated carbonates). The measured ^{14}C content of the sample in year 1950 AD is corrected for the decay of ^{14}C (with the correct decay constant) during the time that has elapsed since the sample was formed, t_i:

$$^{14}\delta_N^i = {}^{14}a_N^i - 1$$

$$^{14}a_N^i = {}^{14}a_N \exp\{-(t_i - 1950)/8267\}$$

$$= F^{14}C\exp\{cal\text{BP}/8267\}$$

where $T_{1/2}/\ln 2$ = 8267 yr for $T_{1/2}$ = 5730 yrs and *cal*BP is the calendar age (cal BP) of the sample.

4.2 Precision and accuracy of measured radiocarbon ages

Precision characterises the degree of agreement among a series of individual measurements, i.e. the uncertainty of the measurement and is often quoted as the one-sigma error. This includes statistical error of counting atoms (AMS) or beta particles as well as uncertainty of measuring standards and blank values included in the calculation of radiocarbon ages. The counting error can be reduced by improved counting statistics. This can be achieved by increasing counting time. In the AMS technique, this is usually limited by the sample size as well as performance and stability of the AMS device.

Accuracy describes the difference between the calculated radiocarbon and the true age of a sample. This is independent of the measurement precision, i.e. radiocarbon ages can be very precise but their accuracy might be low or vice versa (SCOTT et al. 2007a). Radiocarbon laboratories check their accuracy using measurements of known age samples (for example a set of C samples available from IAEA). Moreover, regular proficiency checks known as inter-lab comparison are performed (SCOTT 2003a,b,c; SCOTT et al. 2004). Recently these comparison measurements were extended to various types of samples (NAYSMITH et al. 2007; SCOTT et al. 2007b).

4.3 Calibration of radiocarbon ages

Due to the variability of the atmospheric ^{14}C content and the used convention discussed above, radiocarbon ages are only 'defined' values and require calibration in order to obtain calendar ages. Calibration of radiocarbon ages compensates for both the error introduced by conventional (Libby) half-life $T_{1/2}$ and for the temporal variability of the atmospheric ^{14}C content.

Calibration is a mathematical procedure that places the measured radiocarbon ages (taken with their error) on the experimentally drawn curve. In the probabilistic calibration procedure, calendar ages, corresponding to the radiocarbon age obtained for the measured material, are given with the probability distribution (68% and 95% confidence intervals for 1 sigma and 2 sigma error, respectively) (Stuiver & Reimer 1986, 1989). The calibrated radiocarbon ages are then reported as 'cal AD/BC' or 'cal BP' (calendar years BP). Because of the wiggles on the calibration curve, the transfer to calendar time scale may have a complicated probability distribution (Fig. 5).

Nowadays, calibration can be done using calibration software available via the web site of the *Radiocarbon* journal (http://www.radiocarbon.org). The calibration data used by most of the programs are based on the calibration data sets prepared and published by the International Calibration Group (INTCAL). The most recent set of data IN-

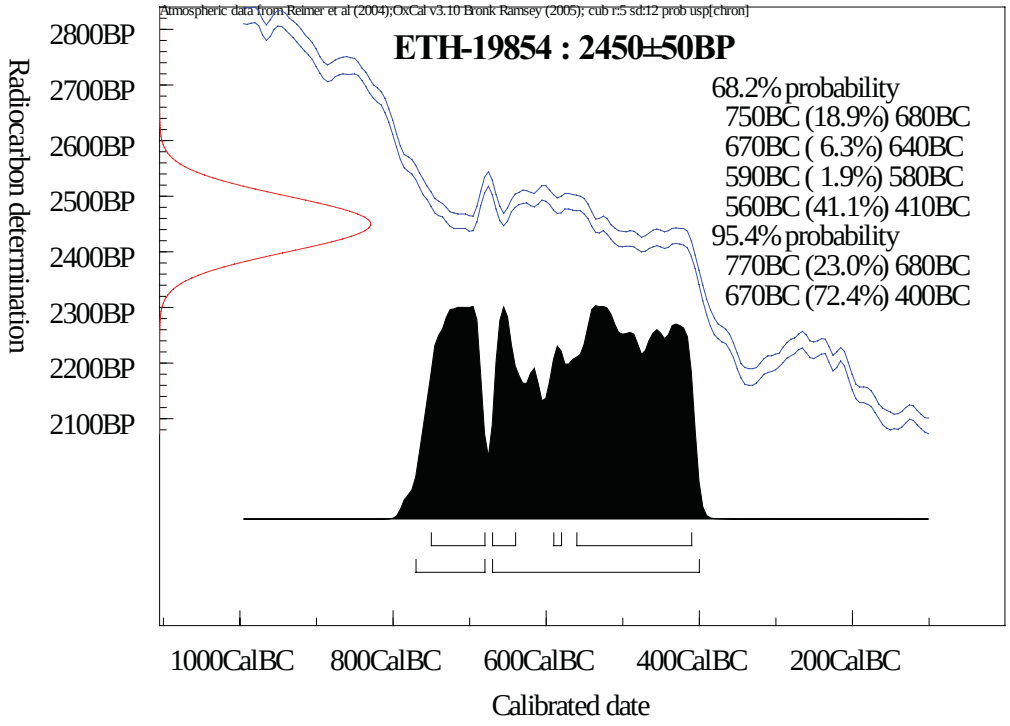

Fig. 5: Example of calibration of radiocarbon age (one of the samples from Ulandryk series, Hajdas et al. 2004b), which is in the range of an age plateau (see text). The complex nature of the calibration curve (wiggles) results in multiple calendar age intervals.

Abb. 5: Beispiel für die Kalibrierung eines Radiokohlenstoffalters (eine der Proben aus der Ulandryk Serie, Hajdas et al. 2004b), welches sich im Bereich eines Altersplateaus befindet (s. Text). Die komplexe Natur der Kalibrierungskurve („wiggles") resultiert in einer Anzahl von möglichen Kalenderjahr-Intervallen.

TCAL04 was published in 2004 (HUGHEN et al. 2004b; REIMER et al. 2004a). The current state of the calibration curve and efforts to extend it to the limits of the method will be discussed later.

5 Sample types and preparation techniques

During the six decades of radiocarbon dating, the method has evolved towards more sophisticated applications that, in many cases, require very small sample sizes. The ultimate goal is to obtain a material for radiocarbon dating that is free of foreign carbon i.e., contaminants. Because carbon is such a common element in the environment, removing either modern (high amount of ^{14}C) or ancient (free of ^{14}C) contaminations has always been a challenging task. An overview of sample preparation presented here is relevant to both conventional and AMS sample preparation laboratories. The focus is however set on samples prepared for the AMS technique because many applications nowadays involve only minute sample amounts. While previous sample treatments were designed to remove contamination assuming that the material has been part of a closed system, present preparation involves evaluation of possible sources of contamination as well as extraction of the fractions that will give the most accurate age estimates. This requires understanding of the environment in which the dated material had been formed and preserved until sampling.

5.1 Sample types

The common types of samples include charcoal, wood, bones, animal tissue, textiles, paper, macroscopic remains of the plants (leaves, fruits, flowers), carbonates (corals, sediments, stalagmites and stalactites), water, air and organic matter from various sediments, soil, palaeosol and peat deposits. Depending on the sample type, an appropriate treatment is chosen to select the most relevant fraction of carbon, which will yield the accurate age of the studied object.

5.2 Sources of contamination

Modern dust that includes particles of, for example, hair, tissue, paper or pollen grains, is the most common source of contamination with modern carbon. In addition, bacterial growth might contaminate sediments and other organic matter during storage. Therefore, freezing or drying of the material to be dated is recommended.

Carbonates and humic acids infiltrate natural environments over the years during which the sample material has been buried in geological or archaeological settings. Diagenesis is the source of contamination that is introduced into the molecular structure of the material to be dated and such effects may often remain unnoticed. The process of exchange of carbon might lead to contamination with either young or old carbon. The most common problem in dating archaeological samples is degradation of bones. While buried in soil, they may incorporate humic acids from the environment. Another example found in geological applications is dissolution and re-crystallization of carbonates. Different types of carbonates may be affected to different degrees.

Conservative substances used to preserve artefacts or bones will introduce either modern or old carbon. Substances which had been used in the past cannot always be tracked down and therefore a range of solvents is used that should remove most commonly used conservative substances. A Soxhlet extraction of contaminants is routinely applied in many laboratories to pre-treat wood, bone and textile samples. Some geological samples also require such treatment if they were buried in bituminous sediments.

5.3 Treatment methods

As the sources and types of contamination vary, so do the methods of pre-treatment developed in order to provide the most accurate radiocarbon ages. The first step in applying these methods is an assessment made on the degree of contamination. Recent samples such as well-preserved wood and charcoal, as well

as textiles and in some cases bones, are usually viewed as intact materials where contaminants remain outside molecular structure of organic matter (M methods). In such cases macroscopic methods, which have been used for many decades by radiocarbon laboratories, are applied (Van Klinken & Hedges 1998). A small but ever increasing portion of samples are pre-treated at the molecular level where specific compounds are isolated, allowing more accurate dating of specific material such as degenerated bones, organic compounds in soil or deep-sea sediments (S-methods). With the exception of dating alpha-cellulose, isolation of specific compounds from a sample for dating would require an AMS facility to handle samples as small as mg and µg of carbon. The development of gas ion sources will allow an omission of the graphitisation process, which is limited by sample size, and thus direct measurement on CO_2 samples as small as a couple of micrograms.

5.3.1 Mechanical cleaning

Sample material will undergo visual examination after its arrival in the laboratory. All visible contaminants are removed under a binocular and the surface of the sample is cleaned if necessary. A short cleaning in an ultrasonic bath is applied to charcoal, textiles, wood and shells of molluscs and foraminifera to remove dust particles, etc. Some laboratories apply vacuuming of textiles surface because an ultrasonic bath might destroy and create a mash of the material. In the case of solid surfaces such as bones or corals, sand blasting is used to clean the surface (Paterne et al. 2004). Soft materials such as sediments have their surfaces scraped. In the case of small plant fragments washed out of sediments, remains of aquatic plants must be removed with tweezers (Hajdas 1993; Hajdas et al. 1993). Rootlets that might have grown in the layer are removed from peat or soil samples by sieving.

5.3.2 The acid-alkali-acid (AAA) method

The AAA pre-treatment is known as the standard chemical treatment of organic matter for radiocarbon dating, which is often applied to remove contamination by carbonates and humic acids (De Vries & Barendsen 1954). The first wash in acid solution (Fig. 6) removes carbonate contamination attached to the surface. The duration of this step applied by different laboratories varies depending on the treated material. After washing with distilled water, a treatment with a weak base (for example 0.1 M NaOH) is applied to dissolve humic acids. Following rinsing to neutral pH, the final wash is a repeated with a hot acid bath to remove carbonates that precipitated from modern atmospheric CO_2, which is dissolved in an alkali solution. This step is shorter than the other two and is followed with a final rinsing to neutral pH. The AAA (or ABA, acid-base-acid) method is relatively straightforward, hence commonly used in most laboratories. However, several studies (Hatté et al. 2001, Head & Zhou 2000) have shown that the alkali step of AAA might be responsible for contamination of some material with modern C from atmospheric CO_2 dissolved during this step and incorporated into the sample structure. Such contamination cannot be entirely removed in the last acid wash if the commonly used weak HCl solution is applied. Materials that require such modification of classical AAA treatment include wood, peat and palaeosols, i.e. common objects for radiocarbon dating. The effect of contamination becomes significant when old material is prepared for radiocarbon dating. Hatté et al. (2001) proposed alternative treatments, which can be applied to samples that are susceptible to contamination of their inner structure. These are designed to remove modern carbon in the last step of treatment (modification of the last step of the AAA (Fig. 6)). For example, modern carbonates, which replaced functional groups in the samples of old wood during acid and base steps, can be detached from the structure by stronger agents such as sulphuric acid. In contrast to hydrochloric acid, H_2SO_4 has a stronger ionic affinity for carbonates.

5.3.3 ABOX Acid-Base-Oxidation

Another modification of the AAA (ABA)

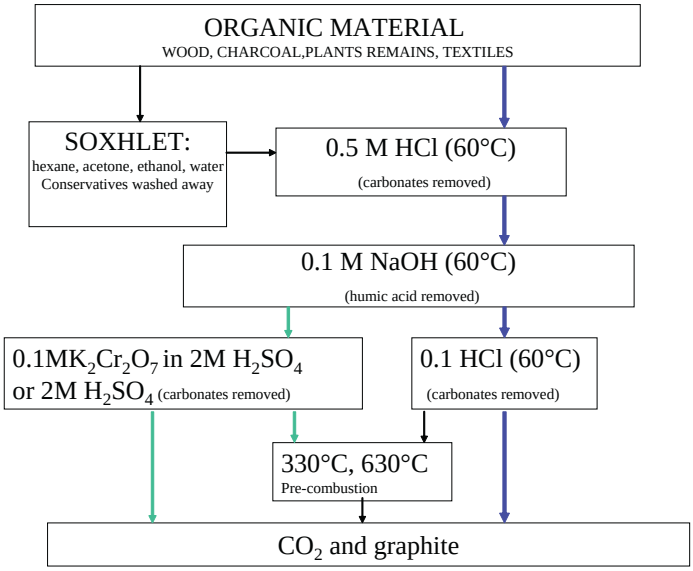

Fig. 6: Overview of pre-treatment methods routinely applied for cleaning organic material. The Soxhlet treatment is applied to material with suspected contamination caused by conservative substances or natural bituminous carbon (see text). The standard AAA treatment (blue path) might be enhanced by pre-combustion steps. ABOX (green path) is usually applied to treatment of material older than 20 ka.

Abb. 6: Überblick über Aufbereitungsmethoden, die routinemäßig für die Reinigung von organischem Material verwendet werden. Die Soxhlet Behandlung wird angewendet an Material, welches vermutlich durch konservierende Substanzen oder natürliches Bitumen verunreinigt ist (s. Text). Die Standard AAA Behandlung (blauer Pfad) kann durch Vorverbrennungsschritte verstärkt werden. ABOX (grüner Pfad), wird überlicherweise für Material verwendet, welches älter als 20 ka ist.

method involves a final oxidising step in the pre-treatment. BIRD et al. (1999) applied two methods of oxidation using a highly oxidising agent of acid dichromate solution (0.1M $K_2Cr_2O_7$ in a 2M solution of H_2SO_4) (Fig. 6), so-called 'wet oxidation', and pre-combustion of the sample in oxygen flow at 330ºC and 630ºC, i.e. temperatures lower than the final combustion at 850ºC. BIRD et al. (1999) used these two methods and showed that the oldest ages of very old charcoal, i.e. the most effective removal of contamination can be obtained when 'wet oxidised' samples are also pre-combusted.

HATTÉ et al. (2001) proposed a replacement of the last hydrochloric wash of peat and paleosols (sediments rich in Fe) by a wash with an oxidising agent such as $K_2Cr_2O_7$. In this study, it was shown that the oxidation process breaks insoluble ferrous compounds that were formed during the alkali step, which could possibly incorporate modern CO_2.

5.3.4 Soxhlet treatment

Samples originating from museums and private collections often have their own history of conservation. In most cases, records of restoration are sparse or non-existent. Materials used as conservative substances contain carbon, which is either of modern or fossil origin and can contaminate samples. Naturally occurring samples can also be contaminated by fossil carbon. The effect has been observed in archaeological samples from Terqa, Syria where asphalt was present in the deposits. Some charcoal samples from this region were dated to be as old as 28,700 BP whereas the archaeological context

was dated to 3000 BP or younger (Venkatesan et al. 1982). Therefore it is advisable to perform Soxhlet treatment of organic matter recovered from soils, sediments and any tar-containing environments.

For Soxhlet treatment, a standard procedure has been developed (Bruhn et al. 2001, Hajdas et al. 2004c) and the most common conservative substances are removed in a sequence of solvents bathing (hexane, acetone and methanol). The sample is placed in the Soxhlet apparatus as shown in Fig. 7 and the liquid is brought to the boiling point. The condensate circulates in the Soxhlet for 30 min so that the sample is immersed in the clean hot solvent almost all the time. Contamination is removed with each spilling of the solvent through the siphon back to the heated bottle.

5.3.5 Leaching surface of carbonate samples

Surface of carbonate samples such as tufa, corals and shells may be contaminated due to diagenic processes. In order to remove such contamination, samples are cleaned mechanically (using an ultrasonic bath) and subjected to various leaching procedures, which involve acid and/or H_2O_2 solution. The degree of leaching varies, depending on the material dated. Burr et al. (1992) showed that 80 % leaching of coral surfaces yields satisfactory ages. Ages of ostracode shells from sediments of Mono Lake became older as the shells were successively dissolved (Fig. 8) (Hajdas et al. 2004d).

5.3.6 Bone organic fraction

Bone contains mainly mineralised hydroxylapatite and carbonate-apatite as well as partly fluorapatite and chlorapatite, which are bound to a matrix of collagen. Collagen makes up to 20 % of dried, defatted fresh bone. A smaller fraction of the organic matrix is formed by non-collagen proteins such as osteocalcin or ferritin.

Most laboratories employ the method developed by Longin (1971) (Fig. 9). Bones are first crushed or ground in a mill to speed up the dissolution in acid. This step removes contaminants but may remove collagen as well. Therefore, time and acid strength should be controlled during the process.

Gelatine is obtained by dissolution of collagen in a weak acid (Longin 1971). The demineralised sample is placed in 0.01N HCl solution and left at 58ºC for 18-24 hr. The solution is then filtered and freeze-dried (Fig. 9) prior to combustion. In order to remove potential contamination of the bone, additional separation techniques have been developed. A modification of the Longin (1971) method, including

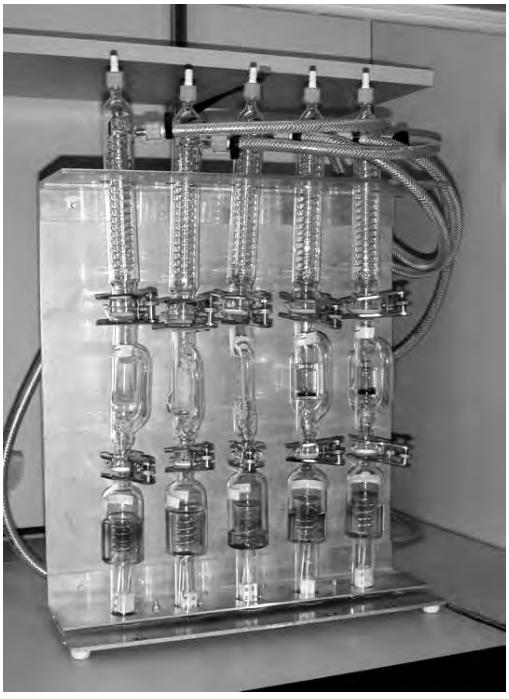

Fig. 7: Soxhlet preparation system at the ETH lab. The sample holders (middle part) are placed above a boiling solvent (lower part). The vapours of the solvent are cooled (upper part) and precipitated into the sample holder.

Abb. 7: Soxhlet Aufbereitungssystem im Labor der ETH. Die Probenhalter (mittlerer Teil) werden oberhalb eines kochenden Lösungsmittels platziert (unterer Teil). Der Dampf des Lösungsmittels wird gekühlt (oberer Teil) und schlägt sich im Probenhalter nieder.

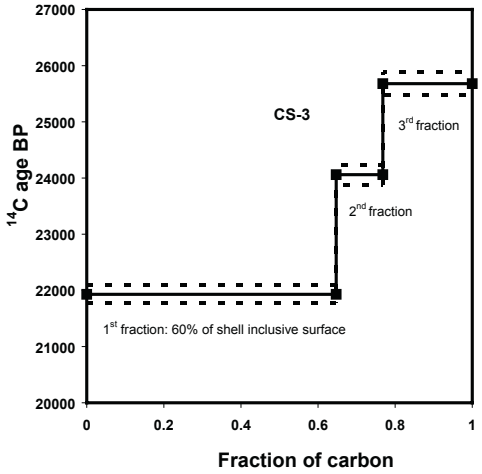

Fig. 8: Effect of consecutive leaching on radiocarbon age of ostracode shells from Carlson Sink, Mono Lake, USA (HAJDAS et al. 2004d).

Abb. 8: Effekt des fortlaufenden Ablaugens auf Radiokohlenstoffalter von Ostrakodenschalen aus Carlson Sink, Mono Lake, USA (HAJDAS et al. 2004d).

a short treatment of 'collagen' with a base solution prior to gelatinisation, has been proposed by ARSLANOV & SVEZHENTSEV (1993). This procedure was adopted by HAJDAS ET AL. (2007) and PIOTROWSKA & GOSLAR (2002) and proved very effective in removing contamination. Separation of molecular masses by ultra-filtration was proposed by BROWN et al. (1988) and improved providing very promising results (HIGHAM et al. 2006a, 2006b). The procedure of ultra-filtration involves separation of molecular masses because those of peptides are heavier than the possible contaminant of humic and fulvic acids. The liquid is placed in ultra-filtration tubes with a 30 kDa filter (Viva Spin or Millipore) and centrifuged at 4000 rpm for 15 to 30 min (depending on the volume of the tube). In effect, molecules heavier than 30 kDa will remain above whereas the smaller (contamination fraction) will pass through the filter and be discarded. The heavier fraction obtained is freeze-dried and then subjected to combustion.

6 Site and sample specific problems of radiocarbon dating

In order to obtain the most accurate ages and reliable chronologies for the studied objects or sites (sedimentary records), appropriate material must be sampled for radiocarbon dating. For lake sediments, terrestrial macrofossils should be sampled to avoid potential 'hard water' effects caused by old carbonates built into organic matter of aquatic plants (HAJDAS et al. 1993, 1995, 1998). The presence of old carbon dissolved from bedrock is different from site to site and the 'hard water' effect may range from hundreds of years to nil. More locally, radiocarbon ages of organic matter can also be influenced due to volcanic (^{14}C free) CO_2 added to the atmosphere or dissolved in water. For example, remains of aquatic plants found in sediments of Lake Monticchio (Italy) were more than 10,000 ^{14}C yr older compared to terrestrial macrofossils in the same sediment layer (HAJDAS et al. 1998). Another source of old carbon has been observed in polar regions where slow decomposition of organic matter and longevity of some species of mosses might result in older radiocarbon ages (HUMLUM et al. 2005). Similarly, too old ages are observed when redeposited or re-used material is dated. The best example is the 'old wood' effect known in dating wooden artefacts.

For marine records, hand picked foraminifer shells of plankton living in the upper layer of the ocean are usually used for dating. The radiocarbon age of water in this layer varies from 400 to 1200 ^{14}C yr. Correction for the marine reservoir effect is based on measurements of marine radiocarbon ages of material with known age (REIMER & REIMER 2001). Other problems in dating marine records are related to bioturbation and poor preservation of shells as discussed by BROECKER et al. (1999, 2006).

7 Graphite preparation for AMS ^{14}C measurements

For AMS measurements of ^{14}C /^{12}C ratios, the autochthonous carbon present in the sample

material has to be transformed into pure graphite. The first step in this process is obtaining CO_2 by either combustion (organic matter) or acidification (shells and inorganic sediments).
For combustion, dried organic matter is weighed and placed in a quartz glass tube, which contains wire-formed CuO for oxidation of the material that is sealed after the tube is evacuated. Silver wire or powder is added together with the sample to bind SO_2 and other halogen gases that could poison the graphitisation reaction. The sealed tubes are placed in an oven at 950ºC for 2 hr. Carbonate samples are placed in a special chamber, which is evacuated, then mixed with concentrated phosphoric acid and dissolved. The resulting CO_2 is then purified and frozen using liquid nitrogen (Hajdas et al. 2004d). The experimental details are given in Hajdas et al. (2004c).
Most of the AMS laboratories use the graphitisation method described by Vogel et al. (1984), where the reaction of $CO_2 + 2\ H_2$ (heated to 580 to 600ºC for ca. 2 to 4 hr) over catalyst (cobalt or iron powder) results in reduction to C and H_2O. The graphite that forms on the surface of the catalyst is then pressed onto a target designed for AMS measurement.
Measurements of the $^{14}C/^{12}C$ and $^{13}C/^{12}C$ ratios of the samples to be dated are determined relative to the respective NBS oxalic acid I or oxalic acid II standard values. Chemistry blanks prepared from natural graphite, coal or marble (for example the C-1 standard of IAEA, Vienna) is usually analysed in order to determine contamination introduced during sample preparation. All samples (unknowns, standards and blanks) of one series are measured several times (typically three or four). The total measuring time per sample is around 30 to 40 min. For details of measurements performed at the AMS facility at the ETH Zurich see Bonani et al. (1987) and Synal et al. (1997, 2007).

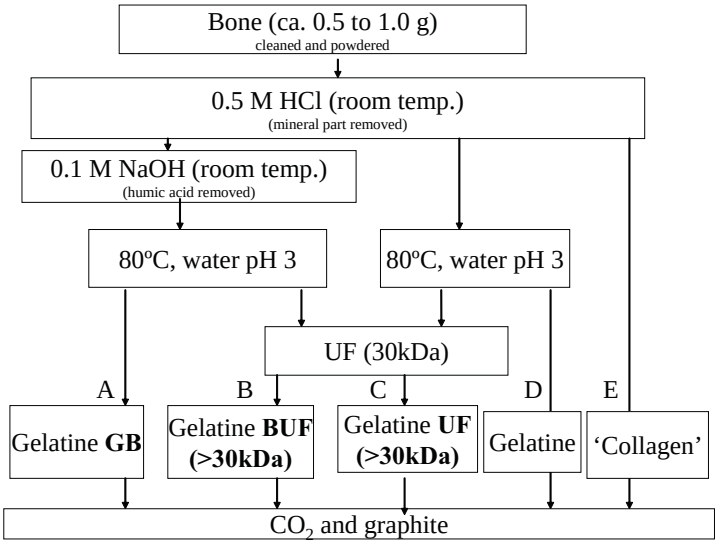

Fig. 9: Overview of bone treatment (organic fraction): path A: modified Longin method (Arslanov & Svezhentsev 1993), path B: modified Longin method combined with Ultra Filtration, path C: Longin method + Ultra-Filtration (Brown et al. 1988), path D: Longin method (Longin 1971), path E: 'collagen'.

Abb. 9: Überblick über der Aufbereitung von Knochen (organische Fraktion): Pfad A: modifiziertes Longin-Verfahren (Arslanov & Svezhentsev 1993), Pfad B: modifiziertes Longin-Verfahren kombiniert mit Ultra-Filtration, Pfad C: Longin-Verfahren+Ultra-Filtration (Brown et al. 1988), Pfad D: Longin-Verfahren (Longin 1971), Pfad E: 'Kollagen'.

8 Calibration issues

8.1 ^{14}C age 'plateaux', rapid 'jumps' and 'wiggles'

Precise radiocarbon dating of certain periods of interest may be complicated by extreme variability of atmospheric ^{14}C content present at times in the radiocarbon calibration curve. These complications arise from variations in atmospheric ^{14}C content caused by the changes in the production rate and changes in the carbon cycle and are known as 'wiggles' in the calibration curve. Radiocarbon age 'plateaux', for example, caused by a decrease in the atmospheric ^{14}C concentration, appears as a slowing down of the ^{14}C clock such as one that occurred at 2500-2400 BP, i.e. between 700 BC and 400 BC ('Hallstatt plateau') (Fig. 10). In effect, similar radiocarbon ages may appear to correspond to a range of up to 500 calendar years. The opposite is observed when atmospheric ^{14}C levels increase so that the ^{14}C clock appears to speed up. Therefore, due to the 'wiggles', a single radiocarbon age may correspond to more than one calendar age range or the ^{14}C clock may even appear to be reversed with respect to actual time.

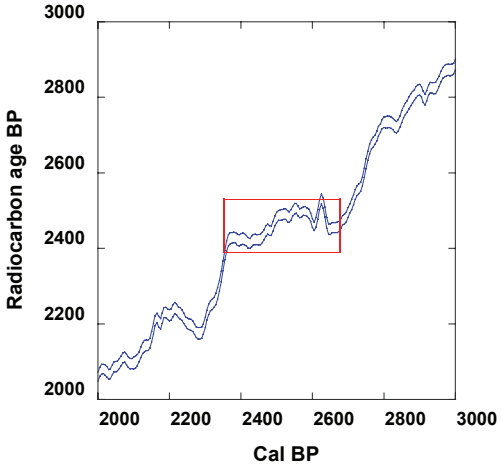

Fig. 10: Radiocarbon age plateau at 2400-2500 BP (700 BC and 400 BC) known as a 'Hallstatt plateau' marked on the calibration curve of INTCAL04 (REIMER et al. 2004a).

Abb. 10: Radiokohlenstoff Altersplateau zwischen 2400 und 2500 BP (700 BC bis 400 BC), bekannt als "Hallstatt Plateau", markiert auf der Kalibrierungskurve INTCAL04 (REIMER et al. 2004a).

The set of radiocarbon ages obtained on a trunk of a larch tree found in Scythian tombs/kurgans of Altai Mountains illustrates the effect the age plateaus can have on the precision of calendar ages and shows how the wiggle match can help to resolve it. Eleven out of sixteen calibrated ages fall on the 2400-2500 BP age plateau. In effect, the calibrated ages of all these samples range from 700 BC to 400 BC (Fig. 11). However, a χ^2 fit of the age sequence to the calibration curve resulted in a precise dating of the last ring to be 2267 $^{+13}/_{-21}$ cal BP (317 $^{+13}/_{-21}$ BC) (Fig. 12), which was presumably the year when the kurgan was built (HAJDAS et al. 2004b).

Another method to improve calendar chronologies, despite the ^{14}C plateaux, is the use of models such as wiggle-matching or calibration models, where additional information about the samples (sequence order) might be applied to reduce the intervals of calibrated ages (RAMSEY et al. 2001). This Bayesian approach to calibration of radiocarbon ages (BUCK et al. 1996) is now included in calibration programs such as BCal (http://bcal.sheffield.ac.uk) (BUCK et al. 1999), OxCal (RAMSEY 2008) or Bpeat (BLAAUW & CHRISTEN 2005). 'Wiggle-matching' with the Bpeat program has been applied to develop age-depth models of Holocene peat sections from the Netherlands (BLAAUW et al. 2007). The high-resolution radiocarbon dating combined with Bayesian modelling was used to establish chronology of climatic events of Kaipo Bog (New Zealand) (HAJDAS et al. 2006). Similarly, the late Glacial sedimentary record of Hauterive/Rouges-Terres, Lake Neuchâtel (CH) (HAJDAS et al. 2004a) were radiocarbon dated and the age model was built using Bayesian model of OxCal v3 program (RAMSEY 2001).

8.2 Extension of the calibration curve

The history of variations in atmospheric ^{14}C production during the last 12,400 years is based on tree ring measurements and dendrochronol-

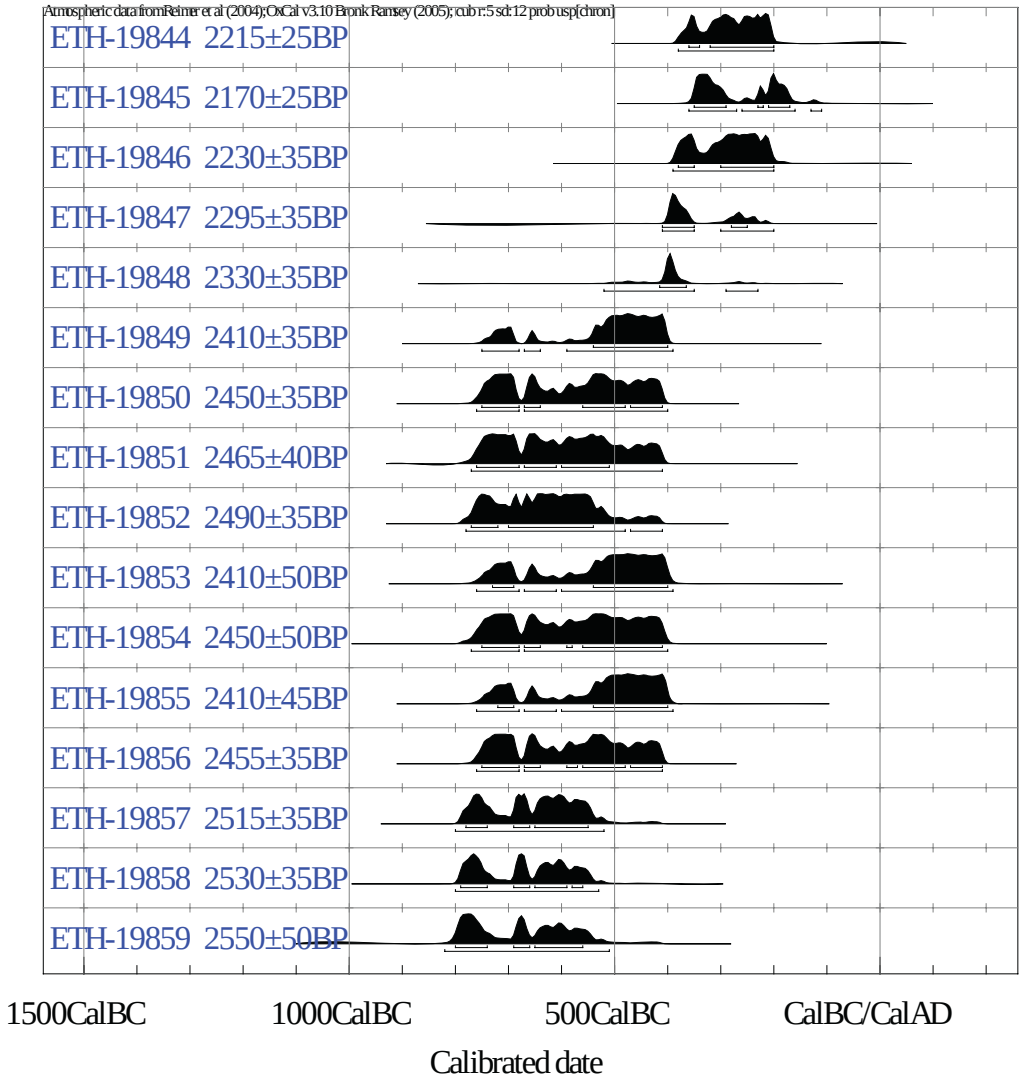

Fig. 11: Results of calibration of radiocarbon ages obtained for a tree ring sequence of samples from a larch tree recovered from a kurgan (burial mound) in Ulandryk (Altai Mountains) (HAJDAS et al. 2004b). Note the wide ranges of calibrated age intervals obtained for radiocarbon ages hitting the plateau (see text). An exception is the sample ETH-19848, 2330 ± 35 BP, as this age corresponds to a steep slope on the calibration curve

Abb. 11: Ergebnisse der Kalibrierung von Radiokohlenstoffaltern für Proben aus einer Baumringsequenz aus einer Lärche, die aus einem Kurgan (Grabhügel) aus Ulandryk (Altai Gebirge) geborgen wurde (HAJDAS et al. 2004b). Bemerkenswert ist der breite Bereich an kalibrierten Altersintervallen für Radiokohlenstoffaltern, die auf Plateaus liegen (siehe Text). Eine Ausnahme ist Probe ETH-19848, 2330 ± 35 BP, weil diese Probe mit einem steilen Abfall in der Kalibrationskurve zusammenfällt.

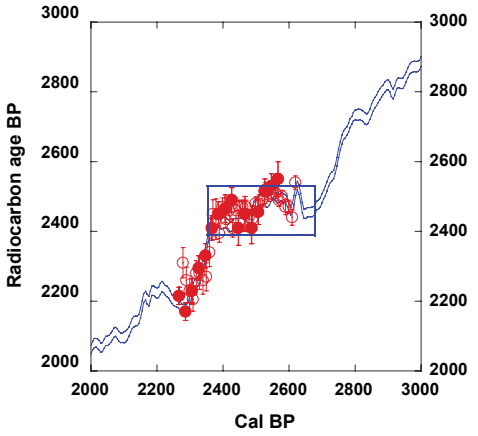

Fig. 12: Results from the Ulandryk kurgan (Fig. 11) fitted to the calibration curve (see text): filled circles (HAJDAS et al. 2004b) and open circles (KUZMIN et al. 2004). The last ring is dated to 2267 $^{+13}/_{-21}$ cal BP (317 $^{+13}/_{-21}$ BC).

Abb. 12: Ergebnisse für den Ulandryk Kurgan (Abb. 11) projiziert auf die Kalibrierungskurve (siehe Text): ausgefüllte Kreise (HAJDAS et al. 2004b) und offene Kreise (KUZMIN et al. 2004). Der letzte Ring wurde auf 2267 $^{+13}/_{-21}$ cal BP (317 $^{+13}/_{-21}$ BC) datiert.

ogy. However, the older part of the calibration has to be based on records other than the trees. The radiocarbon ages of foraminifera shells from sediments of Cariaco Basin and measurements of ^{14}C on U/Th dated corals, all corrected for corresponding local reservoir age, have been used to construct the late glacial and glacial part of the calibration curve (12,400-26,000 cal BP) (REIMER et al. 2004b) (Fig. 13). In addition to the atmospheric calibration curve, a global mix layer marine reservoir age has been modelled and used for construction of a marine calibration (HUGHEN et al. 2004b).

Extension of the calibration curve to the limits of the radiocarbon method is of great interest to the wide range of palaeoclimate studies and archaeological research. Corals, marine and lake sediments and stalagmites may provide continuous records of ^{14}C changes (Fig. 14). In addition, Marine Isotope Stage 3 Kauri wood found in bogs of New Zealand is being studied for this purpose (HOGG et al. 2007, TURNEY et al. 2007). In the future, an updated data set of INTCAL04 will allow conversion of radiocarbon ages older than 21000 BP to the estimated (not yet calibrated) calendar ages (RAMSEY et al. 2006).

Another problem of the calibration curve that must be considered is the reconstruction of the temporal as well as spatial variations of the marine reservoir effect. Variations documented for specific locations and periods (for summary see REIMER & REIMER 2001) may affect radiocarbon-based chronologies of the marine records. Efforts are being made to reconstruct such variations using high-resolution chronologies of marine records (BONDEVIK et al. 1999, 2001, 2006; MANGERUD et al. 2006) or to model it (FRANKE et al. 2008).

9 Summary and outlook

As long as carbon-bearing material is available, radiocarbon dating methods allow measurement of the isotopic composition of the material, which is only limited to the materials formed during the last 50-55 ka. The measured ^{14}C /^{12}C ratio relative to the reference material allows calculation of the radiocarbon age. However, due to the complicated history of ^{14}C, this age requires translation to the calendar age.

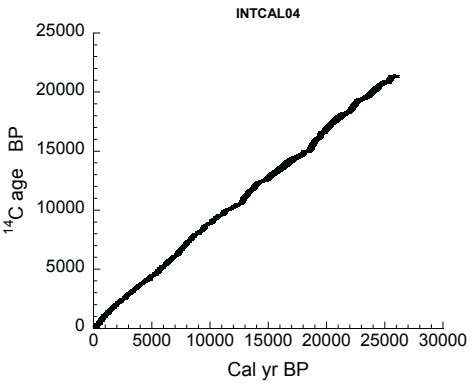

Fig. 13: Radiocarbon calibration curve of INCAL04 (REIMER et al. 2004a).

Abb. 13: Radiokohlenstoff-Kalibrierungskurve INTCAL04 (REIMER et al. 2004a).

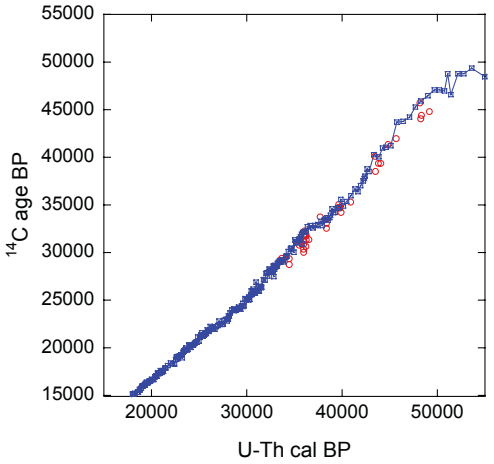

Fig. 14: Reconstruction of past variation in ^{14}C content based on measurements of foraminifera (squares) from Cariaco Basin; with the calendar time scale obtained by climatic correlation to U/Th dated stalagmites from the Hulu Cave (Hughen et al. 2006; Wang et al. 2001). Included are also corals ages (circles) dated by both radiocarbon and U/Th (Fairbanks et al. 2005).

Abb. 14: Rekonstruktion vergangener Variationen im ^{14}C Gehalt basierend auf Messungen von Foraminiferen (Vierecke) aus dem Cariaco Becken, die durch Klimatische Proxy mit der Kalender-Zeitreihe U/Th-datierter Stalagmiten aus der Hulu Cave korreliert wurden (Hughen et al. 2006; Wang et al. 2001) und Korallen (Kreise). Zudem sind Korallenalter enthalten, die sowohl durch Radiokohlenstoff als auch U/Th datiert wurden (Fairbanks et al. 2005).

Sampling and sample preparation are important steps in obtaining reliable radiocarbon ages. Measurements and error analysis, corrections for fractionation and reservoir effect are the next steps that are followed by the calibration of the radiocarbon age. From the very beginning of the method, all these components have been under constant development. Improved preparation techniques allow the selection of material free of contamination that is most suitable for dating. Twenty-five years ago, the development of the AMS revolutionised radiocarbon dating allowing for analyses on samples containing only a few mg of carbon (as compared to grams needed for conventional radiocarbon dating method). Calibration issues were also recognised and great efforts of many international groups resulted in the calibration curves that are presently in use. This work is being continued and remains a great challenge to the radiocarbon dating community.

During the last ten years, novel solutions in the AMS technique resulted in lowering energies needed for successful separation of C isotopes. Radiocarbon-dating dedicated small AMS setups are becoming a reality, allowing for higher throughput and shorter turnaround time of samples (Suter et al. 2007; Synal et al. 2007). Moreover, sophisticated preparative methods allow for separation of carbon at the molecular level (e.g., Eglinton et al. 1996, Ingallis et al. 2004, Von Reden et al. 1998), providing opportunity for tracing contamination. The AMS systems that operate with a gas ion source allow measurements to be performed on CO_2 (Ruff et al. 2007). Samples containing few micrograms of C are combusted and their isotopic composition is measured without the graphitisation step involved. This technical development marks another revolution in radiocarbon dating that will allow radiocarbon dating at the molecular level. Thanks to this development, the great value of ^{14}C as an environmental tracer is becoming very appealing in addition to its usefulness as a dating tool.

Acknowledgments

Special thanks to all the colleagues from the AMS facility at ETH Zurich for support of my ^{14}C research of the last 20 years. Liping Zhou and Anne Hormes provided very helpful reviews of this manuscript.

References

Arnold, J. R. & Libby, W. F. (1949): Age Determinations by Radiocarbon Content - Checks with Samples of Known Age. – Science, 110: 678-680.

Arslanov, K. A. & Svezhentsev, Y. S. (1993): An Improved Method for Radiocarbon Dating Fossil Bones. – Radiocarbon, 35: 387-391.

BEER, J., SIEGENTHALER, U., BONANI, G., FINKEL, R. C., OESCHGER, H., SUTER, M. & WOLFLI, W. (1988): Information on Past Solar-Activity and Geomagnetism from Be-10 in the Camp Century Ice Core. – Nature, 331: 675-679.

BIRD ,M. I., AYLIFFE, L. K., FIFIELD, L. K., TURNEY, C.S.M., CRESSWELL. R.G., BARROWS. T. T. & DAVID. B. (1999): Radiocarbon dating of "old" charcoal using a wet oxidation, stepped-combustion procedure. – Radiocarbon. 41: 127-140.

BLAAUW, M., BAKKER, R., CHRISTEN, J.A., HALL, V.A. & VAN DER PLICHT, J. (2007): A Bayesian framework for age modeling of radiocarbon-dated peat deposits: Case studies from the Netherlands. – Radiocarbon, 49: 357-367.

BLAAUW, M. & CHRISTEN, J.A. (2005): Radiocarbon peat chronologies and environmental change. –Journal of the Royal Statistical Society Series C-Applied Statistics, 54: 805-816.

BONANI, G., BEER, J., HOFMANN, H., SYNAL, H. A., SUTER, M., WÖLFLI, W., PFLEIDERER, C., JUNGHANS, C. & MÜNNICH, K.O. (1987): Fractionation, precision and accuracy in ^{14}C and ^{13}C measurements. – Nuclear Instruments and Methods in Physics Research, B29: 87-90.

BONDEVIK, S., BIRKS, H.H., GULLIKSEN, S. & MANGERUD, J. (1999): Late Weichselian marine C-14 reservoir ages at the western coast of Norway. – Quaternary Research, 52: 104-114.

BONDEVIK, S., MANGERUD, J., BIRKS, H.H., GULLIKSEN, S. & REIMER, P. (2006): Changes in North Atlantic Radiocarbon Reservoir Ages During the Allerød and Younger Dryas. – Science, 312: 1514-1517.

BONDEVIK, S., MANGERUD, J. & GULLIKSEN, S. (2001): The marine C-14 age of the Vedde Ash Bed along the west coast of Norway. – Journal of Quaternary Science, 16: 3-7.

BROECKER, W., BARKER, S., CLARK, E., HAJDAS, I. & BONANI, G. (2006): Anomalous radiocarbon ages for foraminifera shells. – Paleoceanography 21: PA2008, doi:10.1029/2005PA001212.

BROECKER, W., MATSUMOTO, K., CLARK, E., HAJDAS, I. & BONANI, G. (1999): Radiocarbon age differences between coexisting foraminiferal species. – Paleoceanography, 14: 431-436.

BROWN, T. A., NELSON, D.E., VOGEL, J.S. & SOUTHON, J.R. (1988): Improved Collagen Extraction by Modified Longin Method. – Radiocarbon, 30: 171-177.

BRUHN, F., DUHR, A., GROOTES, P.M., MINTROP, A. & NADEAU, M.J. (2001): Chemical removal of conservation substances by 'soxhlet'-type extraction. – Radiocarbon, 43: 229-237.

BUCK, C.E., CHRISTEN, J.A. & JAMES, G.N. (1999): BCal: an on-line Bayesian radiocarbon calibration tool. – Internet Archaeology 7: http: //intarch.ac.uk/journal/issue7/buck/.

BUCK, C.E., CAVANAGH, W.G. & LITTON, C.D. (1996): The Bayesian Approach to Interpreting Archaeological Data. – 377 S.; Chichester (Wiley).

BURR, G.S., EDWARDS, R.L., DONAHUE, D.J., DRUFFEL, E.R.M. & TAYLOR, F.W. (1992): Mass-Spectrometric C-14 and U-Th Measurements in Coral. – Radiocarbon, 34: 611-618.

CHANNELL, J.E.T., STONER , J.S., HODELL, D.A. & CHARLES, C.D. (2000): Geomagnetic paleointensity for the last 100 kyr from the sub-antarctic South Atlantic: A tool for inter-hemispheric correlation. – Earth and Planetary Science Letters, 175: 145-160.

CRAIG, H. (1953): The Geochemistry of the Stable Carbon Isotopes. – Geochimica Et Cosmochimica Acta, 3: 53-92.

CRAIG, H. (1954): Carbon-13 in Plants and the Relationships between Carbon-13 and Carbon-14 Variations in Nature. – Journal of Geology, 62: 115-149.

DE VRIES, H.L. & BARENDSEN, G.W. (1954): Measurements of Age by the Carbon-14 Technique. – Nature, 174: 1138-1141.

ELINGTON, T.I, ALUWIHARE L.I., BAUER J.E., DRUFFEL E.R.M. & MCNICHOL, A.P. (1996): Gas chromatographic isolation of individual compounds from complex matrices for radiocarbon dating. – Analytical Chemistry 68: 904-912.

FAIRBANKS, R.G., MORTLOCK, R.A., CHIU, T.-C., CAO, L., KAPLAN, A., GUILDERSON, T.P., FAIRBANKS, T.W., BLOOM, A.L., GROOTES, P.M. & NADEAU, M.-J. (2005): Radiocarbon calibration curve spanning 0 to 50,000 years BP based on paired 230Th/234U/238U and 14C dates on pristine corals. – Quaternary Science Reviews, 24: 1781-1796.

FINKEL, R.C. & SUTER, M. (1993): AMS in the Earth Sciences:Technique and Applications. – Advances in Analytical Geochemistry, 1: 1-114.

FRANKE, J., PAUL, A. & SCHULZ, M. (2008): Modeling variations of marine reservoir ages during the last 45 000 years. – Climate of the Past Discussions, 4: 81–110.

GODWIN, H. (1962): Half-Life of Radiocarbon. – Nature, 195: 984

HAJDAS, I. (1993): Extension of the radiocarbon calibration curve by AMS dating of laminated sediments of lake Soppensee and lake Holzmaar. – Diss. ETH Nr.10157 thesis: 147 S.; ETH Zurich.

Hajdas, I., Ivy, S.D., Beer, J., Bonani, G., Imboden, D., Lotter, A.F., Sturm, M. & Suter, M. (1993): Ams Radiocarbon Dating and Varve Chronology of Lake Soppensee - 6000 to 12000 C-14 Years BP. – Climate Dynamics, 9: 107-116.

Hajdas, I., Zolitschka, B., Ivy-ochs, S.D., Beer, J., Bonani, G., Leroy, S.A.G., Negendank, J.W., Ramrath, M. & Suter, M. (1995): Ams Radiocarbon Dating of Annually Laminated Sediments from Lake Holzmaar, Germany. – Quaternary Science Reviews, 14: 137-143.

Hajdas, I., Bonani, G., Zolitschka, B., Brauer, A. & Negendank, J.W. (1998): C-14 ages of terrestrial macrofossils from Lago Grande di Monticchio (Italy). – Radiocarbon, 40: 803-808.

Hajdas, I., Bonani, G., Hadorn, P., Thew, N., Coope, G.R. & Lemdahl, G. (2004a): Radiocarbon and absolute chronology of the Late-Glacial record from Hauterive/Rouges-Terres, Lake Neuchatel (CH). – Nuclear Instruments and Methods in Physics Research Section B: Beam Interactions with Materials and Atoms, 223-224: 308-312.

Hajdas, I., Bonani, G., Slusarenko, I.Y. & Seifert, M. (2004b): Chronology of Pazyryk 2 and Ulandryk 4 Kugrans based on high resolution radiocarbon dating and dendrochronology -a step towards precise dating of Scythian Burials. – In: Scott, E.M. (ed.): Impact of the Environment on the Human Migration in Eurasia: 107-116; Printed in the Netherlands (Kluwer Academic Publishers).

Hajdas, I., Bonani, G., Thut, J., Leone, G., Pfenninger, R. & Maden, C. (2004c): A report on sample preparation at the ETH/PSI AMS facility in Zurich. – Nuclear Instruments and Methods in Physics Research Section B: Beam Interactions with Materials and Atoms, 223-224: 267-271.

Hajdas, I., Bonani, G., Zimmerman, S.H., Mendelson, M. & Hemming, S. (2004d): C-14 ages of ostracodes from pleistocene lake sediments of the western Great Basin, USA-Results of progressive acid leaching. – Radiocarbon, 46: 189-200.

Hajdas, I., Lowe, D.J., Newnham, R.M. & Bonani, G. (2006): Timing of the late-glacial climate reversal in the Southern Hemisphere using high-resolution radiocarbon chronology for Kaipo bog, New Zealand. – Quaternary Research, 65: 340-345.

Hajdas, I., Bonani, G., Furrer, H., Mader, A. & Schoch, W. (2007): Radiocarbon chronology of the mammoth site at Niederweningen, Switzerland: Results from dating bones, teeth, wood, and peat. – Quaternary International, 164-65: 98-105.

Hatté, C., Morvan, J., Noury, C. & Paterne, M. (2001): Is classical acid-alkali-acid treatment responsible for contamination? An alternative proposition. – Radiocarbon, 43: 177-182.

Head, M.J. & Zhou, W. J. (2000): Evaluation of NaOH leaching techniques to extract humic acids from palaeosols. – Nuclear Instruments & Methods in Physics Research Section B-Beam Interactions with Materials and Atoms, 172: 434-439.

Higham, T., Ramsey, C.B., Karavanic, I., Smith, F.H. & Trinkaus, E. (2006a): Revised direct radiocarbon dating of the Vindija G(1) upper Paleolithic Neandertals. – Proceedings of the National Academy of Sciences of the United States of America, 103: 553-557.

Higham, T.F.G., Jacobi, R.M. & Ramsey, C.B. (2006b): AMS radiocarbon dating of ancient bone using ultrafiltration. – Radiocarbon, 48: 179-195.

Hogg, A.G., Fifield, L.K., Turney, C.S.M., Palmer, J.G., Galbraith, R. & Baillie, M.G.K. (2006): Dating ancient wood by high-sensitivity liquid scintillation counting and accelerator mass spectrometry - Pushing the boundaries. – Quaternary Geochronology, 1: 241-248.

Hogg, A. G., Fifield, L.K., Palmer, J.G., Turney, C.S.M. & Galbraith, R. (2007): Robust radiocarbon dating of wood samples by high-sensitivity liquid scintillation spectroscopy in the 50-70 kyr age range. – Radiocarbon, 49: 379-391.

Hua, Q. & Barbetti, M. (2004): Review of tropospheric bomb C-14 data for carbon cycle modeling and age calibration purposes. – Radiocarbon 46: 1273-1298.

Hughen, K., Lehman S., Southon J., Overpeck J., Marchal O., Herring C. & Turnbull J. (2004a): C-14 activity and global carbon cycle changes over the past 50,000 years. – Science 303: 202-207.

Hughen, K.A., Baillie, M.G.L., Bard, E., Beck, J.W., Bertrand, C.J.H., Blackwell, P.G., Buck, C.E., Burr, G.S., Cutler, K.B., Damon, P.E., Edwards, R.L., Fairbanks, R.G., Friedrich, M., Guilderson, T.P., Kromer, B., McCormac, G., Manning, S., Ramsey, C.B., Reimer, P.J., Reimer, R.W., Remmele, S., Southon, J.R., Stuiver, M., Talamo, S., Taylor, F.W., van der Plicht, J. & Weyhenmeyer, C.E. (2004b): Marine04 marine radiocarbon age calibration, 0-26 cal kyr BP. – Radiocarbon, 46: 1059-1086.

Hughen, K., Southon, J., Lehman, S., Bertrand, C. & Turnbull, J. (2006): Marine-derived C-

14 calibration and activity record for the past 50,000 years updated from the Cariaco Basin. – Quaternary Science Reviews, 25: 3216-3227.

HUMLUM O., ELBERLING B., HORMES A., FJORDHEIM K., HANSEN O. H. & HEINEMEIER J. (2005): Late-Holocene glacier growth in Svalbard, documented by subglacial relict vegetation and living soil microbes. – Holocene 15: 396-407.

INGALLS, A.E., ANDERSON, R.F. & PEARSON, A. (2004): Radiocarbon dating of diatom-bound organic compounds.-Marine Chemistry, 92: 91-105.

JULL, A.J.T. & BURR, G. S. (2006): Accelerator mass spectrometry: Is the future bigger or smaller? – Earth and Planetary Science Letters, 243: 305-325.

KROMER B. & MÜNNICH O. (1992): CO_2 gas proportional counting in radiocarbon dating--review and perspective. In: TAYLOR, R.E., LONG, A. & KRA, R.S. (eds) Radiocarbon after four decades. An interdisciplinary perspective: 184-197; New York (Springer Verlag)

KUZMIN, Y.V., SLUSARENKO, I.Y., HAJDAS, I., BONANI, G. & CHRISTEN, J.A. (2004): The comparison of C-14 wiggle-matching results for the 'floating' tree-ring chronology of the Ulandryk-4 burial ground (Altai mountains, Siberia). – Radiocarbon, 46: 943-948.

LAJ, C., KISSEL, C., MAZAUD, A., CHANNELL, J.E.T. & BEER, J. (2000): North Atlantic palaeointensity stack since 75 ka (NAPIS-75) and the duration of the Laschamp event. – Philosophical Transactions of the Royal Society of London Series a-Mathematical Physical and Engineering Sciences, 358: 1009-1025.

LAJ, C., KISSEL, C., SCAO, V., BEER, J., THOMAS, D.M., GUILLOU, H., MUSCHELER, R. & WAGNER, G. (2002): Geomagnetic intensity and inclination Variations at Hawaii for the past 98 kyr from core SOH-4 (Big Island): a new study and a comparison with existing contemporary data. – Physics of the Earth and Planetary Interiors, 129: 205-243.

LEVIN, I., HAMMER, S., KROMER, B. & MEINHARDT, F. (2008): Radiocarbon observations in atmospheric CO2: Determining fossil fuel CO2 over Europe using Jungfraujoch observations as background. – Science of The Total Environment, 391: 211-216.

LEVIN, I. & HESSHAIMER, V. (2000): Radiocarbon - A unique tracer of global carbon cycle dynamics. – Radiocarbon, 42: 69-80.

LEVIN, I. & KROMER, B. (2004): The tropospheric (CO2)-C-14 level in mid-latitudes of the Northern Hemisphere (1959-2003). – Radiocarbon, 46: 1261-1272.

LIBBY, W.F., ANDERSON, E.C. & ARNOLD, J.R. (1949): Age Determination by Radiocarbon Content - World-Wide Assay of Natural Radiocarbon. – Science, 109: 227-228.

LONGIN, R. (1971): New Method of Collagen Extraction for Radiocarbon Dating. – Nature, 230: 241-242.

MANGERUD, J., BONDEVIK, S., GULLIKSEN, S., KARIN HUFTHAMMER, A. & HOISAETER, T. (2006): Marine 14C reservoir ages for 19th century whales and molluscs from the North Atlantic. – Quaternary Science Reviews, Critical Quaternary Stratigraphy, 25: 3228-3245.

MANN, W.B. (1983): An International Reference Material for Radiocarbon Dating. – Radiocarbon, 25: 519-527.

MASARIK, J. & BEER, J. (1999): Simulation of particle fluxes and cosmogenic nuclide production in the Earth's atmosphere. – Journal of Geophysical Research, 104: 12099-12111.

MCCORMAC, F.G., HOGG, A.G., BLACKWELL, P.G., BUCK, C.E., HIGHAM, T.F.G. & REIMER, P.J. (2004): SHCal04 Southern Hemisphere calibration, 0-11.0 cal kyr BP. – Radiocarbon, 46: 1087-1092.

MOOK, W.G. & VAN DER PLICHT, J. (1999): Reporting C-14 activities and concentrations. – Radiocarbon, 41: 227-239.

NAYSMITH, P., SCOTT, E.M., COOK, G.T., HEINEMEIER, J., VAN DER PLICHT, J., VAN STRYDONCK, M., RAMSEY, C.B., GROOTES, P.M. & FREEMAN, S.P.H.T. (2007): A cremated bone intercomparison study. – Radiocarbon, 49: 403-408.

NYDAL, R., GULLIKSEN, S., LOVSETH, K. & SKOGSETH, F.H. (1984): Bomb C-14 in the Ocean Surface 1966-1981. – Radiocarbon, 26: 7-45.

NYDAL, R. & LOVSETH, K. (1965): Distribution of Radiocarbon from Nuclear Tests. – Nature, 206: 1029.

NYDAL, R. & LOVSETH, K. (1983): Tracing Bomb C-14 in the Atmosphere 1962-1980. – Journal of Geophysical Research-Oceans and Atmospheres, 88: 3621-3642.

NYDAL, R., LOVSETH, K. & SKOGSETH, F.H. (1980): Transfer of Bomb C-14 to the Ocean Surface. – Radiocarbon, 22: 626-635.

OLSSON, I. U., KARLEN, I. & STENBERG, A. (1966): Radiocarbon Variations in Atmosphere. – Tellus, 18: 293.

PATERNE, M., AYLIFFE, L.K., ARNOLD, M., CABIOCH, G., TISNERAT-LABORDE, N., HATTE, C., DOUVILLE,

E. & Bard, E. (2004): Paired C-14 and Th-230/U dating of surface corals from the Marquesas and Vanuatu (sub-equatorial Pacific) in the 3000 to 15,000 cal yr interval. – Radiocarbon, 46: 551-566.

Pawelczyk, S. & Pazdur, A. (2004): Carbon. isotopic composition of tree rings as a tool for biomonitoring CO2 level. – Radiocarbon, 46: 701-719.

Piotrowska, N. & Goslar, T. (2002): Preparation of bone samples in the Gliwice radiocarbon laboratory for AMS radiocarbon dating. – Isotopes in Environmental and Health Studies, 38: 267-275.

Ramsey, C.B. (2001): Development of the radiocarbon calibration program. – Radiocarbon, 43: 355-363.

Ramsey, C.B., Buck, C.E., Manning, S. W., Reimer, P. & van der Plicht, H. (2006): Developments in radiocarbon calibration for archaeology. – Antiquity, 80: 783-798.

Ramsey, C.B., van der Plicht, J. & Weninger, B. (2001): 'Wiggle matching' radiocarbon dates. – Radiocarbon, 43: 381-389.

Ramsey, C.B. (2008): Deposition models for chronological records. – Quaternary Science Reviews, 27: 42-60.

Reimer, P.J., Baillie, M.G.L., Bard, E., Bayliss, A., Beck, J.W., Bertrand, C.J.H., Blackwell, P.G. & Buck, C.E. (2004a): IntCal04 Terrestrial Radiocarbon Age Calibration, 0-26 Cal Kyr BP. – Radiocarbon, 46: 1029-1058.

Reimer, P.J., Baillie, M.G.L., Bard, E., Bayliss, A., Beck, J.W., Bertrand, C.J.H., Blackwell, P.G., Buck, C.E., Burr, G.S., Cutler, K.B., Damon, P.E., Edwards, R.L., Fairbanks, R.G., Friedrich, M., Guilderson, T.P., Hogg, A.G., Hughen, K.A., Kromer, B., McCormac, G., Manning, S., Ramsey, C.B., Reimer, R.W., Remmele, S., Southon, J.R., Stuiver, M., Talamo, S., Taylor, F.W., van der Plicht, J. & Weyhenmeyer, C.E. (2004b): IntCal04 terrestrial radiocarbon age calibration, 0-26 cal kyr BP. – Radiocarbon, 46: 1029-1058.

Reimer, P.J., Brown, T.A. & Reimer, R.W. (2004c): Discussion: Reporting and calibration of post-bomb C-14 data. – Radiocarbon, 46: 1299-1304.

Reimer, P.J. & Reimer, R.W. (2001): A marine reservoir correction database and on-line interface. – Radiocarbon, 43: 461-463.

Rom, W., Brenninkmeijer, C.A.M., Ramsey, C.B., Kutschera, W., Priller, A., Puchegger, S., Rockmann, T. & Steier, P. (2000): Methodological aspects of atmospheric (CO)-C-14 measurements with AMS. – Nuclear Instruments & Methods in Physics Research Section B-Beam Interactions with Materials and Atoms, 172: 530-536.

Rozanski, K., Levin, I., Stock, J., Falcon, R.E.G. & Rubio, F. (1995): Atmospheric (CO2)-C-14 variations in the Equatorial region. – Radiocarbon, 37: 509-515.

Ruff, M., Wacker, L., Gaggeler, H.W., Suter, M., Synal, H.A. & Szidat, S. (2007): A gas ion source for radiocarbon measurements at 200 kV. – Radiocarbon, 49: 307-314.

Scott, E.M. (2003a): Part 2: The Third International Radiocarbon Intercomparison (TIRI). – Radiocarbon, 45: 293-328.

Scott, E.M. (2003b): Section 1: The Fourth International Radiocarbon Intercomparison (FIRI). – Radiocarbon, 45: 135-150.

Scott, E.M. (2003c): Section 2: The Results. – Radiocarbon, 45: 151-157.

Scott, E. M., Boaretto, E., Bryant, C., Cook, G.T., Gulliksen, S., Harkness, D.D., Heinemeier, J., McGee, E., Naysmith, P. & Possnert, G. (2004): Future needs and requirements for AMS 14C standards and reference materials. – Nuclear Instruments and Methods in Physics Research Section B: Beam Interactions with Materials and Atoms, 223-224: 382-387.

Scott, E.M., Cook, G.T. & Naysmith, P. (2007a): Error and uncertainty in radiocarbon measurements. – Radiocarbon, 49: 427-440.

Scott, E.M., Cook, G.T., Naysmith, P., Bryant, C. & O'Donnell, D. (2007b): A report on phase 1 of the 5th International Radiocarbon Intercomparison (VIRI). – Radiocarbon, 49: 409-426.

Siegenthaler, U., Heimann, M. & Oeschger, H. (1980): C-14 Variations Caused by Changes in the Global Carbon-Cycle. – Radiocarbon, 22: 177-191.

Spalding, K.L., Bhardwaj, R.D., Buchholz, B.A., Druid, H. & Frisen, J. (2005a): Retrospective birth dating of cells in humans. – Cell, 122: 133-143.

Spalding, K.L., Buchholz, B.A., Bergman, L.-E., Druid, H. & Frisen, J. (2005b): ForensicsAge written in teeth by nuclear tests. – Nature, 437: 333-334.

Stuiver, M. & Polach, H.A. (1977): Reporting of C-14 Data - Discussion. – Radiocarbon, 19: 355-363.

Stuiver, M. & Reimer, P. (1989): Histograms Obtained from Computerized Radiocarbon Age Calibration. – Radiocarbon, 31: 817-823.

STUIVER, M. & REIMER, P.J. (1986): A Computer-Program for Radiocarbon Age Calibration. – Radiocarbon, 28: 1022-1030.

SUESS, H.E. (1955): Radiocarbon Concentration in Modern Wood. – Science, 122: 415-417.

SUTER, M., DOBELI, M., GRAJCAR, M., MULLER, A., STOCKER, M., SUN, G., SYNAL, H.-A. & WACKER, L. (2007): Advances in particle identification in AMS at low energies. – Nuclear Instruments and Methods in Physics Research Section B: Beam Interactions with Materials and Atoms, Accelerator Mass Spectrometry - Proceedings of the Tenth International Conference on Accelerator Mass Spectrometry, 259: 165-172.

SYNAL, H.-A., STOCKER, M. & SUTER, M. (2007): MICADAS: A new compact radiocarbon AMS system. – Nuclear Instruments and Methods in Physics Research Section B: Beam Interactions with Materials and Atoms, Accelerator Mass Spectrometry - Proceedings of the Tenth International Conference on Accelerator Mass Spectrometry, 259: 7-13.

SYNAL, H.A., BONANI, G., DOBELI, M., ENDER, R.M., GARTENMANN, P., KUBIK, P.W., SCHNABEL, C. & SUTER, M. (1997): Status report of the PSI/ETH AMS facility. – Nuclear Instruments & Methods in Physics Research Section B-Beam Interactions with Materials and Atoms, 123: 62-68.

TAYLOR, R.E., LONG, A. & KRA, R.S. (1992): Radiocarbon after Four Decades. – 596 S., New York (Springer-Verlag).

TURNEY, C.S.M., FIFIELD, L.K., PALMER, J.G., HOGG, A.G., BAILLIE, M.G.L., GALBRAITH, R., OGDEN, J., LORREY, A. & TIMS, S.G. (2007): Towards a radiocarbon calibration for oxygen isotope stage 3 using New Zealand kauri (Agathis australis). – Radiocarbon, 49: 447-457.

VAN DER PLICHT, J. & HOGG, A. (2006): A note on reporting radiocarbon. – Quaternary Geochronology, 1: 237-240.

VAN KLINKEN, G.J. & HEDGES, R.E.M. (1998): Chemistry strategies for organic C-14 samples. – Radiocarbon, 40: 51-56.

VENKATESAN, M.I., LINICK, T.W., SUESS, H.E. & BUCCELLATI, G. (1982): Asphalt in C-14-Dated Archaeological Samples from Terqa, Syria.-Nature, 295: 517-519.

VOELKER, A.H.L., GROOTES, P.M., NADEAU, M.J. & SARNTHEIN, M. (2000): Radiocarbon levels in the Iceland Sea from 25-53 kyr and their link to the Earth's magnetic field intensity. – Radiocarbon, 42: 437-452.

VOGEL, J.S., SOUTHON, J.R., NELSON, D.E. & BROWN, T.A. (1984): Performance of Catalytically Condensed Carbon for Use in Accelerator Mass-Spectrometry. – Nuclear Instruments & Methods in Physics Research Section B-Beam Interactions with Materials and Atoms, 233: 289-293.

VOGT, S., HERZOG, G.F. & REEDY, R.C. (1990): Cosmogenic Nuclides in Extraterrestrial Materials. – Reviews of Geophysics, 28: 253-275.

VON REDEN, K.F., MCNICHOL, A.P., PEARSON, A. & SCHNEIDER, R.J. (1998): C-14 AMS measurements of <100 mu g samples with a high-current system. – Radiocarbon, 40: 247-253.

WAGNER, G., BEER, J., LAJ, C., KISSEL, C., MASARIK, J., MUSCHELER, R. & SYNAL, H.-A. (2000): Chlorine-36 evidence for the Mono Lake event in the Summit GRIP ice core. – Earth and Planetary Science Letters, 181: 1-6.

WANG, Y.J., CHENG, H., EDWARDS, R.L., AN, Z. S., WU, J. Y., SHEN, C.C. & DORALE, J.A. (2001): A high-resolution absolute-dated Late Pleistocene monsoon record from Hulu Cave, China. – Science, 294: 2345-2348.

Eiszeitalter und Gegenwart Quaternary Science Journal	**57/1–2**	25–51	*Hannover 2008*

Magnetic dating of Quaternary sediments, volcanites and archaeological materials: an overview

Ulrich Hambach, Christian Rolf & Elisabeth Schnepp *)

Abstract: Magnetic dating includes all approaches dealing with the temporal variation of the Earth's magnetic field (EMF) as well as with the application of climate dependent variations of rock magnetic properties of sedimentary sequences and their correlation to independently dated palaeoclimatic archives. Palaeomagnetism has an outstanding impact on geosciences in general and especially on Quaternary chronology and palaeoclimate research. Palaeomagnetic dating employs the temporal variation of the direction as well as the intensity of the EMF on time scales from 10^2 to 10^7 years. The well-known temporal pattern of reversals of the EMF on time scales from 10^4 to 10^7 years and the shorter secular variation (amplitude 10-30°, time scale 1 to 10^3 years) provide an excellent tool for stratigraphic subdivisions. Records of the intensity variations of the EMF as well as the indirect dating by means of correlating rock magnetic property variations from sedimentary archives to dated palaeoclimatic records also serve as dating tools. Field methods as well as laboratory methods and techniques in data analysis will not be discussed in this paper. It is our aim to give a short and subjective overview on palaeomagnetism and magnetic susceptibility stratigraphy as dating tools in Quaternary science.

[Magnetische Datierung quartärer Sedimente, Vulkanite und archäologischer Materialien: Ein Überblick]

Kurzfassung: Unter magnetischer Datierung versteht man sowohl die Verfahren, die die zeitlichen Variationen des Erdmagnetfeldes (EMF) zur Altersbestimmung benutzen, als auch die Verwendung der klimaabhängigen Änderungen der gesteinsmagnetischen Parameter und ihre Korrelation mit unabhängig datierten paläoklimatischen Archiven. Die Paläomagnetik hat einen herausragenden Einfluss auf die Geowissenschaften genommen und im Besonderen zur Etablierung der Chronologie des Quartärs und der Paläoklimaforschung beigetragen. Die paläomagnetische Datierung benutzt die zeitlichen Variationen der Richtung wie der Intensität des EMFs auf Zeitskalen von 10^2 bis 10^7 Jahren. Das wohlbekannte zeitliche Muster von Polaritätswechseln des EMFs auf Zeitskalen von 10^4 bis 10^7 Jahren wie auch die Säkularvariation (Amplitude 10-30°, Zeitskala 1 bis 10^3 Jahre) stellen ein hervorragendes Werkzeug für die Unterteilung von sedimentären oder vulkanischen Gesteinsabfolgen dar. Aufzeichnungen der Änderungen der Intensität des EMFs sowie die indirekte Datierungen über den Vergleich der Variation gesteinsmagnetischer Parameter in Sedimentarchiven mit anderen datierten Paläoklimaserien können ebenfalls zur Datierung herangezogen werden. Weder die Methoden im Gelände und im Labor, noch die Techniken der Datenanalyse werden in dieser Publikation angesprochen. Unser Ziel ist vielmehr, einen kurzen und subjektiven Überblick über die Paläomagnetik bzw. magnetische Suszeptibilitätsstratigraphie als Datierungswerkzeug in der Quartärforschung zu geben.

Keywords: magnetic dating, Quaternary, palaeomagnetism, secular variation, magnetic susceptibility, stratigraphy

* Addresses of authors: U. Hambach, Chair of Geomorphology, Laboratory for Palaeo- and Enviro-Magnetism (PUM), University of Bayreuth, 94450 Bayreuth, Germany. E-Mail: ulrich.hambach@uni-bayreuth.de; C. Rolf, Leibniz Institute for Applied Geosciences (GGA), Stilleweg 2, 30655 Hannover, Germany. E. Schnepp, Chair of Geophysics, University of Leoben, Gams 45, 8130 Frohnleiten, Austria

1 Introduction

Palaeomagnetism, as a generic term for several sub-disciplines in geomagnetism (e.g., magnetostratigraphy, apparent polar wander, archaeomagnetism), is an essential part of geosciences. Its outstanding impact on geosciences in general and on the development of the model of plate tectonics in particular is widely appreciated. Rock magnetism (environmental magnetism) became famous in Quaternary research after its successful application as magnetic susceptibility stratigraphy for indirect dating of Asian loess deposits and their correlation to the global ice volume record.

The success and achievements of palaeo- and rock magnetism in earth sciences are amongst others, proven by the plenitude of monographs on these topics. For a deeper insight into the methods of palaeomagnetism, we refer to following textbooks without any claim for completeness (in chronological order): Collinson et al. (1967), McElhinny (1973), Stacey & Banerjee (1974), Collinson (1983), Tarling (1983), Thompson & Oldfield (1986), Soffel (1991), Butler (1992), Van der Voo (1993), Opdyke & Channell (1996), Dunlop & Özdemir (1997), Tauxe (1998), Maher & Thompson (1999), McElhinny & McFadden (2000), Evans & Heller (2003), Lanza & Meloni (2006).

Field methods as well as laboratory methods and techniques in data analysis will not be discussed here. For these topics we refer to textbooks (e.g., Collinson 1983; Butler 1992).

This paper does not want to appear as a textbock in miniature. The aim of this paper is to give a short overview on palaeomagnetism and magnetic susceptibility stratigraphy as dating tools in Quaternary science and to draw the reader's attention to the possibilities and problems of the methods.

2 The Earth's magnetic field

Our planet is surrounded by a magnetic field. The intensity of the Earth's magnetic field (EMF) on its surface is extremely weak

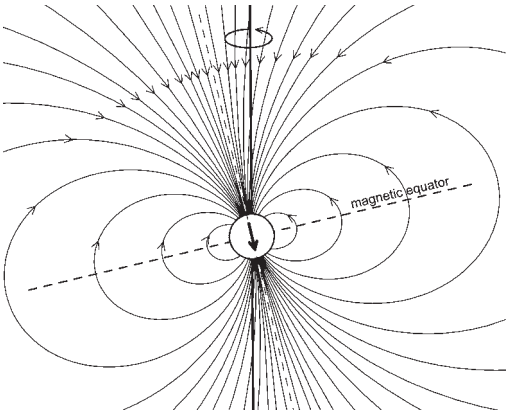

Fig. 1: Sketch of the Earth magnetic field (EMF) lines displaying its dipole character. Note the deviation of the dipole axis (dashed line) from the Earth's rotation axis. Redrawn from Schnepp (2007).

Abb. 1: Skizze der Feldlinien des Erdmagnetfeldes (EMF), welche den Dipolcharakter des Feldes anzeigt. Zu beachten ist auch, dass die Dipolachse (gestrichelte Linie) im Vergleich zur Rotationsachse der Erde geneigt ist (nach Schnepp 2007).

(30.000 – 60.000 $*10^{-9}$ (nano) Tesla) compared with technically used magnetic fields. It is, for example, several hundred times weaker than the field between the poles of a toy horseshoe magnet (Jacobs 1994). Monitoring the EMF in observatories all over the world during the last 400 years demonstrates its dominant dipole character. This dipole is inclined by about 10° against the rotation axis of the Earth (Fig. 1) today. The main elements (components) of the geomagnetic field vector are declination (D) and inclination (I) measured in degrees, the intensity of the total field (F) described by the horizontal component (H) and the vertical component (Z) pointing downwards into the Earth on the northern hemisphere (Fig. 2a). Declination describes the deviation of a compass needle (magnetic north) from true (geographic) north. Inclination is the angle between the horizontal plane and the total field vector, measured positive into the Earth. At the magnetic poles, the magnetic needle of an inclinometer points vertically; the horizontal intensity is zero, while total intensity reaches the maximum. At the magnetic equator, the

inclination is zero and the horizontal component is about half of the intensity at the pole. Accordingly, inclination as well as F, H and Z depend on the geographic latitude (Fig. 2b).

The elements of the geomagnetic field vary on time scales ranging from days to tens of millions of years owing to complex magneto-hydrodynamic processes that generate the geodynamo in the outer liquid core of the earth. The extent of these temporal changes is dependent upon the location on Earth due to non-dipole sources of the EMF. In terms of directional changes with time, we have to differentiate between three features: the most prominent is called geomagnetic polarity reversal, meaning a 180° flip of declination and a change of sign of the inclination (Fig. 3), i.e. the dipole would point to the geographic North Pole in Figure 1. The duration of such a transition is in the order of 10^3 to 10^4 years. Superimposed to this relatively abrupt and large change during a reversal, is a background variability of angular variation (10-30°) called secular variation (SV). This movement of the geomagnetic elements occurs on time scales from 1 to 10^3 years. The third feature is called geomagnetic excursion. This describes an incomplete reversal or a short time interval of anomalously high secular variation (more than 30°). This phenomenon is not fully understood at present. The strength of the field vector (intensity) varies with time on the same time scales, but the long-term behaviour is not well understood, because the little data that is available is also poor. Secular variation of intensity is in the order of ± 50 % of the present field strength, while during excursions and reversals a strong decay in intensity down to about 10 % of the present intensity is observed (Merrill et al. 1996). Palaeointensity is much more difficult to measure and its palaeomagnetic determination needs more complicated procedures than determination of palaeodirection. While measurements of the palaeofield direction are quick and applicable to most kinds of rocks, special conditions are needed for a successful determination of the absolute palaeointensity.

It is the main task of palaeomagnetism to identify the ancient geomagnetic direction and in-

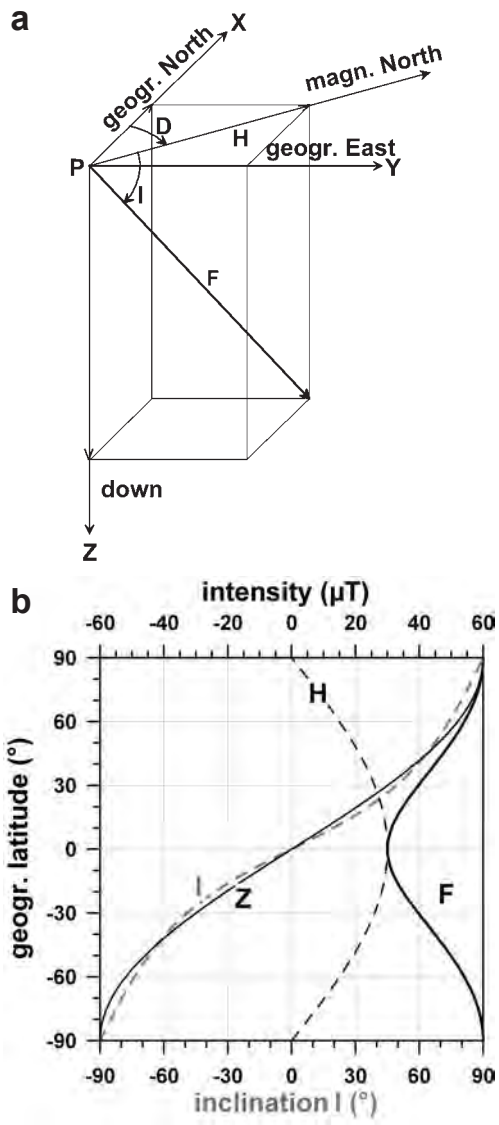

Fig. 2: (a) Earth magnetic elements shown in a Cartesian coordinate system at a point P of the Earth's surface (redrawn from Schnepp, 2007), (b) dependence of inclination (I) as well as total (F), horizontal (H) and vertical (Z) intensity (black) on geographic latitude.

Abb. 2: (a) Die erdmagnetischen Elemente sind in einem kartesischen Koordinatensystem für einen Punkt P auf der Erdoberfläche dargestellt (verändert nach Schnepp 2007); (b) zeigt den Zusammenhang zwischen Inklination (I) bzw. Total- (F), Horizontal- (H) und Vertikalintensität (Z, jeweils schwarz) und der geographischen Breite .

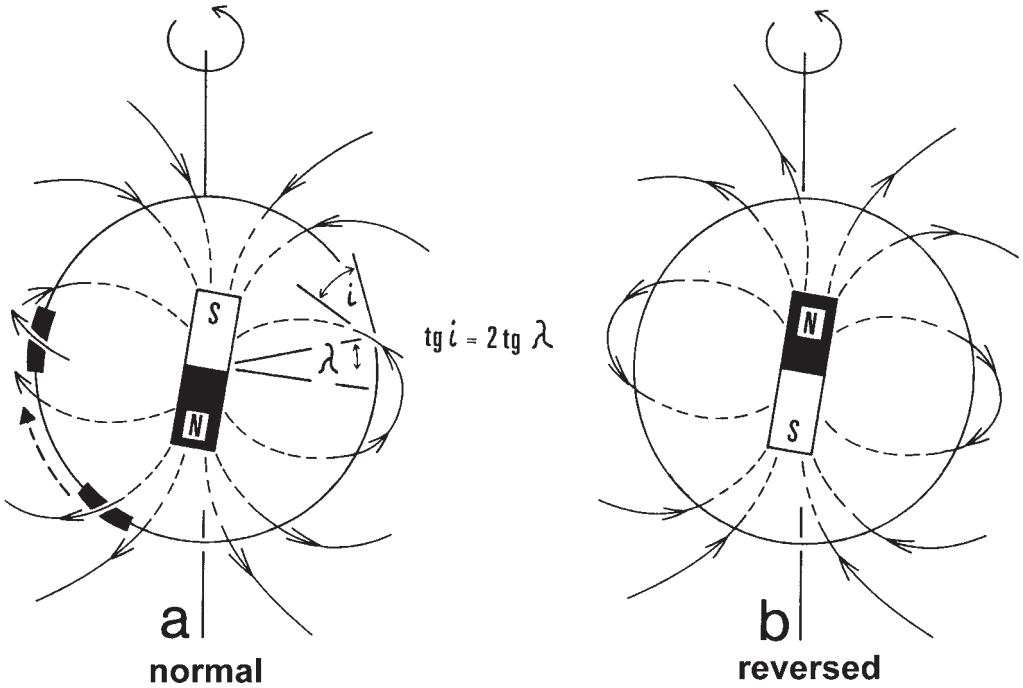

Fig. 3: Sketch of the Earth's magnetic dipole field in normal (a) and reversed (b) state. The bar magnet in the Earth's centre symbolizes the virtual dipole moment which is the main element of the EMF. Note the orientation of magnetic South and North. Also given is the dependence (dipole formula, see Fig. 2 (a)) of inclination (i) on geomagnetic latitude (λ). Redrawn from Hambach & Krumsiek (2000).

Abb. 3: Skizze des magnetischen Dipolfeldes der Erde mit normaler (a) bzw. inverser (b) Polarität. Der Stabmagnet im Erdmittelpunkt symbolisiert das axiale virtuelle Dipolmoment, den Hauptterm des EMFs. Zu beachten ist die Orientierung von magnetisch Süd und Nord. Weiterhin ist der Zusammenhang (Dipolformel, vergl. auch Abb. 2 (a)) von Inklination (i) und geographischer Breite (λ) angegeben (nach Hambach & Krumsiek, 2000).

tensity at the moment of formation of the rocks under investigation and to derive a chronology of temporal changes of these elements. This knowledge of the temporal geomagnetic field in the past offers chronometric possibilities on various geologic time scales. For chronological investigations, the use of quite short-lasting subchrons or even magnetic excursions is more effective than the use of chrons. In the following chapters, we will give examples and simple explanations for the use of the temporal change of elements of the geomagnetic field as dating tools in Quaternary research. In doing so, we will focus on examples from continental sedimentary archives and archaeomagnetic studies. For a deepened insight on palaeomagnetism see, for example, Butler (1992) and on the temporal characteristics of the geomagnetic field we refer to Channell et al. (2004a), Gubbins (2008) and Jacobs (1994).

3 Remanence acquisition

All information carried by the main elements of the geomagnetic field described above can be stored in almost every rock type and up to ages of more than billions of years. The carriers of the magnetic memory in rocks are ferrimagnetic and antiferromagnetic minerals. These are iron minerals, exclusively iron oxides/hydroxides

and sulphides, with special lattice properties that enable the storage of magnetic information over geological time at ambient temperature. For simplicity, we will call them magnetic minerals in the following (*sensu strictu*). We will give only a short introduction into the processes responsible for remanence acquisition. For a detailed description, we refer to the literature mentioned above (e.g., Butler 1992).

3.1 Magmatic rocks

In magmatic rocks, as well as in heated archaeological materials, a so-called thermoremanent magnetization (TRM) or thermoremanence carries the ancient signal of the EMF. A TRM is produced by cooling to temperatures below the Curie temperature (CT) in the presence of a magnetic field. The CT is a mineral specific temperature, generally lower than 700° C, below which the minerals become magnetic. The TRM at surface temperature can be stable over geological time and resistant to magnetic fields after original cooling. Best long-term recorders are flood basalt provinces with long-lasting volcanic activity such as the Deccan traps in India (Courtillot et al. 1986) or volcanites on Gran Canaria (Leonhardt et al. 2002). In case of rapid and frequent eruptions, it is even possible to record a complete change of polarity (Leonhardt et. al. 2002; Leonhardt & Soffel 2002). A TRM can also be the result of a metamorphic overprint, if the reached temperatures and/or time spans are sufficient.

3.2 Archaeological materials

Because rapid cooling of lava flows takes place on time scales of hours to years, a lava flow provides a spot reading of the EMF elements, which is stored as the TRM. The same happens when a hearth, oven, kiln or any other artificially fired structure is heated and cooled down in the EMF. They will obtain a TRM parallel to the EMF. For soil, clay or loam, apart from detrital or diagenetic Fe-bearing minerals, new magnetic minerals are formed under the influence of fire and hence the magnetism of the material is considerably enhanced (Le Borgne 1955). The TRM carried by young lavas or archaeological material is normally very stable and only minor secondary magnetisation components are observed.

3.3 Sediments

Sediments are able to record information about the EMF by a depositional process called acquisition of post-depositional remanent magnetisation (PDRM). During deposition and diagenesis, detrital magnetic minerals may become aligned parallel to the EMF and the sediment acquires the primary PDRM. Most of the detrital minerals involved in this process acquired their primary magnetic moment by thermal processes and carry therefore a stable TRM. In comparison to the thermal remanent magnetisation described earlier, the PDRM is normally less intensive and stable (for fundamentals see e.g., Hamano (1980) and Tucker (1980)). There are several processes that may weaken the primary (quasi-synsedimentary) magnetisation, for example bioturbation, compaction or alteration of magnetic minerals by changing chemical environments. As described by several authors (e.g., Bleil & von Dobeneck 1999; Evans & Heller 2003; Roberts & Winklhofer 2004) the most effective handicap against recording of short lasting subchrons is the lock-in mechanism. This mechanism describes the fixing of the magnetic remanence in sediments. Remanence locking does not happen immediately during deposition at or near to the sediment water interface, but needs a specific amount of sediment (lock-in depth) superposed to force dewatering, which in turn hinders grain rotation. The required lock-in time in case of fine grained clastics varies depending on grain size and sedimentation rate and was found to be in the order of 150 years in lake sediments with high sedimentation rates (Stockhausen 1998). Due to this process, it may happen that the lock-in depth (height of sediment necessary to fix magnetic remanence) needs more time to be collected than a subchron lasts. In that case, such a subchron may be entirely suppressed or masked. This is even more valid for the shorter

excursions of the magnetic field, which - if recorded and well dated - are excellent time markers.
The precipitation and growth of magnetic minerals during diagenesis and weathering is also an important process of remanence acquisition. This chemical process may lead to a stable so-called chemical remanent magnetisation (CRM). A CRM may occur in all kind of rocks at any time, if the environmental conditions are appropriate.

4 Methods in palaeomagnetic dating

Palaeomagnetic dating includes all approaches dealing with the temporal variation of the direction as well as with the intensity of the EMF on time scales from 10^2 to 10^7 years. On time scales of only a few million years, the well-known temporal pattern of reversals of the EMF provides an excellent tool for the subdivision of sedimentary sequences as well as volcanic rocks. Short-lived changes of the EMF (in the order of 10^3 years) in direction and intensity are called geomagnetic excursions, as stated above. If their chronology is known, they are perfect time markers, especially in sequences that are hardly datable by other methods. Records of the intensity variations of the EMF retrieved from sediments (relative palaeointensity), volcanic rocks and archaeological items (absolute palaeointensity) may also serve as dating tools and their application in stratigraphic studies is continuously increasing.

4.1 Magnetic polarity stratigraphy

Magnetic polarity stratigraphy or magnetostratigraphy is based on the temporal pattern of the reversals of the EMF as documented in the geomagnetic polarity timescale (GPTS). In the 1960s, it was found that sea floor spreading at mid-ocean ridges led to the characteristic bilateral symmetric 'stripes' of normal and reversed polarised oceanic crust. This pattern is measurable by ship based magnetometers and provides the basis for the GPTS (e.g., Cox et al. 1967). The GPTS serves as the main 'levelling rule' for the magnetic polarity stratigraphy from the recent back to the Early Jurassic (Fig. 4, 5).
Magnetic polarity stratigraphy is one of the excellent and independent tools (among others, e.g., oxygen isotope stratigraphy and orbitally tuned cyclo-stratigraphy) available for retrieving chronometric information, especially from sedimentary sequences. Magnetic polarity stratigraphy capitalises on the fact that the polarity of the EMF is recorded in rocks shortly after deposition. A distinction is drawn between chrons (10^5 – 10^7 years duration) and subchrons (10^4 – 10^5 years long). The first four chrons are usually named after famous geomagnetists (Brunhes, Matuyama, Gauss, Gilbert) and subchrons are named after the geographic location of their first discovery (Jaramillo, Olduvai). Both chrons and subchrons are helpful time markers, if recorded and classifiable (Channell et al. 2004a, Fig. 5).
The chronologic system used in magnetostratigraphy was determined simultaneously with its development. A GPTS (Fig. 5) labelled with names was originally based on magnetic remanence data from continental volcanic sequences dated with K-Ar ages and it is mainly used in investigations of Quaternary and Early Tertiary rocks (Cox et al. 1967; Mankinen & Dalrymple 1979). In contrast, a GPTS with a numerical system, based on the scheme used for labelling the marine magnetic anomalies, is used for roughly the last 160 Ma, the time span with substantial portions of oceanic crust remaining in ocean basins (Cande & Kent 1995). The magnetic field anomalies are interpreted to be due to reversals of the geomagnetic field as recorded in the rocks of the oceanic crust (Fig. 4). A more detailed discussion about the nomenclature and evolution of the different GPTSs in use can be found e.g. in Jacobs (1994), McElhinny & McFadden (2000) or Opdyke & Channell (1996).
Combining GPTS and Milankovitch climate cyclicity improved application and led to a powerful geochronometer called the astronomical polarity timescale (APTS). APTS has improved accuracy of chronology for the Pliocene and Pleistocene and is now even used for calibrating high-precision radiometric dating (e.g., Bassinot et al. 1994; Kent 1999).

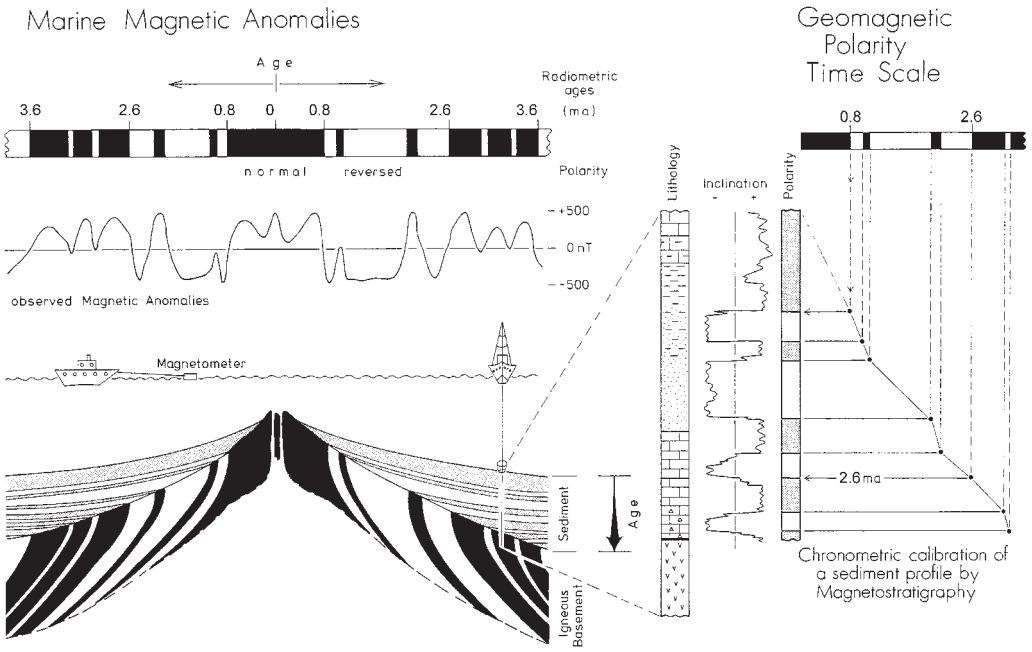

Fig. 4: Sea floor spreading at mid-ocean ridges leads to the characteristic bilateral symmetric 'stripes' of normal and reversed polarised oceanic crust. This pattern is measurable by ship-based magnetometers and provided the basis for the Geomagnetic Polarity Time Scale (GPTS). The GPTS serves as the 'levelling rule' for the magnetic polarity stratigraphy. From Hambach & Krumsiek (2000).

Abb. 4: Die Bildung von neuem Ozeanboden (sea floor spreading) an den mittelozeanischen Rücken führt zu den charakteristischen, bilateralen, symmetrischen ‚Streifen' von normal und invers magnetisierter ozeanischer Kruste. Dieses Muster wird mit Seemagnetik gemessen und lieferte die Basis für die geomagnetische Polaritätszeitskala (GPTS). Die Magnetostratigraphie benutzt die GPTS zur Kalibration der Zeit (aus Hambach & Krumsiek, 2000).

4.1.1 Magnetic polarity stratigraphy in sedimentary archives

With respect to sediments, the situation is generally complex. Firstly, in limnic and marine sediments, conditions for recording the complete succession of changes in the EMF prevail frequently (Channell 1999; Clement & Kent 1987; Frank et al. 2007; Nowaczyk et al. 1994), in contrast to fluvial continental sedimentation, which is very often far from being continuous. In their milestone publication about Chinese loess, Heller & Liu (1982) were able to demonstrate the great potential of Quaternary continental sediments for magnetostratigraphy. This was the starting point for a great variety of studies in Quaternary sediments all over the world (e.g., Langereis et al. 1997; Rolph 1993; Rösler et al. 1997; Worm et al. 1998; see textbooks by Evans & Heller 2003 and Opdyke & Channell 1996). Secondly, remanence lock-in of sediments (see chapter 3.1) does not happen immediately after deposition but needs a specific amount of sediment superposed to force dewatering (e.g., Bleil & von Dobeneck 1999; Butler 1992; Evans & Heller 2003; Tauxe 1998).

In the following, we will discuss some exemplary studies in which magnetic polarity stratigraphy was successfully applied to continental sediments. Though there have been many attempts to date Quaternary sediments

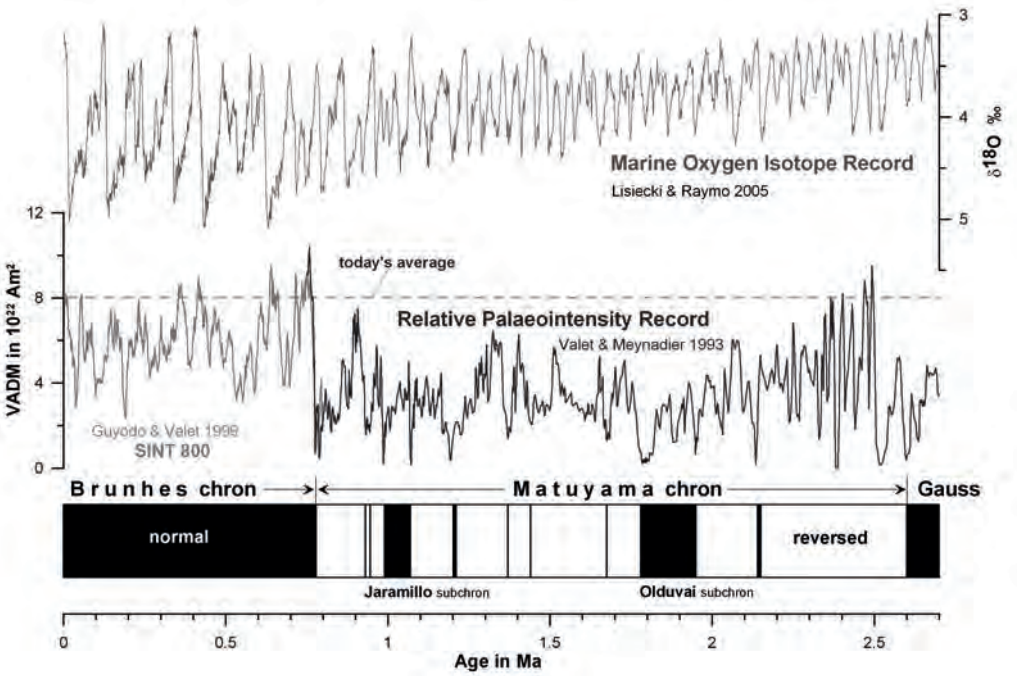

Fig. 5: The GPTS of the Quaternary is characterised by the normal Brunhes and the reversed Matuyama chron, of which the latter is interrupted by several subchrons. A record of Earth's magnetic axial dipole moment (VDAM) temporal variations is also shown. Note that the minima in RPI go together with polarity changes and that today's dipole moment is relatively high compared to most of the length of the Quaternary. The marine oxygen isotope record shows the evolution of the global ice volume and thus of the global climate. Data from Channell et al. (2004a) [GPTS], Valet & Meynadier (1993) and Guyodo & Valet (1999) [relative palaeointensity, RPI] and Lisiecki & Raymo (2005) [marine oxygen isotopes].

Abb. 5: Die GPTS des Quartärs unterteilt sich im Wesentlichen in die normale Brunhes- und die inverse Matuyama-Chrone, letztere ist von mehreren Subchronen unterbrochen. Eine Kurve der zeitlichen Änderung des Dipolmoments der Erde ist ebenfalls dargestellt. Man beachte das zeitgleiche Auftreten von Polaritätswechseln und Minima des Dipolmoments. Weiterhin beachtenswert ist die Stärke des heutigen Dipolmoments der Erde im Vergleich zu der während des Quartärs. Die marine Sauerstoffisotopenkurve zeigt die Entwicklung der globalen Eisvolumina und somit des globalen Klimas. Daten von Channell et al. (2004a) [GPTS], Valet & Meynadier (1993) und Guyodo & Valet (1999) [relative Paläointensität, RPI] and Lisiecki & Raymo (2005) [marine oxygen isotopes].

by palaeomagnetic methods in the last decades, the success story of magnetic polarity dating in continental Quaternary sequences started with the seminal work of Friedrich Heller and Tung-Sheng Liu assigning the Chinese loess to the Quaternary time table and correlating it with the global ice volume record (Heller & Liu 1982, 1984). For further reading we refer to Evans & Heller (2003) and Heller & Evans (1996).

In active orogenic belts such as the Alpine range, sedimentary sequences very often reveal only incomplete records representing short time intervals. Even though a polarity change is identified, due to the indistinguishability of magnetic polarity patterns for the last 3 million years (mainly because of negligible small tectonic movements of the European plate) the acquired data cannot be unambiguously assigned to any interval of the GPTS without further chronological information. Magnetic polarity stratigraphy on glacial sediments of the Iller-Lech-Platte showed problems in determination

of palaeodirections for these sediments carrying a remanence of weak intensity and difficulties on stratigraphic interpretation due to incompleteness of the profiles. However, it was possible to find the Matuyama-Brunhes boundary in two profiles on the Zusam gravel plain and to date it to older than 780 ka (Strattner & Rolf 1995).

Worm et al. (1998) studied a more than 4 km thick succession of delta sediments from Bangladesh that was devoid of firm dating through biostratigraphy or other methods. Applying classical magnetic polarity stratigraphy, a Lower Pleistocene to Lower Pliocene age could be assigned for the whole sequence. This new and reliable age model inferred a sedimentation rate of 1.2 m ka^{-1}, which appears to be one of the highest sedimentation rates in Earth history that was sustained for millions of years.

Pleistocene fluvial sequences in the eastern part of the Pannonian Basin were studied in order to establish a palaeoclimatic framework for the region (Nador et al. 2003). Magnetostratigraphy indicates that the sediment sequences span the last 2.6 Ma without significant hiatuses (Cooke et al. 1979). Comparison of systematic variations in magnetic susceptibility with changes in grain size distribution revealed Milankovitch-scale cyclicity in sedimentation. Comparison of pollen and gastropod paleoecological data with the magnetic susceptibility proxies suggests that climate was a major allogenic control factor on the cyclicity. This study convincingly demonstrates the potential of magnetic dating techniques even in fluvial sequences, which are important palaeoclimate archives on the continents.

The Quaternary stratigraphy of the North Sea and surrounding areas received essential support through magnetostratigraphic investigations. Maher & Hallam (2005) were able to determine stable magnetic polarities from discontinuous sediment sequences, of Plio/Pleistocene age, occurring onshore around the southern North Sea margins. The reliable palaeomagnetic polarity determinations were used, in combination with biostratigraphic data and in comparison with the GPTS, to ascribe correlations and absolute ages, which shed a new light, especially on the Quaternary stratigraphy of East Anglia.

The lower Rhine Embayment and the Rhine-Meuse-Delta in the Netherlands are complex sedimentary systems which recorded environmental changes of the Rhine catchment including even parts of the Alps (Preusser 2008). Their chronology is largely based on magnetostratigraphic studies (e.g. Boenigk & Frechen 2005; Zagwijn 1992), which provide the only time constraints especially for the Lower Pleistocene.

Magnetostratigraphic and rock magnetic investigations performed on fluvial sediments from the Ludwigshafen-Parkinsel drilling project (Upper Rhine Graben (URG), Germany) show the change from mainly locally controlled sedimentation from the graben margins to a more distinct alpine controlled sedimentation at a depth of 177 m by magnetic data (Rolf et al. 2008). Based on lithostratigraphic correlation with other sedimentary records from the URG and also based on palynological evidence, this event happened at the end of the Late Pliocene at the top of a normally polarised core interval (end of the Gauss Chron?). The well documented characteristic change in magnetomineralogy from goethite to greigite almost at the same stratigraphic level, was interpreted solely as a climatic signal, which can be correlated with the global climate change at ~2.6 Ma that is well documented in a wide range of sedimentary environments (e.g. deep-sea sediments, loess).

The chronology of early humans in Europe is intrinsically tied to the results of palaeomagnetic investigations at the excavation sites. From Dmanisi, Georgia, several findings of *Homo erectus* are reported from sediments containing a reversal and resting on normally polarised basalt. Supported by the faunal context, an age slightly younger than the Olduvai subchron was inferred making these human remains from Dmanisi the oldest in Eurasia (Gabunia et al. 2000). At Atapuerca, Spain, human remains (*Homo erectus*?) were found in cave debris that are reversely polarised. Combined bio- and magnetostratigraphy prove here

the existence of early humans already well before the Matuyama-Brunhes boundary (Pares & Perez-Gonzalez 1995). Also, the age of the earliest "German", the *Homo heidelbergensis* was constrained by palaeomagnetism. The investigation of several sedimentary units above and below the sand beds in which the jaw was found exhibit only normal polarity, assigning this beds doubtless to the Brunhes chron (Hambach et al. 1992; Wagner et al. 1997).

4.1.2 Magnetic polarity dating of magmatic rocks

Volcanic rocks are normally stable and firm recorders of the EMF. Yet due to the relatively short duration of volcanic activities compared to quasi-continuous recorders such as sediments, the magnetic information very often only represents spot-readings of the EMF and shorter reversals were frequently not recorded. If by chance a volcano was active during the life-time of an excursion or subchron, it might be possible to identify them (see chapter 4.1.3).

The volcanic oceanic crust represents by far the most important archive for the history of the EMF, going back to about 160 Ma at least. Sea floor spreading at mid-ocean ridges led to the characteristic bilateral symmetric 'stripes' of normal and reversed polarised oceanic crust. This pattern is measurable by ship-based magnetometers and provided the basis for the Geomagnetic Polarity Time Scale (GPTS) (Fig. 4). The GPTS serves as the 'levelling rule' for the magnetic polarity stratigraphy and its development started in the sixties of the last century. The beginning, however, was the work of Allen Cox who systematically measured volcanic rocks, which were dated by the contemporaneously improved K-Ar dating techniques. His early GPTS covered only the last 5 Ma, but allowed the determination of spreading rates, which in turn lead to the extrapolation of the GPTS back to the Early Jurassic (Cox et al. 1967; Opdyke & Channell 1996).

There are numerous magnetostratigraphic studies of volcanic sequences on continents. We would like to highlight the extensive work that was done on the Deccan traps in India (Courtillot et al. 1986). Only magnetic polarity was able to prove the unexpected short eruption interval for this immense amount of lava. In only about 1 Ma, exactly around the Cretaceous-Tertiary boundary, the complete succession of trap basalts were erupted and possibly contributed to the vast extinction event at the end of the Mesozoic.

Leonhardt et al. (2002) studied a continuous series of 87 lava flows from the mid-Miocene shield basalts of Gran Canaria. The sequence covers a reversal of the EMF from reverse to normal. Intermediate directions of the field are recorded in 34 lava flows and in addition to the reversal, three excursions (see chapter 4.1.3) are recorded. The results impressively demonstrate the potential of magnetic polarity studies for temporally highly resolved volcanic sequences and their relevance for understanding the processes controlling the geodynamo. Conventional K-Ar dating techniques are unable to resolve short-lived volcanic events and very often suggest continuous volcanic activity in a given time span. Palaeomagnetic data from the Quaternary alkali basaltic volcanic field of the Perşani Mountains, Romania, revealed sites with normal, transitional (excursional) and reversed polarity (Fig. 6). The combination of K-Ar dating with palaeomagnetic polarity determinations allowed the discrimination of short-lived volcanic phases of only a few thousand years duration, well beyond the precision of K-Ar dating (Panaiotu et al. 2004).

4.1.3 Geomagnetic Excursions as time markers

As discussed above, the shape of the EMF varies on time scales ranging from days to tens of millions of years. Long periodic amplitudinal and directional variations as polarity changes and even polarity transitions, as well as medium to long periodic secular variations (see chapter 4.2) are relatively well-known phenomena (Merrill et al. 1996). However, prominent short-lived features (< 5 ka) such as magnetic polarity episodes and reversal excursions are only rarely

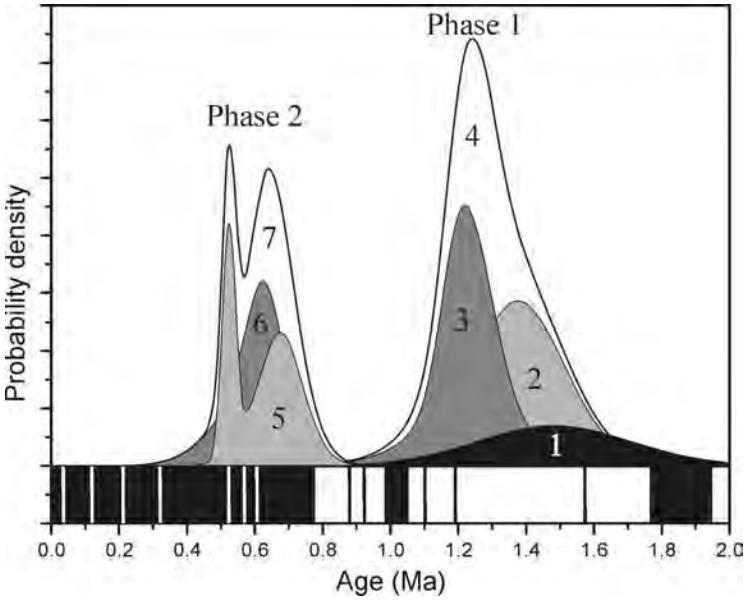

Fig. 6: Distribution of K-Ar ages from the Perşani Mountains, Romania. This alkali basaltic volcanic field revealed sites with normal, transitional (excursional) and reversed polarity. The individual density distributions display populations of normal, transitional (excursional) and reversed polarity sites separated (1-3, 5-6) and combined (4, 7). The combination of K-Ar dating with palaeomagnetic polarity determinations allows the discrimination of short-lived volcanic phases of only a few thousand years duration, well beyond the precision of K-Ar dating. Thin white and black bands are short lived polarity excursions (white) or subchrons (black, Matuyama). From Panaiotu et al. (2004).

Abb. 6: Verteilung der K-Ar-Alter der Perşani Berge, Rumänien. Dieses alkalibasaltische Vulkanfeld enthält Vulkanite mit normaler, transitionaler (exkursionaler) und inverser Polarität. Die Verteilungen zeigen Populationen mit normaler, transitionaler (exkursionaler) und inverser Polarität im Einzelnen (1-3, 5-6) bzw. die Gesamtverteilungen (4, 7). Die Kombination von K-Ar-Altern und der Bestimmung der magnetischen Polarität erlaubt die Unterscheidung von kurzen vulkanischen Phasen mit nur einigen Tausend Jahren Dauer, die durch die K-Ar-Datierung allein nicht aufgelöst werden können. Schmale weiße und schwarze Bänder sind kurzlebige Polaritätsexkursionen (weiß) oder Subchrons (schwarz, Matuyama). Aus Panaiotu et al. (2004).

documented. These rare features of the EMF, so-called geomagnetic events, are characterised by large deviations from the dipole direction often associated with a low relative palaeointensity. Most of them are found in the Brunhes chron (since 780 ka ago) where several have been documented in sedimentary and volcanic rocks. The reports include short-term reversals, which probably occur globally (e.g. Blake polarity episode), and reversal excursions whose extension is possibly regionally restricted (e.g. Fram Strait episode?). The significance and interpretation of geomagnetic events, and to a certain extent even their interpretation as real manifestations of the EMF, is still open to debate (Laj & Channell, 2007). Geomagnetic excursions probably originate from incomplete reversals that employ only a polarity change in the liquid outer, but not in the solid inner core (Gubbins 1999). Thus, the older picture of the geomagnetic field having long periods of stable polarity may not be correct; instead, the field appears to suffer many dramatic changes in direction and reduction in intensity.

The most significant progress in our understanding of temporal variations of the EMF

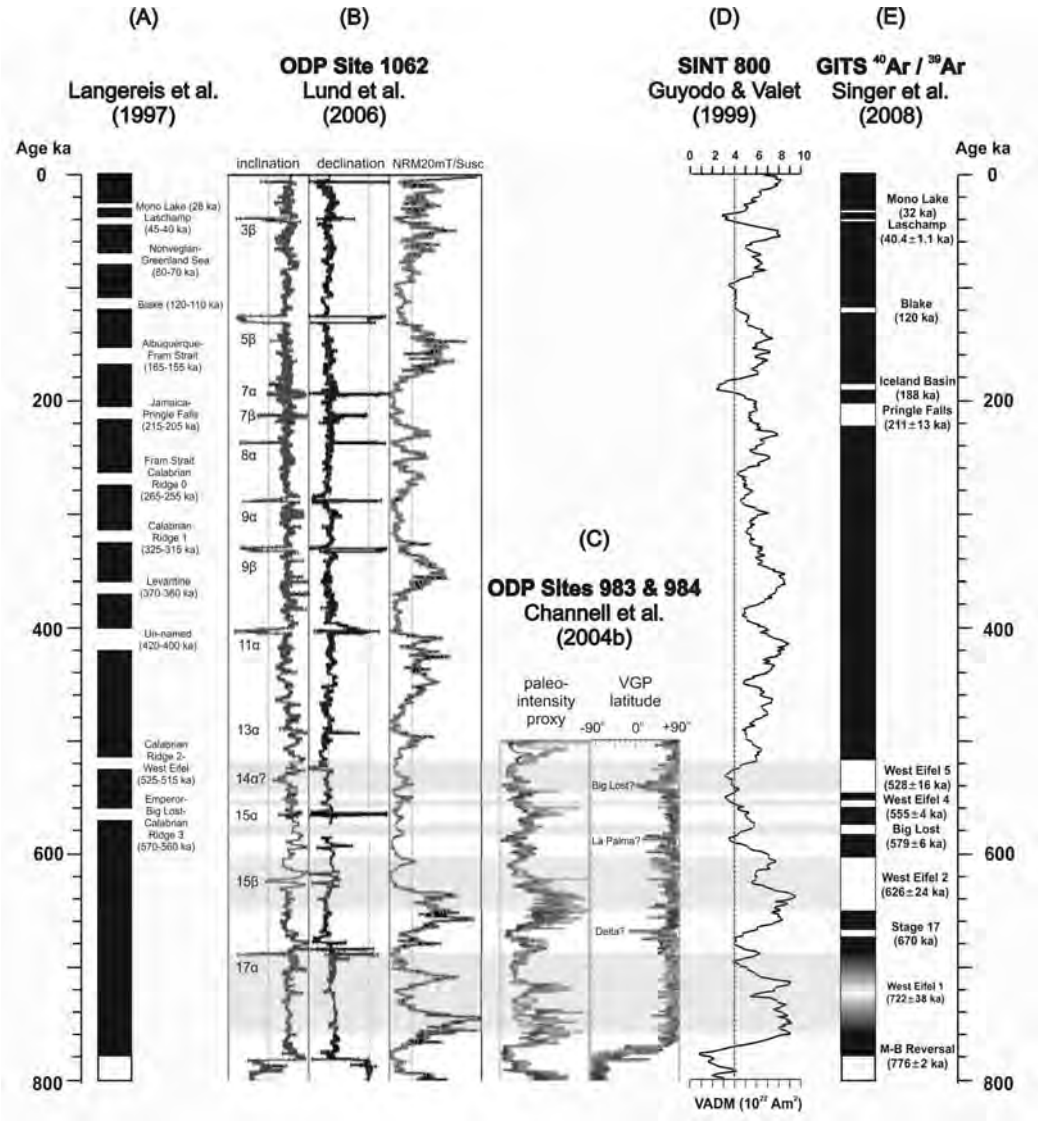

Fig. 7: Records of geomagnetic excursions and palaeointensity during the Brunhes Chron. Records are from: A) LANGEREIS et al. (1997), B) LUND et al. (2006), C) CHANNELL et al. (2004b), D) GUYODO & VALET (1999), and E) Geomagnetic Instability Time Scale (GITS) based on $^{40}Ar/^{39}Ar$ dated volcanic rocks plus excursions in marine sediment cores that have been dated via continuous oxygen isotope-based astrochronology (e.g. CHANNELL et al. 2004a). Redrawn from SINGER et al. (2008).

Abb. 7: Aufzeichnungen der geomagnetischen Exkursionen während der Brunhes-Chron. Die Kurven stammen von: A) LANGEREIS et al. (1997), B) LUND et al. (2006), C) CHANNELL et al. (2004b), D) GUYODO & VALET (1999), und E) Geomagnetische Instabilitätszeitskala (GITS) basierend auf $^{40}Ar/^{39}Ar$ datierten vulkanischen Gesteinen und Exkursionen aufgezeichnet in marinen Sedimentkernen, die mit einer kontinuierlichen astrochronologischen Sauerstoffisotopenkurve datiert wurden (z.B. CHANNELL et al. 2004a). Nach SINGER et al. (2008).

during the last decade stems from marine sedimentary records. This comes from relative palaeointensity curves in particular (see chapter 4.3), but some directional records also suggest that the processes that generate the EMF are highly dynamic and that temporal variations occur on a much shorter time scale than previously thought possible (Guyodo & Valet 1999; Lund et al. 2006; Nowaczyk et al. 1994). However, while changes of the virtual axial dipole moment (VADM) account for the global nature of apparently most of the (relative) minima of the relative palaeointensity variations, not all geomagnetic events or excursions in the Brunhes chron could be traced globally (Fig. 7).

Nevertheless, combined evidence suggest that at least 10 polarity events or excursions exist in the Brunhes chron, which are often not primarily preserved and / or diagenetically overprinted in most of sedimentary environments due to the palaeoclimatic conditions under which they were recorded (e.g., Bleil & von Dobeneck 1999; Langereis et al. 1997). However, an impressive record of well documented excursions has been published in the last years. Langereis et al. (1997) gave a thorough review of Brunhes age excursions and reported several new ones from a detailed study of an eastern Mediterranean piston core. Precisely calibrated astronomical reversal boundaries and ages for short-lived subchrons and polarity episodes in the Matuyama chron were published by Horng et al. (2002). The Ocean Drilling Program (ODP) recovered many long sediment sequences from around the world that contain medium- to high-resolution paleomagnetic records of Brunhes ages. Lund et al. (2006) collected the evidence for 17 excursions younger than the last reversal from these records and provided accurate ages based on oxygen isotope chronostratigraphies. From a marine core off Portugal going back to 400 ka, Thouveny et al. (2004) documented eight lows in relative palaeointensity. Four of these lows mark already well-known events and were also accompanied by directional excursions, which points to their global nature. From the ODP site 919, located in the Northern Atlantic, Channell (2006) found additional evidence for four already well documented excursions of the last 250 ka. This interval contains at least five polarity episodes with global evidence. From young to old these are: Mono Lake (32-34 ka), Laschamp (40-42 ka), Blake (115-120 ka), Icelandic Basin (~185 ka) and Pringle Falls (205-225 ka) (Channell 2006). In recent years, Brad Singer pointed out the instability of the dominant normal polarity of the Brunhes chron. Singer and his co-workers applied precise $^{40}Ar/^{39}Ar$ isochron dating on volcanic rocks containing excursional palaeomagnetic records. Combining their data with records from sediments, they constructed a Geomagnetic Instability Time Scale (GITS) for the Brunhes Chron (Singer et al. 2008, Fig. 7).

Geomagnetic excursions have even been reported from loess profiles. The earliest evidence dates back to the seventies and was later confirmed by numerous papers published in the mid 1990s (e.g., Reinders & Hambach 1995, and references therein; Evans & Heller 2001, for review and further reading). Recently, Pilipenko et al. (2006) and Zhu et al. (2006) presented records containing excursional directions from loess sections in the Ukraine and the Chinese loess plateau, proving that even loess units can record short-term features of the EMF.

We will not provide any listing of Brunhes excursions that could be useful stratigraphic markers, because their exact ages and timing as well as their global or only regional nature are still under debate. Therefore, we would like to draw the reader's attention to some recently published papers (e.g., Channell 2006; Lund et al. 2006; Singer et al. 2008) and we encourage them to follow the forthcoming relevant publications.

In the context of geomagnetic excursions, the possible link between climate and EMF is being increasingly addressed. Already Worm (1997) suggested "a link between geomagnetic reversals and events and glaciations" following the observation of a concomitant incidence of geomagnetic polarity events and sediments indicating periods of cold climate. The occurrence of excursions and reversals with the obliquity signal of the Earth's orbit was tested by Fuller (2006). His results have shown that

the strongest minima in the palaeomagnetic intensity records correlate with obliquity minima and suggest that precession provides some power to the geodynamo. In their study of a well dated marine core off Portugal, Thouveny et al. (2004) made the interesting observation that relative palaeointensity lows often coincide with the end of interglacial or interstadial stages. They found, furthermore, a dominant period in the relative palaeointensity record of about 100 ka and a phase shift between the $\delta^{18}O$ and the relative palaeointensity record in the order of 18 ka. Both findings may suggest the dependence of Earth's climate system and EMF upon the same driving process.
However, possible interactions between the Earth's climate system, the geodynamo and solar activity can presently not be proven. Further evidence and models have to be awaited. The papers of Courtillot et al. (2007) and Fuller (2006) give an up-to-date summary of the current state of discussion.

4.2 Secular variation

The shortest with palaeomagnetic techniques resolvable temporal variation of the EMF is a lower angular variation (10-30°) called secular variation (SV) occurring on time scales from 1 to 10^3 years. The SV of the EMF provides insight into processes in the outer liquid core of the Earth. Therefore, considerable effort has been undertaken to map the palaeomagnetic SV with high temporal resolution over long time-intervals from sites all over the world (e.g., Lund 1996; Stockhausen 1998). However, even for a relatively large area such as Europe, only few records exist that are considerable longer than the Holocene, or extend into the early Upper Pleistocene (Brandt et al. 1999; Thouveny et al. 1990).
SV is observed today by magnetic observatories, which are spread over the globe as well as by satellites, i.e. CHAMP or OERSTEDT (Olsen et al. 2006). Historic measurements of SV go back in time only 400 years (Jackson et al. 2000), whereas archaeomagnetic data cover the past two or three millennia for Europe (De Marco et al. 2008a; Gallet et al. 2002; Gómez-Paccard et al. 2006a, b; Márton & Ferencz 2006; Schnepp & Lanos 2005, 2006; Tema et al. 2006; Zananiri et al. 2007) and for America (Bowles et al. 2002, Sternberg 1989) and go back about 8000 years for a few places, i.e. Bulgaria (Kovacheva et al. 1998) (Fig. 9). Secular variation master curves have been obtained from many places on Earth with a broad range of time resolution and directional fidelity. An overview of the data sets obtained for the past 7000 years was given by (Korte et al. 2005). Well-defined archaeomagnetic secular variation curves have time resolutions in the order of 50-100 years. SV data from sediments often cover much longer time intervals, but here the time resolution as well as preciseness of the direction is lower (Fig. 8). While the so-called archaeomagnetic dating, which is also possible for lavas (Tanguy et al. 2003), provides a date with error margins (Lanos 2004; Le Goff et al. 2002), SV dating for lake sediments uses wiggle matching in order to correlate sedimentary profiles.

4.2.1 Dating with secular variation

Dating with secular variation (SV) is possible on time scales from decades to millennia for the past 50 ka. It can be applied to young volcanic rocks, lake sediments with high sedimentation rates, baked in-situ archaeological structures and, with limitations, to displaced ceramic material.
The dating process depends strongly on the material to be dated. Continuous data series obtained from sediments require wiggle matching techniques in order to replace depth by a time scale calibrated with SV patterns, whereas in contrast, volcanic rocks or archaeological materials provide spot readings of the direction (intensity), which allow calculation of a probability distribution of age, but does not necessarily provide a single date.

4.2.1.2 Archaeomagnetic dating

Archaeomagnetic dating uses detailed regional calibration curves with an error envelope (Fig.

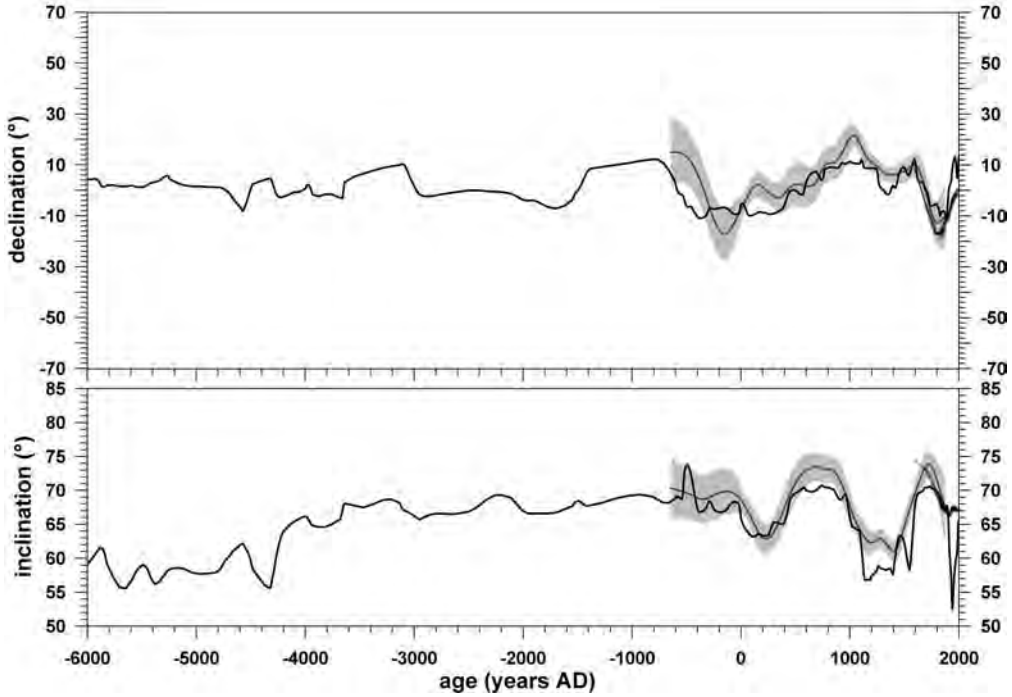

Fig. 8: Declination and inclination (black curves) for the past 6000 years obtained from paleomagnetic measurements of the Holzmaar sediments (Stockhausen 1998). The curves are shown in comparison with the German archaeomagnetic secular variation curve (Schnepp & Lanos 2005, see also Fig. 9, grey curves with 95% error envelope). In order to match the variation pattern, the time scale of the sediment curve was shifted by 125 years to younger dates.

Abb. 8: Deklination und Inklination (schwarze Kurven) der vergangenen 6000 Jahre, die aus paläomagnetischen Untersuchungen der Holzmaarsedimente gewonnen wurden (Stockhausen 1998). Die Kurven sind im Vergleich mit der deutschen archäomagnetischen Säkularvariationskurve (Schnepp & Lanos 2005, siehe auch Abb. 9, graue Kurven mit 95% Fehlerband) gezeigt. Damit die Variationsmuster der Sediment- und der archäomagnetischen Kurven zusammenpassen, wurde die Sedimentkurve um 125 Jahre zu jüngeren Altern hin verschoben.

8). This dating compares directions and intensities of unknown age against the curves and a probability distribution of age is obtained. Additional constraints (archaeological finds, stratigraphy) allow a reduction in ambiguity. Archaeomagnetic dating can be applied to in-situ fired structures and, with limitations, also to displaced material as potsherds or bricks. Whereas the polarity time scale is valid for the complete Earth, because a polarity reversal is a worldwide phenomenon, secular variations show regional patterns that cannot be transferred over very far distances (Casas & Incoronato 2007). Accordingly, a reference curve is required, which is valid for the region in which the archaeological structure was found or in which the displaced material was produced; for archaeomagnetic dating applications. Reference curves must be established first by studying the direction and/or intensity of well dated archaeological material for a certain region, before archaeomagnetic dating is possible (e.g., De Marco et al. 2008b).

Due to the lock-in mechanism in sediments mentioned above, a shift between archaeomagnetic SV variation curves and sedimentary

secular variation curves is observed, which has to be taken into account, if time resolutions below 500 years are required.
Besides archaeomagnetic reference curves, which are made for dating in specific regions, global models of the EMF are available (Korte & Constable 2005; Korte et al. 2005), which allow the calculation of secular variation curves for any place. The use of such model curves for dating purposes results in very uncertain ages. This has to be avoided for all regions from which no or only few data exist for the requested time interval.

4.2.1.3 Secular variation dating in sedimentary archives

In limnic and marine sediments, conditions for recording the complete succession of temporal changes of the EMF prevail frequently over diagenesis and other secondary processes. Normally, two questions are addressed before a palaeomagnetic record is analysed with respect to the underlying physical processes. Firstly, the crucial determination of a depth to time transformation to construct a well-defined time-series usually requires a multi-disciplinary approach, and several years, too. The second question addresses the nature of the record: how and when was the natural remanent magnetisation acquired; is it contemporaneous with the sedimentary matrix? If not, what is the time lag between sedimentation and remanence acquisition? In other words: is it possible to verify that a geological archive carries a record of the past variations of the EMF? Conventional techniques such as the stacking of multiple data from one lake (sedimentary environment) are used for such an evaluation. Supplementary arguments are then drawn from rock magnetic studies to construct plausibility arguments as to the origin of the stacked signal.
Warved sediments from the Eifel Maar lakes have been successfully used to retrieve reliable SV records for geomagnetic as well as for stratigraphic studies. The best record of the Holocene SV for Central Europe was derived from a thorough study of three Maar lakes from the West-Eifel (Germany) (Stockhausen 1998, see Fig. 8). Zolitschka et al. (2000) applied multiple dating methods and interlake comparison in order to establish a robust chronology for a Late Weichselian continental paleoclimate record from the Eifel Maar Lakes. Dating by means of SV serves here for the chronostratigraphic frame especially for the older part (10 – 23 ka) of the succession.
Reinders et al. (submitted) presented the so far "oldest" SV record for Germany from cores of the dry Maar Jungfernweiher in the southern West Eifel Volcanic Field. The record covers the time interval from approx. 60 – 100 ka and revealed a time interval of low SV which could be used to correlate the record to the SV records of Lac du Bouchet in Central France as well as to Lago Grande de Montichio in South Italy by wiggle matching (Brandt et al. 1999; Thouveny et al. 1990).

4.3 Dating by means of relative palaeointensity records

Not only the direction, but also the intensity of the EMF at a given point at the Earth's surface provides important information about the EMF itself. As the direction, the intensity also undergoes temporal variations. During a polarity reversal, the intensity goes down, probably to less than 10 % of the average values before or after the reversal (e.g., Jacobs 1994). The EMF also weakens dramatically (Fig. 5 and 7) during geomagnetic excursions (see chapter 4.1.3). The variation of the EMF intensity within the Brunhes normal chron is quite well-known and provides a tool for relative stratigraphic dating.
Absolute palaeointensity can be determined from magmatic rocks as well as from heated archaeological materials by simulating the remanence acquisition process in the laboratory (e.g., Schnepp & Hradetzky, 1994). In sediments, however, only a relative approximation for the intensity of the EMF at the time shortly after deposition is possible. For this purpose, the determined magnetic remanence is normalised by a measure for the concentration of magnetisable minerals in the sediment (Tauxe

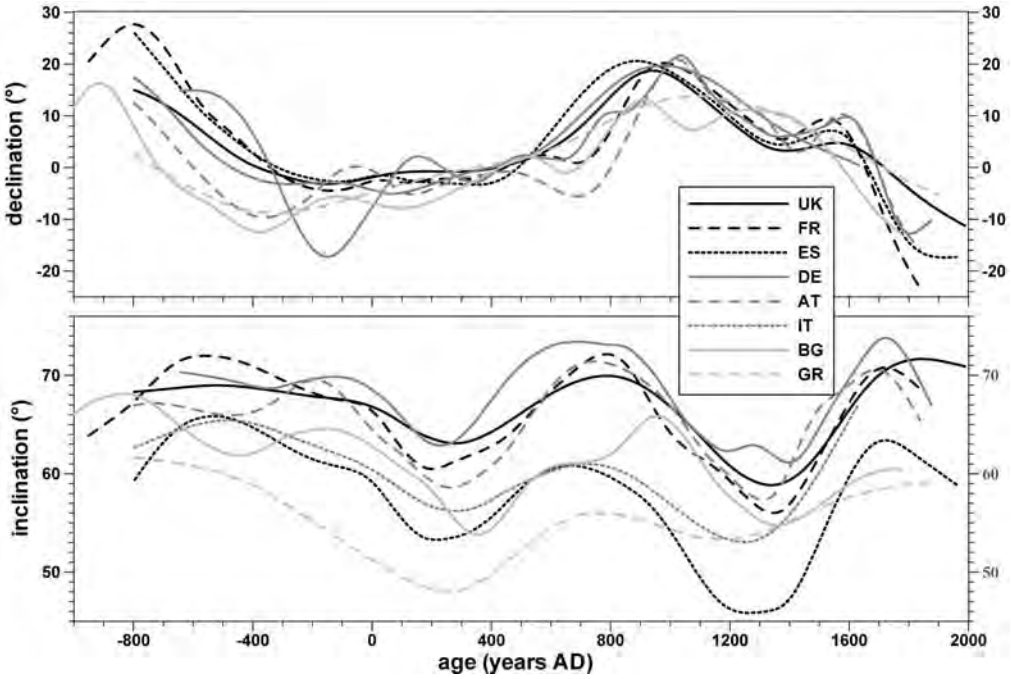

Fig. 9: Declination and inclination for archaeomagnetic secular variation reference curves are plotted versus time for several European countries: United Kingdom (UK, Zananiri et al. 2007), France (FR) and Spain (ES, Gómez-Paccard et al., 2006a, b), Germany (DE, Schnepp & Lanos 2005), Austria (AT, Schnepp & Lanos 2006), Italy (IT, Tema et al. 2006), Bulgaria (BG, Lanos 2004) and Greece (GR, De Marco et al., 2008a).

Abb. 9: Deklination und Inklination aufgetragen gegen die Zeit der archäomagnetischen Säkularvariations-referenzkurven für verschiedenen europäische Länder: Vereinigtes Königreich (UK, Zananiri et al. 2007), Frankreich (FR) und Spanien (ES, Gómez-Paccard et al. 2006a, b), Deutschland (DE, Schnepp & Lanos 2005), Österreich (AT, Schnepp & Lanos 2006), Italien (IT, Tema et al. 2006), Bulgarien (BG, Lanos 2004), und Griechenland (GR, De Marco et al. 2008a).

1998). The result is a relative palaeointensity (RPI) record that shows variations in the order of ten thousands to thousands of years (Fig. 5). Valet & Meynadier (1993) published one of the first long RPI records, which goes back 4 Ma and covers the whole Quaternary. For the past 800 ka, Guoyodo & Valet (1999) built a stack of globally distributed marine RPI records. This synthetic intensity record (SINT 800) is the best 'master curve' presently available on this timescale (Fig. 5). Short-lived variations in SINT 800, however, seem to be suppressed due to the stacking process. A very detailed data set with high temporal resolution covering the last 75 ka for the North Atlantic realm (North Atlantic PalaeoIntensity Stack, NAPIS) was published by Laj et al. (2000) and was extended later on to a global stack (Global PalaeoIntensity Stack, GLOPIS, Laj et al. 2004). High-resolution reconstruction of cosmogenic nuclide concentrations along sedimentary archives is an alternative approach for documenting past magnetic field changes. This approach is being increasingly applied in the study of marine as well as ice cores (e.g. Carcaillet et al. 2004).

Recent studies of high-resolution RPI records from European loess sites contain evidence for multiple RPI lows between approximately 22 and 45 ka, including the "Mono Lake" and

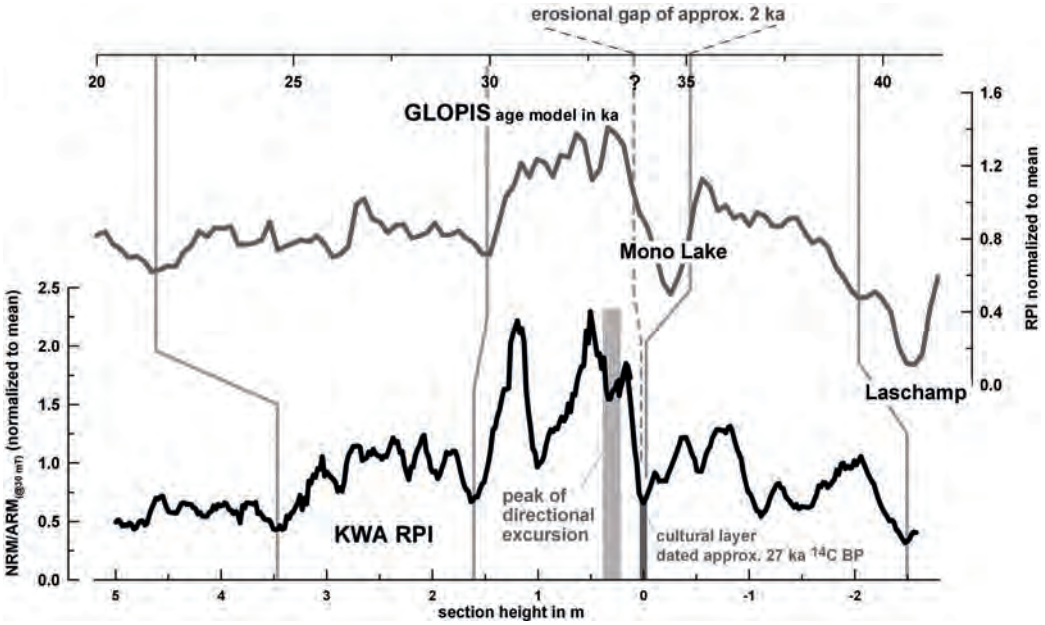

Fig. 10: A relative palaeointensity (RPI) record from a loess section in Krems (Lower Austria) and the Global Palaeointensity stack (GLOPIS). The Mono Lake and Laschamp geomagnetic excursions are characterised by pronounced intensity lows. Age (GLOPIS) and depth (from left: shallow, young to right: deep, old) are plotted on the abscissa vs. the RPI. Light grey lines indicate suggested correlations; a cultural layer dated by radiocarbon is indicated. From HAMBACH et al. (submitted).

Abb. 10: Die relative Paläointensität (RPI) gemessen an einem Lössprofil aus Krems (Niederösterreich) und der Global Palaeointensity stack (GLOPIS). Die geomagnetische Mono-Lake- und die Laschamp-Exkursion werden durch deutlich hervortretende Abschwächungen der Intensität charakterisiert. Alter (GLOPIS) bzw. Tiefe (von links (jung bzw. hangend) nach rechts (alt bzw. liegend)) sind auf der Abszisse gegen die RPI abgetragen. Hellgrau gestrichelte Linien verbinden die vorgeschlagene Korrelation der Kurven; eine mit Radiokohlenstoff datierte Kulturschicht ist angegeben. Aus HAMBACH et al. (submitted).

"Laschamp" geomagnetic excursions. The best documented RPI record stems from an archaeological site in Krems (Austria). The age model is based on AMS radiocarbon dates from cultural layers as well as on optical stimulated luminescence dating and RPI correlation to the GLOPIS stack. The investigation of the palaeomagnetic signal resulted in a reliable and comparable RPI record (Fig. 10). This high-resolution palaeomagnetic record clearly emphasises the yet largely undiscovered but high potential of quasi-continuously deposited loess sites, which contain archaeological materials for palaeomagnetic studies (HAMBACH et al. submitted; ZEEDEN et al. 2008).

5 Magnetic susceptibility stratigraphy

Nowadays, magnetic properties of sediments and soils are widely used in Quaternary palaeoclimatic, as well as in geoarchaeological, research to characterise the palaeoenvironment and to indirectly date sedimentary sequences. Magnetic property variations with depth/time in sedimentary sequences are mainly climatically controlled and therefore can serve as relative dating tools if the timing of palaeoclimatic variations is known independently.

Palaeomagnetism and enviromagnetism use the same physical methods and similar technologies, but deal with fundamentally differ-

ent phenomena. Palaeomagnetism is based on the fact that rocks can provide a record of the temporal variations of the EMF: Sediments may be regarded in this case as 'tape recorders' of the past EMF which we can decipher with palaeomagnetic methods. By knowing its temporal variations, one can indirectly date these sediments while correlating their records with 'master curves' (e.g., Butler 1992, Schnepp et al. 2004).

Enviromagnetism, the magnetism of sediments and soils (rock and mineral magnetism applied to environmental questions), however, describes the occurrence, abundance and properties of iron-bearing minerals in the environment: When we study the magnetic properties of sediments and soils as proxies for environmental change, we study the physical (magnetic) properties of the 'tape' itself and not the 'music', which is recorded on it (e.g., Evans & Heller 2003).

Magnetic grains, exclusively iron oxides/hydroxides and sulphides, occur virtually ubiquitously in Quaternary sediments, soils, dusts and organisms, albeit often in minor or trace concentrations. After sedimentation or reworking, they undergo diagenesis and pedogenesis when, for example, more humid conditions predominate, which is reflected in physical-chemical alterations of the sediment or soil. These alterations can also result in transformation, depletion as well as enhancement of magnetic minerals. Especially ferrimagnetic minerals react in ambient laboratory magnetic fields (measurement of magnetic susceptibility, MS) several orders of magnitude more strongly than other iron-bearing minerals. Thus, already very small amounts of magnetic minerals control the magnetic properties of sediments or soils. Furthermore, they may act as sensitive magnetic recorders of palaeoclimatic and palaeoenvironmental change. Changes in climate as well as human occupations produce changes in the environment, including sedimentary and soil-forming environments. Thus, magnetic information from a wide range of marine as well as continental sedimentary archives reflects alternating warm/humid and cold/dry climates during the Quaternary.

Therefore, MS and other magnetic parameters as functions of depth in sedimentary archives can serve as proxies for palaeoclimatic variations also on the continents and allow for a close match with the isotope records from Greenland and Antarctic ice cores as well as with all kinds of high-resolution palaeoclimatic archives on millennial scales.

Loess is by far the most important terrestrial archive that provides detailed palaeoclimatic information for the whole Quaternary and in China goes back to even the Pliocene. Heller & Liu (1984) first used magnetic susceptibility variations in Chinese loess to correlate the loess deposits to marine records. The MS variations in the loess-palaeosol couplets in the Chinese loess plateau resemble the pattern of the global ice volume record with higher values in palaeosols (interglacials) and lower values in loess (glacials). In China, magnetic susceptibility was found to reflect the intensity of pedogenesis, which in turn leads to enhancement of magnetic minerals in soils. However, in other parts of the world under different climatic conditions, even depletion of the magnetic fraction could be observed. Furthermore, the wind strength during dust transport and loess deposition also seems to control the magnetic mineralogy. With stronger winds, minerals with higher density such as iron oxides are enriched during aeolian transport. For a detailed discussion of these phenomena, we refer to Evans & Heller (2001, 2003).

The enhancement of magnetic minerals in loess during pedogenesis is by far the most important process that defines the magnetic properties of most loess deposits. The models that deal with the enhancement processes are essential for understanding the direct mineralogical reasons for magnetic susceptibility enhancement. The formation of ferrimagnetic minerals in the course of pedogenesis is the most important mechanism. Its rate and the equilibrium between the formation of magnetite/maghemite and other Fe-minerals are controlled by conditions in the soil environment such as temperature, moisture, pH and content of organic matter (Evans & Heller 2001). The most widely

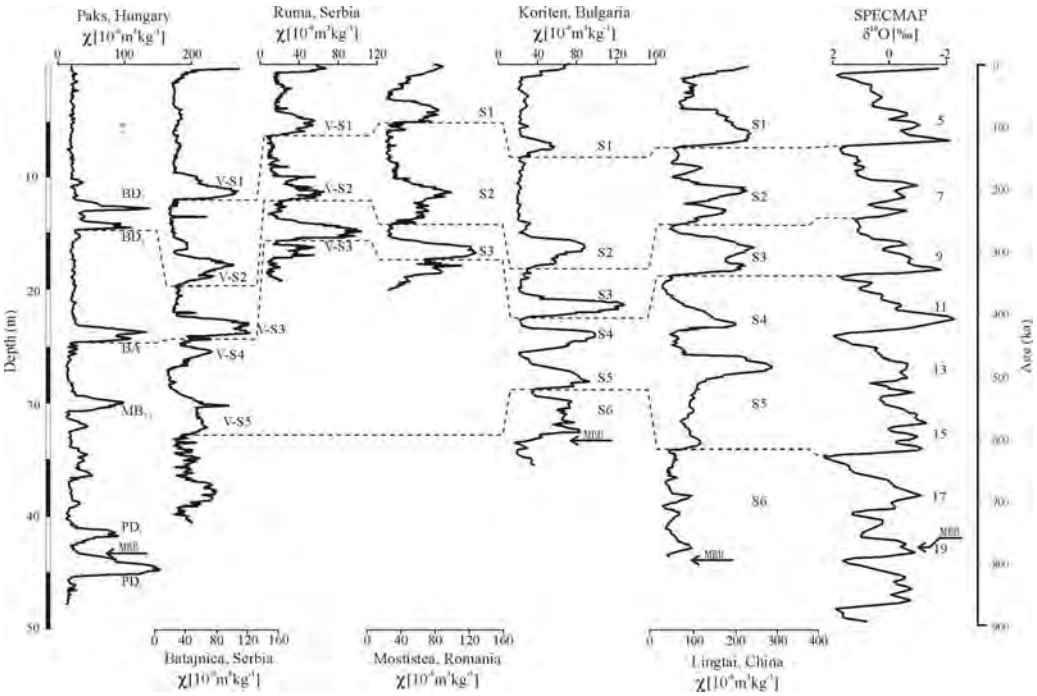

Fig. 11: Correlation of magnetic susceptibility records from Paks (SARTORI et al. 1999), Batajnica, Ruma (MARKOVIĆ et al. 2006), Mostistea (PANAIOTU et al. 2001) and Koriten (JORDANOVA & PETERSEN 1999), with the astronomically calibrated MS curve of the Chinese loess site Lingtai (SUN et al. 2006) and with the SPECMAP oxygen isotope record (IMBRIE et al. 1984). Note that all SE-European sections are plotted on the depth scale of the loess profiles at Paks. From MARKOVIC et al. (submitted).

Abb. 11: Korrelation von magnetischen Suszeptibilitäts Kurven aus Paks (SARTORI et al. 1999), Batajnica, Ruma (MARKOVIĆ et al. 2006), Mostistea (PANAIOTU et al. 2001) und Koriten (JORDANOVA & PETERSEN 1999) mit der astronomisch kalibrierten MS Kurve des chinesischen Lössprofils Lingtai (SUN et al. 2006) und mit der SPECMAP Sauerstoffisotopenkurve (IMBRIE et al. 1984). Zu beachten ist, dass alle SE-europäischen Profile mit dem Tiefenmaßstab des Lössprofils Paks gezeichnet wurden. Aus MARKOVIC et al. (submitted).

accepted model (CHEN et al. 2005; EVANS & HELLER 2001; MAHER 1998; THOMPSON & OLDFIELD 1986) assumes alternating reducing and oxidizing conditions in the beginning, which leads to a release of Fe^{2+} from the weathering of iron minerals. For the whole process, the relevance of iron-reducing bacteria is stressed by several authors (CHEN et al. 2005; EVANS & HELLER 2003; MAHER 1998). Finally, magnetite of extremely fine grain size is formed by dehydration and is still susceptible for dissolution. Only further oxidation to maghemite results in a more stable ferrimagnetic mineral giving the palaeosols in loess their magnetic characteristics (BUGGLE et al. in press; MAHER 1998).

Many previous investigations of loess-palaeosol sequences around the world have used MS as a basis for differentiating widespread loess and palaeosol units, correlating them regionally and relating them to the deep-sea isotope stratigraphy (e.g., HELLER & EVANS 1996; EVANS & HELLER 2001). Recently thick loess deposits from the Carpathian region were also studied using magnetic proxies. The application of the Chinese loess stratigraphical scheme (HELLER & LIU 1984) necessitates a serious revision of the earlier chronostratigraphic interpreta-

tions of the loess-palaeosol sequences in the Danube basins. In Figure 11, MS records from loess sections from the Middle and Lower Danube Basin (Hungary and Serbia to Romania and Bulgaria) are presented. The more than 40 m thick loess-palaeosol sequences on the Danube banks near Batajnica, Serbia, are characterised by sharp environmental differences between high dust accumulation rates during the glacials and reduced dust fluxes in the periods of palaeosol formation (Markovic et al., submitted). The correlation of the MS record at Batajnica to other records from the region as well to the global ice volume record (Imbrie et al. 1984), leads to a revised chronostratigraphic frame that yields deposition of loess during the last five interglacial-glacial cycles. This example demonstrates on the one hand the potential of MS stratigraphy as an indirect dating tool for the Middle and Upper Pleistocene across Eurasia and on the other hand its potential for analysing the long-term environmental dynamics within the context of regional, continental and global climate changes.

6 Summary and outlook

In our overview, we pointed out the potential of the largely underdeveloped application of magnetic dating techniques in the Quaternary. Though magnetic dating is already well established for marine sediments and volcanic rocks, in terrestrial sedimentary archives and for archaeological materials, its implementation is far from exhausted. Since the early 1980s, magnetostratigraphic and magnetic susceptibility dating has been extensively applied to Asian loess sequences. However, their applications to other loess provinces around the world and to other terrestrial sedimentary archives still lacks a breakthrough. While the refinement of the geomagnetic polarity time scale for the past 200 Ma has slowed down in recent times, a new potential seems to arise from the geomagnetic instability time scale for the past few Ma. High precision $^{40}Ar/^{39}Ar$ isochron dating now allows the correlation of geomagnetic excursions recorded in volcanic rocks with the worldwide relative palaeointensity stack of marine sequences. This provides a new and additional possibility for magnetostratigraphic dating for the Quaternary. The use of geomagnetic excursions as time markers in the Brunhes and Matuyama chrons, in combination with relative palaeointensity records derived from the same archives, will open a new perspective for dating of Middle and Lower Pleistocene sequences which are hardly datable by other methods.

As the Quaternary is the first period in Earth's history in which the climate and the biosphere are influenced by non-system players (humans), the knowledge about past climates is essential for our understanding of future climate change. Magnetic dating techniques are among the few dating methods, which can be applied to a wide range of geological archives and that can help us to decipher what happened in the past and can help improve predictions of future climate changes.

We have hopefully demonstrated the success and achievements of palaeo- and rock magnetism in earth science in general and for Quaternary research in particular and we would be very pleased, if our contribution publicises magnetic dating techniques to a broader geoscientific audience.

Acknowledgements

The authors would like to thank, first of all, Frank Preusser, the editor of this special volume of Quaternary Science Journal (Eiszeitalter und Gegenwart). Without his persistent encouragement and never ending patience, this paper would never have been finished. Constructive reviews by Thomas Fredrichs, Robert Scholger and an anonymous reviewer significantly improved the quality of the manuscript.

References

Bassinot, F. V., Labryie, L. D., Vincent, E., Quidelleur, X., Shackleton, N. J. & Lancelot, Y. (1994): The astronomical theory of climate and

the age of Brunhes-Matuyama magnetic reversal. – Earth Planetary Science Letters, 126: 91-108.

Bleil, U. & von Dobeneck, T. (1999): Geomagnetic events and relative paleointensity records – Clues to high resolution paleomagnetic chronostratigraphies of Late Quaternary marine sediments? - In: Fischer, G. & Wefer, G. (eds.): Use of proxies in Paleoceanography: Examples from the South Atlantic: 635-665; Berlin (Springer Verlag).

The Pliocene and Quaternary fluvial archives of the Rhine system. – Quaternary Science Reviews, 25: 550-574.

Boenigk, W. & Frechen, M. (2005): The Pliocene and Quaternary fluvial archives of the Rhine system. – Quaternary Science Reviews, 25: 550-574.

Bowles, J., Gee, J., Hildebrand, J. & Tauxe, L. (2002): Archaeomagnetic intensity results from California and Ecuador: evaluation of regional data. – Earth and Planetary Science Letters, 203: 967-981.

Brandt, U., Nowaczyk, N. R., Ramrath, A., Brauer, A., Mingram, J., Wulf, S. & Negendank, J. F. W. (1999): Palaeomagnetism of Holocene and Late Pleistocene sediments from Lago di Mezzano and Lago Grande di Monticchio (Italy): initial results. – Quaternary Science Reviews, 18: 961-976.

Buggle, B., Hambach, U., Glaser, B., Gerasimenko, N., Marković, S., Glaser, I., Zöller, L. (in press): Stratigraphy and spatial and temporal paleoclimatic trends in East European loess paleosol sequences. – Quaternary International (2008), doi:10.1016/j.quaint.2008.07.013.

Butler, R. F. (1992): Paleomagnetism: magnetic domains to geological terranes. – 319 S.; Boston (Blackwell). [available online – http: //www.geo.arizona.edu/Paleomag/book/]

Cande, S. C. & Kent, D. V. (1995): Revised calibration of the geomagnetic polarity timescale for the Late Cretaceous and Cenozoic. – Journal of Geophysical Research, B100: 6093-6095.

Carcaillet, J. T., Bourle`s, D. L. & Thouveny, N. (2004): Geomagnetic dipole moment and ^{10}Be production rate intercalibration from authigenic ^{10}Be/^{9}Be for the last 1.3 Ma. – Geochemistry, Geophysics, and Geosystems, 5, Q05006, doi: 10.1029/2003GC000641.

Casas, L. & Incoronato, A. (2007): Distribution analysis of errors due to relocation of geomagnetic data using the 'Conversion via Pole' (CVP) method: implications on archaeomagnetic data. – Geophysical Journal International, 169 (2): 448-454, doi:10.1111/j.1365-246X.2007.03346.x.

Channell, J. E. T. (1999): Geomagnetic paleointensity and directional secular variation at Ocean Drilling Program (ODP) site 984 (Bjorn Drift) since 500 ka: comparisons with ODP site 983 (Gardar drift). – Journal of Geophysical Research B: Solid Earth, 104, (B10): 22937-22951.

Channell, J. E. T. (2006): Late Brunhes polarity excursions (Mono Lake, Laschamp, Iceland Basin and Pringle Falls) recorded at ODP Site 919 (Irminger Basin). – Earth and Planetary Science Letters, 244: 378-393.

Channell, J. E. T., Curtis, J. H. & Flower, B. P. (2004b): The Matuyama-Brunhes boundary interval (500-900 ka) in North Atlantic drift sediments. – Geophysical Journal International, 158: 489-505.

Channell, J. E. T., Kent, D. V., Lowrie, W. & Meert, J. G. (2004a): Timescales of the paleomagnetic field. - 320 S.; Washington DC (American Geophysical Union).

Chen, T., Xu, H., Xie, Q., Chen, J., Ji, J. & Lu, H. (2005): Characteristics and genesis of maghemite in Chinese loess and paleosols; mechanism for magnetic susceptibility enhancement in paleosols. – Earth Planetary Science Letters, 240, (3-4): 790-802.

Clement, B. M. & Kent, D. V. (1987): Short polarity intervals within the Matuyama: transition field records from hydraulic piston cored sediments from the North atlantic. – Earth and Planetary Science Letters, 91: 253-264.

Collinson, D. W., Creer, K. M. & Runcorn, S. K. (1967): Methods in Palaeomagnetism. - 609 S.; Amsterdam, New York (Elsevier).

Collinson, D. W. (1983): Methods in Rock Magnetism and Paleomagnetism. – 503 S.; London, New York (Chapman and Hall).

Cooke, H.B.S., Hall, J.M. & Ronai, A. (1979): Paleomagnetic, sedimentary and climatic records from boreholes at Devavanya and Vesztö, Hungary. – Acta Geologica Hungarica, 22: 89–109.

Courtillot, V., Besse, J., Vandamme, D., Montigny, R., Jaeger, J.-J. & Cappetta, H. (1986): Deccan flood basalts at the Cretaceous/Tertiary boundary? – Earth and Planetary Science Letters, 80: 361-374.

Courtillot, V., Gallet, Y., Le Mouël, J.-L., Fluteau, F. & Genevey, A. (2007): Are there connections between the Earth's magnetic field and climate? – Earth and Planetary Science Letters, 253: 328–339.

Cox, A., Dalrymple, G. B. & Doell, R. (1967): Reversals of the Earth´s Magnetic Field. – Scientific American, 216: 44-54.

De Marco, E., Spassov, S., Kondopoulou, D., Zananiri, I. & Gerofoka, E. (2008a): Archaeomagnetic study and dating of a Hellenistic site in Katerini (N. Greece). – Physics and Chemistry of the Earth, 33: 481-495, doi:10.1016/j.pce.2008.02.017.

De Marco, E., Spatharas, V., Gómez-Paccard, M., Chauvin, A. & Kondopoulou, D. (2008b): New archaeointensity results from archaeological sites and variation of the geomagnetic field intensity for the last 7 millennia in Greece. – Physics and Chemistry of the Earth, 33: 578-595, doi: 10.1016/j.pce.2008.02.025.

Dunlop, D. J. & Özdemir, Ö. (1997): Rock Magnetism: Fundamentals and frontiers. – 573 S.; Cambridge (Cambridge University Press).

Evans, M. E. & Heller, F. (1994): Magnetic enhancement and palaeoclimate: study of a loess/palaeosol couplet across the loess plateau of China. – Geophysical Journal International, 117: 257-264.

Evans, M. E. & Heller, F. (2001): Magnetism of loess/palaeosol sequences: Recent developments. – Earth-Science Reviews, 54: 129-144.

Evans, M. E. & Heller, F. (2003): Environmental Magnetism - Principles and Applications of Enviromagnetics. – 299 S.; San Diego, (Academic Press).

Frank, U., Nowaczyk, N. R. & Negendank, J. (2007): Palaeomagnetism of greigite bearing sediments from the Dead Sea, Israel. – Geophysical Journal International, 168: 904-920.

Fuller, M. (2006): Geomagnetic field intensity, excursions, reversals and the 41,000-yr obliquity signal. – Earth and Planetary Science Letters, 245: 605–615.

Gabunia, L., Vekua, A., Lordkipanidze, D., Swisher, C.C., Ferring, R., Justus, A., Nioradze, M., Tvalchrelidze, M., Anton, S.C., Bosinski, G., Joris, O., de Lumley, M.A., Majsuradze, G. & Mouskhelishvili, A. (2000): Earliest Pleistocene hominid cranial remains from Dmanisi, Republic of Georgia: Taxonomy, geological setting, and age. – Science, 288: 1019-1025.

Gallet, Y., Genevey, A. & Le Goff, M. (2002): Three millennia of directional variation of the Earth's magnetic field in western Europe as revealed by archaeological artefacts. – Physics of the Earth and Planetary Interiors, 131: 81-89.

Gómez-Paccard, M., Catanzariti, G., Ruiz-Martínez, V. C., McIntosh, G., Núnez, J. I., Osete, M. L., Chauvin, A., Lanos, P., Tarling, D. H., Bernal-Casasola, D., Thiriot, J. & Group, A. W. (2006a): A catalogue of Spanish archaeomagnetic data. – Geophysical Journal International, 166: 1125-1143, doi: 10.1111/j.1365-246X.2006.03020.x.

Gómez-Paccard, M., Chauvin, A., Lanos, P., McIntosh, G., Osete, G., Catanzariti, M. L., Ruiz-Martínez, V. C & Núñez, J. I. (2006b): First archaeomagnetic secular variation curve for the Iberian Peninsula: Comparison with other data from Western Europe and with global geomagnetic field models. – Geochemistry, Geophysics, Geosystems G³, 7: Q12001, doi: 10.1029/2006GC001476.

Gubbins, D. (1999): The distinction between geomagnetic excursions and reversals. – Geophysical Journal International, 137 (1): F1– F4.

Gubbins, D. (2008): Geomagnetic reversals. – Nature Earth Science, 452: 165-167.

Guyodo, Y. & Valet, J-P. (1999): Global changes in intensity of the Earth's magnetic field during the past 800 kyr. – Nature, 399: 249-252.

Hamano, Y. (1980): An experiment on the post-depositional remanent magnetization in artificial and natural sediments. – Earth and Planetary Science Letters, 51: 221-232.

Hambach, U. & Krumsiek, K. (2000): Magnetische Polaritätsstratigraphie. – In: Stratigraphische Kommission Deutschlands (ed.): Stratigraphie von Deutschland III - Die Kreide in der Bundesrepublik Deutschland. – Courier Forschungsinstitut Senckenberg, 226: 51-59, Frankfurt.

Hambach, U., Mangini, A., Wagner, G. A. & Zöller, L. (1992): Physikalische Altersbestimmung der Schichtenfolge von Mauer. – In: Beinhauer, K. W. & Wagner, G. A. (eds): Schichten von Mauer (85 Jahre *Homo erectus heidelbergensis*). – 192 S., Reiß-Museum Mannheim.

Hambach, U., Zeeden, C., Hark, M., Zöller, L., Neugebauer-Maresch, C., Einwögerer, T., Händel, M. & Simon, U. (submitted): A High resolution palaeointensity record from a Lower Austrian last glacial loess site: implications for Upper Palaeolithic chronologies. – Quartär.

Heller, F. & Evans, M. E. (1996): Magnetoklimatologie: Mineralmagnetismus und Eiszeiten. – Naturwissenschaften, 83: 97-102.

Heller, F. & Liu, T.-S. (1982): Magnetostratigraphical dating of loess deposits in China. – Nature, 300 (5891): 431-433.

Heller, F. & Liu, T.-S. (1984): Magnetism of Chinese loess deposits. – Geophysical Journal of the Royal Astronomic Society, 77: 125-141.

Horng, C.-S., Lee, M.-Y., Pälike, H., Wie, K.-Y., Liang, W.-T., Iizuka,Y. & Torii, M. (2002): Astronomically calibrated ages for geomagnetic

reversals within the Matuyama chron. – Earth Planets Space, 54: 679-690.

Imbrie, J., J. D. Hays, D. G. Martinson, A. McIntyre, A. C. Mix, J. J. Morley, N. G. Paces, W. L. Prell & Shackleton, N.J. (1984): The orbital theory of Pleistocene climate: Support from a revised chronology of the marine δ18O record.- In: Milankovitch and Climate, Part I, edited by A. Berger et al.: 269-305; Norwell, Massachusates (D. Reidel).

Jackson, A., Jonkers, A. R. T. & Walker, M. R. (2000): Four centuries of geomagnetic secular variation from historical records. - Philosophical Transactions of the Royal Society of London, Series A, 358: 957-990.

Jacobs, J. A. (1994): Reversals of the Earth's magnetic field. Second edition. - 346 S.; Cambridge (Cambridge University Press).

Jordanova, D. & Petersen, N. (1999): Paleoclimatic record from a loess-soil profile in northeastern Bulgaria II. Correlation with global climatic events during the Pleistocene. – Geophysical Journal International, 138: 533-540.

Kent, D.V. (1999): Orbital tuning and geomagnetic polarity timescales. – Philosophical Transactions of the Royal Society of London, Series A, 357: 1995-2007.

Korte, M. & Constable, C. (2005): Continuous geomagnetic field models for the past 7 millennia: 2. CALS7K. – Geochemistry, Geophysics, Geosystems G^3, 6: 1-18, Q02H16, doi:10.1029/2004GC000801.

Korte, M., Genevey, A., Constable, C. G., Frank, U. & Schnepp, E. (2005): Continuous geomagnetic field models for the past 7 millennia: 1. A new global data compilation. – Geochemistry, Geophysics, Geosystems G^3, 6 (2): 1-32, Q02H15, doi:10.1029/2004GC000800.

Kovacheva, M., Jordanova, N. & Karloukovski, V. (1998): Geomagnetic field variations as determination from Bulgarian archaeomagnetic data. Part II: the last 8000 years. – Surveys in Geophysics, 19: 431-460.

Laj, C. & Channell, J.E.T. (2007): Geomagnetic Excursions. – In: Schubert, G. (ed.): Treatise on Geophysics, 5: 373-416, Amsterdam (Elsevier) .

Laj, C., Kissel, C. & Beer, J. (2004): High resolution global paleointensity stack since 75 kyr (GLOPIS-75) calibrated to absolute values. – In: Channell, J. E. T., Kent, D. V., Lowrie, W. & Meert, J. G. (eds): Timescales of the Paleomagnetic Field. – Geophysical Monograph Series, 145: 255-265; Washington, DC (American Geophysical Union).

Laj, C., Kissel, C., Mazaud, A., Channell, J. E. T. & Beer, J. (2000): North Atlantic palaeointensity stack since 75ka (NAPIS-75) and the duration of the Laschamp event. – Philosophical Transactions: Mathematical, Physical and Engineering Sciences, 358: 1009-1025.

Langereis, C. G., Dekkers, M. J., de Lange, G. J., Paterne, M. & van Santvoort, P. J. M. (1997): Magnetostratigraphy and astronomical calibration of the last 1.1 Myr from an eastern Mediterranean piston core and dating of short events in the Brunhes. – Geophysical Journal International, 129: 75-94.

Lanos, P. (2004): Bayesian inference of calibration curves: application to archaeomagnetism. In: Buck, C. E. & Millard, A. R. (eds.): Tools for Constructing Chronologies: Crossing Disciplinary Boundaries. - Series: Lecture Notes in Statistics, 177: 43-82; London (Springer-Verlag).

Lanza, R. & Meloni, A. (2006): The Earth´s Magnetism: An introduction for geologists. - 278 S.; Berlin, Heidelberg, New York (Springer).

Le Borgne, E. (1955): Susceptibilité magnetique anormale du sol superficial. – Annales Geophysicae, 11: 399–419.

Le Goff, M., Gallet, Y., Genevey, A. & Warmé, N. (2002): On archaeomagnetic secular variation curves and archaeomagnetic dating. – Physics of the Earth and Planetary Interiors, 134: 203-211.

Leonhardt, R., Matzka, J., Hufenbecher, F., Soffel, H. C. & Heider, F. (2002): A reversal of the Earth´s magnetic field recorded in mid-Miocene lava flows of Gran Canaria: Paleodirections. - Journal of Geophysical Research, 107 (B1): EPM 7-1 EPM 7-12.

Leonhardt, R. & Soffel, H. C. (2002): A reversal of the Earth's magnetic field recorded in mid-Miocene lava flows of Gran Canaria: Paleointensities. - Journal of Geophysical Research, 107 (B11): 1053-1064, doi: 10.1007/s00531-006-0089-3.

Lisiecki, L. E., & Raymo, M. E. (2005): A Pliocene-Pleistocene stack of 57 globally distributed benthic d18O records. – Paleoceanography, 20: PA1003, doi:10.1029/2004PA001071.

Lund, S. P. (1996): A comparison of Holocene paleomagnetic secular variation records from North America. – Journal of Geophysical Research, 101 (B4): 8007-8024.

Lund, S. P., Stoner, J. S., Channell, J. E. T. & Acton, G. (2006): A summary of Brunhes paleomagnetic field variability recorded in ODP Cores. – Physics of the Earth and Planetary Interiors, 156: 194-204.

Maher, B. A. (1998): Magnetic properties of modern soils and Quaternary loessic paleosols: Paleoclimatic implications. – Palaeogeography, Palaeoclimatology, Palaeoecology, 137: 25-54.

Maher, B. A. & Hallam, D. F. (2005): Palaeomagnetic correlation and dating of Plio/Pleistocene sediments at the southern margins of the North Sea Basin. – Journal of Quaternary Science, 20: 67–77.

Maher, B. A. & Thompson, R. (1999): Quaternary climates, environments and magnetism. –399 S.; Cambridge (University Press).

Mankinen, E. A. & Dalrymple, G. B. (1979): Revised geomagnetic polarity time scale for the Interval 0-5 m.y. B.P. – Journal of Geophysical Research, 84 (B2): 615-626.

Marković, S. B., Hambach, U., Catto, N., Jovanović, M., Buggle, B., Machalett, B., Zöller, L., Glaser, B. & Frechen, M. (submitted): The Middle and Late Pleistocene loess sequences at Batajnica, Vojvodina, Serbia.

Marković, S. B., Oches, E., Sümegi, P., Jovanović, M. & Gaudenyi, T. (2006): An introduction to the Upper and Middle Pleistocene loess-paleosol sequences of Ruma section (Vojvodina, Yugoslavia). – Quaternary International, 149: 80-86.

Márton, P. & Ferencz, E. (2006): Hierarchical versus stratification statistical analysis of archaeomagnetic directions: the secular variation curve for Hungary. – Geophysical Journal International, 164: 484-489, doi: 10.1111/j.1365-246X.2006.02873.x.

McElhinny, M. W. (1973): Palaeomagnetism and Plate Tectonics. – 358 S.; London (Cambridge University Press).

McElhinny, M. W. & McFadden, P. L. (2000): Paleomagnetism: Continents and Oceans. – 386 S.; San Diego, San Francisco, New York, Boston, London, Sydney, Tokyo (Academic Press).

Merrill, R. T., McElhinny, M. W. & McFadden, P. L. (1996): The Magnetic Field of the Earth: Paleomagnetism, the Core, and the Deep Mantle. – International Geophysical Series, 63. – 531 S.; San Diego (Academic Press).

Nador, A., Lantos, M., Toth-Makk, A. & Thamo-Bozso, E. (2003): Milankovitch-scale multiproxy records from fluvial sediments of the last 2.6 Ma, Pannonian Basin, Hungary. – Quaternary Science Reviews, 22: 2157-2175.

Nowaczyk, N. R., Frederichs, T. W., Eisenhauer, A. & Gard, G. (1994): Magnetostratigraphic data from late Quaternary sediments from the Yermak Plateau, Arctic Ocean: evidence for four geomagnetic polarity events in the last 170 ka of the Brunhes Chron. – Geophysical Journal International, 117: 453-471.

Olsen, N., Lühr, H., Sabaka, T. J., Mandea, M., Rother, M., Tøffner-Clausen, L. & Choi, S. (2006): CHAOS – A Model of Earth's Magnetic Field derived from CHAMP, Ørsted, and SAC-C magnetic satellite data. – Geophysical Journal International, 166: 67-75, doi: 10.1111/j.1365-246X.2006.02959.x.

Opdyke, N. D. & Channell, J. E. T. (1996): Magnetic Stratigraphy. – 346 S; San Diego (Academic Press).

Panaiotu C. G., Panaiotu, C. E., Grama, A. & Necula C (2001): Paleoclimatic record from a loess-paleosol profile in southeastern Romania. – Physics and Chemistry of the Earth (A) 26: 893-898.

Panaiotu, C. G., Pecskay, Z., Hambach, U., Seghedi, I., Panaiotu, C. E., Tetsumaru, I., Orleanu, M. & Szakacs, A. (2004): Short-lived quaternary volcanism in the Persani Mountains (Romania) revealed by combined K-Ar and paleomagnetic data. – Geologica Carpathica, 55: 333-339.

Pares, J. M. & Perez-Gonzalez, A. (1995): Paleomagnetic age for hominid fossils at Atapuerca archaeological site, Spain. – Science, 269: 830-832.

Pilipenko, O. V., Abrahamsen, N. & Trubikhin, V. M. (2006): Petro- and Paleomagnetic Investigations of Tuzla Section Sediments (Krasnodarsk Territory). – Izvestiya, Physics of the Solid Earth, 42: 344-356.

Preusser, F. (2008): Characterisation and evolution of the River Rhine system. – Netherlands Journal of Geosciences, 87: 7-19.

Reinders, J. & Hambach, U. (1995): A geomagnetic event recorded in loess deposits of the Tönchesberg (Germany): identification of the Blake magnetic polarity episode. – Geophysical Journal International, 122: 407-418.

Reinders, J., Hambach, U., Sirocko, F., Rolf, C. & Nowaczyk, N. R. (submitted): A 50m Record of Palaeomagnetic Secular Variation retrieved from Laminated Sediments from an Eifel Maar Lake (Germany) – Evidence for a Time Interval with Low Palaeosecular Variation During MIS5.

Roberts, A. P. & Winklhofer, M. (2004): Why are geomagnetic excursions not always recorded in sediments? Constraints from post-depositional remanent magnetization lock-in modelling. – Earth and Planetary Science Letters, 227: 345-359.

Rolf, C., Hambach, U. & Weidenfeller, M. (2008): Rock and palaeomagnetic evidence for the Plio-Pleistocene palaeoclimatic change recorded in Upper Rhine Graben sediments (Core Ludwigshafen-Parkinsel). – Netherlands Journal of Geosciences, 87: 41-50.

Rolph, T. C. (1993): The Matuyama-Jaramillo R-N transition recorded in a loess section near Lanzhou, P. R. China. – Journal of Geomagnetism and Geoelectricity, 45: 301-318.

Rösler, W., Metzler, W. & Appel, E. (1997): Neogene magnetic polarity stratigraphy of some fluviatile Siwalik sections, Nepal. – Geophysical Journal International, 130: 89-111.

Sartori, M., Heller, F., Forster, T., Borkovec, M., Hammann, J. & Vincent, E. (1999): Magnetic properties of loess grain size fractions from section Paks (Hungary). – Physics of the Earth and Planetary Interiors, 116: 53-64.

Schnepp, E. (2007): Archäomagnetische Datierung in Deutschland und Österreich. – Archäologisches Korrespondenzblatt, 37: 313-320.

Schnepp, E. & Hradetzky, H. (1994): Combined paleointensity and $^{39}Ar/^{40}Ar$ age spectrum data from volcanic rocks of the West Eifel field (Germany): Evidence for an early Brunhes geomagnetic excursion. – Journal of Geophysical Research, 99: 9061-9076.

Schnepp, E. & Lanos, P. (2005): Archaeomagnetic secular variation in Germany during the past 2500 years. – Geophysical Journal International, 163: 479-490.

Schnepp, E. & Lanos, P. (2006): A preliminary secular variation reference curve for archaeomagnetic dating in Austria. – Geophysical Journal International, 166: 91-96.

Schnepp, E., Pucher, R., Reinders, J., Hambach, U., Soffel, H. & Hedley, I. (2004): A German catalogue of archaeomagnetic data. – Geophysical Journal International, 157: 64-78.

Singer, B., Hoffman, K., Schnepp, E. & Guillou, H. (2008): Multiple Brunhes Chron Excursions Recorded in the West Eifel (Germany) Volcanics: Support for Long-Held Mantle Control Over the Non-Axial Dipole Field. – Physics of the Earth and Planetary Interiors, doi:10.1016/j.pepi.2008.05.001.

Soffel, H. C. (1991): Paläomagnetismus und Archäomagnetismus. – 276 S.; Heidelberg (Springer).

Stacey, F. D. & Banerjee, S. K. (1974): The Physical Principles of Rock Magnetism. – 195 S.; Amsterdam (Elsevier).

Sternberg, R. S. (1989): Archaeomagnetic paleointensity in the American Southwest during the past 2000 years. – Physics of the Earth and Planetary Interiors, 56: 1-17.

Stockhausen, H. (1998): Geomagnetic palaeosecular variation (0–13000 year BP) as recorded in sediments from three maar lakes from the West Eifel (Germany). – Geophysical Journal International, 135: 898–910.

Strattner, M. & Rolf, C. (1995): Magnetostratigraphische Untersuchungen an pleistozänen Deckschicht-Profilen im bayerischen Alpenvorland. – Geologica Bavarica, 99: 55-101.

Sun, Y., Clemens, S. C., An, Z. & Yu, Z. (2006): Astronomical timescale and palaeoclimatic implication of stacked 3.6-Myr monsoon records from the Chinese Loess Plateau. – Quaternary Science Reviews, 25: 33-48.

Tanguy, J.-C., Le Goff, M., Principe, C., Arrighi, S., Chillemi, V., Paiotti, A., La Delfa, S. & Patanè, G. (2003): Archeomagnetic dating of Mediterranean volcanics of the last 2100 years: validity and limits. – Earth and Planetary Science Letters, 211: 11-124.

Tarling, D. H. (1983): Palaeomagnetism: Principles and Applications in Geology, Geophysics und Archaeology. – 379 S.; London, New York (Chapman & Hall).

Tauxe, L. (1998): Paleomagnetic principles and practice. - In: Nolet, G. (ed.): Modern Approaches in Geophysics, 17. – 299 S.; Princeton (Kluwer Academic Publisher).

Tema, E., Hedley, I. & Lanos, P. (2006): Archaeomagnetism in Italy: A compilation of data including new results and a preliminary Italian Secular Variation curve. – Geophysical Journal International, 167: 1160-1171, doi: 10.1111/j.1365-246X.2006.03150.x.

Thompson, R. & Oldfield, F. (1986): Environmental magnetism. – 227 S.; London (Allen and Unwin).

Thouveny, N., Creer, K. M. & Blunk, I. (1990): Extension of the Lac du Bouchet palaeomagnetic record over the last 120000 years. – Earth and Planetary Science Letters, 97: 140-161.

Thouveny, N., Carcaillet, J., Moreno, E., Leduc, G. & Nerini, D. (2004): Geomagnetic moment variation and paleomagnetic excursions since 400 kyr BP; a stacked record from sedimentary sequences of the Portuguese margin. – Earth and Planetary Science Letters, 219: 377-396.

Tucker, P. (1980): A grain mobility model of post-depositional realignment. – Geophysical Journal

of the Royal Astronomical Society, 63: 149-163.

Van der Voo, R. (1993): Paleomagnetism of the Atlantic, Tethys and Iapetus Oceans. – 411 S.; Cambridge (Cambridge University Press).

Valet, J.-P. & Meynadier, L. (1993): Geomagnetic field intensity and reversals during the past four million years. – Nature, 366: 234-238.

Wagner, G. A., Fezer, F., Hambach, U., von Königswald, W. & Zöller, L. (1997): Das Alter des *Homo heidelbergensis* von Mauer. – In: Wagner, G. A. & Beinhauer, K. W. (eds): *Homo heidelbergensis* von Mauer: Das Auftreten des Menschen in Europa: 124-143, Heidelberg.

Worm, H.-U., Ahmed, A. M. M., Ahmed, N. U., Islam, H. O., Hambach, U. & Lietz, J. (1998): Large sedimentation rate in the Bengal delta: magnetostratigraphic dating of Cenozoic sediments from north-eastern Bangladesh. – Geology, 26: 487-490.

Zagwijn, W. H. (1992): The beginning of the ice age in Europe and its major subdivisions. – Quaternary Science Reviews, 11: 583-591.

Zananiri, I., Batt, C. M., Lanos, P., Tarling, D. H. & Linford, P. (2007): Archaeomagnetic secular variation in the UK during the past 4000 years and its application to archaeomagnetic dating. – Physics of the Earth and Planetary Interiors, 160: 97-107.

Zeeden, C., Hambach, U., Reddersen, B., Fülling, A., Hark, M., Nowaczyk, N., Fuchs, M. & Zöller, L. (2008): High resolution paleonintensity records from European last glacial loess sites. – Geophysical Research Abstracts, Vol. 10: EGU2008-A-10564, 2008; SRef-ID: 1607-7962/gra/EGU2008-A-10564.

Zhu, R., Liu, Q., Pan, Y. Deng, C. & Sun, J. (2006): Identifying the origin of the magnetic directional anomalies recorded in the Datong loess profile, north-eastern Chinese loess plateau. – Geophysical Journal International, 164: 312-318.

Zolitschka, B., Brauer, A., Negendank, J. F.W., Stockhausen, H. & Lang, A. (2000): Annually dated late Weichselian continental paleoclimate record from the Eifel, Germany. – Geology, 28: 9, 783-786.

Eiszeitalter und Gegenwart Quaternary Science Journal	57/1–2	52–76	Hannover 2008

^{230}Th/U-dating of fossil corals and speleothems

Denis Scholz & Dirk Hoffmann *)

Abstract: Both marine and terrestrial carbonates can be precisely dated by U-series disequilibrium methods in the age range <600 ka (thousands of years). Here we focus on ^{230}Th/U-dating of reef corals and speleothems. The requirements, potential but also the problems of ^{230}Th/U-dating of both archives are presented and discussed. Fossil reef corals are used as indicators for past sea level fluctuations and as high-resolution palaeoclimate archives. These applications require precise and accurate dating, which can be achieved using ^{230}Th/U-dating. However, many fossil corals show evidence for post-depositional open-system behaviour. This limits the accuracy of ^{230}Th/U-ages of fossil corals rather than the analytical precision. We present and discuss the currently available methods to identify altered corals and also review three recently developed open-system dating approaches. Speleothems are very important climate archives because they are found in most continental areas and can be used to investigate and directly compare spatially variable climate conditions. They usually show no evidence for open-system behaviour but may contain significant amounts of initial detrital ^{230}Th. We discuss the currently available correction techniques and methods to derive the most reliable ages. Furthermore, we give an overview of the state of the art techniques for U-series isotopes measurements.

[^{230}Th/U-Datierung fossiler Korallen und Speläotheme]

Kurzfassung: Marine und terrestrische Karbonate können im Altersbereich von bis zu 600.000 Jahren mit Uranreihen-Ungleichgewichtsmethoden sehr präzise datiert werden. In diesem Artikel wird die ^{230}Th/U-Datierung von Riffkorallen und Speläothemen dargestellt. Anforderungen, Potenzial aber auch Probleme der Datierung beider Archive werden eingehend diskutiert. Fossile Riffkorallen werden sowohl als Anzeiger der Meeresspiegelschwankungen der Vergangenheit als auch als Paläoklimaarchiv mit sehr hoher Auflösung genutzt. Für beide Anwendungen werden äußerst präzise und zuverlässige Alter benötigt, die mit der ^{230}Th/U-Methode bestimmt werden können. Viele fossile Riffkorallen zeigen jedoch Anzeichen von nachträglicher diagenetischer Veränderung, welche die Genauigkeit der ^{230}Th/U-Alter mehr limitiert als die Messgenauigkeit. Die Methoden zur Identifikation diagenetisch veränderter Korallen werden dargestellt, und drei in den letzten Jahren entwickelte Methoden zur Datierung von Korallen, die sich als offene Systeme verhalten haben, werden diskutiert. Speläotheme sind bedeutende Klimaarchive, da sie in fast allen Gegenden vorkommen, was es ermöglicht, Klimaveränderungen in verschiedenen Gebieten zu untersuchen und direkt miteinander zu vergleichen. Sie zeigen in der Regel keine Anzeichen für nachträgliche Störungen des U-Th-Systems können aber in Einzelfällen signifikante Mengen von initialem ^{230}Th enthalten. Die gängigen Korrekturverfahren und Methoden, um zuverlässige Datierungen zu erhalten, werden dargestellt. Weiterhin geben wir einen Überblick über die derzeitigen Methoden zur Messung von Uranreihenisotopen.

Keywords: ^{230}Th/U-dating, fossil corals, speleothems, palaeoclimate reconstruction, mass spectrometry

* Addresses of authors: Denis Scholz, Heidelberg Academy of Sciences, Im Neuenheimer Feld 229, 69120 Heidelberg, Germany. E-Mail: Denis.Scholz@iup.uni-heidelberg.de; Dirk Hoffmann, Bristol Isotope Group, School of Geographical Sciences, University of Bristol, University Road, BS8 1SS, Bristol, United Kingdom. E-mail: Dirk.Hoffmann@bristol.ac.uk

1 Introduction

Palaeoclimate archives such as ice cores, deep sea sediments or speleothems provide important insights about natural climate variability, which are urgently needed to understand the mechanisms driving our climate system and hence to quantify and potentially predict (anthropogenic) future climate change. A key aspect of palaeoclimate reconstruction is the accurate determination of the *timing* of past climate changes, which provides fundamental information about the phasing of change and, therefore, about potential links between climate in different regions or between climate and the forcing mechanisms driving it (Henderson 2006).

Carbonates such as corals or speleothems can be accurately and precisely dated using U-series disequilibrium methods. This method is based on the radioactive decay of radionuclides within the naturally occurring decay chains. There are three decay chains, each starts with an actinide nuclide (i.e., ^{238}U, ^{235}U, and ^{232}Th) having a long half live (all have $T_{1/2} > 7 \times 10^8$ a) and ultimately ends with different stable isotopes of lead (Fig. 1). In an undisturbed system all daughter nuclides reach a state of radioactive equilibrium with the parent nuclide after a few million years. Natural processes that fractionate the nuclides within a decay chain result in a disequilibrium between the activity of the parent and the daughter isotopes. The return to equilibrium then allows quantification of time and, thus, dating of the timing of chemical or physical fractionation (Bourdon et al. 2003).

U-series disequilibrium dating methods can, in principle, be applied to all materials that form accompanied by a constrained parent-daughter disequilibrium, such as marine carbonates (reef and deep sea corals, carbonate bank sediments, molluscs and foraminifera), lacustrine carbonates (tufa and inorganically precipitated sediments), terrestrial carbonates (speleothems and travertine) and peat deposits (Geyh 2008). However, U-series dating of each of these materials is associated with particular problems. For example, mollusc shells and foraminifera were shown to take up and exchange U after deposition violating the basic closed-system assumption of U-series dating (next section). Hence, U-series dating cannot be reliably applied to these materials. Reef building corals and speleothems (i.e., secondary carbonates precipitated in caves), however, can be accurately and precisely dated using U-series methods. For these materials U-series dating methods are widely used because they provide by far the most reliable and precise ages for samples younger than 600 ka (thousands of years). Here, we focus on mass spectrometric U-series dating of corals and speleothems. A review of ^{230}Th/U-dating of other marine and terrestrial carbonates is given by Edwards et al. (2003).

Fossil reef corals were successfully dated for the first time with U-series methods by Barnes et al. (1956) using alpha-counting techniques, followed by numerous studies in the 1960's and 1970's (e.g., Broecker et al. 1968; Mesolella et al. 1969). With the advent of modern thermal ionisation mass spectrometry (TIMS, section 2.3.2) the precision of U-series dating significantly improved. This led to increasing research on fossil reef corals and the application for sea level reconstruction in the late 1980's and early 1990's (e.g., Bard et al. 1990; Chappell & Polach 1991; Chen et al. 1986; Edwards et al. 1986; Gallup et al. 1994).

The potential of using U-series dated proxy records in speleothems, such as oxygen and carbon isotopes for palaeoclimate reconstruction was already indicated by the pioneering work in the 1960's and 1970's (e.g., Hendy & Wilson 1968). Within the past two decades improvements in analytical techniques allowed (i) more precise ^{230}Th/U-ages to be obtained from much smaller sample sizes and (ii) a variety of proxies to be measured at very high spatial resolution (i.e., in the range of μm). Because speleothems are found in most continental areas, spatially variable climate changes can be investigated and directly compared. Thus, it has recently been hypothesized that for palaeoclimate research, the next two decades might be „the age of the speleothem" (Henderson 2006).

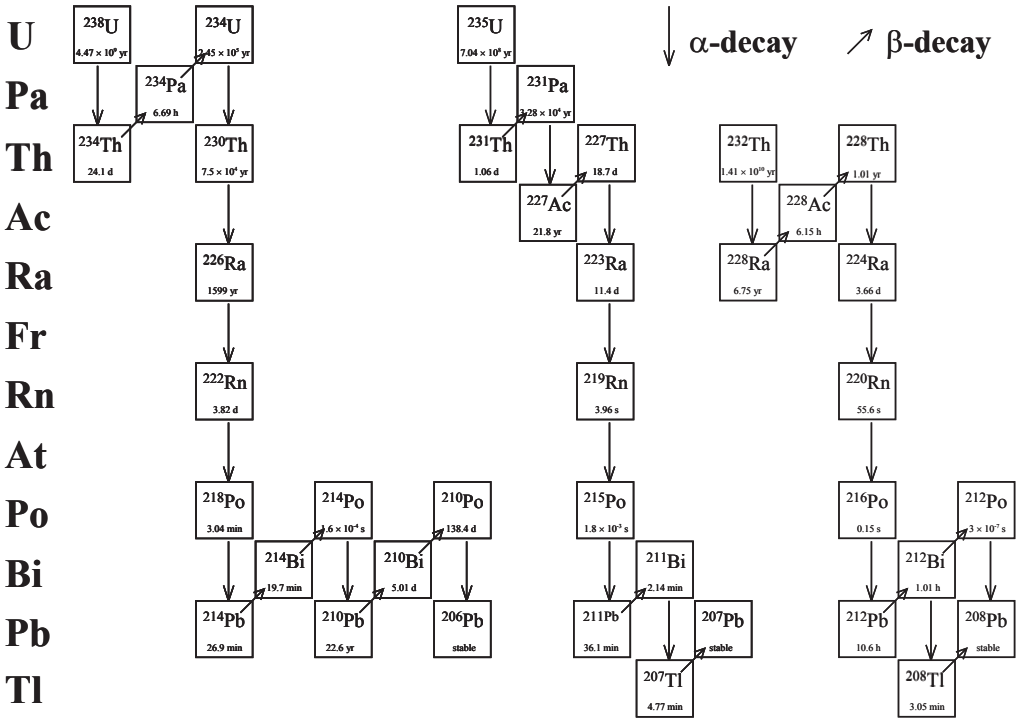

Fig. 1: Schematic drawing of the ^{238}U, ^{235}U and ^{232}Th decay chains (from SCHOLZ 2005). The half-lives of the nuclides are indicated in the boxes.

Abb. 1: Schematische Darstellung der Zerfallsreihen von ^{238}U, ^{235}U und ^{232}Th. Die Halbwertszeiten sind in den jeweiligen Boxen angegeben.

2 Basics

2.1 Geochemistry of U and Th

Typical U concentrations of the continental crust range from 0.1 to 6 µg/g. ^{238}U is the most abundant U isotope (99.2745 %), and ^{232}Th is the most abundant Th isotope (~100 %). The average Th/U weight ratio in crustal rocks is ~3.5 (WEDEPOHL 1995). The half-lives of ^{238}U ($T_{1/2} = 4.4683 \times 10^9$ a, JAFFEY et al. 1971), ^{235}U ($T_{1/2} = 0.70381 \times 10^9$ a, JAFFEY et al. 1971), and ^{232}Th ($T_{1/2} = 14.01 \times 10^9$ a, HOLDEN 1990) are much longer than those of their daughters in the decay chain (Fig. 1). Thus, the activities of parent and daughter isotopes reach a state of secular equilibrium in naturally occurring undisturbed materials within several million years. However, natural processes can disrupt the state of equilibrium, which is the key of the U-series disequilibrium dating methods. A state of disequilibrium in the ^{238}U decay chain can either result from elemental fractionation of Th from U or from isotope fractionation between ^{234}U and ^{238}U.

The elemental fractionation is a result of the different geochemical behaviour of U and Th. U mainly exists in two oxidation states in nature (U^{4+} and U^{6+}), and at the Earth's surface it is dominant in its soluble U^{6+} form. It is soluble as uranyl ion $(UO_2)^{2+}$ and in various uranyl carbonate forms (IVANOVICH & HARMON 1992). In a reducing environment, however, it occurs mainly in the U^{4+} state where it is insoluble and, thus, far less mobile than U^{6+}. In contrast, Th,

which occurs in terrestrial material mainly in the 4+ oxidation state, is insoluble in natural waters (Ivanovich & Harmon 1992), and, thus, under natural conditions usually transported in minerals or adsorbed onto particles. As a consequence, groundwater, fluvial water and seawater contain dissolved U but essentially no Th. Hence, in contrast to U, Th is not incorporated in secondary carbonates during their formation resulting in an initial Th/U disequilibrium.

Fractionation of ^{234}U and ^{238}U is produced by the α-recoil effect. An α-decay (e.g., decay of ^{238}U, Fig. 1) results in the emission of a He nucleus with finite kinetic energy. This has a twofold effect: (i) The daughter nuclide is slightly displaced from its parent's original site and, thus, either directly ejected into an adjacent phase or more easily removed subsequently. (ii) The crystal lattice is damaged by the α-particle along the trajectory (Bourdon et al. 2003). Therefore, the daughter nuclide is subsequently more easily mobilized than its parent e.g., during weathering processes. As a consequence, ^{234}U/^{238}U isotope ratios of ground and river water are usually higher than the equilibrium value (Chabaux et al. 2003; Porcelli & Swarzenski 2003).

2.2 Calculation of ^{230}Th/U-ages

The activity, A, of a number of atoms of a radioactive nuclide, N, is defined as the number of decay events per unit of time:

$$A = \frac{dN}{dt} = -\lambda N \,, \qquad (1)$$

where λ is the decay constant defined as ln(2)/$T_{1/2}$.

In the following, activities and activity ratios are indicated by parenthesis, e.g., (^{238}U). The temporal development of the activities of the individual isotopes within a decay chain is described by a system of differential equations, which can be solved by standard methods (Ivanovich & Harmon 1992).

In contrast to U, Th is not incorporated in secondary carbonates. Thus, the initial activity of ^{230}Th, $(^{230}\mathrm{Th})_{init.}$, is zero. If we further assume that the decay system remains closed after deposition (i.e., both U and Th isotopes are neither lost nor gained) and take into account that the half-live of ^{238}U is much longer than that of ^{234}U and ^{230}Th (Fig. 1), the development of (^{234}U/^{238}U) and (^{230}Th/^{238}U) is described by equations (2) and (3) (see Ivanovich & Harmon 1992, for derivation):

$$\left(\frac{^{234}U}{^{238}U}\right)(t) = \left(\left(\frac{^{234}U}{^{238}U}\right)_{init.} - 1\right) \; e^{-\lambda_{234}\, t} + 1 \qquad (2)$$

$$\left(\frac{^{230}Th}{^{238}U}\right)(t) = (1 - e^{-\lambda_{230}\, t}) + \left(\left(\frac{^{234}U}{^{238}U}\right)(t) - 1\right)\frac{\lambda_{230}}{\lambda_{230} - \lambda_{234}}(1 - e^{-(\lambda_{230} - \lambda_{234})\, t}), \qquad (3)$$

where $(^{234}\mathrm{U}/^{238}\mathrm{U})_{init.}$ is the initial (^{234}U/^{238}U) activity ratio, and the λ_i are the decay constants for ^{230}Th and ^{234}U, respectively. The most recent values for the decay constants of ^{230}Th and ^{234}U are $\lambda_{230} = 9.1577 \times 10^{-6}$ a^{-1} and $\lambda_{234} = 2.8263 \times 10^{-6}$ a^{-1} (Cheng et al. 2000). Note that Eqs. (2) and (3) are only valid if two basic assumptions are fulfilled: (i) no presence of initial ^{230}Th and (ii) the system remains closed after deposition. If one of these assumptions is violated, the resulting ^{230}Th/U-age might be biased substantially and, thus, without significance. However, if both assumptions are fulfilled, the measurement of (^{234}U/^{238}U) and (^{230}Th/^{238}U) allows the calculation of the time since the formation of the sample. Fig. 2 shows the temporal development of (^{230}Th/^{238}U) and (^{234}U/^{238}U) for two different values of (^{234}U/^{238}U)$_{init.}$.

(^{234}U/^{238}U) is often given in the δ-notation in per mil:

$$\delta^{234}U = \frac{\left(\frac{^{234}U}{^{238}U}\right) - \left(\frac{^{234}U}{^{238}U}\right)_{eq}}{\left(\frac{^{234}U}{^{238}U}\right)_{eq}} \cdot 1000$$

$$= \left(\left(\frac{^{234}U}{^{238}U}\right) - 1\right) \cdot 1000\,, \qquad (4)$$

where $(^{234}U/^{238}U)_{eq}$ indicates $(^{234}U/^{238}U)$ in secular equilibrium.

Eq. (2) alone cannot be used for age calculations because $(^{234}U/^{238}U)_{init.}$ is generally not known. Fortunately, Eq. (3) only requires the present $(^{230}Th/^{238}U)$ and $(^{234}U/^{238}U)$ of the sample to solve for age, which can both be measured. Since Eq. (3) cannot be analytically solved for t, the age calculation must be done either graphically or numerically. The corresponding error of the age can be calculated using numerical methods, such as Monte-Carlo simulation (LUDWIG 2003). A common way to visualize the temporal development of the activity ratios is to plot $(^{234}U/^{238}U)$ vs. $(^{230}Th/^{238}U)$ (Fig. 3).

2.3 Analytical techniques

^{230}Th/U-dating requires precise and accurate measurement of the relevant U and Th isotope abundances to obtain the isotope activity ratios needed to calculate an age according to Eqs. (2) and (3). The isotopes ^{238}U, ^{234}U, ^{230}Th have a different atomic mass and all decay by alpha emission (Fig. 1). Two methods are commonly used for U and Th isotope measurements: alpha spectrometry and mass spectrometry. Both techniques require prior chemical separation and purification of U and Th from the $CaCO_3$ matrix (IVANOVICH & HARMON 1992). A detailed description of the sample preparation chemistry is given by HOFFMANN (in press). Since U and Th behave differently during separation and purification, a tracer (or „spike“) is required, such as a solution of ^{236}U and ^{229}Th with known accurately calibrated U-Th ratio. A defined

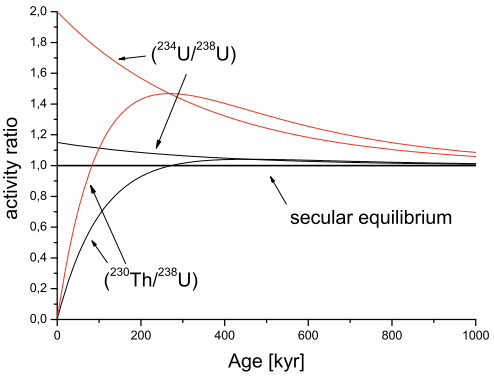

Fig. 2: Temporal development of $(^{234}U/^{238}U)$ and $(^{230}Th/^{238}U)$ under closed system conditions with no initial Th. Two cases of initial $(^{234}U/^{238}U)$ are shown: $(^{234}U/^{238}U)_{init.} = 1.15$ (black line) and $(^{234}U/^{238}U)_{init.} = 2.0$ (red line). The development of $(^{230}Th/^{238}U)$ depends on that of $(^{234}U/^{238}U)$ (Eq. (3)), which in turn depends on $(^{234}U/^{238}U)_{init.}$ (Eq. 2). The limit of the dating range is reached when secular equilibrium is established. It is obvious that the dating range depends on $(^{234}U/^{238}U)_{init.}$. For marine samples, which usually have $(^{234}U/^{238}U)_{init.} = 1.15$ (black line, see next section), the dating range is ~600,000 a (EDWARDS et al. 2003). For other samples, such as speleothems, higher values of $(^{234}U/^{238}U)_{init.}$ can be found, and older samples may still be datable.

Abb. 2: Zeitliche Entwicklung der Aktivitätsverhältnisse $(^{234}U/^{238}U)$ und $(^{230}Th/^{238}U)$ unter Annahme eines geschlossenen Systems. Es werden zwei Fälle unterschieden: $(^{234}U/^{238}U)_{init.} = 1.15$ (schwarze Kurve) and $(^{234}U/^{238}U)_{init.} = 2.0$ (rote Kurve). Die Entwicklung von $(^{230}Th/^{238}U)$ hängt von der von $(^{234}U/^{238}U)$ ab, welche wiederum von $(^{234}U/^{238}U)_{init.}$ abhängt. Die Grenze der Datierbarkeit ist erreicht, wenn sich das säkulare Gleichgewicht eingestellt hat. Es ist offensichtlich, dass diese Grenze von $(^{234}U/^{238}U)_{init.}$ abhängt. Für marine Proben, die in der Regel ein initiales $(^{234}U/^{238}U)$ Aktivitätsverhältnis von 1.15 haben (schwarze Kurve, s. nächster Abschnitt), ist das Limit der Datierungsmethode ca. 600 000 Jahre (EDWARDS et al. 2003). Für andere Proben, wie z.B. Speläotheme, sind höhere Werte für $(^{234}U/^{238}U)_{init.}$ nicht ungewöhnlich. In diesen Fällen können auch ältere Proben noch datiert werden.

quantity of the tracer needs to be added to the sample prior to the separation procedure (isotope-dilution technique). Hence, additionally to the above mentioned isotopes, the abundances of ^{236}U (and/or ^{233}U) and ^{229}Th also have to be determined. Furthermore, ^{232}Th is measured as a proxy for detrital components.

2.3.1 Alpha spectrometry

Radioactive decay of the isotopes mentioned above is accompanied by the emission of an alpha particle with isotope specific energy. Thus, one possibility of measuring the relative isotope abundances is alpha spectrometry. However, alpha spectrometry is meanwhile of minor importance for ^{230}Th/U-dating of corals and speleothems due to the limits in precision and requirements in sample sizes. In brief, after separation, U and Th fractions are deposited as a thin layer on a flat surface such as metal planchet, e.g., by electrodeposition. The planchet is then placed in a sample chamber at high vacuum beneath a detector, which detects the occurrence and energy of alpha particles. A U or Th isotope measurement takes a few days, and the precision is in the range of a few percent, which limits the dating range to 300 ka. Another disadvantage of alpha spectrometry compared to mass spectrometry is the rather big sample size required for one measurement (usually more than 1 µg total U).

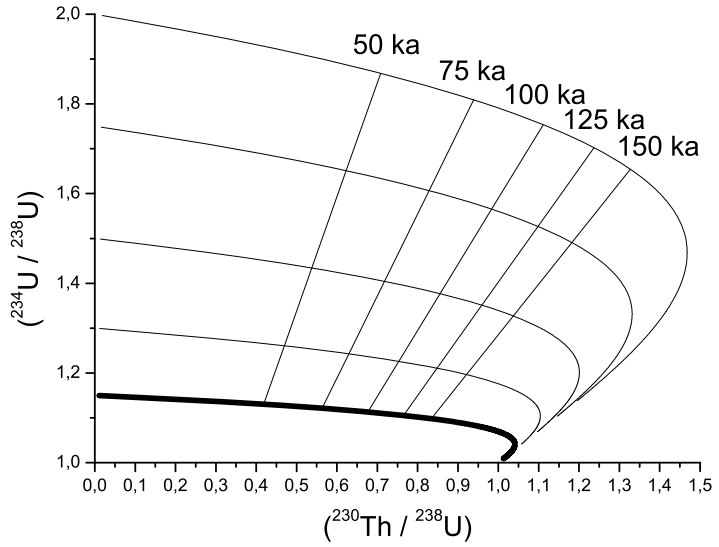

Fig. 3: (^{234}U/^{238}U) vs. (^{230}Th/^{238}U) plot for different values of $(^{234}U/^{238}U)_{init.}$. Each curve starts with (^{230}Th/^{238}U) = 0 but with another value of $(^{234}U/^{238}U)_{init.}$. The bold curve corresponds to $(^{234}U/^{238}U)_{init.} = 1.15$, the value measured on modern sea water, and represents the seawater evolution curve. All curves finally converge to secular equilibrium. The vertically tilted straight lines represent isochrons for a specific age as indicated by the corresponding labels. All combinations of activity ratios of an isochron correspond to the same age. This plot is very useful to detect post-depositional open-system behaviour (next section).

Abb. 3: (^{234}U/^{238}U) vs. (^{230}Th/^{238}U) Diagramm für verschiedene Werte von $(^{234}U/^{238}U)_{init.}$. Jede Kurve startet bei (^{230}Th/^{238}U) = 0 jedoch mit einem anderen Wert für $(^{234}U/^{238}U)_{init.}$. Die fettgedruckte Kurve gilt für $(^{234}U/^{238}U)_{init.} = 1.15$, welches der heutige Wert von Meerwasser ist, und heißt daher *seawater evolution curve*. Alle Kurven konvergieren gegen das säkulare Gleichgewicht. Die vertikalen Gerade sind Isochronen für die angegebenen Alter. Alle Kombinationen von Aktivitätsverhältnissen auf einer Isochrone entsprechen dem gleichen Alter. Dieses Diagramm ist sehr nützlich, um nachträgliche Störungen des Systems zu erkennen (s. nächster Abschnitt).

2.3.2 Mass spectrometry

^{230}Th/U-dating is now largely done using mass spectrometry. Thus, this technique is presented in more detail here. Basically, a mass spectrometer directly measures the relative isotope abundances via the mass to charge ratio of ionised isotopes in a sample. The concept was first introduced almost a century ago in 1913 by Thompson. It is based on the deflection of charged particle beams in a magnetic field depending on the mass to charge ratio. A review of early developments of mass spectrometry can be found in DE LAETER (1998). Technical advances in thermal ionisation mass spectrometry (TIMS) in the 1980´s led to a significant improvement in precision and detection limits (EDWARDS et al. 1987. In the last 10–15 years further improvements in plasma source mass spectrometry, especially the advent of multi collector inductively coupled plasma mass spectrometry (MC-ICPMS) led to a further shift to this technique (e.g., GOLDSTEIN & STIRLING 2003; HALLIDAY et al. 1998). Here we focus on TIMS and MC-ICPMS because those are currently the most important techniques for high precision U and Th isotope measurements.

The basic concept of mass spectrometry is: (i) ionisation of isotopes, (ii) acceleration of the charged particles using a high potential difference, and (iii) the separation of charged particle beams with different mass to charge ratio in a magnetic field. The intensities of the separated ion beams then have to be detected to obtain the relative abundance. Thus, there are three main parts of a mass spectrometer: ion source, mass analyser and detector system.

A TIMS is a solid source mass spectrometer. The purified U and Th solutions are placed on a filament, e.g., made of Rhenium, which is placed in the ion source of the mass spectrometer. The sample chamber is evacuated to high vacuum, and the filament then heated by an electric current. Atoms are thermally released from the filament and a certain proportion (<1 %) also ionised. The ions are accelerated by a high potential in the ion source, and the ion beam is focused into the mass analyser section. The mass analyser of a TIMS is a magnetic field. Typically, a U or Th isotope measurement takes a few hours. The total U needed for one analysis is in the range of a few tens to hundreds of nanograms, and precisions of a few per mil can be achieved.

A MC-ICPMS is a plasma source mass spectrometer. The ion source consists of a torch, in which an Ar plasma is generated by a radio frequency (RF) coil. The purified U and Th sample is dissolved in a weak acid, and these solutions are nebulised in a spray chamber and mixed with Ar sample gas. The mixture is then injected into the plasma, which has a temperature of about 8000 K, and almost completely ionised (>90 %). The ions are transferred from the plasma at atmospheric pressure into the mass spectrometer at high vacuum via the interface region, where more than 90 % of the ions are lost. Inside the mass spectrometer an extraction voltage accelerates the ions via electrical lenses into the mass-analyser section. A modern MC-ICPMS is usually equipped with a combination of an electrostatic analyser (ESA) and magnetic analyser (Nier-Johnson geometry). In contrast to TIMS, the ESA, which is essentially an energy filter, is needed because of the larger energy spread of the ions. The ionisation and transfer efficiency of a modern MC-ICPMS is in the range of 1 %. The measurement time of one U or Th sample is 10-20 minutes with precisions comparable to TIMS. For MC-ICPMS ^{230}Th/U-dating typically a total U load of about 5 – 10 ng is needed (HOFFMANN et al. 2007). Further details can be found in GOLDSTEIN & STIRLING (2003).

The detector system is largely the same for TIMS and MC-ICPMS. It is usually a combination of Faraday cup detectors and ion counter devices. Ion beam intensities larger than 1 mV can be measured on Faraday cups. Small ion beams are detected using ion counters, such as secondary electron multipliers or Daly detectors. U isotopes, for example, are usually measured with a combination of an ion counting system for the minor ^{234}U and ^{236}U isotopes and Faraday cups for the more abundant ^{235}U and ^{238}U isotopes. The isotope beams are ideally measured simultaneously (static) to avoid

biases by unstable beam intensities. If the detector system has only one ion counter, two static measurements are done, one with ^{234}U on the ion counter and ^{238}U on a Faraday cup and another with ^{236}U on the ion counter and ^{238}U on a Faraday cup. The measured raw isotope ratios need to be corrected for several instrumental biases, such as ion-counter-Faraday-cup gain, ion counter darknoise, Faraday cup baseline, peak tailing („abundance sensitivity") and mass fractionation (e.g., Hoffmann et al. 2007).
In summary, precise and accurate U-Th isotope ratio measurements can be done with TIMS and MC-ICPMS, with MC-ICPMS allowing the use of smaller sample sizes. An accurate correction of instrumental biases and accurately calibrated spikes are essential for reliable dating results. Currently, the limit for ^{230}Th/U-dating is in the range of approximately 600 ka.

3 ^{230}Th/U-dating of reef corals

3.1 ^{238}U, ^{234}U and ^{230}Th in seawater

River runoff from the continents is the dominant supply of U to the oceans with an estimated flux of ~11×10^9 g/a (± 35 %) (Ivanovich & Harmon 1992). Additional sources of U in the ocean are, e.g., wind-blown dust and groundwater discharge. While the former is unlikely to be significant (<3 % of the riverine U flux), the latter is very difficult to estimate because both the total flux and the average U concentration of groundwater are poorly known. U is mainly removed from the oceans into reducing marine sediments where U becomes insoluble in the U^{4+} state. The oceanic U budget is in balance within the level of uncertainty, and seawater has a near constant U concentration of 3.3 ppb (Chen et al. 1986) indicating a residence time of ~400 ka.
Seawater (^{234}U/^{238}U) is elevated compared to secular equilibrium, which is related to the α-recoil effect in minerals on the continents and in marine sediments. Most measured seawater (^{234}U/^{238}U) values are around 1.146 (Chen et al. 1986; Robinson et al. 2004a), one study yielded a slightly higher value (1.149 ± 0.002, Delanghe et al. 2002). All these values are calculated using the half-lives reported by Cheng et al. (2000).
Potential changes in palaeo seawater (^{234}U/^{238}U) with *time* are most likely to be induced by changes in the riverine input, and several studies used models to place limits on how much marine (^{234}U/^{238}U) could have changed over Late Quaternary time scales (e.g., Chen et al. 1986; Hamelin et al. 1991; Richter & Turekian 1993). These studies revealed that seawater δ^{234}U should not have changed more than 10-20 ‰ compared to its modern value during the last several hundred ka. This is further confirmed by U-series analysis of U-rich slope sediments suggesting that seawater δ^{234}U remained within 15 ‰ of its modern value within the last 360 ka (Henderson 2002). Recent studies indicate shifts in seawater (^{234}U/^{238}U) at times of major glacial-interglacial transitions involving large variations in sea levels (Esat & Yokoyama 2006; Robinson et al. 2004b), but during periods of high sea level (i.e., interglacials) seawater δ^{234}U should have been in the range of 146 ± 10 ‰.
Th generally exists as a neutral hydroxide species in the oceans and is highly insoluble. Because of its high particle reactivity, it has a distinct tendency to become incorporated in colloids or adsorbed onto particle surfaces (Ivanovich & Harmon 1992). Thus, ^{230}Th produced by decay of ^{234}U in the water column is rapidly removed by sorption to particles, which settle from the water column. The average residence time of Th in seawater is estimated as ~20 a (Henderson & Anderson 2003) resulting in (^{230}Th/^{238}U) values that are 105 times lower than secular equilibrium (Moore 1981).

3.2 Incorporation of U-series isotopes into reef corals

The dominant form of U in seawater is the large uranyl carbonate anion $UO_2(CO_3)_3^{4-}$, and with descending pH, the species $UO_2(CO_3)_3^{2-}$ and $UO_2(CO_3)_3^{0}$ prevail. A comparison of several U substitution mechanisms showed that U incorporation into reef corals occurs most likely according to the following reaction (Shen & Dunbar 1995; Swart & Hubbard 1982):

$$CaCO_3 + UO_2(CO_3)_2^{2-} \rightleftarrows CaUO_2(CO_3)_2 + CO_3^{2-} \quad (5)$$

A variety of studies showed that the U/Ca ratio of scleractinian corals is controlled by the absolute U concentration of seawater (SHEN & DUNBAR 1995; SWART & HUBBARD 1982), water temperature (MIN et al. 1995; SHEN & DUNBAR 1995), coral growth rate, and coral species (CROSS & CROSS 1983). However, despite of these effects molar U/Ca ratios of surface corals are within about 30% of the seawater value of 1.3×10^{-6} (EDWARDS et al. 2003). Isotope fractionation between ^{234}U and ^{238}U seems not to occur during coral growth, which is demonstrated by the good agreement of the average $\delta^{234}U$ value measured on modern corals (i.e., 146.6 ± 1.4 ‰, DELANGHE et al. 2002) with the seawater value.

Molar $^{232}Th/^{238}U$ values of young surface corals are typically slightly lower than seawater values (CHEN et al. 1986). This shows that U and Th are not largely fractionated during aragonite formation and are incorporated into coral skeletons in their proportions in seawater. Consequently, the low ($^{230}Th/^{238}U$) activity ratio in seawater leads to close to zero initial ($^{230}Th/^{238}U$) activity ratio in corals, which is one of the basic premises for U-series dating.

3.3 Reliability of $^{230}Th/U$-coral ages

The reliability of U-series ages of fossil reef corals depends on the validity of the two basic premises of $^{230}Th/U$-dating. As discussed in the previous section, most reef building surface corals do not contain substantial initial ^{230}Th. Comparison of $^{230}Th/U$-ages of corals with ages known a priori from counting of annual density bands showed that initial ^{230}Th levels are negligible in corals containing less than 100 pg/g of ^{232}Th (EDWARDS et al. 2003). ^{232}Th concentrations between several hundred and 1000 pg/g (COBB et al. 2003) or even higher (SCHOLZ et al. 2004; STIRLING et al. 1998) have been reported. However, values of this magnitude still do not result in significant shifts in $^{230}Th/U$-ages for corals older than several ka, because the initial ^{230}Th will be negligible compared to that produced by decay of ^{234}U. Only for very young corals (i.e., younger than a few thousand years) high ^{232}Th content indicates the presence of significant levels of initial ^{230}Th and makes an appropriate correction necessary. This requires knowledge of the initial ($^{230}Th/^{232}Th$) activity ratio. Investigation of samples with known age showed isotopic $^{230}Th/^{232}Th$ ratios between 0 and 2×10^{-5} for marine and $\sim 4 \times 10^{-6}$ for terrestrial sources (COBB et al. 2003). With these values upper and lower limits for the correction can be estimated.

The validity of the closed-system assumption is more difficult to assess. During periods of low sea level (e.g., glacial periods) most fossil reef corals were exposed to meteoric water for a substantial period of time. This bears the risk of the aragonitic coral skeletons being recrystallised to calcite by dissolution or reprecipitation processes. Because calcite was shown to incorporate much less U than aragonite (REEDER et al. 2000), such processes are supposed to be accompanied with significant loss of U. Therefore, the calcite content of fossil corals is used as an indication for post-depositional recrystallisation and should not exceed 1%. The calcite content of a coral matrix can be precisely determined by X-ray diffraction (XRD).

Another test for open-system behaviour is the comparison of the total U content of fossil corals and their modern counterparts. Numerous studies on various coral species showed that the primary U concentration ranges from 1.5 to 4 µg/g (e.g., AMIEL et al. 1973; CROSS & CROSS 1983; GVIRTZMAN et al. 1973; SWART & HUBBARD 1982), and within one coral specimen variations of several percent are possible (MIN et al. 1995; SHEN & DUNBAR 1995). Due to the rather large variability of U concentration in modern corals the total U content can only serve as a broad indicator for open system behaviour. Nevertheless, post-depositional uptake and/or loss of U might result in substantial age bias. For example, SCHOLZ et al. (2007) presented evidence for post-depositional U redistribution in coral reefs on Barbados, which leads to a maximum age bias of 30 ka for corals

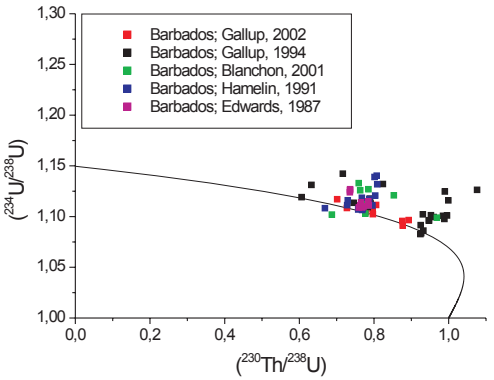

Fig. 4: A compilation of the activity ratios measured on fossil reef corals from Barbados, West Indies. The error bars are smaller than the plot-symbols. All corals are of the genus *Acropora palmata*. It is evident that most corals plot above the seawater evolution curve and, thus, have elevated initial (^{234}U/^{238}U). Data are taken from Blanchon & Eisenhauer (2001), Edwards et al. (1987), Gallup et al. (2002; 1994) and Hamelin et al. (1991).

Abb. 4 : Zusammenstellung von gemessenen Aktivitätsverhältnissen an fossilen Riffkorallen von Barbados. Die Fehlerbalken sind kleiner als die Symbole. Alle Korallen gehören zu der Gattung *Acropora palmata*. Es ist offensichtlich, dass die meisten Datenpunkte oberhalb der *seawater evolution curve* liegen und somit erhöhte $(^{234}U/^{238}U)_{init.}$ haben. Die Daten stammen aus Blanchon & Eisenhauer (2001), Edwards et al. (1987), Gallup et al. (2002; 1994) und Hamelin et al. (1991).

from Marine Isotope Stage (MIS) 6.5 (~175 ka before present). Elevated ^{232}Th can also be related to post-depositional contamination from detrital sources and, therefore, be an indication for open-system behaviour.

However, post-depositional open-system behaviour needs to be reliably identified in corals. Because corals incorporate ^{234}U and ^{238}U in the same ratio as they occur in modern seawater, the initial coral (^{234}U/^{238}U), which can be calculated using the ^{230}Th/U-age in Eq. (2), should agree with modern seawater (^{234}U/^{238}U). Equivalently, the (^{230}Th/^{238}U) and (^{234}U/^{238}U) activity ratios of a fossil coral should plot on the seawater evolution curve, which describes the temporal development of activity ratios under closed-system conditions with the initial (^{234}U/^{238}U) of modern seawater (bold line in Fig. 3). A significant deviation of the initial (^{234}U/^{238}U) from the seawater value indicates open-system behaviour and the ^{230}Th/U-age has to be considered non-reliable.

However, the analytical precision of mass spectrometric analyses indicates that initial (^{234}U/^{238}U) varies significantly between different corals and that in fact most fossil reef corals display initial (^{234}U/^{238}U) in excess of modern seawater and recent corals (e.g., Bard et al. 1992; Bard et al. 1991; Edwards et al. 1987; Hamelin et al. 1991; Henderson et al. 1993; Ku et al. 1990) (Fig. 4).

All coral data shown in Fig. 4 correspond to past sea level highstands, i.e., MIS 5 and 7. As discussed in Section 3.1, seawater (^{234}U/^{238}U) should have been within 1 % of the modern value during such periods. Thus, the large variation in initial (^{234}U/^{238}U) of corals cannot reflect changes in the marine U isotopic composition and is a clear evidence for open-system behaviour. The fact that even samples, which are apparently pristine according to mineralogical criteria, show elevated initial (^{234}U/^{238}U) suggests that the isotopic system is more sensitive to post-depositional changes than any petrographic or general geochemical parameter (Chen et al. 1991; Zhu et al. 1993). Therefore, the premise of closed-system behaviour is not generally warranted for fossil reef corals, and the accuracy of ^{230}Th/U-ages is more limited due to the isotopic anomalies than analytical precision (Bard et al. 1992; Stirling et al. 1995).

To detect diagenetically altered corals, various reliability criteria were developed (e.g., compare Stirling et al. 1998), and only ^{230}Th/U-ages that fulfil these criteria are believed to be *strictly* reliable:

a) Initial (^{234}U/^{238}U) within a specific range of modern seawater (^{234}U/^{238}U)
b) U content within the range of modern analogues from the same region
c) ^{232}Th concentrations lower than 1 ppb
d) Calcite content lower than 1 %
e) Primary aragonitic textures

An additional rigorous test for open-system behaviour is combined ^{231}Pa/U and ^{230}Th/U-dating (EDWARDS et al. 2003). The application of both dating methods to the same coral sample allows identification of isotopically altered corals, which otherwise would have passed all criteria. Recent measurements on 14 corals with initial δ^{234}U values within 8‰ of modern seawater from Barbados showed that six had discordant ^{231}Pa/U and ^{230}Th/U-ages (CUTLER et al. 2003; GALLUP et al. 2002). This demonstrates processes that have affected Pa, Th, and/or U, but not δ^{234}U (EDWARDS et al. 2003).

3.4 Open-system dating of fossil reef corals

Since obviously most fossil corals show evidence for post-depositional diagenesis, an approach to reliably date these corals would represent a major improvement. Therefore it is a current research focus to understand the mechanisms of coral diagenesis on U-Th isotopes and develop correction techniques for open-system dating.

Several authors have proposed diagenetic scenarios, such as post-depositional U and Th gain/loss to explain the observed isotopic anomalies in fossil reef corals (e.g., BAR-MATTHEWS et al. 1993; CHEN et al. 1991; FRUIJTIER et al. 2000; HAMELIN et al. 1991; HENDERSON et al. 1993). Most diagenetically altered fossil reef corals show elevated initial δ^{234}U. Several studies detected a correlation between δ^{234}U and the ^{230}Th/U-age (FRUIJTIER et al. 2000; STEIN et al. 1993; ZHU et al. 1993) and also between δ^{234}U and (^{230}Th/^{238}U) (GALLUP et al. 1994; SCHOLZ et al. 2004; STIRLING et al. 1998; THOMPSON et al. 2003; VILLEMANT & FEUILLET 2003). Other studies, however, found no general correlations (CHEN et al. 1991).

BENDER et al. (1979) were the first who presented a diagenetic open-system model for fossil reef corals. They assumed that all corals suffered continuous addition of ^{234}U and ^{230}Th. Subsequently, KU et al. (1990) proposed a model, based on gain or loss of both ^{234}U and ^{238}U through continuous exchange with U in groundwater or soil water. GALLUP et al. (1994) detected a rough correlation between initial δ^{234}U and ^{230}Th/U-age in Barbados corals. On the basis of the observed relation between (^{234}U/^{238}U) and (^{230}Th/^{238}U) (Fig. 3), they modelled the diagenetic processes assuming continuous addition of ^{234}U and ^{230}Th. However, this model has two serious problems: (i) it is difficult to show that the diagenetic trends are such as described by the model when there are a only limited number of coeval corals. Furthermore, in many cases corals do not show the same diagenetic trends or no trend at all (EDWARDS et al. 2003; POTTER et al. 2004; SCHOLZ et al. 2004; SCHOLZ et al. 2007). (ii) It is not reasonable that ^{234}U and ^{230}Th should be added at similar rates because of their very different chemical behaviour (Section 2.1). In theory, the redistribution of these isotopes should rely on transport by groundwater or porewater, but the model results suggest that the different solubilities of U and Th do not play a significant role in how they are transported and deposited. GALLUP et al. (1994) proposed that the nuclides are transported on particles in the water, such as organic colloids. Many authors have proposed mechanisms to explain this problem. CHEN et al. (1991) proposed that some ^{238}U, ^{234}U, and ^{230}Th may be leached out of one part of the coral by chemical reactions and deposited onto another part. As a mechanism for ^{234}U addition they proposed that ^{234}Th as the recoil daughter nuclide of ^{238}U (Fig. 1) is likely to be hydrolysed and adsorbed onto a solid surface before decaying to ^{234}U.

More recently, three models dealing with open-system behaviour of fossil reef corals were published (SCHOLZ et al. 2004; THOMPSON et al. 2003; VILLEMANT & FEUILLET 2003). The model of VILLEMANT & FEUILLET (2003) takes into account possible initial ^{230}Th excess and continuous selective redistribution (i.e., gain and/or loss) of ^{234}U, ^{234}Th, and ^{230}Th controlled by α-recoil processes. The THOMPSON et al. (2003) model explains the positive correlation between (^{234}U/^{238}U) and (^{230}Th/^{238}U) by coupled addition of particle-reactive ^{234}Th and ^{230}Th, which is produced by decay of dissolved U and α-recoil mobilisation of U daughters. In

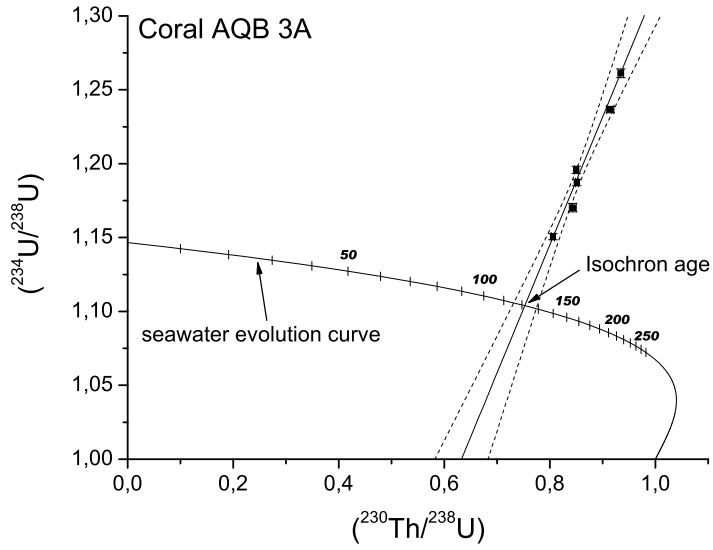

Fig. 5: (taken from Scholz & Mangini 2006): Isochron plot for coral AQB 3A from Aqaba, Jordan (Scholz et al. 2004). The activity ratios measured in six different sub-samples show a high linear correlation between (^{234}U/^{238}U) and (^{230}Th/^{238}U) (R = 0.99). The labels on the seawater evolution curve represent the corresponding ^{230}Th/U-ages in ka. The isochron age is calculated from the intersect of the isochron with the seawater evolution curve. The dashed curves represent confidence bands at 95% confidence level. Isochron age errors can be calculated from the intersects of the confidence bands with the seawater evolution curve.

Abb. 5: (übernommen aus Scholz & Mangini 2006): Isochronen Diagramm für Koralle AQB 3A aus Aqaba, Jordanien (Scholz et al. 2004). Die Aktivitätsverhältnisse, die an sechs verschiedenen Teilproben der Koralle gemessen wurden, zeigen eine starke lineare Korrelation zwischen (^{234}U/^{238}U) and (^{230}Th/^{238}U) (R = 0.99). Die Beschriftungen an der *seawater evolution curve* zeigen die entsprechenden ^{230}Th/U-Alter in ka. Das Isochronen Alter wird aus dem Schnittpunkt der Isochrone mit der *seawater evolution curve* berechnet. Die gestrichelten Kurven sind die entsprechenden 95%-Konfidenzbänder. Der Fehler des Isochronenalters wird aus den Schnittpunkten des Konfidenzbänder mit der seawater evolution curve bestimmt.

contrast to Gallup et al. (1994), the authors of both models suggest that their models can be used to correct ^{230}Th/U-ages of samples with initial δ^{234}U deviating from the modern seawater value. They term these ages *open-system ages*. Because both models assume very similar redistribution mechanisms, the calculated ^{230}Th/U-ages are similar. Corals that were affected by other diagenetic processes (e.g., gain/loss of U) cannot be dated because the models take only into account the described redistribution process. Thus, such corals must be rejected, e.g., by application of standard screening criteria (Section 3.3). However, there are problems with the α-recoil based models: (i) The trends between (^{234}U/^{238}U) and (^{230}Th/^{238}U) observed at different localities worldwide are not the same. In general, the data points from a given terrace are not all co-linear within analytical error, as required for an exact ^{230}Th/U-age correction with these models (Edwards et al. 2003). (ii) Impossibly large volumes of carbonate are necessary to maintain the concentration of dissolved U required to produce the isotopic anomalies observed in most fossil reef corals (Thompson et al. 2003).

Scholz et al. (2004) proposed a different model to date diagenetically altered reef corals. They assumed that different sub-samples of an individual coral gained different amounts of

U with high ($^{234}U/^{238}U$), possibly followed by U loss proportional to U gain. This results in a linear correlation between ($^{230}Th/^{238}U$) and ($^{234}U/^{238}U$), similar to the models of THOMPSON et al. (2003) and VILLEMANT & FEUILLET (2003). In contrast to these models, however, the slope of the addition line (referred to as isochron) is not defined by the model but depends on the timing of U gain and loss, respectively, and hence, on the specific diagenetic history of the analysed coral. The isochron is obtained from a linear fit of the data on a ($^{234}U/^{238}U$) vs. ($^{230}Th/^{238}U$) diagram, and the coral isochron age is calculated from the intersect of the isochron with the seawater evolution curve (Fig. 5).

The isochron model (SCHOLZ et al. 2004) can also explain the activity ratios of fossil corals plotting below the seawater evolution curve if one assumes that the gained U has a lower ($^{234}U/^{238}U$) activity ratio than the coral. Because coral isochron dating does not account for elevated ^{232}Th and aragonite recrystallisation, prior screening with standard screening criteria is still required. The isochron age error is calculated by propagation of the uncertainties of the isochron (SCHOLZ & MANGINI 2006).

Meanwhile, the three open-system models have been applied in several studies to derive palaeoclimatic information (ANDERSEN et al. 2008; FELIS et al. 2004; FRANK et al. 2006; POTTER et al. 2004; THOMPSON & GOLDSTEIN 2005; THOMPSON & GOLDSTEIN 2006; WAELBROECK et al. 2008). However, both conventional $^{230}Th/U$-dating and the three open-system models are associated with specific problems. For example, investigation of several sub-samples from the same coral specimen has shown that the real age uncertainty of both conventional $^{230}Th/U$-ages and the open-system ages calculated by the THOMPSON et al. (2003) model is substantially larger than suggested by the quoted uncertainties (SCHOLZ & MANGINI 2007). In addition, the widely used „strict" reliability criteria are not sufficient to identify all corals that were altered by other diagenetic processes than assumed by the models (SCHOLZ & MANGINI 2007). In general, all models should only be applied to coral data, which have been demonstrated to be altered by the underlying processes. Application to published coral data may result in both wrong $^{230}Th/U$-ages and substantial underestimation of the age uncertainty (SCHOLZ & MANGINI 2007).

After all, despite of almost 40 years of intensive examination of the U-series systematics of fossil reef corals, a number of aspects that produce the diagenetic alterations have not been satisfactorily explained so far. Thus, it has been extremely difficult to develop a general correction technique for diagenetically altered fossil reef corals, although several promising models have been proposed.

4 $^{230}Th/U$-dating of speleothems

4.1 Growth and occurrence of speleothems

Speleothems such as stalagmites, stalactites or flowstones are secondary cave deposits and grow in karst areas in almost all parts of the world. A detailed overview of the different forms of speleothems is given e.g. by HILL & FORTI (1997). In brief, speleothem growth can be explained as follows: Meteoric water seeps through the soil above a cave and becomes enriched in CO_2 due to the high pCO_2 of the soil zone, which results from the respiration of plant roots and decay of organic material. In the soil zone pCO_2 levels can reach values of up to 100,000 ppm (MCDERMOTT 2004). This results in the production of carbonic acid according to Eq. (6):

$$H_2O + CO_{2(aq)} \rightleftarrows H_2CO_3, \quad (6)$$

which dissociates according to Eqs. (7) and (8):

$$H_2O + H_2CO_3 \rightleftarrows HCO_3^- + H_3O^+ \quad (7)$$

$$H_2O + HCO_3^- \rightleftarrows CO_3^{2-} + H_3O^+ \quad (8)$$

Calcium carbonate is dissolved as described by Eq. (9), when the highly corrosive percolating water comes into contact with the carbonate bedrock:

$$CO_2 + H_2O + CaCO_3 \rightleftarrows Ca^{++} + 2HCO_3^- \quad (9)$$

The resulting equilibrium concentration of Ca^{++} and HCO_3^- in the drip water depends on several parameters such as temperature, pCO_2 and whether dissolution occurs in a closed or an open system (Kaufmann 2003; McDermott 2004). The pCO_2 of cave air is usually higher than atmospheric pCO_2 but, depending of the degree of cave ventilation, much lower than in the soil zone. Thus, the CO_2 dissolved in the water entering the cave degases to the cave atmosphere. The drip water becomes supersaturated with respect to calcite, and $CaCO_3$ precipitates forming speleothems.

Stalagmite growth was first quantitatively described by Dreybrodt (1988; 1999). More recently, several models were developed describing the growth rate and shape of stalagmites depending on cave temperature, drip rate, pCO_2 of both the soil zone and the cave and also the mixing parameter, which accounts for mixing of the impinging drop with the existing solution film on top of the stalagmite (Kaufmann 2003; Mühlinghaus et al. 2007; Romanov et al. 2008b).

4.2 U incorporation into speleothems

Dissolution of the carbonate bedrock above the cave also results in accumulation of traces of several elements in the drip water, such as Mg, Sr, Ba and also U. Their concentration in the drip water mainly depends on their concentration in the host rock and the corresponding partitioning coefficient. The trace elements are then co-precipitated with speleothem calcite. Thus, the U-concentration in speleothems ranges from near zero to more than 100 µg/g (Ford & Williams 2007).

The U and Th isotopes, which are relevant for ^{230}Th/U-dating (Fig. 1, Section 2.2), are in secular equilibrium in the host rock (Fig. 2) because the karst bedrock usually has an age of several million years. However, due to the different geochemical behaviour of U and Th (Section 2.1) the activity ratios established in the percolating cave drip water are substantially different from secular equilibrium. Th is insoluble in natural water and, thus, the (^{230}Th/^{238}U) of drip water is zero - one of the basic premises for ^{230}Th/U-dating. In contrast, the (^{234}U/^{238}U) of drip water is usually larger than secular equilibrium due to the preferential leaching of ^{234}U resulting from α-recoil (Section 2.1), unless the host rock is already depleted in ^{234}U. The (^{234}U/^{238}U) of drip water depends on (i) the age of the bedrock and (ii) the time available for the dissolution of the bedrock. In theory, slowly percolating water and, thus, a long residence time should result in high drip water (^{234}U/^{238}U). In contrast, high rainfall events and, as a consequence, fast percolating waters and, thus, a short residence time should result in (^{234}U/^{238}U) close to secular equilibrium. However, unambiguous interpretation of (^{234}U/^{238}U) and quantification of the responsible processes remain difficult (Porcelli & Swarzenski 2003). In any case, drip water (^{234}U/^{238}U) can vary substantially for different cave systems and is also usually not constant in time for an individual cave. Thus, there is no uniform initial (^{234}U/^{238}U) for speleothems like e.g. for marine carbonates, such as reef corals (Section 3). This does not affect the application of ^{230}Th/U-dating to speleothems because the initial (^{234}U/^{238}U) is not needed for the age calculation (Eq. 3).

4.3 Reliability of speleothem ^{230}Th/U-ages

Again, the speleothem sample has to meet the two basic premises of ^{230}Th/U-dating. The validity of the first assumption (i.e., no initial ^{230}Th) is usually assessed by measuring the concentration of detrital ^{232}Th. The second assumption is more difficult to verify. As mentioned in the previous section, there is no general initial (^{234}U/^{238}U) as for marine carbonates, which could be used as a reliability criterion. However, due to their natural occurrence in caves speleothems are not as exposed to meteoric waters as e.g. reef corals. Thus, even very old stalagmites are usually very well preserved and show no evidence for post-depositional diagenesis (Woodhead et al. 2006).

However, violation of one of the basic premises cannot be a priori excluded and the reliability of ^{230}Th/U ages needs to be assessed. Initial ^{230}Th

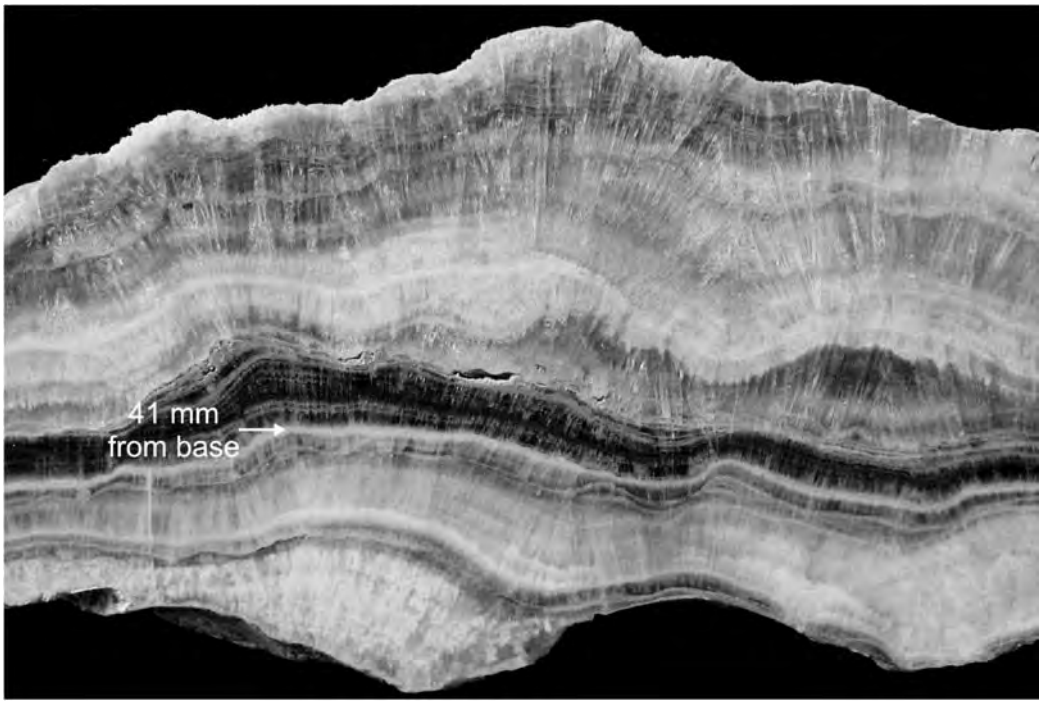

Fig. 6: Flowstone SPA 59 from Spannagel cave, Austrian Alps. There are clearly visible distinct growth layers. The chronology of SPA 59 is shown in Fig. 7. The picture was provided by C. Spötl.

Abb. 6: Flowstone SPA 59 aus der Spannagel Höhle in den österreichischen Alpen. Unterschiedliche Wachstumslagen sind sehr gut zu erkennen. Das Altersmodell für SPA 59 ist in Abb. 7 dargestellt. Das Foto wurde von C. Spötl zur Verfügung gestellt.

(i.e., not produced by in situ decay of ^{234}U and ^{238}U in the sample) is generally accompanied by a larger amount of ^{232}Th because the $^{230}Th/^{232}Th$ isotope ratio in most crustal materials is around 5×10^{-6} (WEDEPOHL 1995). For $^{230}Th/U$-dating the ^{232}Th concentration of a sample is routinely also measured in addition to the isotopes required for the age calculation (Section 2.3). Samples containing more than an acceptable value of initial ^{230}Th can be identified based on the assumption that detrital ^{232}Th is accompanied by ^{230}Th in a defined ratio. However, it is not possible to correct the measured ($^{230}Th/^{238}U$) using a universally applicable ($^{230}Th/^{232}Th$) ratio because this ratio varies substantially in possible detrital source materials. Two correction procedures were suggested: (i) correction for detrital contamination using an a priori estimate of the isotopic composition of the detrital phase and the corresponding uncertainty (HELLSTROM 2006; LUDWIG 2003), and (ii) direct determination of the isotopic composition of the detrital phase using isochron techniques (BECK et al. 2001; LUDWIG 2003; LUDWIG & TITTERINGTON 1994). The $^{230}Th/U$-ages of speleothems with ($^{230}Th/^{232}Th$) within a range that indicates significant Th contamination (i.e., ($^{230}Th/^{232}Th$) < 100 – 300, RICHARDS & DORALE 2003) should either be corrected for the effect of contamination or rejected (HELLSTROM 2006).

A criterion to test the reliability of the $^{230}Th/U$-ages of speleothems is that the ages must be in stratigraphic order. Basically, the $^{230}Th/U$-age of the upper layers must be younger than that of those below because stalagmites grow from the bottom up depositing growth layers (KAUFMANN 2003; MÜHLINGHAUS et al. 2007; ROMANOV et al. 2008b) (Fig. 6). Thus, the ages down the growth axis of a stalagmite must

become progressively older. Age inversions of dated layers, i.e., a ^{230}Th/U-age of a sub-sample that is significantly older or younger than suggested by the stratigraphy, indicate that at least one of the determined ages is wrong. This may have several reasons: (i) Post-depositional open-system behaviour, i.e., violation of the closed-system assumption, (ii) inadequate correction for detrital contamination, (iii) underestimation of the age uncertainty resulting either from the analysis itself or the applied correction for contamination, or (iv) a mistake during the analysis or the sample preparation. In any case, age inversions have to be cross-checked by analysis of additional samples from the same horizon. Otherwise, they must be accounted for by assigning the corresponding ages with an appropriately enlarged age uncertainty.

4.4 Speleothem age-distance model

To determine the age of a stalagmite at the depths of the proxy measurements, an age model is constructed, which mathematically describes the relationship between the distance from the top/bottom of the stalagmite and the age of the stalagmite. However, although an increasing number of papers presenting high precision ^{230}Th/U ages of speleothems were published in the last decade, a standard approach to derive an age model on the basis of the measured ages (compare Fig. 6) has not been established yet. Some authors use linear interpolation of the ^{230}Th/U-ages between the depth of the dated samples (Wang et al. 2005), others apply least squares polynomial fits (Spötl & Mangini 2002). Other studies, in turn, apply various kinds of smoothing splines (Spötl et al. 2006; Vollweiler et al. 2006) or even more sophisticated methods (Drysdale et al. 2005; Drysdale et al. 2004; Genty et al. 2006) based on the general growth systematics of speleothems (Kaufmann 2003). The age model is crucial because the timing or duration determined for a specific event, e.g., indicated by a peak in a stable isotope curve, depends on the method used to calculate the age model. This is especially problematic because ^{230}Th/U-dating is usually not performed at the depth of the corresponding peak. Thus, a generalised method to construct speleothem age models is desirable, which would not only guarantee the comparability of stalagmite records from different laboratories but also make the most efficient use of the U-series ages. A general approach to estimate the uncertainty of stalagmite age models is also needed (Drysdale et al. 2004; Genty et al. 2006; Heegaard et al. 2005; Spötl et al. 2006).

4.5 ^{230}Th/U-dating of speleothems and palaeoclimate reconstruction

The chronology of speleothem growth provides important palaeoclimatic information. For example, the timing of speleothem growth itself is related to the climatic conditions above the cave. In cold and/or dry environments even a slight cooling/drying may result in a cessation of speleothem growth (Holzkämper et al. 2004; Holzkämper et al. 2005; Spötl et al. 2006). Timing of speleothem formation can also be related to global climate and sea level changes (Bard et al. 2002; Richards et al. 1994). Speleothems found in submerged caves indicate that the caves were not flooded at some time in the past because speleothems only form when the cave is air filled. Therefore, in tectonically stable regions the timing of the growth of speleothems collected from submerged caves unambiguously indicates that the cave was above sea level and constrains times of lower sea levels.

Furthermore, the speleothem growth rate is related to precipitation intensity, temperature and vegetation cover above the cave, which in turn is related to climate (Drysdale et al. 2005; Drysdale et al. 2004; McDermott 2004; Mühlinghaus et al. 2007).

An accurate and precise chronology is essential for using speleothems as palaeoclimate archives. Speleothems provide numerous proxies of palaeoclimate, which can be measured with very high spatial resolution (Henderson 2006). Most palaeoclimate studies using speleothems apply precisely dated high-resolution stable isotope profiles (i.e., δ^{18}O and δ^{13}C), which have contributed much information to the un-

derstanding of the climate system within the last decade (BAKER et al. 2007; CRUZ JR et al. 2005; DRYSDALE et al. 2005; FLEITMANN et al. 2003; GENTY et al. 2003; HOLZKÄMPER et al. 2004; MANGINI et al. 2005; NEFF et al. 2001; NIGGEMANN et al. 2003b; NIGGEMANN et al. 2003a; PARTIN et al. 2007; SPÖTL & MANGINI 2002; SPÖTL et al. 2002; WANG et al. 2004; WANG et al. 2005; ZANCHETTA et al. 2007). The $\delta^{13}C$ signal recorded in speleothems depends on several parameters both in the soil zone and in the cave (MCDERMOTT 2004) and is, therefore, complicated to interpret. However, the understanding of the effects influencing stalagmite $\delta^{13}C$ has improved in recent years (MICKLER et al. 2004; MICKLER et al. 2006; MÜHLINGHAUS et al. 2007; ROMANOV et al. 2008a). In combination with a thorough monitoring of the studied cave system the application of $\delta^{13}C$ for palaeoclimate reconstruction is possible (BAR-MATTHEWS et al. 2000; DRYSDALE et al. 2004; FRISIA et al. 2006; GENTY et al. 2006; GENTY et al. 2003; MÜHLINGHAUS et al. 2007). High resolution trace element profiles may reveal variation in precipitation intensity (HUANG & FAIRCHILD 2001; JOHNSON et al. 2006; ROBERTS et al. 1998; TREBLE et al. 2003; VERHEYDEN et al. 2000).

4.6 ^{230}Th/U-dating of speleothem SPA 59

We present a case study of ^{230}Th/U-dating of a flow stone (SPA 59) collected in the Spannagel cave, Austrian Alps. The present mean annual temperature in the cave is around 2°C and, thus, just above the freezing point. Since speleothems do not form below this point, periods of speleo-

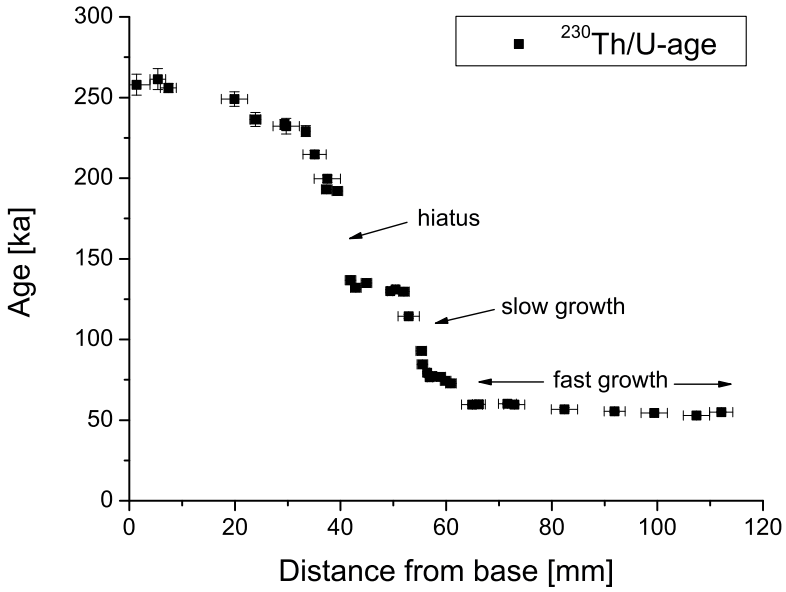

Fig. 7: TIMS ^{230}Th/U-dating results for flowstone SPA 59 from Spannagel cave (modified after HOLZKÄMPER et al. 2005). The speleothem grew in several phases between 50 and 270 ka, which correspond to interglacials as defined in the SPECMAP chronology (IMBRIE et al. 1984). Periods of fast and slow growth, respectively, as well as a longer hiatus between ~140 and ~190 ka are indicated.

Abb. 7: TIMS ^{230}Th/U-Datierungsergebnisse für Flowstone SPA 59 aus der Spannagel Höhle (geändert nach HOLZKÄMPER et al. 2005). Dieser Speläothem wuchs in mehreren Phasen zwischen 50 und 270 ka, die entsprechenden Interglazialen in der SPECMAP Chronologie zugeordnet werden können (IMBRIE et al. 1984). Phasen schnellen bzw. langsamen Wachstums sowie ein längerer Hiatus zwischen 140 und 190 ka sind eingezeichnet.

them formation correspond to past warm phases (Holzkämper et al. 2005; Spötl et al. 2007). Thus, the timing of the beginning and end of speleothem growth, respectively, is of particular interest. A chronology based on TIMS ^{230}Th/U-dating of SPA 59 was previously published by Holzkämper et al. (2005). More recently a high spatial resolution MC-ICPMS ^{230}Th/U-dating study of the hiatus between MIS 7 and 5 was performed by Hoffmann et al. (submitted).

The spatial resolution of ^{230}Th/U dating that can be achieved depends on the sampling as well as the mass spectrometry technique that is used. There is a variety of different techniques to obtain sub-samples from speleothems. Usually a stalagmite is cut in two halves along the growth axis and the surface is then polished to identify growth layers. Samples for ^{230}Th/U-dating can be taken from a growth layer by a handheld drill. A disadvantage of this sampling technique is that the obtained powders are prone to contamination and cannot be cleaned prior to chemical treatment. Another possibility is to cut slices from the speleothem and then cut subsamples, e.g., using a band saw. The obtained solid pieces of carbonate can be chemically cleaned prior to further analytical work. This technique, however, is more destructive than using a handheld drill.

Fig. 6 shows the section of flowstone SPA 59 from Spannagel cave, Austrian Alps, analysed by Holzkämper et al. (2005). The corresponding TIMS ^{230}Th/U-dating results, based on 37 analyses along the 11 cm of growth are presented in Fig. 7. TIMS results were obtained on sample sizes between 50 and 200 mg, which were sampled using a band saw. The flowstone formed between 260 and 55 ka, mostly during the warm phases of Marine Isotope Stages (MIS) 7, 5 and 3. There are substantial differences in growth rates, with fast growth around 250, 135 and 55 ka. In contrast growth was very slow between 125 and 75 ka. Furthermore, there is a distinct 55 ka long hiatus between 190 and 135 ka.

SPA 59 has an exceptionally high U concentration (between 10 and 168 µg/g, Holzkämper et al. 2005) allowing the use of samples smaller than 1 mg for MC-ICPMS analysis. Hence, ^{230}Th/U-dating can be performed at very high spatial resolution. Hoffmann et al. (submitted) cut a 1 mm thick sample slice off the flowstone section previously analysed by Holzkämper et al. (2005) for high spatial resolution MC-ICPMS ^{230}Th/U dating. Six carbonate pieces of 0.5 – 1 mg were then cut from SPA 59 between 39 and 44 mm from the base at a spatial resolution of 0.8 mm using a diamond coated wire saw (Fig. 8). The sample pieces were cleaned by ultrasonication in ultra-pure water to remove potential surface contamination or residuals from the cutting process. The dried small pieces were stripped off the section with a razorblade and weighed before processing through U and Th separation and purification chemistry and MC-ICPMS analysis (Hoffmann 2008). Fig. 9 shows the high resolution dating results in comparison with the previous TIMS chronology. The dating results agree well both below and above a white layer at the position of the hiatus indicated in Fig. 7, though the data were obtained in two different laboratories using different spikes and mass spectrometric techniques. However, the higher spatial resolution obtained using MC-ICPMS shows a dating problem associated with the white layer according to the stratigraphy criterion. Samples taken from the white layer are not in stratigraphic order. The ^{230}Th/U-age at 40 mm from base is apparently too old and another sample, taken at 41 mm, is out of range for ^{230}Th/U dating (Fig. 9). This indicates U loss, which is supported by lower U concentration in the white area (39 and 13 µg/g, respectively) compared to the clear and dense crystal below and above the white layer (64 and 134 µg/g, respectively). Thus, this section cannot be reliably dated by the ^{230}Th/U-method. The problem was not recognised in the study of Holzkämper et al. (2005) because they used larger sample sizes and TIMS.

Current research is concerned with MC-ICPMS ^{230}Th/U dating of microsamples, e.g., using a micromill or the laser ablation technique to further increase spatial resolution. Microsamples of SPA 59 with masses of about 0.09 - 0.1 mg can be prepared using a micromill. Micromill sam-

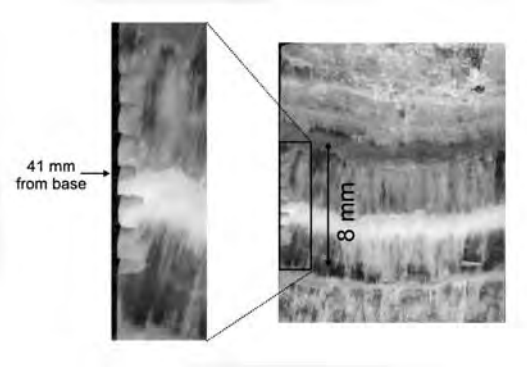

Fig. 8: A 1 mm thick slice of flowstone SPA 59. The white layer in the middle is at 41 mm from base at the position of the hiatus between MIS 7 and MIS 5. Six samples of a weight of about 1 mg were cut using a wire saw. The wire saw cuts are shown in the enlarged section. The small pieces between the cuts were stripped off and analysed for U-Th using MC-ICPMS.

Abb. 8: 1 mm dicke Scheibe von Flowstone SPA 59. Die weiße Lage in der Mitte befindert sich in 41 mm Abstand von der Basis in der Position der Wachstumsunterbrechung zwischen MIS 7 und MIS 5. Mit einer Drahtsäge wurden sechs Proben von ca. 1 mg herausgesägt. Die Schnitte der Säge sind in der vergrößerten Darstellung zu sehen. Die kleinen Karbonatstücke zwischen den Schnitten wurden entnommen und mittels MC-ICPMS auf ihren U- und Th-Gehalt untersucht.

pling procedures for ^{230}Th/U-dating are similar to those outlined in CHARLIER et al. (2006) for Sr isotope measurements (HOFFMANN et al. submitted). The laser ablation (LA) technique allows fast and direct ^{230}Th/U dating of speleothems without prior chemical separation at a spatial resolution of a few hundred µm. The precision of LA-MC-ICPMS can be similar to alpha spectrometry with samples sizes orders of magnitudes smaller (HOFFMANN et al. submitted).

5 Conclusions

Both fossil reef corals and speleothems are important archives of the climate of the past and can be reliably dated using U-series disequilibrium methods. The dating range of the ^{230}Th/U-method is between 500 and 600 ka depending on both analytical precision and initial (^{234}U/^{238}U). Using state of the art mass spectrometric techniques such as TIMS and MC-ICPMS, accurate and very precise ages can be obtained. However, several criteria must be fulfilled to obtain reliable ages.

Most fossil corals show evidence for post-depositional diagenetic alteration, which is an indication for open-system behaviour. There have been several reliability criteria established to identify unaltered corals, but these are not able to detect all altered corals (SCHOLZ & MANGINI 2007). Several open-system dating models have been developed to calculate reliable ages from altered corals (SCHOLZ et al. 2004; THOMPSON et al. 2003; VILLEMANT & FEUILLET 2003), but each model is associated with specific problems and should only be applied if the underlying assumptions are valid (SCHOLZ & MANGINI 2007). The understanding of the mechanisms of coral diagenesis and the development of appropriate correction approaches is a major goal of current research.

Most speleothems show no evidence for post-depositional open-system behaviour but some may contain significant amounts of initial ^{230}Th, indicated by elevated ^{232}Th content. There are two correction approaches available to account for detrital contamination: (i) Direct determination of the isotopic composition of the detrital phase using isochron techniques or (ii) correction using an a priori estimate of the ^{230}Th/^{232}Th composition of the detrital phase with the corresponding uncertainty. The application of both approaches results in increased age uncertainty. Although an increasing number of speleothem studies with high precision ^{230}Th/U dating have been published in the last decade, a standard approach for the derivation of an age model on the basis of the determined ages has not been established yet. This is one of the goals of current research concerning ^{230}Th/U-dating of speleothems. Very high spatial resolution dating using laser ablation and micromill techniques with precisons comparable to alpha spectrometry are currently being developed (HOFFMANN 2008; HOFFMANN et al. submitted).

If the above mentioned criteria are met, it is

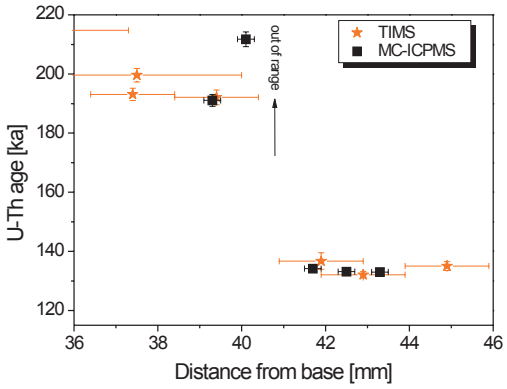

Fig. 9: TIMS and MC-ICPMS ^{230}Th/U-dating results for SPA 59. Below and above the white layer the results are in good agreement. However, sub-samples taken from the white layer are not in stratigraphic order indicating U loss.

Abb. 9: Ergebnisse der TIMS bzw. MC-ICPMS ^{230}Th/U-Datierung von SPA 59. Oberhalb und unterhalb der weißen Lage stimmen die Ergebnisse beider Methoden gut überein. Proben, die aus der weißen Lage entnommen wurden, stimmen nicht mit der Stratigraphie überein, was ein Anzeichen für nachträglichen U Verlust ist.

possible to derive very accurate and precise ^{230}Th/U-ages of both reef corals and speleothems. Their accuracy depends on several factors, such as the accuracy of the spike calibration and the correction of instrumental biases.

Acknowledgements

We would like to thank Frank Preusser for inviting us to write this article. Christoph Spötl kindly provided flowstone SPA 59 and the picture presented as Fig. 6. Thomas Felis kindly made available coral AQB 3A. Denis Scholz is funded by the DFG Research Group 668 (DAPHNE). Dirk Hoffmann is funded by the Leverhulme Trust. Thorough reviews of Mebus Geyh and Peter Rowe helped to improve the manuscript.

References

Amiel, A.J., Miller, D.S. & Friedman, G.M. (1973): Incorporation of uranium in modern corals. – Sedimentology, 20: 523-528.

Andersen, M.B., Stirling, C.H., Potter, E.-K., Halliday, A.N., Blake, S.G., McCulloch, M.T., Ayling, B.F. & O'Leary, M. (2008): High-precision U-series measurements of more than 500,000 year old fossil corals. – Earth and Planetary Science Letters, 265: 229-245.

Baker, A., Asrat, A., Fairchild, I.J., Leng, M.J., Wynn, P.M., Bryant, C., Genty, D. & Umer, M. (2007): Analysis of the climate signal contained within δ^{18}O and growth rate parameters in two Ethopian stalagmites. – Geochimica et Cosmochimica Acta, 71: 2975-2988.

Bar-Matthews, M., Wasserburg, G.J. & Chen, J.H. (1993): Diagenesis of fossil coral skeletons: Correlation between trace elements, textures, and ^{234}U/^{238}U. – Geochimica et Cosmochimica Acta, 57: 257-276.

Bar-Matthews, M., Ayalon, A. & Kaufman, A. (2000): Timing and hydrological conditions of Sapropel events in the Eastern Mediterranean, as evident from speleothems, Soreq cave, Israel. – Chemical Geology, 169: 145-156.

Bard, E., Hamelin, B. & Fairbanks, R.G. (1990): U-Th ages obtained by mass spectrometry in corals from Barbados: sea level during the past 130,000 years. – Nature, 346: 456-458.

Bard, E., Fairbanks, R.G. & Hamelin, B. (1992): How accurate are the U-Th ages obtained by mass spectrometry on coral terraces. – In: Kukla, G. & Went, E. (eds.): Start of a Glacial: 15-21; Berlin (Springer-Verlag).

Bard, E., Antonioli, F. & Silenzi, S. (2002): Sea-level during the penultimate interglacial period based on a submerged stalagmite from Argentarola Cave (Italy). – Earth and Planetary Science Letters, 196: 135-146.

Bard, E., Fairbanks, R.G., Hamelin, B., Zindler, A. & Hoang, C.T. (1991): Uranium-234 anomalies in corals older than 150,000 years. – Geochimica et Cosmochimica Acta, 55: 2385-2390.

Barnes, J.W., Lang, E.J. & Potratz, H.A. (1956): The ratio of ionium to uranium in coral limestone. – Science, 124: 175-176.

Beck, J.W., Richards, D.A., Edwards, R.L., Silverman, B.W., Smart, P.L., Donahue, D.J., Herrera-Osterheld, S., Burr, G.S., Calsoyas, L., Jull, A.J.T. & Biddulph, D. (2001): Extremely large variations of atmospheric C-14 concentration during the last glacial period. – Science, 292: 2453-2458.

Bender, M.L., Fairbanks, R.G., Taylor, F.W., Matthews, R.K., Goddard, J.G. & Broecker, W.S. (1979): Uranium-series dating of the Pleistocene

reef tracts of Barbados, West Indies. – GSA Bulletin, 90: 577-594.

BLANCHON, P. & EISENHAUER, A. (2001): Multi-stage reef development on Barbados during the Last Interglaciation. – Quarternary Science Rewiews, 20: 1093-1112.

BOURDON, B., TURNER, S.P., HENDERSON, G.M. & LUNDSTROM, C.C. (2003): Introduction to U-series geochemistry. – In: BOURDON, B., HENDERSON, G.M., LUNDSTROM, C.C. & TURNER, S.P. (Eds.): Uranium-series Geochemistry: 1-21; Washington, DC (Mineralogical Society of America).

BROECKER, W.S., THURBER, D.L., GODDARD, J.G., KU, T.-L., MATTHEWS, R.K. & MESOLELLA, K.J. (1968): Milankovich hypothesis supported by precise dating of coral reefs and deep sea sediments. – Science, 159: 297-300.

CHABAUX, F., RIOTTE, J. & DEQUINCEY, O. (2003): U-Th-Ra Fractionation during weathering and river transport. – In: BOURDON, B., HENDERSON, G.M., LUNDSTROM, C.C. & TURNER, S.P. (Eds.): Uranium-series Geochemistry: 533-576; Washington, DC (Mineralogical Society of America).

CHAPPELL, J. & POLACH, H. (1991): Post-glacial sea-level rise from a coral record at Huon Peninsula, Papua New Guinea. – Nature, 349: 147-149.

CHARLIER, B.L.A., GINIBRE, C., MORGAN, D., NOWELL, G.M., PEARSON, D.G., DAVIDSON, J.P. & OTTLEY, C.J. (2006): Methods for the microsampling and high-precision analysis of strontium and rubidium isotopes at single crystal scale for petrological and geochronological applications. – Chemical Geology, 232: 114-133.

CHEN, J.H., EDWARDS, R.L. & WASSERBURG, G.J. (1986): ^{238}U-^{234}U-^{232}Th in seawater. – Earth and Planetary Science Letters, 80: 241-251.

CHEN, J.H., CURRAN, H.A., WHITE, B. & WASSERBURG, G.J. (1991): Precise chronology of the last interglacial period: ^{234}U-^{230}Th data from fossil coral reefs in the Bahamas. – GSA Bulletin, 103: 82-97.

CHENG, H., EDWARDS, R.L., HOFF, J., GALLUP, C.D., RICHARDS, D.A. & ASMEROM, Y. (2000): The half-lives of uranium-234 and thorium-230. – Chemical Geology, 169: 17-33.

COBB, K.M., CHARLES, C.D., CHENG, H., KASTNER, M. & EDWARDS, R.L. (2003): U/Th-dating living and young fossil corals from the central tropical Pacific. – Earth and Planetary Science Letters, 210: 91-103.

CROSS, T.S. & CROSS, B.W. (1983): U, Sr and Mg in Holocene and Pleistocene corals *A. palmata* and *M. annularis*. – Journal of Sedimentary Petrology, 53: 587-594.

CRUZ JR, F.W., BURNS, S.J., KARMANN, I., SHARP, W.D., VUILLE, M., CARDOSO, A.O., FERRARI, J.A., SILVA DIAS, P.L. & VIANA JR, O. (2005): Insolation-driven changes in atmospheric circulation over the past 116,000 years in subtropical Brazil. – Nature, 434: 63-66.

CUTLER, K.B., EDWARDS, R.L., TAYLOR, F.W., CHENG, H., ADKINS, J., GALLUP, C.D., CUTLER, P.M., BURR, G.S. & BLOOM, A.L. (2003): Rapid sea-level fall and deep-ocean temperature change since the last interglacial period. – Earth and Planetary Science Letters, 206: 253-271.

DE LAETER, J.R. (1998): Mass spectrometry and geochronology. – Mass Spectrometry Reviews, 17: 97-125.

DELANGHE, D., BARD, E. & HAMELIN, B. (2002): New TIMS constraints on the uranium-238 and uranium-234 in seawaters from the main ocean basins and the Mediterranean Sea. – Marine Chemistry, 80: 79-93.

DREYBRODT, W. (1988): Processes in Karst Systems. - 288 pp.; Berlin (Springer).

DREYBRODT, W. (1999): Chemical kinetics, speleothem growth and climate. – Boreas, 28: 347-356.

DRYSDALE, R.N., ZANCHETTA, G., HELLSTROM, J.C., FALLICK, A.E. & ZHAO, J.-X. (2005): Stalagmite evidence for the onset of the Last Interglacial in southern Europe at 129 ± ka. – Geophysical Research Letters, 32: L24708.

DRYSDALE, R.N., ZANCHETTA, G., HELLSTROM, J.C., FALLICK, A.E., ZHAO, J.-X., ISOLA, I. & BRUSCHI, G. (2004): Palaeoclimatic implications of the growth history and stable isotope ($\delta^{18}O$ and $\delta^{13}C$) geochemistry of a Middle to Late Pleistocene stalagmite from central-western Italy. – Earth and Planetary Science Letters, 227: 215-229.

EDWARDS, R.L., CHEN, J.H. & WASSERBURG, G.J. (1986): ^{238}U-^{234}U-^{230}Th-^{232}Th systematics and the precise measurement of time over the past 500,000 years. – Earth and Planetary Science Letters, 81: 175-192.

EDWARDS, R.L., GALLUP, C.D. & CHENG, H. (2003): Uranium-series dating of marine and lacustrine carbonates. – In: BOURDON, B., HENDERSON, G.M., LUNDSTROM, C.C. & TURNER, S.P. (Eds.): Uranium-series Geochemistry: 363-405; Washington, DC (Mineralogical Society of America).

EDWARDS, R.L., CHEN, J.H., KU, T.-L. & WASSERBURG, G.J. (1987): Precise Timing of the Last Interglacial Period from Mass Spectrometric

Determination of Thorium-230 in Corals. – Science, 236: 1547-1553.

Esat, T.M. & Yokoyama, Y. (2006): Variability in the uranium isotopic composition of the oceans over glacial-interglacial timescales. – Geochimica et Cosmochimica Acta, 70: 4140-4150.

Felis, T., Lohmann, G., Kuhnert, H., Lorenz, S.J., Scholz, D., Pätzold, J., Al-Rousan, S.A. & Al-Moghrabi, S.M. (2004): Increased seasonality in Middle East temperatures during the last interglacial period. – Nature, 429: 164-168.

Fleitmann, D., Burns, S.J., Mudelsee, M., Neff, U., Kramers, J., Mangini, A. & Matter, A. (2003): Holocene Forcing of the Indian Monsoon Recorded in a Stalagmite from Southern Oman. – Science, 300: 1737-1739.

Ford, D.C. & Williams, P.W. (2007): Karst Hydrogeology & Geomorphology. 576 pp.; Chichester (John Wiley & Sons).

Frank, N., Turpin, L., Cabioch, G., Blamart, D., Tressens-Fedou, M., Colin, C. & Jean-Baptiste, P. (2006): Open system U-series ages of corals from a subsiding reef in New Caledonia: Implications for sea level changes and subsidence rate. – Earth and Planetary Science Letters, 249: 274-289.

Frisia, S., Borsato, A., Mangini, A., Spötl, C., Madonia, G. & Sauro, U. (2006): Holocene climate variability in Sicily from a discontinuous stalagmite record and the Mesolithic to Neolithic transition. – Quaternary Research, 66: 388-400.

Fruijtier, C., Elliott, T. & Schlager, W. (2000): Mass-spectrometric ^{234}U-^{230}Th ages from the Key Largo Formation, Florida Keys, United States: Constraints on diagenetic age disturbance. – GSA Bulletin, 112 (2): 267-277.

Gallup, C.D., Edwards, R.L. & Johnson, R.G. (1994): The timing of High Sea Levels over the past 200,000 years. - Science, 263: 796-800.

Gallup, C.D., Cheng, H., Taylor, F.W. & Edwards, R.L. (2002): Direct Determination of the Timing of Sea Level Change During Termination II. – Science, 295: 310-313.

Geyh, M.A. (2008): ^{230}Th/U dating of interglacial and interstadial fen peat, lignite: Potential and limits. - Quaternary Science Journal (Eiszeitalter und Gegenwart, 57/1-2: 77-94.

Genty, D., Blamart, D., Ouahdi, R., Gilmour, M., Baker, A., Jouzel, J. & Van-Exter, S. (2003): Precise dating of Dansgaard-Oeschger climate oscillations in western Europe from stalagmite data. – Nature, 421: 833-837.

Genty, D., Blamart, D., Ghaleb, B., Plagnes, V., Causse, C., Bakalowicz, M., Zouari, K., Chkir, N., Hellstrom, J.C., Wainer, K. & Bourges, F. (2006): Timing and dynamics of the last deglaciation from European and North African δ^{13}C stalagmite profiles – comparison with Chinese and South Hemisphere stalagmites. - Quaternary Science Reviews, 25: 2118-2142.

Goldstein, S.J. & Stirling, C.H. (2003): Techniques for measuring uranium-series nuclides: 1992-2002. – In: Bourdon, B., Henderson, G.M., Lundstrom, C.C. & Turner, S.P. (Eds.): Uranium-Series Geochemistry: 23-57; Washington, DC (Mineralogical Society of America).

Gvirtzman, G., Friedman, G.M. & Miller, D.S. (1973): Control and distribution of uranium in coral reefs during diagenesis. – Journal of Sedimentary Petrology, 43: 985-997.

Halliday, A.N., Lee, D.C., Christensen, J.N., Rehkamper, M., Yi, W., Luo, X.Z., Hall, C.M., Ballentine, C.J., Pettke, T. & Stirling, C. (1998): Applications of multiple collector-ICPMS to cosmochemistry, geochemistry, and paleoceanography. – Geochimica et Cosmochimica Acta, 62: 919-940.

Hamelin, B., Bard, E., Zindler, A. & Fairbanks, R.G. (1991): ^{234}U/^{238}U mass spectrometry of corals: How accurate is the U-Th age of the last interglacial period? – Earth and Planetary Science Letters, 106: 169-180.

Heegaard, E., Birks, H.J.B. & Telford, R.J. (2005): Relationships between calibrated ages and depth in stratigraphical sequences: an estimation procedure by mixed-effect regression. – The Holocene, 15: 612-618.

Hellstrom, J.C. (2006): U-Th dating of speleothems with high initial ^{230}Th using stratigraphical constraint. – Quaternary Geochronology, 1: 289-295.

Henderson, G.M. (2002): Seawater (^{234}U/^{238}U) during the last 800 thousand years. – Earth and Planetary Science Letters, 199: 97-110.

Henderson, G.M. (2006): Caving in to new chronologies. – Science, 313: 620-622.

Henderson, G.M. & Anderson, R.F. (2003): The U-series toolbox for paleoceanography. – In: Bourdon, B., Henderson, G.M., Lundstrom, C.C. & Turner, S.P. (eds.): Uranium-series Geochemistry: 493-531; Washington, DC (Mineralogical Society of America).

Henderson, G.M., Cohen, A.S. & O'Nions, R.K. (1993): ^{234}U/^{238}U ratios and ^{230}Th ages for Hateruma Atoll corals: implications for coral diagenesis and seawater ^{234}U/^{238}U ratios. – Earth and Planetary Science Letters, 115: 65-73.

HENDY, C.H. & WILSON, A.T. (1968): Palaeoclimatic data from speleothems. - Nature, 219: 48-51.

HILL, C.A. & FORTI, P. (1997): Cave Minerals of the World. – 463 pp.; (Nat. Speleological Society, 2nd edition).

HOFFMANN, D.L. (2008): ^{230}Th isotope measurements of femtogram quantities for U-series dating using multi ion counting (MIC) MC-ICPMS. – International Journal of Mass Spectrometry, **275**: 75–79.

HOFFMANN, D.L., SPÖTL, C. & MANGINI, A. (submitted): Comparison of high spatial resolution MC-ICPMS U-Th dating of a U rich speleothem using laser ablation, micromill and conventional sampling techniques. – Chemical Geology.

HOFFMANN, D.L., PRYTULAK, J., RICHARDS, D.A., ELLIOTT, T., COATH, C.D., SMART, P.L. & SCHOLZ, D. (2007): Procedures for accurate U and Th isotope measurements by high precision MC-ICPMS. – International Journal of Mass Spectrometry, 264: 97-109.

HOLDEN, N.E. (1990): Total half-lives for selected nuclides. – Pure & Applied Chemistry, 62: 941-958.

HOLZKÄMPER, S., SPÖTL, C. & MANGINI, A. (2005): High-precision constraints on timing of Alpine warm periods during the middle to late Pleistocene using speleothem growth periods. – Earth and Planetary Science Letters, 236: 751-764.

HOLZKÄMPER, S., MANGINI, A., SPÖTL, C. & MUDELSEE, M. (2004): Timing and progression of the Last Interglacial derived from a high alpine stalagmite. – Geophysical Research Letters, 31: L07201.

HUANG, Y. & FAIRCHILD, I.J. (2001): Partitioning of Sr^{2+} and Mg^{2+} into calcite under karst-analogue experimental conditions. – Geochimica et Cosmochimica Acta, 65: 47-62.

IMBRIE, J., HAYS, J.D., MCINTYRE, A., MIX, A.C., MORLEY, J.J., PISIAS, N.G., PRELL, W.L. & SHACKLETON, N.J. (1984): The orbital theory of Pleistocene climate: Support from a revised chronology of the marine δ^{18}O record. – In: BERGER, A., IMBRIE, J., HAYS, J., KUKLA, G.J. & SALTZMAN, E. (eds.): Milankovitch and Climate: 269-305; Boston (D. Reidel).

IVANOVICH, M. & HARMON, R.S. (1992): Uranium-series Disequilibrium: Applications to Earth, Marine, and Environmental Sciences. – 911 pp.; Oxford (Oxford University Press).

JAFFEY, A.H., FLYNN, K.F., GLENDENIN, L.E., BENTLEY, W.C. & ESSLING, A.M. (1971): Precision Measurement of Half-Lives and Specific Activities of ^{235}U and ^{238}U. – Physical Reviews, C4: 1889-1906.

JOHNSON, K.R., HU, C., BELSHAW, N.S. & HENDERSON, G.M. (2006): Seasonal trace-element and stable-isotope variations in a Chinese speleothem: The potential for high-resolution paleomonsoon reconstruction. – Earth and Planetary Science Letters, 244: 394-407.

KAUFMANN, G. (2003): Stalagmite growth and palaeo-climate: the numerical perspective. – Earth and Planetary Science Letters, 214: 251-266.

KU, T.-L., IVANOVICH, M. & LUO, S. (1990): U-Series dating of Last Interglacial high sea stands: Barbados revisited. – Quaternary Research, 33: 129-147.

LUDWIG, K.R. (2003): Mathematical-statistical treatment of data and errors for ^{230}Th/U geochronology. – In: BOURDON, B., HENDERSON, G.M., LUNDSTROM, C.C. & TURNER, S.P. (eds.): Uranium-series Geochemistry: 631-656; Washington, DC (Mineralogical Society of America).

LUDWIG, K.R. & TITTERINGTON, D.M. (1994): Calculation of ^{230}Th/U isochrons, ages, and errors. – Geochimica et Cosmochimica Acta, 58: 5031-5042.

MANGINI, A., SPÖTL, C. & VERDES, P. (2005): Reconstruction of temperature in the Central Alps during the past 2000 yr from a δ^{18}O stalagmite record. – Earth and Planetary Science Letters, 235: 741-751.

MCDERMOTT, F. (2004): Palaeo-climate reconstruction from stable isotope variations in speleothems: a review. – Quaternary Science Reviews, 23: 901-918.

MESOLELLA, K.J., MATTHEWS, R.K., BROECKER, W.S. & THURBER, D.L. (1969): The astronomical theory of climatic change: Barbados Data. – Journal of Geology, 77: 250-274.

MICKLER, P.J., STERN, L.A. & BANNER, J.L. (2006): Large kinetic isotope effects in modern speleothems. – GSA Bulletin, 118: 65-81.

MICKLER, P.J., BANNER, J.L., STERN, L., ASMEROM, Y., EDWARDS, R.L. & ITO, E. (2004): Stable isotope variations in modern tropical speleothems: Evaluating equilibrium vs. kinetic isotope effects. – Geochimica et Cosmochimica Acta, 68: 4381-4393.

MIN, G.R., EDWARDS, R.L., TAYLOR, F.W., RECY, J., GALLUP, C.D. & BECK, J.W. (1995): Annual cycles of U/Ca in coral skeletons and U/Ca thermometry. – Geochimica et Cosmochimica Acta, 59: 2025-2042.

MOORE, W.S. (1981): The thorium isotope content of ocean water. – Earth and Planetary Science Letters, 53: 419-426.

Mühlinghaus, C., Scholz, D. & Mangini, A. (2007): Modelling stalagmite growth and $\delta^{13}C$ as a function of drip interval and temperature. – Geochimica et Cosmochimica Acta, **71**:2780–2790.

Neff, U., Burns, S.J., Mangini, A., Mudelsee, M., Fleitmann, D. & Matter, A. (2001): Strong coherence between solar variability and the monsoon in Oman between 9 and 6 kyr ago. – Nature, 411: 290-293.

Niggemann, S., Mangini, A., Richter, D.K. & Wurth, G. (2003a): A paleoclimate record of the last 17,600 years in stalagmites from the B7-cave, Sauerland, Germany. – Quaternary Science Reviews, 22: 555-567.

Niggemann, S., Mangini, A., Mudelsee, M., Richter, D.K. & Wurth, G. (2003b): Sub-Milankovitch climatic cycles in Holocene stalagmites from Sauerland, Germany. – Earth and Planetary Science Letters, 216: 539-547.

Partin, J.W., Cobb, K.M., Adkins, J.F., Clark, B. & Fernandez, D.P. (2007): Millenial-scale trends in west Pacific warm pool hydrology since the Last Galcial Maximum. – Nature, 449: 452-456.

Porcelli, D. & Swarzenski, P.W. (2003): The behaviour of U- and Th-nuclides in groundwater. – In: Bourdon, B., Henderson, G.M., Lundstrom, C.C. & Turner, S.P. (eds.): Uranium-series Geochemistry: 317-361; Washington, DC (Mineralogical Society of America).

Potter, E.-K., Esat, T.M., Schellmann, G., Radtke, U., Lambeck, K. & McCulloch, M.T. (2004): Suborbital-period sea-level oscillations during marine isotope substages 5a and 5c. – Earth and Planetary Science Letters, 225: 191-204.

Reeder, R.J., Nugent, M., Lamble, G.M., Tait, C.D. & Morris, D.E. (2000): Uranyl incorporation into calcite and aragonite: XAFS and luminescence studies. – Environmental Science & Technology, 34: 638-644.

Richards, D.A. & Dorale, J.A. (2003): Uranium-series chronology and environmental applications of speleothems. – In: Bourdon, B., Henderson, G.M., Lundstrom, C.C. & Turner, S.P. (eds.): Uranium-series Geochemistry: 407-460; Washington, DC (Mineralogical Society of America).

Richards, D.A., Smart, P.L. & Edwards, R.L. (1994): Maximum sea levels for the last glacial period from U-series ages of submerged speleothems. – Nature, 367: 357-360.

Richter, F.M. & Turekian, K.K. (1993): Simple models for the geochemical response of the ocean to climatic and tectonic forcing. – Earth and Planetary Science Letters, 119: 121-131.

Roberts, M.S., Smart, P.L. & Baker, A. (1998): Annual trace element variations in a Holocene speleothem. – Earth and Planetary Science Letters, 154: 237-248.

Robinson, L.F., Belshaw, N. & Henderson, G.M. (2004a): U and Th concentrations and isotope ratios in modern carbonates and waters from the Bahamas. – Geochimica et Cosmochimica Acta, 68: 1777-1789.

Robinson, L.F., Henderson, G.M., Hall, L. & Matthews, I. (2004b): Climatic control of riverine and seawater uranium-isotope ratios. – Science, 305: 851-854.

Romanov, D., Kaufmann, G. & Dreybrodt, W. (2008a): $\delta^{13}C$ profiles along growth layers of stalagmites: Comparing theoretical and experimental results. – Geochimica et Cosmochimica Acta, 72: 438-448.

Romanov, D., Kaufmann, G. & Dreybrodt, W. (2008b): Modeling stalagmite growth by first principles of chemistry and physics of calcite precipitation. – Geochimica et Cosmochimica Acta, 72: 423-437.

Scholz, D. (2005): U-series dating of diagenetically altered fossil reef corals and the application for sea level reconstruction.Dissertation, Naturwissenschaftlich-Mathematische Gesamtfakultät der Universität Heidelberg, 172 pp.

Scholz, D. & Mangini, A. (2006): Estimating the uncertainty of coral isochron U-Th ages. – Quaternary Geochronology, 1: 279-288.

Scholz, D. & Mangini, A. (2007): How precise are U-series coral ages? – Geochimica et Cosmochimica Acta, 71: 1935-1948.

Scholz, D., Mangini, A. & Felis, T. (2004): U-series dating of diagenetically altered fossil reef corals. – Earth and Planetary Science Letters, 218: 163-178.

Scholz, D., Mangini, A. & Meischner, D. (2007): U-redistribution in fossil reef corals from Barbados, West Indies, and sea level reconstruction for MIS 6.5. – In: Sirocko, F., Claussen, M., Litt, T. & Sanchez-Goni, M.F. (eds.): The climate of past Interglacials: 119-140; Amsterdam (Elsevier).

Shen, G.T. & Dunbar, R.B. (1995): Environmental controls on uranium in reef corals. – Geochimica et Cosmochimica Acta, 59: 2009-2024.

Spötl, C. & Mangini, A. (2002): Stalagmite from the Austrian Alps reveals Dansgaard-Oeschger events during isotope stage 3: Implications for the absolute chronology of Greenland ice cores. – Earth and Planetary Science Letters, 203: 507-518.

SPÖTL, C., MANGINI, A. & RICHARDS, D.A. (2006): Chronology and paleoenvironment of Marine Isotope Stage 3 from two high-elevation speleothems, Austrian Alps. – Quaternary Science Reviews, 25: 1127-1136.

SPÖTL, C., HOLZKÄMPER, S. & MANGINI, A. (2007): The Last and the Penultimate Interglacial as recorded by speleothems from a climatically sensitive high-elevation cave site in the Alps. – In: SIROCKO, F., CLAUSSEN, M., LITT, T. & SANCHEZ-GONI, M.F. (eds.): The climate of past Interglacials: 471-491; Amsterdam (Elsevier).

SPÖTL, C., MANGINI, A., FRANK, N. & EICHSTÄDTER, R. (2002): Start of the Last Interglacial at 135 kyr B.P.: Evidence from a high-Alpine speleothem. – Geology, 30: 815-818.

STEIN, M., WASSERBURG, G.J., AHARON, P., CHEN, J.H., ZHU, Z.R., BLOOM, A. & CHAPPELL, J. (1993): TIMS U-series dating and stable isotopes of the last interglacial event in Papua New Guinea. – Geochimica et Cosmochimica Acta, 57: 2541-2554.

STIRLING, C.H., ESAT, T.M., MCCULLOCH, M.T. & LAMBECK, K. (1995): High-precision U-series dating of corals from Western Australia and implications for the timing and duration of the Last Interglacial. – Earth and Planetary Science Letters, 135: 115-130.

STIRLING, C.H., ESAT, T.M., LAMBECK, K. & MCCULLOCH, M.T. (1998): Timing and duration of the Last Interglacial: evidence for a restricted interval of widespread coral reef growth. – Earth and Planetary Science Letters, 160: 745-762.

SWART, P.K. & HUBBARD, J.A.E.B. (1982): Uranium in scleractinian coral skeletons. – Coral Reefs, 1: 13-19.

THOMPSON, W.G. & GOLDSTEIN, S.J. (2005): Open-system coral ages reveal persistent suborbital sea-level cycles. – Science, 308: 401-404.

THOMPSON, W.G. & GOLDSTEIN, S.L. (2006): A radiometric calibration of the SPECMAP timescale. – Quaternary Science Reviews, 25: 3207-3215.

THOMPSON, W.G., SPIEGELMANN, M.W., GOLDSTEIN, S.L. & SPEED, R.C. (2003): An open-system model for U-series age determinations of fossil corals. – Earth and Planetary Science Letters, 210: 365-381.

TREBLE, P.C., SHELLEY, J.M.G. & CHAPPELL, J. (2003): Comparison of high resolution sub-annual records of trace elements in a modern (1911-1992) speleothem with instrumental climate data from southwest Australia. – Earth and Planetary Science Letters, 216: 141-153.

VERHEYDEN, S., KEPPENS, E., FAIRCHILD, I.J., MCDERMOTT, F. & WEIS, D. (2000): Mg, Sr and Sr isotope geochemistry of a Belgian Holocene speleothem: implications for paleoclimate reconstructions. – Chemical Geology, 169: 131-144.

VILLEMANT, B. & FEUILLET, N. (2003): Dating open systems by the ^{238}U-^{234}U-^{230}Th method: application to Quaternary reef terraces. – Earth and Planetary Science Letters, 210: 105-118.

VOLLWEILER, N., SCHOLZ, D., MÜHLINGHAUS, C., MANGINI, A. & SPÖTL, C. (2006): A precisely dated climate record for the last 9 kyr from three high alpine stalagmites, Spannagel Cave, Austria. – Geophysical Research Letters, 33: L20703.

WAELBROECK, C., FRANK, N., JOUZEL, J., PARRENIN, F., MASSON-DELMOTTE, V. & GENTY, D. (2008): Transferring radiometric dating of the last interglacial sea level high stand to marine and ice core records. – Earth and Planetary Science Letters, 265: 183-194.

WANG, X., AULER, A.S., EDWARDS, R.L., CHENG, H., CRISTALLI, P.S., SMART, P.L., RICHARDS, D.A. & SHEN, C.-C. (2004): Wet periods in northeastern Brazil over the past 210 kyr linked to distant climate anomalies. – Nature, 432: 740–743.

WANG, Y., CHENG, H., EDWARDS, R.L., HE, Y., KONG, X., AN, Z., WU, J., KELLY, M.J., DYKOSKI, C.A. & LI, X. (2005): The Holocene Asian Monsoon: Links to solar changes and North Atlantic climate. – Science, 308: 854-857.

WEDEPOHL, H.K. (1995): The composition of the continental crust. – Geochimica et Cosmochimica Acta, 59: 1217-1232.

WOODHEAD, J., HELLSTROM, J.C., MAAS, R., DRYSDALE, R.N., ZANCHETTA, G., DEVINE, P. & TAYLOR, E. (2006): U–Pb geochronology of speleothems by MC-ICPMS. – Quaternary Geochronology, 1: 208-221.

ZANCHETTA, G., DRYSDALE, R.N., HELLSTROM, J.C., FALLICK, A.E., ISOLA, I., GAGAN, M.K. & PARESCHI, M.T. (2007): Enhanced rainfall in the Western Mediterranean during deposition of sapropel S1: stalagmite evidence from Corchia cave (Central Italy). – Quarternary Science Reviews, 26: 279-286.

ZHU, Z.R., WYRWOLL, K.-H., COLLINS, L.B., CHEN, J.H., WASSERBURG, G.J. & EISENHAUER, A. (1993): High-precision U-series dating of Last Interglacial events by mass spectrometry: Houtman Abrolhos Islands, Western Australia. – Earth and Planetary Science Letters, 118: 281-293.

Eiszeitalter und Gegenwart Quaternary Science Journal	57/1–2	77–94	Hannover 2008

^{230}Th/U dating of interglacial and interstadial fen peat and lignite: Potential and limits

Mebus A. Geyh *)

Abstract: The state-of-the-art and potential of the ^{230}Th/U disequilibrium method are discussed for the dating of fen peat and lignite. Recommendations are given for the collection of suitable samples. The numerous interfering factors in ^{230}Th/U dating of fen peat show that a rigorous examination of the reliability of the measured data sets is required if reliable ^{230}Th/U ages are to be obtained. The accuracy of such ^{230}Th/U ages allows a reliable correlation of interglacial and interstadial deposits to the warm periods documented in the SPECMAP timescale but does not yet allow detailed temporal resolution.

[^{230}Th/U-Altersbestimmung interglazialer und interstadialer Niedermoortorfe und Ligniten: Potential und Grenzen]

Kurzfassung: Der Stand und die Zukunft der Altersbestimmung von Niedermoortorf und Lignit mit der ^{230}Th/U-Ungleichgewichtsmethode werden diskutiert. Empfehlungen zur Auswahl der Probeentnahmestellen und zur Entnahme von geeigneten Proben werden gegeben. Aufgrund der zahlreichen negativen Einflussmöglichkeiten ist eine gründliche Eignungsprüfung der gemessenen Aktivitätsverhältnisse von Uran und Thorium solcher Proben notwendig, um zuverlässige Alter bestimmen zu können. Die Datierungsgenauigkeit ist ausreichend, um interglaziale und interstadiale Ablagerungen sicher den Warmperioden der SPECMAP-Zeitskala zuzuordnen, noch nicht aber, um sie zeitlich auflösen zu können.

Keywords: ^{230}Th/U dating, fen peat, lignite, minimum age

1 Basic principles of ^{230}Th/U dating

Peat deposits are important archives of Pleistocene climate change but correlation of individual records with long-term archives such as marine oxygen isotope records (SPECMAP; Martinson et al. 1987) remains tentative. Correlations based on palynological and stratigraphic studies are usually based on certain pre-assumptions and can hence not provide any independent age constrains. Sound numerical dating methods seem to be suitable tools to achieve a reliable correlation between the marine and terrestrial climatic records. One of them is the ^{230}Th/U dating method. It is suitable for all materials that accumulated uranium during their formation and have not been affected by post-sedimentary processes that would mobilise uranium and thorium. When this is the case, the sampled material can be expected to have behaved as a closed system with respect to uranium and/or thorium during ageing. Moreover, it should not be older than 350-500 ka (Ivanovich & Harmon 1992; Bourdon et al. 2000).

The ^{230}Th/U dating method is based on the radioactive decay series of ^{238}U. The first long-lived daughter isotope ^{234}U ($\tau = 2.4525 \times 10^2$ ka, Cheng et al. 2000) decays into the isotope ^{230}Th ($\tau = 75.69$ ka, Cheng et al. 2000) with the

*Address of autor: M. A. Geyh, Rübeland 12, 29308 Winsen/Aller, Germany.
E-Mail: Mebus.geyh@t-online.de

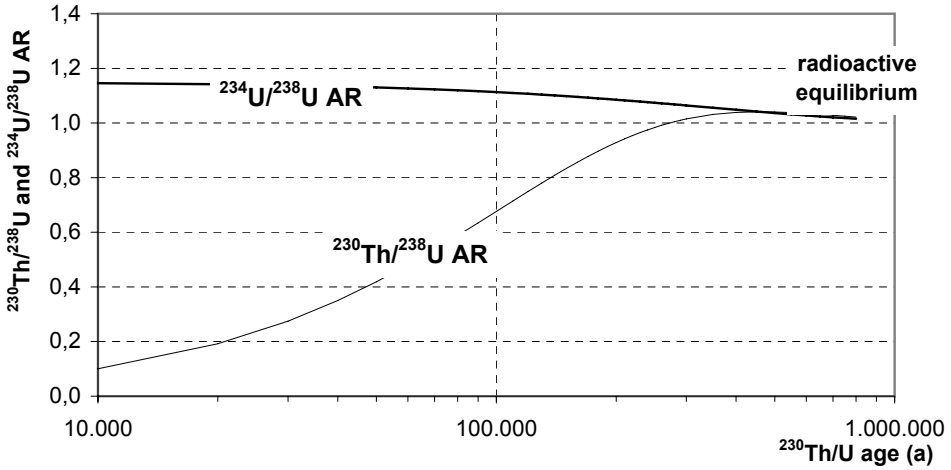

Fig. 1: Change in the $^{230}Th/^{238}U$ and $^{234}U/^{238}U$ activity ratios with increasing age for an initial $^{234}U/^{238}U$ AR of 1.15 (corresponding to the mean of marine sediments).

Abb. 1: Änderung der $^{230}Th/^{238}U$- und $^{234}U/^{238}U$-Aktivitätsverhältnisse mit der Alterung für ein initiales $^{234}U/^{238}U$-Aktivitätsverhältnis von 1,15 (entsprechend dem Mittelwert mariner Sedimente).

emission of an alpha particle. The half-life of ^{238}U ($\tau = 4.468 \times 10^9$ a) is considerably longer than that of ^{234}U. As a consequence, radioactive equilibrium is established after about one million years in most geologically old rocks and sediments. At radioactive equilibrium, all members of the decay series have the same specific activity (which is the decay rate per mass unit), i.e., the activity ratios of any two of the series members are equal to one.

Radioactive equilibrium can be disturbed by geochemical processes if the members of the radioactive series have certain geochemical properties. An example is the uranium and thorium isotopes of the uranium-238 decay series. U(VI) ions are soluble in oxygenated water while thorium is practically insoluble. Hence, during weathering, uranium tends to be dissolved in water and thorium bound by clay minerals.

Uranium dissolved in groundwater can be incorporated into new systems. Examples are speleothems, foraminifera and fen peat. The most simple $^{230}Th/U$ dating model assumes that the new system initially contains only uranium. Radioactive disequilibrium exists between ^{238}U and ^{230}Th during ageing. The numerical $^{230}Th/U$ clock starts at zero and a $^{230}Th/^{238}U$ activity ratio (AR) = 0. The radioactive disequilibrium between ^{230}Th and ^{238}U continues and evolves during ageing. A new radioactive equilibrium is approached after 350-500 ka. This process can be used to date sample material and is described by Equation 1, which has to be solved iteratively. Activity ratios are given in square brackets and $\lambda = \ln 2/\tau$:

$$(1) \qquad \left[\frac{^{230}Th}{^{238}U}\right] = (1 - e^{-\lambda_{230} \cdot t}) + \left(\frac{^{234}U}{^{238}U} - 1\right) \cdot \frac{\lambda_{230}}{\lambda_{230} - \lambda_{234}} \cdot (1 - e^{-(\lambda_{230} - \lambda_{234}) \cdot t})$$

The change in the $^{230}Th/^{238}U$ AR with age t is shown in Figure 1 assuming an initial $^{234}U/^{238}U$ AR of 1.15, which is characteristic for most marine carbonates. The $^{234}U/^{238}U$ AR of samples from terrestrial environments covers a wide range between 1 and 20. The most rapid change in the $^{230}Th/^{238}U$ AR takes place between 50,000 and about 200,000 years. The maximum age that can be measured by any dating method is the minimum age of the sample. For the radiometric and mass spectrometric $^{230}Th/U$ dating methods, this maximum age is about 350 ka and about 500 ka, respectively (Chapter 7).

Kaufman & Broecker (1965) introduced an isotope-ratio evolution plot in which the ^{234}U/^{238}U AR is plotted versus the ^{230}Th/^{238}U AR. It shows the variation of these two ARs with increasing age. Each initial ^{234}U/^{238}U AR yields a separate evolution line. All meet the point (1,1) at radioactive equilibrium, i.e., at infinite age. The ARs of coeval samples fit straight lines of their corresponding ages, which are termed "isochrons" (Fig. 2).

2 Fen peat and lignite for ^{230}Th/U dating

The history of ^{230}Th/U dating of fen peat began with a study by Titayeva (1966). Her efforts failed as the analyzed Holocene peat was too young for ^{230}Th/U dating. But Titayeva recognised that "excess" (detrital) thorium and uranium have to be taken into account for ^{230}Th/U dating of fen peat. The first ^{230}Th/U ages of this material were published by Vogel & Kronfeld (1980). Because the ages were not corrected for detrital thorium and uranium, as suggested by Titayeva (1966), their results were not acceptable by Quaternary geologists. The first chronostratigraphically satisfactory ^{230}Th/U ages of fen peat were determined by van der Wijk et al. (1986) and Heinjes & van der Plicht (1992).
Fen peat and lignite have a potential for ^{230}Th/U dating because the fulvic and humic acids they contain have an extremely large capacity for forming complexes with uranium dissolved in groundwater. Moreover, in the reducing milieu of peat, soluble U(VI) is reduced to U(IV) and bound in very stable, immobile uranyl organic complexes. As a result fen peat may have uranium concentrations of up to 100 ppm.
The following scenario of fen peat formation is the basis for ^{230}Th/U dating of fen peat and lignite. Figure 3 shows a schematic section of a growing fen moss in a shallow lake. During its growth, uranium dissolved in groundwater enters the moss and is tightly bound to fulvic and humic acids. Before the peat has been compacted, groundwater can enter even deeper parts of the moss. In the terminal stage, organic material fills the entire volume of the lake. In the succeeding glacial period, the organic deposits are covered by mineral soil and compacted.
Figure 4 shows a section of interglacial fen peat sandwiched between detrital material above and below. The uranium dissolved in the groundwater seeping through the bottom and top mineral cover layers during the period of ageing is continuously absorbed in the bottom and top parts of the peat. It has been empirically found that the corresponding rim layers are seldom thicker than 10 cm. The organic material in the rim layers behaves as an open system with respect to uranium and is not datable. As a

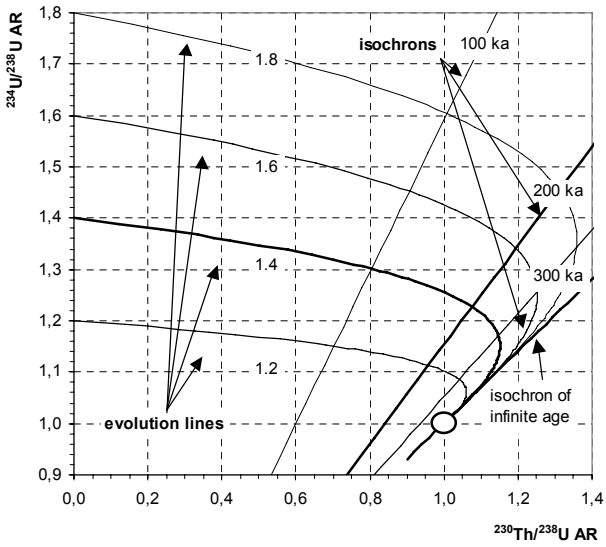

Fig. 2: Variation of the ^{234}U/^{238}U AR and the ^{230}Th/^{238}U AR with increasing age. Every initial ^{234}U/^{238}U AR yields an evolution line. All of them meet at the point (circle at 1,1) at infinite age, i.e. at radioactive equilibrium. The ARs of coeval samples plot on straight lines called isochrons (Kaufman & Broecker 1965).

Abb. 2: Entwicklung der ^{234}U/^{238}U- und ^{230}Th/^{238}U-Aktivitätsverhältnisse mit wachsenden Alter. Jedes ^{234}U/ ^{238}U AR liefert eine eigene Entwicklungslinie, die wie alle anderen bei unendlichem Alter im Punkt 1,1 (Kreis) enden. Die Aktivitätsverhältnisse gleich alter Proben liegen auf Geraden, den Isochronen (Kaufman & Broecker 1965).

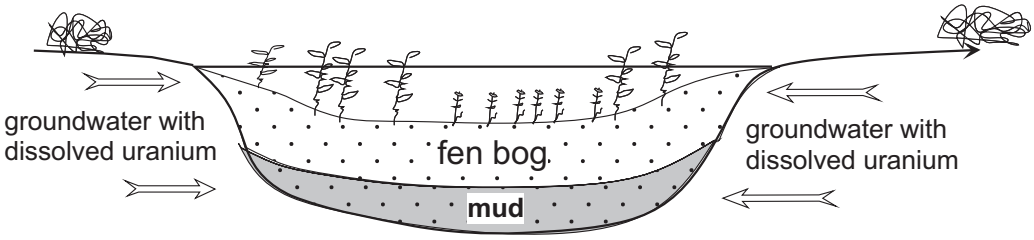

Fig. 3: Accumulation of uranium bound to fulvic and humic acids in fen peat during the peat formation in a shallow lake.

Abb. 3: Akkumulation von im Grundwasser gelöstem Uran an Fulvo- und Huminsäuren des Niedermoortorfs während der Entwicklung eines Niedermoores im flachen See.

consequence, groundwater entering the central part of fen peat more than 20-cm-thick should be free of uranium and the central part remains a closed system with respect to uranium. It is suitable for ^{230}Th/U dating.

The uranium and thorium data determined in a chronological study of the Netiesos interglacial site in Lithuania by GAIGALAS et al. (2005) is used in the following as a case study to illustrate the ^{230}Th/U dating of fen peat and lignite. The authors determined an ESR age on freshwater mollusc shells of 101.5 ± 11.5 ka. Six samples were collected between 30 and 55 cm depth. All were analyzed using the L/L (leachate/leachate) method (SCHWARCZ & LATHAM 1989; KAUFMAN 1993); the two outer samples (from 30 and 55 cm depth) were not analyzed with the total sample dissolution (TSD) method (BISCHOFF & FITZPATRICK 1991; LUO & KU 1991). The U and Th isotope ratios were measured radiometrically at St. Petersburg University and summarized with 2σ standard deviations in a research report (Table 1). The standard deviations of these results deviate slightly from those published by GAIGALAS et al. (2005). The reason is unknown.

3 Factors that interfere with ^{230}Th/U dating of fen peat and lignite

There are two main factors which render ^{230}Th/U age determination difficult or even impossible:

1. Open-system conditions with respect to uranium and thorium, as well as

Tab. 1: Isotopenergebnisse der Niedermoorproben von Netiesos in Litauen (GAIGALAS et al. 2005).

No.	name	depth (cm)	ash (%)	^{238}U ± 2σ (dpm/g)	^{230}Th/^{238}U ± 2σ	^{234}U/^{238}U ± 2σ	^{230}Th/^{232}Th ± 2σ
5133	L-1	30-35	50.4	0.537 ± 0.011	0.655 ± 0.032	1.194 ± 0.068	1.824 ± 0.081
5134	L-2	35-40	51.9	0.572 ± 0.018	0.617 ± 0.022	1.079 ± 0.047	1.555 ± 0.043
5135	L-3	40-45	49.7	0.494 ± 0.017	0.666 ± 0.029	1.119 ± 0.053	1.437 ± 0.059
5136	L-4	45-50	49.3	0.728 ± 0.022	0.657 ± 0.030	1.088 ± 0.046	1.790 ± 0.100
5137	L-5	50-55	47.3	0.640 ± 0.018	0.672 ± 0.031	1.136 ± 0.044	1.748 ± 0.107
5138	L-6	55-60	45.8	0.477 ± 0.008	0.755 ± 0.021	1.105 ± 0.026	1.545 ± 0.053
5129	T-2	35-40	51.9	1.582 ± 0.049	0.825 ± 0.032	1.001 ± 0.044	1.584 ± 0.075
5130	T-3	40-45	49.7	1.446 ± 0.034	0.900 ± 0.025	1.014 ± 0.033	1.240 ± 0.026
5131	T-4	45-50	49.3	2.009 ± 0.052	0.833 ± 0.025	1.030 ± 0.038	1.448 ± 0.036
5132	T-5	50-55	47.3	1.786 ± 0.039	0.843 ± 0.026	1.029 ± 0.032	1.352 ± 0.043

2. Detrital contamination with allochthonous ^{230}Th.

Open system conditions: Fen peat and lignite theoretically offers a chemically ideal milieu for closed-system conditions with respect to uranium. In contrast to carbonates (e.g., corals, foraminifera, speleothem), the reducing milieu of the peat means that any uranium present is reduced to insoluble U(IV), which form stable complexes with inorganic and organic ligands, such as humic and fulvic acids. Moreover, movement of humic acids over large distances and, therefore, post-depositional displacement of uranium can be largely excluded in the confined conditions of interglacial peat deposits. Likewise, α-recoil only moves the uranium daughter isotopes over distances that are smaller than the common sample volume of several cm^3 (Henderson & Slowey 2000). According to the above-described scenario for the formation of interglacial fen peat deposits, the central part may be considered as a closed system with respect to uranium and thorium. However, there are several possible situations in which this may not be true. Some fen peat deposits contain thin sand layers which may be conduits for oxygenated groundwater to the middle of the deposit. In the peat adjacent to these layers, open-system conditions with respect to uranium may have been present. Occasionally samples from the central part of a deposit without visible stratigraphic peculiarities yield outlier ^{230}Th/U ages. A possible explanation is that permafrost might have expanded the frozen fen peat and on warming voids were created into which groundwater containing uranium could have penetrated before the peat was recompacted. Detailed descriptions of the sampling site may help correlate outlier ^{230}Th/U ages to stratigraphic peculiarities. There are other scenarios which may occur in permafrost regions (Schirrmeister et al. 2002). For example, superficial peat layers may become dry down to a depth of 1-2 m during the summer months, allowing oxygenated melt water to enter the deep parts of the deposit.

Many dated interglacial peat deposits in western Asia have been exposed along river banks. If the river rises above the level of the peat layers, samples collected from up to several decimetres depth may have been affected by river water. Exposed fen peat deposits well above the present river level might also have been affected by seeping rainwater. Only drill cores of sufficient length seem to guarantee suitable peat samples.

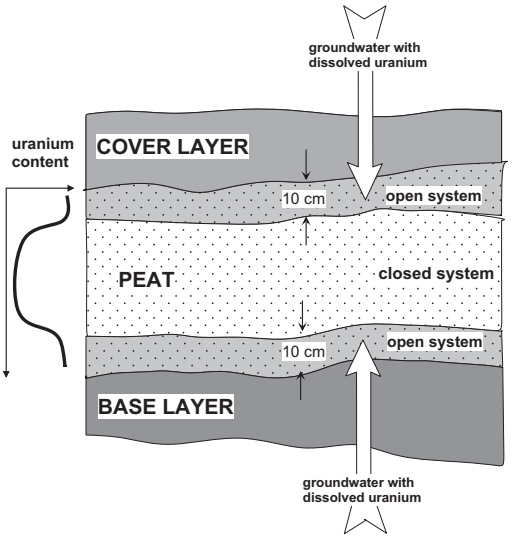

Fig. 4: Schematic of a section through a layer of interglacial fen peat: Samples suitable for ^{230}Th/U dating can only be expected in the central part of the organic deposit. The top and bottom 10 cm in most cases behaved as open systems with respect to uranium during ageing and are, therefore, unsuitable for ^{230}Th/U dating.

Abb. 4: Schematisiertes interglaziales Niedermoorprofil: Geeignete Proben für die ^{230}Th/U-Altersbestimmung können nur im zentralen Bereich des Torfes erwartet werden. Die Randbereiche von 10 cm Mächtigkeit im Hangenden und Liegenden des Torfes bilden gewöhnlich offene Systeme für Uran und erweisen sich deshalb für die ^{230}Th/U-Datierung als ungeeignet.

Thorium typically exists in the +4 and +5 oxidation states. The ions are readily hydrolyzed and either precipitate or are adsorbed on detrital particulates (inorganic or organic), clay minerals and iron (oxy)hydroxides. Thorium ions can be transported with humic acids (Richards & Dorale 2003). But movement of humic acids in confined peat beds can be excluded.

Detrital contamination with allochthonous ^{230}Th: Airborne dust or water-borne fine-grained material may become incorporated during the formation of fen peat. These contaminants usually contain thorium, which is often bound to detrital clay. The presence of ^{230}Th in the detrital material means that the ^{230}Th/U clock shows ^{230}Th/U ages that are too old. The allochthonous (detrital) ^{230}Th decays during ageing while the content of radiogenic ^{230}Th increases as a result of the decay of ^{234}U. Hence the ^{230}Th/U age error due to detrital contamination decreases with increasing age. The age error caused by an initial detrital ^{230}Th content is often large and may amount to several 1000 years up to 100,000 years. Therefore, the two or more sources of ^{230}Th (one radiogenic and at least one detrital) have to be distinguished and quantified for correction of the ^{230}Th/U ages.

Limits on the $^{230}Th/U$ method for the dating of peat and lignite: The above-described scenario of both accumulation and binding of uranium in fen peat limits the use of the ^{230}Th/U dating method for this material. Accurate ^{230}Th/U ages of sublayers cannot be expected. During the growth of the moss the peat remains very porous and groundwater or lake water containing dissolved uranium may enter even deeper layers. Hence the ^{230}Th/U ages will always be younger than the actual ones. Moreover, as fen peat formation is restricted to shallow lakes, which exist mainly at the end of the interglacial or interstadial periods, the corresponding organic deposits often represent the end of the peat-formation period or the interglacial period rather than the beginning. Hence, suitable material of palynologically distinct sub-layers of the first part of the interglacial period can seldom be provided.

Exclusion of raised-bog peat from $^{230}Th/U$ dating: Raised-bog peat receives uranium mainly from particulate matter in precipitation. Therefore, the concentration is usually low and there may be different sources of thorium and uranium with different isotopic compositions. Moreover, as raised bog peat is often only

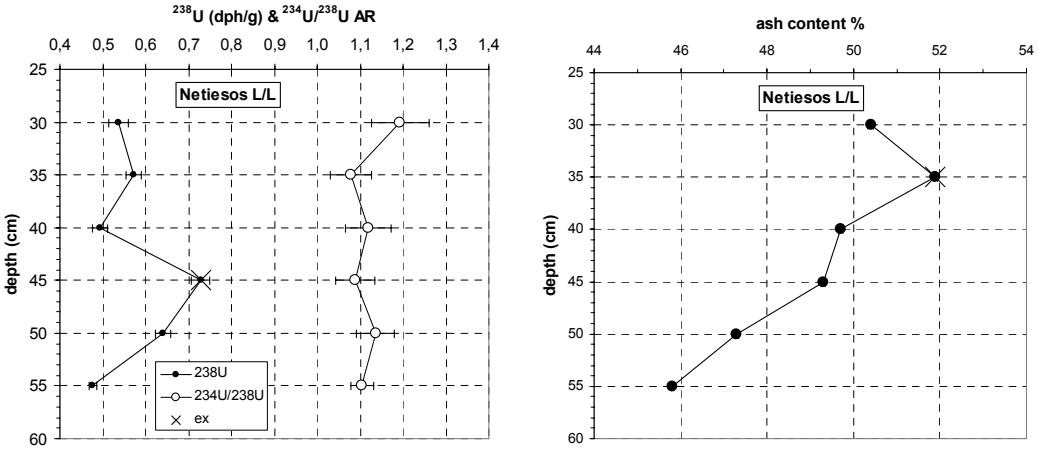

Fig. 5: Depth profiles of the specific ^{238}U activity, the ^{234}U/^{238}U AR and the ash content at the Netiesos site in Lithuania (GAIGALAS et al. 2005). Samples L-4 and L-5 (crossed dots) have a slightly elevated specific ^{238}U activity. This indicates that the premises of ^{230}Th/U dating are potentially violated.

Abb. 5: Die Tiefenprofile der spezifischen ^{238}U-Aktivität, des ^{234}U/^{238}U-Aktivitätsverhältnisses und des Aschegehalts vom Profil Netiesos in Litauen (GAIGALAS et al. 2005). Die Proben L-4 und L-5 (angekreuzte Punkte) haben eine leicht erhöhte ^{238}U-Konzentration und damit ein geringes Potential, für die ^{230}Th/U-Datierung geeignet zu sein.

weakly decomposed and the content of humic acids is low the ability to absorb actinides is limited. As a consequence, all attempts to date raised-bog peat using the ^{230}Th/U dating method have failed.

4 Determination of the reliability of data sets for the ^{230}Th/U dating of fen peat and lignite

Based on the above-described scenario for fen peat formation and the numerous factors that interfere with ^{230}Th/U dating of fen peat, it is necessary to identify and to discard data sets from samples that are not suitable for ^{230}Th/U dating. Such sample material does not fulfil the two basic premises of this dating method: (1) It has behaved as an open system with respect to uranium (and thorium) and/or (2) it contained more than one detrital contaminant.

Three simple tests are used for the initial reliability determination: depth profiles of (i) uranium concentration or specific ^{238}U activity, (ii) ^{234}U/^{238}U AR, and (iii) ash content.

Uranium-depth profiles may show up samples which behaved as an open system with respect to uranium on the basis of elevated uranium concentration relative to the base level in the central part of the peat profile. The ^{234}U/^{238}U AR in the top and bottom rim layers can be expected to differ from the central part if ^{234}U was preferentially leached or accumulated. The third test is determination of the ash content of the sample: an elevated ash content may indicate the presence of sand layers.

Figure 5 shows the results of the three tests for the Netiesos site (Gaigalas et al. 2005). The ^{238}U activity of samples L-4 and L-5 (45 and 50 cm) are 30-40 % above the other samples and therefore these samples potentially violate the two basic premises for ^{230}Th/U dating. The authors do not describe any disturbance of the stratigraphy, and therefore other information is necessary to determine which samples need to be excluded from the age determination. For example, the decrease in ash content with depth points to the possibility of open-system conditions in the upper part of the peat.

Examination of 222 data sets obtained from 33 fen peat sections in Eurasia (e.g. Arslanov 2005) has yielded evidence that ^{230}Th/U ages can be satisfactorily correlated with the SPECMAC chronology even from samples with considerably elevated or depleted uranium concentrations, or from samples with anomalous ^{234}U/^{238}U ARs or that contain a high ash content. Hence, the three tests do not reliably identify samples that do not fulfil the basic premises for ^{230}Th/U dating.

More sophisticated tests are required. The theoretical background was developed in the 1960s.

Kaufman & Broecker (1965) introduced the concept of a binary mixture of radiogenic ^{230}Th and allochthonous detrital ^{232}Th. If the latter has only one source, the proportion of detrital ^{230}Th can be estimated via the thorium concentration or the ^{232}Th activity. As the half-life of ^{232}Th is very large ($\tau = 14.01\times10^9$ a), it behaves similar to a stable isotope. Hence, its activity has not changed during the aging of the sample and hence is a measure of the initial detrital ^{230}Th content in the sample. One of the main tasks of ^{230}Th/U dating of fen peat and lignite is to determine the initial ^{230}Th/^{232}Th AR (thorium index) in order to correct the corresponding ages for the detrital contamination (Chapter 5).

The principal feature of binary mixing is that any two properties of the two components show a linear correlation. Hence, the plot of any two isotope ratios of uranium and/or thorium in peat samples – according to the Kaufman & Broecker concept – must also yield a straight line. If this requirement is not fulfilled, the basic premises for ^{230}Th/U dating are not fulfilled: The material did not behave as a closed system with respect to uranium and thorium and/or there were more than two sources of detrital ^{230}Th.

In 1970, Osmond et al. (1970) developed two mixing plots: ^{230}Th/^{238}U AR versus ^{232}Th/^{238}U AR (Osmond-I plot) and ^{234}U/^{238}U AR versus ^{232}Th/^{238}U AR (Osmond-II plot) (Figs. 6 and 7 bottom). Rosholt (1976) introduced two additional plots, the Rosholt-I (^{230}Th/^{232}Th AR versus ^{238}Th/^{232}Th AR) and Rosholt-II plots

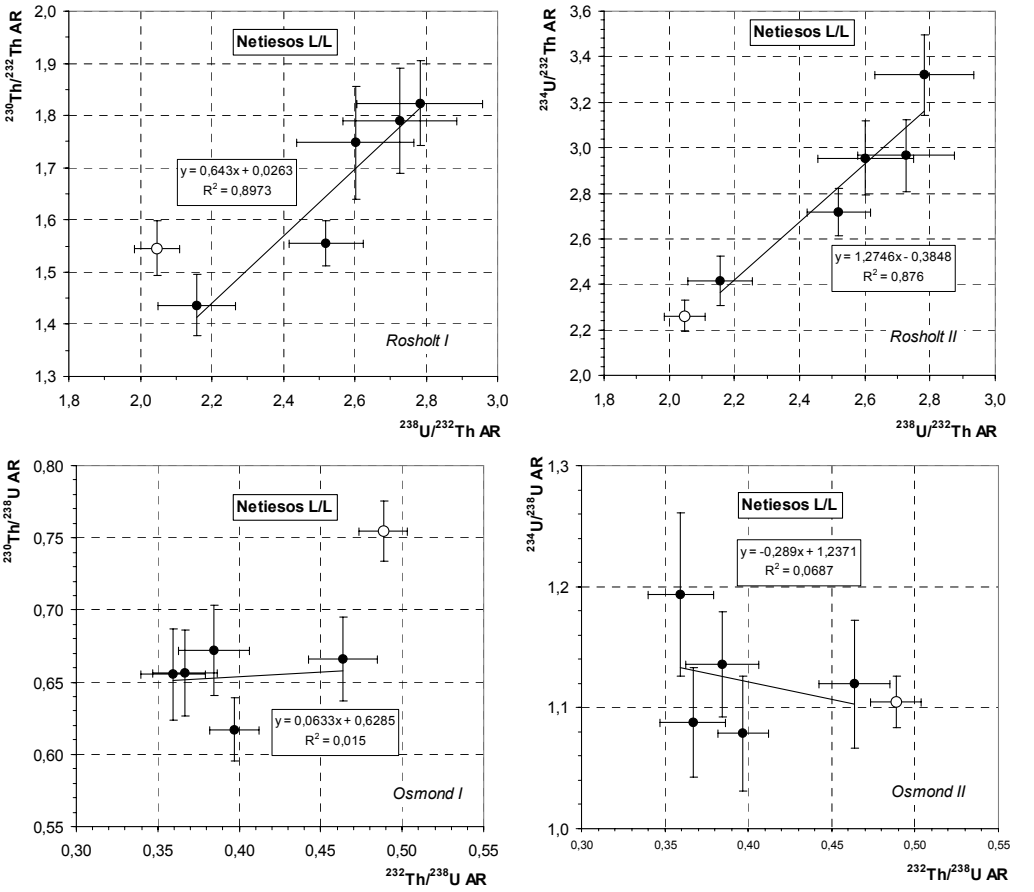

Fig. 6: Top: Rosholt I and Rosholt II plots (ROSHOLT 1976) of the L/L data from the Netiesos site in Lithuania (GAIGALAS et al. 2005): The slopes of the mixing lines equal the $^{230}Th/^{234}U$ AR and the $^{234}U/^{238}U$ AR, respectively, and the y-intercepts give the $^{230}Th/^{232}Th$ AR and $^{234}U/^{232}Th$ ARs. The data for sample L-6 (open circle) does not fit the "isochron" and was not used for the $^{230}Th/U$ age calculation.

Bottom: Osmond I und Osmond II plots (OSMOND et al. 1970) of the L/L data from the Netiesos site in Lithuania (GAIGALAS et al. 2005): The slopes of the mixing lines give the $^{230}Th/^{232}Th$ AR and the $^{234}U/^{232}Th$ AR, respectively, and the y-intercepts provide the $^{230}Th/^{238}U$ AR and $^{234}U/^{238}U$ AR. The data for sample L-6 (open circle) does not fit the mixing lines and was not used for the $^{230}Th/U$ age calculation.

Abb. 6: Oben: Rosholt-I und Rosholt-II-Diagramme (ROSHOLT 1976) der L/L-Daten vom Netiesos-Profil in Litauen (GAIGALAS et al. 2005): Die Steigungen der beiden Mischgeraden liefern die Aktivitätsverhältnisse $^{230}Th/^{234}U$ und $^{234}U/^{238}U$ sowie die Y-Achsenabschnitte die $^{230}Th/^{232}Th$- und $^{234}U/^{232}Th$-Aktivitätsverhältnisse. Der Datensatz der Probe L-6 (weißer Kreis) liegt jenseits der „Isochrone" und wurde bei der Berechnung des $^{230}Th/U$-Alters nicht berücksichtigt.

Unten: Osmond-I und Osmond-II-Diagramme (OSMOND et al. 1970) der L/L-Daten vom Netiesos-Profil in Litauen (GAIGALAS et al. 2005): Die Steigungen der beiden Mischgeraden liefern die Aktivitätsverhältnisse $^{230}Th/^{232}Th$ und $^{234}U/^{232}Th$ sowie die Y-Achsenabschnitte die $^{230}Th/^{238}U$- und $^{234}U/^{238}U$-Aktivitätsverhältnisse. Der Datensatz der Probe L-6 (weißer Kreis) liegt jenseits der Mischgerade und wurde nicht bei der Berechnung des $^{230}Th/U$-Alters berücksichtigt.

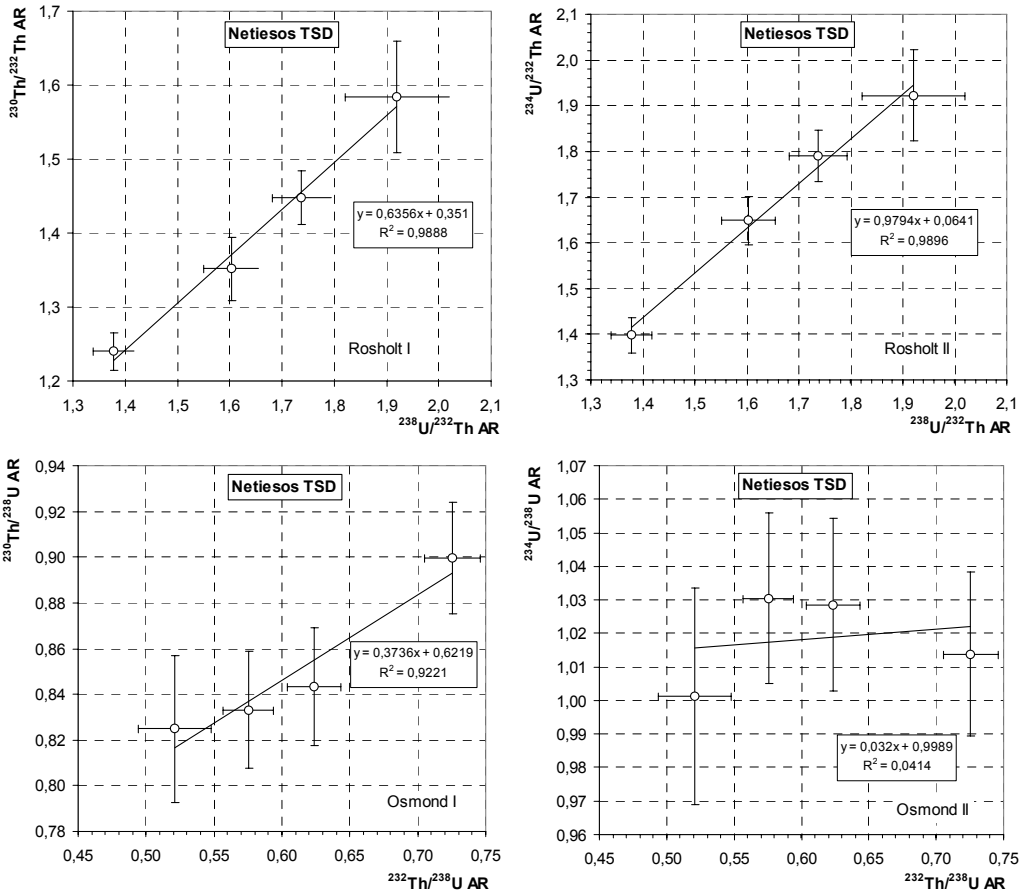

Fig. 7: Top: Rosholt I and Rosholt II plots (Rosholt 1976) of the TSD data from the Netiesos site in Lithuania (Gaigalas et al. 2005): The slopes of the mixing lines equal the ^{230}Th/^{234}U AR and the ^{234}U/^{238}U AR, respectively, and the y-intercepts give the ^{230}Th/^{232}Th AR and ^{234}U/^{232}Th AR. All data points are on the mixing lines within their uncertainty intervals and are used to calculate ^{230}Th/U ages.

Bottom: Osmond I und Osmond II plots (Osmond et al. 1970) of the TSD data from the Netiesos data in Lithuania (Gaigalas et al. 2005): The slopes of the mixing lines give the ^{230}Th/^{232}UTh AR and the ^{234}U/^{232}Th AR, respectively, and the y-intercepts provide the ^{230}Th/^{238}U AR and ^{234}U/^{238}U AR. All data points are on the mixing lines within their uncertainty intervals and are used to calculate ^{230}Th/U ages.

Abb. 7: Oben: Rosholt-I und Rosholt-II-Diagramme (Rosholt 1976) der TSD-Daten vom Netiesos-Profil in Litauen (Gaigalas et al. 2005): Die Steigungen der beiden Mischgeraden liefern die Aktivitätsverhältnisse von ^{230}Th/^{234}U und ^{234}U/^{238}U sowie die Y-Achsenabschnitte die ^{230}Th/^{232}Th- und ^{234}U/^{232}Th-Aktivitätsverhältnisse. Alle Datensätze genügen den Mischgeraden und den Kriterien der ^{230}Th/U-Methode.

Unten: Osmond-I und Osmond-II-Diagramme (Osmond et al. 1970) der TSD-Daten vom Netiesos-Profil in Litauen (Gaigalas et al. 2005): Die Steigungen der beiden Mischgeraden liefern die Aktivitätsverhältnisse ^{230}Th/^{232}Th und ^{234}U/^{232}Th sowie die Y-Achsenabschnitte die ^{230}Th/^{238}U- und ^{234}U/^{238}U-Aktivitätsverhältnisse.

($^{234}U/^{232}Th$ AR versus $^{238}U/^{232}Th$ AR; Figs. 6 and 7 top). The Rosholt-I plot is often incorrectly referred to as an "isochron" plot. The slope of the least-squares fitted straight line in a plot of the $^{230}Th/^{232}Th$ versus $^{238}U/^{232}Th$ activity ratios of coeval samples equals the $^{230}Th^{*}/^{234}U$ AR of the radiogenic $^{230}Th^{*}$ and its intercept on the y-axis equals the decay-corrected initial $^{230}Th/^{232}Th$ AR (detrital correction factor = *f*). The Rosholt-II plot yields the present $^{234}U/^{238}U$ AR. Both ARs are required to calculate the $^{230}Th/U$ ages (Eq. 1). An "isochron" slope of 0 corresponds to a $^{230}Th/U$ age of zero; an "infinite" age has a slope of 1 (radioactive equilibrium).

Figures 6 and 7 show two sets of the four Rosholt-Osmond plots of the ARs obtained from the uranium and thorium analyses of the fen peat at the Netiesos site using the L/L and TSD methods. The displacement of any pair of AR values from any of the four mixing lines indicates that the corresponding sample may not fulfill the basic premises for $^{230}Th/U$ dating. Especially, the Rosholt I and II plots give "a misleading impression of an well-defined isochron for data of little statistical power" (LUDWIG 2003). LUDWIG mentions three factors as the reason. (1) The $^{238}U/^{232}Th$ and $^{234}U/^{232}Th$ ARs tend to reflect the U/Th element ratio. The abundances of both ^{234}U and ^{230}Th of non-zero-age materials are generally highly correlated with the concentration of uranium. Therefore, the scatter of the $^{238}U/^{232}Th$ AR greatly amplifies even a dubious isochron trend. As a result the correlation coefficient of the Rosholt isochrons are usually higher than 0.90 and also considerably greater than those of the Osmond plots. (2) The ARs, especially if measured radiometrically, are highly correlated if the denominator isotope ^{232}Th activity is low. Due to the large analytical error the data scatter along lines subparallel to most isochrons and paradoxically strengthen the visual impression of an isochron. 3) The data points of radiometrically measured ARs plotted with error ranges appear to fall more precisely on the regression line than the error ranges imply, even if there is much more scatter than the errors would otherwise indicate ("zero"-correlation problem; CHAYES 1949, 1971).

To obtain a well defined mixing line, (LUDWIG & TITTERINGTON 1994), data sets from at least two coeval samples with widely differing detrital ^{230}Th content must be available. In the case of fen peat, a much larger number of samples should be analysed.

Coeval samples with similar detrital contamination yield a data cluster, which excludes the possibility of a mixing line. Moreover, the y-axis intercept of the mixing line must be positive, as a decay-corrected negative initial $^{230}Th/^{232}Th$ AR is theoretically excluded. The mean of negative decay-corrected AR values can be accepted only if its confidence interval includes zero.

The four mixing plot tests – especially those by Osmond – are a sensitive check for identifying unsuitable data sets. However, it is recommended to include the three simple tests described above in a rigorous examination of the reliability of U/Th age data. Moreover, supplementary tests should be found which also allow an objective and reproducible identification of suitable and unsuitable data sets.

5 Detrital contamination and the correction factors

According to the KAUFMAN & BROECKER (1965) concept, the radiogenic ^{230}Th activity ($[^{230}Th]^{*}$) can be calculated from the measured activity $[^{230}Th]$ as follows:

$$(2) \qquad [^{230}Th]^{*} = [^{230}Th] - [^{232}Th] \cdot f_o \cdot e^{-\lambda_{230} \cdot t}$$

$$= [^{230}Th] - f \times [^{232}Th],$$

where f_o is the initial $^{230}Th/^{232}Th$ AR and *f* is the decay-corrected f_o.

Any correction of radiometrically determined $^{230}Th/U$ ages for detrital ^{230}Th is negligible if the measured $^{230}Th/^{232}Th$ AR of any sample is smaller than 20 because in this case the detrital ^{230}Th activity is very low.

The detritus-corrected ^{234}U activity ($[^{234}U]^{*}$) can be calculated from the Rosholt II plot using an analogous equation:

$$(3) \qquad [^{234}U]^{*} = [^{234}U] - [^{232}Th] \cdot g_o \cdot e^{-\lambda_{234} \cdot t}$$
$$= [^{234}U] - g \cdot [^{232}Th],$$

where g_o is initial ^{234}U/^{232}Th AR and g is the decay-corrected g_o.

Both of these equations to correct for detrital thorium and detrital uranium assume there was only source of contamination.

No detrital correction is needed if most of the samples contain little or no detrital contamination and inferring effects can be excluded, like in the case for speleothems and or corals. In such cases the slope of the mixing lines of the Rosholt-I and Rosholt-II plots equal the ^{230}Th/^{238}U AR and ^{234}U/^{238}U AR, respectively, which are required to calculate the ^{230}Th/U age (Equation 1). The computer program ISOPLOT (Ludwig 2003) can be used to calculate the corrected ^{230}Th/U age and its standard deviation. The theoretical background for calculating the "error-correlated" standard deviation is given by Ludwig & Titterington (1994) and Ludwig (2001; 2003).

In the case of fen-peat dating a statistical check of the individual ^{230}Th/U ages is recommended in order to identify outliers. This cannot be done with the ISOPLOT program. Therefore, Equations 2 and 3 should be applied to each data set of peat and lignite samples (Geyh 1994; 2001). The required f and g values and their standard deviations are obtained from the intercept of the mixing lines with the y-axis of the Rosholt-I and Rosholt-II plots or the iterative approximation of the decay-corrected initial ^{230}Th/^{232}Th AR described below. The standard deviation of the detritus-corrected ^{230}Th activity is calculated using the usual error propagation equations. In most cases the correction for detrital uranium is not necessary because the ^{234}U/^{238}U AR and ^{232}Th/^{238}U AR do not correlate for most peat samples. This is also the case for the Netiesos site (Figs. 6 and 7 bottom).

An independent approach to the determination of the detrital correction factor f is to approximate the decay-corrected initial ^{230}Th/^{232}Th AR iteratively. The ^{230}Th/^{232}Th AR and ^{234}U/^{232}Th AR

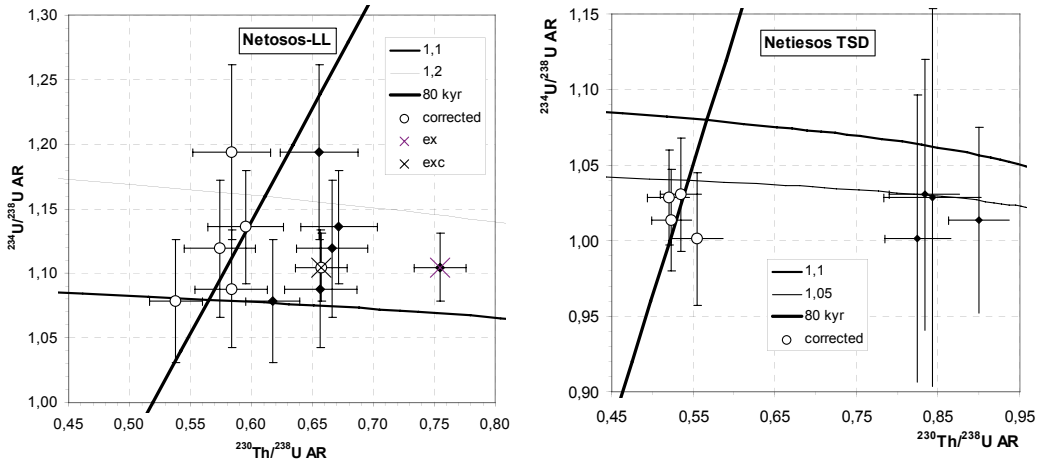

Fig. 8: Isotope-ratio evolution plot: Scatter of the L/L (left) and TSD ARs and their standard deviations in the ^{230}Th/^{232}Th- ^{234}U/^{232}Th diagram for the Netiesos site in Lithuania (Gaigalas et al. 2005). This scatter decreases with increasing detrital correction factor. The L/L data of sample L-6 (crossed symbols) remains far from the cluster.

Abb. 8: Isotopen-Evolutionsdiagramm: Die Streuweite der L/L- und TSD-Aktivitätsverhältnisse des Netiesos-Profils in Litauen (Gaigalas et al. 2005) nimmt im ^{230}Th/^{232}Th- ^{234}U/^{232}Th-Diagramm mit steigendem detritischen Korrekturfaktor ab. Die L/L-Daten der Probe L-6 (gekreuzter Punkt) bleibt der Punkthäufung fern.

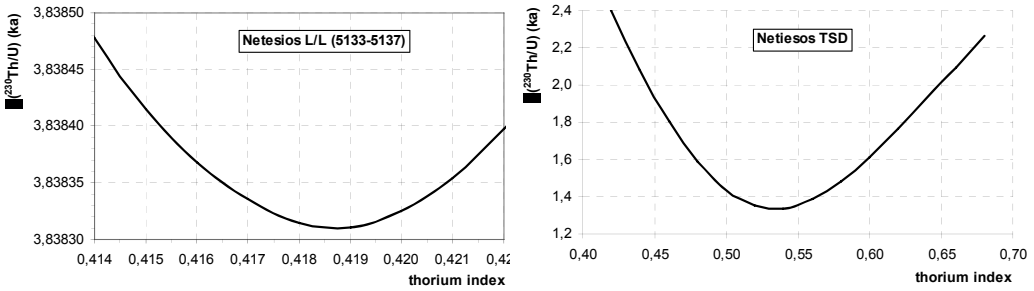

Fig. 9: The scatter represented by the standard deviations of the iteratively corrected L/L and TSD ^{230}Th/U ages of the Netiesos site in Lithuania (GAIGALAS et al. 2005) approaches a minimum at f(L/L) = 0.412 ± 0.080 and f(TSD) = 0.534 ± 0.011. The values for sample L-6 were discarded.

Abb. 9: Streuweite der iterativ-korrigierten ^{230}Th/U-Alter vom Netiesos-Profil in Litauen (GAIGALAS et al. 2005) erreicht Minima bei f(L/L) = 0.412 ± 0.080 bzw. f(TDS) = 0.534 ± 0.011. Der Datensatz der Probe L-6 wurde ausgeschlossen.

of coeval samples containing contamination from different sources scatter widely. Iteratively increasing the detrital correction factor *f* causes the points to move to the left in the isotope-ratio evolution plot of KAUFMAN & BROECKER (1965). The higher the detrital contamination the faster the points move to the left. The optimum detrital correction factor *f* is obtained when the points of the cluster are the closest together. The points in the cluster move further apart when the *f* value is increased beyond the value for the minimum width of the cluster. An elliptical shape of the cluster is caused by differences in the initial ^{234}U/^{238}U AR (Fig. 8). An effect resulting from α-recoil as observed in carbonates (HENDERSON & SLOWEY 2000) cannot be completely excluded for fen peat.

A plot of the standard deviation of the ^{230}Th/U age versus the *f* value provides a measure of the scatter of the individual ages. For the case study from the Netiesos site , the scatter of the L/L and TSD ^{230}Th/U ages approaches a minimum at *f(L/L)* = 0.412 ± 0.080 and *f(TSD)* = 0.534 ± 0.011 (Fig. 9). The plots again show that sample L-6 does not fulfill the premises for ^{230}Th/U dating.

An iterative method developed to determine the decay-corrected initial ^{230}Th/^{232}Th AR provides an additional test for a rigorous examination of the reliability of the data sets (GEYH 2001). The iteratively detritus-corrected ^{230}Th/U ages plotted against the iteratively determined detrital correction factor yields lines with different slopes. If all samples behaved as closed systems with respect to uranium and only one detritus component was present in the samples, the lines should intersect at only one point – the actual *f* value. If one or more lines do not pass through this point the corresponding sample is identified as unsuitable.

For the case study of the Netiesos site, the bold line for sample L-6 in the L/L plot belongs to outlier data which do not fulfill the premises of the ^{230}Th/U dating method. This line does not pass through the common intersection point.

6 ^{230}Th/U age and random uncertainty

The data sets suitable for calculation of a ^{230}Th/U age and its standard deviation are selected on the basis of the rigorous examination of their reliability described above. The detrital correction is applied to each measured ^{230}Th activity (Equation 2; Chapter 5) and the ^{230}Th/U ages are calculated using Equation 1. The χ^2 test is then applied to the corrected ^{230}Th/U ages, outliers are discarded, and the mean ^{230}Th/U age is calculated. The standard deviation of the mean ^{230}Th/U age is obtained using the Gaussian method for error determination of the ^{230}Th/U ages of the samples.

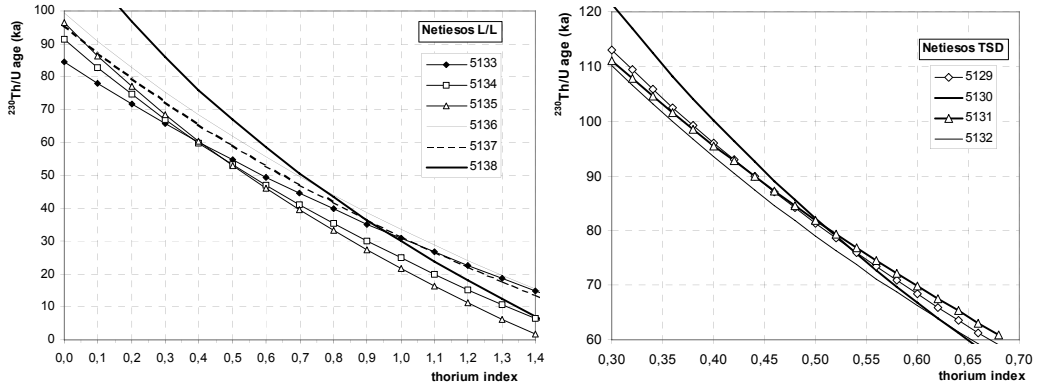

Fig. 10: Change of the detritus-corrected ^{230}Th/U ages with the iteratively increased f. Five lines of the L/L data and all lines of the TSD data have common intersection points at 61.6 ka and 76.4 ka, respectively. The bold line of the sample L-6 does not.

Abb. 10: Änderung der detritus-korrigierten ^{230}Th/U-Alter bei iterativ erhöhtem f-Wert. Fünf Linien der L/L-Daten und alle der TSD-Daten haben nahe zusammen liegende Schnittpunkte bei 61.6 ka und 76.4 ka. Die dicke Linie des L/L-Datensatzes der Probe L-6 liefert davon entfernte Schnittpunkte.

7 Minimum ^{230}Th/U age of samples

The limited precision of uranium and thorium isotope activity measurements means that there is an upper limit of the ^{230}Th/U age that can be determined. This limit is the minimum ^{230}Th/U age of a sample, corresponding to the maximum ^{230}Th/U age that can be determined with the ^{230}Th/U dating method. This minimum ^{230}Th/U age is expressed, for example, as >350 ka. Surprisingly, minimum ages are usually not estimated.

The isotope-ratio evolution plot of KAUFMAN & BROECKER (1965) can be used to develop a method for calculating the minimum ^{230}Th/U age (GEYH & MÜLLER 2005). X in Equation 1 is replaced by ^{230}Th/^{238}U AR and Y by the decay-corrected initial ^{234}U/^{238}U AR. Thus,

$$(4) \qquad X = \frac{\lambda_{230}}{\lambda_{23o} - \lambda_{234}}(Y-1)\cdot (1-e^{-(\lambda_{230}-\lambda_{234})\cdot t}) + (1-e^{-\lambda_{23o}\cdot t})$$

The decay-corrected initial ^{234}U/^{238}U (Y) is given by

$$(5) \qquad Y = (Y_o - 1)\cdot e^{-\lambda_{234}\cdot t} + 1$$

The uranium and thorium ARs of an infinitely old sample are given by a straight line in the isotope-ratio evolution plot. The equation for this isochron is derived from Equation 4 assuming an age $t = \infty$:

$$(6) \qquad X = \frac{\lambda_{230}}{\lambda_{230} - \lambda_{234}}\cdot Y - \frac{\lambda_{234}}{\lambda_{230} - \lambda_{234}} + 1$$

The ellipse defined by the X and Y random uncertainties of any data point should touch but never cut the infinite-age isochron. When the infinite-age isochron is tangent to the ellipse of the X and Y random uncertainties, the minimum ^{230}Th/U age t_{min} of the sample can be determined from the X_{min} and Y_{min} (Fig. 11). The equation of the ellipse with maximum axis lengths of $\pm 2\sigma X$ and $\pm 2\sigma Y$ around X_{min} and Y_{min} is given by

$$(7) \qquad \left(\frac{X - X_{\min}}{2\sigma X}\right)^2 + \left(\frac{Y - Y_{\min}}{2\sigma Y}\right)^2 = 1$$

Equations 4-7 are solved iteratively by decreasing or increasing the age until the error ellipse of a date touches the infinite-age isochron. A detritus-corrected ^{230}Th/U date is considered reasonable if it is smaller than the corresponding minimum ^{230}Th/U sample age t_{min} (GEYH &

MÜLLER 2005). Otherwise the result has to be expressed as the minimum ^{230}Th/U age.

8 Precision and accuracy of ^{230}Th/U dating of fen peat

The precision and accuracy of ^{230}Th/U dating of fen peat may be illustrated by three case studies. GAIGALAS et al. (2005) published L/L and TSD ^{230}Th/U ages of 108.8 ± 8.7 ka and 80.3 ± 5.9 ka, respectively, for fen peat deposits at the Netiesos site in Lithuania. The higher value from the L/L data was obtained after rejection of the data from the uppermost (L-1: 30 cm) and lowermost (L-6: 55 cm) peat samples. A rigorous examination of the sample data sets was not carried out. The decision to reject these two values was based neither on an elevated ^{238}U activity nor on ash content (Fig. 5).

A rigorous check of the reliability of the L/L data sets identified only sample L-6 as unsuitable for ^{230}Th/U dating. The L-6 data do not fit the mixing lines of the Rosholt-I and Osmond-I plots (Fig. 6), no minimum cluster size was found when the L-6 data was included in the evolution plot (Fig. 8), and in the iterative plot the L-6 line does not pass through the common intersection point of the L-1 to L-5 lines. Sample L-2 has a slightly elevated ash content (Fig. 5) and its AR values do not fit well the mixing lines of the Rosholt-I and Osmond-I plots (Fig. 7). Other indications that L-2 is unsuitable were not found.

A rigorous check of the reliability of the TSD data sets does not identify any outliers. The ^{230}Th/U age was calculated with the Equations 1 and 2 and yielded 78.4 ± 4.3 ka and a detrital correction factor of 0.519 ± 0.161. The χ^2 test applied to the four data sets yields $\chi^2 = 0.4$. Iterative evaluation yielded an age of 76.4 ± 1.3 ka with a detrital correction factor of 0.534 ± 0.010.

A ^{230}Th/U age of 72.6 ± 10.0 ka and a detrital correction factor of 0.268 ± 0.365 and a χ^2 = 0.8 were calculated using Equations 1 and 2, discarding the data from samples L-2 and L-6. Iterative evaluation yielded a detrital correction factor f = 0.456 ± 0.060. An age of 77.0 ± 11.1 ka and a detrital correction factor f = 0.199 ± 0.381 (χ^2 = 0.4) were obtained when only the data from sample L-6 was discarded and the iterative evaluation yielded f = 0.419 ± 0.080. Disregarding sample L-6 shifts the calculated lines in the Rosholt-I and Osmond-I of the L/L data plots to the right and downwards, respectively. This yields an acceptable ^{230}Th/U age of 77.0 ± 11.1 ka. It is in agreement with the TSD ^{230}Th/U age of 78.4 ± 4.3 ka. This age falls within the time span of MIS 5a (Brørup interstadial) between 76 and 78 ka of the SPECMAP time scale (MARTINSON et al. 1987).

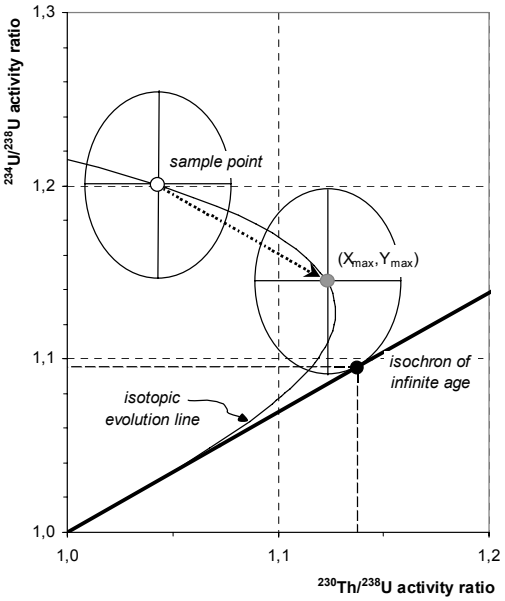

Fig. 11: Isotope-ratio evolution plot (KAUFMAN & BROECKER 1965) to determine the minimum ^{230}Th/U age t_{min} of a sample. When the data point (open circle) moves on the evolution line to the right with increasing age (grey circle) until its ellipse of 2σ X and Y uncertainties touches the infinite-age isochron (grey circle), the corresponding X_{min} = ^{230}Th/^{238}U AR and Y_{min} = ^{234}U/^{238}U AR yield the minimum age t_{min}.

Abb. 11: Isotopenentwicklungsdiagramm nach KAUFMAN & BROECKER (1965) zur Bestimmung des methodischen Minimum-^{230}Th/U-Alters einer Probe. Der weiße Punkt bewegt sich mit wachsendem Alter auf der Entwicklungslinie bis zu dem grauen Punkt, an dem die Ellipse der 2σ Y- und Y-Standardabweichungen die Isochrone für unendliche Alter trifft (schwarzer Punkt). Die entsprechenden X_{min} = ^{230}Th/^{238}U- und Y_{min} = ^{234}U/^{238}U- Aktivitätsverhältnisse liefern das Minimum-^{230}Th/U-Alter der Probe.

The second case study presented here was the first attempt to check whether it is possible to date fen peat and lignite by the ^{230}Th/U dating method (Geyh 2001). Eemian peat deposits in Europe seemed to be the most suitable for this as they contain the only Quaternary interglacial material that can be palynologically firmly identified and related to the SPECMAP timescale (Geyh 2001). Unfortunately, no cores were available and all samples were collected from exposures with the associated risk of interfering processes.

Seven sites in Germany yielded a mean ^{230}Th/U age of 111.9 ± 1.2 ka for the detritus-corrected ^{230}Th/U ages and 114.4 ± 1.9 ka using Equations 1 and 2. The agreement is good but the ages are below what is expected from SPECMAP chronology. There are several possible reasons for this. The data sets were not subjected to a rigorous reliability test. The samples might not have completely fulfilled the two basic premises for ^{230}Th/U dating due to the lack of optimum sampling conditions. In any case, the ^{230}Th/U ages and their standard deviations for these seven sites may be considered as representative of the attainable accuracy of ^{230}Th/U dating of fen peat. The precision, however, is good enough to firmly assign the dated Eemian interglacial deposits to MIS 5e but is not sufficient to assign a precise chronological age to sub-layers.

In the third case study, the ^{230}Th/U ages for Holsteinian/Hoxnian Interglacial peat were obtained from drill cores and agree better with the SPECMAP chronology (Geyh & Müller 2005). The Hoxnian Interglacial in England has been correlated with the Holsteinian Interglacial (Turner 1970). A mean ^{230}Th/U age of 317 ± 14 ka was obtained from the fen peat at Tottenhill in the Nar Valley of NW Norfolk (Rowe et al. 1997). The ^{230}Th/U ages from the Marks Tey site in the UK, which has been palynologically classified as Holsteinian, (Rowe et al. 1999), have a very low precision and could be interpreted only by using a probabilistic approach. The authors concluded that these deposits correlate with MIS 11 or some older stage with 87 % confidence. Using Equations 4 to 7, ^{230}Th/U minimum ages of >165 to >245 ka were obtained for their data (Geyh & Müller 2005). This implies that the measured U and Th data reliably allow only the statement that the geological age of the Holsteinian samples is greater than MIS 7.

B

The Bossel site about 30 km west of Hamburg contains two organic layers: one above and one below the sediments of the Holsteinian Sea. This location became the reference site for the Holsteinian Interglacial in northern Germany as declared by the European Commission on the Stratigraphy of the Quaternary. The "isochron" plot of the AR of ten samples from both peat layers yielded a mean detritus-corrected ^{230}Th/U age of 323 ± 5 ka with individual detritus-corrected ^{230}Th/U ages between 298 and 347 ka. The lower peat layer yielded a mean detritus-corrected ^{230}Th/U age of 312 ± 3 ka with individual detritus-corrected ^{230}Th/U ages between 293 and 369 ka. The four ^{230}Th/U ages of the upper peat layer yielded a detritus-corrected mean age of 327+50/-37 ka.

These case studies provide evidence that ^{230}Th/U dating of fen peat and lignite does not yield high-precision ages. The accuracy may be around 10,000 a. But this is adequate to reliably relate any interglacial peat deposit to only one of the documented warm periods of the SPECMAP chronology (Martinson et al. 1987).

9 Sampling, analysis and isotope ratio determination

To fulfil the requirements for isochron^{230}Th/U dating the samples must be coeval from the same interglacial or interstadial. For this it is sufficient to take samples from anywhere within the centre of the fen peat deposit. Rim layers of at least 10 cm thickness have to be excluded from the analysis. It is recommended to take the samples from a monolith or a drill core. At least four samples with a wide range of concentration of the detrital contamination, but even better more should be dated.

The sample preparation is more or less the same for both measurement methods for determining the ARs and consists of several steps. Ultrapure

acids which are free of even traces of uranium and thorium have to be used. The chemical preparation should be done in a clean-air laboratory in order to lower the risk of any detrital contamination. This is especially important if small samples are treated for measurement in a TIMS (thermal-ion mass spectrometer) or MC-ICP-MS (multi-collector inductively coupled plasma mass spectrometer). In radiometric laboratories repeated and comprehensive contamination tests have to be carried out.

Preferentially, peat should be treated by "total sample dissolution" (TSD) (BISCHOFF & FITZPATRICK 1991; LUO & KU 1991). This method includes both lattice-bound and adsorbed thorium. Empirically it has been found that ^{230}Th/U ages obtained by the "leachate/leachate" method (SCHWARCZ & LATHAM 1989; KAUFMAN 1993) often deviate from the palynologically expected age and do not fit the SPECMAP timescale. Selective leaching of peat samples does not adequately separate the radiogenic and detrital ^{230}Th components. In addition, the radiogenic ^{230}Th may become readsorbed on detrital material during incomplete dissolution. The following steps are taken in the "total sample dissolution" method:

- The samples of 3-5 g of fresh or 0.3-0.5 g of dry peat are taken from visibly undisturbed micro ranges within monoliths or cores.
- The surface of each sample is removed. The peat is then broken into pieces, dried and ignited in a quartz tube at a maximum temperature of about 800 °C in a stream of oxygen to burn all organic material. Insoluble glass beads do not form below this temperature and, therefore, loss of uranium and thorium is avoided.
- The weighed peat ash is treated with NaOH in order to remove traces of humic acids. The residue is completely dissolved in a con. HF/HNO_3/HCL mixture to completely dissolve uranium and thorium. If the L/L technique is applied, the sample is leached with a HNO_3/HCl mixture for at least 6 h. Next, 0.5 mL of a ^{229}Th spike and 0.5 mL of a ^{233}U/^{236}U double spike are added as a check of thermal fractionation in the ion source. The solution is heated with an infrared lamp for up to 20 h in order to ensure perfect mixing of sample and spike.
- The leachate is separated from the residue by centrifuging.
- Uranium and thorium are co-precipitated with $Fe(OH)_3$.
- The precipitate is dissolved in con. HNO_3.
- Uranium and thorium are separated from the mixture by standard ion-exchange chemistry using an actinide-specific resin (DOWEX 1×8 100-200 mesh). Thorium is eluted from the column by dilute HCl, uranium is then removed with HBr.

^{230}Th/U age determinations are preferentially done now by TIMS and MC-ICP-MS. Details are given by SCHOLZ & HOFFMANN (2008). Radiometric measurements of the ARs require at least ten times more material and are less precise by one order of magnitude. The extracted uranium and thorium are electroplated on stainless steel discs. The latter are put into an alpha spectrometer and the emitted alpha particles are counted. Due to the long ^{230}Th half-life of 75,690 ka, only one out of 6×10^6 atoms of ^{230}Th decays during the common measurement time of one week. Hence, especially the counting statistics limits the precision of radiometric ^{230}Th/U ages.

10 Conclusions

Interglacial fen peat and lignite with ages of up to 350-500 ka can be dated with the ^{230}Th/U dating method. The main prerequisite is that the samples are collected from the parts of a deposit that behaved as closed system with respect to uranium during ageing and have no more than one detrital component. In the case of fen peat, the bottom and top rim layers of about 10 cm have to be discarded. Drill cores yield better samples than monoliths collected from exposed outcrops. Small samples of a few cm^3 (about 1 g of dry peat) are sufficient for TIMS and MC-ICP-MS ^{230}Th/U dating. Radiometric ^{230}Th/U dating requires at least ten times more material. The coeval samples should have a wide range in the amount of detrital contamination. A

single uranium and thorium isotope analysis of peat does not yield a reliable ^{230}Th/U age. The TSD analytical method seems to be superior to the L/L method. Reliable ^{230}Th/U ages, however, always require a comprehensive and rigorous reliability check of the measured data in order to identify samples that were unsuitable for ^{230}Th/U dating. The accuracy of ^{230}Th/U ages of fen peat and lignite is around 10 ka, which is sufficient for reliable correlation with the warm periods of the global marine δ^{18}O chronology.

Acknowledgement

I sincerely thank Dr. Denis Scholz, University Heidelberg. He read the paper very critically and made many valuable suggestions which substantially improved the manuscript. Clark Newcomb kindly overtook the final reading.

References

Arslanov, Kh. A. (2005): Interim Report INTAS Project 01-0675 of the CR2 Team. May 1, 2004 to April 30, 2005 (unpublished).

Bischoff, J.L. & Fitzpatrick, J.A. (1991): U-series dating of impure carbonates: An isochron technique using total-sample dissolution. – Geochimica Cosmochimica Acta, 55: 543-554.

Bourdon, B., Henderson, G.M., Lundstrom, C.C. & Turner, S.P. (eds.) (2000): Uranium-series Geochemistry. – Reviews in Mineralogy and Geochemistry, 52: 656 pp.; Washington, D.C. (Mineralogical Society of America).

Chayes, F. (1949): On ratio correlation in petrography. – Journal of Geology, 57: 239-254.

Chayes, F. (1971): Ratio Correlation. A Manual for Students of Petrology and Geochemistry: 99 pp.; Chicago (University Chicago Press).

Cheng, H., Edwards, R.L., Hoff, J., Gallup, C.D., Richards, D.A. & Asmeron, Y. (2000): The half-lives of uranium-234 and thorium-230. – Chemical Geology (Isotope Geoscience Section), 169: 17-33.

Gaigalas, A., Arslanov, K.A., Maksimov, F.E., Kuznetsov, V.Y., Chernov, S.B. & Melesyté, M. (2005): Results of uranium-thorium isochron dating of Netiesos section peat-bog in south Lithunia. – Geologija, 51: 29-38.

Geyh, M.A. (1994): Precise "Isochron"-Derived Detritus-Corrected U/Th Dates. – 16th Radiocarbon Conference in Groningen, June 1997: poster.

Geyh, M.A. (2001): Reflections on the ^{230}Th/U dating of dirty material. – Geochronometria, 20: 9-14.

Geyh, M.A. & Müller, H. (2005): Numerical ^{230}Th/U dating and a palynological review of the Holsteinian/Hoxnian Interglacial. – Quaternary Science Reviews, 24: 1861-1872.

Heijnis, H. & van der Plicht, J. (1992): Uranium/thorium dating of Late Pleistocene peat deposits in NW Europe, uranium/ thorium isotope systematics and open-system behaviour of peat layers.– Chemical Geology (Isotope Geoscience Section), 94: 161-171.

Henderson, G.M. & Slowey, N.C. (2000): Evidence from U-Th dating against northern hemisphere forcing of the penultimate deglaciation. – Nature, 404: 61-66.

Ivanovich, M. & Harmon, R.S. (eds.) (1992): Uranium-Series Disequilibrium (2nd ed.): 910 p.; Oxford (Clarendon).

Kaufman, A. (1993): An evaluation of several methods for determining ^{230}Th/U ages in impure carbonates. – Geochimica Cosmochimica Acta, 57: 2303-2317.

Kaufman, A. & Broecker, W.S. (1965): Comparison of Th^{230} and C^{14} ages for carbonate materials from lakes Lahontan and Bonneville. – Journal of Geophysical Research, 70: 4039-4054.

Ludwig, K.R. (2001): ISOPLOT 2.49. – Special Publication, 1a: 58 p.; Berkeley (Geochronology Center).

Ludwig, K.R. (2003): 16 Mathematical-statistical treatment of data and errors for ^{230}Th/U geochronology. – In: Rosso, J.J. & Ribbe, P.H. (eds): Reviews in Mineralogy and Geochemistry: Uranium-Series Geochemistry, 52: 631-656.

Ludwig, K.R. & Titteringon, D.M. (1994): Calculation of ^{230}Th/U isochrons, ages, and errors. – Geochimica Cosmochimica Acta, 58: 5031-5042.

Luo, S. & Ku, T.-L. (1991): U-series isochron dating: A generalized method employing total-sample dissolution. – Geochimica Cosmochimica Acta, 55: 555-564.

Martinson, D.G., Pisias, N.G., Hays, J.D., Imbrie, J., Moore, Jr., Th.C. & Shackleton, N.J. (1987): Age dating and the orbital theory of the ice ages: development of a high-resolution 0 to 300,000-year chronostratigraphy. – Quaternary Research, 27: 1-29.

Osmond , J.K., May, J.P. & Tanner, W.F. (1970): Age of the Cape Kennedy barrier and lagoon complex.

– Journal of Geophysical Research, 75: 469-479.

RICHARDS, D.A. & DORALE, J.A. (2003): Uranium-series chronology and environmental applications of speleothems. Uranium-series Geochemistry. – In: BOURDON, B., HENDERSON, G.M., LUNDSTROM, C.C. & TURNER, S.P. (eds.): Reviews in Mineralogy and Geochemistry, 52: 407-459; Washington, D.C. (Mineralogical Society of America).

ROSHOLT, J.N. (1976): ^{230}Th/U dating of travertine and caliche rinds. – The Geological Society of America, Abstracts and Program, 8: 1076 p.

ROWE, P.J., RICHARDS, D.A., ATKINSON, T.C., BOTTRELL, S.H. & CLIFF, R.A. (1997): Geochemistry and radiometric dating of a Middle Pleistocene peat. – Geochimica et Cosmochimica Acta, 61: 4201-4211.

ROWE, P.J., ATKINSON, T.C. & TURNER, C. (1999): U-series dating of Hoxnian interglacial deposits at Marks Tey, Essex, England. – Journal of Quaternary Science, 14: 693-702.

SCHOLZ, D. & HOFFMANN, D. (2008): ^{230}Th/U dating of fossil corals and speleothems. – Quaternary Science Journal (Eiszeitalter & Gegenwart), 57/1-2: 52–76.

SCHWARCZ, H.P. & LATHAM, A.G. (1989): Dirty calcites: 1. Uranium-series dating of contaminated calcite using leachates alone.– Chemical Geology (Isotope Geoscience Section), 80: 35-43.

SCHIRRMEISTER, L., OEZEN, D. & GEYH, M.A. (2002): ^{230}Th/U dating of frozen peat, Bil'shoy Lyakhovsky Island (northern Sibiria). – Quaternary Research, 57: 253-258.

TITAYEVA, N.A. (1966): Possibility of absolute dating of organic sediments by the ionium method. – Geokhimiya, 10: 1183-1191 (English translation at 941-950).

TURNER, C. (1970): The Middle Pleistocene deposits at Marks Tey, Essex. – Philosophical Transactions of the Royal Society of London, Series B, 257: 373-440.

VAN DER WIJK, A., EL-DAOUSHY, F., ARENDS, A. R. & MOOK, W.G. (1986): Dating peat with U/Th disequilibrium: Some geochemical considerations. – Chemical Geology (Isotope Geoscience Section), 59: 283-292.

VOGEL, J.C. & KRONFELD, J. (1980): A new method for dating peat. – South African Journal of Science, 76: 557-558.

YORK, D. (1969): Least square fitting of a straight line with correlated errors. – Earth Planetary Science Letters, 5: 320-324.Table 1.

Eiszeitalter und Gegenwart Quaternary Science Journal	57/1–2	95–149	Hannover 2008

Luminescence dating: basics, methods and applications

Frank Preusser, Detlev Degering, Markus Fuchs, Alexandra Hilgers, Annette Kadereit, Nicole Klasen, Matthias Krbetschek, Daniel Richter & Joel Q.G. Spencer*)

Abstract: Luminescence dating is a tool frequently used for age determination of Quaternary materials such as archaeological artefacts, volcanic deposits and a variety of sediments from different environmental settings. The present paper gives an overview of the physical basics of luminescence dating, the necessary procedures from sampling to age calculation, potential problems that may interfere with correct age calculation as well as procedures to identify and resolve those problems. Finally, a brief summary of the most common fields of application is given ranging from artefacts to the variety of different sediments suitable for luminescence dating.

[Lumineszenzdatierung: Grundlagen, Methoden und Anwendungen]

Kurzfassung: Lumineszenzdatierung ist eine häufig angewendete Methode zur Altersbestimmung quartärer Materialien, wie z.B. archäologischer Artefakte, vulkanischer Ablagerungen oder von Sedimenten unterschiedlicher Ablagerungsräumen. Das vorliegende Manuskript gibt einen Überblick über die physikalischen Grundlagen der Lumineszenzdatierung, erläutert die notwendigen Prozeduren von der Probennahme bis hin zur Altersberechnung, diskutiert potenzielle Probleme die eine korrekte Altersberechnung beeinträchtigen können und stellt Verfahren vor, mit denen diese Probleme erkannt und beseitigt werden können. Abschließend wird ein kurzer Überblick über die gängigsten Anwendungsgebiete gegeben, von Artefakten bis hin zu verschiedenen Sedimenten, die für Luminszenzdatierung geeignet sind.

Keywords: Luminescence, physical dating methods, archaeology, geosciences, Quaternary

*Addresses of authors: F. Preusser, Institut für Geologie, Universität Bern, Baltzerstrasse 1+3, 3012 Bern, Switzerland. E-Mail: preusser@geo.unibe.ch; D. Degering, Verein für Kernverfahrenstechnik und Analytik Rossendorf e.V., Postfach 510119, 01314 Dresden, Germany. E-Mail: detlev.degering@vkta.de; M. Fuchs, Lehrstuhl für Geomorphologie, Universität Bayreuth, Universitätsstrasse 30, 95440 Bayreuth, Germany. E-Mail: markus.fuchs@uni-bayreuth.de, present address: Department of Geology, University of Cincinnati, Cincinnati, OH 45221, USA; A. Hilgers, Geographisches Institut, Universität zu Köln, Albertus-Magnus-Platz, 50923 Köln, Germany. E-Mail: a.hilgers@uni-koeln.de; A. Kadereit, Lumineszenzlabor des Geographischen Instituts der Universität Heidelberg, Im Neuenheimer Feld 348, 69120 Heidelberg, Germany. E-Mail: a.kadereit@mpi-hd.mpg.de; N. Klasen, Fachbereich Geographie, Deutschhausstrasse 10, 35032 Marburg, Germany. E-Mail: nicole.klasen@staff.uni-marburg.de; M. Krbetschek, Sächsische Akademie der Wissenschaften zu Leipzig, Forschungstelle Geochronologie Quartär, TU Bergakademie Freiberg, Institut für Angewandte Physik, Bernhard-von-Cotta Strasse 4, 09596 Freiberg, Germany. E-Mail: quatmi@physik.tu-freiberg.de; D. Richter, Max-Planck-Institute for Evolutionary Anthropology, Department of Human Evolution, Deutscher Platz 6, 04103 Leipzig, Germany. E-Mail: drichter@eva.mpg.de; J. Q. G. Spencer, Institut für Geologie und Paläontologie, Leopold-Franzens-Universität Innsbruck, Innrain 52, 6020 Innsbruck, Austria, present address: Department of Geology, Kansas State University, 108 Thompson Hall, Manhattan, KS 66506-3201, USA. E-Mail: joelspen@ksu.edu

1 Introduction

Luminescence techniques enable evaluation of the time that has elapsed since mineral grains crystallised, were last exposed to daylight or heated to a few hundred degrees Celsius. The method uses an optically and thermally sensitive light or *luminescence* signal in minerals such as quartz and feldspar. During exposure to light or heat the luminescence signal within the grains is erased (optically bleached or thermally annealed) until it is completely removed (zeroed) (Fig. 1). Once the grains are sealed from daylight and remain at normal environmental temperatures, the luminescence signal accumulates again, being induced by naturally occurring radioactivity. For dating, the amount of absorbed energy per mass of mineral (1 J kg^{-1} = 1 Gy (Gray)) due to natural radiation exposure since zeroing - known as the palaeodose - is determined by comparing the natural luminescence signal of a sample with that induced by artificial irradiation. Several laboratory techniques have been developed to accomplish the necessary stimulation and recording of the weak but measurable luminescence emitted from minerals. The time elapsed since the last daylight exposure or heating is calculated by dividing the palaeodose by the dose rate, the latter representing the amount of energy deposited per mass of mineral due to radiation exposure acting on the sample over a certain time (Gy a^{-1}). This relation is represented by the following simple equation:

$$\text{Luminescence age (a)} = \frac{\text{Palaeodose (Gy)}}{\text{Dose rate (Gy a}^{-1}\text{)}} \quad (1)$$

Luminescence dating has been applied to a wide range of topics within Quaternary research such as landscape evolution, palaeoclimate, geohazards and (geo)-archaeology, and has undergone several important methodological refinements since its early days. One of the first publications suggesting the use of thermoluminescence (TL) as a research tool was by DANIELS et al. (1953) and a few years later TL was used to date ceramics (GRÖGLER et al. 1958; AITKEN et al. 1964, 1968). An important benchmark was the application of TL to the dating sediments (WINTLE & HUNTLEY 1979, 1980; WINTLE 1980). Another breakthrough came with the introduction of optical stimulation by both visible (HUNTLEY et al. 1985) and infrared light (HÜTT et al. 1988). More recent advances concern the development of measurement procedures. Of these, notable developments are the use of a single aliquot (DULLER 1991; MURRAY & WINTLE 2000), as well as single grain dating techniques (MURRAY & ROBERTS 1997; DULLER et al. 2000), new analytical tools such as linearly modulated luminescence (BULUR 1996), radiofluorescence (KRBETSCHEK et al. 2000; ERFURT et al. 2003) and spatially-resolved luminescence (GREILICH et al. 2002; GREILICH & WAGNER 2006).

The aim of the present paper is to give an overview of the method as a whole with particular emphasis towards non-luminescence specialist researchers interested in the application of luminescence dating in Quaternary research. It is neither intended to give a full literature review nor to explain every technical aspect in too much detail but rather to give the reader

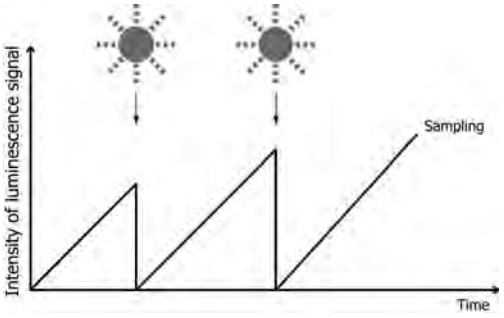

Fig. 1: The basic principle of luminescence dating: zeroing of the signal during daylight exposure (or by heating) and subsequent accumulation of the signal with time, when the material is sealed from daylight and not exposed to heat.

Abb. 1: Die Grundlage der Lumineszenzdatierung: Nullstellung des Signals während Tageslichtexposition (oder durch Erhitzen) und anschließende Akkumulierung des Signals während der Zeit, in der das Material vor Sonnenlicht geschützt bzw. keiner Erhitzung ausgesetzt ist.

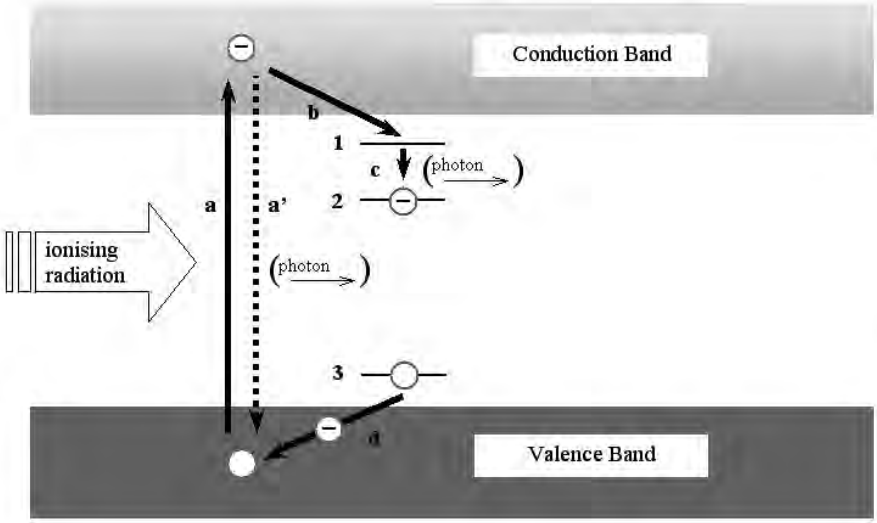

Fig.2.1: Basic processes leading to a latent luminescence signal (schematic):
a – A valence electron is excited by ionising radiation, and has sufficient energy to reach the conduction band, leaving a hole in the valence band.
a' – Most of the excited electrons dissipate their energy by recombining immediately with a hole in the valence band; the transition is sometimes accompanied by photon emission.
b, c – Prompt transition of a few excited electrons into localised energy states below the band edge resulting in electron trapping; light is potentially emitted during these processes..
d – A hole in the valence band may be filled by electrons from localised levels above the valence band edge; hence the hole transfers from the valence band to the localised level.

Abb. 2.1: Grundlegende Prozesse, die zu einem latenten Lumineszenzsignal führen (schematisch):
a – Ein Elektron aus dem Valenzband wird durch ionisierende Strahlung angeregt, es besitzt ausreichend Energie um das Leitungsband zu erreichen und hinterlässt ein Loch im Valenzband.
a'– Die Mehrheit der angeregten Elektronen verliert ihre Energie durch unverzügliche Rekombination mit einem Loch im Valenzband; dieser Übergang ist mitunter mit der Emission von Photonen verbunden.
b, c – Spontane Übergänge einiger angeregter Elektronen in lokalisierte Energiezustände unterhalb der Bandkante („Fallen") führen zu stabilem Elektroneneinfang; zum Teil wird bei diesen Prozessen Licht emittiert.
d – Ein Loch im Valenzband kann durch Elektronen aus lokalisierten Niveaus oberhalb der Valenzbandkante aufgefüllt werden; damit geht das Loch vom Valenzband in den lokalisierten Zustand über.

a firm grounding for the potential, limitations and modern approaches of quality control in luminescence dating of Quaternary materials.

2 Physical background

2.1 Origin of the luminescence signal

The process behind the phenomenon of luminescence is best described by the energy-level representation of insulating solids (Figs. 2.1 and 2.2). The basic mechanism is that ionising radiation causes the excitation of atoms within the crystal lattice, leading to activated electrons at higher energy states. The vast majority of the activated electrons leave the activated states instantaneously, but some charge is captured at electronic levels below the edge of the conduction band (Fig. 2.1 a-c). These levels are called *electron traps*. The charge deficit creates a hole

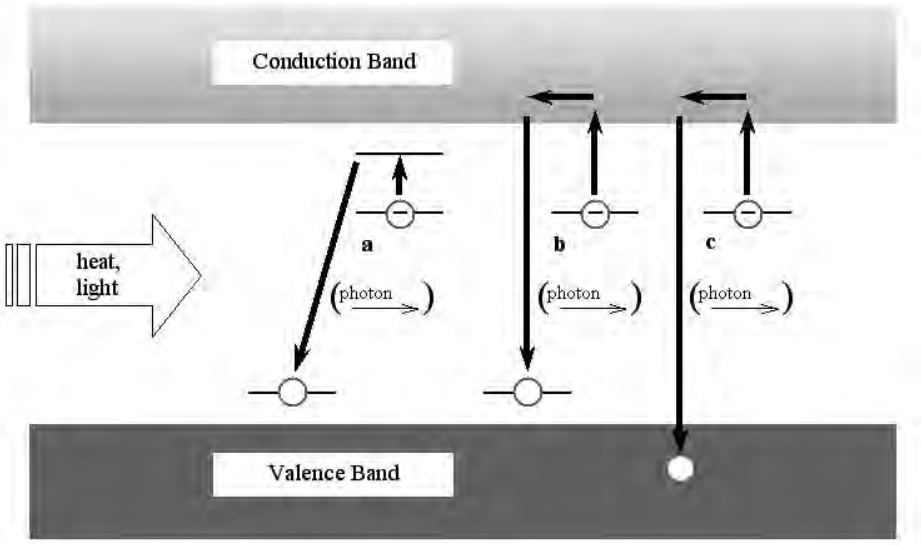

Fig. 2.2: Stimulation of luminescence by heat and light. Possible processes leading to the emptying of trap levels after excitation by light or heat (schematic):
a, b – Recombination with localised holes above the valence band edge; a) the electron is first transferred to an unstable level below the conduction band; b the recombines via the conduction band.
c – Recombination with a hole in the valence band.
The energy loss may be released in the form of light (= luminescence).

Abb. 2.2: Lumineszenzanregung durch Wärme oder Licht. Mögliche Prozesse, die zum Entleeren der Fallenniveaus nach Anregung durch Licht oder Hitze führen (schematisch):
a, b – Rekombination mit lokalisierten Löchern oberhalb der Valenzbandkante ; im Fall a wird das Elektron zuerst in einen instabilen Zustand unterhalb des Leitungsbandes transferiert, in Fall b rekombiniert es über das Leitungsband.
c – Rekombination mit einem Loch im Valenzband.
Der Energieverlust kann als Licht freigesetzt werden (= Lumineszenz).

in the valence band, which may move to form *recombination centres* within the band gap (Fig. 2.1 d). Both electron traps and recombination centres are linked to lattice defects such as oxygen vacancies or foreign atoms (e.g., Al^{3+} instead of Si^{4+} in the quartz lattice). It is important to note that various types of defects exist in the different minerals used in luminescence dating and that the energy representation shown in Fig. 2 very much simplifies the complex situation found in natural minerals. In reality, several kinds of traps and recombination centres exist (cf., CHEN & MCKEEVER 1997; KRBETSCHEK et al. 1997; MCKEEVER & CHEN 1997; MCKEEVER 2001). A basic characterisation of an electron trap is its energetic depth below the conduction band. The trap depth represents the energy necessary to lift the electron from the trap back to the conduction band. Only electrons captured at traps of a certain depth (in energy terms ~1.6 eV or more) remain captured for several million years, which is the prerequisite for dating Quaternary materials since the possibility of charge leakage is less likely for longer storage times (AITKEN 1998). With time, more and more electrons will be captured at the traps within a crystal and so the latent luminescence signal within the mineral will increase. Since the number of traps is limited the latent luminescence cannot increase indefinitely but

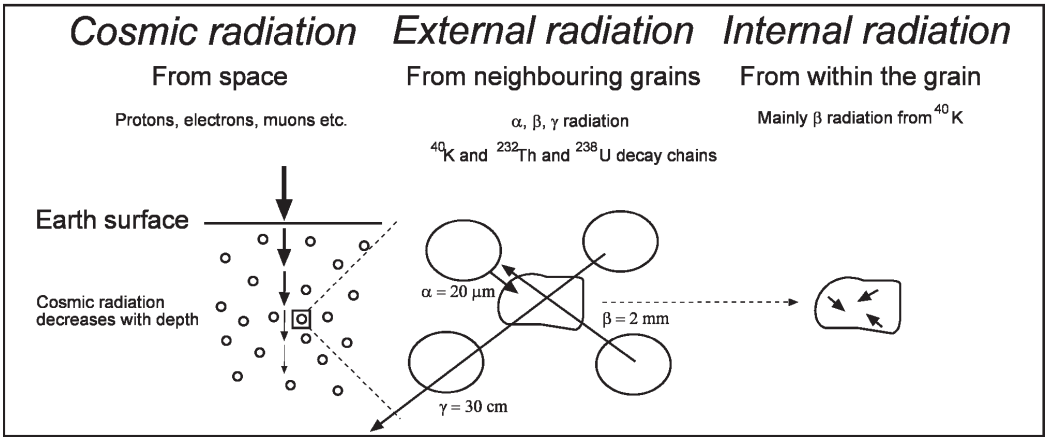

Fig. 3: Different components relevant for the calculation of dose rate for luminescence dating.

Abb. 3: Verschiedene Komponenten, die für die Berechnung der Dosisleistung relevant sind.

will reach a saturation value (saturation dose). Electrons are released from the traps once the mineral is exposed to a particular stimulation energy (Fig. 2.2). In this context it is necessary to consider that the depth of a trap defines the kind of stimulation the captured electron is sensitive to. The deeper the trap, the higher is the required stimulation energy. Once the electron has been lifted to the appropriate recombination level within or below the conduction band, there is a certain probability that it will recombine at an electron hole (recombination centre) and in doing so, release some of the stored energy in the form of light. It is this light released during the recombination process that is referred to as luminescence, and is dependent in various ways on whether TL, optically stimulated luminescence (OSL), etc., is used as the stimulation method. The intensity of light emitted by a sample during stimulation is proportional to the number of recombining electrons and, hence, proportional to the amount of electrons trapped prior to stimulation. The latter is a function of both time and the number of electrons trapped per time interval, which in turn is a function of the dose rate. As a consequence, the intensity of emitted luminescence is linked to the total energy imparted to the mineral due to radioactive exposure since the signal was last zeroed via sufficient stimulation energy.

2.2 Environmental dose rate

Natural ionising radiation occurs in the form of alpha, beta and gamma radiation and cosmic rays (Fig. 3). Alpha radiation consists of Helium nuclei (He^{2+}) that have a penetration depth in sediment of about 20 µm and hence penetrate only the outer part of sand-sized mineral grains. Beta particles (electrons) and gamma rays (photons) have a much higher penetration depth in sediments, of the order of a few mm or dm, respectively, and thus pervade the whole mineral. Because of their small size compared to the penetration depth of alphas, silt and clay-sized particles are completely penetrated by all three types of radiation. In addition to their low penetrating power, a further important factor in the context of dosimetry is that alpha particles induce less luminescence signal, with respect to the absorbed energy, being usually only about 5–20 % compared to beta and gamma radiation (Aitken 1998).

With regard to dating, the environmental dose rate comprises internal, external and cosmic dose rate components. Internal dose rate originates from radioactive elements that may be present within the lattice of the luminescent mineral. Most important is the contribution from ^{40}K when using alkali feldspars as natural dosimeters. In quartz, the contribution of inter-

nal dose rate to the total dose rate is usually considered to be negligible. External dose rate comprises all radiation acting on the luminescent grain from the surrounding sediment, and is derived from ^{40}K, abundant in some feldspars, micas and clay minerals, and the isotopes of the $^{238}U/^{235}U$ and ^{232}Th decay chains. Uranium and Thorium are found at relatively high concentrations in zircon and some exotic minerals, but are ubiquitously present in low concentrations in a variety of common minerals such as carbonates (uranium) and clay minerals. A minor contribution to the total dose rate comes from the presence of ^{87}Rb (typically < 1 %). The contribution from other radioactive elements is so small that it is usually neglected. For calculating external dose rate the moisture content of the sediments is of great importance, as the attenuation of ionising radiation is much greater if the pores in the sediment are filled with water rather than air. Cosmic radiation consists of a variety of different particles such as neutrons, muons, electrons and photons that constantly penetrate the Earth's surface. Due to the nature of the Earth's magnetic field and absorption by the atmosphere, the intensity of cosmic radiation increases pole-wards and with altitude; overburden by both sediment and water (e.g., in lake or marine environments) will shield the sample and reduce the strength of cosmic radiation.

3 Luminescent minerals and their properties

Although a variety of minerals show the phenomenon of luminescence, the application of luminescence for dating purposes is, so far, mainly limited to quartz and feldspar. This is due to their abundance in sediments at most geological settings, as well as their ability to fulfil the requirements of sensitivity to radiation dose and behavioural characteristics. They are also sufficiently resistant to weathering compared to, for example, carbonates, which are also known to carry a luminescence signal (e.g., WIESER et al. 1993; CARMICHAEL et al. 1994). Furthermore, the luminescence signal in both feldspar and quartz is sufficiently bleachable by daylight, is stable over long periods of time, and signal growth can be readily described using mathematical functions for the physical behavior. The dating potential of other minerals such as zircon (TEMPLER & SMITH 1988; SMITH et al. 1991; VAN ES et al. 2000) and halite (BAILEY et al. 2000) was initially tested but little systematic work has been carried out so far to investigate the potential of these minerals in more detail. The following briefly describes the key properties of quartz and feldspar and discusses their advantages and disadvantages for dating.

3.1 Quartz

Quartz is presently the mineral favoured for dating by many luminescence specialists. Beside its common occurrence in sediments, resistance to weathering and relatively well investigated luminescence properties, this is in particular due to the fact that it is not effected by the phenomenon of anomalous fading, as is at least some feldspar (see section 6.3). Due to these advantages, most research during the past decade has concentrated on developing quartz luminescence dating with special attention paid to the development of procedures to determine the palaeodose (e.g., WINTLE & MURRAY 2006). However, there are a few circumstances when quartz may not be the mineral of choice and it appears that many problems related to quartz have only more recently been identified. First of all, there are some geological settings, although relatively rare, where quartz does not occur due to the alkaline composition of the host rock. In other areas, luminescence from feldspar inclusions within the quartz may complicate the detection of the luminescence originating from the quartz itself. Although procedures have been suggested to deal with feldspar inclusions (WALLINGA et al. 2002) these are not straightforward. It has also been shown that quartz of volcanic origin may display anomalous fading (BONDE et al. 2001; TSUKAMOTO et al. 2007) and this problem needs to be addressed in future research. A further problem, possibly related to a young sedimentary history of the grain, is

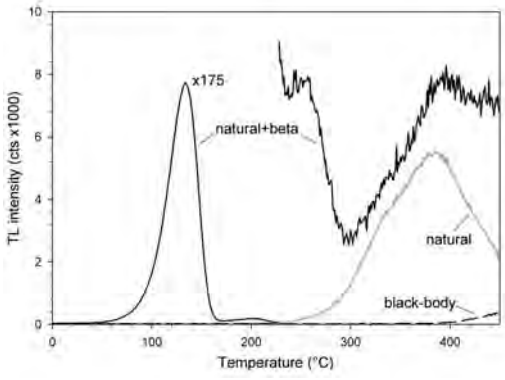

Fig. 4: Natural and artificial TL glow curve and black body radiation of a quartz sample from Nigeria (Gumnior & Preusser 2007).

Abb. 4: Natürliche und künstlich induzierte TL-Glühkurve und Schwarzkörperstrahlung einer Quarz-Probe aus Nigeria (Gumnior & Preusser 2007).

that quartz from some areas, shows rather low, if any, luminescence (e.g., Lukas et al. 2007) and changes in sensitivity that are not able to be corrected for (Preusser et al. 2006). Thermal transfer of charge from light-insensitive to light-sensitive traps, that may cause palaeodose overestimation, has also been reported in this context (Rhodes & Bailey 1997; Rhodes 2000). A considerable disadvantage of quartz is that the saturation dose, when all traps are captured by electrons, and, as a consequence, its potential dating range, is usually up to one order of magnitude lower than that of feldspar.

3.2 Feldspars

Potassium-rich feldspars are commonly used in luminescence dating studies. The disadvantages of using Na-rich feldspars for dating are discussed in Krbetschek et al. (1997) and only a few studies have focussed on this mineral (e.g., Krause et al. 1997). The major advantages of feldspar are that it typically has bright luminescence signals and a higher saturation dose, which allows the potential to date much older deposits than with quartz. Another advantage is that a substantial proportion of the dose rate comes from ^{40}K within the feldspar, which lowers the uncertainty from external dose rate, in particular due to variations in past sediment moisture. A disadvantage that has often been attributed to feldspar is that its optical signal is less light sensitive compared to quartz (Godfrey-Smith et al. 1988; Wallinga 2002a), although this does not appear to be supported by other experimental evidence which shows a similar resetting behaviour for both minerals (Preusser 1999a; Klasen et al. 2006).
The major problem in feldspar dating is the loss of part of the signal with time, a phenomenon referred to as anomalous fading (Wintle 1973), which affects feldspars of at least some geological origins and causes an underestimation of the luminescence age if this is not corrected for. This will be discussed in more detail below (section 6.3).

4 Luminescence methods

Luminescence dating comprises a range of different but related phenomena. The fact that a strict nomenclature is not always adhered to and that some techniques are not often used may cause some confusion to the non-specialist. The following nomenclature refers to the most-widely used terminology and the techniques used in luminescence dating are described (Table 1).

4.1 Thermoluminescence (TL)

The term thermoluminescence (TL) describes the light emitted by a mineral, other than incandescence or black body radiation, when heated. The light originates from captured electrons being freed due to heat stimulation and subsequent recombination. Thus, it is also (and more correctly) referred to as thermally-stimulated luminescence (TSL) although this term is not often used. In addition to sensitivity to heat, a number of the electrons are also sensitive to optical activation, and this has also been utilised in the dating of sediments by TL. In practice, the sample is typically heated from ambient temperature to 450°C while the emitted photons are detected by a photomulti-

Table 1: Summary of the different methods used in luminescence dating.

Tab. 1: Zusammenfassung der verschiedenen Methoden der Lumineszenzdatierung.

Abbrev.	Method	Main application	Primary Reference
TL	Thermoluminescence	Dating heated materials	AITKEN et al. (1964)
ITL	Isothermal TL	Experimental (quartz)	JAIN et al. (2005)
OSL	Optically stimulated lum.	Dating sediments (quartz)	HUNTLEY et al. (1985)
IRSL	Infrared stimulated lum.	Dating sediments (feldspar)	HÜTT et al. (1988)
IR-RF	Infrared radiofluorescence	Dating sediments (feldspar)	TRAUTMANN et al. (1999a)
LM-OSL	Linearly modulated OSL	Analytical tool (quartz)	BULUR (1996)
HR-OSL	Spatially resolved lum.	Dating rock surfaces	GREILICH et al. (2002)
TT-OSL	Thermally transferred OSL	Experimental (quartz)	WANG et al. (2006 a)

plier tube and subsequently counted. The first measurement of TL empties the electron traps after which a second heated measurement is undertaken to record the unwanted light signal due to black body radiation or incandescence. This starts to grow around 400°C when using blue-violet detection filters, and the sum of this is subtracted from the first signal (Fig. 4). The different TL peaks of the glow curve represent different trap populations, with electrons from "shallow" traps recombining at lower stimulation temperatures than those from "deep" traps at higher temperatures, and a comparison of naturally and artificially induced TL reveals information about the stability of different signal components. This characteristic is utilised to identify the appropriate thermal pre-treatment for reliable measurement, and to investigate the extent to which a sample was zeroed by the natural heating/bleaching process.

TL was the only method used in retrospective dosimetry and luminescence dating until the mid-1980s, and was originally developed for the dating of ceramics (AITKEN et al. 1964), although it was also used later to date volcanic rocks (e.g., HWANG 1970; MAY 1979; RAYNAL et al. 1982), heated artefacts and sediments (HUXTABLE et al. 1978) as well as aeolian deposits (e.g., WINTLE & HUNTLEY 1979, 1980; WINTLE 1981; SINGHVI et al. 1982). However, of the applications mentioned above it is only the TL dating of ceramics and heated artefacts that remains in regular use today, while the dating of sediments using TL was largely abandoned in the mid-1990s as it presents a significant disadvantage compared to optical dating. This arises is because part of the thermally stimulated luminescence signal is not sensitive to natural daylight, on which sediments rely on for zeroing or bleaching. Thermal stimulation releases trapped charges associated with both light-sensitive and light-insensitive components and so can lead to potentially severe age overestimates. Under optimum experimental settings, i.e. direct sunlight exposure of min-

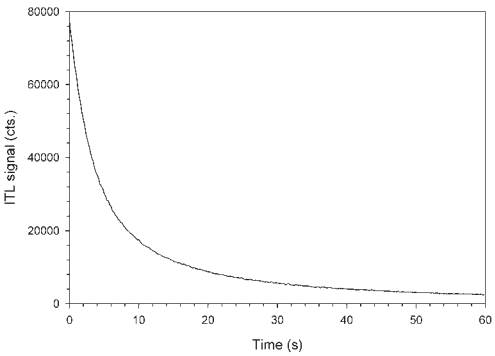

Fig. 5: Natural isothermal decay curve of a quartz sample from Nigeria (GUMNIOR & PREUSSER 2007), preheated at 230°C for 10 s and measured at 325°C.

Abb. 5: Natürliches isothermales Zerfallsignal einer Quarz Probe aus Nigeria (GUMNIOR & PREUSSER 2007), die bei 230°C für 10 s vorgeheizt und anschliessend bei 325°C gemessen wurde.

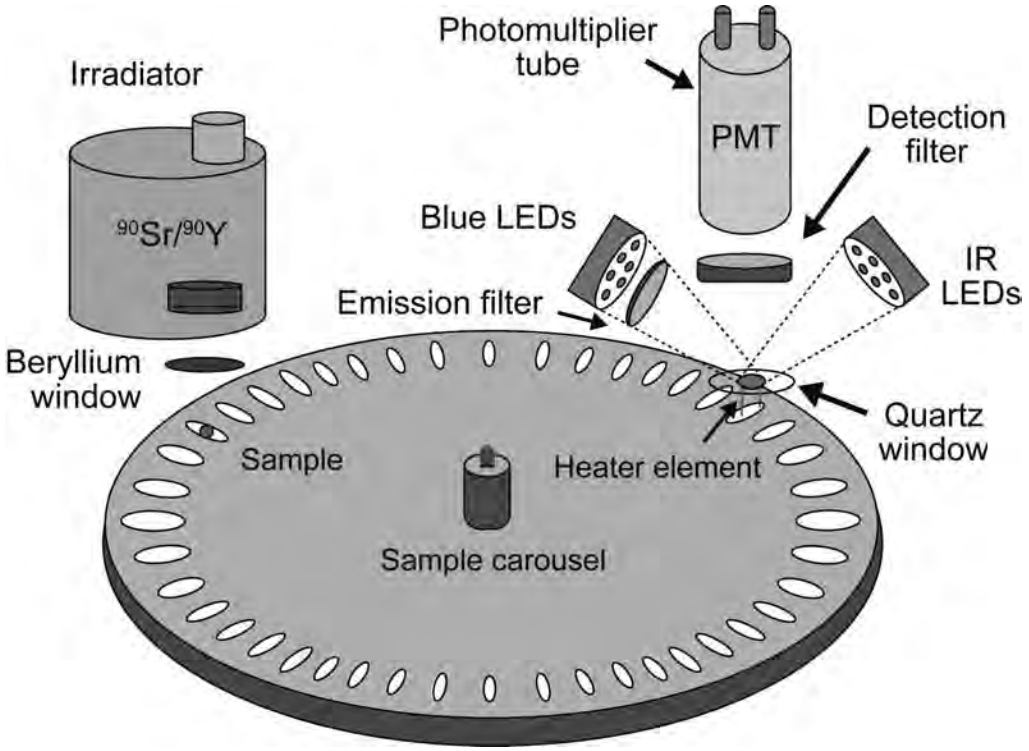

Fig. 6: Sketch showing the basic features of a TL/OSL reader (redrawn after Risø National Laboratory).

Abb. 6: Die Skizze zeigt den grundlegenden Aufbau eines TL/OSL Gerätes (umgezeichnet nach Risø National Laboratory).

eral grains, it will take several hours for the TL signal to be reduced to a small residual signal while the optical signal is almost fully reset within a few minutes (Godfrey-Smith et al. 1988).

A modification of the classical TL approach is the isothermal TL (ITL) method, in which TL is recorded while the sample is held at a constant or isothermal temperature (Jain et al. 2005; Huot et al. 2006) (Fig. 5). The advantage of this method is that a specific trap population is emptied while deeper traps are not stimulated. In contrast to TL it is thus possible to focus on a trap population with certain physical properties. A first test study indicated that the potential of the method lies in the prospect of increasing the age range towards older samples (Jain et al. 2005; Choi et al. 2006a), although, while some tests on quartz showed quite promising results, other test studies identified several problems and age overestimates in comparison to optical dating (Buylaert et al. 2006). Nevertheless, ITL appears to be an interesting approach with some potential, especially for older sedimentary samples and heated objects.

4.2 Optical stimulation

The most important breakthrough in recent years in luminescence dating has been the use of optical stimulation (optical dating). This area of luminescence dating mainly comprises stimulation by visible light as introduced by Huntley et al. (1985), and by infrared (IR) as first described by Hütt et al. (1988), may be collectively referred to as photoluminescence or photon-stimulated luminescence (PSL). The

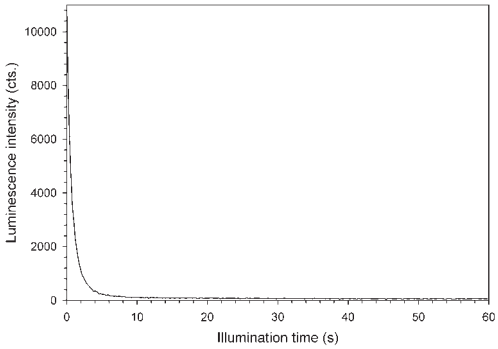

Fig. 7: OSL decay curve of a quartz sample from Nigeria (GUMNIOR & PREUSSER 2007) resulting from blue diode stimulation. Sample preheated at 230°C for 10 s and measured at 125°C.

Abb. 7: OSL-Zerfallskurve einer Quarz-Probe aus Nigeria (GUMNIOR & PREUSSER 2007), stimuliert mit blauen Dioden. Die Probe wurde bei 230° vorgeheizt und bei 125°C gemessen.

advantage of any optical method is that only the light-sensitive part of the luminescence signal is stimulated, which for sedimentary deposits considerably minimises the problem of incomplete bleaching of the luminescence signal prior to deposition. Furthermore, more reliable and precise methods for determining the palaeodose have been developed since the mid-1990s and have revolutionised luminescence dating. These methods will be described below. Regardless of what kind of photon-stimulation is used, optical filters are placed between the sample and the light-sensitive surface of the photomultiplier tube to minimise crosstalk between light from the stimulation source and light emitted from the sample (Fig. 6). When optical excitation begins the latent luminescence in the mineral will start to decay, resulting in a so-called decay curve recorded by the photomultiplier (Fig. 7).

4.2.1 Optically stimulated luminescence (OSL)

The term optically stimulated luminescence (OSL) is used here only with reference to stimulation by visible light, although in some literature OSL is used as an umbrella term for all light stimulation including IR wavelengths. Stimulation by visible light is conducted by exposing the sample to a laser beam, the light of a filtered halogen lamp or to high-power light emitting diodes (LEDs), the latter being the latest and most versatile development, and hence used in the majority of currently manufactured luminescence readers (Fig. 6). The width of the excitation waveband differs for different stimulation sources but all lie in the green to blue part of the spectrum, i.e. between 420-550 nm. Both quartz and feldspar respond to stimulation within this waveband although for dating applications it is principally used for OSL measurements of quartz. Light of longer wavelengths becomes increasingly inefficient at stimulating OSL in quartz, whereas wavelengths in the near infrared excite luminescence in feldspars due to one or more excitation resonances. Light emissions for OSL from quartz are detected in the ultraviolet range.

4.2.2 Infrared stimulated luminescence (IRSL)

In contrast to visible light, low-energy photons from the IR band will stimulate luminescence in feldspars but not in quartz (HÜTT & JAEK 1989). The most common term for this phenomenon is infrared stimulated luminescence (IRSL) although some researchers refer to it as IR-OSL or IR-PSL. Stimulation uses either an IR laser or IR diodes, the latter now being the most commonly used. The fact that quartz does not respond to IR stimulation is regularly used to check quartz-separates for feldspar contamination. One advantage of feldspar stimulation with IR is that it allows the detection of different recombination processes in feldspars with different physical properties that are reflected by distinct light emission in the UV, blue, yellow and red emission bands (KRBETSCHEK et al. 1997). The potential of comparing different emission bands, in particular in the context of detecting and overcoming fading of feldspar IRSL (see below), is not yet fully utilised as only a few studies have so far compared the

various sample emissions (e.g., Krause et al. 1997; Preusser 1999b; Preusser et al. 2003). Recent research has focused on IRSL red emissions and it is expected that the apparent stability of the IRSL signal in this part of the spectrum may overcome problems related to signal stability, i.e. regarding fading and resulting age underestimation (Fattahi & Stokes 2003 a, b; Stokes & Fattahi 2003). However, the detection of red IRSL from feldspars using conventional luminescence readers presents some problems, and the use of more sophisticated instrumentation has shed doubt on its stability (Baril & Huntley, 2003). Spectral measurements in this study identified a very low stability of the red (about 700 nm) IRSL emission of feldspars.

4.2.3 Infrared radiofluorescence (IR-RF)

Infrared radiofluorescence (IR-RF) dating was first introduced by Trautmann et al. (1999a) and was referred to as radioluminescence (RL) dating. Because the underlying physical process of this type of luminescence is quite different from that associated with TL, OSL and IRSL dating, the change in nomenclature was useful to physically distinguish this more recently developed dating method (Erfurt & Krbetschek 2003b). In IR-RF dating the palaeodose is determined by a (IR emitting) fluorescence process, i.e. a prompt radiative charge transition. An emission at 865 nm during excitation by ionising radiation is typical for potassium feldspars (orthoclase, microcline) only. The physical basis of this phenomenon and methodological aspects of its application in dating were investigated to develop a reliable new technique for age determination of sediments (Schilles et al. 1999; Trautmann et al. 1999a, b; Krbetschek et al. 2000; Schilles & Habermann 2000; Trautmann et al. 2000; Trautmann 2000; Erfurt 2003, Erfurt & Krbetschek 2003a). The IR emission can be interpreted as the transition of electrons from the conduction band into a particular kind of electron trap. During ionising irradiation a number of electrons reach the conduction band from which they promptly recombine with luminescence centres and emit visible (VIS) fluorescence or transfer to that electron trap by emission of near-IR fluorescence (cf., process c in Fig. 2.1). The trap is probably the same as stimulated by IRSL (process a in Fig. 2.2). Compared to OSL and IRSL, the IR-RF signal bleaches slightly more slowly under light exposure although much faster than TL. As the RF-dose characteristics in quartz are far more complex and variable than in K-rich feldspars (Krbetschek & Trautmann 2000), the majority of studies have so far concentrated on feldspars.

Palaeodose determination based on the phenomenon of IR-RF of potassium feldspars has different advantages compared to TL, OSL and IRSL. Firstly it is a direct measure of the electron density of a (well defined) trap, which does not rely on the conventional luminescence centres (which, as shown, can fade). This also explains why IR-RF dose response curves decrease with increasing dose (Fig. 8) – if the electron trap is empty (zero or low dose) the number of transitions into the traps are high (large signal), if the trap is filling up, the signal decreases due to the decreasing number of free traps. Another advantage of this method is that luminescence stimulation and dose accumulation are applied at the same time. This allows continuous measurement and the recording of a very high number of dose points (Fig. 8) and follows a strict stretched single-exponential decay curve for physically defined reasons. Furthermore, single aliquot regeneration procedures (see Section 5.3) are used for dose determination (Erfurt & Krbetschek 2003b) and also contribute to high precision in palaeodose estimates using the IR-RF method.

The measurement of an IR luminescence emission itself however, together with its low dynamic range and the special procedure of dose application and measurement is not a simple task and requires special instrumentation (Erfurt et al. 2003), which is not commercially available, and explains why this method is broadly accepted (Bøtter-Jensen et al. 2003a; Geyh 2005) but only carried out at

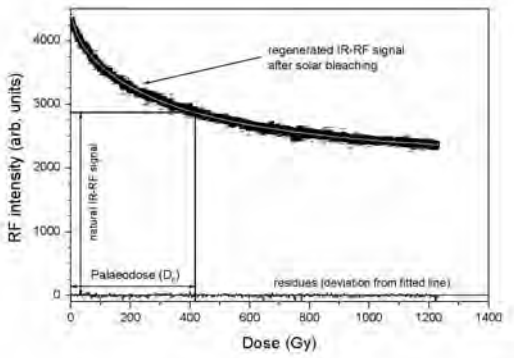

Fig. 8: IR-RF single aliquot regeneration dose response curve of a fluvial sample from central Germany (open cast mine Delitzsch) used to determine the palaeodose (IRSAR-protocol by ERFURT & KRBETSCHEK 2003b). Note the high number of dose points and how the bottom curve (residual: deviations from the fitted line) shows good agreement to the fitted stretched-single –exponential decay curve. The low dynamic range of the IR-RF signal can also be seen.

Fig. 8: IR-RF – Dosisfunktion eines Einzelpräparates einer fluviatilen Probe aus Mitteldeutschland (Tagebau Delitzsch), verwendet zur Bestimmung der Paläodosis (IRSAR-Protokoll nach ERFURT & KRBETSCHEK 2003b). Man beachte die große Zahl an Dosispunkten und die durch die untere Linie (Residuen: Abweichung von der angepassten Kurve) gezeigte gute Übereinstimmung mit der Anpassung an eine gestreckt einfach-exponentiell absinkende Kurve. Der geringe dynamische Umfang des IR-RF-Signals ist ebenfalls sichtbar.

one luminescence dating laboratory (Freiberg, Germany). Its dating-range spans 20 ka to about 350 ka in most cases and as far back as 500 ka with low dose rates. The IR-RF signal stability has been proven through different physical experiments, and also shows a good agreement with independent age control up to 250-300 ka (ERFURT et al. 2003; DEGERING & KRBETSCHEK 2007). It has so far been applied to sediment dating where the signal is optically reset but can also be used to date thermally reset events. DEGERING & KRBETSCHEK (2007) and KRBETSCHEK et al. (2008) have published data of limnic, fluvial and other water-lain sediments back to about 350 ka. Developments in instrumentation including the application of single grain dating, for which the first successful experiments have been made, will improve this method with regard to its precision and the potential to extend the age range.

4.2.4 Linearly modulated OSL (LM-OSL)

In contrast to "conventional" optical stimulation where the energy of the stimulation source is kept constant (continuous wave, CW-OSL), in linearly modulated OSL (LM-OSL) the stimulation power from the LEDs is ramped slowly (typically over 10^3 to 10^4 s) in a linear fashion from zero to some preset value (BULUR 1996; BULUR et al. 2000). The result of this slow increase of stimulation intensity is that in quartz the trapped charge is released first from shallow, and subsequently to deeper traps. This procedure results in overlapping peaks of luminescence emission related to different traps (in some sense similar to TL peaks). Due to the overlap of different components it is necessary to apply mathematical deconvolution to the LM-OSL data to discriminate between different components (cf., CHOI et al. 2006b). The result of this fitting gives information on the presence of different OSL components in a particular sample (Fig. 9), which are grouped according to when they occur during LM-OSL. Fast, medium and slow components have been identified, with the latter consisting of up to five individual subcomponents (JAIN et al. 2003; SINGARAYER & BAILEY 2003), and all of which have different light sensitivities (BAILEY et al. 1997). The first of these is the fastest emission and it follows that this is the easiest to optically bleach in the natural sedimentary environment. Whether or not these different components originate from the same or different optical charge traps is still not fully understood. It is important to note that not all components are present in quartz of different geological origin (Fig. 9) and that the relation between sample properties and different trap populations remains vague. Furthermore, due to uncertainties related to mathematical deconvolution, LM-OSL has rarely been used for direct dating purposes. However, LM-OSL

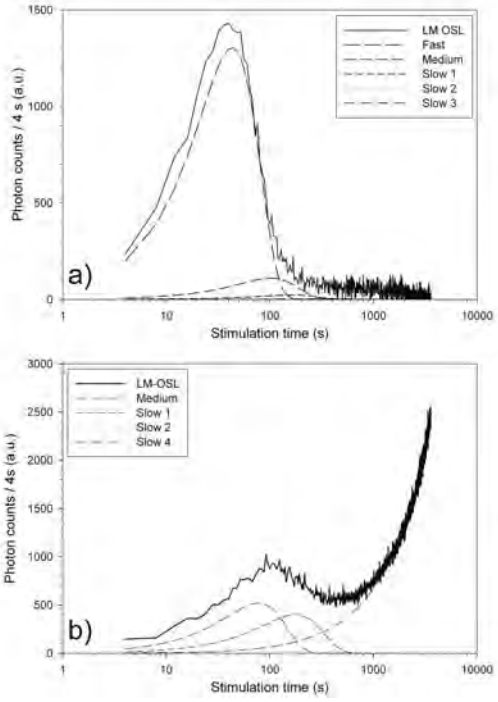

Fig. 9: Deconvoluted LM-OSL curve for (a) well-behaved Australian quartz and (b) quartz sample from Bavaria. The fast component that dominates the signal in sample (a) is not present in sample (b), which is dominated by an unstable medium component.

Abb. 9: Entfaltete LM-OSL Kurve für (a) einen australischen Quarz mit guten und (b) einen Quarz aus Bayern mit schlechten Lumineszenzeigenschaften. Die schnelle Komponente die das Signal in Probe (a) dominiert ist in Probe (b) nicht vorhanden; diese wird durch eine instabile mittlere Komponente dominiert.

is an extremely useful tool for characterising the properties of individual samples and can be used to detect the potential for poor behaviour in quartz, in an early phase of the dating process, although most important is the use of the fast component in circumventing problems of partial bleaching.

4.2.5 Spatially-resolved luminescence (HR-OSL)

A novel approach in luminescence is high resolution spatially-resolved luminescence (HR-OSL) dating of stone surfaces (Greilich 2004; Greilich et al. 2002, 2005; Greilich & Wagner 2006). Similar to sediment dating, the aim is to determine the time when a stone surface was last exposed to daylight. The upper and lower surface of a granitic block, for example, will be shielded from daylight after erecting the wall of a historic monument. Dating the last daylight exposure of mineral grains within construction material hence reflects the age of a building. Besides archaeology, the approach also has great potential for geological applications, as sediments often contain pebbles and boulders.
Optical dating of stone surfaces requires new approaches to sample preparation, palaeodose measurement and dose rate determination. In contrast to conventional luminescence dating, stone surfaces are kept intact to ensure only the grains exposed to light during the construction process are analysed. Because samples remain intact, this method has the great advantage that all information on the micro-dosimetric field is preserved; a detail which is destroyed during the traditional sample preparation. Aliquots are prepared by retrieving small drill cores (diameter ~10 mm) from a stone surface, cutting a thin slice (~ 2 mm thick) from the surface end of the core and mounting this slice in a specially designed metal holder after which, the luminescence measurements basically follow the single-aliquot regenerative-dose (SAR) protocol (see Section 5.2). However, the conventional way of measuring bulk luminescence signals using a photomultiplier tube is not appropriate for a stone surface with varying minerals and grain-size. In contrast, detection of the luminescence signal is achieved by means of a charged-coupled device (CCD) chip, which permits spatial resolution down to 25 µm x 25 µm. This produces a large amount of data (several thousand data points per individual measurement) and data management and analysis require a special software program (Greilich et al. 2006). This software allows production of palaeodose values for each of the many picture elements, filtering of data and statistical analyses that can be spatially resolved for each pixel and then displayed in histograms.

The same spatial resolution for palaeodose calculation is needed for dose rate determination. This is achieved by using an energy dispersive X-ray analysis detector mounted on a scanning electron microscope (SEM-EDX) for the determination of the potassium content of feldspar grains. A special variant of fission-track analysis using tracks induced by fast neutrons is used to determine dose rates from uranium and thorium (WAGNER et al. 2005). From the spatially-resolved palaeodose and dose-rate data, luminescence ages are calculated for each of the analysed grains from a drill-core surface-slice. The last daylight exposure of a stone surface is calculated by combining data of several individually drilled samples.

4.2.6 Thermally transferred OSL

A new approach in the optical dating of quartz is the thermally transferred OSL (TT-OSL) technique (WANG et al. 2006 a). This method makes use of the two components of the thermally transferred OSL signal, which can be divided into the recuperated OSL signal and the basic transferred signal (AITKEN 1998). The recuperated OSL signal is generated by electrons being transferred via optical stimulation from the OSL traps into thermally unstable traps (refuge traps) (WANG et al. 2006a). After the OSL traps are emptied (through light exposure), the transfer from the refuge traps into the OSL traps is generated by thermal treatment. The subsequent light exposure results in a recuperated OSL signal, which is less sensitive compared to the OSL signal (WANG et al. 2006b), and is believed to have the potential to date samples beyond the level of saturation of the fast component of the OSL signal used in a common SAR-procedure (WANG et al. 2007). In contrast, the basic transfer signal derives from electrons trapped in light-insensitive traps and is released into light-sensitive traps by preheating and therefore inapplicable for dating. WANG et al. (2007) presented a SAR procedure using the recuperated OSL signal for palaeodose determination and showed agreement with OSL results.

5 Luminescence procedures

Several values are required to calculate a luminescence age and are either taken from empirical observations or are derived from mathematical expressions. These values are either associated with the determination of palaeodose and the reliability of this measurement or are used for the calculation of a dose rate. The following section gives a brief overview of how these values are determined, how they are taken into account in the age model and which values give information on the reliability of the applied dating procedures.

5.1 Sampling

A first and important point in any dating process is correct sampling. It is mandatory to collect detailed information on the geological context (including photographs, detailed field notes and so forth), particularly concerning the environment of sedimentary deposition and sediment overburden (sample depth below surface, indication for post-sedimentary disturbance, hiatuses, sedimentation cycles). Present and past hydrological conditions (sediment moisture) of the sample need to be assessed as far as possible. To ensure a uniform radiation field, the sample should be taken from a homogenous layer with a thickness of at least 50 cm. If no such layer is available, on-site measurement of gamma radiation (using a portable gamma spectrometer or a gamma counter) should be utilised to minimise the impact of inhomogeneity on dose rate calculation. Samples used for the determination of palaeodose have to be taken without exposing the material to daylight, and is usually achieved by forcing opaque metal or plastic tubes into a freshly cleaned exposure. Material from both ends of the tubes, which is likely to have had some daylight exposure, is discarded for palaeodose measurements but can be used for dose rate determination. Some laboratories require additional material for dose rate determination, particularly when high-resolution gamma spectrometry measurements are performed, but this

material need not be protected from daylight exposure. It is strongly recommended that researchers having little experience in sampling for luminescence dating should contact an expert prior to sample collection to get information on specific requirements.

5.2 Sample preparation

Prior to any luminescence measurements, a preparation procedure is carried out to retrieve quartz and K-feldspar separates. All preparation work for the determination of the palaeodose is carried out under subdued laboratory illumination to avoid any loss of luminescence. Most luminescence facilities have either red or orange low intensity lights installed. The first steps include treatment by HCl and H_2O_2 to remove carbonates and organic material, respectively, always followed by washing with deionised water. A particular grain size is then isolated by either sieving (sand-size grains) or settling (silt). For sand sized grains, quartz and K-feldspar separates are isolated using heavy liquids with densities of 2.58 g cm^{-3}, 2.62 g cm^{-3} and 2.70 g cm^{-3} (Mejdahl 1985). Treating the quartz fraction with concentrated HF acid etches the surface of the quartz by about 10 µm to minimise the alpha-luminescence and also to minimise feldspar minerals by dissolution (plagioclase has a similar density as quartz), followed by treatment with HCl to remove any fluorides that may have formed during etching and dissolution. Etching with 10 % HF is often applied to remove the outer part of K-feldspar grains and etching with either HF (at various concentrations) or H_2SiF_6 is used to isolate fine-grain quartz separates (cf., Mauz & Lang 2004). Alternatively, one can also use polymineral fine-grain samples for palaeodose determination. In such samples the IRSL signal will usually be dominated by feldspar emissions as quartz is not sensitive to

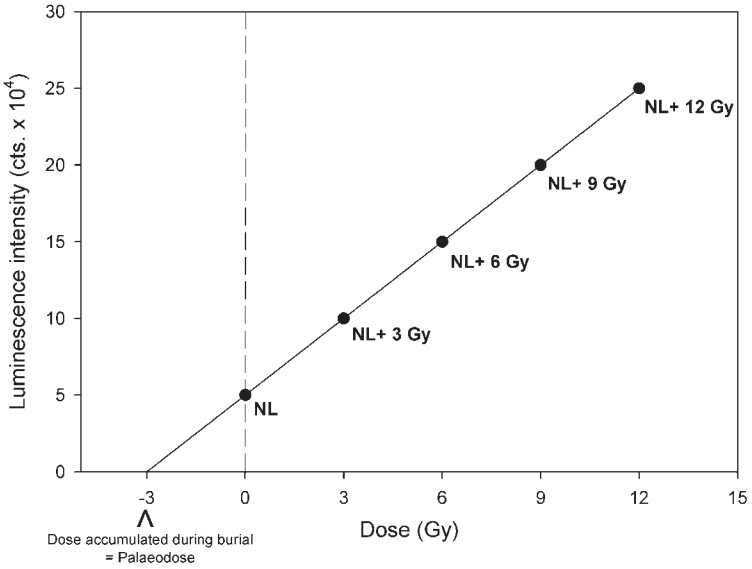

Fig. 10: Additive-dose response curve. Different laboratory doses are added to the natural signal (NL) to characterise the increase of luminescence intensity with dose. The best fitting function is then extrapolated to calculate the dose absorbed during burial (palaeodose).

Abb. 10: Dosisfunktion nach der additiven Methode. Verschiedene Dosiswerte werden im Labor zum natürlichen Signal (NL) hinzugefügt um das Anwachsen der Lumineszenz mit zunehmender Dosis zu charakterisieren. Die beste Kurvenanpassung an die Messwerte wird dann extrapoliert, um die Dosis zu bestimmen, die während der Lagerungszeit absorbiert wurde (Paläodosis).

IR stimulation. In all approaches the grains are mounted on ~10 mm diameter stainless steel or aluminium discs. Fine-grained silts are left to slowly settle (usually through a small vial of acetone) onto the discs; a silicon spray is used to mount sand-sized grains. With sand-sized grains, circular templates are commonly used to determine the quantity of mounted grains.

5.3 Determination of the palaeodose

Measurements are carried out on specialised luminescence equipment and further information regarding technical details about the most commonly used device manufactured by the Risø National Laboratory is found in BØTTER-JENSEN et al. (2003b). The machine consists of a measurement chamber equipped with a sample changer, a sample heating device, stimulation sources (laser or LEDs), a detection unit (photomultiplier tube and optical filters) and, usually in all laboratories, an integrated irradiation source ($^{90}Sr/^{90}Y$ beta source) (Fig. 6). In multiple aliquot dating (see below) irradiation is often carried out using external radioactive sources.

In principle there are two different approaches to determine the palaeodose: additive dose and regenerative dose. For both approaches, a so-called dose response curve is calculated reflecting the increase of latent luminescence in the mineral grains with increasing dose. In the additive dose approach an artificial laboratory-induced signal is added to the natural signal (Fig. 10), while in the regenerative dose method the latent luminescence signal is first removed and the sample is then irradiated and a laboratory signal regenerated (Fig. 11). The advantage of the regenerative method is that no extrapolation of the dose response curve is necessary. This fitting of the curve can cause significant uncertainties in the additive dose approach, especially where data are scattered or for older samples where the growth curve reaches saturation. Small fitting errors can produce large errors in palaeodose determination. The disadvantage of the regenerative method is that the process of zeroing the signal in the grains has been proven to often change the luminescence properties of a sample. If such changes in luminescence sensitivity are not corrected for, the palaeodose will be systematically under- or overestimated (WINTLE 1997).

Regardless of which approach is being used, the measurement of palaeodose comprises three different steps: irradiation, preheating and measurement of luminescence. Irradiation is carried out to induce a latent luminescence signal in the grains and is performed by using either beta sources (external or integrated in the luminescence reader) or external gamma sources. During artificial irradiation all traps, including those unstable over longer time periods, capture electrons. To allow comparison with the palaeodose absorbed over the burial time, the unstable component of the luminescence signal has to be removed, and is achieved by heating the sample (between 200°C and 300°C for usually 10 s, or several hours at temperatures of about 150°C) causing eviction of the electrons caught at shallow traps. Once this preheating of the sample has been performed, the luminescence is measured by stimulating the sample with either heat or light.

5.3.1 Multiple aliquot techniques

Up to the late 1990s, most luminescence dating studies used multiple aliquot approaches. With this method, determination of the palaeodose is carried out using several (usually five) subsamples (aliquots) for the different irradiation doses. The average of these individual dose groups is then used for the construction of a dose response curve. The major disadvantage of a multiple aliquot approach is that each aliquot often behaves differently (due to e.g., variable sensitivity changes, incomplete and variable bleaching, etc.) giving rise to scatter in the data. For this reason, a relatively large uncertainty is often associated with mathematical fitting of dose response curves constructed by multiple aliquot approaches. Furthermore, it has been shown that samples are often affected by changes in luminescence sensitivity when using regenerated doses and this approach should not be used if this change cannot be

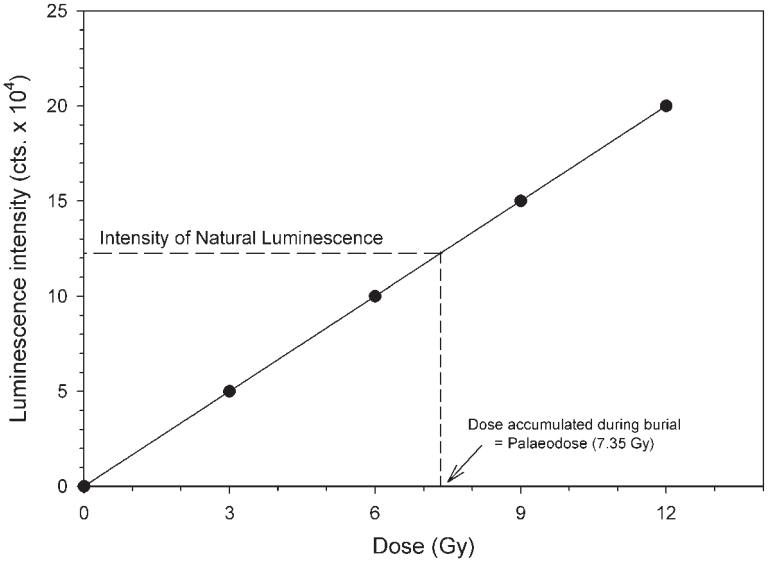

Fig. 11: Regenerative-dose response curve describing the increase of luminescence with dose. Once the natural luminescence signal has been erased by either light or heat exposure, different laboratory doses are administered to the aliquots, and the luminescence response to these used to construct a curve of best fit. The intensity of the natural luminescence signal (dotted line) is then projected onto this to determine the dose absorbed during burial (palaeodose) using interpolation.

Abb. 11: Dosisfunktion nach der regenerativen Methode. Mit verschiedenen Dosiswerten werden im Labor Einzelpräparate bestrahlt, deren Lumineszenzsignal zuvor durch Licht oder Wärme gelöscht wurde. Damit soll das Anwachsen des Lumineszenzsignals mit der Dosis bestimmt werden. Die Intensität des natürlichen Lumineszenzsignals (gestrichelte Linie) wird dann auf die beste Kurvenanpassung projiziert, um die Dosis durch Interpolation zu bestimmen, die während der Lagerungszeit akkumuliert wurde (Paläodosis).

corrected (Duller 1994; Wintle 1997). The major disadvantage with the additive dose approach as mentioned above is the uncertainty of extrapolation with particular regard to older samples.

5.3.2 Single aliquot techniques

When Huntley et al. (1985) published their benchmark paper on optical dating, they already mentioned the possibility of using single aliquot approaches. The main aspect of any such approach is that all measurements are carried out on a single portion or aliquot of the same grains, which circumvents the problem of individual luminescence properties of grains from different aliquots. Several approaches were tested in the 1990s, most of which contributed to the improvement of methodology but included methodological problems that threw doubt on the use of these approaches in routine dating applications (e.g., Duller 1991; Mejdahl & Bøtter-Jensen 1994; Zander et al. 2000). A major breakthrough was made with the development of the single-aliquot regenerative-dose (SAR) technique that was mainly developed and further refined by Murray & Wintle (2000, 2003). As this method is now used in most dating applications by the majority of laboratories world-wide, the principles and procedures will be described in some detail below. A more detailed review focussing on technical details has been presented by Wintle & Murray (2006).

The basic idea behind the SAR technique is to utilise a regenerative dose approach and correct

for any sensitivity change that may occur in the course of the measurement procedure. To carry out this sensitivity correction, a so-called test dose, which remains constant during the whole protocol, is administered after measuring each regenerative (including natural and zero) dose (Fig. 12). The luminescence intensity resulting from each regenerative dose (L_x) is normalised by the luminescence intensity of the following test dose (T_x) and the ratio L_x/T_x, which represents the sensitivity-corrected luminescence signal, is used to construct a dose response curve (Fig. 13). For suitable curve fitting, construction of the latter requires at least three different regenerative dose points (plus a zero dose point). Flexibility in the SAR protocol permits an increase in the number of dose points if required, and can be used to improve the mathematical fitting of the dose response curve when a sample is approaching saturation.

The performance of each individual SAR cycle is verified by two internal tests: recuperation and recycling. The first test considers the signal from an aliquot given zero regenerative dose and then the same test dose as every other SAR cycle, for which L_0/T_0 should be close to 0.00. Values above zero indicate that an unwanted signal was induced by preheating the sample prior to measurement (recuperation), and MURRAY & WINTLE (2000) suggest that recuperation should not exceed 5 % of the natural sensitivity corrected signal intensity (L_N/T_N). If recuperation exceeds this value, it is necessary to modify the protocol by either changing the preheat procedure or by adding a so-called "hot-bleach" (illuminating the sample at elevated temperature) to avoid any such effect (MURRAY & WINTLE 2003). The second test (recycling ratio) confirms whether correction for sensitivity change was successful. This test is carried out by measuring the luminescence response to the same regenerative dose at the beginning, and then again at the end of the SAR cycle (Fig. 13). If the sensitivity correction was successful, the ratio of the two measurements will be unity. MURRAY & WINTLE (2000) suggest discarding any measurements where the recycling ratio is >10 % from unity (i.e., 0.90 < recycling ratio < 1.10).

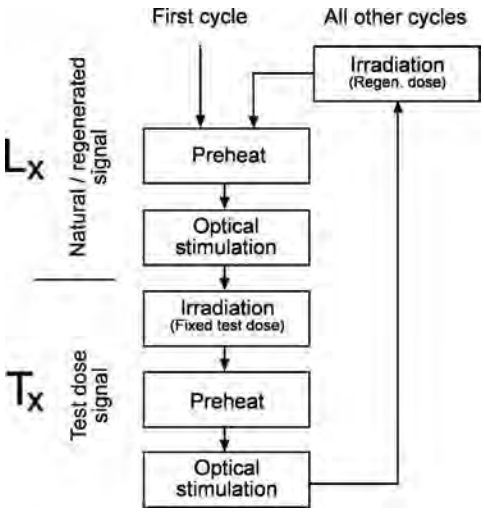

Fig. 12: Overview of the single-aliquot regenerative-dose (SAR) protocol (MURRAY & WINTLE 2000). L_x describes the luminescence signal of the natural sample (L_N) or different regenerative doses (e.g., $L_{10\ Gy}$). T_x is the luminescence response to a constant test dose (e.g., 2 Gy) that is measured after the natural and each regenerative dose.

Abb. 12: Überblick über das Einzelproben-Protokoll mit regenerierter Dosis (SAR) (MURRAY & WINTLE 2000). L_x ist das Lumineszenzsignal der natürlichen Probe (L_N) bzw. verschiedener regenerierter Dosispunkte (z.B., $L_{10\ Gy}$). T_x ist das Lumineszenzsignal, das aus der Bestrahlung mit einer konstanten Testdosis (z.B. 2 Gy) gewonnen wird. Dieses Signal wird nach der natürlichen Lumineszenz und nach jedem regenerierten Dosispunkt gemessen.

In addition to these quality controls performed during every SAR measurement, a series of further tests have been developed to ensure the reliability of the measurement procedure. If these tests do not provide acceptable results it is necessary to modify the measurement procedure. In this context it is important to recognise that, due to the nature of the signal and the variety of sediment sources, luminescence properties of minerals are different in different geological settings. Hence, it is mandatory to carry out a rigorous testing program for all dating projects (e.g., BLAIR et al. 2005; KLASEN et al. 2006).

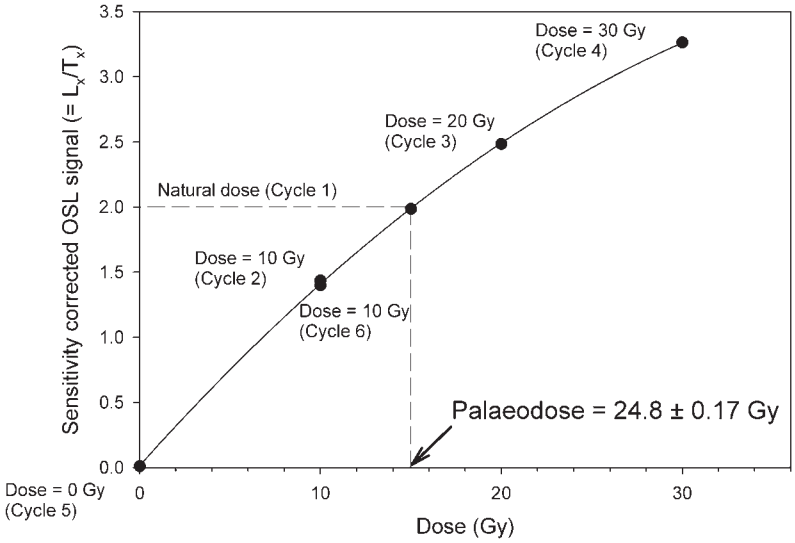

Fig. 13: A typical SAR-generated dose response curve. The ratio of L_x / T_x (e.g., L_{10} / T_{10}) is plotted versus applied regenerative dose. L_N / T_N is then projected onto this curve to determine the palaeodose through interpolation. The lowest regenerative dose is measured twice, at the beginning and end of each individual SAR cycle, to ensure that sensitivity changes have been sufficiently corrected for. The ratio of these two measurements is referred to as the *recycling ratio* and should be within 10 % of unity.

Abb. 13: Eine typische Dosisfunktion, die mit dem SAR-Protokoll gewonnen wurde. Der Quotient L_x / T_x (z. B., L_{10} / T_{10}) wird gegen die regenerierte Dosis aufgetragen. L_N / T_N wird dann auf diese Kurve projiziert um die Paläodosis durch Interpolation zu bestimmen. Das Signal der niedrigsten regenerierten Dosis wird zweimal, am Anfang und am Ende jedes einzelnen SAR-Zyklus, gemessen, um zu überprüfen, ob Sensitivitätsänderungen hinreichend korrigiert wurden. Das Verhältnis dieser wiederholten Messungen wird Wiederfindungsverhältnis (recycling ratio) genannt und sollte um weniger als 10% von Eins abweichen.

A basic requirement that proves the suitability of the SAR protocol is that a known dose that is administered in the laboratory can be retrieved by the measurement procedure (Roberts et al. 1999; Wallinga et al. 2000). For testing this, a so-called dose recovery test is carried out during which the natural signal is first optically erased and then a known laboratory dose is given to the sample. This known dose is then treated as the natural dose in the SAR protocol and the ratio of measured/given dose should be unity if the procedure works correctly, and repeating this test for a sample gives information on the best achievable precision. This very much depends on the luminescence properties of the sample, especially luminescence intensity. Reported values range between relative standard deviations of a few percent, e.g. 4 % for Dutch aeolian sands (Vandenberge et al. 2003), to between 10-15 % found for glacial deposits from Switzerland (Preusser et al. 2007).

A major problem that can, at least in some areas, interfere with correct determination of the palaeodose and is not directly detectable in standard SAR measurements is basic thermal transfer (Rhodes & Pownall 1994; Rhodes & Bailey 1997; Rhodes 2000). The phenomenon is similar to the effect of recuperation (cf., Aitken 1998) and has a major effect on the natural sample but not on subsequent regenerative dose measurements (Rhodes 2000). A simple test to identify if thermal transfer affects a sample is carried out by erasing the latent luminescence and then measuring the apparent palaeodose (Fig. 14). Where the apparent palaeodose is significantly > 0 Gy this is due to a transfer of

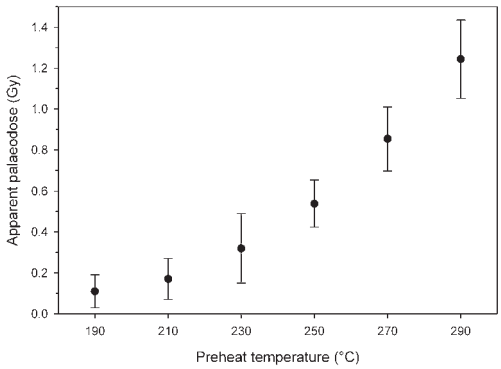

Fig. 14: Plot of palaeodose versus preheat temperature for a sample in which the OSL signal was zeroed by previous optical stimulation (thermal transfer test). The increase of apparent palaeodose results from an OSL signal that is induced by thermal transfer of electrons from light-insensitive to light-sensitive traps.

Abb. 14: Abhängigkeit der ermittelten Paläodosis von der Vorheiztemperatur für eine Probe, deren OSL-Signal durch vorherige optische Anregung auf Null gesetzt wurde (Test des thermischen Transfers) Das Anwachsen der scheinbaren Paläodosis resultiert aus einem OSL Signal, welches durch thermischen Transfer von Elektronen aus lichtinsensitiven in lichtsensitive Fallen hervorgerufen wird.

charge from hard-to-bleach to easy-to-bleach traps. Most studies that have reported significant thermal transfer are related to quartz with a young sedimentary history, i.e. proglacial deposits (RHODES & POWNALL 1994; RHODES & BAILEY 1997; RHODES 2000; PREUSSER et al. 2006), although other studies have shown that thermal transfer may be negligible for some proglacial sediments (e.g., KLASEN et al. 2006; PREUSSER et al. 2007). The test described above is a quick and effective way to exclude the presence of thermal transfer.

A further test exists to check whether the applied preheating procedure is sufficient to remove unstable signal components in the artificially induced signal (AITKEN 1985). For this, the palaeodose is determined for a series of different preheat temperatures (Fig. 15). If all the unstable charge is removed, the calculated palaeodose should not change with increasing preheat temperature. However, it is possible that the phenomenon of thermal transfer is also present and in this case a compromise between a preheat procedure suitable to remove all unstable charge but without causing significant thermal transfer is necessary.

For feldspar samples, storage tests are carried out to monitor the short-term stability of the artificially-induced luminescence signal. This is carried out because feldspars can sometimes be affected by a phenomenon referred to as anomalous fading that describes a loss of signal with time (WINTLE 1973) (see section 6.3).

5.4 Determination of the dose rate

After obtaining the palaeodose, the next step in age determination for a sample requires assessment of the rate at which the radiation dose was delivered to the mineral grains. Similar to the palaeodose this assessment is made over the burial period, being the time since the sample last saw daylight during transport and deposition or since it was last exposed to heat. In most cases, the accumulated dose per unit time, the dose rate, is constant and the age t of a sample is simply calculated from the measured palaeodose D according to Equation 1. A minor component of the dose rate is produced by ionising cosmic radiation and can be estimated from geographic position and burial depth of the sampled material (PRESCOTT & HUTTON 1994) (Fig. 16). The larger part originates from the natural radionuclide ^{40}K and from the uranium and thorium decay series.

In principle, there are three ways to determine this contribution by either measuring the dose rate (a) directly in the sediment using dosimeters, (b) by measuring alpha, beta and gamma dose rates using radiation counting devices, or (c) by analysing the activity and/or concentration of the dose rate relevant nuclides followed by determination of the dose rate using well-established conversion factors. In practice, most laboratories use the last approach. Within the calculation some general assumptions are made for convenience (AITKEN 1985):

– The material is isotropic and homogenous

with respect to the distribution of the sources of ionising radiation.
– The investigated system is indefinitely expanded.
– All radionuclide concentrations are constant in time.

Infinite system dose rates are easily calculated from the specific activities of the radionuclides using conversion factors tabulated in the literature (cf., Adamiec & Aitken 1998). Moisture corrections as described in Aitken (1985) are necessary to consider the radiation attenuation by pore water. Inhomogeneity due to grain size, pore volume and moisture distributions, as well as of the mineral composition are removed in multi-grain samples by averaging over a large number of grains. An inhomogeneity remains between the radionuclide content of the investigated grain itself (causing the internal dose) and the averaged irradiation from all sources outside the grain (the external dose). This effect is dealt with using a correction factor, which denotes the ratio of the actual absorbed dose to the theoretical one of an infinite system. Furthermore, the influence of HF etching of grain surfaces can be taken into account by such a factor. Calculated correction values were originally reported by Mejdahl (1979) and Bell (1979, 1980) and more recently determined by Monte Carlo simulations (Brennan et al. 1991, Brennan 2003).

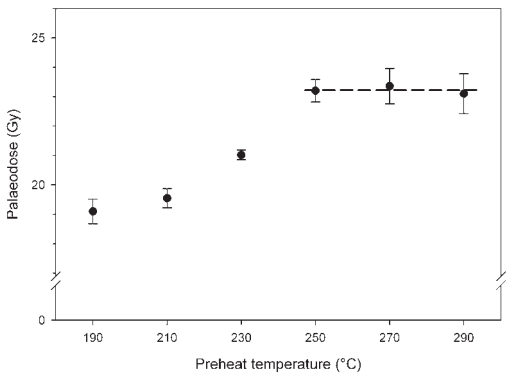

Fig. 15: Preheat tests are performed to determine the thermal pre-treatment that erases all thermally unstable luminescence components in a sample. In this example, palaeodose remains constant for preheat temperatures of 250°C and above (preheat plateau).

Abb. 15: Vorheiztests werden durchgeführt, um diejenige thermische Vorbehandlung zu ermitteln, mit der alle thermisch instabilen Lumineszenzkomponenten in der Probe entfernt werden. In diesem Beispiel bleibt die Paläodosis konstant für Vorheiztemperaturen ab 250°C (Vorheizplateau).

There is a variety of methods that can be utilised for radionuclide analysis in this context (cf., Singhvi & Krbetschek 1996). Most commonly used are inductively-coupled-plasma mass-spectrometry (ICP-MS), high-resolution gamma spectrometry, neutron activation analysis (NAA) and flame photometry (for K only). To check the performance of the procedures certified reference materials are available for all methods. ICP-MS has three main advantages: (a) small sample size (< 1 g required), (b) low detection limit and (c) high precision. The disadvantages of ICP-MS are: (a) small sample size can be a problem if the sediment exposure is inhomogeneous, (b) total dissolution of the sample, especially if zircon is present, is not straightforward, (c) measuring K by ICP-MS is rather problematic (cf., Preusser & Kasper 2001) and (d) this method does not give any information concerning whether radioactive disequilibrium is present in the uranium and thorium decay chains. High-resolution gamma spectrometry is rather time-intensive (each measurement takes at least a day) and requires usually at least 100 g of sample material. Larger sample sizes do, however, reduce uncertainty due to inhomogeneity. The most important advantage of gamma spectrometry is related to the assessment of possible radioactive disequilibrium in the thorium and uranium decay chains (see section 6.4).

The internal dose rate contribution is usually considered to be negligible for quartz grains. In K-feldspars it is often estimated from the stoichiometry of the mineral. Dütsch & Krbetschek (1997) proposed a method for the direct determination of the internal potassium concentration of feldspar grains by studying the peak position of the red radiophosphorescence at about 720 nm. This method was successfully

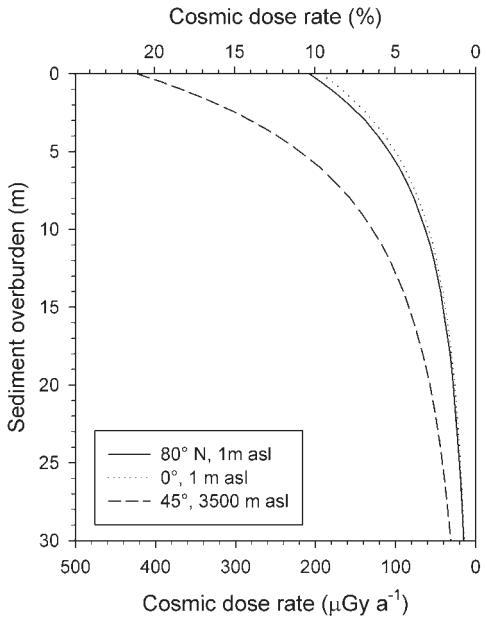

Fig. 16: Dependency of cosmic dose rate on geographic location and sediment overburden, with examples illustrated for sea-level at both high latitude and an equatorial position, as well as a mid latitude position at high altitude. Longitude has a negligible effect on cosmic dose rate. The lower x-axis gives absolute values while the upper x-axis indicates the relative contribution from cosmic rays for a generic sample reflecting a typical sediment with a mean dose rate of 2 mGy a^{-1}.

Abb. 16: Abhängigkeit der kosmischen Dosisleistung von der geographischen Position und der Sedimentüberdeckung. Dargestellt sind Beispiele für hohe Breiten bzw. am Äquator auf Meeresniveau sowie eine Position in den mittleren Breiten in großer Höhe. Der Längengrad hat einen vernachlässigbaren Effekt auf die kosmische Dosisleistung. Die untere x-Achse enthält Absolutwerte, während die obere x-Achse den relativen Beitrag der kosmischen Strahlung für eine Probe mit einer für viele Sedimente typischen mittleren Dosisleistung von 2 mGy a^{-1} anzeigt.

applied to sediments with non-stochiometric K contents (DEGERING & KRBETSCHEK 2007).

5.5 Age calculation

Once both the palaeodose and all dose-rate relevant information are available the luminescence age of a sample together with its uncertainty can be calculated (cf., Aitken 1985). In single aliquot dating, the technique now used by the majority of luminescence dating laboratories, the palaeodose is assessed from many replicated single aliquots. Several statistical methods have been developed to analyse luminescence data and determine the palaeodose. For those samples shown to be completely bleached prior to deposition, some form of central tendency approach is used such as (weighted) arithmetic mean, median or a central age model (cf., Galbraith et al. 1999; Bailey & Arnold 2006). For the palaeodose values determined using any of these approaches standard deviation and standard error are then determined (cf., Geyh 2008). For incompletely bleached samples determination of the palaeodose is more complex (see sections 6.1 and 6.2). For dose rate calculation, the results of measuring dose rate relevant elements (K, Th, U) are combined with the contribution from cosmic radiation and several sample specific factors such as grain size and moisture content have also to be considered (see sections 5.4 and 6.4). These quite complex calculations are usually carried out using special computer programs such as AGE (by R. Grün, Canberra) or ADELE (G. Kuhlig, Freiberg).

6 Problems hindering accurate age determination

6.1 Incomplete bleaching

One of the major problems in luminescence dating is incomplete resetting or bleaching of the latent signal. For sediments, this can occur when the grains are exposed to adequate daylight conditions for too little time and/or if the grains have been transported and deposited by water. Incomplete bleaching is a particular problem for sediments from glacial environments as well as for some fluvial and hill-slope deposits. For all such deposits it is mandatory to investigate if the sample has been completely bleached prior to deposition or not and several approaches exist for doing so.

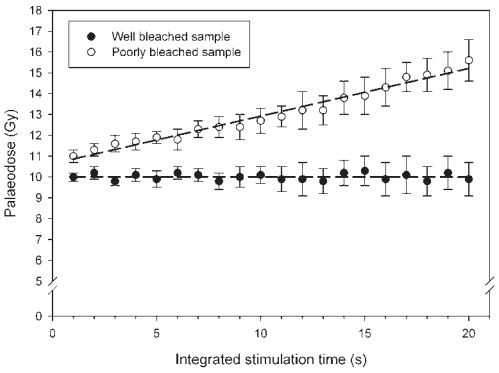

Fig. 17: Shine plateau tests for two samples indicating completely (plateau) and incompletely (increasing palaeodose values) bleached samples. The presence of a shine plateau does not guarantee that a sample has been completely bleached prior to deposition, where they may be potential interference from an unstable signal component.

Abb. 17: Ausleuchtplateautests für zwei Proben, die auf eine vollständig (flaches Plateau) bzw. unvollständig (ansteigende Paläodosiswerte) gebleichte Probe hinweisen. Das Vorhandensein eines Ausleuchtplateaus belegt jedoch nicht zweifelsfrei, dass eine Probe vor der Ablagerung vollständig gebleicht wurde, da mögliche Störungen durch instabile Signalkomponenten vorliegen können.

One approach is to plot palaeodose as a function of optical stimulation time (in the case of OSL and IRSL) or temperature (in the case of TL). The basic idea behind this approach is that the signal during initial stimulation and at lower temperature, respectively, is more light-sensitive than the subsequent following signal (Li 1991, Singhvi & Lang 1998, Bailey 2003a, b). As a consequence, one would expect an increase of palaeodose with stimulation time (temperature) for incompletely bleached samples and a flat shine-plateau-plot for samples that were completely reset at deposition (Fig. 17). Unfortunately, this approach has not been proven to ubiquitously identify incomplete bleaching (e.g., Fiebig & Preusser 2007). Hence, a flat shine-plateau may only be interpreted as evidence for, but not proof of complete bleaching.

The alternative and recently more widely used approach is based on the assumption that sediment grains are not only incompletely, but differentially bleached prior to deposition. This means that the luminescence signal may be completely bleached in some of the grains while the remaining may carry varying amounts of residual signal. When measuring several individual grains from a sample, the lower values in a distribution of doses will most likely represent the grains that were zeroed while the upper values in the distribution will reflect grains that had residual luminescence at deposition (Murray et al. 1995). Typically, a completely bleached sample is expected to reveal a Gaussian distribution while incompletely bleached samples should show a positively skewed distribution of palaeodose estimates (Fig. 18). Although many studies have demonstrated Gaussian distributions for samples with the same radiation dose, recent work indicates that in some cases a Gaussian distribution may not be a sufficient criterion for identifying completely bleached samples (Fuchs et al. 2007).

If a sample has been identified as being incompletely bleached the age estimate based on the mean palaeodose for all aliquots has to be considered as the maximum deposition age. To determine the true burial palaeodose the dose distribution must be investigated further, and for this, it is necessary to measure at least a few dozen individual palaeodose estimates to ensure a substantial statistical basis. The different statistical approaches to extract the true burial palaeodose from the distribution of differentially bleached samples will not be discussed in detail here, we would refer the reader to the overview by Bailey & Arnold (2006). For the time being we have to consider that none of the approaches has proven to ubiquitously provide the correct result when compared to independent age control. Dating results for samples taken from certain environments, in particular proglacial settings, should be considered carefully until more sophisticated methods are available. As each sample has its own sedimentary history, it is advisable to date several

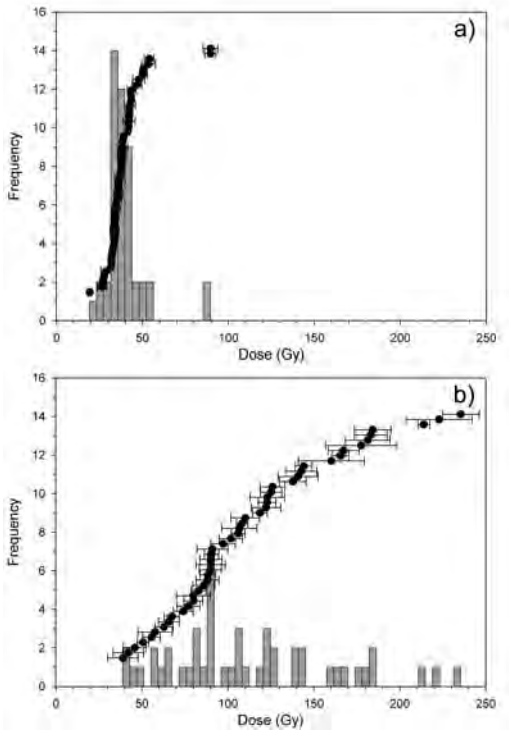

Fig. 18: Scatter of repeated palaeodose measurements for (a) a relatively well-bleached and (b) very poorly bleached sample. While sample (a) displays a symmetric distribution with only two aliquots having significantly higher doses, aliquots of sample (b) show a large scatter in palaeodose values. Both samples are from last glacial (Würmian, ca. 24 ka old) proglacial sediments from Switzerland (from PREUSSER et al. 2007).

Abb. 18: Streuung wiederholter Paläodosismessungen für (a) eine relative gut gebleichte und (b) eine sehr schlecht gebleichte Probe. Während Probe (a) eine symmetrische Verteilung mit nur zwei Aliquots bei signifikant höheren Dosiswerten zeigt, weisen die Aliquots der Probe (b) ein deutlich höheres Streuen der Paläodosiswerte auf. Beide Proben sind aus proglazialen Sedimenten der letzten Vergletscherung (Würmeiszeit, ca. 24 ka alt) aus der Schweiz entnommen worden (aus PREUSSER et al. 2007).

samples from the same sedimentary layer and cross-check the results, and will in most cases help to prove if the age can be considered reliable or needs to be interpreted with caution.

Earlier studies also explored the lower light sensitivity of TL compared to optical signals. For example, WINTLE et al. (1993) compared TL and IRSL of colluvial samples and found that TL ages are up to 10 ka higher than IRSL ages, although IRSL ages also overestimated the expected age and demonstrated that the approach can only be used for sediments where incomplete bleaching is of minor importance such as loess.

Different grain size fractions may also show different degrees of bleaching, with generally two different fractions used in luminescence dating: fine grains (4-11 μm) and coarse grains (90-200 μm). For alluvial sediments, several case studies have shown that the coarser grains appear to be better bleached than finer fractions (e.g., OLLEY et al. 1998; TRUELSEN & WALLINGA 2003) although relatively little systematic work has been carried out on this issue.

6.2 Scatter of single aliquot and single grain palaeodose values

Multiple replicates of palaeodose measurements on sub-samples from the same sediment sample always show a certain variation among the individual estimates, the causes of which are not all fully understood or quantified at present. One major demand in luminescence studies is to assess the extent of the scatter in palaeodose distributions and determine whether the extent of such scatter represents the natural variation of the dose absorbed during burial. If such a baseline variation is known, additional sources of scatter between palaeodose estimates, in particular caused by incomplete resetting of the luminescence signal prior to burial or pedogenesis (see below), can be identified and discriminated outside of this natural baseline variation (GALBRAITH et al. 2005). Only if these requirements are fulfilled can the true palaeodose accumulated during burial be extracted from complex dose-distributions. One important issue in this context is that the spread in palaeodose is very much dependent on the number of grains on the measured aliquot (WALLINGA 2002b). With regard to aliquot size, it is also important to recognise that only a small proportion of all grains show

a measurable optical signal (cf., Duller 2004), hence, the luminescence signal from small aliquots most likely originates from a few or even single grains only. For large aliquots, containing several hundred or thousand of grains, the variation of natural palaeodose will be relatively small, whereas for small aliquots the variation will increase, and for single grains will increase still further. For example, the variation in palaeodose values observed for some fine-grain aliquots, which contain hundreds of thousands of grains, can be less than 1 %. On the other hand, a scatter of 20-30 % for small aliquots (less than 50 grains) of bright Australian aeolian quartz has been reported (Lomax et al. 2003, 2007), although the OSL characteristics of this material are considered to be very suitable. Poorly behaved dim quartz grains, for example from the foreland of the Swiss Alps, show an even higher variation (Preusser et al. 2007).

Four different major sources may cause broad and complex palaeodose distributions and these are: (a) laboratory reproducibility of the measurement; (b) partial bleaching; (c) post-depositional sediment mixing caused by bioturbation or similar phenomena; and (d) variation in the distribution of radioactivity within the sediment (microdosimetry).

Reproducibility of the laboratory measurements can easily be determined for each individual sample with a dose recovery test (section 5.3.2). Depending on the particular properties of the minerals investigated and on aliquot size, this typically varies from about 5 % to 15 % (cf., Preusser et al. 2007). This is much less than the spread of palaeodose values observed in many natural samples. Incomplete bleaching of the luminescence signal, as discussed above, can result in a substantial scatter of palaeodose values resulting in overestimation of OSL ages. Additionally, pedo-/bioturbation can have an important effect on dose distributions, in particular for sandy deposits such as aeolian dunes (Bateman et al. 2003). Pedoturbation is common in former drylands that have later experienced increased humidity resulting in high floral and faunal occupation (Bateman et al. 2007). The most common effect of pedoturbation will be contamination of older sediment by younger surficial material. This will cause a negatively skewed dose distribution where the lower palaeodose values are not representative of the variation in true burial dose. In contrast, partial bleaching will cause a positively skewed dose distribution where the true burial dose lies in the lower dose region, while the upper part of the distribution represents grains that where incompletely zeroed at deposition.

A source that may cause variation of palaeodose is inhomogeneity of exposure to beta irradiation from grain-to-grain within sediments (microdosimetry). This occurs due to the fact that radioactive elements are sufficiently abundant in only a few minerals such as K-feldspar (^{40}K) and zircon (^{238}U and ^{232}Th), so-called "hotspots" of radioactivity. As beta particles penetrate to only a few mm within typical sediment, grains proximal to hotspots will be exposed to a much higher dose rate than other grains and hence absorb more dose during burial. Although the majority of causes of natural variation of palaeodose are difficult to constrain, it is likely that the effect of microdosimetry may be inversely related to the number of hotspots within the sediment matrix. Mayya et al. (2006) calculated that inhomogeneous microdosimetry will cause positively skewed palaeodose distributions and that the effect on the standard deviation for repeated single grain measurements may be between 18 % and 46 %, being inversely dependent on the K-content of the sediment.

6.3 Anomalous fading

The phenomenon of anomalous fading was first observed by Wintle (1973) in a study of TL dating of sanidine. Fading is a loss of luminescence signal with time; this implies that some of the electrons captured at traps are unstable and do not possess the trap lifetime exhibited by the majority of electrons in the trap. The effect in a dating application will be that the laboratory induced signal from a particular trap will originate from both stable and unstable charge,

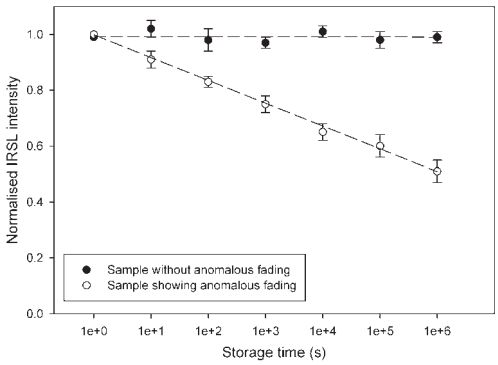

Fig. 19: In the presence of anomalous fading laboratory irradiation will produce a signal that decays (fades) over time. This same unstable signal is not present in the natural sample and, as a consequence, the absorbed palaeodose and hence the age of the sample will be underestimated.

Abb. 19: Bei vorhandenem anormalem Ausheilen (Fading) produziert die Laborbestrahlung ein Signal, welches mit der Zeit zerfällt. Dieses instabile Signal ist in der natürlichen Probe nicht vorhanden. Daraus resultiert, dass die absorbierte Paläodosis und somit das Alter der Probe unterschätzt werden.

whereas the natural signal from the same trap will derive only from the stable charge. The same artificial radiation dose will produce a much higher signal than that resulting from natural irradiation and, as a consequence, the palaeodose will be underestimated as will the age of the sample (Fig. 19).

Preheating the samples prior to measurement (section 5.3) will remove most of the unstable charge, but several studies have shown that this unwanted charge may remain even after applying rigorous thermal pre-treatments. One possible fading mechanism that has been suggested is attributed to the tunnelling of electrons (e.g., VISOCEKAS 1985), whereby charge tunnels between traps and luminescence centres rather than recombining via the conduction band. While the phenomenon is normally only attributed to feldspars, recent publications imply that it may also exist in volcanic quartz (BONDE et al. 2001; TSUKAMOTO et al. 2007). With regard to feldspar, there is much debate over whether fading affects this mineral ubiquitously (e.g., HUNTLEY & LAMOTHE 2001) or, if it is related to feldspar of specific geological origin and, at least partly, inappropriate laboratory procedures. With regard to the latter, two issues are of major relevance. Firstly, the thermal pretreatment must be long enough, and the temperature high enough to remove thermally unstable components. Secondly, KRBETSCHEK et al. (1997) have shown that unstable components in feldspars are mainly related to emissions in the UV band, and recommend that these emissions should be avoided, suggesting either the use of short-wave blocking optical filters (e.g., a Schott GG400) or interference filters that only allow transmission of emissions in a very narrow band. While studies implementing these recommendations often produce ages consistent with independent age control (e.g., CLARKE & RENDELL 2003; PREUSSER 2003), those studies incorporating the UV emissions have reported significant underestimation of luminescence ages (e.g., HUNTLEY & LAMOTHE 2001).

Nevertheless, further studies utilising a restricted detection window have still observed fading of feldspars in their samples (e.g., WALLINGA et al. 2007), and this may be related to the measurement of feldspars of volcanic origin, which have been shown to be predominantly affected by fading, and may be due to the disordered crystal lattice in volcanic minerals resulting from rapid cooling and crystallisation (SPOONER 1994). This may also explain the fading observed in volcanic quartz.

Storage tests performed at either room or elevated temperature indicate whether a sample is affected by fading (AITKEN 1985; SPOONER 1992), and are a suitable approach as it is expected that fading components decay on a logarithmic scale (VISOCEKAS 1985, 2002; SPOONER 1994). Where fading is observed in samples it is possible to calculate the rate of fading per decade and use it to correct the age (HUNTLEY & LAMOTHE 2001; AUCLAIR et al. 2003; LAMOTHE et al. 2003). LAMOTHE et al. (2003) undertook fading correction for samples both on the linear part of the dose response curve and for geologically old sediments in luminescence field saturation. However, a recent study by WALLINGA et al. (2007) dem-

onstrated that the applied fading correction was not sufficient to account for the offset between feldspar and quartz ages. More research in this area is necessary to fully utilise the potential of feldspars in dating; in particular the higher saturation dose and hence increased dating range.

6.4 Accurate dose rate determination

Besides the problems associated with the determination of the dose absorbed during burial (palaeodose) there are also potential errors related to the correct calculation of dose rate, some of the most important of which are discussed in the following.

6.4.1 Alpha efficiency

Alpha particles produce much less luminescence signal compared to beta and gamma rays, and so the effective dose from alpha irradiation is therefore multiplied by a factor that reflects this lower ionisation efficiency; this factor, referred to as the a-value, is usually < 0.1 (Aitken & Bowman 1975).

For sand-size minerals, for which most research has concentrated during the last decade, a-values are of minor importance as alpha particles penetrate only the outer ca. 10 µm of the grain, and the outer rim of such grains is usually removed by HF etching during sample preparation. When measuring fine-silt grains, for example when dating loess, lacustrine sediments or fine silicate inclusions from ceramics, the the a-value is of major importance. For such materials it is recommended that the a-value is determined for each individual sample, which involves comparison of laboratory-induced luminescence due to both alpha and beta radiation (e.g. Aitken 1985).

6.4.2 Internal K-content

With regard to the internal dose rate of feldspar, there is the potential to underestimate the K-concentration where chemical analyses (e.g. AAS) or beta counting are used, and is is due to the fact that potassium content lower than the stochiometric maximum can be caused by contamination of the sample by, for example, quartz that is often found in the feldspar fraction, but is not relevant for palaeodose determination. An extended chemical analysis (e.g. K, Na, Ca, Al, Si concentration), the use of micro-probe equipment and the calculation of a theoretical feldspar composition may overcome this problem to some extent (Dütsch & Krbetschek 1997).

6.4.3 Sediment moisture

Another major uncertainty is associated with the moisture content of a sample during burial Water in the sediment pores absorbs much more radiation than air and so the effective dose acting on a grain is higher in sediments with low moisture content compared to a similar saturated sediment (Fig. 20). In age calculation, an average value for moisture over the whole burial time is usually assumed, but the lack of information concerning the extent of moisture variation throughout the burial period means that this is often the greatest source of uncertainty in a luminescence age. The present moisture content of the sample is often used as a guideline for age calculation but it is crucial that potential changes in the hydrological conditions are carefully considered during sampling. It is often also

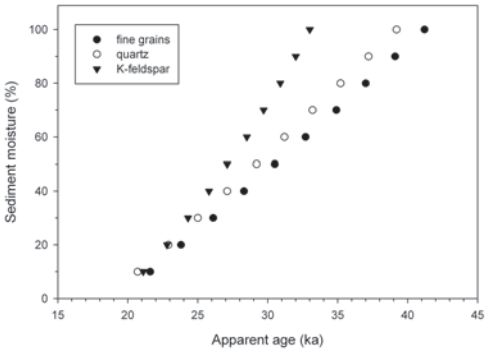

Fig. 20: Impact of sediment moisture on calculated luminescence age.

Abb. 20: Einfluss der Sedimentfeuchte auf das berechnete Lumineszenzalter.

appropriate to measure water up-take capability of samples to give an estimate of maximum moisture content (cf., AITKEN 1998). For example, fluvial sediments are usually water saturated directly after burial but the height of the water table may change when rivers incise or terraces are tectonically up-lifted. In such cases the sediment may be above the water table for a significant part of the burial period and pores may be only partially filled with water. In lacustrine settings, pore space will decrease with on-going consolidation of the sediment as discussed in the context of luminescence dating by JUSCHUS et al. (2007). Uncertainties related to sediment moisture are most important for water-lain sediments but can in principle also be significant in certain other sedimentary settings such as coastal deposits or sediments that have been affected by permafrost in the past.

6.4.4 Cosmic dose rate

The contribution of cosmic radiation to the total dose rate is usually calculated according to the sampling depth and geographical position of the sampling site following PRESCOTT & HUTTON (1994). The dynamic character of sedimentary systems with repeated events of erosion and accumulation results in variation of the thickness of the overburden above a buried sediment sample. Therefore, the contribution of cosmic rays to the total dose rate of the sample is not constant over the entire period of burial time, but may vary significantly. Such fluctuation in the overburden thickness is less significant in sedimentary environments where the contribution of cosmic rays to the total dose is generally low. Frequently the proportion measures less than 10 %. However in quartz-rich aeolian dune sand system the dose rate tends to be low and the cosmic ray contribution to the annual dose can be a major component of the total dose rate. In such cases a substantial error in total dose rate calculation and, hence, luminescence age can be introduced if the cosmic dose contribution is calculated using present sampling depth. To provide a more accurate dose rate assessment the burial history of a sample should be taken into account, as far as this can be reconstructed (MUNYIKWA 2000).

6.4.5 Radioactive disequilibria

Special attention must be directed to sediments exhibiting radioactive disequilibria since the prerequisite of constant radionuclide concentrations does not hold (cf., KRBETSCHEK et al. 1994). The radioactive elements of uranium and thorium are the beginning members or 'parents' of three decay series starting with the isotopes ^{238}U, ^{235}U and ^{232}Th. Their half-lives are of the order of 10^9 to 10^{10} years and thus they are still present in nature. These parent radionuclides and their stable end 'daughter' products of ^{206}Pb, ^{207}Pb and ^{208}Pb, respectively, are linked together by decay chains including several daughter isotopes of various elements but with half-life times much shorter than 10^9 years. Table 2 gives the physical and chemical properties of the most significant members of ^{238}U and ^{232}Th decay series in dose-rate determination.

In an undisturbed geological situation the activities within each decay series are in 'radioactive equilibrium', characterised by equal activities of all involved nuclides. Physical and chemical differentiation processes lead to a loss of this balance and to radioactive disequilibria. In closed systems the balance is restored on a time scale of the order of ca. five half-lives of the radionuclide concerned. Open systems can reach stationary states if geochemical properties do not change with time. As a consequence of the time dependent change in activities in the case of radioactive disequilibria, the external dose rate also becomes a function that varies with time. Equation (1) must then be replaced by an iteration technique which searches for the point in time t, at which equation (2) holds:

$$\int_{t_0}^{t_0+t} \dot{D}(\tau)d\tau = D \qquad (2)$$

where t_0 is the moment of sample bleaching. In the case of radioactive disequilibria one needs: (a) preferably an analysis of all long-lived ra-

Table 2: Physical and chemical properties of the dosimetrically most significant isotopes of ^{238}U and ^{232}Th decay series.

Tab. 2: Physikalische und chemische Eigenschaften der dosimetrisch wichtigsten Isotope der ^{238}U und ^{232}Th Zerfallsreihen.

Decay series	Nuclide	Half life	Significant Properties
^{238}U series	^{238}U	$4.5 \cdot 10^9$ a	Actinide, heavy metal, forms organic complexes, valence states U(IV) (low solubility) and U(VI) (soluble as uranyl ion $(UO_2)^{2+}$)
	^{234}U	$2.5 \cdot 10^5$ a	
	^{230}Th	$7.5 \cdot 10^4$ a	Actinide, tetravalent, low solubility
	^{226}Ra	$1.6 \cdot 10^3$ a	Earth alkali metal, soluble
	^{222}Rn	3.8 d	Inert gas
	^{210}Pb	22 a	Heavy metal, forms organic complexes
^{232}Th series	^{232}Th	$1.4 \cdot 10^{10}$ a	cf. ^{230}Th
	^{228}Ra	5.8 a	cf. ^{226}Ra
	^{228}Th	1.9 a	cf. ^{230}Th

dionuclides; and (b) a model of the possible activity evolutions in the past in agreement with both the geochemical parameters of the system and with the modern radionuclide contents.

Low-level high-resolution gamma spectrometry is suitable for multi-nuclide analyses, mostly fulfilling criterium (a). Generally, this method is suitable for determination of the following long-lived nuclides (in some cases with the use of short-lived daughter nuclides): ^{238}U, (^{230}Th), ^{226}Ra, ^{210}Pb from ^{238}U series, ^{228}Ra, ^{228}Th from ^{232}Th series and ^{40}K.

The time evolution of radioactive disequilibria in closed systems and in special types of open systems can be analytically solved. Mathematically, the solution for each activity term is a superposition of exponential decays with coefficients containing the initial activities, the decay constants and exchange parameters in open systems (Degering & Krbetschek 2007).

Modelling the disequilibrium in the past is based upon assumptions concerning the value of the prevailing parameters and their variability with time. In most cases this results in a more or less broad range of possible time evolutions, leading to the current radionuclide concentrations. In comparison to ages ignoring disequilibria, the uncertainty in age increases but so too does reliability.

In recent years several samples exhibiting radioactive disequilibria have been accurately dated when compared to independent age control from radiocarbon dating. From these investigations some indications of "suspicious" systems and their treatment can be derived:

– Organic substances tend to accumulate complex-forming elements like uranium or lead. Since the solubility of U and Th are very different, organic sediments like peat often show strong U/Th imbalance. The most important is $^{234}U/^{230}Th$ disequilibrium and is definitely predictable for closed systems (Degering & Krbetschek 2007).
– Changes in the moisture content or in the groundwater level may lead to variable redox conditions and hence changes between open and closed system characteristics. Especially for fine grain dating, the dosimetric consequence of variable moisture is a variable attenuation of the external irradiation with time. The resulting enhanced uncertainty in the dating result can only be reduced by applying a model considering this variation (Preusser & Degering 2007).

– Calcareous material deposits containing, for example, mollusc shells or corals are able to exchange radionuclides with their environment. Reasonable explanations of the modern radionuclide contents partly require the assumption of an open system, mainly connected with uranium uptake after deposition. The clear reconstruction of the evolution of disequilibrium in the past is hardly practical here. A careful investigation should include the calculation of borderline cases to give an impression of the likely span of reliable ages (ZANDER et al. 2007).

7 Suitable materials

Up until the 1980s most research in luminescence dating had focused on fundamental problems and the application of TL for dating heated objects and volcanic deposits as well as some initial work on TL dating of sediments (cf., AITKEN 1985). Since the introduction of optical dating (using IR and visible light) most research has focused on the dating of sediments, in particular in the context of palaeoclimate change as well as archaeology (Table 3, 4). General overviews on early work are provided by PRESCOTT & ROBERTSON (1997), AITKEN (1998) or STOKES (1999) and the following sections will concentrate on benchmark publications and the most recent developments.

7.1 Archaeological materials

A wealth of archaeological materials can be dated with luminescence methods. Apart from unheated sediments (see section 7.3) containing archaeological remains, two main categories can be distinguished: (1) heated sediment e.g. ceramics, pottery, bricks, fire places, fire pits, hearths, kilns; and (2) heated rocks e.g. flint, chert, quartzite, quartz, silcrete, sandstone and other rock materials. An additional category includes man made materials such as slag and walls constructed from rock materials.

The association of dated material and human occupation is always a key question when applying chronometric dating methods in establishing the age of archaeological sites or, in other words, the relationship between the event dated and the question asked has to be clearly shown. However, it is often only through luminescence on heated materials that an age of an archaeological event can directly be provided (cf., RICHTER 2007; ALPERSON-AFIL et al. 2007 for discussion of natural fires).

Table 3 lists the commonly used materials/samples in luminescence dating, together with the appropriate method and the event dated, which is sometimes not evident at first sight. In some cases it is important to take the life time of an artefact or feature into consideration, e.g. a kiln could have been used for an extended period of time, but in general only its last use can be dated and not the time of construction. Or in the case of dating rock surfaces, the time since the last exposure to light is dated, which can be the time of construction or destruction of a monument. Ceramics could be much younger than an associated construction or much older, e.g. when they are discarded in a pit or trench from older deposits and are therefore out of context. The depositional age of sediment infill provides age information concerning abandonment rather than construction, e.g. of a trench or pit. Anthropogenic sediments or sediments altered by human occupation are difficult to date with luminescence methods. It is therefore often advisable to select more suitable sedimentological units bracketing the archaeological layer of interest and thus OSL dating can provide *termini post quem* and *ante quem* age estimates.

Heated rocks are usually dated by TL but if the material is sufficiently sensitive OSL methods can be applied as well. In such cases, bleaching during excavation might be a major concern (e.g., TRIBOLO 2003), although flint, for example, has been shown to be insensitive to optical stimulation (POOLTON et al. 1995). Conversely, TL of flint is very hard to bleach by light for most samples from a highly diverse material group (RICHTER et al. 1999).

The first luminescence ages on archaeological material were obtained using TL on ceramics by GRÖGLER et al. (1958). TL dating of ceram-

Table 3: Overview of different dating applications for archaeological materials by luminescence methods.

Tab. 3: Überblick über die verschiedenen Anwendungsbereiche der Lumineszenzmethoden zur Datierung archäologischer Materialien.

Material	Material details	Method	Dated event	Interpreted as time of	Archaeological example
Brick	Quartz, feldspar	TL/OSL	Last firing	Manufacture	Bailiff & Holland (2000)
Brick surface	Quartz, feldspar	OSL	Last exposure	Construction; repair; destruction	Bailiff & Holland (2000)
Ceramic, pottery, tile	Quartz, feldspar	TL/OSL	Last firing	Manufacture; authenticity	Barnett (2000)
Daub (burnt)	Quartz, feldspar	TL/OSL	Last heating	Destruction	Quickert et al. (2003)
fFgurine	Quartz, feldspar	TL/OSL	Last heating	Manufacture; authenticity	Zink & Porto (2005)
Hearth stone	Sandstone, limestone, granite (quartz, feldspar)	TL/OSL	Last heating	Last use	Ichikawa & Nagatomo (1978)
Kiln	Quartz, feldspar	TL	Last firing	Last use	Hong et al. (2001)
Lithic artefact (heated)	Flint, chert, quartzite, quartz, silcrete	TL	Last heating	Discard	Richter et al. (2007)
Limestone (heated)	Calcite, quartz	TL	Last heating	Last use	Roque et al. (2001)
Mortar	Quartz, feldspar	TL/OSL	Last light exposure	Building	Goedicke (2003)
Oven	Quartz, feldspar	TL	Last firing	Last use	Roque et al. (2002)
Pit/trench infill	Quartz, feldspar	OSL	Last light exposure	Abandonment; infilling	Lang & Wagner (1996)
Rock surface	Granite, marble, limestone (quartz, feldspar, calcite)	OSL/TL	Last light exposure	Construction; destruction	Greilich et al. (2005, 2006); Liritzis & Vafiadou (2005)
Sediment (burnt)	Quartz, feldspar	TL/OSL	Last heating	Last use	Godfrey-Smith & Shalev (2002)
Sediment, aeolian	Quartz, feldspar	OSL	Last light exposure	Deposition	Jacobs et al. (2003 a,b)
Sediment, colluvial	Quartz, feldspar	OSL	Last light exposure	Deposition	Lang & Hönscheidt (1999)
Sediment, fluvial	Quartz, feldspar	OSL	Last light exposure	Deposition	Folz et al. (2001)
Slag	Quartz	TL	Last firing	Last use	Haustein et al. (2003)
Wasp nest	Quartz, feldspar	OSL	Last light exposure	Building	Yoshida et al. (2003)

ics and pottery soon became the backbone for establishing many archaeological chronologies in the world, but with the increased precision of archaeological dating (including seriation etc.) and the possibility of providing calendar ages by calibrating radiocarbon data, the application of TL dating of ceramics and pottery became less important from the 1980s onward. However, BARNETT (2000) used TL to verify the typo-chronologies for the British Late Bronze and Iron Age, using both shards that were diagnostic by their shape and/or decoration, as well as those that were undiagnostic (fabric based chronology), and it was shown that the established chronology for diagnostic pottery was supported by the TL results. As the conditions for luminescence dating were not different for the diagnostic samples, it was concluded on the other hand that the accuracy of chronologies based on fabric only required refinement (BARNETT 2000).

Establishing the timing of construction, repair and destruction of parts of the medieval citadel of Termez in Usbekistan was attempted by VIELLEVIGNE et al. (2006), who showed the feasibility of a combined OSL and TL approach on different bricks, that could be related to the reuse of older bricks, as was also done by BAILIFF & HOLLAND (2000).

The correlation of features considered to be fire places, hearths or fire pits, which lie close to an archaeological settlement site but lack remains like hearth stones, is often difficult to establish. The heat-reddened rim and infill of a pit from an Early Bronze Age context at Ashkelon Marina in Israel was dated with TL additive methods and OSL by GODFREY-SMITH & SHALEV (2002). While the TL age for the heated sediment agrees well with radiocarbon data, the TL result for the pit infill is greatly overestimated and clearly shows that this method is inappropriate for unheated sediment. On the other hand an OSL age for the pit infill agrees well with the TL age of the heat-reddened rim, suggesting the pit was rapidly filled after disuse and confirming the likely function of the fire pits for early copper smelting technology.

TL-dating of domestic ovens for the Neolithic site of Dikili Tash in Greece (ROQUE et al. 2002) provided confidence in the often assumed association of radiocarbon dating samples with occupational levels and strengthens the Neolithic chronological framework for that region. It is possible to establish the authenticity of figurines and ceramics using TL and OSL, although an accurate date cannot usually be given due to the lack of knowledge of the precise radiation field of each individual object. ZINK & PORTO (2005) investigated a large collection of Tanagra figurines and used probability statistics to distinguish fake from authentic ones.

Quartz pebbles from the site of Pedra Furada in Brazil were dated with TL techniques by VALLADAS et al. (2003). These pebbles are assumed to have been used as hearthstones and/or for heating liquids. The site of Pedra Furada is controversial because of the claim that it has a much greater antiquity than the time generally recognised for the arrival of humans in the Americas. While the TL age estimates prove the antiquity of the heating, the question of the anthropogenic use of the pebbles cannot be solved solely by establishing the time when fire occurred (VALLADAS et al. 2003). Sandstones are the most common material used to establish the age of distinct hearths but limestone was more frequently used to construct fireplaces in the Palaeolithic. The feasibility of using TL for dating heated limestone is reported by ROQUE et al. (2001) from the Upper Palaeolithic site of Combe Saunière in France.

TL dating of heated flint plays a major role in establishing the relationships in time between tool assemblages, technocomplexes and hominid species, under the assumption that the time difference between archaeological material surrounding the intrusive burial and skeletal material is negligible. Heated flints from layers containing Middle Palaeolithic artefacts in several caves in Israel which are associated with Neanderthal remains in some and with modern humans in others were dated (VALLADAS et al. 1987; 1988, 1999; MERCIER et al. 1993). These dates provide evidence for an extended overlap of several thousand years of the two species within a relatively small region. In general, TL

Table 4: Overview of different applications of luminescence methods for dating sediments (n.a. = not available).

Tab. 4: Überblick über verschiedene Anwendungsgebiete der Lumineszenz zur Datierung von Sedimenten.

Sediment type	Severity	Most common problem	Pioneering study	Review
Loess	Minor		TL: Wintle (1981)	Singhvi et al. (2001)
Aeolian sand	Minor		TL: Singhvi et al. (1982)	Singhvi et al. (2001)
Fluvial deposits	Average	Partial bleaching	TL: Forman et al. (1988) OSL: Perkins & Rhodes (1994)	Wallinga (2002 a)
Hillslope sediments	Average	Partial bleaching	IRSL: Wintle et al. (1993)	Fuchs & Lang (2008)
Lacustrine sediments	Average	Sediment moisture	TL: Berger (1990)	n.a.
Proglacial deposits	Challenging	Partial bleaching	TL: Gemmell (1985) IRSL: Hütt & Jungner (1992)	n.a.
Coastal deposits	Average	Radioactive disequilibria	TL: Balescu et al. (1991)	n.a.
Deep sea sediments	Average	Radioactive disequilibria	TL: Wintle & Huntley (1979)	n.a.

methods are used to establish the age of individual archaeological layers and thus help to establish the chronologies of technocomplexes beyond the range of radiocarbon dating, e.g. for the middle Palaeolithic chronology of Western Europe (Richter et al. 2007). Recently, a SAR protocol employing red TL was developed, which allows the dating of small samples of heated flint, thus increasing the number of Palaeolithic sites, which could be dated (Richter & Krbetschek 2006). Mastering fire is regarded as one of the hallmarks in human evolution and certainly played an important role in dramatic changes in human behaviour connected with diet, defence and social interaction. Analysis of lithics suspected of having been heated using TL helped provide evidence for the controlled use of fire at the Acheulian site of Gesher Benot Ya'aqov in Israel, where distinct clustering of heated and non-heated materials reveal the positions of former fire places (Alperson-Afil et al. 2007). TL dating of heated flint can also be used to verify the integrity of an archaeological site or layer. Results of heated flint from an assemblage dated by Debenham (1994) provided evidence of an otherwise unobserved severe mixing of a Palaeolithic site.

Slags are often the only remains from archaeometallurgical activities and the association of dates obtained from materials in the vicinity is often questioned. The application of a combination of the red TL with a SAR protocol on extracted quartz by Haustein et al. (2003) showed a fair agreement in comparison with independent age control.

Determining the age when a wall was built, a megalith was erected, repair work or destruction took place, or even when rocks were moved and discarded or reused is of great importance in archaeology. The recent development by Greilich et al. (2005, 2006) on the OSL dating of surface exposure is a significant development. These authors were able to establish surface exposure ages of granitic surfaces from rocks used to construct some of the Nasca geoglyphs. These results were contrasted by the surface exposure age of rocks which were unmoved for several 10^3 years. But even standard TL and OSL methods are capable of producing reasonable age estimates of surface exposure of

Neolithic as well as Greek monuments (LIRITZIS & VAFIADOU 2005).

7.2 Volcanic deposits

The dating of volcanic deposits was developed in the early 1970s, soon after the successful application of TL to date archaeological materials. Despite the fact that anomalous fading appears to affect most volcanic feldspar (WINTLE 1973), and possibly volcanic quartz as well, (TSUKAMOTO et al. 2007) more than 50 studies have been published on the dating volcanic deposits. A comprehensive review on studies carried out in the 1970-90s is provided by FATTAHI & STOKES (2003b). TL dates have been used to establish chronological frameworks for volcanic activity in areas such as the Massif Central, France (VERNET et al. 1998) and China (LI & YIN 2001). While FATTAHI & STOKES (2003b) summarise good consistency of TL ages with independent age control for several dating studies, problems with anomalous fading occurred in many other studies. An important aspect is the use of the red emission from feldspar, which has proven to be more stable than other TL emissions (e.g. FATTAHI & STOKES 2000; MIALLIER et al. 2004; GANZAWA et al. 2005; BASSINET et al. 2006). However, relatively little research has been carried out and to date only a few research groups have focused on this topic.

7.3 Sediments

7.3.1 Loess

Loess was among the first sediments that were systematically dated by luminescence methods, in particular by TL (e.g., WINTLE 1981; WINTLE 1990). In most early dating studies, the optically insensitive TL signal was determined by laboratory bleaching using UV lamps (or by using daylight) and used to define the zero point of the dose response curve (WINTLE & HUNTLEY 1979). This total bleach approach assumes that all light-sensitive TL is removed from the grains during transportation and this has been investigated by plotting palaeodose versus TL-temperature for the samples investigated (the so-called plateau test). It has been demonstrated that partial bleaching is of minor importance for loess that has been deposited by aeolian processes but can be relevant for re-worked loess.

A frequent problem has been a systematic underestimation of TL (e.g., ZHOU et al. 1995), the reason for which is not fully understood. This may be related in part to the use of UV filters for luminescence detection, which allow an unstable UV emission from feldspathic minerals to be transmitted. However, as many other studies have provided dates consistent with independent age control and geological time models it also became evident that the application of luminescence (both TL and optical stimulation) is apparently restricted to the last glacial cycle (i.e. the last 130 ka). A comprehensive review of the work carried out in the 1980-90s is provided by SINGHVI et al. (2001).

More recently, single-aliquot methodology, in particular for quartz, has been applied to loess to improve both the precision and reliability of the chronology as well as to extend the datable age range. ZANDER et al. (2000) compared single-aliquot sand-size quartz OSL and multiple-aliquot silt-size polymineral IRSL and TL on samples from a site in Czech Republic. They found good consistency for the different methods but higher precision of the quartz ages. WATANUKI et al. (2005) dated a loess sequence in Japan applying the SAR methodology on quartz and polymineral fine-grain extracts. They produced reliabile quartz ages as old as 500 ka with independent age control from tephra chronology. Polymineral fine-grain ages, which have been measured using the UV emission band, are underestimated by 10-20 % in this study. A similar approach has been tested by WATANUKI et al. (2003) and WANG et al. (2006a) on Chinese loess and these authors also identified a systematic underestimation of polymineral ages using UV emissions. A comprehensive summary of previous work on luminescence dating of Chinese loess is provided by STEVENS et al. (2007). These authors

also conclude, using high resolution sampling for OSL dating, that loess accumulation has been episodic and not continuous during the last glacial cycle, in contrast to many previous assumptions. Buylaert et al. (2007) concluded that the SAR procedures used in their studies do not allow dating beyond the Last Interglacial, and yielded a systematic underestimation of quartz OSL ages, for example, an OSL age of 112 ± 7 ka and fading corrected IRSL age of 301 ± 30 ka for loess from below the Brunhes/Matuyama (B/M) boundary.

Present work is focusing on extending the dating range in Chinese loess by developing new measuring techniques such as red TL from quartz (Lai & Murray 2006; Lai et al. 2006) and thermally-transferred OSL (Wang et al. 2007). The latter in particular looks rather promising, with Wang et al. (2006b) reporting a mean TT-OSL age of 771 ± 15 ka for loess from the B/M boundary.

7.3.2 Aeolian sand

Due to the aeolian transport processes of saltation, raptation (creep) and suspension the sediment grains are most likely exposed to sufficient light for optical re-setting of the luminescence signal prior to burial, and so poor bleaching is rarely a problem in aeolian materials (Duller 2004). As aeolian environments provide ideal conditions for the application of luminescence dating, a vast number of dating studies on dune sands has been carried out during the past decades since Singhvi et al. (1982) published the first study on aeolian sand dunes from Rajhastan, India. Since then, luminescence dating has been used to constrain the chronology of aeolian sands in a variety of drylands such as the Kalahari (Stokes et al. 1997a; Telfer & Thomas 2007), Namib (Bristow et al. 2005, 2007), Sahara (Lancaster et al. 2002; Bubenzer et al. 2007), Sahel (Stokes et al. 2004), Arabian (Preusser et al. 2002; Stokes & Bray 2005), Taklamakan (Yang et al. 2006) and Australian (Gardner et al. 1987; Nanson et al. 1992; Twidale et al. 2001; Lomax et al. 2003; Fitzsimmons et al. 2007;) deserts. Furthermore, several studies have focussed on aeolian sand deposits in former periglacial regions such as those in the European sand belt (Dijkmans et al. 1992; Bateman 1998; Bateman & Van Huissteden 1999; Hilgers et al. 2001; Vandenberghe et al. 2004; Hilgers 2007; Kasse et al. 2007), the Pampa of Argentina (Tripaldi & Forman 2007) and in North America (Stokes et al. 1997b; Feathers et al. 2006; Forman et al. 2006).

Compared to water-lain deposits luminescence dating of aeolian sand, especially considering the recent advances in methodology (e.g. SAR protocol), is relatively straightforward as partial bleaching is not usually a major concern for such sediments. However, aeolian deposits play a major role in understanding the complexity of dose distributions and hence in improving the accuracy and precision of luminescence dating (Bateman et al. 2003; Vandenberghe et al. 2003; Lomax et al. 2007; see Section 6.4 for details). Aeolian deposits are also important in studies that have explored the possibilities of extending the minimum and maximum age limits. For example, Ballarini et al. (2007) successfully explored the potential to date dune sand as young as 10 a. Some of the oldest luminescence ages (in this case TL) ever published have been determined for stranded beach dunes from SE Australia that yielded ages as old as 800 ka (Huntley et al. 1993; Huntley & Prescott 2001). More recently, Rhodes et al. (2006) provided OSL ages of about 500 ka for aeolian deposits from Morrocco and a single age of 1 Ma, the latter being from inversely magnetised sediments attributed to the Matuyama chron. These latter two examples are, however, exceptional due to the low dose rate (< 1 mGy a^{-1}) of the investigated sediments, and saturation of the luminescence signal will be reached earlier at higher dose rates.

Dunes are complex and composite features formed during several events of deposition which may have been interrupted by episodes of erosion, and as such represent inherently discontinuous archives, which complicate the interpretation of OSL records in terms of their significance for palaeoclimate or pal-

aeoenvironmental reconstructions. Thus, any interpretation of OSL data has to be done in the context of the complete environmental system, including the effective geomorphological processes (e.g., BUBENZER et al. 2007). Various approaches are taken to minimise this problem and to optimise the value of luminescence dating results. The necessity of an increase of samples analysed per dune as well as the investigation of several dunes within a dune field to obtain not only detailed but informative records of aeolian processes in a certain area have been demonstrated for example by TELFER & THOMAS (2007) and HILGERS (2007). The combination of ground-penetrating radar (GPR) and OSL dating provides a powerful tool to reveal the dynamic history of dunes. Based on the GPR profiles of the internal structure of the dunes sampling locations for OSL dating can be determined (e.g., BRISTOW et al. 2007).

7.3.3 Fluvial deposits

Most of the early studies using TL for dating fluvial and other water-lain sediments revealed age overestimations due to incomplete bleaching of the signal prior to deposition (e.g., FORMAN et al. 1988). With the advent of OSL methodology the dating of waterlain sediments was reconsidered, but took nearly a decade from the breakthrough publication of HUNTLEY et al. (1985) to the first systematic studies on dating waterlain deposits. For example, PERKINS & RHODES (1994) used multiple-aliquot methodology to date sandy River Thames sediments and achieved a good consistency with independent age control. Nevertheless, up to the late 1990s fluvial and in particular glaciofluvial sediments (see section 7.3.6) have been considered rather challenging and the reliability of optical dating of such deposits has been considered questionable at least.

However, it has been the dating of fluvial deposits that led to a major improvement in luminescence methodology with the development of single aliquot techniques (see section 5.3.2). One of the pioneering studies was that of MURRAY et al. (1995) who investigated submodern fluvial sediments from Australia using a modified version of the so-called SARA protocol (MEJDAHL & BØTTER-JENSEN 1994), a technique that is only infrequently used nowadays. The study by MURRAY et al. (1995) was the first in which a large number (>100) of individual palaeodose values were calculated for individual samples. As already indicated by DULLER (1994), it was demonstrated that samples not fully zeroed consist of a mixture of grains having a different degree of bleaching, including grains that have been completely bleached at deposition. Hence, the scatter of several individual palaeodose values will be broad and positively skewed for incompletely bleached samples, and tight and normally distributed for well-bleached samples (cf., OLLEY et al. 1998, 1999). A comprehensive review on the problems and potential of optical dating of fluvial deposits has been provided by WALLINGA (2002a) and the following discussion will concentrate on a few aspects only.

As a major concern has always been the degree of resetting of the optical signal prior to deposition, several studies have investigated the resetting of modern analogues. For example, STOKES et al. (2001) observed a monotonic decrease of apparent palaeodose in modern deposits of the River Loire downstream from the source, with values close to zero for transport distances of more than 300 km. Consequently, STOKES et al. (2001) concluded that the resetting of the OSL signal in a large drainage basin is much more likely than considered from many earlier studies. This assertion was later confirmed by SINGARAYER et al. (2005) who identified different resetting for individual components of the OSL signal. FUCHS et al. (2005) investigated the degree of zeroing in deposits of the 2002 millennium flood in Saxony and compared quartz and feldspar signals. These authors observed residual ages of 0.14-0.45 ka for silt-size quartz and 1.12-4.00 ka for polymineral fine-grains for samples from the River Elbe. For the River Rote Weißeritz, where sand-size grains have been investigated, residual ages of 0.36-0.83 ka for quartz and 2.12-4.67 ka for feldspar have been calculated. Similar low residual quartz OSL ages are reported for mod-

ern deposits of River Ahr in western Germany (Choi et al. 2007). On the other hand, Fiebig & Preusser (2007) observed rather high residual ages in some of the young deposits of the River Danube, parts of which were deposited by the floods in 2002. For some of these samples residual ages are as high as several 10 ka. However, these exceptional values are probably the result of an artificial input of sediment to prevent riverbed erosion.

During the last decade OSL dating has been applied to the reconstruction of the fluvial history in several regions, both in large drainage systems such as River Rhine (e.g., Wallinga et al. 2004, 2007; Busschers et al. 2005; Schokker et al. 2005), Loire (Colls et al. 2001) and Mississippi (Rittenour et al. 2005) as well as small scale catchments, for example, in Lincolnshire, England (Briant et al. 2004) or the Klip River, South Africa (Rodnight et al. 2006). Besides work in the middle latitudes, luminescence dating has also frequently been applied to date fluvial dynamics in the semi-arid subtropics in regions such as the Chad Basin (Gumniour & Preusser 2007), Death Valley (Sohn et al. 2007) and, in particular, on the Indian Subcontinent (e.g., Juyal et al. 2000; Jain & Tandon 2003).

7.3.4 Hillslope deposits

The term hillslope deposits describes sediments that are eroded from and transported along hillslopes by running water or gravity and that usually form wedge-shaped deposits on the foot-slope. Such deposits are often referred to as colluvium although the term is inconsistently used by different researchers. First successful studies on dating colluvial samples were carried out by Forman et al. (1988) on colluvium from the US using TL. Later, Wintle et al. (1993) and Botha et al. (1994) applied IRSL dating to sediments from South Africa. Detailed reviews on dating hillslope deposits are provided by Lang et al. (1999) and Fuchs & Lang (2008).

The major limitation in dating hillslope deposits is incomplete bleaching of the luminescence signal, due to the fact that several processes are involved in the formation of hillslope deposits such as soil erosion (ploughing, sheet and rill erosion), mass movements (sliding, falling) and soil creep (e.g. solifluction). Many of these processes cause downslope movement of sediment as a rather compact block such as in the case of sliding. Hence, with respect to daylight bleaching, only a small fraction of the sediment in the colluviation process (i.e. only the outer layer of sediment grain on a rigid block) will be exposed to daylight. If material is transported by water (e.g., sheet erosion), the intensity and spectral composition of the daylight is subdued by the usually high suspended load (Ditlefsen 1992). Another problem is related to coagulation of grains that hampers sufficient zeroing of the luminescence signal, because the inner grains of an aggregate are shielded from daylight exposure (Lang & Wagner 1996). Furthermore, due to the usually rather small catchments of colluvial systems sediment transport distance tends to be relatively small, decreasing the probability of efficient bleaching as the duration of light exposure will be relatively short.

Despite these shortcomings, there are many examples of successful luminescence dating of colluvium, which might be explained by two controlling factors. Firstly, hillslope deposits are usually repeatedly reworked, which increases the probability of daylight exposure. Secondly, bioturbation and mechanical processes in the soil as well as cultivation ensure that mineral grains are frequently exposed to daylight before the sediment grains are eroded and transported. Nevertheless, investigating the degree of bleaching prior to deposition, as described in section 6.1, is a fundamental requirement in dating colluvial deposits.

Although luminescence dating of hillslope deposits is rather challenging, it has been applied to a variety of case studies worldwide. The first systematic study by Wintle et al. (1993) and Botha et al. (1994) correlated sediments and soils with dryer or wetter climatic periods of the Late Quaternary in South Africa and describe in detail the complexity of slope evolution processes. Similar studies have been car-

ried out by, for example, CLARKE et al. (2003) in the UK and ERIKSSON et al. (2000) in Tanzania. Another application of dating hillslope deposits was in the context of palaeoseismicity research as vertical displacement along faults scarp leads to its erosional degradation. This potential was first explored by PORAT et al. (1996) on colluvial sediments associated with fault scarp activities for estimating seismic hazards. These authors established an earthquake chronology with four large earthquakes for the period 37 – 14 ka and five smaller earthquakes more recently. PORAT et al. (1997) confirmed the suitability of luminescence dating in palaeoseismic research but PORAT et al. (2001) found a slope-face dependency for the bleaching degree of colluvial sediments, with colluvial sediments from south-facing scarps being better bleached than colluvium derived from north-facing scarps. Studies in a similar context have been provided by LU et al. (2002) for China and FATTAHI et al. (2006) for Iran.

Increased sediment transport down-slope can also be induced by human activity, in particular during the Holocene. Widespread clearance of woodlands and associated soil erosion typically causes increased erosion along hillslopes, for example, when humans established permanent settlements and agriculture. Among the first studies was that by LANG (1994) who investigated colluvial sediments derived from a loess-covered landscape in southwest Germany, and this was followed by similar studies (e.g., KADEREIT et al. 2002). A frequency distribution of IRSL ages from the area revealed that increased colluviation coincides with phases of higher population density and show that the intensity of farming activities is the main trigger for soil erosion (LANG 2003). In a study in Greece, FUCHS et al. (2004) and FUCHS & WAGNER (2005) applied the SAR protocol to the quartz coarse grain fraction for reconstructing Holocene soil erosion and to elucidate the interaction of humans and environment since Neolithic times. Colluviation strongly fluctuated in the course of the Holocene, with a sharp increase during the Early Neolithic and the onset of agricultural activities. Further periods of increased deposition of hillslope sediments are the Middle and Late Bronze Age, the Roman period and the period since the sixteenth century AD (FUCHS 2007). Similar studies have been carried out, for example, in Romania (KADEREIT et al. 2006) and in Belgium (ROMMENS et al. 2007)

7.3.5 Lacustrine sediments

Relatively few studies have been reported on attempts to date lacustrine sediments, although such deposits are important archives of past environmental change and hence relevant for reconstructing Quaternary climate history. Early work by KRONBORG (1983) and BERGER (1990) studied the amount of resetting of TL in modern sediments and on dating deposits of known age. Both studies have highlighted the potential as well as the limitations of TL. With the introduction of OSL new dimensions were added to the dating of water-lain sediment due to the higher bleachability of the optical signal (HUNTLEY et al. 1985). DITLEFSEN (1992) experimentally investigated the bleaching of sediment in suspension demonstrating that the optical signal is almost completely bleached in dilute suspensions within a few hours, little bleaching has been observed in dense suspensions. KRAUSE et al. (1997) used IRSL to date lake deposits from Antarctica and compared four different emission bands (280, 330, 410, 560 nm), with the inconsistent results of palaeodose (D_e) measurements being attributed to different bleaching characteristics of the different emission bands.

Late Glacial to Holocene sediments from Lake Holzmaar, Germany, gave IRSL ages consistent with varve chronology for samples with low concentrations of biogenic material. Inaccurate ages obtained for organic rich samples are explained by problems with dose rate determination (LANG & ZOLITSCHKA 2001). THOMAS et al. (2003) applied different approaches to date lacustrine deposits from Greece revealing an underestimation of polymineral fine grain IRSL and post-IR OSL UV emissions compared to quartz OSL ages and radiocarbon chronology.

It was demonstrated that the underestimation of IRSL ages was due to anomalous fading that was observed in storage tests. However, the presence of fading is probably explained by using IRSL UV emissions or by a specific geological setting at that particular site since other studies on dating lacustrine sediments using blue emissions have provided correct age estimates (Doran et al. 1999; Wolfe et al. 2000; Berger & Doran 2001; Berger et al. 2004). Vandergoes et al. (2005) dated a 150 000 year old lake record from Okarito Pakihi, New Zealand and got IRSL and post-IR OSL ages in agreement with the results of radiocarbon dating, tephra chronology and the chronological time frame deduced from comparison with pollen records from ocean sediment. Juschus et al. (2007) found SAR IRSL ages consistent with the age model proposed from several proxies tuned to regional insolation.

While all the examples given above are from humid regions in the middle to high latitudes, a few studies have used luminescence methodology to date ancient lake deposits from arid zones. The particular advantages of luminescence are that it circumvents contamination problems that often affect radiocarbon in arid environments and extends the dating range beyond the few 10 ka possible with radiocarbon. However, only very few studies have utilised this potential so far, in particular Radies et al. (2005) who dated lake deposits of the Early Holocene humid period in Oman and Armitage et al. (2007) who demonstrated that a lake occupied the Fazzan Basin, Libyan Sahara, during the Early Holocene, the Last Interglacial and probably during Marine Isotope Stage (MIS) 11.

7.3.6 Proglacial deposits

Some of the first attempts to date glaciofluvial deposits were carried out by Gemmell (1985, 1994) who investigated the resetting of the luminescence signal in modern samples. Mejdahl (1991) compared TL and radiocarbon ages of Late Glacial sediments applying different bleaching techniques. Berger & Easterbrook (1993) and Berger & Eyles (1994) dated glaciogenic and water-lain sediments from the Western Washington, British Columbia and Toronto area. Hütt & Jungner (1992) compared TL and IRSL dating of Late Glacial sediments but their results were overestimated due to partial bleaching. Duller (1994) investigated the bleaching characteristics of glaciofluvial feldspars and identified two different types of partial bleaching: one type showing grains that were incompletely bleached to the same amount (type A) and the other type showing a mixture of grains containing a majority of completely bleached grains, together with some insufficiently bleached grains (type B). He concluded that successful IRSL dating of glaciogenic sediments that were deposited only a few kilometres in front of the ice sheet is unlikely (Duller et al. 1995). Further investigations compared the resetting of TL, IRSL and OSL signals in modern and ancient fluvial and glaciofluvial sediments from Switzerland and Northern Germany (Preusser 1999c). Dating results reveal that the sediments from Switzerland were completely bleached while those from Northern Germany were not, for most samples investigated. These results were additionally supported by further investigations of Preusser (2003) and Preusser et al. (2003, 2005a). Dating glaciofluvial deposits from New Zealand showed problems due to low luminescence sensitivity of the quartz grains (Preusser et al. 2005b, 2006). Beside the problem of insufficient resetting prior to deposition, which leads to age overestimation, the influence of 'thermal transfer' as reported by Rhodes & Bailey (1997) causes an overestimation of the expected age on the investigated sediments. OSL dating of glaciogenic deposits from Northern Eurasia were presented by Larsen et al. (1999) and Svendsen et al. (2004) as well as Forman (1999), Forman et al. (1999, 2002) and Mangerud et al. (2001) implicating glacier advances during the Late Saalian, the Early Weichselian, the Middle Weichselian and the Late Weichselian. Optical dating of proglacial and glaciofluvial sediments from inneralpine valleys and the Alpine Foreland provided dif-

ferent problems with low quartz luminescence sensitivity and partial bleaching (KLASEN et al. 2006, 2007). While samples from the inneralpine valleys can be assigned to bleaching type B (DULLER 1994), incompletely bleached samples from the Alpine foreland consist of grains being reset to the same amount and are therefore assigned to type A (DULLER 1994). For these samples, calculating a mean palaeodose is challenging, and the methods of OLLEY et al. (1998) and GALBRAITH et al. (1999) which extract individual palaeodose values out of a positively skewed distribution, failed due to the fact that distributions are Gaussian. This is supported by investigations of FUCHS et al. (2007) who reported that partially bleached samples can also be represented by normal distributions. Therefore, frequency distributions should be regarded very carefully when used for the interpretation of bleaching characteristics. Additionally, quartz samples from the northern Alpine Foreland appear not to contain any 'fast component' within the OSL-signal (cf., BULUR et al. 2000). Applying SAR- methodology to these samples resulted in an underestimation of the age of the sediment as this protocol is designed for samples dominated by a 'fast component' (KLASEN 2007). DULLER (2006) investigated glaciogenic deposits from Chile and Scotland using single grain optical dating, and shoedg that grains were commonly affected by low luminescence sensitivity. Nevertheless, DULLER (2006) concluded that the single grain methodology is the method of choice to detect partial bleaching. Despite this, PREUSSER et al. (2007) determined OSL ages consistent with radiocarbon ages for proglacial sediments from Switzerland using small aliquots.

7.3.7 Coastal (water-lain) deposits

The pioneering study on dating coastal deposits was carried out by BALESCU et al. (1991) on raised interglacial beaches from the Channel Region (France, Belgium). These authors used TL from feldspars detected in the UV band and found residual ages of no more than a few ka in modern deposits. However, TL ages of older deposits were underestimated by up to 40 %. BALESCU & LAMOTHE (1992) later demonstrated that ages consistent with stratigraphy are obtained when blue TL emissions are used for dating. The same authors calculated a minimum age of 271 ± 36 ka for the marine Herzeele Formation in northern France that is interpreted as being of Holsteinian age (BALESCU & LAMOTHE 1993). The first applications of IRSL to coastal sediments reveal a good consistency with TL and independent age control (BALESCU & LAMOTHE 1994; BALESCU et al. 1997). In another early study, MAUZ et al. (1997) used TL from quartz separates to date littoral deposits from southern Italy revealing that eustatic oscillations deduced from a deep ocean sediment proxy are not completely recorded within the inner shelf deposits. MAUZ & HASLER (2000) found evidence from both feldspar IRSL and quartz TL dating for relatively high sea-level (-15 m) during early MIS 3 (ca. 50 ka ago) in the Mediterranean although this is inconsistent with that from the Huon Peninsular of New Guinea.

While the studies summarised above used multiple-aliquot approaches, more recent studies have used single-aliquot methodology. RICHARDSON (2001) investigated the degree of resetting in modern intertidal deposits from England and Wales revealing substantial residual ages in many of the samples, especially for those deposited by turbid water suspension. The author also highlights the potential problem associated with estimating the correct average water content during burial for samples from such environments. HONG et al. (2003), however, found clear evidence for complete bleaching of sub-modern tidal-flat deposits from Korea and report ages between 40-120 a. Excellent consistency of OSL and ^{210}Pb as well as ^{137}Cs dating of sub-modern estuarine sediments from Denmark has been shown by MADSEN et al. (2005, 2007) with OSL ages ranging from a few years to about 1000 a. The age of near-surface samples in one core is 9 ± 3 a and 7 ± 4 a in another, indicating that partial bleaching does not apparently have any major affect in such environments. The applicability

of OSL for dating young tidal flat deposits has also been demonstrated for the Frisian Coast, Germany, where age control is available from radiocarbon dating of peat (Mauz & Bungenstock 2007). Zander et al. (2007) showed that Holocene coastal sediments from the Persian Gulf that are affected by radioactive disequilibrium in the Uranium decay chain due to high amounts of calcareous material (shell debris etc.) can still be correctly dated using OSL.

Murray & Funder (2003) dated several samples from an Eemian site in Denmark to test the accuracy of OSL dating. Although the mean age of the individual samples is 119 ± 6 ka including systematic uncertainties and, hence, in acceptable agreement with the expected age of the sediment (128-132 ka), there is a suggestion that OSL may systematically underestimate the true age by about 10 % percent. This question has been addressed by Murray et al. (2007) who dated an Eemian site in northern Russia consisting of foreshore marine deposits with an expected age of about 130 ka. The mean of 16 OSL ages determined for this deposit was 112 ± 7 ka (including systematic uncertainties) showing a similar underestimation to that of the site in Denmark. The authors discuss several possible explanations for the apparent underestimation of OSL ages, among which are changes in sensitivity of the natural signal at the beginning of the SAR procedure, which is not corrected for, contamination of the stable fast component of the OSL signal by less-stable components as well as open system radionuclide behaviour and inaccurate estimates of long-term water content.

7.3.8 Deep sea sediments

One of the first applications of TL dating on sediments was on deep ocean deposits (Wintle & Huntley 1979, 1980; Berger et al. 1984). More recently, Stokes et al. (2003) used SAR methodology on silt-size quartz gathered from two cores from the Arabian Sea where age control is provided by radiocarbon, tephrachronology and a correlative marine-proxy age model. The investigated silt is interpreted as dust input from the Arabian Peninsula transferred by aeolian processes into the ocean. In this study, particular attention was paid to radioactive disequilibria that are a major potential error source in dating deep ocean sediments. The nine OSL ages obtained by Stokes et al. (2003) are, with one exception, in good agreement with independent age control and demonstrate the potential of OSL to date deep ocean sediments. Olley et al. (2004) applied sand-size single-grain quartz for dating a core off the NW Australian coast, and these authors also found good consistency of OSL with radiocarbon ages but highlight that partial bleaching may be important, even for grains that underwent long distance aeolian transport. Berger (2006) carried out a test study on a variety of cores from the Arctic Ocean and found varying levels of signal resetting in different regions. Using a new technique enabled correct dates for the Late Holocene deposits to be established. This study demonstrated the potential but also highlighted the problems associated with dating samples from the Arctic Ocean, which are probably related to sediment input through glacial transport (e.g., ice raft). Kortekaas et al. (2007) dated a core covering the last 15 ka from the Arkona Basin, Baltic Sea, using fine-sand quartz (63-100 μm). These authors observed a good agreement between OSL and radiocarbon age from bivalve mollusc shells, although radiocarbon ages on bulk sediment samples were between 1000 and 3000 a higher than OSL and bivalve ages. The incorporation of reworked material in the bulk samples is suggested as the cause for overestimation.

8 Summary and outlook

Luminescence dating allows the dating of mineral crystallisation, heating to a few 100°C or the last daylight exposure of sediment grains. It covers the time range from a few years or decades up to several hundred-thousand years. Luminescence dating represents a suite of related techniques, all of which provide an estimate of radiation history due to accumulation of trapped charges in mineral lattices. During the last de-

cade, several methods have been developed that have considerably improved the reliability and precision of luminescence dating. It is highly recommended that information with regard to tests of quality assurance is included when publishing the results of luminescence dating.

Recent research is focusing on improved and innovative procedures of both palaeodose and dose rate determination. For palaeodose determination, it is necessary to better understand the sources of variation observed for individual palaeodose estimates determined for the same sample, especially to quantify the effect of microdosimetry. Furthermore, it is expected that it may be possible to extend the upper dating limit using approaches such as thermally-transferred OSL in quartz or by using a more stable luminescence emission, such as the red emission band of feldspars. With regard to dose rate determination, improvements in the handling of radioactive disequilibria and variation in sediment moisture may help to further improve the precision and accuracy of luminescence dating.

Acknowledgements

The authors thank Sven Lukas and Michaela Ustaszewski for their comments on earlier versions of the manuscript and in particular Sally Lowick for final language corrections..

References

ADAMIEC, G. & AITKEN, M.J. (1998): Dose-rate conversion factors: update. – Ancient TL, 16: 37-50.

AITKEN, M.J. (1985): Thermoluminescence dating. – 359 S.; London (Academic Press).

AITKEN, M.J. (1998): An introduction to optical dating. – 267 S.; Oxford (University Press).

AITKEN, M.J., REID, J. & TITE, M.S. (1964): Thermoluminescence dating of ancient ceramics. – Nature, 202: 1032.

AITKEN, M.J., ZIMMERNANN, D.W. & FLEMING, S.J. (1968): Thermoluminescence dating of ancient pottery. – Nature, 219: 442.

AITKEN, M.J. & BOWMANN, S.G.E. (1975): Thermoluminescence dating: assessment of alpha particle contribution. – Archaeometry, 17: 132-138.

ALPERSON-AFIL, N., RICHTER D. & GOREN-INBAR, N. (2007): Phantom hearths and controlled use of fire at Gesher Benot Ya'Aqov, Israel. – Paleoanthropology: 1-15.

ARMITAGE, S.J., DRAKE, N.A., STOKES, S., EL-HAWAT, A., SALEM, M., WHITE, K., TURNER, P. & MCLAREN, S.J. (2007): Multiple phases of north African humidity recorded in lacustrine sediments from the Fazzan Basin, Libyan Sahara. – Quaternary Geochronology, 2: 181-186.

AUCLAIR, M., LAMOTHE, M. & HUOT, S. (2003): Measurement of anomalous fading for feldspar IRSL using SAR. – Radiation Measurements, 37: 487-492.

BAILEY, R.M. (2003a): Paper I: The use of measurement-time dependent single-aliquot equivalent-dose estimates from quartz in the identification of incomplete signal resetting. – Radiation Measurements, 37: 673-683.

BAILEY, R.M. (2003b): Paper II: The interpretation of measurement-time-dependent single-aliquot equivalent-dose estimates using predictions from a simple empirical model. – Radiation Measurements, 37: 685-691.

BAILEY, R.M., SMITH, B.W, RHODES, E.J. (1997): Partial bleaching and the decay form characteristics of quartz OSL. – Radiation Measurements, 27: 123-136.

BAILEY, R.M., ADAMIEC, G. & RHODES, E.J. (2000): OSL properties of NaCl relative to dating and dosimetry. – Radiation Measurements, 32: 717-723.

BAILEY, R.M. & ARNOLD, L.J. (2006): Statistical modelling of single grain quartz D-e distributions and an assessment of procedures for estimating burial dose. – Quaternary Science Reviews, 25: 2475-2502.

BAILIFF, I.K. & HOLLAND, N. (2000): Dating bricks of the last two millennia from Newcastle upon Tyne: a preliminary study. – Radiation Measurements, 32: 615-619.

BALESCU, S., PACKMAN, S.C. & WINTLE, A.G. (1991): Chronological separation of interglacial raised beaches from Northwestern Europe using thermoluminescence. – Quaternary Research, 35: 91-102.

BALESCU, S. & LAMOTHE, M. (1992): The blue emission of K-feldspar coarse grains and its potential for overcoming TL age underestimation. – Quaternary Science Reviews, 11: 45-51.

BALESCU, S. & LAMOTHE, M. (1993): Thermoluminescence dating of the Holsteinian marine formation of Herzeele, northern France. – Journal of Quaternary Science, 8: 117-124.

Balescu, S. & Lamothe, M. (1994): Comparison of TL and IRSL age estimates of feldspar coarse grains from waterlain sediments. – Quaternary Science Reviews, 13: 437-444.

Balescu, S., Lamothe, M. & Lautridou, J.P. (1997): Luminescence evidence for two Middle Pleistocene interglacial events at Tourville, northwestern France. – Boreas, 26: 61-72.

Ballarini, M., Wallinga, J., Wintle, A.G. & Bos, A.J.J. (2007): Analysis of equivalent-dose distributions for single grains of quartz from modern deposits. – Quaternary Geochronology, 2: 77-82.

Baril, M.R & Huntley, D.J. (2003): Infrared stimulated luminescence and phosphorescence spectra of irradiated feldspars. – Journal of Physics: Condensed Matter, 15: 8029-8048.

Barnett, S.M. (2000): Luminescence dating of pottery from later prehistoric Britain. – Archaeometry, 42: 431-457.

Bassinet, C., Mercier, N., Miallier, D., Pilleyre, T., Sanzelle, S. & Valladas, H. (2006): Thermoluminescence of heated quartz grains: Intercomparisons between SAR and multiple-aliquot additive dose techniques. – Radiation Measurements, 41: 803-808.

Bateman, M.D. (1998): The origin and age of coversand in north Lincolnshire, UK. – Permaforst and Periglacial Processes, 9: 313-325.

Bateman, M.D. & Van Huissteden, J. (1999): The timing of last-glacial periglacial and aeolian events, Twente, eastern Netherlands. – Journal of Quaternary Science, 14: 277-283.

Bateman, M.D., Frederick, C.D., Jaiswal, M.K. & Shingvi, A.S. (2003): Investigations into the potential effects of pedoturbation on luminescence dating. – Quaternary Science Reviews, 22:1169-1176.

Bateman, M.D., Boulter, C.H., Carr, A.S., Frederick, C.D., Peter, D. & Wilder, M. (2007): Detecting post-depositional sediment disturbance in sandy deposits using optical luminescence. – Quaternary Geochronology, 2: 57-64.

Bell, W.T. (1979): Attenuation factors for the absorbed radiation dose in quartz inclusions for thermoluminescence dating. – Ancient TL, 8: 2-13.

Bell, W.T. (1980): Alpha dose attenuation in quartz grains for thermoluminescence dating. – Ancient TL, 12: 4-8.

Berger, G.W. (1990): Effectiveness of natural zeroing of the thermoluminescence in sediments. – Journal of Geophysical Research, 95: 12375-12397.

Berger, G.W. (2006): Trans-arctic-ocean tests of fine-silt luminescence sediment dating provide a basis for an additional geochronometer for this region. – Quaternary Science Reviews, 25: 2529-2551.

Berger, G.W., Huntley, D.J. & Stipp, J.J. (1984): Thermoluminescence studies on a ^{14}C-dated marine core. – Canadian Journal of Earth Science, 21: 1145-1150.

Berger, G.W. & Easterbrook, D.J. (1993): Thermoluminescence dating tests for lacustrine, glaciomarine and floodplain sediments from Western Washington and British Columbia. – Canadian Journal of Earth Sciences, 30: 1815-1828.

Berger, G.W. & Eyles, N. (1994): Thermoluminescence chronology of Toronto-area Quaternary sediments and implications for the extent of the midcontinent ice sheets(s). – Geology, 22: 31-34.

Berger, G.W. & Doran, P.T. (2001): Luminescence-dating zeroing tests in Lake Hoare, Taylor Valley, Antarctica. – Journal of Paleolimnology, 25: 519-529.

Berger, G.W., Melles, M., Banerjee, D., Murray, A.S. & Raab, A. (2004): Luminescence chronology of non-glacial sediments in Changeable Lake, Russian High Arctic, and implications for limited Eurasian ice-sheet extent during the LGM. – Journal of Quaternary Science, 19: 513-523.

Blair, M.W., Yukihara, E.G. & McKeever, S.W.S. (2005): Experiences with single-aliquot OSL procedures using coarse-grain feldspars. – Radiation Measurements, 39: 361-374.

Bonde, A., Murray, A. & Friedrich, W.L. (2001): Santorini: Luminescence dating of a volcanic province using quartz? – Quaternary Science Reviews, 20: 789-793.

Botha, G.A., Wintle, A.G. & Vogel, J.C. (1994): Episodic late Quaternary paleogully erosion in northern KwaZulu-Natal, South Africa. – Catena, 23: 327–340.

Bøtter-Jensen, L., McKeever, S.W.S. & Wintle, A.G. (2003a): Optically Stimulated Luminescence Dosimetry. – 355 S.; Amsterdam (Elsevier).

Bøtter-Jensen, L., Andersen, C.E., Duller, G.A.T. & Murray, A.S. (2003b): Developments in radiation, stimulation and observation facilities in luminescence measurements. – Radiation Measurements, 37: 535-541.

Brennan, B.J. (2003): Beta doses to spherical grains. – Radiation Measurements, 37: 299-303.

Brennan, B.J., Lyons, R.G. & Phillips, S.W. (1991): Attenuation of alpha particle track dose for

spherical grains. – Nuclear Tracks and Radiation Measurements, 18: 249-253.

BRIANT, R.M., COOPE, G.R., PREECE, R.C., KEEN, D.H., BOREHAM, K.S., GRIFFITHS, H.I., SEDDON, M.B., GIBBARD, P.L. (2004): Fluvial system response to Late Devensian (Weichselian) aridity, Baston, Lincolnshire, England. – Journal of Quaternary Science, 19: 479-495.

BRISTOW, C.S, LANCASTER, N. & DULLER, G.A.T. (2005): Combining ground penetrating radar surveys and optical dating to determine dune migration in Namibia. – Journal of the Geological Survey, London, 162: 315-321.

BRISTOW, C.S., DULLER, G.A.T. & LANCASTER, N. (2007): Age and lateral migration of linear dunes in the Namib Desert. – Geology, 35: 555-558.

BUBENZER, O., BESLER, H. & HILGERS, A. (2007): Filling the gap: OSL data expanding ^{14}C Chronologies of Late Quaternary Environmental Change in the Libyan Desert. – Quaternary International, 175: 41-52.

BULUR, E. (1996): An alternative technique for optically stimulated luminescence (OSL) experiment. – Radiation Measurements, 26: 701-709.

BULUR, E., BØTTER-JENSEN, L. & MURRAY, A.S. (2000): Optically stimulated luminescence from quartz measured using linear modulation technique. – Radiation Measurements, 32: 407-411.

BUSSCHERS, F.S., WEERTS, H.J.T., WALLINGA, J., KASSE, C., DE WOLF, H. & COHEN, K.M. (2005): Sedimentary architecture and optical dating of Middle and Late Pleistocene Rhine-Meuse deposits – fluvial response to climate change, sea-level fluctuations and glaciation. – Netherlands Journal of Geosciences (Geologie en Mijnbouw), 84: 25-41.

BUYLAERT, J.P., MURRAY, A.S., HUOT, S., VRIEND, M.G.A., VANDENBERGHE, D., DE CORTE, F. & VAN DEN HAUTE, P. (2006): A comparison of quartz OSL and isothermal TL measurements on Chinese loess. – Radiation Protection Dosimetry, 119: 474-478.

BUYLAERT, J.P., VANDENBERGHE, D., MURRAY, A.S., HUOT, S., DE CORTE, F. & VAN DEN HAUTE, P. (2007): Luminescence dating of old (> 7 ka) Chinese loess: A comparison of single-aliquot OSL and IRSL techniques. – Quaternary Geochronology, 2: 9-14.

CARMICHAEL, L.A., SANDERSON, D.C.W. & NIRIAIN, S. (1994): Thermoluminescence measurement of calcite shells. – Radiation Measurements, 23: 455-463.

CHEN, R. & MCKEEVER, S.W.S. (1997): Theory of Thermoluminescence and related phenomena. – 576 S.; Singapore (World Scientific Singapore).

CHOI, J.H., MURRAY, A.S., CHEONG, C.-S., HONG, D.G. & CHANG, H.W. (2006a): Estimation of equivalent dose using quartz isothermal TL and the SAR procedure. – Quaternary Geochronology, 1: 101-108.

CHOI, J.H., DULLER, G.A.T. & WINTLE, A.G. (2006b): Analysis of quartz LM-OSL curves. – Ancient TL, 24: 9-20.

CHOI, S.-W., PREUSSER, F. & RADTKE, U. (2007): Dating of river Rhine Lower Terrace sediments from the Middle Rhine area, Germany. – Quaternary Geochronology, 2: 137-142.

CLARKE, M.L. & RENDELL, H.M. (2003): Late Holocene dune accretion and episodes of persistent drought in the Great Plains of Northeastern Colorado. – Quaternary Science Reviews, 22: 1051-1058.

CLARKE, M.L., VOGEL, J.C., BOTHA, G.A. & WINTLE, A.G. (2003): Late Quaternary hillslope evolution recorded in eastern South African colluvial badlands. – Palaeogeography, Palaeoclimatology, Palaeoecology, 197: 199-212.

COLLS, A.E., STOKES, S., BLUM, M. & STRAFFIN, E. (2001): Ag limits on the Late Quaternary evolution of the upper Loire River. – Quaternary Science Reviews, 20: 743-750.

DANIELS, F., BOYD, C.A. & SAUNDERS, D.F. (1953): Thermoluminescence as a research tool. – Science, 117: 343-349.

DEBENHAM, N.C. (1994): A guide to TL dating flint assemblages. – In: ASHTON, N. & DAVID, A. (eds) Stories in stone. Lithic Studies Society Occasional Paper 4: 4-6.

DEGERING, D. & KRBETSCHEK, M. R. (2007): Dating of Interglacial deposits by luminescence methods. – In: SIROCKO, F., CLAUSSEN, M., SANCHEZ GONI, M.F. & LITT, T. (eds.): The Climate of Past Interglacials: 157-172; Amsterdam (Elsevier).

DIJKMANS, J.W.A., VANMOURIK, J.M. & WINTLE, A.G. (1992): Thermoluminescence dating of aeolian sands from polycyclic soil profiles in the southern Netherlands. – Quaternary Science Reviews, 11: 85-92.

DITLEFSEN, C. (1992): Bleaching of K-feldspars in turbid water suspensions: A comparison of photo- and thermoluminescence signals. – Quaternary Science Reviews, 11: 33-38.

DORAN, P.T., BERGER, G.W., LYONS, W.B., WHARTON, R.A., DAVISSON, M.L., SOUTHON, J. & DIBB, J.E.

(1999): Dating Quaternary lacustrine sediments in the McMurdo Dry Valleys, Antarctica. – Palaeogeography, Palaeoclimatology, Palaeoecology, 147: 223-239.

Duller, G.A.T. (1991): Equivalent dose determination using single aliquots. – Nuclear Tracks and Radiation Measurements, 18: 371-378.

Duller, G.A.T. (1994): Luminescence dating of sediments using single aliquots: new procedures. – Quaternary Science Reviews, 13: 149-156.

Duller, G.A.T (2004): Luminescence dating of Quaternary sediments: recent advances. – Journal of Quaternary Science, 19: 183-192.

Duller, G.A.T (2006): Single grain optical dating of glacigenic deposits. – Quaternary Geochronology, 1: 296-304.

Duller, G.A.T., Wintle, A.G. & Hall, A.M. (1995): Luminescence dating and its application to key pre-late Devensian sites in Scotland. – Quaternary Science Reviews, 14: 495-519.

Duller, G.A.T., Bøtter-Jensen, L & Murray, A.S. (2000): Optical dating of single sand-sized grains of quartz: sources of variability. – Radiation Measurements, 32: 453-457.

Dütsch, C. & Krbetschek, M.R. (1997): New methods for a better internal K-40 dose rate determination. – Radiation Measurements, 27: 377-381.

Erfurt, G. (2003): Infrared luminescence of Pb^{+} centres in potassium-rich feldspars. – Physica status solidi (a), 200: 429-438.

Erfurt, G. & Krbetschek, M.R. (2003a): Studies on the physics of the infrared radioluminescence of potassium feldspar and on the methodology of its application to sediment dating. – Radiation Measurements, 37: 505-510.

Erfurt, G. & Krbetschek, M.R. (2003b): IRSAR - A single-aliquot regenerative-dose dating protocol applied to the infrared radiofluorescence (IR-RF) of coarse-grain K feldspar. – Ancient TL, 21: 25-43.

Erfurt, G., Krbetschek, M.R., Bortolot, V.J. & Preusser, F. (2003): A fully automated multi-spectral radioluminescence reading system for geochronology and dosimetry. – Nuclear Instruments and Methods in Physic Research, B 207: 487-499.

Eriksson M.G., Olley J.R. & Payton R.W. (2000): Soil erosion history in central Tanzania based on OSL dating of colluvial and alluvial hillslope deposits. – Geomorphology, 36: 107-128.

Fattahi, M. & Stokes, S. (2000): Extending the time range of luminescence dating using red TL (RTL) from volcanic quartz. – Radiation Measurements, 32: 479-485.

Fattahi, M. & Stokes, S. (2003a): Red luminescence from potassium feldspar for dating applications: a study of some properties relevant for dating. – Radiation Measurements, 37: 647-660.

Fattahi, M. & Stokes, S. (2003b): Dating volcanic and related sediments by luminescence methods: a review. – Earth Science Reviews, 62: 229-264.

Fattahi, M., Walker, R., Hollingsworth, J., Bahroudi, A., Nazari, H., Talebian, M., Armitage, S. & Stokes, S. (2006): Holocene slip-rate on the Sabzevar thrust fault, NE Iran, determined using optically stimulated luminescence (OSL). – Earth and Planetary Science Letters, 245: 673–684.

Feathers, J.K., Rhodes, E.J., Huot, S. & Mcavoy, J.M. (2007): Luminescence dating of sand deposits related to late Pleistocene human occupation at the Cactus Hill Site, Virginia, USA. – Quaternary Geochronology, 2: 167-187.

Fiebig, M. & Preusser, F. (2007): Investigating the amount of zeroing in modern sediments of River Danube, Austria. – Quaternary Geochronology, 2: 143-149.

Fitzsimmons, K.E., Bowler, J.M., Rhodes, E.J. & Magee, J.M. (2007): Relationships between desert dunes during the late quaternary in the Lake Frome region, Strzelecki Desert, Australia. – Journal of Quaternary Science, 22: 549-558.

Folz, E., Bodu, P., Bonte, P., Joron, J.L., Mercier, N. & Reyss, J.L. (2001): OSL dating of fluvial quartz from Le Closeau, a Late Paleolithic site near Paris - comparison with 14C chronology. – Quaternary Science Reviews, 20: 927-933.

Forman, S.L. (1999): Infrared and red stimulated luminescence dating of Late Quaternary near-shore sediments from Spitsbergen, Svalbard. – Arctic Antarctic and Alpine Research, 31: 34-49.

Forman, S.L., Jackson, M.E., McCalpin, J. & Maat, P. (1988): The potential of using thermoluminescence to date buried soils developed on colluvial and fluvial sediments from Utah and Colorado, U.S.A.: Preliminary results. – Quaternary Science Reviews, 7: 287-293.

Forman, S.L., Ingólfsson, O., Gataullin, V., Manley, W.F. & Lokrantz, H. (1999): Late Quaternary stratigraphy of western Yamal Peninsula, Russia: New constraints on the configuration of the Eurasian ice sheet. – Geology, 27: 807-810.

Forman, S.L., Ingólfsson, O., Gataullin, V., Manley, W.F. & Lokrantz, H. (2002): Late Quaternary stratigraphy, glacial limits and paleoenvironments of the Marresale area, western Yamal

Peninsula, Russia. – Quaternary Research, 57: 355-370.

FORMAN, S.L., SPAETH, M., MARIN, L., PIERSON, J., GOMEZ, J., BUNCH, F. & VALDEZ, A. (2006): Episodic Late Holocene dune movements on the sand-sheet area, Great Sand Dunes National Park and Preserve, San Luis Valley, Colorado, USA. – Quaternary Research, 66: 97-108.

FUCHS, M. (2007): An assessment of human versus climatic impacts on Holocene soil erosion in NE Peloponnese, Greece. – Quaternary Research, 67: 349-356.

FUCHS, M., LANG, A. & WAGNER, G.A. (2004): The history of Holocene soil erosion in the Phlious Basin, NE-Peloponnese, Greece, provided by optical dating. – The Holocene, 14: 334-345.

FUCHS, M. & WAGNER, G.A. (2005): Chronostratigraphy and geoarchaeological significance of an alluvial geoarchive: Comparative OSL and AMS 14C dating from Greece. – Archaeometry, 47: 849-860.

FUCHS, M., STRAUB, J. & ZÖLLER, L. (2005): Residual luminescence signals of recent river flood sediments: A comparison between quartz and feldspar of fine- and grain-sized sediments. – Ancient TL, 23: 25-20.

FUCHS, M., WODA, C. & BÜRKERT, A. (2007): Chronostratigraphy of a sediment record from the Hajar mountain range in the north Oman: Implications for optical dating of insufficiently bleached sediments. – Quaternary Geochronology, 2: 202-207.

FUCHS, M. & LANG, A. (2008): Luminescence dating of hillslope deposits - a review. – Geomorphology. (in press).

GALBRAITH, R.F., ROBERTS, R.G., LASLETT, G.M., YOSHIDA, H. & OLLEY, J.M. (1999): Optical dating of single and multiple grains of quartz from Jinmium Rock Shelter, Northern Australia: Part 1, Experimental design and statistical models. – Archaeometry, 41: 339-364.

GALBRAITH, R.F., ROBERTS, R.G. & YOSHIDA, H. (2005): Error variation in palaeodose estimates from single aliquots of quartz: a fractorial experiment. – Radiation Measurements, 39: 289-307.

GANZAWA, Y., FURUKAWA, H., HASHIMOTO, T., SANZELLE, S., MIALLIER, D. & PILLEYRE, T. (2005): Single grains dating of volcanic quartz from pyroclastic flows using Red TL. – Radiation Measurements, 39: 479-487.

GARDNER, G.J., MORTLOCK, A.J., PRICE, D.M., READHEAD, M.L. & WASSON, R.J. (1987): Thermoluminescence and radiocarbon dating of Australian desert dunes. – Australian Journal of Earth Sciences, 34: 343-357.

GEMMELL, A.M.D. (1985): Thermoluminescence dating of glacially transported sediments: Some considerations. – Quaternary Science Reviews, 7: 227-285.

GEMMELL, A.M.D. (1994): Environmental controls on the TL age of modern (zero-age) proglacial outwash sediments. – Quaternary Science Reviews, 13: 485-489.

GEYH, M.A. (2005): Handbuch der physikalischen und chemischen Altersbestimmung. – Wissenschaftliche Buchgesellschaft, Darmstadt, 211 S.

GEYH, M.A. (2008): The handling of numerical ages and their random errors. – Quaternary Science Journal (Eiszeitalter & Gegenwart), 57/1-2: 239–252.

GODFREY-SMITH, D.I., HUNTLEY, D.J. & CHEN, W.H. (1988): Optical dating studies of quartz and feldspar sediment extracts. – Quaternary Science Reviews, 7: 373-380.

GODFREY-SMITH, D.I. & SHALEV, S. (2002): Determination of usage and absolute chronology of a pit feature at the Ashkelon Marina, Israel. – Geochronometria, 21: 163-166.

GOEDICKE, C. (2003): Dating historical calcite mortar by blue OSL: results from known age samples. –Radiation Measurements, 37: 409-415.

GREILICH, S. (2004): Über die Datierung von Gesteinsoberflächen mittels optisch stimulierter Lumineszenz. – Dissertation Universität Heidelberg: 143 S.

GREILICH, S., GLASMACHER, U.A. & WAGNER, G.A. (2002): Spatially resolved detection of luminescence: a unique tool for archaeochronometry. – Naturwissenschaften, 89: 371-375.

GREILICH, S. & WAGNER, G.A. (2006): Development of a spatially resolved dating technique using HR-OSL. – Radiation Measurements, 41: 738 – 743.

GREILICH, S., GLASMACHER, U.A. & WAGNER, G.A. (2005): Optical dating of granitic stone surfaces. – Archaeometry, 47: 645-665.

GREILICH, S., HARNEY, H.-L., WODA, C. & WAGNER, G.A. (2006): AgesGalore – a software program for evaluating spatially resolved luminescence data. – Radiation Measurements, 41: 726-735.

GRÖGLER, N., HOUTERMANS, F.G. & STAUFFER, H. (1958): Radiation damage as a research tool for geology and prehistory. – 5a Rass Internazion Elettr Nucl Sezione Nucleare Rome: 5-15.

GUMNIOR, M. & PREUSSER, F. (2007): Late Quaternary river development in the southwestern Chad Ba-

sin: Luminescence chronology from the Komadugu palaeofloodplain (NE-Nigeria). – Journal of Quaternary Science, 22: 709-719.

Haustein, M., Roewer, G., Krbetschek, M.R. & Pernicka, E. (2003): Dating archaeometallurgical slags using thermoluminescence. – Archaeometry, 44: 519-530.

Hilgers, A. (2007): The chronology of Late Glacial and Holocene dune development in the northern Central European lowland reconstructed by optically stimulated luminescence (OSL) dating. – PhD. Thesis University of Cologne: 353 S., URN: urn:nbn:de:hbz:38-21788, URL: http://kups.ub.uni-koeln.de/volltexte/2007/2178.

Hilgers, A., Murray, A.S., Schlaak, N. & Radtke, U. (2001): Comparison of quartz OSL protocols using lateglacial and Holocene dune sands from Brandenburg, Germany. – Quaternary Science Reviews, 20: 731-736.

Hong, D.G., Yi, S.B., Galloway, R.B., Tsuboi, T. & Hashimoto, T. (2001): Optical dating of archaeological samples using a single aliquot of quartz stimulated by blue light. – Journal of Radioanalytical and Nuclear Chemistry, 247: 179-184.

Hong, D.G., Choi, M.S., Han, J.-H. & Cheong, C.-S. (2003): Determination of sedimentation rate of recently deposited tidal flat, western coast of Korea, using IRSL dating. – Quaternary Science Reviews, 22: 1185-1189.

Huntley, D.J., Godfrey-Smith, D.I. & Thewalt, M.L.W. (1985): Optical dating of sediments. – Nature, 313: 105-107.

Huntley, D.J., Hutton, J.T. & Prescott, J.R. (1993): The stranded beach dune sequence of south-east Australia – A test of thermoluminescence dating, 0-800 ka. – Quaternary Science Reviews, 12: 1-20.

Huntley, D.J. & Prescott, J.R. (2001): Improved methodology and new thermoluminescence ages for the dune sequence in south-east South Australia. – Quaternary Science Reviews, 20: 687-699.

Huntley, D.J. & Lamothe, M. (2001): Ubiquity of anomalous fading in K-feldspars and the measurement and correction for it in optical dating. – Canadian Journal of Earth Sciences, 38: 1093-1106.

Huot, S., Buylaert, J.-P. & Murray, A.S. (2006): Isothermal thermoluminescence signals from quartz. – Radiation Measurements, 41: 796-802.

Hütt, G., Jaek, I. & Tchonka, J. (1988): Optical dating – K-feldspars optical-response stimulation spectra. – Quaternary Science Reviews, 7: 381-385.

Hütt, G. & Jaek, J. (1989): Infrared stimulated photoluminescence dating of sediments. – Ancient TL, 7: 48-51.

Hütt, G. & Jungner, H. (1992): Optical and TL dating on glaciofluvial sediments. – Quaternary Science Reviews, 11: 161-163.

Huxtable, J., Aitken, M.J. & Bonhommet, N. (1978): Thermoluminescence dating of sediment baked by lava flows of Chaine des Puy. – Nature, 275: 207-209.

Hwang, F.S.W. (1970): Thermoluminescence dating applied to volcanic lava. – Nature, 227: 940-941.

Ichikawa, Y. & Nagatomo, T. (1978): Thermoluminescence dating of burnt sandstones from Senpukuji Cave. – PACT, Revue du groupe européen d'études pour les techniques physiques, chimiques et mathématiques appliquées à l'archéologie, 2: 165-174.

Jacobs, Z., Duller, G.A.T. & Wintle, A.G. (2003a): Optical dating of dune sand from Blombos Cave, South Africa: I - multiple grain data. – Journal of Human Evolution, 44: 599-612.

Jacobs, Z., Duller, G.A.T. & Wintle, A.G. (2003b): Optical dating of dune sand from Blombos Cave, South Africa: II - single grain data. – Journal of Human Evolution, 44: 613-625

Jain, M. & Tandon, S.K. (2003): Fluvial response to Late Quaternary climate changes, western India. – Quaternary Science Reviews, 22: 2223-2235.

Jain, M., Murray, A.S. & Bøtter-Jensen, L. (2003): Characterisation of blue-light stimulated luminescence components in different quartz samples: implications for dose measurement. – Radiation Measurements, 37: 441-449.

Jain, M., Bøtter-Jensen, L., Murray, A.S., Denby, P.M., Tsukamoto, S. & Gibling, M.R. (2005): Revisiting TL: dose measurement beyond the OSL range using SAR. – Ancient TL, 23: 9-24.

Juschus, O. Preusser, F., Melles, M. & Radtke, U. (2007): Applying SAR-IRSL methodology for dating fine-grain sediments from Lake El'gygytgyn, northeastern Siberia. – Quaternary Geochronology, 2: 187-194.

Juyal, N., Raj, R., Maurya, D.M., Chamyal, L.S. & Singhvi, A.K. (2000): Chronology of Late Pleistocene environmental changes in the lower Mahi basin, western India. – Journal of Quaternary Science, 15: 501-508.

Kadereit, A., Lang, A., Müth, J., Hönscheidt, S. & Wagner, G.A. (2002): IR-OSL-dated colluvial sediments as a key to Holocene landscape re-

construction. Case studies from SW-Germany. – Zeitschrift für Geomorphologie N.F., 128: 191-207.

KADEREIT, A., SPONHOLZ, B., RÖSCH, M., SCHIER, W., KROMER, B. & WAGNER, G.A. (2006): Chronology of Holocene environmental changes at the tell site of Uivar, Romania, and its significance for late Neolithic tell evolution in the temperate Balkans. – Zeitschrift für Geomorphologie N.F., 142: 19-45.

KASSE, C., VANDENBERGHE, D., DE CORTE, F. & VAN DEN HAUTE, P. (2007): Late Weichselian fluvio-aeolian sands and coversands of the type locality Grubbenvorst (southern Netherlands): sedimentary environments, climate record and age. – Journal of Quaternary Science, 22: 695-708.

KLASEN, N. (2007): Lumineszenzdatierung glazifluvialer Sedimente im nördlichen Alpenvorland. – PhD. Thesis University of Cologne: 210 S., URL: http://kups.ub.uni-koeln.de/volltexte/2008/2293.

KLASEN, N., FIEBIG, M., PREUSSER F. & RADTKE, U. (2006): Luminescence properties of glaciofluvial sediments from the Bavarian Alpine Foreland. – Radiation Measurements, 41: 866-870.

KLASEN, N., FIEBIG, M., PREUSSER F., REITNER, J.M. & RADTKE, U. (2007): Luminescence dating of proglacial sediments from the Eastern Alps. – Quaternary International, 164/165: 21-32.

KORTEKAAS, M., MURRAY, A.S., SANDGREN, P. & BJÖRK, S. (2007): OSL chronology for a sediment core from the southern Baltic Sea: A continuous sedimentation record since deglaciation. – Quaternary Geochronology, 2: 95-101.

KRAUSE, W.E., KRBETSCHEK, M.R. & STOLZ, W. (1997): Dating of Quaternary lake sediments from the Schirmacher oasis (east Antarctica) by infrared stimulated luminescence (IRSL) detected at the wavelength of 560 nm. – Quaternary Science Reviews, 16: 387-392.

KRONBORG, C. (1983): Preliminary results of age determination by TL of interglacial and interstadial sediment. – PACT journal, 9: 595-605.

KRBETSCHEK, M.R., RIESER, U., ZÖLLER, L. & HEINICKE, J. (1994): Radioactive disequilibria in palaeodosimetric dating of sediments. – Radiation Measurements, 23: 485-489.

KRBETSCHEK, M.R., GÖTZE, J., DIETRICH, A. & TRAUTMANN, T. (1997): Spectral information from minerals relevant for luminescence dating. – Radiation Measurements, 27: 695-748.

KRBETSCHEK, M.R. & TRAUTMANN, T. (2000): A spectral radioluminescence study for dating and dosimetry. – Radiation Measurements, 32: 853-857.

KRBETSCHEK, M. R., TRAUTMANN, T., DIETRICH, A. & STOLZ, W. (2000): Radioluminescence dating of sediments: methodological aspects. – Radiation Measurements, 32: 493-498.

KRBETSCHEK, M.R., DEGERING, D. & ALEXOWSKY, W. (2008): Infrarot-Radiofluoreszenz-Alter (IR-RF) unter-saalezeitlicher Sedimente Mittel- und Ostdeutschlands. – Zeitschrift der Deutschen Gesellschaft für Geowissenschaften, 109 (in press).

LAI, Z.P. & MURRAY, A. (2006): Red TL of quartz extracted from Chinese loess: Bleachability and saturation dose. – Radiation Measurements, 41: 836-840.

LAI, Z.P., MURRAY, A.S., BAILEY, R.M., HUOT, S. & BØTTER-JENSEN, L. (2006): Quartz red TL SAR equivalent dose overestimation for Chinese loess. – Radiation Measurements, 41: 114-119.

LAMOTHE, M., AUCLAIR, M., HAMZAOUI C. & HUOT, S. (2003): Towards a prediction of long-term anomalous fading of feldspar IRSL. – Radiation Measurements, 37: 493-498.

LANCASTER, N., KOCUREK, G., SINGHVI, A., PANDEY, V., DEYNOUX, M., GHIENNE, J.F. & LO, K. (2002): Late Pleistocene and Holocene dune activity and wind regimes in the western Sahara Desert of Mauritania. – Geology, 30: 991-994.

LANG, A. (1994): Infra-red stimulated luminescence dating of Holocene reworked silty sediments. – Quaternary Science Reviews, 13: 525-528.

LANG, A. (2003): Phases of soil erosion-derived colluviation in the loess hills of Southern Germany. – Catena, 51: 209-221.

LANG, A. & WAGNER, G.A. (1996): Infrared stimulated luminescence dating of archaeosediments. –Archaeometry, 38: 129-141.

LANG, A. & HÖNSCHEIDT, S. (1999): Age and source of colluvial sediments at Vaihingen-Enz, Germany. –Catena, 38: 89-107.

LANG, A., MOYA, J., COROMINAS, J., SCHROTT, L. & DIKAU, R. (1999): Classic and new dating methods for assessing the temporal occurrence of mass movements. – Geomorphology, 30: 33-52.

LANG, A. & ZOLITSCHKA, B. (2001): Optical dating of annually laminated lake sediments: A test case from Holzmaar/Germany. – Quaternary Science Reviews, 20: 737-742.

LARSEN, E., LYSÅ, A., DEMIDOV, I., FUNDER, S., HOUMARK-NIELSEN, M., KJAER, K.H. & MURRAY, A.S. (1999): Age and extent of the Scandinavian ice sheet in northwest Russia. – Boreas, 28: 115-132.

Li, S.-H. (1991): Removal of the thermally unstable signal in optical dating of K-feldspar. – Ancient TL, 9: 26-29.

Li, S.-H. & Yin, G.M. (2001): Luminescence dating of young volcanic activity in China. – Quaternary Science Reviews, 20: 865-868.

Liritzis, I. & Vafiadou, A. (2005): Dating by luminescence of ancient megalithic masonry. – Mediterranean Archaeology and Archaeometry, 5: 25-38.

Lomax, J., Hilgers, A., Wopfner, H., Grün, R., Twidale, C.R. & Radtke, U. (2003): The onset of dune formation in the Strzelecki Desert, South Australia. – Quaternary Science Reviews, 22: 1067-1076.

Lomax, J., Hilgers, A., Twidale, C.R., Bourne, J.A. & Radtke, U. (2007): Treatment of broad palaeodose distributions in OSL dating of dune sands from the western Murray Basin, South Australia. – Quaternary Geochronology, 2: 51-56.

Lu, Prescott, J.R., Hua, Z., Jie, C. & Lanying, W. (2002): Optical dating of colluvial deposits from Xiyangfang, China, and the relation to palaeo-earthquake events. – Quaternary Science Reviews, 21: 1087–1097.

Lukas, S., Spencer, J.Q.G., Robinson, R.A.J. & Benn, D.I. (2007): Problems associated with luminescence dating of Late Quaternary glacial sediments in the NW Scottish Highlands. – Quaternary Geochronology, 2: 243-248.

McKeever, S. (2001): Optically stimulated luminescence dosimetry. – Nuclear Instruments and Methods in Physics Research B, 184: 29-54.

McKeever, S. & Chen., R. (1997): Luminescence Models. – Radiation Measurements, 27: 625-661.

Madsen, A.T., Murray, A.S., Andersen, T.J., Pejrup, M. & Breuning-Madsen, H. (2005): Optically stimulated luminescence dating of young estuarine sediments: a comparison with 210Pb and 137Cs dating. – Marine Geology, 214: 251-268.

Madsen, A.T., Murray, A.S., Andersen, T.J. & Pejrup, M. (2007): Optical dating of young tidal sediments in the Danish Wadden Sea. – Quaternary Geochronology, 2: 89-94.

Mangerud, J., Astakhov,V.I., Murray, A.S. & Svendsen, J.I. (2001): The chronology of a large ice-dammed lake and the Barents–Kara Ice Sheet advances, Northern Russia. – Global and Planetary Change, 31: 321-336.

Mauz, B., Buccheri, G., Zöllerm L. & Greco, A. (1997): Middle to Upper Pleistocene morphostructural evolution of the NW-coast of Sicily: Thermoluminescence dating and palaeontological-statigraphical evaluations of littoral deposits. – Palaeogeography, Palaeoclimatology, Palaeoecology, 128: 269-285.

Mauz, B. & Hasler, U. (2000): Luminescence chronology of Late Pleistocene raised beaches in southern Italy: new data of relative sea-level changes. – Marine Geology, 170: 187-203.

Mauz, B. & Lang, A. (2004): Removal of the feldspar-derived luminescence component from polymineral fine silt samples for optical dating applications: evaluation of chemical treatment protocols and quality control procedures. – Ancient TL, 22: 1-8.

Mauz, B. & Bungenstock, F. (2007): How to reconstruct trends of late Holocene relative sea level: A new approach using tidal flat clastic sediments and optical dating. – Marine Geology, 237: 225-237.

May, R.J. (1979): Thermoluminescence dating of Hawaiian basalt. – Geological Survey Professional Paper, 1095: 47 S.

Mayya, Y.S., Mortekai, P., Murari, M.K. & Singhvi, A.K. (2006): Towards quantifying beta microdosimetric effects in single-grain quartz dose distribution. – Radiation Measurements, 41: 1032-1039.

Mejdahl, V. (1979): Thermoluminescence dating: Beta-dose attenuation in quartz grains. – Archaeometry, 21: 61-72.

Mejdahl, V. (1985): Thermoluminescence dating of partially bleached sediments. – Nuclear Tracks and Radiation Measurements, 10: 711-715.

Mejdahl, V. (1991): Thermoluminescence dating of lateglacial sand sediments. – Nuclear tracks and Radiation Measurements, 18: 71-75.

Mejdahl, V. & Bøtter-Jensen, L. (1994): Luminescence dating of archaeological materials using a new techniques based on single aliquot measurements. – Quaternary Science Reviews, 13: 551-554.

Mercier, N., Valladas, H., Bar-Yosef, O., Vandermeersch, B., Stringer, C.B. & Joron, J.-L. (1993): Thermoluminescence date for the mousterian burial site of Es-Skhul, Mt. Carmel. – Journal of Archaeological Science 20: 169-174.

Miallier, D., Condomines, M., Pilleyre, T., Sanzelle, S. & Guittet J. (2004): Concordant thermoluminescence and U-238-Th-230 ages for a trachytic dome (Grand Sarcoui) from the Chaine des Puys (French Massif Central). – Quaternary Science Reviews, 23: 709-715.

MUNYIKWA, K. (2000): Cosmic ray contribution to environmental dose rates with varying overburden thickness. – Ancient TL, 18: 27-34.

MURRAY, A.S., OLLEY, J.M. & CAITCHEON, G.G. (1995): Measurement of equivalent doses in quartz from contemporary water-lain sediments using optically stimulated luminescence. – Quaternary Science Reviews, 14: 365-371.

MURRAY, A.S. & ROBERTS, R.G. (1997): Determining the burial time of single grains of quartz using optically stimulated luminescence. – Earth and Planetary Science Letters, 152: 163-180.

MURRAY, A.S. & WINTLE, A.G. (2000): Luminescence dating of quartz using an improved single-aliquot regenerative-dose protocol. – Radiation Measurements, 33: 57-73.

MURRAY, A.S. & WINTLE, A.G. (2003): The single aliquot regenerative dose protocol: potential for improvements in reliability. – Radiation Measurements, 37: 377-381.

MURRAY, A.S. & FUNDER, S. (2003): Optically stimulated luminescence dating of a Danish Eemian coastal marine deposit: a test of accuracy. – Quaternary Science Reviews, 22: 1177-1183.

MURRAY, A.S., SVENDSEN, J.I., MANGERUD, J. & ASTAKHOV, V.I. (2007): Testing the accuracy of quartz OSL dating using a known-age Eemian site on the river Sula, northern Russia. – Quaternary Geochronology, 2: 102-109.

NANSON, G.C, CHEN, X.Y. & PRICE, D.M. (1992): Lateral migration, thermoluminescence chronology and colour variation of longitudinal dunes near Birdsville in the Simpson Desert, Central Australia. - Earth Surface Processes and Landforms, 17: 807-819.

OLLEY, J., CAITCHEON, G. & MURRAY, A.S. (1998): The distribution of apparent dose as determined by optically stimulated luminescence in small aliquots of fluvial quartz: implications for dating young sediments. – Quaternary Science Reviews, 17: 1033-1040.

OLLEY, J.M., CAITCHEON, G.G. & MURRAY, A.S. (1999): The origin of dose distribution in fluvial sediments, and the prospect of dating single grains from fluvial deposits using optically stimulated luminescence. – Radiation Measurements, 30: 207-217.

OLLEY, J.M., DE DEKKER, P., ROBERTS, R.G., FIFIELD, L.K., YOSHIDA, H. & HANCOCK, G. (2004): Optical dating of deep-sea sediments using single grains of quartz: a comparison with radiocarbon. – Sedimentary Geology, 169: 175-189.

PERKINS, N.K. & RHODES, E.J. (1994): Optical dating of fluvial sediments from Tattershall, U.K. – Quaternary Science Reviews, 13: 517-520.

POOLTON, N.R.J., BØTTER-JENSEN, L. & RINK, W.J. (1995): An optically stimulated luminescence study of flint related to radiation dosimetry. – Radiation Measurements, 24: 551-555.

PORAT, N., WINTLE, A.G., AMIT, R. & ENZEL, Y. (1996): Late Quaternary earthquake chronology from luminescence dating of colluvial and alluvial deposits of the Arava Valley, Israel. – Quaternary Research, 46: 107-117.

PORAT, N., AMIT, R., ZILBERMAN, E. & ENZEL, Y. (1997): Luminescence dating of fault-related alluvial fan sediments in the southern Arava valley, Israel. – Quaternary Science Reviews, 16: 397-402.

PORAT, N., ZILBERMAN, E., AMIT, R. & ENZEL, Y. (2001): Residual ages of modern sediments in an hyperarid region, Israel. – Quaternary Science Reviews, 20: 795-798.

PRESCOTT, J.R. & HUTTON, J.T. (1994): Cosmic ray contributions to dose rates for luminescence and ESR dating: large depths and long term variations. – Radiation Measurements, 23: 497-500.

PRESCOTT, J.R. & ROBERTSON, G.B. (1997): Sediment dating by luminescence: A review. – Radiation Measurements, 27: 893-922.

PREUSSER, F. (1999a): Bleaching characteristics of some optically stimulated luminescence signals. – Ancient TL, 17: 11-14.

PREUSSER, F. (1999b): Luminescence dating of fluvial sediments and overbank deposits from Gossau, Switzerland: fine grain dating. – Quaternary Science Reviews, 18: 217-222.

PREUSSER, F. (1999c): Lumineszenzdatierung fluviatiler Sedimente - Fallbeispiele aus der Schweiz und Norddeutschland. – Kölner Forum für Geologie und Paläontologie, 3: 63 S.

PREUSSER, F. (2003): IRSL dating of K-rich feldspars using the SAR protocol: Comparison with independent age control. – Ancient TL, 21: 17-23.

PREUSSER, F., RADIES, D. & MATTER, A. (2002): A 160,000-Year record of dune development and atmospheric circulation in Southern Arabia. – Science, 296: 2018-2020.

PREUSSER, F. & KASPER, H.U. (2001): Comparison of dose rate determination using high-resolution gamma spectrometry and inductively coupled plasma - mass spectrometry. – Ancient TL, 19: 19-23.

PREUSSER, F., GEYH, M.A. & SCHLÜCHTER, Ch. (2003): Timing of Late Pleistocene climate change in

lowland Switzerland. – Quaternary Science Reviews, 22: 1435-1445.

Preusser, F., Drescher-Schneider, R., Fiebig, M. & Schlüchter, Ch. (2005a): Re-interpretation of the Meikirch pollen record, Swiss Alpine Foreland, and implications for Middle Pleistocene chronostratigraphy. – Journal of Quaternary Science, 20: 607-620.

Preusser, F., Andersen, B.G., Denton, G.H. & Schlüchter, Ch. (2005b): Luminescence chronology of Late Pleistocene glacial deposits of North Westland, New Zealand. – Quaternary Science Reviews, 24: 2207-2227.

Preusser, F., Ramseyer, K. & Schlüchter, Ch. (2006): Characterization of low OSL intensity quartz from the New Zealand Alps. – Radiation Measurements, 41: 871-877.

Preusser F., Blei, A., Graf, H. & Schlüchter, Ch. (2007): Luminescence dating of pro-glacial sediments from Switzerland. – Boreas, 36: 130-142.

Preusser, F. & Degering, D. (2007): Luminescence dating of the Niederweningen mammoth site, Switzerland. – Quaternary International, 164-165: 106-112.

Quickert, N.A., Godfrey-Smith, D.I. & Casey, J.L. (2003): Optical and thermoluminescence dating of Middle Stone Age and Kintampo bearing sediments at Birimi, a multi-component archaeological site in Ghana. – Quaternary Science Reviews, 22: 1291-1297.

Radies, D., Hasiotis, S.T, Preusser, F., Neubert, E. & Matter, A. (2005): Paleoclimatic significance of Early Holocene faunal assemblages in wet interdune deposits of the Wahiba Sand Sea, Sultanate of Oman. – Journal of Arid Environments, 62: 109-125.

Raynal, J.P., Daugas, J.P., Paquereau, M.M., Miallier, D., Fain, J. & Sanzelle, S. (1982): 1st dating of the basaltic maar of Clermont-Ferand, Puy-de-Dome, France. – Comptes rendus de l'Academie des Sciences Serie II, 295: 1011-1014.

Rhodes, E.J. (2000): Observations of thermal transfer OSL signals in glacigenic quartz. – Radiation Measurements, 32: 595-602.

Rhodes, E.J. & Pownall, L. (1994): Teroing of the OSL signal in quartz from young glaciofluvial sediments. – Radiation Measurements, 23: 581-585.

Rhodes, E.J. & Bailey, R.M. (1997): The effect of thermal transfer on the zeroing of quartz from recent glaciofluvial sediments. – Quaternary Science Reviews, 16: 291-298.

Rhodes, E.J., Singarayer, J.S., Raynal, J.-P., Westaway, K.E. & Sbihi-Alaoui, F.Z. (2006): New age estimates for the Palaeolithic assemblages and Pleistocene succession of Casablanca, Morocco. – Quaternary Science Reviews, 25: 2569-2585.

Richardson, C.A. (2001): Residual luminescence signals in modern coastal sediments. – Quaternary Science Reviews, 20: 887-892.

Richter, D. (2007): Advantages and limitations of Thermoluminescence Dating of heated flint from Palaeolithic sites. – Geoarchaeology 22: 671-683

Richter, D., Krbetschek, M.R., Rieser, U., Trautmann, T. & Wagner, G.A. (1999) Spectral investigation of the thermoluminescence of heated flint (silex). – Quaternary Science Review, 18: 279-285.

Richter, D. & Krbetschek, M. (2006): A new Thermoluminescence dating technique for heated flint. –Archaeometry, 48: 695-705.

Richter, D., Mercier, N., Valladas, H., Jaubert, J., Brugal, J.-P., Kervazo, B., Reyss, J.L., Joron, J.L., Wagner, G.A. & Texier, P.-J. (2007): Thermoluminescence dating of heated flint from the Mousterian Site of Bérigoule, Murs, Vaucluse, France. – Journal of Archaeological Sciences, 34: 532-539.

Rittenour, T.M., Goble, R.J. & Blum, M.D. (2005): Development of an OSL chronology for Late Pleistocene channel belts in the lower Mississippi valley, USA. – Quaternary Science Reviews, 24: 2539-2554.

Roberts, R.G., Galbraith, R.F., Olley, J.M., Yoshida, H. & Laslett, G.M. (1999): Optical dating of single and multiple grains of quartz from jinmium rock shelter, northern Australia, part 2, Results and implications. – Archaeometry, 41: 365-395.

Rodnight, H., Duller, G.A.T., Wintle, A.G. & Tooth, S. (2006): Assessing the reproducibility and accuracy of optical dating. – Quaternary Geochronology, 1: 109-120.

Rommens, T., Verstraeten, G., Peeters, I., Poesen, J., Govers, G., Van Rompaey, A., Mauz, B., Packman, S. & Lang, A. (2007): Late-Holocene evolution of a dry valley in the loess region of central Belgium. – The Holocene, 9: 777-788.

Roque, C., Guibert, P., Vartanian, E., Bechtel, F. & Schvoerer, M. (2001): Thermoluminescence-dating of calcite: Study of heated limestone fragments from Upper Paleolithic Layers at Combe Sauniere, Dordogne, France. – Quaternary Science Reviews, 20: 935-938.

ROQUE, C., GUIBERT, P., VARTANIAN, E., BECHTEL, F., TREUIL, R., DARCQUE, P., KOUKOULI-CHRYSSANTHAKI, H. & MALAMIDOU, D. (2002): The chronology of the Neolithic sequence at Dikili Tash, Macedonia, Greece. TL dating of domestic ovens. – Archaeometry, 44: 613-633.

SCHILLES, T. & HABERMANN, J. (2000): Radioluminescence dating: the IR emission of feldspar. – Radiation Measurements, 32: 679-683.

SCHILLES, T., LANG, A., HABERMANN, J. & RIESER, U. (1999): Improved single aliquot dating applications using a new highly efficient modular luminescence reader. – Radiation Protection Dosimetry, 84: 363-366.

SCHOKKER, J., CLEVERINGA, P., MURRAY, A.S., WALLINGA, J. & WESTERHOFF, W.E. (2005): An OSL dated Middle and Late Quaternary sedimentary record in the Roer Valley Graben (southeastern Netherlands). – Quaternary Science Reviews, 24: 2243-2264.

SINGARAYER, J.S. & BAILEY, R.M. (2003): Further investigations of the quartz optically stimulated luminescence components using linear modulation. – Radiation Measurements, 37: 451-458.

SINGARAYER, J.S., BAILEY, R.M., WARD, S. & STOKES, S. (2005): Assessing the completeness of optical resetting of quartz OSL in the natural environment. – Radiation Measurements, 40: 13-25.

SINGHVI, A.K., SHARMA, Y.P. & AGRAWAL, D.P. (1982): Thermo-Luminescence dating of sand dunes in Rajasthan, India. – Nature, 295: 313-315.

SINGHVI, A.K. & KRBETSCHEK, M.R. (1996): Luminescence dating: A review and a perspective for arid zone sediments. – Annals of Arid Zone, 35: 249-279.

SINGHVI, A.K. & LANG, A. (1998): Improvements in infra-red dating of partially bleached sediments - the "Differential Partial Bleach Technique". – Ancient TL, 16: 63-71.

SINGHVI, A.K., BLUSZCZ, A., BATEMAN, M.D. & RAO, M.S. (2001): Luminescence dating of loess-palaeosol sequences and coversands: methodological aspects and palaeoclimatic implications. – Earth Science Reviews, 54: 193-211.

SMITH, B.W., WHEELER, G.C.W.S., RHODES, E.J. & SPOONER, N.A. (1991): Luminescence dating of zircon using an imaging photon detector. – Nuclear Tracks and Radiation Measurements, 18: 273-278.

SOHN, M.F., MAHAN, S.A., KNOTT, J.R. & BOWMAN, D.D. (2007): Luminescence ages for alluvial-fan deposits in Southern Death Valley: Implications for climate-driven sedimentation along a tectonically active mountain front. – Quaternary International, 166: 49-60.

SPOONER, N.A. (1992): Optical dating – preliminary-results on the anomalous fading of luminescence from feldspars. – Quaternary Science Reviews, 11: 139-145.

SPOONER, N.A. (1994): The anomalous fading of infrared-stimulated luminescence from feldspars. – Radiation Measurements, 23: 625-632.

STEVENS, T., THOMAS, D.S.G., ARMITAGE, S.J., LUNN, H.R. & LU, H. (2007): Reinterpreting climate proxy records from late Quaternary Chinese loess: A detailed OSL investigation. – Earth Science Reviews, 80: 111-136.

STOKES, S. (1999): Luminescence dating applications in geomorphological research. – Geomorphology, 29: 153-171.

STOKES, S., THOMAS, D.S.G. & WASHINGTON, R. (1997a): Multiple episodes of aridity in southern Africa since the last interglacial period. – Nature, 388: 154-158.

STOKES, S., KOCUREK, G., PYE, K. & WINSPEAR, N.R. (1997b): New evidence for the timing of aeolian sand supply to the Algodones dunefield and East Mesa area, southeastern California, USA. – Palaeogeography, Palaeoclimatology, Palaeoecology, 128: 63-75.

STOKES, S, BRAY, H.E. & BLUM, M.D. (2001): Optical resetting in large drainage basins: tests of zeroing assumptions using single-aliquot procedures. – Quaternary Science Reviews, 20: 879-885.

STOKES, S. & FATTAHI, M. (2003): Red emission luminescence from quartz and feldspar for dating applications: an overview. – Radiation Measurements, 37: 383-395.

STOKES, S., INGRAM, S., AITKEN, M.J., SIROCKO, F., ANDERSON, R. & LEUSCHNER, D. (2003): Alternative chronologies for Late Quaternary (Last Interglacial-Holocene) deep sea sediments via optical dating of silt-sized quartz. – Quaternary Science Reviews, 22: 925-941.

STOKES, S., BAILEY, R.M., FEDOROFF, N. & O'MARAH, K.E. (2004): Optical dating of aeolian dynamism on the West African Sahelian margin. – Geomorphology, 59: 281-291.

STOKES, S. & BRAY, H.E. (2005): Late pleistocene eolian history of the liwa region, Arabian Peninsula. – Geological Society of America Bulletin, 117: 1466-1480.

SVENDSEN, J.I., ALEXANDERSON, H., ASTAKHOV, V.I., DEMIDOV, I., DOWDESWELL, J.A., FUNDER, S., GATAULLIN, V., HENRIKSEN, M., HJORT,CH.,

Houmark-Nielsen, M., Hubberten, H.W., Ingólfsson, O., Jakobsson, M.,. Kjær, K.H., Larsen, E., Lokrantz, H., Lunkka, J.P., Lyså, A., Mangerud, J., Matiouchkov, A., Murray, A.S., Möller, P., Niessen, F., Nikolskaya, O., Polyak, L., Saarnisto, M., Siegert, Ch., Siegert, M.J., Spielhagen, R.F. & Stein, R. (2004): Late Quaternary ice sheet history of northern Eurasia. – Quaternary Science Reviews, 23: 1229-1271.

Telfer, M.W. & Thomas, D.S.G. (2007): Late Quaternary linear dune development of the southwestern Kalahari: Implications for aeolian palaeoclimatic reconstructions and predictions of future dynamics. – Quaternary Science Reviews, 26: 2617-2630.

Templer, R.H. & Smith, B.W. (1988): Auto-regenerative TL dating with zircon inclusions from fired materials. – Nuclear Tracks and Radiation Measurements, 14: 329-332.

Thomas, P.J., Murray, A.S. & Sandgren, P. (2003): Age limit and age underestimation using different OSL signal from lacustrine quartz and polymineral fine grains. – Quaternary Science Reviews, 22: 1139-1143.

Trautmann, T. (2000): A study of radioluminescence kinetics of natural feldspar dosimeters: experiments and simulations. – Journal of Physics D: Applied Physics, 33: 2304-2310.

Trautmann, T., Krbetschek, M.R., Dietrich, A. & Stolz, W. (1999a): Radioluminescence dating: a new tool for Quaternary geology and archaeology. – Naturwissenschaften, 86: 441-444.

Trautmann, T., Krbetschek, M.R., Dietrich, A. & Stolz, W. (1999b): Feldspar radioluminescence: A new dating method and its physical background. – Journal of Luminescence, 85: 45-58.

Trautmann, T., Krbetschek, M.R., Dietrich, A. & Stolz, W. (2000): The basic principal of radioluminescence dating and a first model approach. – Radiation Measurements, 32: 487-492.

Tribolo, C. (2003): Apport des méthodes de la luminescence a la chronologie des techno-facies du Middle Stone Age associés aux premiers hommes modernes du sud de l'Afrique. – PhD thesis,. Universitö de Bordeaux I, 236 S.

Tripaldi, A. & Forman, S.L. (2007): Morphology and chronology of Late Quaternary dune fields of western argentina. – Palaeogeography, Palaeoclimatology, Palaeoecology, 251: 300-320.

Truelsen, J. & Wallinga, J. (2003): Zeroing of the OSL signal as a function of grain size: Investigating bleaching and thermal transfer for a young fluvial sample. – Geochronometria, 22: 1-8.

Tsukamoto, S., Murray, A. S., Huot, S., Watanuki, T., Denby, P. M. & Bøtter-Jensen, L. (2007): Luminescence property of volcanic quartz and the use of red isothermal TL for dating tephras. – Radiation Measurements, 42: 190-197.

Twidale, C.R., Prescott, J.R., Bourne, J.A. & Williams, F.M. (2001): Age of desert dunes near Birdsville, southwest Queensland. – Quaternary Science Reviews, 20: 1355-1364.

Valladas, H., Joron, J.-L., Valladas, G., Arensburg, B., Bar-Yosef, O., Belfer-Cohen, A., Goldberg, P., Laville, H., Meignen, L., Rak, Y., Tchernov, E., Tillier, A.-M. & Vandermeersch, B. (1987): Thermoluminescence dates for the neanderthal burial site at Kebara in Israel. – Nature, 330: 159-160.

Valladas, H., Reyss, J.-L., Joron, J.-L., Valladas, G., Bar-Yosef, O. &, Vandermeersch, B. (1988): Thermoluminescence dating of mousterian ‚Proto-Cro-Magnon' remains from Israel and the origin of modern man. – Nature, 331: 614-616.

Valladas, H., Mercier, N., Froget, L., Hovers, E., Joron, J.-L., Kimbel, W.H. & Rak, Y. (1999): TL Dates for the Neanderthal Site of the Amud Cave, Israel. – Journal of Archaeological Science, 26: 259-268.

Valladas, H., Mercier, N., Michab, M., Joron, J.-L., Reyss, J.-L. & Guidon, N. (2003): TL age-estimates of burnt quartz pebbles from the Toca do Boqueirao da Pedra Furada (Piaui, Northeastern Brazil). – Quaternary Science Reviews, 22: 1257-1263.

Vandenberghe, D., Hossain, S.M., De Corte, F. & Van den haute, P. (2003): Investigations on the origin of the equivalent dose distribution in a Dutch coversand. – Radiation Measurements, 37: 433-439.

Vandenberghe, D., Kasse, C., Hossain, S.M., De Corte, F., Van den Haute, P., Fuchs, M. & Murray, A.S. (2004): Exploring the method of optical dating and comparison of optical and C-14 ages of Late Weichselian coversands in the southern Netherlands. – Journal of Quaternary Science, 19: 73-86.

Vandergoes, M., Newnham, R., Preusser, F., Hendy, C., Lowell, T., Fitzsimons, S., Hogg, A., Kasper, H.U. & Schlüchter, Ch. (2005): Southern Ocean terrestrial record showing local modification of glacial-interglacial climate signals. – Nature, 436: 242-245.

VAN ES, H.J., DEN HARTOG, H.W., DE MEIJER, R.J., VENEMA, L.B., DONOGHUE, J.F. & ROZENDAAL, A. (2000): Assessment of the suitability of zircons for thermoluminescence dating. – Radiation Measurements, 32: 819-823.

VERNET, G., RAYNAL, J.P., FAIN, J., MIALLIER, D., MONTRET, M., PILLEYRE, T. & SANZELLE, S. (1998): Tephrostratigraphy of the last 160 ka in western Limagne (France). – Quaternary International, 47/48: 139-146.

VIELLEVIGNE, E., GUIBERT, P., ZUCCARELLO, A.G. & BECHTEL F (2006): The potential of optically stimulated luminescence for medieval building: A case study at Termez (Uzbeskistan). – Radiation Measurements, 41: 991-994.

VISOCEKAS, R. (1985): Tunneling radiative recombination in Labadorite – its association with anomalous fating of Thermoluminescence. – Nuclear Tracks and Radiation Measurements, 10: 521-529.

VISOCEKAS, R. (2002): Tunnelling in afterglow, its coexistence and interweaving with thermally stimulated luminescence. – Radiation Protection Dosimetry, 100: 45-54.

WAGNER, G.A., GLASMACHER, U.A & GREILICH, S. (2005): Spatially resolved dose rate determination in rocks and ceramics by neutron-induced fission tracks. – Radiation Measurements, 40: 26-31.

WALLINGA, J. (2002a): Optically stimulated luminescence dating of fluvial deposits: a review. – Boreas, 31: 303-322.

WALLINGA, J. (2002b): On the detection of age overestimation using single aliquot techniques. – Geochronometria, 21: 17-26.

WALLINGA, J., MURRAY, A.S. & WINTLE, A.G. (2000): The single-aliquot regenerative-dose (SAR) protocol applied to coarse-grain feldspar. – Radiation Measurements, 32: 529-533.

WALLINGA, J., MURRAY, A.S. & BØTTER-JENSEN, L. (2002): Measurement of the dose in quartz in the presence of feldspar contamination. – Radiation Protection Dosimetry, 101: 367-370.

WALLINGA, J., TÖRNQVIST, T.E., BUSSCHERS, F.S. & WEERTS, H.J.T. (2004): Allogenic forcing of the late Quaternary Rhine-Meuse fluvial record: the interplay of sea-level change, climate change and crustal movements. – Basin Research, 16: 535-547.

WALLINGA, J., BOS, A.J.J., DORENBOS, P., MURRAY, A.S., SCHOKKER, J. (2007): A test case for anomalous fading correction in IRSL dating. – Quaternary Geochronology, 2: 216-221.

WANG, X.L., WINTLE, A.G. & LU, Y.C. (2006a): Thermally transferred luminescence in fine-grained quartz from Chinese loess: Basic observations. – Radiation Measurements, 41: 649-658.

WANG, X.L., LU, Y.C. & WINTLE, A.G. (2006b): Recuperated OSL dating of fine-grained quartz in Chinese loess. – Quaternary Geochronology, 1: 89-100.

WANG, X.L., WINTLE, A.G. & LU, Y.C. (2007): Testing a single-aliquot protocol for recuperated OSL dating. – Radiation Measurements, 42: 380-391.

WATANUKI, T., MURRAY, A.S. & TSUKAMOTO. S. (2003): A comparison of OSL ages derived from silt-sized quartz and polymineral grains from Chinese loess. – Quaternary Science Reviews, 22: 991-997.

WATANUKI, T., MURRAY, A.S. & TSUKAMOTO, S. (2005): Quartz and polymineral luminescence dating of Japanese loess over the last 0.6 Ma: Comparison with an independent chronology. – Earth and Planetary Science Letters, 240: 774-789.

WIESER, A., GÖKSU, H.Y., REGULLA, D.F., FRITZ, P., VOGENAUER, A. & CLARK, I.D. (1993): ESR and TL dating of travertine from Jordan – Complications in palaeodose assessment. – Applied Radiation and Isotopes, 44: 149-152-

WINTLE, A.G. (1973): Anomalous fading of thermoluminescence in mineral samples. – Nature, 245: 143-144.

WINTLE, A.G. (1980): Thermo-Luminescence dating – A review of recent application to non-pottery materials. – Archaeometry, 22: 113-122.

WINTLE, A.G. (1981): Thermo-Luminescence dating of Late Devensian loesses in southern England. – Nature, 289: 479-480.

WINTLE, A.G. (1990): A review of current research on TL dating of loess. – Quaternary Science Reviews, 9: 385-397.

WINTLE, A.G. (1997): Luminescence dating: Laboratory procedures and protocols. – Radiation Measurements, 27: 769-817.

WINTLE, A.G. & HUNTLEY, D.J. (1979): Thermoluminescence dating of a deep-sea sediment core. – Nature, 279: 710-712.

WINTLE, A.G. & HUNTLEY, D.J. (1980): Thermoluminescence dating of ocean sediments. – Canadian Journal of Earth Sciences, 17: 348-360.

WINTLE, A.G., LI, S.H. & BOTHA, G.A. (1993): Luminescence dating of colluvial deposits. – South African Journal of Science, 89: 77-82.

WINTLE, A.G. & MURRAY, A.S. (2006): A review of quartz optically stimulated luminescence characteristics and their relevance in single-aliquot

regeneration dating protocols. – Radiation Measurements, 41: 369-391.

Wolfe, A.P., Fréchette, B., Richard, P.J.H., Miller, G.H. & Forman, S.L. (2000): Paleoecology of a > 90,000-year lacustrine sequence from Fog Lake, Baffin Island, Arctic Canada. – Quaternary Science Reviews, 19: 1677-1699.

Yang, X., Preusser, F. & Radtke, U. (2006): Late Quaternary environmental changes in the Taklamakan Desert, western China, inferred from OSL dated lacustrine and aeolian deposits. – Quaternary Science Reviews, 25: 923-932.

Yoshida, H., Roberts, R.G. & Olley, J.M. (2003): Progress towards single-grain optical dating of fossil mud-wasp nests and associated rock art in northern Australia. – Quaternary Science Reviews, 22: 1273-1278.

Zander, A., Duller, G.A.T. & Wintle, A.G. (2000): Multiple and single aliquot luminescence dating techniques applied to quartz extracted from Middle and Upper Weichselian loess, Zemechy, Czech Republic. – Journal of Quaternary Science, 15: 51-60.

Zander, A., Degering, D., Preusser, F. & Brückner, H. (2007): Optically stimulated luminescence dating of sublittoral and intertidal sediments from Dubai, UAE: Radioactive disequilibria in the uranium decay series. – Quaternary Geochronology, 2: 123-128.

Zhou, L.P., Dodonov, A.E. & Shackleton, N.J. (1995): Thermoluminescence dating of the Orkutsay loess section in Tashkent Region, Uzbekistan, Central Asia. – Quaternary Science Reviews, 14: 721-730.

Zink, A. & Porto, E. (2005): Luminescence dating of the Tanagra terracottas of the Louvre collections. –Geochronometria 24: 21-26.

Eiszeitalter und Gegenwart Quaternary Science Journal	57/1–2	150–178	Hannover 2008

Electron spin resonance (ESR) dating of Quaternary materials

Gerhard Schellmann, Koen Beerten and Ulrich Radtke *)

Abstract: ESR dating has become an efficient tool in earth sciences for geochronological studies on different kinds of littoral deposits (coral reefs terraces, beach ridge systems, aeolianites) during the last ten years. Improvements in annual dose rate (D') estimation and the newly developed approach for equivalent dose (D_E) determination (D_E -D_{max} plot procedure) increase the precision of ESR dating of Holocene and Pleistocene corals as well as marine and terrestrial mollusc shells. This is strongly supported by the comparison of ESR dating results with other numeric dating methods such as radiocarbon and TIMS Uranium series analysis (TIMS $^{230}Th/^{234}U$). The latter is the main focus of this paper. The uncertainties associated in ESR dating of Holocene corals coincide with the variability of ^{14}C ages caused by the marine reservoir effect. The dating of Pleistocene corals permits the differentiation between the main marine isotope stages (MIS) 5, 7, 9, 11 and 13 as well as between sub-stages $5e_{3/2}$ and $5e_1$, 5c, and $5a_2$ and $5a_1$. The average error range when dating corals is between 5 to 8%. Furthermore, ESR dating of marine and terrestrial mollusc shells has yielded some promising results and permits the differentiation between the interglacial MIS 1, 5, 7 and 9 with an average dating error range of 10 to 15%.
ESR dating of quartz is another promising dating technique for Quaternary and even Neogene geological formations. The presence of quartz in volcanic rocks, tephra, fault gouge and sediments (heated or unheated) allows determining the last time of heating, fault movement or sunlight exposure. Although challenged by several experimental issues, ESR dating of quartz is often the only method able to produce numerical ages for older formations.
ESR has also been applied to a wide variety of other materials such as foraminifera, speleothems, travertines, calcretes and tooth enamel. The most common and reliable application is the ESR dating of mammal teeth, which becomes in conjunction with laser ablation U-series dating, an important method for determining the age of archaeological sites beyond the time range of the ^{14}C dating method back to about 200 to 300 ka.

[**Elektronen Spin Resonanz (ESR)-Datierung quartärer Materialien]**

Kurzfassung: ESR hat sich im letzten Jahrzehnt bei der Datierung verschiedenster littoraler Ablagerungen (Korallenriffterassen, Strandwallsysteme, Dünen) als effizientes Datierungswerkzeug etabliert. Verbesserungen in der Bestimmung der jährlichen Dosisleistung (D') und ein neu entwickelter Ansatz zur Bestimmung der Äquivalent Dosis (D_E – D_{max} Verfahren) haben die Präzision der ESR-Datierung sowohl an holozänen und pleistozänen Korallen als auch an marinen und terrestrischen Molluskenschalen verbessert. Dies wurde durch den Vergleich mit anderen numerischen Datierungsverfahren wie Radiokohlenstoff und TIMS-Uranserien-Analyse (TIMS $^{230}Th/^{234}U$) unterstützt. Der Vergleich mit letzterer Methode steht im Fokus dieses Artikels. Die mit der ESR-Methode verbundenen Ungenauigkeiten bei der Datierung holozäner Korallen liegt in der Größenordnung der Variabilität von ^{14}C-Altern, die durch den marinen Reservoireffekt bedingt ist. Die Datierung pleistozäner Korallen erlaubt die Differenzierung der wichtigen marinen Isotopenstadien (MIS) 5,

*Addresses of authors: G. Schellmann, Universität Bamberg, Lehrstuhl Geographie II – Physische Geographie, Am Kranen 1, D-96045 Bamberg. E-Mail: gerhard.schellmann@ggeo.uni-bamberg.de; K. Beerten, Universität zu Köln, Geographisches Institut, Albertus-Magnus-Platz, D-50923 Köln. E-Mail: kbeerten@uni-koeln.de; U. Radtke, Universität zu Köln, Geographisches Institut, Albertus-Magnus-Platz, D-50923 Köln. E-Mail: u.radtke@uni-koeln.de

7, 9,11 und 13 sowie der Untereinheiten $5e_{3/2}$ und $5e_1$, 5c und $5a_1$ und $5a_2$. Der durchschnittliche Fehler bei der Datierung von Korallen liegt zwischen 5 bis 8%. Weiterhin hat die Datierung mariner und terrestrischer Mollusken mittels ESR viel versprechende Resultate geliefert, die eine Differenzierung der Interglaziale MIS 1, 5, 7 und 9 ermöglichen, bei einem Fehler von 10-15%.
Die ESR Datierung von Quarz ist eine weitere viel versprechende Datierungstechnik für quartäre und sogar neogene geologische Formationen. Das Vorkommen von Quarz in vulkanischen Gesteinen, Tephren, Störungen und Sedimenten (thermisch beeinflusst und unbeeinflusst) ermöglicht die zeitliche Bestimmung des letzten Zeitpunkts vor der Erhitzung, Störung oder der Aussetzung von Sonnenlicht. Obwohl durch einige experimentelle Ergebnisse angezweifelt, ist die ESR Datierung von Quarz die einzige Möglichkeit Altersdaten älterer Ablagerungen zu liefern.
ESR wurde auch bei einer Vielzahl anderer Materialien angewendet, wie zum Beispiel Foraminiferen, Speleothemen, Travertinen, Kalkkrusten und Zahnschmelz. Die gebräuchlichste und zuverlässigste Anwendung ist die ESR-Datierung von Mammutstoßzähnen. Im Zusammenspiel mit der Laser-Ablation Uranserien Datierung ist ESR eine wichtige Methode zur Altersbestimmung archäologischer Fundstätten jenseits der Bestimmungsgrenzen der Radiokohlenstoffmethode bis in den Bereich von 200 bis 300 ka.

Keywords: Electron spin resonance, dating, geochronology, Quaternary, littoral

1 Introduction

Although Ikeya (1975) introduced Electron Spin Resonance Spectroscopy (ESR) for dating stalagmites more than 30 years ago, the full potential of this relatively young method is still not fully utilised. Since then, the quality of ESR-spectrometers and the understanding of the structure and behaviour of the ESR signal used for dating have been significantly improved. Detailed overviews about the ESR dating method have been provided by Ikeya (1993), Grün (1989a, 1989b, 2007), Radtke (1989), Jonas (1997) and Rink (1997).
This method is used for a wide variety of materials with most reliable applications on corals, mollusc shells, quartz, foraminifera, speleothems and teeth. In this text, the potential and present restrictions of ESR dating of Quaternary coral, mollusc shells and quartz is illustrated for selected sites and a short review is presented about the relevance of ESR for dating other carbonates (foraminifera, speleothems) and tooth enamel. For further details about problems and further applications of ESR dating including more literature, see e.g. Grün (2007), Blackwell (2006) and Rink (1997).
Regardless of the recent methodological improvements in ESR and its frequent use for dating corals, mollusc shells, quartz and teeth, there is still a huge potential for further development of the method for these and other materials (e.g. Skinner 2000). Similar to all other methods of age determination, ESR dating is confronted by specific methodological problems that cannot be considered in error calculation. This means, as applies for most analytic methods, that high precision does not automatically guarantee the accuracy of an age estimate. The latter is influenced by different geological factors that cannot be quantified and are hence not part of the age and error calculation. In ESR dating, these are mainly diagenetic alterations of the dated material, incomplete resetting of the ESR signal and up-take or loss of radioactive elements (U, Th, K) (Fig. 1). With regard to these problems, proving the reliability of new dating approaches by independent age control is essential. In the context of the ESR method, this is possible using radiocarbon or $^{230}Th/^{234}U$ dating for corals and mollusc shells or luminescence, palaeomagnetics or $^{40}Ar/^{39}Ar$ for dating quartz.

2 Methodology

The ESR dating method is one of several radiation exposure methods based on radiation dosimetry such as thermoluminescence (TL), optically stimulated luminescence (OSL) and radioluminescence (RL). All these methods

use the phenomenon that common minerals act as natural dosimeters. The radiation causes charge (electrons, free radicals) to be trapped at defects in the crystal lattice of a wide range of minerals such as aragonite, calcite and quartz. The amount of trapped charge accumulation increases with time and can be quantified by the ESR measurement.

2.1 Nature of the ESR signal and its quantification

The process of trapping charge results from the interaction of naturally occurring alpha, beta and gamma, and, to some minor extent, cosmic radiation (D'_{cos}, cosmic dose rate) with matter. The first consists of internal radiation from

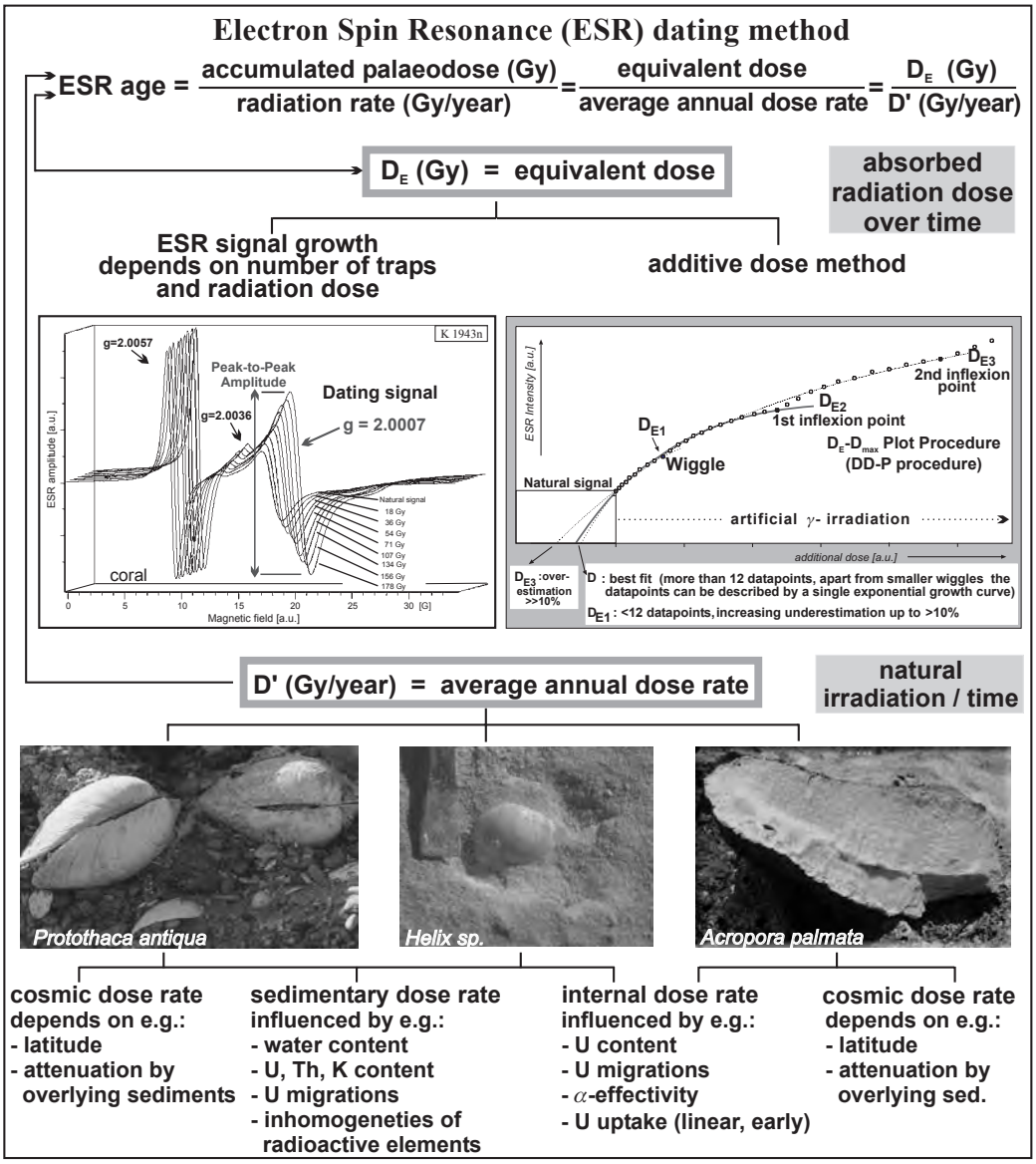

Fig. 1: Generalised principle of ESR dating of aragonitic coral and mollusc shells

Abb. 1: Generalisiertes Schema der ESR-Datierung von Korallen und Muschelschalen.

the mineral itself ($D'_{int.}$, internal dose rate: i.e. Uranium and daughter isotopes, to some extent additionally Th and K in quartz) as well as radiation from the surrounding sediment ($D'_{ext.}$, external dose rate mainly from Uranium and Thorium decay chains and Potassium). Such ionising radiation causes the activation of electrons to an excited energy level. Charge defects in the crystal lattice, so-called traps, capture part of the excited electrons in the band gap. A detailed description of the underlying physical processes is provided by e.g. Grün (1989a, 1989b, 2007), Jonas (1997) und Rink (1997). The amplitude of the ESR signal represents the amount of unpaired electrons at lattice defects (traps). Each material investigated has a characteristic ESR spectrum that may consist of one or several single signals, but not all the individual signals are suitable for dating. Suitable are only ESR signals that are both sensitive to radiation and thermally stable at the prevailing temperature that occurred during deposition and burial. The ESR signal at g = 2.0007 (Fig. 1) is most suitable for dating aragonitic mollusc shells and corals (e.g. Radtke & Grün 1988, Walther et al. 1992, Schellmann & Radtke 1999, 2001). A basic principle in dating biogenic material is that the ESR signal starts to increase after the shell, tooth enamel or coral has been formed.

For ESR dating of quartz, a prerequisite is the existence of a resetting mechanism in nature to zero the ESR signal (and thus the geological clock). In order for the method to be reliable, any pre-existing ESR signals must be erased prior to the event to be dated (Fig. 2). The zeroing process responsible for resetting the geological clock is dependent on the geological context of the quartz mineral. The specific behaviour of ESR centres in quartz allows to determine the moment of the last heating (volcanic rocks, tephra, heated sediments), the moment of the last fault movement (quartz in fault gouges exposed to shearing) and the last exposure to sunlight (sedimentary quartz). The accuracy of the ESR age is dependent on the completeness of the zeroing process. Incomplete signal zeroing will inevitably lead to age overestimates, unless suitable tests can reliably determine the degree of zeroing that may have occurred, through which this can be accounted for.

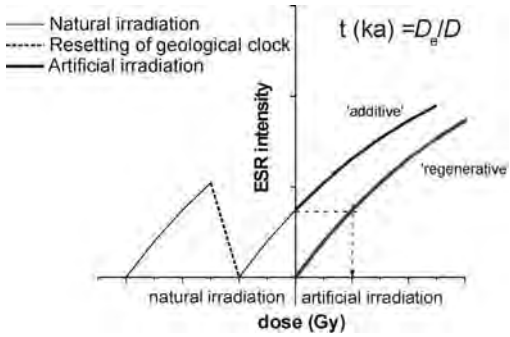

Fig. 2: Generalised principle of ESR dating of quartz. The underlying assumption of ESR dating is that the ESR signal is zeroed prior to the event, which is to be dated (resetting of the geological clock). Subsequently, the ESR signal starts growing again by natural irradiation (left of the intensity axis), until the moment of sampling. In general, there are two methods to infer the accumulated or equivalent dose D_E. In the additive dose method, artificial doses are given on top of the accumulated dose, and the equivalent dose is estimated by extrapolating the growth-curve back to the x-axis (dose-axis). In the regenerative dose method, the signal is zeroed again, and the natural intensity is projected onto the regenerated dose curve to estimate the equivalent dose.

Abb. 2: Generalisiertes Prinzip der ESR-Datierung von Quarz. Die grundlegende Annahme der ESR-Datierung ist, dass das ESR-Signal vor dem zu datierenden Ereignis auf Null gesetzt wird (Zurückstellen der geologischen Uhr). Danach nimmt das ESR-Signal, aufgrund natürlicher Strahlung, bis zum Zeitpunkt der Probennahme wieder zu (linke Seite der ESR Intensitätsachse). Generell gibt es zwei Methode die Akkumulierte oder Äquivalent Dosis (D_E) zu bestimmen. Bei der Additiven Dosis Methode wird auf das natürliche Signal eine künstliche Dosis hinzu gegeben. Die Äquivalent Dosis wird dann durch Abtragen der Wachstumskurve auf der X-Achse bestimmt. Bei der Regenerativen Dosis Methode wird das Signal zuerst auf Null gesetzt und die natürliche Intensität wird auf die regenerative Wachstumskurve projiziert, um die Äquivalent Dosis zu erhalten.

Several ESR centres in quartz have shown to be potential dosimeters of ionising radiation

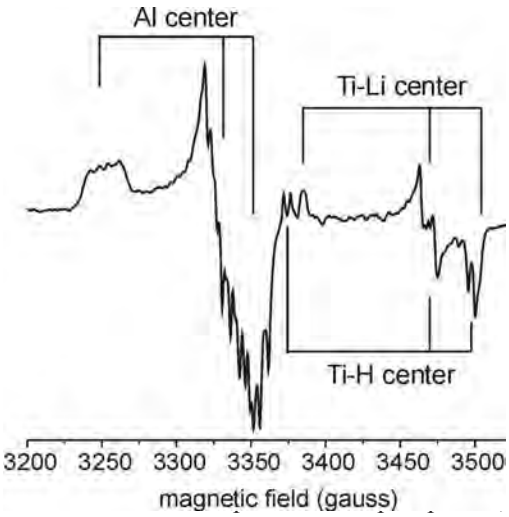

Fig. 3: ESR spectrum of crystalline quartz grains (100-200 µm, 300 mg) at 100 K (Australian sedimentary quartz). Microwave absorption patterns are indicated for the Al-centre, Ti-Li-centre and Ti-H-centre, according to the 3 principal g-values (vertical lines).

Abb. 3: ESR-Spektrum kristalliner Quarzkörner (100-200 µm, 300 µm) bei 100 K (sedimentärer Quarz; Australien). Mikrowellenabsorptionsmuster sind für die Al-, Ti-Li- und Ti-H-Zentren angegeben, bezogen auf die drei grundlegenden g-Werte (vertikale Linien).

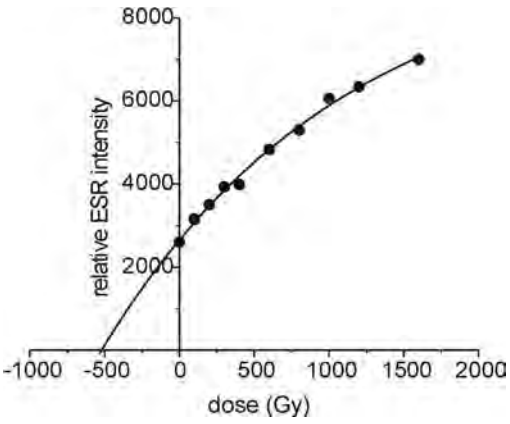

Fig. 4: ESR dose response curve of the Al-centre from an aeolian sample (NWB1, Murray Basin, Australia; unpublished results). The data points are fitted to a rising exponential (GRÜN 1989). Positive values refer to the artificially added doses, while negative values refer to the past irradiation dose. Assuming a dose rate of about 1 Gy ka^{-1}, which is not uncommon in sedimentary contexts, the dose range covered in this example would equal more than 2 million years.

Abb. 4: ESR-Dosisaufbaukurve für das Al-Zentrum gemessen an einem äolischen Sediment (NWB1, Murray Basin, Australien, unveröffentlichte Daten). Die Datenpunkte sind an einen steigenden Exponenten angepasst (GRÜN 1989). Positive Werte beziehen sich auf die künstlich zugegebene Strahlung, wohingegen negative Werte die in der Vergangenheit akkumulierte Dosis repräsentieren. Unter Annahme einer Dosisleistung von ungefähr 1 Gy ka^{-1}, was für sedimentäre Ablagerungen nicht ungewöhnlich ist, deckt die akkumulierte Dosis in diesem Beispiel eine Spanne von mehr als 2 Millionen Jahren ab.

the equivalent of the palaeodose is determined by a so-called additive dose response curve. For this, the sample is irradiated using artificial β- or γ-sources and an individual dose response curve is constructed for each sample. By extrapolation on the x-axis, D_E is calculated (Fig. 1). The equivalent dose of quartz can also be determined using the regenerative dose method, owing to the regeneration characteristics of the paramagnetic defects in the mineral. Following thermal annealing (heating) or optical bleaching, the ESR signal is regenerated with an artificial radioactive source, and the dose is estimated by interpolation of the natural ESR intensity (Fig. 2).

2.2 Dose rate determination

The cosmic dose rate is related to the depth of the sample below surface, latitude and elevation. Further corrections to burial depth may be needed where nearby obstructions or drop-offs in the land surface occur: these are not accounted for by the tables of PRESCOTT & HUTTON (1994). The radioactivity of the surrounding material is either measured in the field using a portable gamma spectrometer or calculated via the determination of the concentration of Potassium, Thorium and

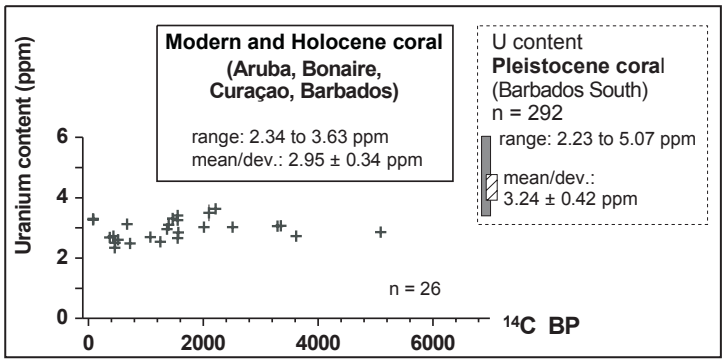

Fig. 5: Uranium content (ppm) of modern, Holocene and Pleistocene corals (slightly modified from Schellmann & Radtke 2003).

Abb. 5: Uran-Gehalte (ppm) moderner, holozäner und pleistozäner Korallen (leicht verändert nach Schellmann & Radtke 2003).

Uranium in the sample. For aragonitic mollusc shells and corals, the internal dose rate is caused almost completely by Uranium. If possible, the Uranium content of each sample should be verified by repeated measurements. In contrast, the internal alpha dose rate in quartz is usually very small in comparison with the external dose rate, allowing it to be neglected in the final age calculation. Most sub-modern, Holocene and Pleistocene corals have Uranium contents of about 3.0 to 3.2 ppm (Fig. 5). It is hence concluded that corals absorb such amounts of Uranium from seawater during their life-time or shortly after their death. Extremely high (up to 5 ppm) and low (below 2.5 ppm) Uranium concentrations are exceptional and at the moment, it can only be speculated about their origin.

For the calculation of ESR ages of corals, an early Uranium up-take and hence a relatively high radiation level from the very beginning can be assumed. This is of importance as ESR ages that are calculated based on an early Uranium up-take model will result in much lower age estimates compared to ages calculated based on the assumption of a linear Uranium uptake. In contrast to this, modern mollusc shells have extremely low Uranium contents of 0.1 to 0.2 ppm (max. 0.7 ppm). Only after an age of more than 2500 yr, do mollusc shells show significantly higher contents of more than 2 ppm Uranium (Fig. 6) and reach levels frequently observed in Pleistocene fossils. This implies that mollusc shells absorb most of the Uranium *post mortem*. However, this delayed up-take of Uranium is negligible for age calculation when dating Pleistocene mollusc shells. For Early to Mid Holocene mollusc shells, which have Uranium contents higher than 0.5 ppm, a delayed up-take of Uranium has to be considered when calculating the internal dose rate. As the exact *post-mortem* up-take of Uranium cannot be reconstructed, the true age will be between the ESR ages estimates calcu-

Table 1: Exemplarily calculation of the effect of different Uranium contents on the ESR age of a Holocene mollusc shell at constant external dose rate. Shown are the age differences that result from linear Uranium up-take and early Uranium up-take, respectively.

Tab. 1: Exemplarische Berechnung zur Verdeutlichung des Einflusses unterschiedlicher Uran-Gehalte auf die ESR-Alter holozäner Muschelschalen unter der Annahme einer konstanten externen Dosisleistung. Sichtbar werden die Altersunterschiede, die aus einer linearen bzw. einer früheren Uranaufnahme resultieren.

U content (ppm)	linear U-uptake model (ESR age diff. to early U-uptake model)
<0.6	same age
0.7	+140 yrs.
1.0	+200 yrs.
1.5	+270 yrs.
2.0	+350 yrs.
2.5	+400 yrs.
3.0	+460 yrs.
3.5	+510 yrs.
4.0	+560 yrs.
4.5	+600 yrs.
5.0	+640 yrs.

lated for linear and early Uranium up-take. For Late Holocene mollusc shells with Uranium contents > 0.5 ppm, linear up-take represents probably the most likely scenario. A detailed discussion of Uranium up-take is provided by JONAS (1997) and RINK (1997). Depending on the contribution of internal dose (= Uranium content of mollusc shell) to the total dose rate, differences in age between the two models will be up to 1000 yr (and more) for samples having a high Uranium content (>5 ppm). For Uranium contents below 0.6 ppm, both models usually result in age estimates consistent within error. Table 1 demonstrates the effect of Uranium up-take on the ESR age of a mid-Holocene mollusc shell.

There are several other potential sources of error associated with dose rate determination that may lead to incorrect ESR ages (Fig. 1). Among these is a change in past sediment water content that can hardly be quantified and may have caused variations in external dose rate. However, this can be accommodated by placing a very large error on the water content in the calculations, for example a value of up to 100% of the water content. Another potential problem can be radioactive disequilibria, i.e. the loss or gain of radioactive elements mainly from the Uranium decay chain (e.g. loss of soluble Uranium). Furthermore, calculation of dose rate for mollusc shells from heterogenous settings, i.e. poorly sorted sand and gravel, is much more insecure than for samples (e.g. land snail shells) from homogenous environments such as aeolianites. Only a few problems are associated with the dose rate determination of

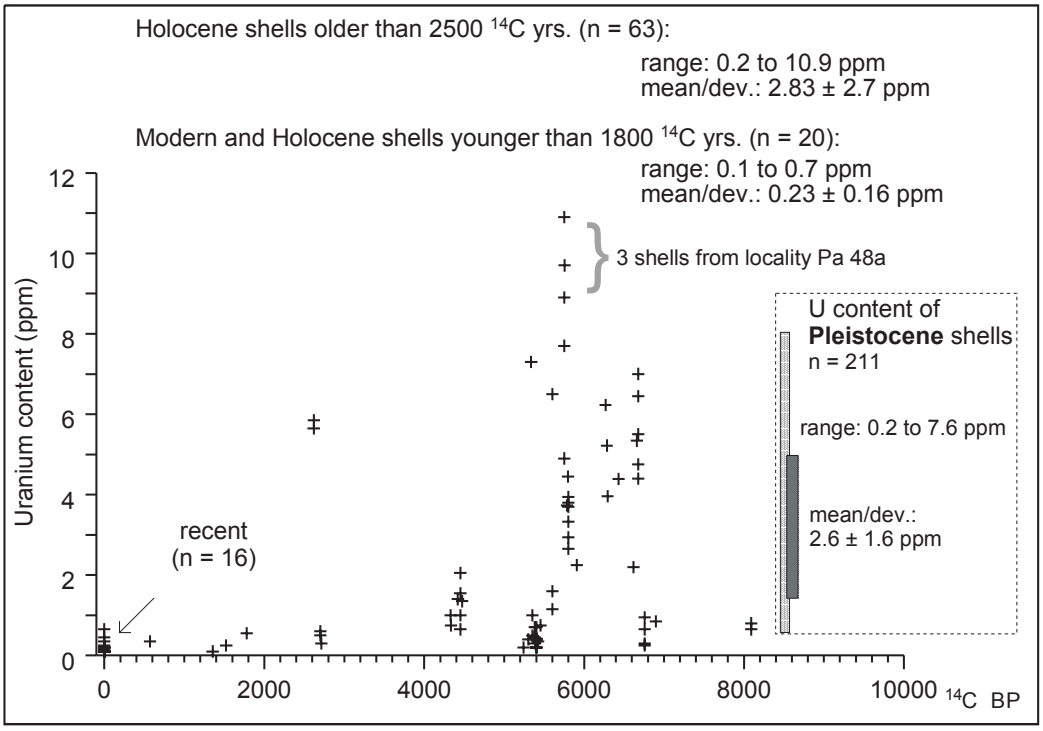

Fig. 6: Uranium content (ppm) of modern, Holocene and Pleistocene mollusc shells from SCHELLMANN & RADTKE (2007). In addition to the Uranium content of radiocarbon dated mollusc shells, values measured for *in situ* bivalve shells that were collected from the same horizons are included.

Abb. 6: Uran-Gehalte (ppm) moderner, holozäner und pleistozäner Muschelschalen (aus SCHELLMANN & RADTKE 2007). Zusätzlich zu den Uran-Gehalten der ^{14}C-datierten Muschelschalen, sind auch die Werte von den *in situ* im gleichen Horizont gefundenen bivalven Schalen angegeben.

corals since only cosmic radiation and internal Uranium are relevant for total dose rate (Fig. 1). The problems of changing water content in the surroundings of the sample and erosive or accumulative processes that may affect cosmic dose calculation have only minor effects.

Supplementary uncertainties in the dose rate for ESR dating of quartz are due to variations in water content and disequilibria in the decay chains of U and Th. Radioactive disequilibrium (i.e. a misbalance between parent and daughter nuclides) might occur if one (or more) of the Th- and/or U-chain members are lost or gained during burial, an effect that would be more pronounced in very permeable sediments. Especially, radionuclides of Rn (gas) and Ra (very leachable), which occur halfway in the U- and Th-chains, could induce disequilibrium. In the case of sediments, it is also possible that disequilibrium already existed at the time of deposition. In order to calculate an accurate dose rate, it is important to check whether any equilibrium exists and if so, whether this equilibrium has remained constant over time. However, in many dating studies, radioactive equilibrium is simply assumed.

A further error source in the calculation of ESR ages is the only poorly known so-called alpha-efficiency, which is also known as k-factor (see Jonas 1997 for details). This value describes the efficiency of α-particles to induce ESR signals compared to other kinds of radiation. Grün (1985) and Grün & Katzenberger (1994) experimentally determined by using a ^{241}Am α-source k-values between 0.07 and 0.10 for mollusc shells. For corals, Radtke & Grün (1988), Grün et al. (1992) and Malmberg & Radtke (2000) determined k-values between 0.05 and 0.07. According to Lyons (1987, cit. in Radtke & Grün 1988) the actual alpha-efficiency of particles from the Uranium decay chain is 20-30 % higher then the values determined using a monoenergetic artificial α-source. Following Grün (2007: 1509), the best k-values for molluscs are 0.07 ± 0.01, for corals 0.06 ± 0.02 and for tooth enamel 0.13 ± 0.02. The influence of uncertainties on the α-efficiency in quartz is reduced because the internal alpha dose rate can usually be neglected (cf. supra). Furthermore, the influence of external alpha rays (several 10 µm) is erased by sample preparation techniques using HF-solutions. As such, in many cases the total dose rate to quartz can be simplified to the sum of the external beta and gamma dose rate and the cosmic dose rate.

3 ESR dating of aragonitic coral and marine and terrestrial mollusc shells

Besides the problems in dose rate determination mentioned above, ESR dating of mollusc shells and corals is associated with another uncertainty that has yet not been quantified. This problem is related to the amplitude of the ESR signal of most mollusc shells, and also rarely for corals, which does not show simple exponential growth to saturation resulting from artificial gamma irradiation. Instead, so-called inflexion points (Fig. 1) have been observed at which signal growth increases suddenly. The physical nature of these inflexion points is yet only poorly understood. Most likely, it results from interference of the ESR dating signal with the so-called a-complex, which shows a relatively higher increase at higher doses and apparently individually disturbs the signal used for dating (Katzenberger & Willems 1988, Barabas et al. 1992). However, it is also possible that inflexion points are related to defects in the crystal lattice that are produced by gamma irradiation (Grün 1990). Attempts to eliminate inflexion points without alternating the ESR dating signal by changing the parameters of the ESR measurement or including thermal pre-treatments have not been successful so far (e.g. Brumby & Yoshida 1994a, Hoffmann et al. 2001, Molodkov et al. 1998). Different preheat temperatures and durations can actually cause significant differences in D_E values and consequently different ESR ages (Schellmann & Radtke 2007). Discontinuous growth of the ESR signal can cause overestimation of calculated D_E of more than 10 % when too high artificial doses are used for construction of the dose response curve (Fig. 1). For determination

of D_E values, only the undisturbed, low-dose part of a dose response curve prior to reaching the first inflexion should be used. Only this part is dominated by the growth of the ESR dating signal and should reflect natural increase. This part of the growth curve can be described by a simple exponential saturation curve. The impact of inflexion points can be minimised by either using several dose points in the lower part of the dose response curve or by applying the standardised procedure of D_E-D_{max}-plots (DDP) (Fig. 1; SCHELLMANN & RADTKE 1999, 2001, 2003). Nevertheless, inflexion points are probably the main reason for age scatter observed in isochronal samples within mollusc bearing sediment layers. Additive dose response curves of corals, on the other hand, rarely show pronounced inflexion points, presumably the reason why ESR dating of isochronal corals scatter much less than molluscs (see below). The D_E values of all ESR ages mentioned here were determined using D_E-D_{max} plots. Prior to this, mollusc and coral samples were ground by hand and sieved to 125-250 µm. At least 20 aliquots with a weight of 0.2000 g were prepared and irradiated using a ^{60}Co-source (Centre of Nuclear Medicine, University of Düsseldorf); dose rate between 0.8 and 2.5 Gy min^{-1}). The maximum irradiation dose was typically between two and three times D_E. Typical parameters on the ESR spectrometer were 10 or 25 mW microwave power, 0.5 or 1.0–1.2 G modulation amplitude, 41.9 s scan-time, 40–50 G scan width and 5 to 40 scans. All D_E values were determined using the programme „Fitsim“ (version 1993) and ESR ages were calculated using the programmes „Data IV“ (version 1990) and „Data V.6“ (version 1999), written by Rainer Grün.

Photo 1: Articulated mollusc shell (*Protothaca antiqua*) in Last Interglacial $T3_{[5]}$ beach deposits near Bustamante, Patagonian Atlantic coast.

Foto 1: Muschelschalen von *Protothaca antiqua* in Lebendstellung in Strandablagerungen des letzen Interglazials $T3_{[5]}$ an der patagonischen Atlantikküste nahe Bustamante.

3.1 Comparing ESR, TIMS Th/U and radiocarbon dating results ages of mollusc shells from Holocene as well as Late and Middle Pleistocene littoral terraces of the Patagonian Atlantic coast

Since several early systematic studies (RADTKE et al. 1981, IKEYA & OMUHRA 1981), dating of molluscs is one of the most common applications of ESR dating and has been applied in several regions worldwide. Particularly typical for the example presented here, the Atlantic coast of Patagonia, is the phenomenon that the coarse littoral beach deposits frequently bear articulated mollusc shells (Photo 1). Such objects are very sensitive to movement and clearly indicate their *in situ* nature. This could be proven by radiocarbon dating of several bivalve mollusc shells found in one sediment layer (SCHELLMANN 1998, SCHELLMANN & RADTKE 2007). The dating of several *in situ* and isochronous mollusc shells (deposited within not more than a few decades) represents an ideal opportunity to test the accuracy of the ESR dating method. With this approach, it is possible to test the reproducibility of ESR dating with special regard to the dating of Pleistocene molluscs, where no other accurate dating methods are available.

Along the Patagonian Atlantic coast, there are several locations where Holocene and Pleistocene littoral deposits with articulated mollusc shells can be found at different elevations. The distribution of raised Pleistocene beach deposits in the Bay of Bustamante is shown in

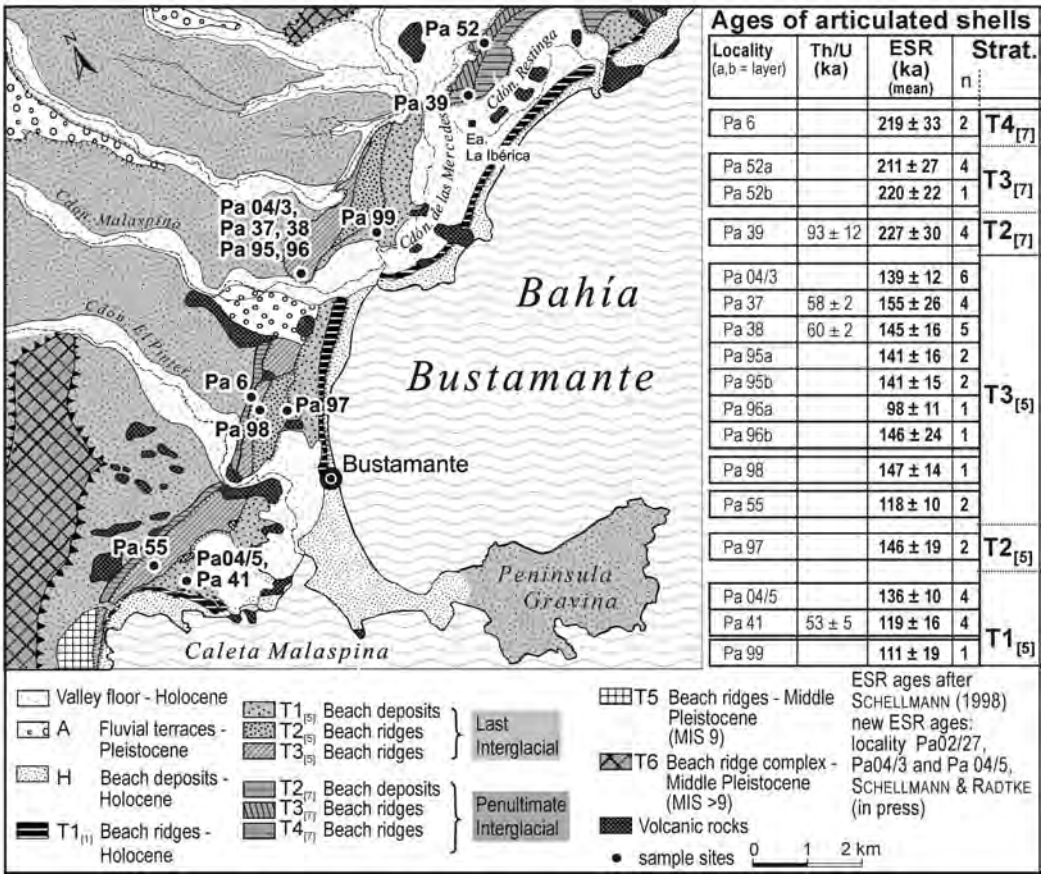

Ages of articulated shells

Locality (a,b = layer)	Th/U (ka)	ESR (ka) (mean)	n	Strat.
Pa 6		219 ± 33	2	$T4_{[7]}$
Pa 52a		211 ± 27	4	$T3_{[7]}$
Pa 52b		220 ± 22	1	
Pa 39	93 ± 12	227 ± 30	4	$T2_{[7]}$
Pa 04/3		139 ± 12	6	$T3_{[5]}$
Pa 37	58 ± 2	155 ± 26	4	
Pa 38	60 ± 2	145 ± 16	5	
Pa 95a		141 ± 16	2	
Pa 95b		141 ± 15	2	
Pa 96a		98 ± 11	1	
Pa 96b		146 ± 24	1	
Pa 98		147 ± 14	1	
Pa 55		118 ± 10	2	
Pa 97		146 ± 19	2	$T2_{[5]}$
Pa 04/5		136 ± 10	4	$T1_{[5]}$
Pa 41	53 ± 5	119 ± 16	4	
Pa 99		111 ± 19	1	

Fig. 7: ESR (mean ages) and TIMS Th/U ages of articulated mollusc shells of Last and Penultimate Interglacial beach ridge systems along the Patagonian Atlantic coast near Bustamante. TIMS Th/U dating by A. Rostami & A. Mangini (Institut für Umweltphysik, Universität Heidelberg); details in SCHELLMANN (1998) and SCHELLMANN & RADTKE (2000).

Abb. 7: ESR (gemittelte Alter) und TIMS Th/U Alter gemessen an Muschelschalen in Lebendstellung aus Strandwallsedimenten des letzen und vorletzen Interglazials entlang der patagonischen Atlantikküste in der Nähe von Bustamante. TIMS Th/U Datierungen wurden von A. Rostami & A. Mangini am Institut für Umweltphysik, Universität Heidelberg durchgeführt. Details bei SCHELLMANN (1998) und SCHELLMANN & RADTKE (2000).

Fig. 7 together with the results of TIMS Th/U and ESR dating, mainly of bivalve molluscs found in the sediments (SCHELLMANN 1998). ESR dating confirms the general morphological and pedostratigraphic differences between the individual beach ridge systems of the area (SCHELLMANN 1998). Beach ridges in distal position to the present shoreline ($T4_{[7]}$ to $T2_{[7]}$) developed during the Penultimate Interglacial (ca. 220,000 yr ago). The beach ridge systems closer to the sea, $T3_{[5]}$ to $T1_{[5]}$ were formed during the Last Interglacial (ca. 130,000 yr ago). The ESR ages are not precise enough to allow a differentiation in age between different beach ridge systems such as $T4_{[7]}$ to $T2_{[7]}$ and $T3_{[5]}$ to $T1_{[5]}$, respectively. Additionally, both Holocene (Fig. 9) and Last Interglacial ESR ages apparently tend to overestimate the real age of the sample. The results of TIMS Th/U however, appear much too young and do not allow a

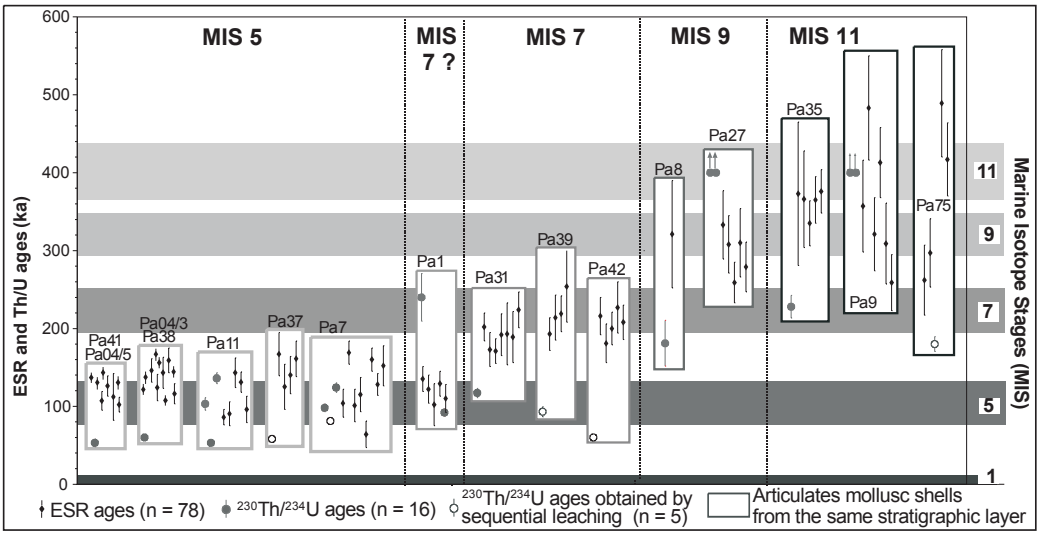

Fig. 8: Comparison of ESR and TIMS Th/U ages of mollusc shells from Late and Middle Pleistocene beach ridge systems along the Patagonian Atlantic Coast. TIMS Th/U dating by A. Rostami & A. Mangini (Institut für Umweltphysik, Universität Heidelberg); details in SCHELLMANN (1998) with additional datings from SCHELLMANN & RADTKE (2007).

Abb. 8: Vergleich der ESR- und TIMS Th/U Alter von Muschelschalen aus spät- und mittelpleistozänen Strandwallsystemen entlang der patagonischen Atlantikküste. TIMS Th/U Datierungen wurden von A. Rostami & A. Mangini am Institut für Umweltphysik, Universität Heidelberg durchgeführt; Details bei SCHELLMANN (1998) mit zusätzlichen Daten aus SCHELLMANN & RADTKE (2007).

differentiation between beach ridge systems of the Last and Penultimate Interglacial (Fig. 7). A similar picture is also revealed when comparing the whole data set of ESR and Th/U dating from different localities along the Patagonian Atlantic coast (Fig. 8). Only the ESR ages allow, with an error of 10-15 %, a geochronological differentiation between Last and Penultimate Interglacial littoral terraces. In cases were several datings are available, a differentiation of beach deposits belonging to Marine Isotope Stage (MIS) 9 is partly possible.

For Holocene mollusc shells, radiocarbon dating can be an independent reliability control for ESR dating. Although such a comparison shows fairly good agreement and reproducibility, it is obvious that significant discrepancies do occur (Fig. 9). It should be kept in mind that articulated mollusc shells within a sediment layer certainly are of the same age. As the external dose rate within the sediment is equal for all samples and possible variations of internal dose rate cannot account for the observed age differences, the variation in age must be related to D_E calculation and some not yet known properties of the ESR dating signal at g = 2.0007. We can conclude that ESR ages of Holocene and Pleistocene mollusc shells can scatter substantially and result in significantly too high age estimates. It is hence necessary to date several shells out of a sediment layer to establish a reliable chronological frame for marine terraces. The given accuracy of ESR dating of mollusc shells will, however, only allow correlating the littoral deposits with certain interglacials but not more precisely.

3.2 ESR dating of Late Pleistocene land snail Helix sp. from aeolianites of the SE coast of Cyprus

Although first ESR dates for mollusc shells

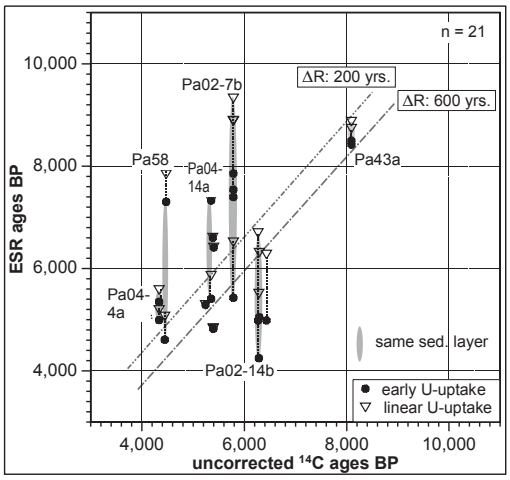

Fig. 9: Comparison of Radiocarbon and ESR ages on articulated Holocene mollusc shells from the Patagonian Atlantic coast (details in Schellmann & Radtke 2007).

Abb. 9: Vergleich von ^{14}C- und ESR-datierten, artikulierten Muschelschalen aus dem Holozän an der patagonischen Atlantikküste (Details bei Schellmann & Radtke 2007).

have been produced by Radtke (1985), little research has been carried out on dating land snails (e.g. Molodkov 1993, Skinner & Shawl 1994, Engin et al. 2006). A comprehensive study on this topic was conducted by Schellmann & Kelletat (2001) on snail shells gathered from aeolianites from the SE coast of Cyprus. The Late Pleistocene aeolianites are spread over several kilometres along the coast and are exposed in cliffs caused by littoral erosion. In some areas, such as along the coast at Nissi Beach (Fig. 10), the basal part of the aeolianite is visible just below present sea level. As the southern coast of Cyprus has only been weakly uplifted since the Last Interglacial (Schellmann & Kelletat 2001), the deposition of the aeolianite probably occurred during times when the sea level was near the coast and therefore only a few ten metres below its present position. During the Late Pleistocene, such sea level stands occurred during the later parts of MIS 5.

Snail shells of *Helix sp*. have been used to confirm this geomorphologic interpretation of the age of the aeolianites by means of geochronology (Fig. 10). According to ESR dating, the deposition of dune sands at Cape Greco took place between ca. 66,000 to 72,000 years ago. At Nissi Beach, snail shells from the aeolianites have been dated to ca. 84,000 to 95,000 yr. According to this data, deposition of the youngest aeolianites took place during the second half of MIS 5 when the sea level was not deeper than some ten metres below the present position (e.g. Thompson & Goldstein 2005; Radtke & Schellmann 2005: 99ff.). Radiocarbon dating of the mollusc shell gave much lower ages (Fig. 10) and cannot be used for geochronological interpretations. This confirms the well-known phenomenon that the upper dating limit of radiocarbon dating of carbonates is often reached at about 25,000 to 30,000 yr (Radtke 1988). The reliability of ESR dating is impressively confirmed at Cape Greco, where the aeolianites are situated on top of beach deposits of the transgression phase of the Last Interglacial (Fig. 8). ESR dates of single shells from these marine deposits indicate an age of 130,000 to 137,000 yr. All together, the results from Cyprus underline the potential of ESR to date terrestrial mollusc shells.

3.3 ESR dating of Pleistocene corals from Barbados

Due to the fact that dose rate determination is relatively unproblematic, as already discussed above, the dating of aragonitic corals has a rather high potential. First test studies on ESR dating of corals were published in the late 1980s (Ikeya & Omuhra 1983, Radtke & Grün 1988, Radtke et al. 1988, Radtke 1989, Grün et al. 1992) and since then, several methodological improvements and the development of more stabile and high-resolution ESR spectrometers have significantly increased the quality of the dating results. It is now not only possible to distinguish between the major periods of high sea level during the last 500,000 yrs but also to differentiate between sub-maxima, for example, during MIS 5 (e.g. Schellmann

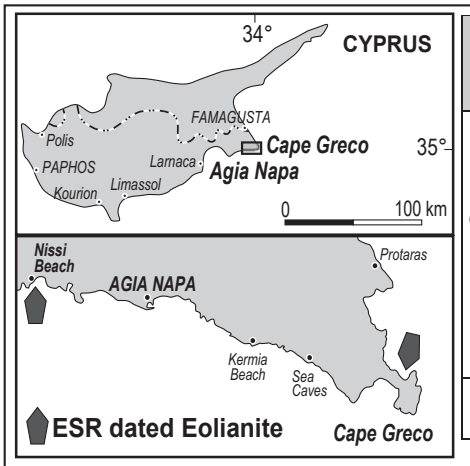

Locality	Lab. No.	Elevation (m asl.)	ESR ages early U. (ka)	±	^{14}C age (a BP)	$\delta^{13}C$
Cape Greco (P1/98, P1/00)	K 2867	14.5	**72**	5	32,500 ± 1800	-8.3
	K 4053	14.5	**67**	6		
	K 2866	11.5	**88**	10	35,000 ± 900	-6.18
	K4052	11.5	**66**	4		
	K 2865	11			29,800 ± 1000	-7.51
	K 4051	11	**70**	7		
	K 4050	11	**71**	6		-8.56
	K 2808	12	**ca. 6.8**		6,376 ± 79	
Nissi Beach	K 4054	≤ 12	**84**	6		
	K 4055	≤ 12	**95**	7		

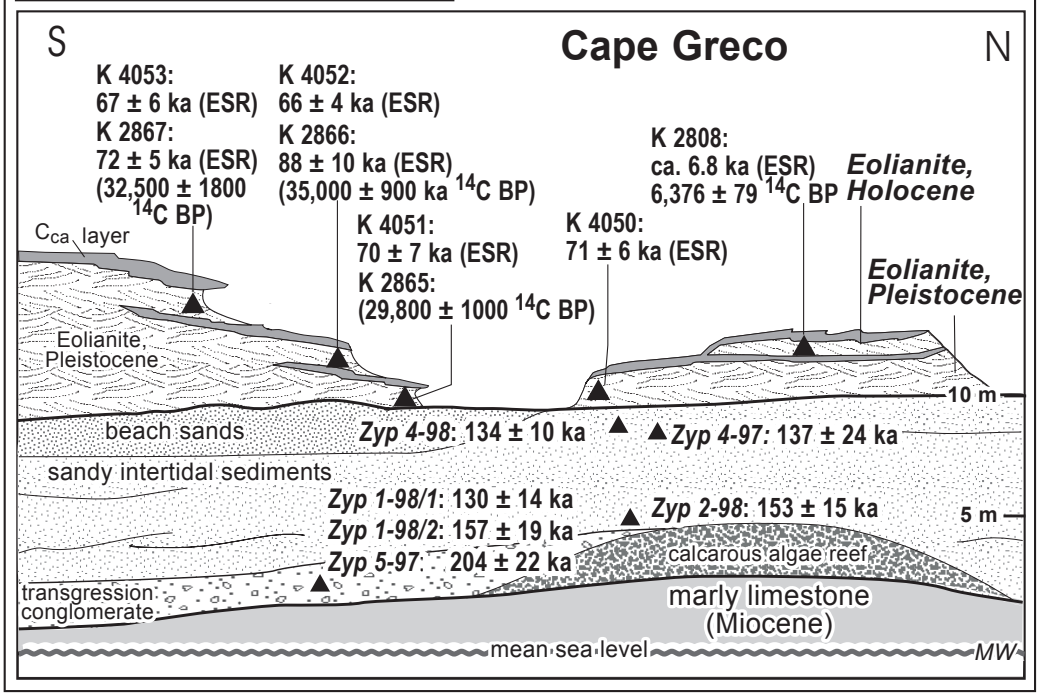

Fig. 10: Radiocarbon and ESR ages of Late Pleistocene aeolianites and beach deposits from the SE coast of Cyprus (SCHELLMANN & KELLETAT 2001).

Abb. 10: ^{14}C- und ESR-Alter spät-pleistozäner äolischer Ablagerungen und Strndablagerungen von der Südost-Küste Zyperns (SCHELLMANN & KELLETAT 2001).

et al. 2004a; SCHELLMANN & RADTKE 2004a). Prerequisite is that numerous corals from one stratigraphic unit and ideally from several locations are dated. Only with this approach, can the effect of weak diagenetic alterations of the coral material and the resulting underestimation of ESR ages be detected from the scatter of individual results. The high quality of ESR dating is proven by comparison with TIMS U/Th dating. For this purpose, up-lifted Late Pleistocene corals from different elevations and age from the southern coast of Barbados

were systematically investigated (Fig. 11). At an elevation of 21 to 43 m above present sea level (asl.), three different coral reefs that formed during the transgression maximum of MIS 5e were identified. Three coral reefs at an elevation between 4 and 17 m asl. are correlated with the sub-maximum of MIS 5c and two further reef terraces at 2-3 m asl. are interpreted to represent sub-stages MIS $5a_1$ and MIS $5a_2$ (Schellmann & Radtke 2004a, Schellmann & Radtke 2004b).

The relatively large scatter of ESR ages determined for individual coral reef terraces is most likely caused by weak diagenetic alterations, which cause re-crystallisation and/or up-take of Uranium. The result is that some ESR ages underestimate the real age of the sample. As a consequence, the oldest ESR samples are more likely to represent the actual age of a coral reef and should hence be used for the chronological interpretation. When more than 20 ESR ages were available for a coral reef terrace, this was accounted for by using the 90 percentile value, and if less than 20 ages were available, then the upper quartile value was used to determine the mean age of the reef. Comparing the results of this approach with the median of U/Th dating shows a rather good concordance (Table 2). Differences in age are on average not more than 3000 yr and hence within the error of ESR dating.

Generally, TIMS U/Th of Late Pleistocene corals is considered to be a highly precise method with analytical errors of < 1 %. However, comparing the results of ESR and TIMS Th/U dating of Last Interglacial corals from Inch Marlowe Point (Fig. 12) and Batts Rock Bay (Fig. 13) reveals that the quality of TIMS U/Th is not better than that of ESR (Schellmann et al. 2004a). At Inch Marlowe Point, ESR ages are about 1000 to 8000 yr younger than TIMS U/Th regardless the actual age of the samples. The upper quartile value of all ESR ages is 73,100 yr and the median of all U/Th ages is 76,700 yr. Interestingly, the spread of individual ages (not considering error) for both methods is about 4000 yr, although all ages were produced on individuals from the same branch of corals and are hence most likely of the same age (grown within not more than a few hundred years). Hence, the high precision of the TIMS U/Th measurements (~ 1 %) apparently does not completely account for the observed scatter in ages of isochronal samples. In contrast, the observed scatter of ESR dating is explained by the relatively high analytical error (low precision) (5-8 %). Hence, when considering the whole data set, the accuracy of

Table 2: ESR ages (upper quartile values) and TIMS U/Th ages (median values) from coral samples from the south and west coast of Barbados. TIMS U/Th dating by E.-K. Potter (Australian National University, Canberra); Details are provided by Schellmann et al. (2004a).

Tab. 2: ESR Alter (Werte oberes Quartil) und TIMS U/Th Alter (gemittelte Werte) von Korallenproben der Süd- und Westküste von Barbados. Die TIMS U/Th-Datierungen wurden von E.-K. Potter (Australian National University, Canberra) durchgeführt. Für weitere Details siehe Schellmann et al. (2004a).

Strat.	Terrace	ESR ages			U/Th ages		
		ka	±	n	ka	±	n
MIS 5a-1	T1a-1	**73.4**	5	14	76.7	0.6	12
MIS 5a-2	T1a-2	**80.9**	5	5	84.2	0.7	4
MIS 5a-2	N2	**85.5**	6	7	84.5	0.8	3
MIS 5c-3	T3	**102.6**	6	8	102.9	1	3
MIS 5c	$N1_{[5c]}$	**108.7**	9	5	105.4	1	7

ESR = Upper quartile value (25% of all ESR ages are ranked above this value)

U/Th = Median of U/Th data with initial delta ^{234}U values between 141 and 157 permil

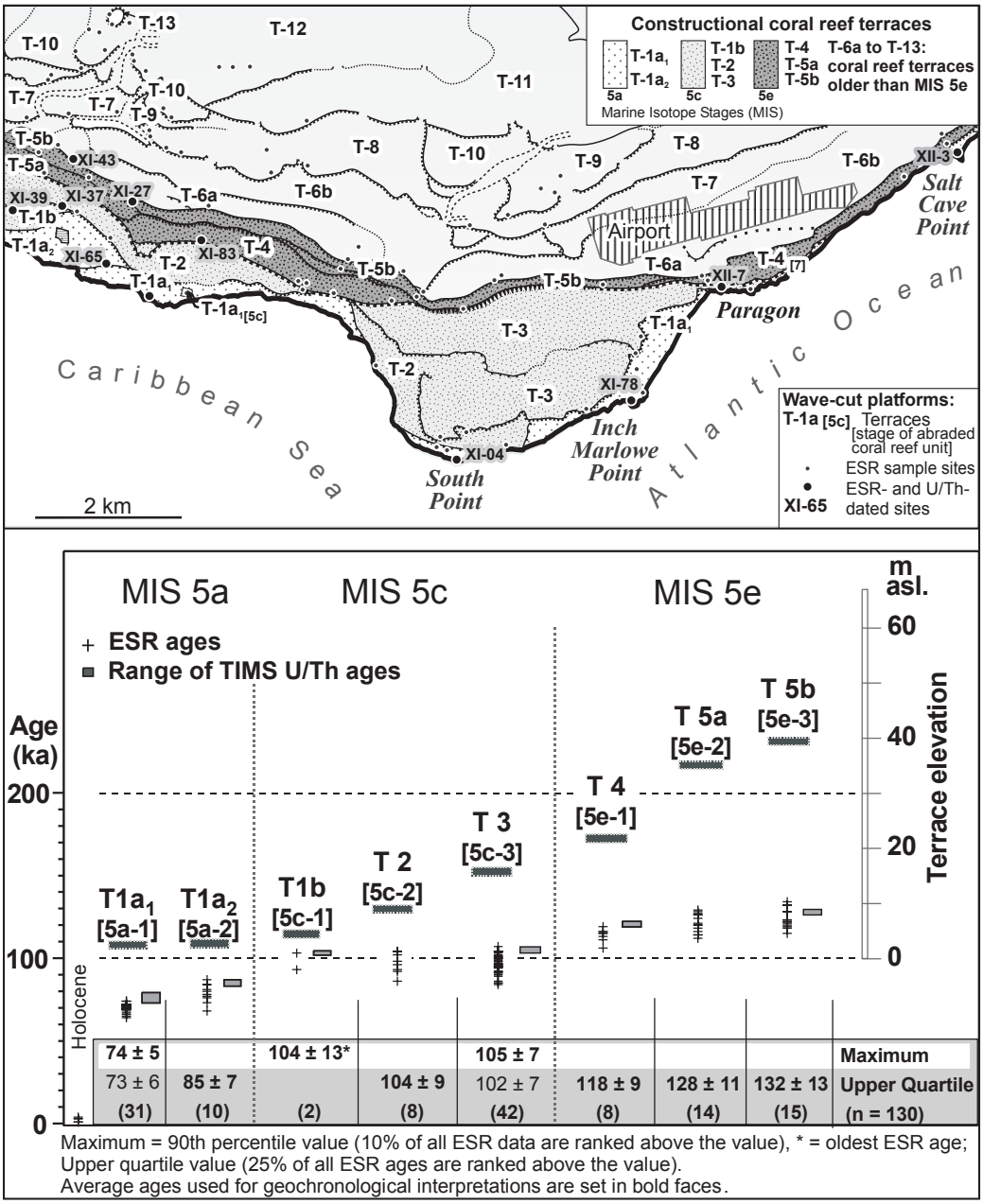

Fig. 11: Coral reef terraces along the southern coast of Barbados with location of ESR and TIMS U/Th dated corals (XI-No. = dated location). TIMS U/Th datings were carried out by E.-K. Potter (Australian National University, Canberra). Details are provided in SCHELLMANN et al. (2004a).

Abb. 11: Korallenriff-Terassen entlang der Südküste von Barbados mit den Entnahmepunkten für die Datierung von Korallen mittels ESR und TIMS U/Th (XI-No. = datierte Lokation). TIMS U/Th-Datierungen wurden von E.-K. Potter (Australian National University, Canberra) durchgeführt. Für weitere Details siehe SCHELLMANN et al. (2004a).

individual TIMS U/Th ages is not better than that of ESR dating. The best possible resolution of both dating methods is also nicely demonstrated for branches of corals sampled at Batts Rock Bay, west coast of Barbados, that were formed during the two sea level sub-maxima of MIS 5c und MIS 5a. According to this data set, both dating approaches are associated with a relatively high non-systematic spread of ages of a few thousand years.

3.4 ESR dating of Holocene corals from the Netherlands Antilles (Aruba, Bonaire, Curaçao)

To further confirm the accuracy of ESR dating, 21 radiocarbon-dated sub-modern, as well as Late and Middle Holocene, coral samples from Tsunami deposits found on Aruba, Bonaire and Curaçao (Netherlands Antilles) were dated by ESR (Fig. 14). The calibrated radiocarbon ages spread between 0 and 3644 years and the ESR ages were between 9 and 3653 yr (not considering the individual uncertainties of each measurement). Despite one sample that is considered an outlier, the ages determined for both methods are consistent within an error range of ca. 250 yr. However, most ESR data shows a tendency towards slightly higher values in ages compared to radiocarbon, which were reservoir corrected assuming that ΔR = -49 (ca. 392 yr). It is likely that the marine reservoir effect did considerably change in the past and that the assumed ΔR-value is not representative for all samples. The calibrated radiocarbon ages may hence not automatically represent the "true" age of a sample. The improved quality of ESR dating is also demonstrated by ESR dating of sub-modern corals that were collected alive by the Zoological Museum of Amsterdam University in the year 1920. For these samples, uncorrected ^{14}C ages were 586 ± 24 and 595 ± 24, respectively. ESR ages were „recent"

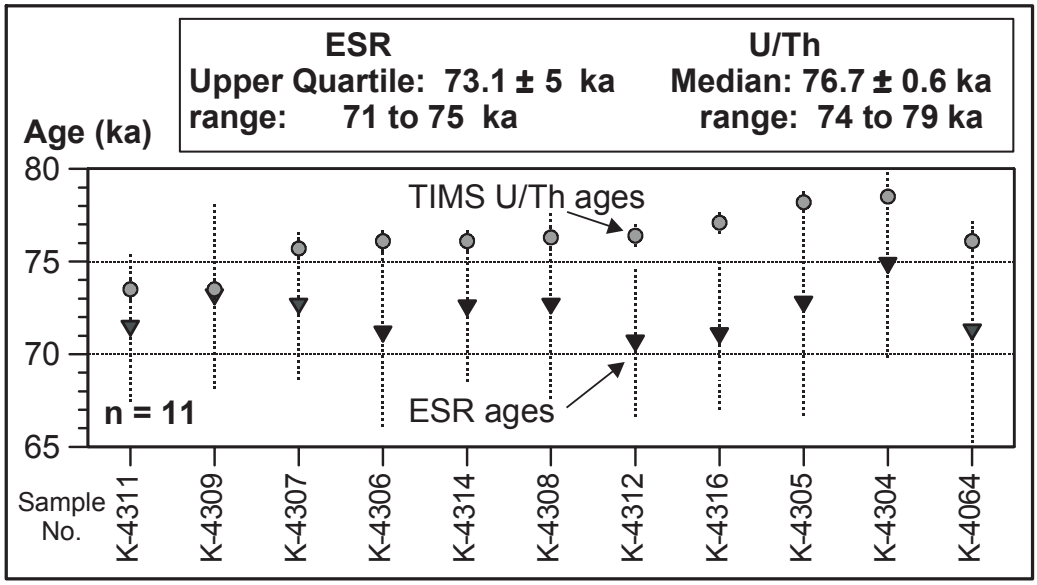

Fig. 12: ESR and TIMS U/Th ages ($\delta^{234}U$ >141 and <157‰) of coral reef terrace T-1a$_1$ near Inch Marlowe Point, southern coast of Barbados. See sample site XI-78 in Fig. 11 (slightly modified after Schellmann et al. 2004a).

Abb. 12: ESR und TIMS U/Th-Alter ($\sigma^{234}U$ >141 and <157 %) der Korallenriffterrasse T-1a bei Inch Marlowe Point an der Südküste von Barbados. Die Lage des Entnahmepunktes XI-78 ist Abb. 12 zu entnehmen (leicht verändert nach Schellmann et al. 2004).

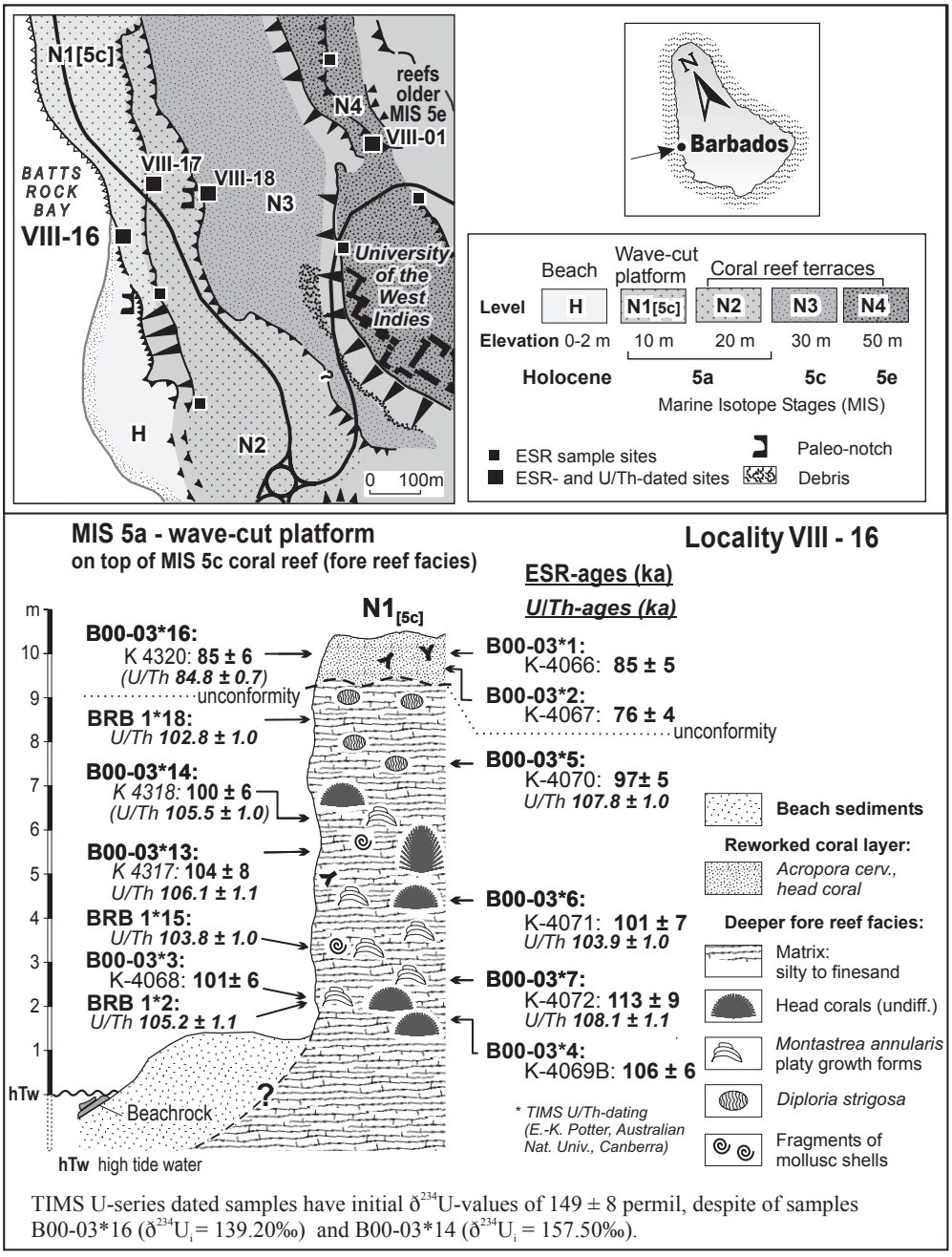

TIMS U-series dated samples have initial $\delta^{234}U$-values of 149 ± 8 permil, despite of samples B00-03*16 ($\delta^{234}U_i$= 139.20‰) and B00-03*14 ($\delta^{234}U_i$ = 157.50‰).

Fig. 13: ESR and TIMS U/Th ages of MIS 5a and MIS 5c coral reefs from Batts Rock Bay. TIMS U/Th datings were carried out by E.-K. Potter (Australian National University, Canberra). Details are provided in SCHELLMANN et al. (2004a).

Abb. 13: ESR- und TIMS U/Th-Alter von Korallenriffen (MIS 5a und MIS 5C) von Batts Rock Bay. Die TIMS U/Th-Datierungen wurden von E.-K. Potter (Australian National University, Canberra) durchgeführt. Für weitere Details siehe SCHELLMANN et al. (2004a).

and 232 ± 22 before present (~ 1778 AD) (Radtke et al. 2003: Table 1). Considering the small amplitude of the ESR dating signal from such young samples, it is astonishing that the ESR ages are much closer to the „real“ age of 1920.

4 ESR dating of quartz

4.1 ESR dating of heated quartz

As ESR signals in quartz usually decay when heated, heating mechanisms in nature may provide an appropriate means of resetting the geological clock, enabling one to establish the age of the (last) heating. For instance, xenolithic quartz in volcanic rocks in the Eifel region (Germany) was successfully dated with the Al-centre (Woda et al. 2001). In general, the ESR ages were in good agreement with independent age control (Ar-Ar) up to 500 ka (Fig. 15).

Similarly, quartz-rich sediments, which were sufficiently heated by overlying lava flows, can be used to estimate the geological age of the lava flow. Miallier et al. (1994a) showed the potential of Ti- and Al-centres to date sediment baked by a Late Pleistocene lava flow by comparison with red TL and other independent age controls. However, dating attempts of heated quartz from a ~ 580 ka pumice ($^{40}Ar/^{39}Ar$) showed scattered ESR underestimates for these centres (Miallier et al. 1994b), leading to the conclusion that the dating range of ESR is below 500 ka for such materials.

ESR results for heated quartz were recently published by Toyoda et al. (2006). In this study, Al- and Ti-centres were used for ESR dating of Quaternary tephra from Japan, in comparison with red TL and other independent age controls (fission track, K/Ar). Although some degree of consistency could be observed for samples younger than 60 ka, the ESR results appeared very scattered, internally (inconsistencies between Al- and Ti-centres) as well as externally (inconsistencies between the ESR and TL data).

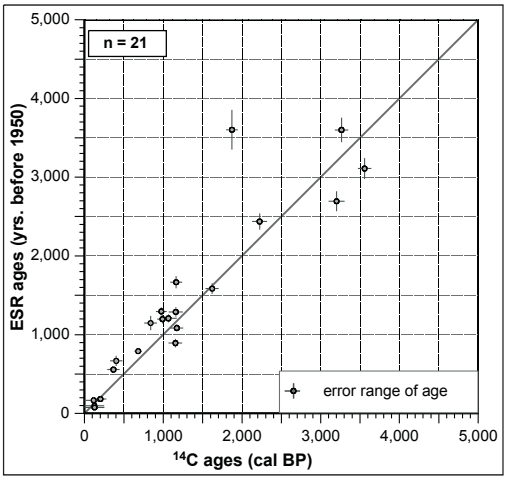

Fig. 14: ESR and radiocarbon ages of Holocene corals from Aruba, Bonaire and Curacao (Netherlands Antilles). Calibrated radiocarbon ages were corrected for marine reservoir effect. Radiocarbon dated coral samples were provided by D. Kelletat & A. Scheffers (Institut für Geographie, Universität Essen); dating and calibration by B. Kromer (Institut für Umweltphysik, Universität Heidelberg); details in Radtke et al. (2003).

Abb. 14: ESR- und ^{14}C-Alter holozäner Korallen aus Aruba, Bonaire und Curacao (Niederländische Antillen). Die kalibrierten ^{14}C-Alter wurden um den marinen Reservoireffekt korrigiert. Die ^{14}C-Alter wurden von D. Kelletat & A. Scheffers (Institut für Geographie, Universität Essen) zur Verfügung gestellt, Datierung und Kalibration durch B. Kromer (Institut für Umweltphysik, Universität Heidelberg). Weitere Details bei Radtke et al. (2003).

Reported ESR ages of heated quartz are often lower for the Al-centre, in comparison with the Ti-centre. This may be due to different thermal stabilities of Al- and Ti-centres (Toyoda & Ikeya 1994). Furthermore, high ambient temperatures such as those in geothermal areas may be sufficient to lower the natural ESR signal of volcanic quartz, eventually leading to age underestimates (Toyoda et al. 1995). Rink (1997) argued that this would lower the ESR dating range of volcanic rocks to around 50-60 ka. Alternatively, age overestimates may result from insufficient signal zeroing of ESR signals before or during the eruption (Woda et al. 2001). Several studies indicate that the

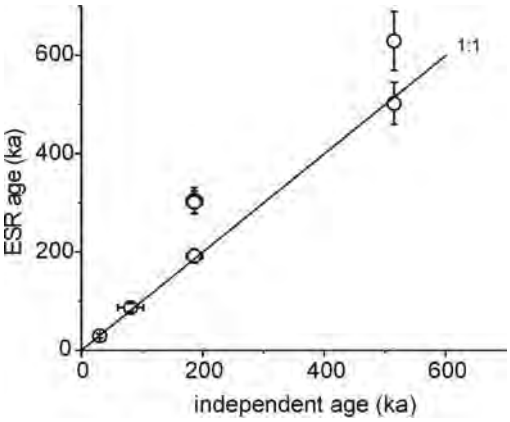

Fig. 15: ESR age plot for samples taken from volcanic deposits in the Eifel region, Germany. Replotted after WODA et al. (2001).

Abb. 15: Darstellung von ESR-Altern aus vulkanischen Ablagerungen der Eifel, Deutschland (aus WODA et al. 2001).

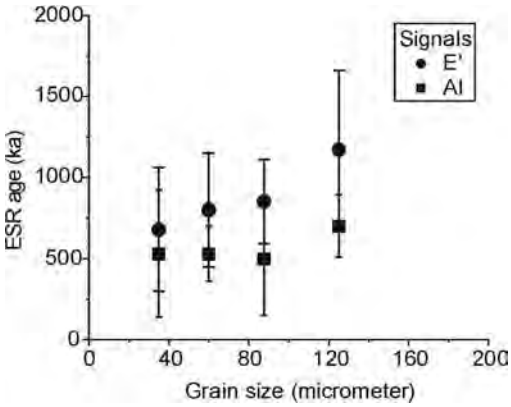

Fig. 16: ESR age plot for fault gouge from the Wangsan Fault (Southern Korea) according to the grain size and the ESR centre used. Note the systematically higher ages for the E'-centre. Replotted after LEE & YANG (2003).

Abb. 16: ESR Alter aus Proben der Wangsan Störung (Süd Korea) bezogen auf die Korngröße und das genutzte ESR Zentrum. Zu beachten sind die systematisch höheren Alter für das E`-Zentrum (nach LEE & YANG 2003).

E'-centre can be used to critically reject insufficiently heated samples (FALGUÈRES et al. 1994, WODA et al. 2001).

4.2 ESR dating of strained quartz

ESR dating of faults is based on the principle of signal zeroing due to fault activity. Fault movements may strain quartz in fault gouge in such a way that the ESR signals are completely zeroed during faulting. Subsequently, the ESR signal starts to grow again, thus allowing the determination of the geological age of the last fault movement. ESR dating of fault gouge is of particular importance in seismic risk assessment. Generally, fault gouge is dated by the ESR plateau method (BUHAY et al. 1988). The methodology involves the use of several ESR centres (usually E'-, OHC- and Al-centres) from different quartz grain size fractions. The idea is that the smaller the grain size, the more the quartz is affected by strain and the more the geological clock has been reset (Fig. 16).

Usually, the best age estimates are obtained from the smallest grain size fractions (LEE & SCHWARCZ 1994). Sometimes however, even the smallest grain size fractions (i.e., around 30 μm) do not reflect the age of the last fault movement. For instance, this was shown by LEE & YANG (2003) in a study on ESR dating of the Wangsan Fault in Southern Korea. Here, ESR ages based on the E'- and Al-centres in quartz from fault gouge cluster around 500-600 ka, but the fault gouge is considered to have been lifted to the surface by later fault movements, which were not strong enough to reset the ESR signals. As such, the reported ESR ages are considered to reflect the latest global reactivation of the fault. In some cases, it appears only possible to calculate maximum ages for the last fault reactivation, as shown by LEE & YANG (2007).

The E_1'-centre is commonly observed in quartz and silica, and has been used to investigate the age of fault movements, heated flint and volcanic ash. However, ESR ages based on this centre should be carefully interpreted because of the possible occurrence of an overlapping unstable signal, the so-called counterfeit E_1'-signal (TOYODA & SCHWARCZ 1994)

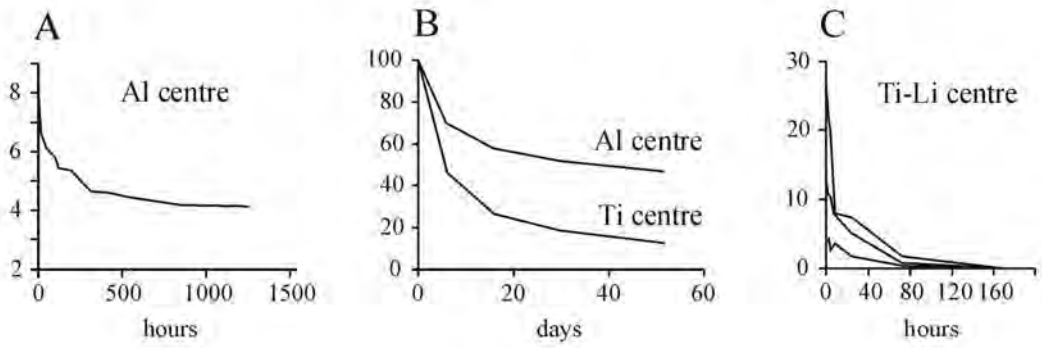

Fig. 17: Simplified bleaching curves for Al- and Ti-centres in quartz. Replotted after A: Laurent et al. (1998), B: Brumby & Yoshida (1994) and C: Toyoda et al. (2000). A: UV-lamp, B: natural sunlight, C: halogen lamp.

Abb. 17: Vereinfachte Bleichkurve für die Al- und Ti-Zentren in Quarz. A: nach Laurent et al. (1998). B: nach Brumby & Yoshida (1994) und C: nach Toyoda et al. (2000). A: UV-Lampe, B. natürliches Sonnenlicht, C: Halogenlampe.

4.3 ESR dating of sedimentary quartz

Quartz grains that are exposed to natural sunlight sufficiently long will have their ESR signals reset to a certain extent during transport, prior to burial (Fig. 17). This important principle forms the basis of ESR dating of sediments. It is one of the most promising sub-disciplines in ESR dating. The specific age range of ESR dating of quartz, possibly up to several Ma, makes sediment dating a potentially very valuable tool, with applications in geology, geography, prehistory and palaeoanthropology. The specific issue in ESR dating of sediments is the extent to which the geological clock is reset to zero, or to a value, which can be determined in the laboratory. Resetting of the geological clock proceeds through sunlight bleaching of ESR centres during transport, prior to burial. Experimental bleaching curves are shown in Fig. 17 for various ESR centres and various artificial light sources. The Al-centre contains an unbleachable residual, whereas Ti-centres can be fully (or to a negligible level) reset. Note that bleaching times are on the order of days to weeks.

4.3.1 Aeolian sediments

The most straightforward application of ESR dating of sedimentary quartz is that of aeolian sediments, because of the sunlight bleaching potential. Several studies report reasonable ESR ages for aeolian sand, based on the Al-centre, in the time frame up to several 100 ka (Yokoyama et al. 1985, Tanaka et al. 1995). Since the Al-centre contains an important unbleachable residual with respect to natural sunlight radiation, it is important to mention that the ESR ages reported in these studies are corrected for this residual. The principle of this method is shown in Fig. 18. Recent investigations in ESR dating of aeolian sand using the Al-centre also include Chinese loess deposits (Yin et al. 2007). Although the results show a strong underestimate relative to the independent age control of the loess, the method seems very promising if the residual dose can be determined very accurately.

The problem of residual doses is less pertinent with Ti-related ESR centres because bleaching studies indicate that the ESR signal can be reset completely or at least to a negligible level with respect to deposits older than Late Pleistocene. Recently for instance, it was shown that in-

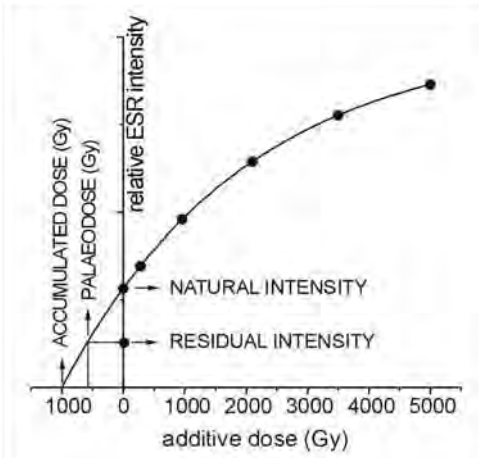

Fig. 18: Correction for the unbleachable residual in ESR dating of quartz sediments using the Al-centre. The residual intensity is measured after prolonged bleaching and this level is used to infer the true palaeodose. Replotted after LAURENT et al. (1998).

Abb. 18: Korrektur unbleichbarer Reste bei der ESR-Datierung von Quarzsedimenten unter Berücksichtigung des Al-Zentrums. Die Restintensität wird nach verlängerter Bleichung gemessen, wobei dieses Niveau zur Bestimmung der Paläostrahlungsrate genutzt wird (nach LAURENT et al. 1998).

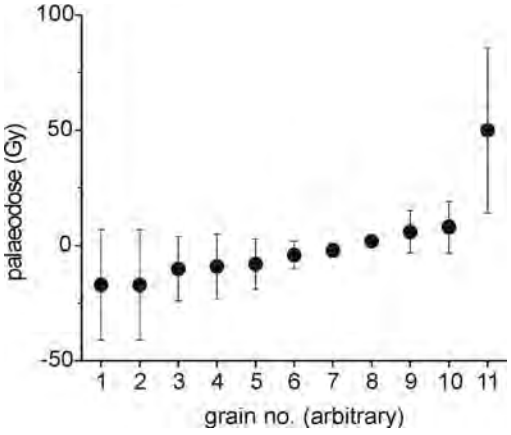

Fig. 19: ESR equivalent dose plot for Ti-centres from individual grains taken from a modern desert surface deposit, Eastern Desert, Egypt. Except for one grain (no. 11), all values are consistent with the expected dose of 0 Gy. Replotted after BEERTEN & STESMANS (2005).

Abb. 19: Darstellung der ESR Äquivalent Dosis für Ti-Zentren, gemessen an Einzelkörner moderner Oberflächenablagerungen aus der Östlichen Wüste, Ägypten. Mit Ausnahme einer Messung (Korn Nr. 11) zeigen alle Messungen konsistente Ergebnisse um den erwarteten Wert von 0 Gy (nach BEERTEN & STESMANS 2005).

dividual quartz grains show non-existing or only very small residual Ti-related doses in an Egyptian desert sand deposit (Fig. 19; BEERTEN & STESMANS 2005).

The potential and problems of multiple grain ESR dating using Ti-centres has been outlined in BEERTEN et al. (2006) for Australian sand dunes up to 350 ka. Large differences are often encountered for individual Ti-related sub-centres in the regenerative dose method, but it is not clear yet whether this is due to sensitivity changes or not. ESR ages based on Ti-H centres seem to underestimate the OSL ages for this profile, whereas the opposite is true for Ti-Li centres. Comparisons with the additive dose method are often hampered by improper dose response showing inflexion points (BEERTEN et al., in press).

The potential and problems of single grain ESR dating using Ti-centres has been outlined in BEERTEN & STESMANS (2007). The first results of this new approach in ESR dating are very promising, but appropriate adaptations in instrumentation and equipment are necessary to make it more flexible and user friendly.

4.3.2 Fluvial and estuarine sediments

ESR dating has been shown to be a useful tool for establishing geochronological frameworks for fluvial and estuarine/marine deposits. Despite proven difficulties with bleaching residuals related to the Al-centre in quartz, this specific ESR centre has been used in many studies to date sedimentary sequences spanning the whole Quaternary period, and even up to the Miocene. A famous example of ESR dating of a fluvial terrace staircase is that from the Somme Basin, France, where consistent ESR results could be obtained relative to biostratigraphi-

cal, archaeological and palaeomagnetic data (Fig. 20; Laurent et al. 1998, Antoine et al. 2000). The same methodology, i.e. ESR of the Al-centre with subtraction of the unbleachable residual, has been used for other terrace staircases as well, with promising results (Voinchet et al. 2004, Bahain et al. 2007, Tissoux et al. 2007). The Al-centre even has the potential to date Plio-Miocene estuarine deposits, as was shown by Laurent et al. (1998). In this study, a consistent ESR dating pattern for deposits from the Tiglian up to the Tortonian (around 8-9 Ma) was obtained.

The quality of the ESR ages from these studies is guaranteed to some extent by bleaching experiments on recent fluvial deposits. Laurent et al. (1998) and Voinchet et al. (2003, 2007) showed that the Al-related ESR signal in quartz is at or very close to the unbleachable residual

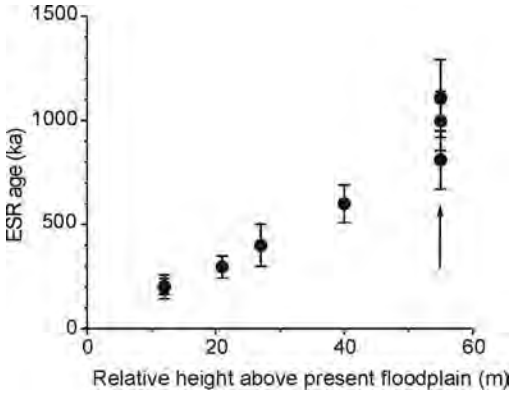

Fig. 20: ESR dating of the River Somme terrace staircase. Replotted from data in Laurent et al. (1998) and Antoine et al. (2000). Only ESR ages on quartz are given. Other age control is available for the terrace sequence. The highest level in this diagram is supposed to be older than the B/M boundary, based on palaeomagnetic measurements. This is confirmed by the ESR dates (see arrow).

Abb. 20: ESR-Daten aus der Somme Terrassenstufe. (nach Laurent et al. 1998 und Antoine et al. 2000). Es sind nur Alter von Datierungen an Quarz dargestellt. Für die Terrassensequenz sind auch andere Alterskontrollen möglich. Für die oberste Stufe wird durch paläomagnetische Altersbestimmung ein Alter älter als die B/M Grenze angenommen. Dies wird durch die ESR-Daten bestätigt (s. Pfeil).

level for various modern (i.e. zero-age) fluvial samples. Another point that should be kept in mind when evaluating such ESR dating results, is the targeted age range. Whereas, due to the slow bleaching behaviour, the Al-centre is probably inappropriate for detailed chronologies in the Late and late Middle Pleistocene, it may be a valuable tool for rough age determinations of extended Early Pleistocene and Pliocene sedimentary sequences, especially if other age-markers or suitable materials for dating are absent. Therefore, the highest potential of the Al-centre could be situated in the Tertiary, where a rough assignment to chronozones could be sufficient to tune estuarine/marine sedimentary sequences to the global sequence-stratigraphic timescale.

However, some fundamental issues in ESR dating using the Al-centre remain ambiguous. First, the determination of the bleaching residual usually proceeds through artificial bleaching experiments using some kind of 'solar simulator'. Up to the present, it is unclear how the irradiation spectrum of the solar lamp influences the magnitude of this residual. Second, the accuracy of the results is only guaranteed if this bleaching residual is a fixed value, in terms of absolute ESR defect concentration, as was pointed out by Brumby & Yoshida (1994b).

Lately, more attention has been paid to the use of Ti-centres for ESR dating of fluvial deposits from terrace staircases as well. A comparative study between ESR dating results of Al- and Ti-centres recently showed that both species have a large potential in geochronological studies (Tissoux et al. 2007). However, from detailed studies it has become clear that individual ages at the single-grain scale may vary considerably if Ti-centres are used (Beerten et al. 2003). Ti-related ESR centres may even contain a small but detectable unbleachable residual, as was recently shown with artificial bleaching experiments on fluvial quartz (Voinchet et al. 2007).

4.3.3 Glacial sediments

Grinding of quartz grains may occur not only

in a fault-related context, but also in some sedimentary environments. Together with sunlight bleaching, such grinding mechanisms could be an effective zeroing mechanism in ESR dating of glacially derived sediments. As such, the Ge-related impurity centre in quartz appears to generate promising results, e.g. in dating Pleistocene glaciations in Central Asia (ZHAO et al. 2006, ZHOU et al. 2006).

Whereas the basis for this specific ESR approach was laid by methodological studies on the behaviour of Ge-centres with respect to sunlight bleaching and pressure (TANAKA et al. 1985, BUHAY et al. 1988, YE et al. 1998), some fundamental points remain unclear. For instance, although growing with small artificial irradiation doses, it appears very difficult to find a natural Ge signal in quartz, as has been pointed out already by RINK (1997). The implication of this observation could be that the Ge centre is not stable at average burial temperatures.

4.4 General remarks

Various methodological issues are common to all types of quartz, irrespective of the geological context. Generally, the additive dose method is used to determine the equivalent dose in quartz. However, sometimes this approach may lead to large uncertainties for samples with a relatively large equivalent dose. In such cases, it would be advantageous to use the regenerative dose method. For ESR centres in quartz, artificial heating may be the most efficient and comfortable way of annealing the signal prior to regenerative dosing. Although this mechanism is not the annealing mechanism in sedimentary environments, this approach is currently being tested for ESR dating of sediments using Ti-related centres (BEERTEN et al. 2006). A major concern here is the possible presence of sensitivity changes (i.e. an alteration of the radiation-sensitivity of the ESR-signal) due to the heating step. Less comfortable in experimental terms, but much more related to the zeroing mechanism in sedimentary environments, is optical bleaching of ESR centres prior to administering the regenerative dose. First results of this approach were recently published for Al-centres in loess (YIN et al. 2007). Unfortunately, the ESR dose response is often found to be problematic in various quartz samples. Sometimes, strong inflexion points are found in the dose response of the Ti-centre and the Al-centre. There are also observations on non-monotonic linear growth of Ti- and Ge-centres, indicating an ESR signal decrease with very high doses of several 1000 Gy (WODA & WAGNER, in press).

5 ESR dating of some other materials (speleothems, foraminifera, tooth enamel)

ESR dating has also been applied to a wide variety of other materials with great importance, especially in palaeoclimatological and archaeological contexts. The most common applications in this framework include speleothems, foraminifera, and tooth enamel.

Many ESR papers have published combined ESR and U-series dating results of speleothems (stalagmites, stalactites), which generally show good agreement. A detailed review is given by RINK (1997: 990f.). Nevertheless, as stated by PIROUELLE et al. (2007), further research is still needed about the best analytical routine for obtaining correct D_E values, which include systematic dating applications coupled with other (e.g. U-series) dating methods. However, as GRÜN (2007: 1512) stated, U series dating of speleothems and other secondary carbonates is much cheaper, faster and more accurate than ESR.

Studies on ESR dating of planctonic foraminifera from a deep-sea sediment core by MUDELSEE et al. (1992) show good agreement with delta ^{18}O stratigraphy. The authors see the possibility to date planctonic foraminifera up to approx. 800 ka by using the ESR signal at g = 2.0036. More recently, HOFFMANN et al. (2001) stated that foraminifera could be dated up to 190 ka, just when using the CO_2^--signal at g = 2.0006. All in all, more studies on well-stratified deep sea cores in combination with independent age controls are needed to show

the potential and the limits of ESR dating of foraminifera.

Lately, ESR dating on human tooth enamel, in conjunction with laser ablation U-series dating, has become an important method for determining the age of human remains back to about 200 to 300 ka, beyond the time range of the ^{14}C dating method (e.g. Grün 2006, 2007; Soressi et al. 2007). Most recently, Grün (2006) gives a detailed description of the ESR dating method itself in application on human teeth, which includes application examples and comparisons with other dating results (^{14}C, U-series, AAR). In addition, Hameau et al. (2007) see a good agreement of coupled ESR/Uranium-series dating of Middle Pleistocene *Rhinocerus* and *Tapirus* tooth enamel on East Java associated with lithic artefacts, which seems to provide a new geochronological framework of human occupation in South-East Asia. Details on ESR dating of teeth are summarized by Grün (2006) and Rink (1997).

There are further materials, e.g. travertines, calcretes or bones, which have been the object of ESR dating. However, the ages are less reliable due to complex Uranium uptake histories, to problems of recrystallisations or to carbonate impurities, which often lead to age underestimations (e.g. Rink 1997; Grün 2007).

6 Summary and outlook

Due the methodological advances of the past decade, ESR dating has become an important geochronological method, especially for dating deposits such as coral reefs and beach ridges as well as quartz from different geological settings. The reliability of ESR dating of carbonates was proven by direct comparison with other dating methods such as radiocarbon and TIMS U/Th. ESR dating of Holocene corals shows accuracy similar to radiocarbon dating when all sources of uncertainty are fully considered. ESR dating of Pleistocene corals allows not only to distinguish between MIS 1, 5, 7, 9, 11 and 13 deposits, but also between sub-stages $5e_{3/2}$, $5e_1$, 5c, $5a_1$ and $5a_2$. The average error of ESR dating of corals is about 5-8%. Late Pleistocene corals can be dated with a similar accuracy as with TIMS U/Th in this time range. The advantage of ESR, however, is that the upper dating limit for corals is probably above 500,000 yr. If diagenesis could be excluded, dating of coral with an age of several million years should be feasible from the physical point of view.

The resolution of ESR dating of molluscs and gastropods is with 10-15 % much lower. Additionally, ages tend to scatter quite substantially, which causes the need to carry out several datings for the same stratigraphic unit to allow accurate geochronological interpretation. Usually it is then possible to correlate layers to certain interglacials periods such as MIS 1, 5, 7 and 9. The high scatter associated with ESR ages of molluscs and gastropods is most likely related to yet not identified problems in palaeodose determination, since problems in dose rate apparently do not account for the scatter.

The examples shown in this paper demonstrate that ESR can be successfully applied to date quartz in various geological contexts. It should be clear that the large age range of ESR dating (up to several Ma), especially in relation to OSL dating (up to several 100 ka), underlines its important position next to other geochronological techniques. However, there are several issues that need further consideration. The accuracy with which the palaeodose can be determined is highly dependent on the degree of resetting of the ESR signal. Some examples show that incomplete resetting could undermine the reliability of the method. Therefore, it is important to incorporate criteria (external and internal) to evaluate the completeness of the zeroing process in nature, such as the plateau method for fault gouge and the use of multiple ESR centres and/or single grain measurements for sediment dating. Cross-checking of the results with independent age control is another crucial step in the development of a reliable ESR dating method. In the case of sediments, reference ages may be provided by luminescence dating (OSL, TL) for Late Pleistocene and in favourable circumstances even Middle Pleis-

tocene deposits. Similarly, ESR dating results of tephra layers could be evaluated against red TL measurements.

The reliability of the palaeodose determination method, purely experimentally, is another concern in ESR dating of quartz. Results of the regenerative dose method and additive dose method should be compared very carefully and a proper annealing mechanism should be looked for in the regenerative dose method (UV-bleaching for sedimentary quartz; thermal annealing for heated quartz). At present, experimental techniques in ESR dating of quartz produce relatively large errors (usually around 15%). In part, this may be related to the dose determination method (i.e. the additive dose technique in the case of older samples), but it is important to verify if intrinsic properties of ESR defects could be the cause of such large errors (i.e. inflexion points). In general, it is believed that the regenerative dose technique may produce much more precise results if there are no sensitivity changes.

There are even more materials, which have the potential for a dating by ESR, however the most reliable applications until now or in the near future seem to be coupled ESR/U-series dating of tooth enamel and perhaps speleothems. A great potential is inherited in ESR dating of foraminifera, which only needs more applications.

In summary, it is clear that the development of the ESR method is far from being complete and it is important to carry out methodological investigations before the full potential of the method can be used.

Acknowledgements

We thank the German Research Foundation (Deutsche Forschungsgemeinschaft, DFG) (grants Ra 383/6-1 to 6-3, Sche 465/2-1) and the Universities of Bamberg, Cologne and Essen for supporting the studies financially during the past years. We are grateful to the Centre of Nuclear Medicine, University of Düsseldorf, for support with ^{60}Co irradiation. Special thanks to Dr. Bernd Kromer (University of Heidelberg) and the Institute of Physics (University of Erlangen) for the Radiocarbon data. We are also grateful to W.J. RINK and an unknown reviewer for their helpful comments. Last, but not least, we would like to say many thanks to Dr. Frank Preusser (University of Bern), who translated large parts of the manuscript, and to Mrs. Karen Schneider (University of Cologne) for polishing the English of the manuscript.

References

ANTOINE, P., LAUTRIDOU, J.P. & LAURENT, M. (2000): Long-term fluvial archives in NW France: response of the Seine and Somme rivers to tectonic movements, climatic variations and sea-level changes. – Geomorphology, 33: 183-207.

BAHAIN, J.J., FALGUÈRES, C., LAURENT, M., VOINCHET, P., DOLO, J.M., ANTOINE P. & TUFFREAU, A. (2007): ESR chronology of the Somme River Terrace system and first human settlements in Northern France. – Quaternary Geochronology, 2: 356-362.

BARABAS, M., BACH, A., MUDELSEE, M. & MANGINI, A. (1992): General properties of the paramagnetic centre at g = 2.0006 in carbonates. – Quaternary Science Reviews, 11: 165-171.

BEERTEN, K. & STESMANS, A. (2005): Single quartz grain ESR dating of a contemporary desert surface deposit, Eastern Desert, Egypt. – Quaternary Science Reviews, 24: 223-231.

BEERTEN, K. & STESMANS, A. (2007): ESR dating of sedimentary quartz: possibilities and limitations of the single grain approach. – Quaternary Geochronology, 2: 373-380.

BEERTEN, K., PIERREUX, D. & STESMANS, A. (2003): Towards single grain ESR dating of sedimentary quartz: first results. – Quaternary Science Reviews, 22: 1329-1334.

BEERTEN, K., LOMAX, J., CLÉMER, K., STESMANS, A. & RADTKE, U. (2006): On the use of Ti centres for estimating burial ages of Pleistocene sedimentary quartz: Multiple-grain data from Australia. – Quaternary Geochronology, 1: 151-158.

BEERTEN, K., RITTNER, S., LOMAX, J. & RADTKE, U. (in press): Dose recovery tests using Ti-related ESR signals in quartz: first results. – Quaternary Geochronology.

Blackwell, B.A.B. (2006): Electron Spin Resonance (ESR) dating in Karst environments. – Acta Carsologica, 35/2: 123-153.

Brumby, S. & Yoshida, H. (1994a): ESR dating of mollusc shell: investigations with modern shell of four species. – Quaternary Science Reviews, 13: 157-162.

Brumby, S. & Yoshida, H. (1994b): An investigation of the effect of sunlight on the ESR spectra of quartz centres: implications for dating. – Quaternary Science Reviews 13, 615-618.

Buhay, W.M., Schwarcz, H.P. & Grün, R. (1988): ESR dating of fault gouge: the effect of grain size. – Quaternary Science Reviews, 7: 515-522.

Engin, B., Kapan-Yeşilyurt, S., Tanner, G., Demirtaş H. & Eken, M. (2006): ESR dating of Soma (Manisa, West Anatolia – Turkey) fossil gastropoda shells. – Nuclear Instruments and Methods in Physics Research B, 243: 397-406.

Falguères, C., Yokoyama, Y. & Miallier, D. (1994): Stability of some centres in quartz. – Nuclear Tracks and Radiation Measurements, 18: 155-161.

Grün, R. (1985): Beiträge zur ESR-Datierung. – Sonderveröffentlichungen des Geologischen Instituts der Universität zu Köln, 59: 1-157.

Grün, R. (1989a): Electron Spin Resonance (ESR) dating. – Quaternary International, 1: 65-109.

Grün, R. (1989b): Die ESR-Altersbestimmungsmethode. – Heidelberg, Berlin (Springer).

Grün, R. (1990): Dose response of the paramagnetic centre at g = 2.0007 in corals. – Ancient TL, 8: 20-22.

Grün, R. (2006): Direct dating of Human Fossils. – Yearbook of Physical Anthropology, 49: 2-48.

Grün, R. (2007): Electron Spin Resonance Dating. – In: Elias, S.A. (ed.): Encyclopedia of Quaternary Science, Vol. 2: 1505-1516; Amsterdam (Elsevier).

Grün, R. & Katzenberger-Apel, O. (1994): An alpha irradiator for ESR dating. – Ancient TL, 12: 35- 38.

Grün, R., Radtke, U. & Omura, A. (1992): ESR and U-series analyses on corals from Huon Peninsula, New Guinea. – Quaternary Science Reviews, 11: 197-202.

Hameau, S., Falguéres, C., Bahain, J.J., Sémah, F., Sémah, A.M., & Dolo, J.M. (2007): ESR dating in Song Terus cave (East Java, Indonesia). – Quaternary Geochronology, 2: 398-402.

Hoffmann, D., Woda, C., Strobl, Ch. & Mangini, A. (2001): ESR-Dating of the Arctic sediment core PS1535 dose-response and thermal behaviour of the CO_2^- signal in foraminifera. – Quaternary Science Reviews, 20: 1009-1014.

Ikeya, M. (1975): Dating a stalactite by electron paramagnetic resonance. – Nature, 255: 48-50.

Ikeya, M. (1993): New applications of Electron Spin Resonance. Dating, dosimetry and microscopy. – Singapore.

Ikeya, M. & Ohmura, K. (1981): Dating of fossil shells with electron spin resonance. – Geology, 89: 247-251.

Ikeya, M. & Ohmura, K. (1983): Comparison of ESR ages of corals from marine terraces with ^{14}C and 230Th/234U ages. – Earth and Planetary Science Letters, 65: 3438.

Jonas, M. (1997): Concepts and methods of ESR dating. – Radiation Measurements, 27: 943-973.

Katzenberger, O. (1989): Experimentelle Untersuchungen zur ESR-Datierung von Molluskenschalen. – Sonderveröffentlichungen des Geologischen Institutes der Universität zu Köln, 72.

Katzenberger, O. & Willems, N. (1988): Interferences encountered in the determination of AD of mollusc samples. – Quaternary Science Reviews, 7: 485-489.

Kinoshita, A., Karmann. I., da Cruz, F.W. (Jr.), Graeff, C.F.O. & Baffa, O. (2005): K-band ESR spectra of calcite stalagmites from southeast and south Brazil. – Applied Radiation and Isotopes, 62: 247-250.

Laurent, M., Falguères, C., Bahain, J.J., Rousseau, L. & Van Vliet Lanoé, B. (1998): ESR dating of quartz extracted from Quaternary and Neogene sediments: method, potential and actual limits. – Quaternary Science Reviews, 17: 1057-1062.

Lee, H.K. & Schwarcz, H.P. (1994). Criteria for complete zeroing of ESR signals during faulting of the San Gabriel fault zone, Southern California. – Tectonophysics, 235: 317-337.

Lee, H.K. & Yang, J.S. (2003): ESR dating of the Wangsan fault, South Korea. – Quaternary Science Reviews, 22: 1339-1343.

Lee, H.K. & Yang, J.S. (2007): ESR dating of the Eupchon fault, South Korea. – Quaternary Geochronology, 2: 392-397.

Lyons, R. (1987): Alpha/gamma response of calcite speleothems as determined by nuclear accelerator techniques. – Fifth Specialist Seminar on TL and ESR dating, 6-10 July 1987, Abstract; Cambridge.

Miallier, D., Sanzelle, S., Falguères, C., Faïn, J., Montret, M., Pilleyre, Th., Soumana, S., Laurent, M., Camus, G. & De Goër de Hervé, A. (1994a): Intercomparisons of red TL and ESR

signals from heated quartz grains. – Radiation Measurements, 23: 143-153.

MIALLIER, D., FAÏN, J., SANZELLE, S., PILLEYRE, TH., MONTRET, M., SOUMANA, S. & FALGUÈRES, C. (1994b). Attempts at dating pumice deposits around 580 ka by use of red TL and ESR of xenolithic quartz inclusions. – Radiation Measurements, 23: 399-404.

MALMBERG, R. & RADTKE, U. (2000): The α-efficiency of corals and its importance for ESR-dating. – Radiation Measurements, 32: 747-750.

MOLODKOV, A. (1993): ESR-Dating of non-marine mollusc shells. – Applied Radiation and Isotopes, 44: 145-148.

MOLODKOV, A., DREIMANIS, A., ABOLTINŠ & RAUKAS, A. (1998): The ESR age of portlandia arctica shells from glacial adeposits of central lativa: an answer to a controversy on the age and genesis of their enclosing sediments. – Quaternary Geochronology, 17: 1077-1094.

MUDELSEE, M., BARABAS, M. & MANGINI, A. (1992): ESR dating of the Quaternary deep-sea sediment core RC17-177. – Quaternary Science Reviews, 11: 181-189.

PIROUELLE, F., BAHAIN, J.J., FALGUÈRES, C. & DOLO, J.M. (2007): Study of the effect of a thermal treatment on the D_E determination in ESR dating of speleothems. – Quaternary Geochronology, 2: 386-391.

PRESCOTT, J.R. & HUTTON, J.T. (1994): Cosmic ray contributions to dose rates for luminescence and ESR dating: large depths and long-term time variations. – Radiation Measurements, 23: 497-500.

RADTKE, U. (1985): Zur zeitlichen Stellung mariner Terrassen auf Fuerteventura (Kanarische Inseln). – Kieler Geographische Schriften, 62: 73-95.

RADTKE, U. (1988): How to avoid useless Radiocarbon dating. – Nature, 333: 307-308.

RADTKE, U. (1989): Marine Terrassen und Korallenriffe - Das Problem der quartären Meeresspiegelschwankungen. Erläutert an Fallstudien aus Chile, Argentinien und Barbados. – Düsseldorfer Geographische Schriften, 27: 245 S.

RADTKE, U. & GRÜN, R. (1988): ESR dating of corals. – Quaternary Science Reviews, 7: 465-470.

RADTKE; U. & SCHELLMANN, G. (2005): Timing and magnitude of sea level change during MIS 5 derived from Barbados coral reef terraces: a critical literature review and new data. – Journal of Coastal Research, SI 42: 52-62.

RADTKE, U., GRÜN, R. & SCHWARCZ, H.P. (1988): Electron spin resonance dating of the Pleistocene coral reef tracts of Barbados. – Quaternary Research, 29: 197-215.

RADTKE, U., HENNIG, G.J., LINKE, W. & MÜNGERSDORF, J. (1981): $^{230}Th/^{234}U$ and ESR-dating of fossil shells in Pleistocene marine terraces (Northern Latium, Central Italy). – Quaternaria, 23: 37-50.

RADTKE, U., SCHELLMANN, G., SCHEFFERS, A., KELLETAT, D., KASPER, H.U. & KROMER, B. (2003): Electron Spin Resonance and Radiocarbon dating of coral deposited by Holocene tsunami events on Curaçao, Bonaire and Aruba (Netherlands Antilles). – Quaternary Science Reviews, 22: 1309-1315.

RINK, W. J. (1997): Electron Spin Resonance (ESR) Dating and ESR applications in Quaternary science and archaeometry. – Radiation Measurements, 27: 975-1025.

SCHELLMANN, G. (1998): Jungkänozoische Landschaftsgeschichte Patagoniens (Argentinien). Andine Vorlandvergletscherungen, Talentwicklung und marine Terrassen. – Essener Geographische Arbeiten, 29: 216 S.

SCHELLMANN, G. & KELLETAT, D. (2001): Chronostratigraphische Untersuchungen litoraler und äolischer Formen und Ablagerungen an der Südküste von Zypern mittels ESR-Altersbestimmungen an Molluscen- und Landschneckenschalen. – Essener Geographische Arbeiten, 32: 75-98.

SCHELLMANN, G. & RADTKE, U. (1999): Problems encountered in the determination of dose and dose rate in ESR dating of mollusc shells. – Quaternary Science Reviews, 18: 1515-1527.

SCHELLMANN, G. & RADTKE, U. (2000): ESR dating stratigraphically well-constrained marine terraces along the Patagonian Atlantic coast (Argentina). – Quaternary International, 68-71: 261-273.

SCHELLMANN, G. & RADTKE, U. (2001): Progress in ESR dating of Pleistocene corals - a new approach for D_E determination. – Quaternary Science Reviews, 20: 1015-1020.

SCHELLMANN, G. & RADTKE, U. (2003): Die Datierung litoraler Ablagerungen (Korallenriffe, Strandwälle, Küstendünen) mit Hilfe der Elektronen-Spin-Resonanz-Methode (ESR). – Essener Geographische Arbeiten, 35: 95-113.

SCHELLMANN G. & RADTKE, U. (2004a): The marine Quaternary of Barbados. – Kölner Geographische Schriften, 81; 137 pp.

SCHELLMANN, G. & RADTKE, U. (2004b): A revised morpho- and chronostratigraphy of the Late and Middle Pleistocene coral reef terraces on South-

ern Barbados (West Indies). – Earth-Science Reviews, 64: 157-187.

Schellmann, G. & Radtke, U. (2007): Zur ESR-Datierung holozäner und jungpleistozäner Muschelschalen – aktuelle Möglichkeiten und Grenzen. – Bamberger Geogr. Schr., 22: 113-152; (in press).

Schellmann, G., Radtke, U., Potter, E.-K., Esat, T. M. & McCulloch, M.T. (2004a): Comparison of ESR and TIMS U/Th dating of marine isotope stage (MIS) 5e, 5c, and 5a coral from Barbados - implications for palaeo sea-level changes in the Caribbean. – Quaternary International, 120: 41-50.

Schellmann G., Radtke, U., Scheffers, A., Whelan F. & Kelletat, D. (2004b): ESR dating of coral reef terraces on Curaçao (Netherlands Antilles) with estimates of Younger Pleistocene sea level elevations. – Journal of Coastal Research, 20: 947-957.

Skinner, A.R. & Shawl, C.E. (1994): ESR dating of terrestrial Quaternary shells. – Quaternary Science Reviews, 13: 679-684.

Skinner, A.R. (2000): ESR dating: is it an 'experimental' technique? – Applied Radiation and Isotopes, 52: 1311-1316.

Soressi, M., Jones, H.L., Rink, W.J., Maureille, B. & Tillier, A.-M. (2007): The Pech-de-l'Azé I Neandertal child: ESR, uranium-series, and AMS ^{14}C dating of its MTA type B context. – Journal of Human Evolution, 52: 455-466.

Tanaka, K., Machette, M.N., Crone, A.J. & Bowman, J.R. (1995): ESR dating of aeolian sand near Tennant Creek, Northern Territory, Australia. – Quaternary Science Reviews, 14: 285-293.

Tanaka, T., Sawada, S. & Ito, T. (1985): ESR dating of Late Pleistocene near-shore and terrace sands in Southern Kanto, Japan. – In: Ikeya, M. & Miki, T. (eds.): ESR Dating and Dosimetry. Ionics: 275-280; Tokyo.

Thompson, W.G. & Goldstein, S.L. (2005): Open-systems coral ages reveal persistent suborbital sea-level cycles. – Science, 308: 401-404.

Tissoux, H., Falguères, C., Voinchet, P., Toyoda, S., Bahain, J.J. & Despriée, J. (2007). Potential use of Ti-center in ESR dating of fluvial sediment. – Quaternary Geochronology, 2: 367-372.

Toyoda, S. & Ikeya, M. (1994). ESR dating of quartz with stable component of impurity centers. – Quaternary Science Reviews, 13: 625-628.

Toyoda, S. & Schwarcz, H.P. (1997). Counterfeit E_1' signal in quartz. – Radiation Measurements, 27: 59-66.

Toyoda, S., Goff, F., Ikeda, S. & Ikeya, M. (1995): ESR dating of quartz phenocrysts in the El Cajete and Battleship Rock Members of Valles Rhyolite, Valles Caldera, New Mexico. – Journal of Volcanology and Geothermal Research, 67: 29-40.

Toyoda, S., Voinchet, P., Falguères, C., Dolo, J.M. & Laurent, M. (2000): Bleaching of ESR signals by the sunlight: a laboratory experiment for establishing the ESR dating of sediments. – Applied Radiation and Isotopes, 52: 1357-1362.

Toyoda, S., Tsukamoto, S., Hameau, S., Usui, H. & Suzuki, T. (2006): Dating of Japanese Quaternary tephras by ESR and luminescence methods. – Quaternary Geochronology, 1: 320-326.

Voinchet, P., Falguères, C., Laurent, M., Toyoda, S., Bahain, J.J. & Dolo, J.M. (2003): Artificial optical bleaching of the Aluminium centre in quartz implications to ESR dating of sediments. – Quaternary Science Reviews, 22: 1335-1338.

Voinchet, P., Bahain, J.J., Falguères, C., Laurent, M., Dolo, J.M., Despriée, J., Gageonnet, R. & Chausse, C. (2004): ESR dating of quartz extracted from Quaternary sediments: application to fluvial terraces systems of Northern France. – Quaternaire, 15: 135-141.

Voinchet, P., Falguères, C., Tissoux, H., Bahain, J.J., Despriée, J. & Pirouelle, F. (2007): ESR dating of fluvial quartz: Estimate of the minimal distance transport required for getting a maximum optical bleaching. – Quaternary Geochronology, 2: 363-366.

Walther, R., Barabas, M. & Mangini, A. (1992): Basic ESR studies on recent corals. – Quaternary Science Reviews, 11: 191-196.

Woda, C., Mangini, A. & Wagner, G.A. (2001): ESR dating of xenolithic quartz in volcanic rocks. – Quaternary Science Reviews, 20: 993-998.

Woda, C. & Wagner, G.A. (2007): Non-monotonic dose dependence of the Ge- and Ti-centres in quartz. – Radiation Measurements, 42: 1441-1452.

Yé, Y., Diao, S., He, J., Gao, J. & Lei, X. (1998): ESR dating studies of palaeo-debris-flow deposits in Dongchuan, Yunnan Province, China. – Quaternary Science Reviews, 17: 1073-1076.

Yin, G., Lin, M., Lu, Y., Li, J. & Han, F. (2007): Preliminary ESR dating results on loess samples from the loess–paleosol sequence at Luochuan, Central Loess Plateau, China. – Quaternary Geochronology, 2: 381-385.

Yokoyama, Y., Falguères, C. & Quaegebeur, J.P., 1985. ESR dating of quartz from Quaternary

sediments: first attempt. – Nuclear Tracks and Radiation Measurements, 10: 921-928.

ZHAO, J., ZHOU, S., HE, Y., YE, Y. & LIU, S. (2006): ESR dating of glacial tills and glaciations in the Urumqi River headwaters, Tianshan Mountains, China. – Quaternary International, 144: 61-67.

ZHOU, S., WANG, X., WANG, J. & XU, L. (2006): A preliminary study on timing of the oldest Pleistocene glaciation in Qinghai–Tibetan Plateau. – Quaternary International, 154-155: 44-51.

Eiszeitalter und Gegenwart Quaternary Science Journal	57/1–2	179–209	Hannover 2008

Surface exposure dating with cosmogenic nuclides

Susan Ivy-Ochs & Florian Kober*)

Abstract: In the last decades surface exposure dating using cosmogenic nuclides has emerged as a powerful tool in Quaternary geochronology and landscape evolution studies. Cosmogenic nuclides are produced in rocks and sediment due to reactions induced by cosmic rays. Landforms ranging in age from a few hundred years to tens of millions of years can be dated (depending on rock or landform weathering rates) by measuring nuclide concentrations. In this paper the history and theory of surface exposure dating are reviewed followed by an extensive outline of the fields of application of the method. Sampling strategies as well as information on individual nuclides are discussed in detail. The power of cosmogenic nuclide methods lies in the number of nuclides available (the radionuclides ^{10}Be, ^{14}C, ^{26}Al, and ^{36}Cl and the stable noble gases ^{3}He and ^{21}Ne), which allows almost every mineral and hence almost every lithology to be analyzed. As a result focus can shift to the geomorphic questions. It is important that obtained exposure ages are carefully scrutinized in the framework of detailed field studies, including local terrace or moraine stratigraphy and regional morphostratigraphic relationships; as well as in light of independent age constraints.

[Oberflächenexpositionsdatierungen mittels kosmogener Nukliden]

Kurzfassung: Im letzten Jahrzehnt hat sich die Methode der Oberflächendatierung mittels kosmogener Nuklide zu einer leistungsfähigen Methode in der Quartärchronologie und quantitativen Landschaftsanalyse entwickelt. Kosmogene Nuklide werden durch kosmische Strahlung in Fest- und Lockergestein gebildet. Die Konzentrationen der kosmogenen Nuklide kann mittels Massenspektrometrie ermittelt werden. Dies ermöglicht - je nach Verwitterungssrate - die Datierung von Landschaftselementen und Landschaftsformen mit Altern zwischen einigen 100 Jahren bis über 10 Millionen Jahren. Neben einem Abriss der historischen Entwicklung und Theorie der Oberflächendatierung mittels kosmogener Nuklide enthält dieser Artikel eine ausführliche Übersicht der zahlreichen Anwendungsgebiete dieser Methode. Probenahmestrategien und die Eigenheiten der einzelnen Nuklide werden im Detail besprochen. Die Vielzahl der mit dieser Methode in den verschiedensten Mineralien bestimmbaren Nuklide (Radionuklide ^{10}Be, ^{14}C, ^{26}Al und ^{36}Cl und Edelgase ^{3}He und ^{21}Ne) erlaubt die Beprobung und Analyse verschiedenster Lithologien. Der erreichte hohe Entwicklungsstand der Methode erlaubt es den Fokus auf die eigentlichen geomorphologischen Fragestellungen zu legen. Die Sensitivität der kosmogenen Oberflächendatierungsmethode muss trotzdem sorgfältig im Rahmen ausführlicher Feldstudien erfolgen, wie zum Beispiel durch die Analyse von lokalen und regionalen Terrassen- oder Moränenstratigraphien oder durch den Vergleich mit anderen Datierungsmethoden.

Keywords: cosmogenic radionuclides, cosmogenic noble gases, surface exposure dating

*Addresses of authors: S. Ivy-Ochs, Institute of Particle Physics, ETH Zurich, 8093 Zurich, Switzerland and Institute of Geography, University of Zurich , 8057 Zurich, Switzerland. E-Mail: ivy@phys.ethz.ch; F. Kober, Institute of Geology, ETH Zurich, 8092 Zurich, Switzerland and Institute of Isotope Geology, ETH Zurich, 8092 Zurich, Switzerland.

1 Introduction and history

Cosmogenic nuclides build-up predictably with time in minerals exposed to cosmic rays. Therefore measuring their concentrations allows determination of how long rocks or sediment have been exposed at or near the surface of the Earth (LAL 1991; GOSSE & PHILLIPS 2001). At present the most commonly utilized nuclides are the radionuclides ^{10}Be, ^{14}C, ^{26}Al, and ^{36}Cl and the stable noble gases ^{3}He and ^{21}Ne (Table 1). Because of the wide variety of nuclides available (with different half-lives or stable) and the fact that they can be measured in a variety of minerals a broad spectrum of geomorphological problems can be addressed (Fig. 1).

By measuring the concentrations of cosmogenic nuclides rock surfaces themselves can be directly dated. This is a unique and powerful tool never before available to geomorphologists. Bedrock landforms, fluvially- or glacially-polished bedrock surfaces, fault footwall faces, and landslide bedrock detachment surfaces can be sampled and dated directly. There is no other method where this is possible. Sedimentary units such as moraines, landslide deposits, fluvial terraces, debris flows or alluvial fans can be directly dated by sampling boulder surfaces or by taking samples made up of numerous clasts. Sites unsuitable for luminescence techniques may be dated with cosmogenic nuclide methods, for example sediments that have not been exposed to light long enough or coarse-grained material. In the past geomorphology has relied on radiocarbon for the indirect dating of landforms. The upper age limit for radiocarbon dating of organic material is about 50 ka, whereas under certain conditions landform ages on the order of tens of millions years can be measured with exposure dating (SCHÄFER et al. 1999; DUNAI et al. 2005). For radiocarbon

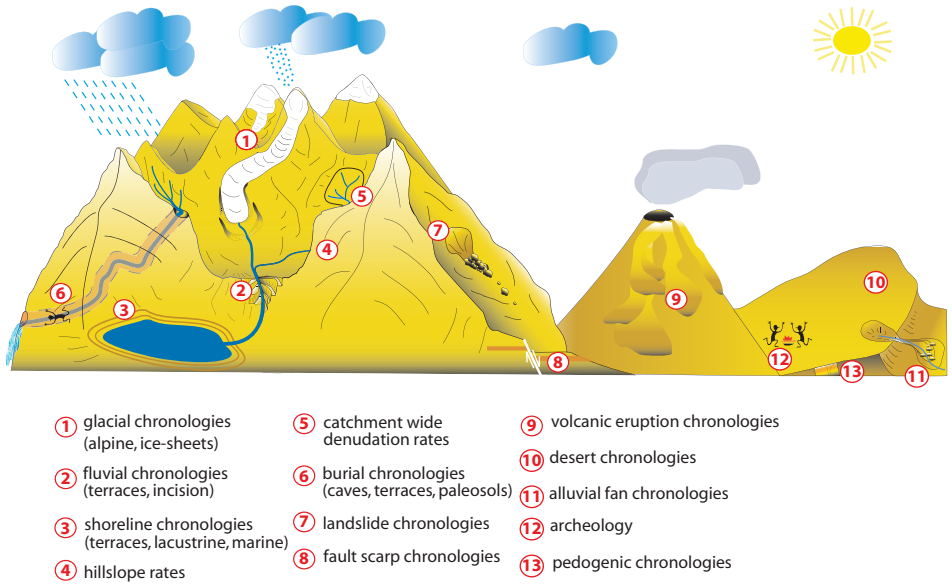

Fig. 1: Schematic diagram showing the various landforms that can be dated and approaches for using cosmogenic nuclides to address questions of timing and rates of landscape change (see also BIERMAN & NICHOLS 2004).

Abb. 1: Überblick über die Landschaftsformen und Landschaftselemente die mittels kosmogener Nuklide datiert oder deren Prozessraten quantifiziert werden können (siehe auch BIERMAN & NICHOLS 2004).

dating organic material must be present in the sediment, which is not the case in most high alpine early Holocene or Lateglacial deposits. Finally organic material included in sediments is not dating the landform itself, the relationship of the organic material to the landform can never be unequivocally established. Entrained wood fragments are simply older than the enclosing sediment.

Because of the presence of higher concentrations (production rates are higher in space than they are on earth) cosmogenic nuclides were initially investigated in lunar and meteorite samples already beginning in the 1950's (Finkel & Suter 1993 and references therein). Earliest attempts to measure cosmogenic nuclides in terrestrial rocks were made by Davis & Schaeffer (1955) and Srinivasan (1976). Davis & Schaeffer (1955) used low-level decay counting to measure ^{36}Cl in a high-Cl phonolite from unglaciated high elevation sites in the Rocky Mountains. In 1976, Srinivasan analyzed the cosmogenic noble gas ^{126}Xe in barite from a sedimentary unit (Srinivasan 1976) and highlighted the potential of noble gases in surface exposure dating (Niedermann 2002). Routine measurement of cosmogenic nuclides and use of cosmogenic nuclides for determination of exposure histories and erosion rates only became possible after the development of accelerator mass spectrometry (AMS), and the construction of high sensitivity noble gas mass spectrometers between 1970 and 1980. These technical developments opened the way to measurements of exceedingly low nuclide concentrations. In the late 1970s first accelerator measurements were reported for ^{14}C (Bennett et al. 1977; Nelson et al. 1977), ^{10}Be (Raisbeck et al. 1978), ^{26}Al (Raisbeck et al. 1979) and ^{36}Cl (Elmore et al. 1979). Early measurements of cosmogenic nuclides in rock and sediment samples were made using ^{3}He (Kurz 1986), ^{10}Be and ^{26}Al (Klein et al. 1982), ^{21}Ne (Marti & Craig 1987), ^{36}Cl (Kubik et al. 1984; Phillips et al. 1986), and ^{14}C (Jull et al. 1992). In 1991, Lal presented detailed terrestrial cosmic ray systematics, setting the standards for production rate and scaling formalisms as well as discussing potential applications and promising nuclide combinations (Lal 1991). Gosse & Phillips (2001) published a comprehensive review of cosmogenic nuclide methods in the Earth Sciences including the appropriate equations. Further summaries are given by Nishiizumi et al. (1993), Cerling & Craig (1994a), Bierman et al. (2002), Morris

Table 1: Nuclide characteristics Mineral-Nuclide overview.

Tab. 1: Überblick über die kosmogenen Nuklide und deren Charakteristika.

Nuclide	Half-life	Other isotopes	meas. method	Target elements	Production rate atoms/g.yr*	Advantages/minerals used	Disadvantages
^{10}Be	1.51 Myr	^{9}Be	AMS	O Si	5	quartz resistant and ubiquitous	low production rate, ^{10}B interference in AMS generally restricted to quartz (no meteoric ^{10}Be)
^{26}Al	716 kyr	^{27}Al	AMS	Si	31	high production rate quartz resistant and ubiquitous	restricted to quartz (low Al) accurate determination of ^{27}Al required
^{36}Cl	301 kyr	^{35}Cl, ^{37}Cl	AMS	Ca K ^{35}Cl	composition dep. e.g. 10 granite e.g. 20 limestone	low detection limit (low AMS Bkgd) any rock type, silicates & carbonates	complicated production ^{36}S interference in AMS accurate determination of total Cl required determination of rock composition required
^{14}C	5.73 kyr	^{12}C, ^{13}C	AMS	O	16	useful for short timescales quartz resistant and ubiquitous	short half-lfe atmospheric ^{14}C contamination
^{3}He	stable	^{4}He	static mass spec.	many	120	high production rate useful for long time scales pyroxene, olivine	diffuses out of quartz or volcanic groundmass radiogenic/nucleogenic/magmatic correction beware pre-exposure
^{21}Ne	stable	^{20}Ne, ^{22}Ne	static mass spec.	Mg Si	20	useful for long time scales, > 50 ka quartz, olivine, pyroxene	nucleogenic/magmatic correction high air background possible beware pre-exposure

*production rates (Gosse & Phillips 2001)

et al. (2002), NIEDERMANN (2002), COCKBURN & SUMMERFIELD (2004). In this review we focus on surface exposure dating of landforms and deposits. The use of cosmogenic nuclides methods in Archeology is discussed in AKÇAR et al. (2008a). Burial dating is dealt with in the paper by DEHNERT & SCHLÜCHTER (2008). For readers interested in the use of cosmogenic nuclides to determine landscape denudation rates we refer to VON BLANCKENBURG (2005), GRANGER (2006; 2007) and GRANGER & RIEBE (2007).

2 Production of cosmogenic nuclides

The Earth is constantly being bombarded by cosmic rays (primarily protons, alpha particles as well as other heavier nuclei). The primary cosmic ray flux consists of galactic and solar cosmic rays with the former clearly being more important for production of cosmogenic nuclides in minerals (LAL & PETERS 1967). Interactions of high-energy cosmic ray particles with nuclei in the Earth's atmosphere result in a cascade of secondary particles (especially neutrons). This means that in traversing the atmosphere, the flux of cosmic ray particles first increases (in the first few kilometers) then steadily decreases. Consequently, nuclide production rates in rocks at the surface of the earth are lower at lower altitude. Primary galactic cosmic rays (especially the lower energy part) are modulated by the Sun's magnetic field. High solar activity reduces the primary cosmic ray flux. Cosmic ray particles are deflected by the Earth's predominantly-dipole magnetic field. The magnetic field impedes and deflects particles with lesser energies at lower latitudes. As a consequence cosmic ray intensity and therefore nuclide production is higher at the poles than at the equator. At sea level production rates are about half at the equator compared to what they are at the poles. The altitude and latitude dependence of cosmogenic nuclide production rates reflects this modulation of the cosmic ray flux by the earth's magnetic field and the atmosphere (Fig. 2) (GOSSE & PHILLIPS 2001, MASARIK et al. 2001). Several physical models have been presented for the scaling of

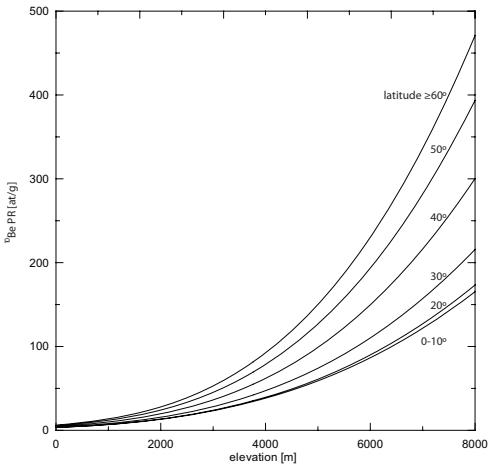

Fig. 2: Production of rate of ^{10}Be in quartz as a function of geomagnetic latitude and altitude (based on STONE 2000). The production rates have been normalized to sea level and high latitude. At low latitude, production rates are lower than at high latitude. Production rates increase exponentially with increasing altitude.

Abb. 2: Produktion von ^{10}Be in Quarz in Abhängigkeit der geomagnetischen Position und Höhe über Meeresspiegel (nach STONE 2000). Die Berechnungen sind skaliert auf Meeresspiegelhöhe und hohe geomagetische Breiten. In niederen Breiten ist die Produktionsrate kleiner als in hohen Breiten. Die Produktionsraten steigen exponentiell mit der Höhe über dem Meer an.

production rates from their sea level and high latitude values to the altitude and latitude of the sampling site (LAL 1991; DUNAI 2000; 2001; STONE 2000; DESILETS & ZREDA 2001; PIGATI & LIFTON 2004; MUZIKAR 2005; DESILETS et al. 2006a) (see detailed discussion in BALCO et al. 2008). Key differences between the systems include the method of modelling the variation of the neutron flux with altitude and how past changes in the magnetic field are incorporated (BALCO et al. 2008). At present most studies use the production rates and scaling system of STONE (2000) for ^{10}Be and ^{26}Al. This allows a certain degree of intercomparison. Although the suitability of this protocol for samples at high altitude is under discussion (see BALCO et al. 2008). In any case it is crucial when

calculating an exposure age to use the same scaling formalities as were used for the original production rate calculations. The University of Washington/CRONUS-Earth website (http://hess.ess.washington.edu/math/) allows the consistent comparison of data from different sites as well as presents detailed discussion of the differences and similarities of the various scaling systems (Balco et al. 2008). Another website where these calculations can be done is cosmocalc.googlepages.com (Vermeesch 2007).

Cosmogenic nuclides are produced within minerals by several reactions (Table 2). These include spallation, muon-induced reactions and low-energy (epithermal and thermal) neutron capture (Lal & Peters 1967). During spallation a secondary cosmic ray neutron with sufficient energy hits the target element and one or more particles are ejected from the nucleus leaving the cosmgenic nuclide in the target element's site in the mineral lattice. Cosmogenic nuclides are also produced through interactions of muons with the target element (capture of slow muons and stopping of fast muons).

Because they are reacting with target elements in rocks the flux of secondary cosmic ray particles decreases (is attenuated) with depth into rock or sediment. Production due to spallation decreases exponentially with depth (Lal 1991) (Fig. 3). Muons are less apt to react than neutrons thus they penetrate deeper into the Earth's surface and production due to muons becomes increasingly important below depths of about 2 m (in a rock of density 2.7 g cm^{-3}). The decrease of production depth profile for muons is described by equations with several exponentionals (Schaller et al. 2001; 2002; Granger & Smith 2000) (see also Dehnert & Schlüchter 2008).

^{36}Cl differs somewhat from the other nuclides. In rocks with sufficient natural Cl (^{35}Cl and ^{37}Cl) ^{36}Cl is produced through low-energy (thermal and epithermal) neutron capture on ^{35}Cl and to a lesser extent on ^{39}K (Table 2); in addition to spallation and muon-related reactions. Low-energy neutrons can diffuse back out of a rock surface (Fabryka-Martin 1988). As a result of this neutron leakage, production of ^{36}Cl by neutron capture peaks about 20 cm down into the rock (Fig. 4). The shape of this curve depends on rock composition (proportion of target elements) and density (Fabryka-Martin 1988; Liu et al. 1994; Phillips et al. 2001). Rocks with little natural Cl will have negligable low-energy neutron capture

Table 2: Main reactions to produce cosmogenic nuclides on the Earth.

Tab. 2: Hauptreaktionen kosmogener Nuklide an der Erdoberfläche.

Target element	Spallation	Negative-muon capture	Low-energy neutron capture
O	$^{16}O(n,2pn)\,^{14}C$	$^{16}O(\mu^-,pn)\,^{14}C$	
	$^{16}O(n,4p3n)\,^{10}Be$	$^{16}O(\mu^-,3p3n)\,^{10}Be$	
Si	$^{28}Si(n,p2n)\,^{26}Al$	$^{28}Si(\mu^-,2n)\,^{26}Al$	
	$^{28}Si(n,2\alpha)^{21}Ne$		
Na	$^{23}Na(n,p2n)^{21}Ne$		
Mg	$^{24}Mg(n,\alpha)^{21}Ne$		
Al	$^{27}Al(n,3p4n)^{21}Ne$		
K	$^{39}K(n,2p2n)\,^{36}Cl$	$^{39}K(\mu^-,p2n)\,^{36}Cl$	$^{39}K(n,\alpha)\,^{36}Cl$
Ca	$^{40}Ca(n,3p2n)\,^{36}Cl$	$^{40}Ca(\mu^-,2p2n)\,^{36}Cl$	
Cl			$^{35}Cl(n,\gamma)\,^{36}Cl$

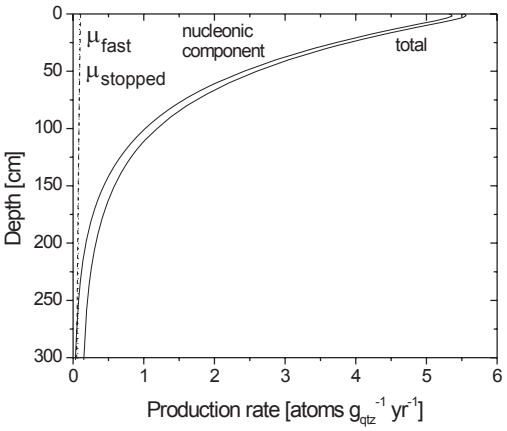

Fig. 3. Production rate of ^{10}Be in quartz as a function of depth at sea level and high latitude. The total production is a composite of the production by neutron spallation, stopped muons, and fast muons.

Abb. 3: Produktion von ^{10}Be in Quarz in Abhängigkeit der Tiefe, skaliert auf Meeresspiegelhöhe und hohe geomagnetische Breiten. Die Gesamtproduktion ist die Summe aus Spallations-, gestoppten und schnellen Muonenreaktionen.

production and the production depth profile will be spallation-dominated and resemble the curve for ^{10}Be (Fig. 3). Complete equations for calculating depth profiles are given in GOSSE & PHILLIPS (2001).

Shielding by surrounding hillslopes and mountains reduces the cosmic ray flux to the sampling site leading to lower production. Similarly dipping of the rock surface decreases the production rate. Shielding corrections are done following DUNNE et al. (1999) (see also GOSSE & PHILLIPS 2001). Calculation of these correction factors is also possible through the internet (http://hess.ess.washington.edu/math/).

Cosmogenic nuclides [atoms g^{-1}] build-up in an exposed rock surface according to the following equation:

$$C_{(t)} = \frac{P_{(0)}}{\lambda + \frac{\rho\varepsilon}{\Lambda}}\left(1 - e^{-\left(\lambda + \frac{\rho\varepsilon}{\Lambda}\right)t}\right) + C_{in}e^{-\lambda t} \qquad \text{Eq. 1}$$

where $P_{(0)}$ [atoms g^{-1} a^{-1}] is the production rate at the sampling site, t [a] is the exposure age of the surface, λ [a^{-1}] is the decay constant, ρ [g cm^{-3}] is the density of the irradiated material, ε [cm a^{-1}] is the erosion rate, and Λ [g cm^{-2}] is the attenuation length. C_{in} [atoms g^{-1}] is the nuclide concentration already present at the beginning of exposure and is called inheritance. The presence of inherited nuclide concentrations will yield ages older than the true age (see also below).

Radionuclides build-up in exposed minerals until secular equilibrium is reached (saturation) which happens after about three to four half-lives. At secular equilibrium the number of nuclides produced per unit time is equivalent to the number that decays; the concentration is at steady state. This is seen in Figure 5 where the the upper concentration growth curve flattens out. When the rock surface is eroding (weathering), both erosion and decay lead to loss of the nuclide. Saturation is reached earlier (after a shorter exposure period) (Fig. 6).

In the first instance, exposure ages are calculated assuming zero inheritance and without erosion such that Eq. 1 simplifies to:

$$C_{(t)} = \frac{P_{(0)}}{\lambda}\left(1 - e^{-\lambda t}\right) \qquad \text{Eq. 2}$$

Eq. 2 is solved for t. The production rate is scaled for site latitude (and when past magnetic field changes are considered longitude), altitude (Fig. 2), as well as, sample thickness, and topographic shielding. The attenuation length is 157 g cm^{-2} and the denstiy of crystalline rock is 2.7 g cm^{-3} (GOSSE & PHILLIPS 2001). As shown in Figure 7 the measured nuclide concentration is a direct measure of the length of the exposure period.

Where field evidence indicates that rock surface weathering (erosion) has been significant, an age is calculated by using an assumed or measured erosion rate with the following equation (Eq. 1 without the inheritance term):

$$C_{(t)} = \frac{P_{(0)}}{\lambda + \frac{\rho\varepsilon}{\Lambda}}\left(1 - e^{-\left(\lambda + \frac{\rho\varepsilon}{\Lambda}\right)t}\right) \qquad \text{Eq. 3}$$

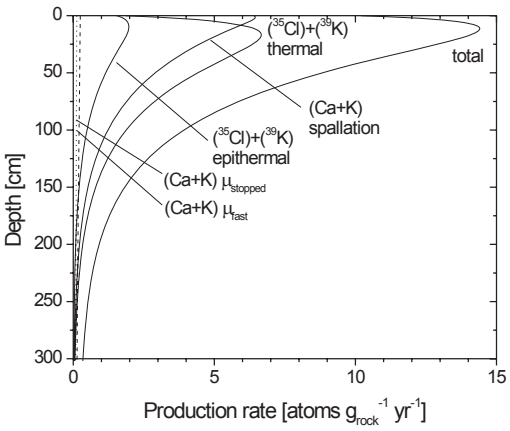

Fig. 4. Production rate of ^{36}Cl in granite with 200 ppm of Cl as a function of depth. The production rates are for sea level and high latitude. The total production is a composite of production by neutron spallation, thermal and epithermal neutrons, stopped and fast muons. The maximum production by thermal neutrons is highest at about 20 cm depth in a rock with a given density of 2.7 g cm^{-3}. Diffusion of thermal neutrons back out of the rock in the uppermost few centimeters causes this reduction in production rate. Variation of production rates with depth calculated after Liu et al. (1994), Stone et al. (1996, 1998), and Phillips et al. (2001).

Abb. 4: Produktion von ^{36}Cl in einem Granit (200 ppm Cl) in Abhängigkeit der Tiefe, skaliert auf Meeresspiegelhöhe und hohe geomagetische Breiten. Die Gesamtproduktion ist die Summe aus Neutronenpallations-, thermischen und epithermischen, sowohl als auch gestoppten und schnellen Muonenreaktionen. Das Maximum der Produktion durch thermische und epithermische Neutronenreaktionen wird in einer Tiefe von 20 cm erreicht (bei einer Dichte von 2.7 g cm^{-3}). Die Diffusion thermischer Neutronen in den oberen Zentimetern des Profils verringert die Gesamtproduktion (berechnet nach Liu et al. (1994), Stone et al. (1996, 1998), and Phillips et al. (2001)).

Crystalline rock surface erosion rates are typically less than 10 mm ka^{-1} (Cockburn & Summerfield 2004). For spallation-dominated nuclides rock surface erosion has the effect of lowering the concentrations so that the measured age is younger than the true period of exposure. For ^{36}Cl exposure dating this is not always the case depending on the relative contribution of production due to low-energy neutron capture and the size of the hump in the depth profile (Fig. 4).

The upper and lower age limits for each nuclide are set by a combination of geological and methodological factors. The lower age limit for ^{10}Be, ^{26}Al and ^{36}Cl is limited predominantly by measurement capabilities. A certain amount of carrier must be added and a certain ratio of radionuclide to stable nuclide must be attained to be above the background levels. Under appropriate conditions exposure ages in the range of several hundred years can be determined (Davis et al. 1999). Upper age limits are constrained by the nuclide half-life and the weathering rate of the rock surface (Fig. 6). In areas where rock weathering is slow exposure ages up to several million years can be determined with ^{10}Be or ^{26}Al; to tens of millions with ^{21}Ne. On the other hand, when a granitic rock surface is weathering at a rate of 5 mm ka^{-1} no ages older than several hundred thousand years can be calculated. But the calculated ages may be minimum ages for that landform. Although the noble gases are stable, they too are affected by erosion and will reach pseudo-saturation just like the radionuclides (Fig. 6).

Often additional information can be gleaned about the history of a rock surface by measuring more than one nuclide (Lal 1991; Nishiizumi et al. 1993; Bierman et al. 1999; Gosse & Phillips 2001). As Eq. 3 contains two unknowns, the age and the erosion rate, using two nuclides can in some settings allow for the determination of both. One way to view two nuclide data (typically Al/Be, Ne/Be) is with the erosion island (or banana) plot (Klein et al. 1986; Lal 1991) (Fig. 8, 9). An important use of the erosion island plot is to readily distinguish data points that represent surfaces that have undergone continuous simple or single stage exposure (plot on or near the erosion island) versus those that reflect complex exposure involving burial (plot below the Al/Be erosion island, above the Ne/Be erosion

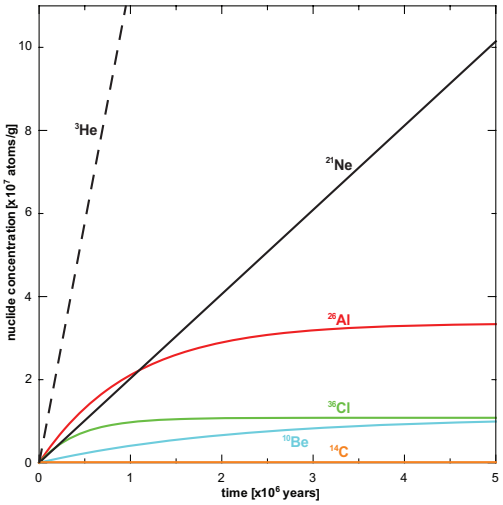

Fig. 5: Increase in concentration of the radionuclides ^{10}Be, ^{26}Al, ^{36}Cl and the stable nuclides ^{3}He and ^{21}Ne with time. Secular equilibrium, where production of radionuclides equals radioactive decay, is approached after 3-4 half-lives. The secular equilibrium concentraton sets the limit of the maximum exposure age that can be determined with a given radionuclide.

Abb. 5: Anstieg der Konzentration der Radionuklide ^{10}Be, ^{26}Al, ^{36}Cl und Edelgase ^{3}He und ^{21}Ne in Abhängigkeit von der Zeit. Ein Gleichgewichtszustand, bei dem die kosmogene Radionuklidproduktion im Gleichgewicht mit dem radioaktiven Zerfall ist, wird nach 3-4 Halbwertszeiten erreicht. Die Gleichgewichtskonzentration bestimmt die maximal mögliche Altersspanne bei der Datierung mit Radionukliden.

island, respectively; Fig. 8, 9) (see DEHNERT & SCHLÜCHTER 2008). Spalling of slabs of rock of tens of centimenters thick may lead to data that plots inside the banana or in the complex field below the banana (BIERMAN et al. 1999; KOBER et al. 2007). The minimum exposure time represented by data plotting below the erosion island is made up of continuous exposure along the outer line (bold black line) followed by burial with complete shielding (zero production). But an infinite number of periods of exposure and burial are possible which require more time (cf. BIERMAN et al. 1999). Indeed data points for rocks or sediment that were exposed then buried can arrive back inside the erosion island after a long enough period of (re)exposure. The erosion island plot can be used to estimate both exposure age and erosion rate, especially at sites where erosion rates are very low and where rocks have been exposed longer than 100 ka, for example in desert environments. For slowly eroding arid and hyperarid environments the use of ^{21}Ne (stable) measured in quartz in concert with ^{10}Be provides increased sensitivity for older, more slowly eroding surfaces (Fig. 9).

The basic assumptions that are implicit in the use of in situ-produced cosmogenic nuclides to address problems of landscape evolution are:

- the half-life of the radionuclide is known,
- production pathways and production rates including their variation in space (including with depth into the rock or sediment) are known,
- the initial nuclide concentration (inheritance) is zero or can be determined or estimated,
- the mineral has remained a closed system, i.e. there has been no gain or loss of the nuclide except due to production or decay (or through erosion).

3 Specific nuclide characteristics

3.1 Radionuclides

AMS (accelerator mass spectrometry) is used to determine concentrations of long-lived radionuclides ^{10}Be, ^{14}C, ^{26}Al, ^{36}Cl by measuring ratios relative to a standard material. In AMS interfering isobars or like-mass molecules are separated at the ion source (when they do not produce negative ions), through mass discrimination with magnetic or electrostatic analyzers (as in traditional mass spectrometry), during stripping and/or during detection (FINKEL & SUTER 1993).

Quartz is used in nearly all ^{10}Be studies. This is because it is a ubiquitous, resistant mineral that can be consistently cleaned of meteoric ^{10}Be. Meteoric ^{10}Be is produced in the atmosphere. Its presence in the analyzed mineral separate

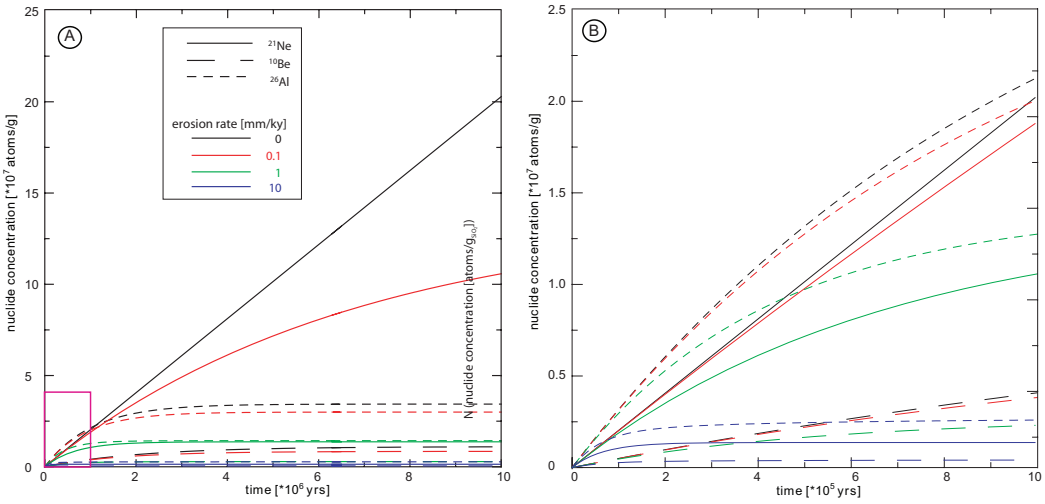

Fig. 6: Increase of the concentrations of ^{10}Be, ^{26}Al, and ^{21}Ne with time taking into account different erosion rates of the exposed surface. Secular equilibrium, where radionuclide gain due to production equals loss due to radioactive decay and erosion, is approached earlier for more rapid erosion rates. A blow-up for the region 0 to 1 Ma is shown.

Abb. 6: Anstieg der Konzentration der Radionuklide ^{10}Be, ^{26}Al und ^{21}Ne in Abhängigkeit von der Zeit und variierenden Erosionsraten an der Erdoberfläche. Ein Gleichgewichtszustand, bei dem die kosmogene Radionuklidproduktion im Gleichgewicht mit radioaktivem Zerfall und der Abnahme durch Erosion ist, wird früher erreicht, je höher die Erosionsrate ist (A). (B) zeigt einen detaillierten Ausschnitt von (A) im Zeitfenster von 0 bis 1 Million Jahre.

would lead to spurious age results. Minerals other than quartz have been tried; for example olivine and pyroxene (Nishiizumi et al. 1990; Blard et al. 2008). It is important to note that in contrast to quartz, these minerals chemically weather to clay minerals, consequently problems removing meteoric ^{10}Be have been reported (Seidl et al. 1997; Ivy-Ochs et al. 1998a). Several groups have tried to measure ^{10}Be in carbonate rocks (Braucher et al. 2005); the affinity of ^{10}Be for clay minerals poses a significant obstacle (Merchel et al. 2008). The use of ^{26}Al is restricted to minerals with low ^{27}Al content. Too much ^{27}Al would yield a ^{26}Al/^{27}Al ratio too low to be measured with AMS. Conveniently, quartz satisfies the requirements for both ^{10}Be and ^{26}Al so that both can be extracted by dissolving a single quartz mineral separate. Pure quartz is obtained by selective chemical dissolution in a hot ultrasonic bath and/or on a shaker table (Kohl & Nishiizumi 1992). Most other minerals dissolve faster than quartz in a dilute HF (ca. 4%) solution. A carrier of ^{9}Be (about half a milligram in solution) is added to the pure quartz mineral separate which is then completely dissolved with concentrated HF and HNO_3. Be and Al are separated and purified with ion exchange methods and selective pH precipitations (Kohl & Nishiizumi 1992; Ivy-Ochs 1996; von Blanckenburg et al. 1996; Bierman et al. 2002) (see also http://depts.washington.edu/cosmolab/chem). Although it has a higher production rate (Table 1), one disadvantage of ^{26}Al is that a separate accurate measurement (with its own uncertainties) is required to determine the ^{27}Al content of the quartz. Ratios of ^{10}Be/^{9}Be or ^{26}Al/^{27}Al are measured with AMS.

Because Cl is hydrophyllic contaminating meteoric ^{36}Cl (or ^{37}Cl or ^{35}Cl) can be removed with rinsing procedures. Under most conditions any rock type or mineral separate can be used

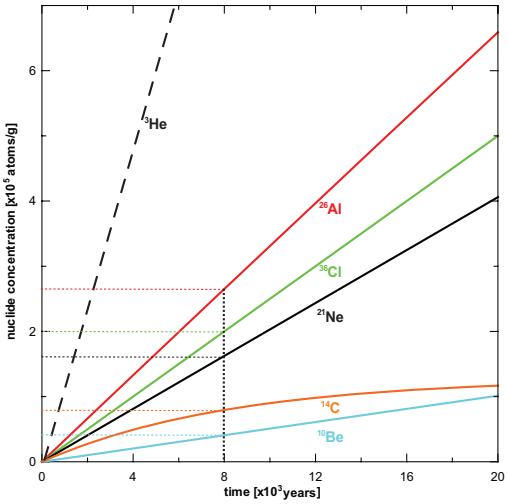

Fig. 7: Close-up of the region 0 to 20,000 years of exposure, illustrating the direct relationship between measured nuclide concentration and exposure age.

Abb. 7: Detaillierter Ausschnitt für das Zeitfenster von 0 bis 20000 Jahren, welcher die direkte Abhängigkeit des Anstiegs der Nuklidkonzentration von der Dauer der Exposition darstellt.

for ^{36}Cl exposure dating. On the other hand if secondary minerals which include meteoric ^{36}Cl precipitate (for example secondary calcite) then the system is no longer closed. Sample preparation procedures for ^{36}Cl are given in ZREDA (1994), IVY-OCHS (1996), STONE et al. (1996, 1998), IVY-OCHS et al. (2004) and DESILETS et al. (2006b) (see also http://depts.washington.edu/cosmolab/chem/). Crushed rock samples are first leached several times to release any non-in situ produced Cl. Several milligrams of carrier (in solution) of known isotopic composition (pure ^{35}Cl, ^{37}Cl, or a mixture of both) are added. Carbonate rocks are dissolved with HNO_3 and silicate rocks with HF. Sulfur is removed by precipitation of $BaSO_4$ (^{36}S interferes with AMS measurement of ^{36}Cl). A crucial improvement in ^{36}Cl methodology is the implementation of isotope dilution. By adding a spike of known isotopic composition but different from the natural ratio of about 3:1 (^{35}Cl:^{37}Cl), both the total rock Cl concentration and ^{36}Cl can be determined in a single target using an AMS set-up, through the measurement of ^{37}Cl/^{35}Cl as well as ^{36}Cl/Cl (ELMORE et al. 1997; IVY-OCHS et al. 2004). This has led to marked improvements in both precision and accuracy in ^{36}Cl results (DESILETS et al. 2006b). Because ^{36}Cl is produced from spallation of Ca and K and low-energy neutron capture on ^{35}Cl and ^{39}K and because each rock has a different chemistry, production rates for ^{36}Cl must be calculated individually. In addition to determination of major element oxides, concentrations of B, Gd, and Sm must be determined. These elements are strong neutron absorbers and influence the proportion of low-energy neutrons that are available for neutron capture reactions on ^{35}Cl and ^{39}K. U and Th concentrations are needed to correct for background (subsurface non-cosmogenic) neutron-capture ^{36}Cl production (FABRYKA-MARTIN 1988).

^{14}C is produced in quartz by spallation of ^{16}O (JULL et al. 1992; LIFTON et al. 2001; YOKOYAMA et al. 2004). Atmospheric ^{14}C contamination is removed from the surfaces and crevices of the quartz grains with acid etching (similar to that used for ^{10}Be studies; KOHL & NISHIIZUMI 1992) and preheating. About five grams of quartz are flux melted in a flow of oxygen (LIFTON et al. 2001) to produce CO_2. which is converted to graphite using standard procedures. Carbon ratios are measured with AMS. The possibility to use a gas ion source for direct analysis of the CO_2 with AMS is an exciting development. Because of difficulties in sample preparation and extraction, ^{14}C is currently used infrequently but has great potential.

3.2 Noble gases

For noble gas studies, mineral separates (tens to hundreds of milligrams) are pre-concentrated using heavy liquids and/or magnetic separation. Quartz is separated using the method of KOHL & NISHIIZUMI (1992). Because of the small amounts necessary mineral separates can also be hand-picked under a binocular microscope. Noble gases are extracted and measured with high sensitivity static noble gas mass spectrometry (NIEDERMANN 2002). Mineral separates

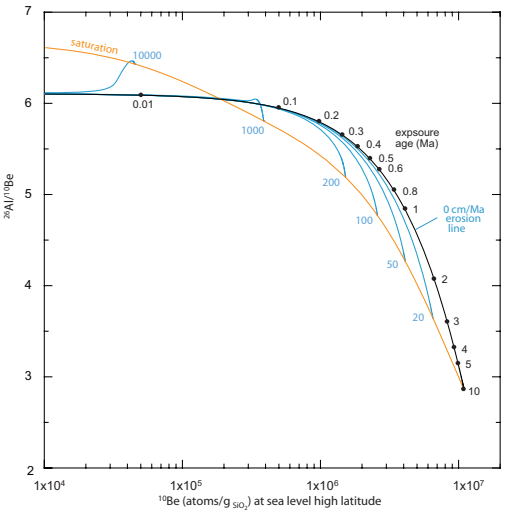

Fig. 8: Plot of $^{26}Al/^{10}Be$ ratios versus ^{10}Be concentration showing the evolution of the $^{26}Al/^{10}Be$ ratios with time. Continuously exposed, non-eroding surfaces evolve along the bold black line. Continuously exposed surfaces eroding with steady-state erosion follow the trajectories (blue lines) that splay downward from the no-erosion line. The red line joins points of final $^{26}Al/^{10}Be$ ratios with the given erosion rates but is not an evolution line. The prescribed area is called the «steady-state erosion island». Samples that plot below the steady-state erosion island experienced a more complex exposure that involves periods of burial (see Dehnert & Schlüchter 2008). Samples may also plot below the erosion island if thick slabs have spalled off.

Abb. 8: Darstellung des Verhältnisses von $^{10}Be/^{26}Al$ zur ^{10}Be-Konzentration, welches die Entwicklung des Verhältnisses von $^{10}Be/^{26}Al$ mit der Zeit aufzeigt (als Funktion der Konzentration). Im Falle einer kontinuierlichen Exposition und Null-Erosion würde eine Probe auf der schwarzen, dicken Linie liegen. Kontinuierliche Exposition mit einer konstanten Erosionsrate würde eine Probe auf Trajektoren (blaue Linien) bewegen, die von der Null-Erosionslinie abzweigen. Die rote Linie verbindet die Endpunkte dieser Trajektoren (Gleichgewichtsendpunkt, Verhältnis von $^{10}Be/^{26}Al$ ist konstant) und ist artifiziell. Das Feld zwischen Null-Erosionslinie und der artifiziellen Linie wird als "Gleichgewichts-Erosionsinsel" bezeichnet. Probenpunkte unterhalb dieser Insel haben eine komplexe Expositionsgeschichte, einschliesslich Perioden mit Abschirmung zur kosmischen Strahlung (siehe auch Dehnert & Schlüchter 2008). Probenpunkte unterhalb der "Gleichgewichts-Erosionsinsel" können auch durch eine schalige Abspaltung vom Festgestein verursacht werden.

are heated to various temperature steps until the final fusion of the sample. Step-wise heating or crushing *in vacuo* are performed to discriminate non-cosmogenic components (nucleogenic, radiogenic, or trapped). Gas purification (separation from e.g., CO_2, water vapour, and heavy noble gases) is accomplished by a combination of cryogenic traps and hot getters.

^{3}He is produced by spallation reactions of nearly all elements. ^{3}He is not measured in quartz as it diffuses out (Trull et al. 1991; Brook & Kurz 1993). Olivine and pyroxene phenocrysts and microphenocrysts are retentive for ^{3}He (Kurz et al. 1990; Cerling & Craig 1994b; Licciardi 1999; Fenton et al. 2001; Marchetti et al. 2005). The presence of radiogenic ^{3}He may limit studies to rocks with young crystallization ages (cf. Niedermann 2002; Williams et al. 2005).

^{21}Ne is produced by spallation of Si, Al, Mg and Na (Table 1) in quartz, olivine, pyroxene and sanidine. An important advantage of ^{21}Ne is that in contrast to ^{3}He it can be measured in quartz (Graf et al. 1991; Staudacher & Allégre 1991). Thus three cosmogenic nuclides, ^{10}Be, ^{26}Al and ^{21}Ne can be determined on aliquots of a single quartz mineral separate (Hetzel et al. 2002a,b; Kober et al. 2007). As ^{14}C is measured in quartz the potential to measure four nuclides in quartz exists. ^{21}Ne is also measured in pyroxene and olivine (Marti & Craig 1987; Staudacher & Allegre 1991; Poreda & Cerling, 1992; Bruno et al. 1997; Schäfer et al. 1999). Kober et al. (2005) showed that the volcanic potassium feldspar sanidine retains ^{21}Ne. By using sanidine one can measure ^{10}Be, ^{36}Cl and ^{21}Ne in aliquots of the same mineral separate (Ivy-Ochs et al. 2007b). Interferences due to trapped and/or nucleogenic (both non-cosmogenic) neon isotopes (Hetzel et al. 2002a) can in most cases be deconvoluted using stepwise heating of mineral separates and plotting data on the three isotope (^{20}Ne, ^{21}Ne, ^{22}Ne) plot (Graf et al. 1991; Niedermann 2002).

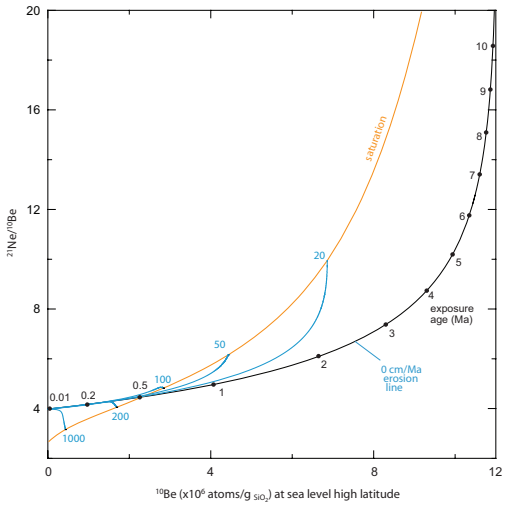

Fig. 9: Plot of ^{21}Ne/^{10}Be ratios versus ^{10}Be concentration showing the evolution of the ^{21}Ne/^{10}Be ratios with time. Continuously exposed, non-eroding surfaces evolve along the bold black line. Continuously exposed surfaces eroding with steady-state erosion follow the trajectories (blue lines) that splay upward from the no-erosion line. The red line joins points of final ^{21}Ne/^{10}Be ratios with the given erosion rates but is not an evolution line. The prescribed area is called the «steady-state erosion island». Samples that plot below the steady-state erosion island experienced a more complex exposure that involves periods of burial. Samples may also plot above the erosion island if thick slabs have spalled off.

Abb. 9: Darstellung des Verhältnisses von ^{21}Ne/^{10}Be zur ^{10}Be-Konzentration, welches die Entwicklung des Verhältnisses von ^{21}Ne/^{10}Be mit der Zeit aufzeigt (s. Legende Fig. 8).

4 Sampling considerations

Cosmogenic nuclides can be used to address a variety of problems in the Earth Sciences (Fig. 1). Two factors are key in deciding which cosmogenic nuclide (Table 1) is best suited to the geological/geomorphological problem at hand: i) the half-life of the nuclide (or stable), and ii) the bedrock geology (mineralogy) of the study area. As described above certain nuclides can only be measured in certain minerals.

Depositional landforms such as moraines (Fig. 10), fluvial terraces or alluvial fans can be dated with cosmogenic nuclides. For the exposure date to represent as close as possible the true formation or abandonment age of the landform, the sampled object (boulder, clasts or bedrock) surface must have i) undergone single-stage exposure (no pre-exposure/inheritance), ii) been continuously exposed in the same position (not shifted), iii) never been covered, and iv) undergone only minimal surface weathering or erosion (not spalled). Sampling large (>1.5 m high), broad, and flat-topped boulders located in stable positions (moraine crest; flat tread of a terrace) best satisfy these conditions. Large boulders have a smaller chance of having sunk in or shifted. To avoid edge effects (MASARIK et al. 2000; MASARIK & WIELER 2003), flat surfaces at least 20-30 cm away from an edge are sampled. Similarly pointed knobs are avoided. Careful scrutiny of candidate boulders may help one to rule out those that have spalled or toppled. The base of boulders is inspected for flakes, although this may be difficult to judge in forested settings. Sample surfaces are evaluated for post-depositional weathering, when there are step-like surfaces the highest one is sampled. A hammer and chisel, a saw or a drill are used to take several hundred grams to 1 kg of the upper few centimeters of the rock surface (Fig. 10). The amount of material needed depends on location (i.e. the local production rate), estimated exposure age and mineralogy (% of the mineral needed) of the sampled surface. Because of the possibility of the data scattering, where enough suitable boulders are present at least three to five different boulders are sampled.

In most data sets the prevalence of ‹›too young›› ages far overshadows ‹›too old›› ages. This has been determined based on independent age controls for the landform (e.g. ^{14}C age for a landslide) or intercomparison of dates from a single or related landform (when inversions occur etc). Most commonly, weathering of the sampled rock surface and/or degradation of the landform leads to «too young›› ages. The magnitude of this effect is related to the age, location (climate, treeline location with respect to the landform), lithology (mineralogy and texture)

and morphology of the landform (flatness of the upper surface steepness of the margins). ‹›Too old ‹› ages arise when the initial nuclide concentration in the sampled rock surface was not zero (inheritance). In boulders, inheritance can be acquired in bedrock exposures before the boulder falls onto the glacier or before the landslide, or when the boulder is reworked from older depo-

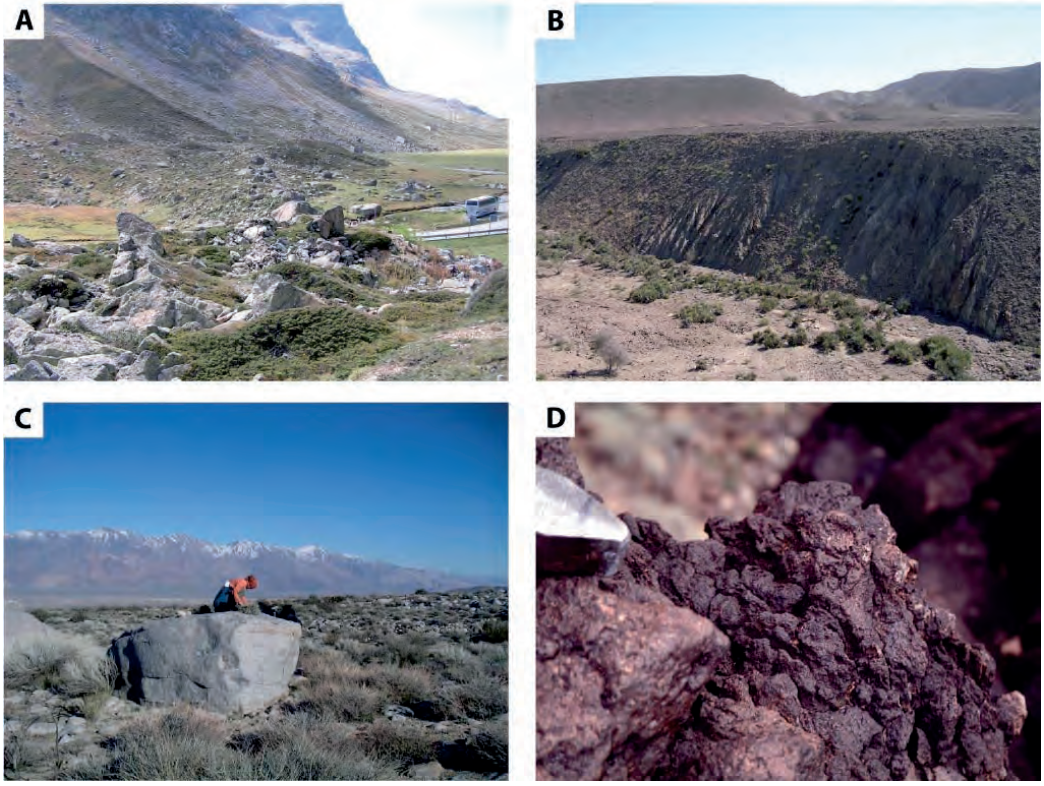

Fig. 10: Examples of exposure dated landforms:
A. View along the boulders making up the latero-terminal moraine complex at Julier Pass, left lateral moraine is seen in the upper left. Numerous boulders were dated with ^{10}Be, ^{26}Al and ^{36}Cl. Exposure dates indicate moraine stabilization at 11.4 ka (Ivy-Ochs et al. 2006),
B. Terrace levels (T2 in the center, T3 in the background) in the Pishamak area, Makran Range, SE Iran, exposure dated with both ^{10}Be and ^{21}Ne (F. Kober, unpublished data),
C. ^{10}Be dated boulder on the Shephard Creek debris-flow fan in Owens Valley (Dühnforth et al. 2008),
D. Pahoehoe flow top from the ca. 90,000 year old (^{3}He) Bar Ten flow, Arizona (Fenton et al. 2001).

Abb. 10: Beispiele von Landformen die mit kosmogenen Nukliden datiert wurden:
A: Blick entlang eines Seiten/Endmoränenkomplexes am Julier Pass, linke Seitenmoräne ist im linken oberen Bildausschnitt. Zahlreiche Blöcke wurden mit ^{10}Be, ^{26}Al und ^{36}Cl datiert. Expositionsalter geben ein Alter von 11400 Jahren an, welches als das Alter der Stabilisierung der Moränen interpretiert wird (Ivy-Ochs et al. 2006).
B: Terrassenniveaus (T2 im Zentrum, T3 im Hintergrund des Bildes) im Gebiet um Pishamak, Makran, SE-Iran, datiert mit ^{10}Be und ^{21}Ne (F. Kober et al. in Bearbeitung).
C: Blöcke eines Schuttstromes auf einem Fächer des Shephard Creeks, Owens Valley (Dühnforth et al. 2008).
D: Oberer Bereich eines Pahoehoe Lavastroms des Bar Ten Stroms, Arizona, datiert auf ca. 90000 Jahre (Fenton et al. 2001).

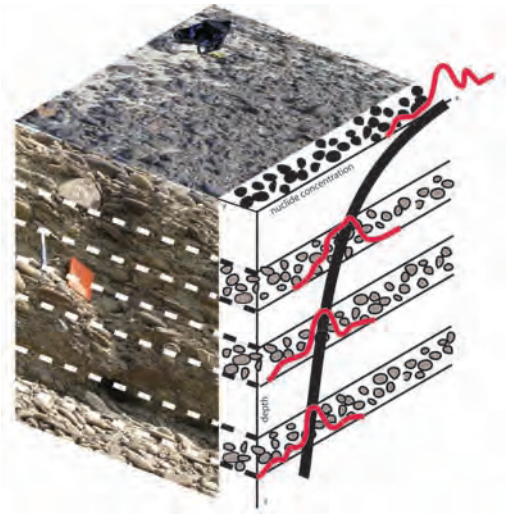

Fig. 11: Schematic sketch of a depth profile (z-axis) and cosmogenic nuclide concentrations (x-axis) in an alluvial sequence deposited in a single event. Red curves show hypothetical frequency distribution of nuclide concentrations of individual clasts, illustrating the need to amalgamate tens of clasts (Anderson et al. 1996; Repka et al. 1997). Amalgamated clast samples taken in certain depth intervals show a decreasing concentration with depth.

Abb. 11: Schematische Darstellung der Nuklidkonzentration (x-Achse) mit der Tiefe (y-Achse) in einer alluvialen Ablagerungsequenz (singuläres Ereignis). Die rote Kurve zeigt die hypothetische Nuklidkonzentrationsverteilung, welche aus einer Anzahl von individuellen Kiesgeröllen gewonnen wurde. Dies zeigt, dass eine Mischung einer größeren Anzahl von Kiesgeröllen zur Datierung nötig ist (Anderson et al. 1996, Repka et al. 1997). Mischproben zeigen eine Abnahme der Nuklidkonzentration mit der Tiefe.

sits. For example boulders can be pushed into new moraines without having their orientation changed (see also Ivy-Ochs et al. 2007a).
Where large boulders are not present amalgamated clast samples are analyzed (Anderson et al.1996; Repka et al. 1997). This method is suitable for older landforms (> 100 ka) that probably never had boulders; for example fluvial terraces. The effects of unrepresentative concentrations (too high or too low) should be smoothed out by the amalgamation of >50 clasts of similar size (several centimeters in diameter) (Anderson et al. 1996; Repka et al. 1997). Clasts are collected from the flat part of the landform surface well away from modifying channels. In many cases the nuclide concentration due to inheritance is revealed by measuring a depth profile. Amalgamated clast samples are taken every 10-20 centimeters down to 2 meters depth (Fig. 11) (Anderson et al. 1996; Repka et al. 1997; Ryerson et al. 2006). Exposure during hill slope erosion, sediment transport, and storage in terraces may result in inheritance in clasts. Scavenging (reworking) of material from older deposits at higher elevation can also lead to inheritance in clasts (Ward et al. 2005). Where field relationships indicate that the top of the depositional surface has undergone little erosion (flat tread morphology as opposed to convex tops on terraces) or little aggradation (minimal silt layer below the top surface pavement) the shape of the depth curve reveals both age and inheritance (Fig. 12). Appropriate sediment densities must be used to calculate the model curves. Commonly the concentration in the upper several tens of centimeters is constant due to mixing (often bioturbation) (Phillips et al. 1998) (Fig. 12). Thick (more than tens of meters) rapidly deposited units may also be burial dated by measuring the concentrations of two nuclides from samples at greater depth (> 10 m) (Granger & Muzikar 2001; Wolkowinsky & Granger 2004; Granger 2006) (see Dehnert & Schlüchter 2008).
Several landscape evolution questions can be addressed by sampling bedrock. Bedrock samples are taken from areas that have never been covered by sediment, ice or snow. This may require sampling a steeply dipping surface and the making of the appropriate sheilding corrections (Nishiizumi et al. 1989; Kelly et al. 2006). In general sampling of steep surface is avoided to circumvent the additional uncertainties associated with the dip correction.

5 Dating of Quaternary landforms

5.1 Glacial landscapes

Surface exposure dating has been used in a broad spectrum of settings in glacial landscapes. This

includes the dating of boulders on moraines (for a recent compilation see Reuther et al. 2006a), boulders on glacial outwash fans (Phillips et al. 1997), boulders on the former margins of ice-dammed lakes (Davis et al. 2006) and boulders deposited during catastrophic outburst of ice-dammed lakes (Cerling et al. 1994; Reuther et al. 2006b). Glacially-polished bedrock is also analyzed for determining rates of ice retreat, and depth of subglacial erosion. The method of burial dating has great potential, especially in the dating of old, buried glacial deposits (see Dehnert & Schlüchter 2008). Balco et al. (2005) used ^{26}Al and ^{10}Be ratios in quartz to determine the age of deeply buried paleosols and underlying till units.

5.1.1 Dating of moraines

Moraines record the location of the margins of a glacier in the past. Changes in glacier volume and length themselves reflect changes in tem-

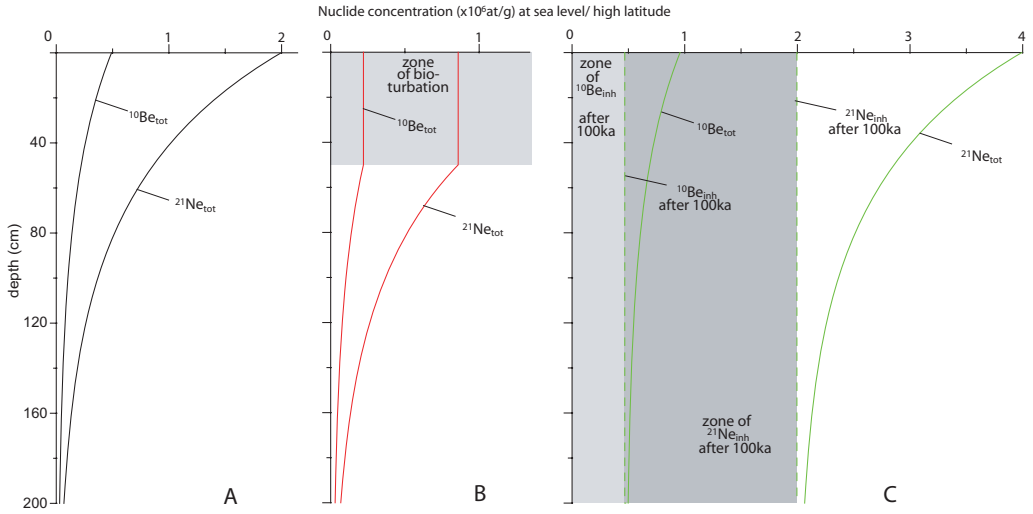

Fig. 12: ^{10}Be and ^{21}Ne concentrations with depth into a rock surface. The nuclide concentration in a sample is a composite of the inherited and the post-depositional nuclide concentration. The inherited concentration can be approximated by measuring several samples from different depths, tens of centimeters apart down to about 2 m.

A. ^{10}Be and ^{21}Ne concentrations in a depth profile after exposure for 100 ka with a constant erosion rate of 0.20 mm/ka.

B. The upper 50 cm have been mixed by bioturbation resulting in constant nuclide concentrations.

C. Curve showing the effect of inheritance on both the ^{10}Be and ^{21}Ne concentrations.

Abb. 12: Entwicklung der Nuklidkonzentration (^{10}Be und ^{21}Ne) in Abhängigkeit von der Tiefe. Die Gesamtnuklidkonzentration ist die Summe aus ererbten Konzentrationen und der Konzentration aus der Produktion nach Ablagerung der Sequenz oder eines vormalig exponierten Tiefenprofils im Festgestein. Die ererbte Nuklidkonzentration kann durch die Beprobung in unterschiedlichen Tiefen (mehrere Proben über eine Tiefe von mindestens 2 m) ermittelt werden.

A. ^{10}Be und ^{21}Ne Nuklidkonzentrationen in einem Tiefenprofil nach einer Expositionszeit von 100000 Jahren unter einer konstanten Erosionsrate von 0,20 mm/1000 Jahre.

B. Der obere Bereich des Profils (50 cm) ist durch Bioturbation homogenisiert, was zu einer konstanten Nuklidkonzentrationen über dieses Intervall führt.

C. Darstellung des Einflusses einer ererbten Nuklidkonzentration auf die ^{10}Be und ^{21}Ne Nuklidkonzentrationen.

perature and precipitation patterns in a region with time (KERSCHNER 2005). Therefore if one can directly date moraines one can construct a chronological structure to past glacier fluctuations and therefore past climatic fluctuations (KERSCHNER & IVY-OCHS 2008). Depending on the detailed structure of the moraine complex the innermost moraine records the onset of glacier downwasting (GOSSE 2005). For example near synchrony of glacier downwasting at the end of the Last Glacial Maximum world-wide has been established with ^{10}Be dating (SCHAEFER et al. 2006). As described above large boulders in stable positions along the moraine crest are sampled preferentially. A boulder must be large and stable enough not to have toppled or shifted and high enough to have protruded above the matrix since moraine deposition (HALLET & PUTKONEN, 1994; PUTKONEN & SWANSON, 2003; PUTKONEN & O'NEAL, 2006). Key limitations include weathering of the boulder surface and degradation of the moraine itself (ZREDA et al. 1994; ZREDA & PHILLIPS, 1995; REUTHER et al. 2006a; IVY-OCHS et al. 2007a). Sampling several small clasts on a young (<20ka) moraine is unlikely to give the depositional age (IVY-OCHS et al. 2007a). Moraines ranging in age from hundreds of years to hundreds of thousands of years in both hemispheres have been dated (e.g. PHILLIPS et al. 1990; IVY-OCHS et al. 1999, 2006; BARROWS et al. 2002; KAPLAN et al. 2004; BRINER et al. 2005; BALCO & SCHAEFER 2006; Akçar et al., 2008b). The older the moraine the greater the spread in ages amongst the exposed boulders. This may make interpretation of the deposition age of moraines that are older than 100 ka difficult (KAPLAN et al. 2005; SMITH et al. 2005). In such cases the oldest age is assumed to be closest to the landform age. But this age may still be a minimum age for the landform.

In a suite of ages from a single moraine outliers that are too old reflect inheritance. Boulders that are deposited in moraines may have acquired inheritance in the bedrock setting or because they are reworked from older moraines. For the case of a boulder suface exposed in the bedrock setting, the amount of inheritance is dependent on how long the bedrock surface was exposed (and the bedrock weathering rate) and how deep the boulder originated inside the bedrock surface (IVY-OCHS et al. 2007a). The effect of this will be greater in younger (Holocene) moraines. Based on a compilation of numerous published moraine boulder exposure ages, PUTKONEN & SWANSON (2003) found that pre-exposure was observed in moraine boulders in only a few percent of cases.

5.1.2 Glacially-modified bedrock surfaces and rates of sub-glacial erosion

Initial deglaciation of the valley bottom and rates of glacier downwasting can be determined by analyzing cosmogenic nuclides in glacially-scoured bedrock surfaces (e.g. roche moutonnées) (GOSSE et al. 1995; GUIDO et al. 2007). However, results from bedrock surfaces should be viewed with caution. If three meters or more of bedrock have not been removed by sub-glacial erosion during the last glaciation, then the rock surface may contain inherited nuclide concentrations. This has been noted where the rock is highly resistant (GUIDO et al. 2007). In the case where the timing of deglaciation is independently known (for example from exposure dating of erratics), the nuclide concentration measured in glacially-scoured bedrock can be used to determine sub-glacial erosion rates. Determined rates are on the order of 0.1 to 1 mm per year (BRINER & SWANSON 1998; COLGAN et al. 2002; FABEL et al. 2004). Direct determination of such rates is only possible with cosmogenic nuclides.

Cosmogenic nuclides have a unique characteristic in that they can be used to elucidate fundamental information about the thermal regime of past ice sheets. Lower ^{26}Al than ^{10}Be concentrations in bedrock reveals areas where ice was frozen to its bed and unerosive (BIERMAN et al. 1999; FABEL et al. 2002; MARQUETTE et al. 2004; STAIGER et al. 2005; SUGDEN et al. 2005; LINGE et al. 2006; PHILLIPS et al. 2006). Production ceased when the surfaces were covered by ice, ^{26}Al decays faster than ^{10}Be thus ^{26}Al/^{10}Be ratios plot below the erosion island (see also DEHNERT & SCHLÜCHTER 2008).

5.2 Alluvial, lacustrine and marine systems

Determining the age of alluvial landforms (for example fluvial terraces and alluvial or debris-flow fans) provides fundamental information about timing and rates of depositional processes. Constructing an age sequence also allows estimation of the contribution of the various external forcing mechanisms, such as tectonically induced base-level or regional slope changes, climatically (discharge) induced or sediment supply dependent variations. Fluvial or marine terraces; or alluvial fans can be dated using depth profiling and measuring one or more nuclides (samples from the upper 2 meters) (Perg et al. 2001; Ward et al. 2005; Ryerson et al. 2006; Frankel et al. 2007) or using burial dating (Wolkowinsky & Granger 2004) (see also Dehnert & Schlüchter 2008).

5.2.1 Wave-cut bedrock platforms and paleoshorelines

Lake and marine paleoshorelines delineate higher water levels and thus record past changes in the balance between precipitation vs. evaporation plus lake drainage and inflow or fluctuations in sea-level, respectively. In order to integrate these periods of lake/sea highstands into existing regional chronologies a time frame is required. Such highstands can be exposure dated in two ways by exposure dating wave-cut bedrock platforms or by determining the age of cobble deposits that mark ancient strandlines.

The only way to directly date a wave-cut bedrock platform is with cosmogenic nuclides. Uplifted marine wave-cut platforms in northern Spain were studied by Alvarez-Marrón et al. (2007) with ^{10}Be, ^{26}Al, and ^{21}Ne. Minimum ages of 1-2 Ma were calculated. Based on a comparison of ^{10}Be and ^{21}Ne data the authors suggested that the surfaces have undergone complex exposure histories and may even be Pliocene in age when the burial time is included. The data of Kong et al. (2007) from wave-cut shore lines of lake Sumxi Co, Western Tibet, agree with regional chronologies; the highest bedrock terrace was formed during enhanced discharge of melting glaciers around 12 ka. This implies that no inherited nuclides were present. Wave-cut bedrock platforms and associated boulders of the Provo shoreline which delineates the latest Pleistocene extent of Lake Bonneville have been dated with a number of cosmogenic nuclides, including ^{3}He (Cerling & Craig 1994a). At that site consistent ages have been obtained with ^{14}C in quartz (Lifton et al. 2001) and ^{10}Be making it an excellent site for production rate determination and nuclide cross-calibrations. Timing of abandonment of the Provo shoreline is known from radiocarbon dating (Godsey et al. 2005).

Cobble and pebble deposits that delineate ancient strandlines can be exposure dated either by analyzing individual clasts or by amalgamating tens of clasts together. Because of the dependency on preservation of the strandlines most of these studies are in arid regions. The primary difficulty in dating such deposits is inheritance. Inheritance is recognized when the clast exposure ages are significantly scattered and/or when they are older than the estimated age of the shoreline based on field relationships or correlations with independently dated sections. Inheritance can be acquired in the catchment when the denudation rate is low. Thus the clasts arrived in the lacustrine system with a non zero initial nuclide concentration. Clasts may have been exposed during intermittent storage in river terraces between erosion in the catchment and final deposition in the shoreline. Finally, inheritance may indicate that clasts were moved from shoreline to shoreline and thus do not give the correct age for the strandline from which they were collected. Matmon et al. (2003) dated five individual chert clasts from the ancient strandline of paleo Lake Lisan age scatter and disagreement with independent age estimates due to inheritance points to intermediate storage of clasts.

5.2.2 Alluvial fans

Patterns of alluvial fan deposition record variations of erosional processes in the fan catchment and changes in incision of the fan head over time (Dühnforth et al. 2008). When individual lobes

can be clearly mapped then surface exposure dating is a useful tool for dating of abandoned fan lobes (DÜHNFORTH et al. 2007). Original depositional forms such as flow snouts and levees are often still present on debris-flow fans that are less than 100 ka old. To date the different fan lobes large boulders in clear position on snout or levee are sampled (BIERMAN et al. 1995; ZEHFUSS et al. 2001; DÜHNFORTH et al. 2007). On older alluvial fans degradation of fan surfaces and boulder grusification leads to smoothing out of the original bar and swale morphology. After a long enough period of time (50 ka?) desert pavement of interlocking clasts develops (RYERSON et al. 2006) with associated desert varnish. In these cases amalgamated clast samples are analyzed. An important question is whether or not the dates represent the interval of lobe construction or whether they point to timing of fan abandonment. Another serious concern for the dating of alluvial and debris-flow fans is inheritance. Similar to the case of the strandline clasts inheritance can have been acquired in the catchment, in intermediate storage, or as clasts are moved from older to younger lobes. Reflecting the bedrock rezeroing effect of glaciers, inheritance is often greater in fans originating in unglaciated catchments.

5.2.3 Fluvial incision rates

Fluvial incision rates and their variation with time are calculated by using the exposure age and height of fluvial (WARD et al. 2005) or strath terraces (BURBANK et al. 1996; LELAND et al. 1998; PRATT-SITAULA et al. 2004; REUSSER et al. 2004). Boulders or amalgamated clast samples on debris-flow deposits on ancient bedrock straths have been dated to determine incision rates (FENTON et al. 2004; MARCHETTI & CERLING 2005). Based on ^{10}Be in samples from three strath terraces REUSSER et al. (2004) reported that incision rates of the Susquehanna River (eastern U.S.A.) more than doubled to 0.5 mm a^{-1}during the last glaciation (32 to 16 ka). In Taiwan ^{36}Cl measured in samples from fluvially-sculpted limestone channel walls in Taroko Gorge indicate incision rates of 26 mm a^{-1} (SCHALLER et al. 2005). Steep gorge walls may provide a more continuous record of incision than strath terraces as the latter is a step-like sequence. In any case it is often difficult to verify that strath terraces were never covered by sediment during their exposure histories. Past incision rates can also be calculated by combining burial ages of cave sediments with the height of the cave above the active river channel (GRANGER et al. 1997; STOCK et al. 2004) (see DEHNERT & SCHLÜCHTER 2008).

5.3 Tectonic and mass movement studies

Cosmogenic nuclides can be used to determine rates of tectonic activity in two ways i) by dating landforms that have been offset by movement along faults and ii) by dating bedrock fault surfaces directly.

5.3.1 Dating of offset landforms

Slip rates on strike-slip faults or rates of uplift on normal faults have been determined by taking the age and offset distances of moraines (LASSERRE et al. 2002; BROWN et al. 2002), fluvial terraces (HETZEL et al. 2002a) and alluvial fans (BIERMAN et al. 1995; SIAME et al. 1997; BROWN et al. 1998; VAN DER WOERD et al. 1998; ZEHFUSS et al. 2001; RITZ et al. 2003; MÉRIAUX et al. 2005; RYERSON et al. 2006; FRANKEL et al. 2007). Cautious interpretation of field evidence for offset distances (piercing point, offset terrace risers vs. treads; offset stream channels) is important (MÉRIAUX et al. 2004).

5.3.2 Direct dating of fault surfaces

Limestone bedrock fault surfaces are dated directly with ^{36}Cl (ZREDA & NOLLER 1998; MITCHELL et al. 2001; BENEDETTI et al. 2002; 2003; PALUMBO et al. 2004). Suitable fault surfaces are several meters high several kilometers long, fresh, and uneroded. Samples are taken at centimeter intervals along the exposed fault surface often with a circular saw. In principle, the recurrence interval of earthquakes along the fault segment can be reconstructed based on step changes in ^{36}Cl concentrations determi-

ned in tens of samples from a single fault face. Earthquakes that occurred as recently as only a thousand years ago are dated. In principle, such a study is also possible with ^{10}Be in quartz, but may be limited by sample preparation time for the large number of samples required. The age of the fault surface that can be determined is controlled by the karst weathering rate of the limestone and is generally restricted to those less than tens of thousands of years old.

5.3.3 Landslides

Landsliding is an important process for the modification of valley slopes and cross profiles, as well as overall landscape denudation especially in steep terrain. By determining the timing of recurrence intervals we can begin to understand the mechanisms of large-scale downslope movement of rock, and the interplay between various possible causes and triggers. These include inherited tectonic structures, debuttressing following retreat of glaciers, climate (precipitation, temperature, permafrost extent etc.), and/or seismic events. Several catastrophic landslides have been dated using cosmogenic nuclides: the Koefels landslide in Austria (Ivy-Ochs et al. 1998b), the Flims landslide in Switzerland (Ivy-Ochs et al. 2008), the Fernpass landslide in Austria (Prager et al. 2008), the Almtal landslide in Austria (van Husen et al. 2007); the Beinn Alligin rock avalanche, in Scotland (Ballantyne & Stone 2004), the Blackhawk landslide in California, U.S.A. (Nichols et al. 2006), several slides in Argentina (Hermanns et al. 2001; 2004), and northern India (Barnard et al. 2001), as well as both deep-seated and shallow landslides in Hong Kong (Sewell et al. 2006).

Although new rock surfaces are created during mass movements, exposure dating of landslides can have mixed results (Ivy-Ochs et al. 2008). Each possible sampling site (bedrock detachment zones, sliding planes, large boulders) has its own advantages and disadvantages. In the breakaway zone recent rockfall can be difficult to identify. Sliding planes with low dip angles may yield too young ages due to past coverage by snow and/or vegetation. Because of the movement mechanisms of landslides, rocks from the outer surface of the pre-slide bedrock frequently end up as boulders on top of the deposit. As a result, «too old» exposure ages with respect to independent age controls occur much more frequently in landslide boulders than in moraine boulders (Nichols et al. 2006; Sewell et al. 2006; Ivy-Ochs et al. 2008). Never-theless exposure dating is an irreplaceable tool in landslide studies, often there is no other way to date the mass movement. Although repeated sliding may be identified during mapping, it is impossible to determine the reccurence interval without direct dating. In the Alps, post-Last Glacial Maximum landsliding in the early Lateglacial cannot be dated with radiocarbon because of a lack of organic material. Holocene landslides can be dated when entrained trees or wood fragments are discovered or by dating basal sediments of impounded lakes. Intercomparison of dating results from various methods allows better constraining of the event age.

5.4 Volcanic sequences

Based on detailed mapping relative eruption sequences are constructed. Lava flows can often be ^{14}C dated with entrained charcoal or by analyzing underlying burnt soil, when such material is found. Time of eruption of lava flows and domes are dated with K/Ar and ^{40}Ar/^{39}Ar (Kelley 2002). Not all flows are suitable for Ar/Ar dating: i) high-K minerals may be lacking, ii) excess Ar or iii) Ar loss may be a problem. As erupted volcanic rocks are newly formed surfaces with no pre-exposure, their initial nuclide concentration is zero, they are well-suited for surface exposure dating. The most challenging aspect is to unequivocally identify the original eruptive surface to sample. This may be established by the presence of primary eruptive features such as spatter (Fig. 10), frothy glassy texture of the cooling rinds on flows or bombs, vesicles near the tops of flows, or the ropey texture of pahoehoe flows (Cerling & Craig 1994a; Fenton et al. 2001; Phillips 2003). Mafic lava flows with olivine and/or

pyroxene phenocrysts or microphenicrysts are dated with ^{3}He and/or ^{21}Ne (Kurz et al. 1990; Anthony & Poths 1992; Cerling & Craig 1994b; Licciardi et al. 1999; 2006; Fenton et al. 2004; Williams et al. 2005; Duffield et al. 2006). ^{21}Ne and ^{10}Be in quartz and/or sanidine phenocrysts have been used to date ignimbrites (welded tuffs) (Libarkin et al. 2002; Kober et al. 2005). Volcanic rocks of intermediate composition lacking quartz or olivine or pyroxene or flows lacking phenocrysts completely can be exposure dated with ^{36}Cl (Phillips 2003; Zreda et al. 1993). This also affords the opportunity for intercomparison between the eruptive (K–Ar or ^{40}Ar/^{39}Ar age) and the exposure age (Fenton et al. 2001; Phillips 2003). For the dating of landforms (moraines, flood deposits, etc.) comprised of volcanic rocks ^{3}He and ^{36}Cl are well suited.

5.5 Ancient Landscapes

It is only since the advent of cosmogenic nuclides that rock surfaces in the arid and hyperarid deserts of southern Africa (Cockburn et al. 1999; 2000; Fleming et al. 1999; Bierman & Caffee 2001), south-central Australia (Bierman & Turner 1995; Bierman & Caffee 2002; Belton et al. 2004), western South America (Nishiizumi et al. 2005; Kober et al. 2007) and Antarctica (Summerfield et al. 1999; Sugden et al. 2005) can be directly dated. The long-lived radionuclides (^{10}Be and ^{26}Al) and especially the noble gases (^{3}He and ^{21}Ne) are well suited to dating landforms that have been exposed for millions of years. Combining nuclides, for example ^{10}Be and ^{26}Al or ^{10}Be and ^{21}Ne, is critical to check for continuous exposure and rule out intermittent coverage. Studies using two or more nuclides indicate that many of the ancient bedrock surfaces in the deserts have been exposed continuously, but are never-theless weathering, albeit remarkably slowly. In most cases only minimum ages can be determined. Maximum erosion rates are calculated by assuming that nuclide concentrations are in steady state. At several of these sites erosion rates range down to less than 1 mm kyr^{-1} (Cockburn & Summerfield 2004). With cosmogenic nuclide methods, fundamental information about the age and mode of formation of ancient landscapes has been gained. High nuclide concentrations measured in Australia led to the conclusion that inselbergs are direct descendents of early Cenozoic or even Mesozoic landforms (Bierman & Caffee 2002). Combined fission-track and low cosmogenic nuclide-derived erosion rates across the Namibian escarpment indicate that great escarpments do not form by rapid (and ongoing) escarpment retreat, but must have formed early on after continental break-up (Cockburn et al. 2000). ^{10}Be in combination with ^{26}Al data showed that many surfaces in Antarctica have experienced single-stage, continuous exposure with remarkably low erosion rates for at least the last several million years (Nishiizumi et al. 1991; Brook et al. 1995; Ivy-Ochs et al. 1995; Summerfield et al. 1999; Matsuoka et al. 2006). The high nuclide concentrations found in rocks in the Dry Valleys Antarctica provide irrefutable support for the premise that the East Antarctic Ice Sheet has been a stable feature since its inception (Schäfer et al. 1999; Ackert & Kurz 2004). Measured pre-Pleistocene apparent exposure ages and corresponding low denudation rates characterize the deserts of northern Chile, despite active uplift (Dunai et al. 2005; Kober et al. 2007; Nishiizumi et al. 2005).

6 Summary and outlook

The ability to use cosmogenic nuclides to determine how long minerals have been exposed at the surface of the earth provides an unrivaled tool for determining ages of landforms and rates of geomorphic processes. Depending or rock and landform weathering rates, landforms ranging in age from a few hundred years to tens of millions of years can be dated. Because of this unique capability, the variety of applications of cosmogenic nuclides will continue to grow. Concern about methodological uncertainties, such as those associated with the production rates, the site latitude and

altitude scaling factors, as well as the effect of past changes in the Earth's magnetic field, has led to the establishment of an international consortium made up of CRONUS-Earth (www.physics.purdue.edu/cronus) and CRONUS-EU (www.cronus-eu.net). Analysis of artificial targets and samples from natural sites with independent age control are underway to refine production rates. Scaling factors are being evaluated with neutron monitors and analysis of same age natural samples taken along altitudinal transects (for example lava flows). Numerical modeling is being used to constrain production rates and scaling factors both now and in the past. The half-lives of radioactive nuclides must be accurately known. In the case of ^{10}Be, two different half-lives have been published, 1.51 and 1.34 Ma (Granger 2006; Nishiizumi et al. 2007). When these factors are better constrained the errors of the final ages will be closer to the range of the AMS and noble gas mass spectrometry measurement uncertainties (of the order of 1-4 %). With improved knowledge of production rates and their scaling to the site, the precision of obtained ages will improve. But the accuracy of the ages remains a question of geological uncertainties. The degradation of both rock surfaces and the landforms with time imposes clear limitations on the time range and accuracy of dating. Similarly, the natural variability of samples depends on landform morphology and its age. Obtained exposure ages must be evaluated individually for conformity with field relationships, including local terrace or moraine stratigraphy and regional morphostratigraphic relationships; as well as with independent age constraints for the same or correlative features. For older landforms (more than a hundred thousand years) measurement of mulitple cosmogenic nuclides can reveal fundamental information, such as non-continuous exposure, which must be factored into interpretations (Alvarez-Marrón et al. 2007; Kober et al. 2007). Cosmogenic nuclides provide a powerful and multifaceted tool whose potential has yet to be fully realized. But this power is tempered with the need for careful sampling based on detailed field mapping.

References

Ackert, R.P. & Kurz, M.D. (2004): Age and uplift rates of Sirius Group sediments in the Dominion Range, Antarctica, from surface exposure dating and geomorphology. – Global and Planetary Change, 42: 207-225.

Akçar, N., Ivy-Ochs, S. & Schlüchter, Ch. (2008a): Application of in-situ produced terrestrial cosmogenic nuclides to archaeology: A schematic review. – Quaternary Science Journal, 57/1-2: 226–238.

Akçar, N., Yavuz, V., Ivy-Ochs, S., Kubik , P.W., Vardar, M., & Schlüchter, Ch. (2008b): A Case for a down wasting mountain glacier during the Termination-I, Verçenik Valley, NE Turkey. – Journal of Quaternary Science, 23: 273-285.

Alvarez-Marrón, J., Hetzel, R., Niedermann, S., Menéndez, R. & Marquineez, J. (2007): Origin, structure and exposure history of a wave-cut platform more than 1 Ma in age at the coast of northern Spain: A multiple cosmogenic nuclide approach. –Geomorphology, 93: 316-334.

Anderson, R.S., Repka, J.L. & Dick, G.S. (1996): Explicit treatment of inheritance in dating depositional surfaces using ^{10}Be and ^{26}Al. – Geology, 24: 47-51.

Anthony, E.Y. & Poths, J. (1992): ^{3}He surface exposure dating and its implications for magma evolution in the Potrillo volcanic field, Rio-Grande Rift, New Mexico, USA. – Geochimica et Cosmochimica Acta, 56: 4105-4108.

Balco, G. & Schaefer, J.M. (2006): Cosmogenic-nuclide and varve chronologies for the deglaciation of southern New England. – Quaternary Geochronology, 1: 15-28.

Balco, G., Stone, J.O., Lifton, N.A. & Dunal, T.J. (2008): A complete and easily accessible means of calculating surface exposure ages or erosion rates from ^{10}Be and ^{26}Al measurements. – Quaternary Geochronology, 3: 174-195.

Balco, G., Stone, J.O.H. & Jennings, C. (2005): Dating Plio-Pleistocene glacial sediments using the cosmic-ray-produced radionuclides ^{10}Be and ^{26}A. – American Journal of Science, 305: 1-41.

Ballantyne, C K. & Stone, J.O. (2004): The Beinn Alligin rock avalanche, NW Scotland: cosmogenic^{10}Be dating, interpretation and significance. – The Holocene, 14: 448-453.

Barnard, P.L., Owen, L.A., Sharma, M.C. & Finkel, R.C. (2001): Natural and human-induced landsliding in the Garhwal Himalaya of northern India. – Geomorphology, 40: 21-35.

BARROWS, T.T., STONE, J.O., FIFIELD, L.K. & CRESSWELL, R.G. (2002): The timing of the Last Glacial Maximum in Australia. – Quaternary Science Reviews, 21: 159-173.

BELTON, D.X., BROWN, R.W., KOHN, B.P., FINK, D. & FARLEY, K.A. (2004): Quantitative resolution of the debate over antiquity of the central Australian landscape: implications for the tectonic and geomorphic stability of cratonic interiors. – Earth and Planetary Science Letters, 219: 21-34.

BENEDETTI, L., FINKEL, R., KING, G., ARMIJO, R., PAPANASTASSIOU, D., RYERSON, F.J., FLERIT, F., FARBER, D. & STAVRAKAKIS, G. (2003): Motion on the Kaparelli fault (Greece) prior to the 1981 earthquake sequence determined from Cl-36 cosmogenic dating. – Terra Nova, 15: 118-124.

BENEDETTI, L., FINKEL, R., PAPANASTASSIOU, D., KING, G., ARMIJO, R., RYERSON, F., FARBER, D. & FLERIT, F. (2002): Post-glacial slip history of the Sparta fault (Greece) determined by Cl-36 cosmogenic dating: Evidence for non-periodic earthquakes. – Geophysical Research Letters, 29: 8, 1246, doi:10.1029/2001GL014510.

BENNETT, C.L., BEUKENS, R.P., CLOVER, M.R., GOVE, H.E., LIEBERT, R.B., LITHERLAND, A.E., PURSER, K.H. & SONDHEIM, W.E. (1977): Radiocarbon dating using electrostatic accelerators - Negative-ions provide the key. – Science, 198: 508-510.

BIERMAN, P. & CAFFEE, M. (2001): Slow rates of rock surface erosion and sediment production across the Namib Desert and Escarpment, Southern Africa. – American Journal of Science, 301: 326-358.

BIERMAN, P. & CAFFEE, M. (2002): Cosmogenic exposure and erosion history of Australian bedrock landforms. - Geological Society of America Bulletin, 114: 787-803.

BIERMAN, P. & NICHOLS, K.K. (2004): Rock to sediment - slope to sea with ^{10}Be-rates of landscape change. – Annual Review of Earth and Planetary Sciences, 32: 215-255.

BIERMAN, P.R., CAFFEE, M.W., DAVIS, P.T., MARSELLA, K., PAVICH, M., COLGAN P., MICKELSON, D. & LARSEN, J. (2002): Rates and timing of earth surface processes from in-situ produced cosmogenic ^{10}Be. – In: GREW, E.S. (ed.): Beryllium: Mineralogy, Petrology, and Geochemistry: Reviews in Mineralogy and Geochemistry, 50: 147-204.

BIERMAN, P.R., GILLESPIE, A.R. & CAFFEE, M.W. (1995): Cosmogenic ages for earthquake recurrence intervals and debris flow fan deposition, Owens Valley, California. – Science, 270: 447-450.

BIERMAN, P.R., MARSELLA, K.A., PATTERSON, C., DAVIS, P.T. & CAFFEE, M. (1999): Mid-Pleistocene cosmogenic minimum-age limits for pre-Wisconsian glacial surfaces in southwestern Minnesota and southern Baffin Island: a multiple nuclide approach. – Geomorphology, 27: 25-39.

BIERMAN, P.R. & TURNER, J. (1995): ^{10}Be and ^{26}Al evidence for exceptionally low rates of Australian bedrock erosion and the likely existence of Pre-Pleistocene landscapes. – Quaternary Research, 44: 378-382.

BLARD, P.H., BOURLÈS, D., PIK, R. & LAVE, J. (2008): In situ cosmogenic ^{10}Be in olivines and pyroxenes. – Quaternary Geochronology, 3: 196-205.

BRAUCHER, R., BENEDETTI, L., BOURLÈS, D., BROWN, E.T. & CHARDON, D. (2005): Use of in situ-produced ^{10}Be in carbonate-rich environments: A first attempt. – Geochimica et Cosmochimica Acta, 69: 1473-1478.

BRINER, J.P., KAUFMANN, D.S., MANLEY, W.F., FINKEL, R.C. & CAFFEE, M.W. (2005): Cosmogenic exposure dating of late Pleistocene moraine stabilization in Alaska. – Geological Society of America Bulletin, 117: 1108-1120.

BRINER, J.P. & SWANSON, T. (1998): Using inherited cosmogenic ^{36}Cl to constrain glacial erosion rates of the Cordilleran ice sheet. – Geology, 26: 3-6.

BROOK, E.J., BROWN, E.T., KURZ, M.D., ACKERT, R.P., RAISBECK, G. & YIOU, F. (1995): Constraints on age, erosion, and uplift of Neogene glacial deposits in the Transantarctic Mountains determined from in situ cosmogenic ^{10}Be and ^{26}Al. – Geology, 23: 1063-1066.

BROOK, E.J. & KURZ, M.D. (1993): Surface-exposure chronology using in-situ cosmogenic ^{3}He in Antarctic quartz sandstone boulders. – Quaternary Research, 39: 1-10.

BROWN, E.T., BENDICK, R., BOURLES, D.L., GAUR, V., MOLNAR, P., RAISBECK, G.M. & YIOU, F. (2002): Slip rates of the Karakorum fault, Ladakh, India, determined using cosmic ray exposure dating of debris flows and moraines. – Journal Geophysical Research, 107: 2192, doi:10.1029/2000JB000100.

BROWN, E.T., BOURLÈS, D. L., BURCHFIEL, B.C., QIDONG, D., JUN, L., MOLNAR, P., RAISBECK, G.M. & YIOU, F. (1998): Estimation of slip rates in the southern Tien Shan using cosmic ray exposure dates of abandoned alluvial fans. – Geological Society of America Bulletin, 110: 377-386.

BRUNO, L.A., BAUR, H., GRAF, T., SCHLÜCHTER, CH., SIGNER, P. & WIELER, R. (1997): Dating of Sirius Group tillites in the Antarctic Dry Valleys with

cosmogenic ^{3}He and ^{21}Ne. – - Earth and Planetary Science Letters, 147: 37-54.

Burbank, D.W., Leland, J., Fielding, E., Anderson, R.S., Brozovic, N., Reid, M.R. & Duncan, C. (1996): Bedrock incision, rock uplift and threshold hillslopes in the northwestern Himalayas. – Nature, 379: 505-510.

Cerling, T.E. & Craig, H. (1994a): Geomorphology and in-situ cosmogenic isotopes. – Annual Review of Earth and Planetary Sciences, 22: 273-317.

Cerling, T.E. & Craig, H. (1994b): Cosmogenic ^{3}He production rates from 39°N to 46°N latitude, western USA and France. – Geochimica et Cosmochimica Acta, 58: 249-255.

Cerling, T.E., Poreda, R.J. & Rathburn, S.L. (1994): Cosmogenic ^{3}He and ^{21}Ne age of the Big Lost River flood, Snake River plain, Idaho. - Geology, 22: 227-230.

Cockburn, H.A.P., Brown, R.W., Summerfield, M.A. & Seidl, M.A. (2000): Quantifying passive margin denudation and landscape development using a combined fission-track thermochronology and cosmogenic isotope analysis approach. – Earth and Planetary Science Letters, 179: 429-435.

Cockburn, H.A.P., Seidl, M.A. & Summerfield, M.A. (1999): Quantifying denudation rates on inselbergs in the central Namib Desert using in situ produced cosmogenic ^{10}Be and ^{26}Al. – Geology, 27: 399-402.

Cockburn, H.A.P. & Summerfield, M.A. (2004): Geomorphological applications of cosmogenic isotope analysis. – Progress in Physical Geography, 28: 1-42.

Colgan, P. M., Bierman, P., Mickelson, D.M. & Caffee, M. (2002): Variation in glacial erosion near the southern margin of the Laurentide ice sheet, south-central Wisconsin, USA; implications for cosmogenic dating of glacial terrains. – Geological Society of America Bulletin, 114: 1581-1591.

Davis, N. K., Locke, W.W., Pierce, K.L. & Finkel, R.C. (2006): Glacial Lake Musselshell: Late Wisconsin slackwater on the Laurentide ice margin in central Montana, USA. – Geomorphology, 75: 330-345.

Davis, P.T., Bierman, P., Marsella, K.A., Caffee, M.W. & Southon, J.R. (1999): Cosmogenic analysis of glacial terrains in the eastern Canadian Arctic; a test for inherited nuclides and the effectiveness of glacial erosion. – Annals of Glaciology, 28: 181-188.

Davis, P.T., Briner, J.P., Coulthard, R.D., Finkel, R.C. & Miller, G.H. (2006): Preservation of Arctic landscapes overridden by cold-based ice sheets. – Quaternary Research, 65: 156-163.

Davis, R. & Schaeffer, O.A. (1955): Chlorine-36 in Nature. – Annals of the New York Academy of Sciences, 62: 107-121.

Dehnert, A. & Schlüchter, Ch. (2008): Sediment burial dating using terrestrial cosmogenic nuclides. – Quaternary Science Journal, 57/1-2: 208–223.

Desilets, D. & Zreda, M. (2001): On scaling cosmogenic nuclide production rates for altitude and latitude using cosmogenic-ray measurements. – Earth and Planetary Science Letters, 193: 213-225.

Desilets, D., Zreda, M., Almasi, P.F. & Elmore, D. (2006a): Determination of cosmogenic ^{36}Cl in rocks by isotope dilution: innovations, validation and error propagation. – Chemical Geology, 233: 185-195.

Desilets, D., Zreda, M. & Pradu, T. (2006b): Extended scaling factors for in situ cosmogenic nuclides: New measurements at low latitude. – Earth and Planetary Science Letters, 246: 265-276.

Duffield, W., Riggs, N., Kaufman, D., Champion, D., Fenton, C., Forman, S., McIntosh, W., Hereford, R., Plescia, J. & Ort, M. (2006): Multiple constraints on the age of a Pleistocene lava dam across the Little Colorado River at Grand Falls, Arizona. – Geological Society of America Bulletin, 118: 421-429.

Dühnforth, M., Densmore, A.L., Ivy-Ochs, S. & Allen, P.A. (2008): Controls on sediment evacuation from glacially modified and unmodified catchments in the eastern Sierra Nevada, California. – Earth Surface Processes and Landforms: in press.

Dühnforth, M., Densmore, A.L., Ivy-Ochs, S., Allen, P.A. & Kubik, P.W. (2007): Timing and patterns of debris flow deposition on Shepherd and Symmes creek fans, Owens Valley, California, deduced from cosmogenic ^{10}Be. – Journal of Geophysical Research-Earth Surface, 112:, F03S15, doi:10.1029/2006JF000562.

Dunai, T.J. (2000): Scaling factors for production rates of in situ produced cosmogenic nuclides: a critical re-evaluation. - Earth and Planetary Science Letters, 176: 157-169.

Dunai, T.J. (2001): Influence of secular variation of the geomagnetic field on production rates of in situ produced cosmogenic nuclides. – Earth and

Planetary Science Letters, 193: 197-212.

DUNAI, T.J., GONZÁLES LOPEZ, G.A. & JUEZ-LARRE, J. (2005): Oligocene–Miocene age of aridity in the Atacama Desert revealed by exposure dating of erosion-sensitive landforms. – Geology, 33: 321-324.

DUNNE, J., ELMORE, D. & MUZIKAR, P. (1999): Scaling factors for the rates of production of cosmogenic nuclides for geometric shielding and attenuation at depth on sloped surfaces. – Geomorphology, 27: 3-11.

ELMORE, D., FULTON, B.R., CLOVER, M.R., MARSDEN, J.R., GOVE, H.E., NAYLOR, H., PURSER, K.H., KILIUS, L.R., BEUKENS, R.P. & LITHERLAND, A.E. (1979): Analysis of Cl-36 in environmental water samples using an electrostatic accelerator. – Nature, 277: 22-25.

ELMORE, D., MA, X., MILLER, T., MUELLER, K., PERRY, M., RICKEY, F., SHARMA, P., SIMMS, P., LIPSCHUTZ, M. & VOGT, S. (1997): Status and plans for the PRIME Lab AMS facility. – Nuclear Instruments & Methods in Physics Research, 123: 69-72.

FABEL, D., HARBOR, J., DAHMS, D., JAMES, A., ELMORE, D., HORN, L., DALEY, K. & STEELE, C. (2004): Spatial patterns of glacial erosion at a valley scale derived from terrestrial cosmogenic ^{10}Be and ^{26}Al concentrations in rock. – Annals of Association of American Geographers, 94: 241-255.

FABEL, D., STROEVEN, A.P., HARBOR, J., KLEMAN, J., ELMORE, D. & FINK, D. (2002): Landscape preservation under Fennoscandian ice sheets determined from in situ produced ^{10}Be and ^{26}Al. – Earth and Planetary Science Letters, 201: 397-406.

FABRYKA-MARTIN, J. (1988): Production of radionuclides in the Earth and the hydrologic significance, with emphasis on chlorine-36 and iodine-129. – PhD thesis. University of Arizona.

FENTON, C.R., POREDA, R.J., NASH, B.P., WEBB, R H. & CERLING, T.E. (2004): Geochemical discrimination of five Pleistocene lava-dam outburst-flood deposits, western Grand Canyon, Arizona. – Journal of Geology 112: 91-110.

FENTON, C.R., WEBB R.H., PEARTHREE, P.A., CERLING, T.E. & Poreda, R.J. (2001): Displacement rates on the Toroweap and Hurricane faults: Implications for Quaternary downcutting in the Grand Canyon, Arizona. – Geology, 29: 1035-1038.

FINKEL, R.C. & SUTER, M. (1993): AMS in the Earth Sciences. – Advances in Analytical Geochemistry, 1: 1-114.

FLEMING, A., SUMMERFIELD, M.A., STONE, J.O., FIFIELD, L.K. & CRESSWELL, R.G. (1999): Denudation rates for the southern Drakensberg escarpment, SE Africa, derived from in-situ-produced cosmogenic ^{36}Cl: initial results. – Journal of the Geological Society, 156: 209-212.

FRANKEL, K.L., BRANTLEY, K.S., DOLAN, J.F., FINKEL, R.C., KLINGER, R.E., KNOTT, J.R., MACHETTE, M.N., OWEN, L.A., PHILLIPS, F.M., SLATE, J.L. & WERNICKE, B.P. (2007): Cosmogenic ^{10}Be and ^{36}Cl geochronology of offset alluvial fans along the northern Death Valley fault zone: Implications for transient strain in the eastern California shear zone. – Journal of Geophysical Research-Solid Earth, 112: B06407, doi: 10.1029/2006JB004350.

GODSEY, H.S., CURREY, D.R. & CHAN, M.A. (2005): New evidence for an extended occupation of the Provo shoreline and implications for regional climate change, Pleistocene Lake Bonneville, Utah, USA. – Quaternary Research, 63: 212-223.

GOSSE, J.C. (2005): The contributions of cosmogenic nuclides to unraveling alpine paleo-glacier histories. – In: HUBER, U.M, BUGMANN, H.K.M & REASONER, M.A (eds.): Global Change and Mountain Regions. A State of Knowledge Overview: 39-50; Dordrecht, (Springer).

GOSSE, J.C., KLEIN, J., EVENSON, E.B., LAWN, B. & MIDDLETON, R. (1995): ^{10}Be Dating of the Duration and Retreat of the Last Pinedale Glacial Sequence. – Science, 268: 1329-1333.

GOSSE, J.C. & PHILLIPS, F.M. (2001): Terrestrial in situ cosmogenic nuclides: theory and application. – Quaternary Science Reviews, 20: 1475-1560.

GRAF, T., KOHL, C.P., MARTI, K. & NISHIIZUMI, K. (1991): Cosmic ray produced neon in Antarctic rocks. – Geophysical Research Letters, 18: 203-206.

GRANGER, D.E. (2006): A review of burial dating methods using ^{26}Al and ^{10}Be. – In: L.L. SIAME, L.L., BOURLÈS, D.L. & BROWN E.T. (eds.): In Situ–Produced Cosmogenic Nuclides and Quantification of Geological Processes, Geological Society of America Special Paper, 415: 1-16.

GRANGER, D. E. (2007): Cosmogenic nuclides - Landscape evolution. – In: ELIAS, S.A. (ed.): Encyclopedia of Quaternary Sciences: 445-452; Amsterdam (Elsevier).

GRANGER, D.E., KIRCHNER, J.W. & FINKEL, R.C. (1997): Quaternary downcutting rate of the New River, Virginia, measured from differential de-

cay of cosmogenic ^{26}Al and ^{10}Be in cave-deposited alluvium. – Geology, 25: 107-110.

Granger, D.E. & Muzikar, P.F. (2001): Dating sediment burial with in situ-produced cosmogenic nuclides: theory, techniques, and limitations. – Earth and Planetary Science Letters, 188: 269-281.

Granger, D.E. & Riebe, C.S. (2007): Cosmogenic nuclides in weathering and erosion. – In Holland H.D.& Turekian, K.K. (eds.): Treatise on Geochemistry, 2nd ed.: 1-43; Amsterdam (Elsevier).

Granger, D.E. & Smith, A.L. (2000): Dating buried sediments using radioactive decay and muogenic production of ^{10}Be and ^{26}Al. – Nuclear Instruments & Methods in Physics Research B, 172: 822-826.

Guido, Z.S., Ward, D.J. & Anderson, R.S. (2007): Pacing the post-Last Glacial maximum demise of the Animas Valley glacier and the San Juan Mountain ice cap, Colorado. – Geology, 35: 739-742.

Hallet, B. & Putkonen, J. (1994): Surface dating of dynamic landforms - young boulders on aging moraines. – Science, 265: 937-940.

Hermanns, R.L., Niedermann, S., Garcia, A.V., Gomez, J.S. & Strecker, M.R. (2001): Neotectonics and catastrophic failure of mountain fronts in the southern intra-Andean Puna Plateau, Argentina. – Geology, 29: 619-622.

Hermanns, R.L., Niedermann, S., Ivy-Ochs, S. & Kubik, P.W. (2004): Rock avalanching into a landslide-dammed lake causing multiple dam failure in Las Conchas valley (NW Argentina) — evidence from surface exposure dating and stratigraphic analyses. – Landslides, 1: 113-122.

Hetzel, R., Niedermann, S., Ivy-Ochs, S., Kubik, P.W., Tao, M. & Gao, B. (2002a): ^{21}Ne verus ^{10}Be and ^{26}Al exposure ages of fluvial terraces: the influence of crustal Ne in quartz. – Earth and Planetary Science Letters, 201: 575-591.

Hetzel, R., Niedermann, S., Tao, M., Kubik, P.W., Ivy-Ochs, S., Gao, B. & Strecker, M.R. (2002b): Low slip rates and long-term preservation of geomorphic features in Central Asia. – Nature, 417: 428-432.

Ivy-Ochs, S. (1996): The dating of rock surface using in situ produced ^{10}Be, ^{26}Al and ^{36}Cl, with examples from Antarctica and the Swiss Alps. – ETH PhD thesis No. 11763, Zürich.

Ivy-Ochs, S., Kerschner, H. & Schlüchter, Ch. (2007a): Cosmogenic nuclides and the dating of Lateglacial and Early Holocene glacier variations: The Alpine perspective. – Quaternary International, 164-65: 53-63.

Ivy-Ochs, S., Kober, F., Alfimov, V., Kubik, P.W. & Synal, H.A. (2007b): Cosmogenic ^{10}Be, ^{21}Ne, and ^{36}Cl in sanidine and quartz from Chilean ignimbrites. – Nuclear Instruments & Methods in Physics Research, B259: 588-594.

Ivy-Ochs, S., Poschinger, A.v., Synal, H.A. & Maisch, M. (2008): Surface exposure dating of the Flims rockslide, Graubünden, Switzerland. – Geomorphology (in press).

Ivy-Ochs, S., Schlüchter, Ch., Kubik, P.W., Denton, G.H. (1999): Moraine exposure dates imply synchronous Younger Dryas glacier advance in the European Alps and in the Southern Alps of New Zealand. – Geografiska Annaler, 81A: 313-323.

Ivy-Ochs, S., Synal, H.A., Roth, C. & Schaller, M. (2004): Initial results from isotope dilution for Cl and ^{36}Cl measurements at the PSI/ETH Zurich AMS facility. – Nuclear Instruments & Methods in Physics Research, B223-24: 623-627.

Ivy-Ochs, S., Schlüchter, Ch., Kubik, P.W., Dittrich-Hannen, B. & Beer, J. (1995): Minimum ^{10}Be exposure ages of early Pliocene for the Table Mountain plateau and the Sirius Group at Mount Fleming, dry valleys, Antarctica. – Geology, 23: 1007-1010.

Ivy-Ochs, S., Kubik, P.W., Masarik, J., Wieler, R., Bruno, L. & Schlüchter, Ch. (1998a): Preliminary results on the use of pyroxene for ^{10}Be surface exposure dating. – Schweizerische Mineralogisch-Petrographische Mitteilungen, 78: 375-382.

Ivy-Ochs, S., Heuberger, H., Kubik, P. W., Kerschner, H., Bonani, G., Frank, M. & Schlüchter, Ch. (1998b): The age of the Koefels event. Relative, ^{14}C and cosmogenic isotope dating of an early Holocene landslide in the Central Apls (Tyrol, Austria). – Zeitschrift für Gletscherkunde und Glazialgeologie, 134: 57-70.

Ivy-Ochs, S., Kerschner, H., Reuther, A., Maisch, M., Sailer, R., Schaefer, J., Kubik, P. W., Synal, H. A. & Schlüchter, Ch. (2006): The timing fof glacier advances in the northern Alpes based on surface exposure dating with cosmogenic ^{10}Be, ^{26}Al, ^{36}Cl and ^{21}Ne. – In: Siame, L.L, Bourlès, D.L. & Brown, E.T. (eds.): In Situ–Produced Cosmogenic Nuclides and Quantification of Geological Processes: Geological Society of America Special Paper, 415: 43-60.

Jull, A.J., Wilson, A.E., Burr, G.S., Toolin, L.J. & Donahue, D.J. (1992): Measurements of cosmo-

genic ^{14}C produced by spallation in high-altitude rocks. – Radiocarbon, 34: 737-744.

KAPLAN, M.R., ACKERT, R.P., SINGER, B.S., DOUGLASS, D.C. & KURZ, M.D. (2004): Cosmogenic nuclide chronology of millennial-scale glacial advances during O-isotope stage 2 in Patagonia. – Geological Society of America Bulletin, 116: 308-321.

KAPLAN, M.R., DOUGLASS, D.C., SINGER, B.S. & CAFFEE, M.W. (2005): Cosmogenic nuclide chronology of pre-last glacial maximum moraines at Lago Buenos Aires, 46 degrees S, Argentina. – Quaternary Research, 63: 301-315.

KELLEY, S. (2002): K-Ar and Ar-Ar. – In: PORCELLI, D., BALLENTINE, C.J., & WIELER, R. (eds.): Noble Gases in Geochemistry and Cosmochemistry: Reviews in Mineralogy & Geochemistry 47: 785-818.

KELLY, M.A., IVY-OCHS, S., KUBIK, P.W., VON BLANCKENBURG, F. & SCHLÜCHTER, CH. (2006): Chronology of deglaciation based on ^{10}Be dates of glacial erosional features in the Grimsel Pass region, central Swiss Alps. – Boreas, 35: 634 - 643.

KERSCHNER, H. (2005): Glacier-climate models as palaeoclimatic information sources: Examples from the Alpine Younger Dryas period. – In: HUBER, U.M., BUGMANN, H.K.M.& REASONER, M.A. (eds.): Global Change and Mountain Regions (A State of Knowledge Overview: 73-82; Dordrecht (Springer).

KERSCHNER, H. & IVY-OCHS, S. (2008): Palaeoclimate from glaciers: Examples from the Eastern Alps during the Alpine Lateglacial and early Holocene. – Global and Planetary Change, 60: 58-71.

KLEIN, J., GIEGENGACK, R., MIDDLETON, R., SHARMA, P., UNDERWOOD, J. & WEEKS, R.A. (1986): Revealing histories of exposure using in situ produced ^{26}Al and ^{10}Be in Libyan desert glass. – Radiocarbon, 28: 547-555.

KLEIN, J., MIDDLETON, R. & TANG, H.Q. (1982): Instrumentation of an FN tandem for the detection of ^{10}Be. – Nuclear Instruments & Methods in Physics Research, 193: 601-616.

KOBER, F., IVY-OCHS, S., LEYA, I., WIELER, R., BAUR, H. & MAGNA, T. (2005): In situ cosmogenic ^{10}Be and ^{21}Ne in sanidine and in situ cosmogenic ^{3}He in Fe-Ti-oxide minerals. – Earth and Planetary Science Letters, 236: 404-418.

KOBER, F., IVY-OCHS, S., SCHLUNEGGER, F., BAUR, H., KUBIK, P.W. & WIELER, R. (2007): Denudation rates and a topography-driven precipitation threshold in northern Chile: multiple cosmogenic nuclide data and sediment yield budgets. – Geomorphology, 83: 97-120.

KOHL, C.P. & NISHIIZUMI, K. (1992): Chemical isolation of quartz for measurement of in-situ-produced cosmogenic nuclides. - Geochimica et Cosmochimica Acta, 56: 3583-3587.

KONG, P., NA, C. G., FINK, D., HUANG, F.X. & DING, L. (2007): Cosmogenic ^{10}Be inferred lake-level changes in Sumxi Co Basin, Western Tibet. – Journal of Asian Earth Sciences, 29: 698-703.

KUBIK, P.W., KORSCHINEK, G. & NOLTE, E. (1984): Accelerator mass-spectrometry with completely stripped ^{36}Cl Ions at the Munich postaccelerator. – Nuclear Instruments & Methods in Physics Research, B229: 51-59.

KURZ, M.D. (1986): Cosmogenic helium in a terrestrial rock. – Nature, 320: 435-439.

KURZ, M.D., COLODNER, D., TRULL, T.W., MOORE, R.B. & O'BRIEN, K. (1990): Cosmic ray exposure dating with in-situ produced cosmogenic ^{3}He: results from young Hawaian lava flows. – Earth and Planetary Science Letters, 97: 177-189.

LAL, D. (1991): Cosmic ray labeling of erosion surfaces: in-situ nuclide production rates and erosion models. – Earth and Planetary Science Letters, 104: 424-439.

LAL, D. & PETERS, B. (1967): Cosmic ray produced radioactivity on the Earth. – Handbuch der Physik: 551-612.

LASSERRE, C., GAUDEMER, Y., TAPPONNIER, P., MÉRIAUX, A.-S., VAN DER WOERD, J., DAOYANG, Y., RYERSON, F.J., FINKEL, R.C. & CAFFEE, M.W. (2002): Fast late Pleistocene slip rate on the Leng Long Ling segment of the Haiyuan fault, Qinghai, China. – Journal of Geophysical Research, 107 2276, doi:10.1029/2000JB000060.

LELAND, J., REID, M.R., BURBANK, D.W., FINKEL, R. & CAFFEE, M. (1998): Incision and differential bedrock uplift along the Indus River near Nanga Parbat, Pakistan Himalaya, from Be-10 and Al-26 exposure age dating of bedrock straths. – Earth and Planetary Science Letters, 154: 93-107.

LIBARKIN, J.C., QUADE, J., CHASE, C.G., POTHS, J. & MCINTOSH, W. (2002): Measurement of ancient cosmogenic ^{21}Ne in quartz from the 28 Ma Fish Canyon Tuff, Colorado. – Chemical Geology, 186: 199-213.

LICCIARDI, J.M., KURZ, M.D., CLARK, P.U. & BROOK E.J. (1999): Calibration of cosmogenic ^{3}He production rates from Holocene lava flows in Oregon, USA, and effects of the Earth' magnetic

field. – Earth and Planetary Science Letters, 172: 261-271.

Licciardi, J.M., Kurz, M.D. & Curtice, J.M. (2006): Cosmogenic ^{3}He production rates from Holocene lava flows in Iceland. – Earth and Planetary Science Letters, 246: 251-264.

Lifton, N.A., Jull, A.J.T. & Quade, J. (2001): A new extraction technique and production rate estimate for in situ cosmogenic ^{14}C in quartz. – Geochimica et Cosmochimica Acta, 65: 1953-1969.

Linge, H., Brook, E.J., Nesje, A., Raisbeck, G., Yiou, F. & Clark, H. (2006): In situ ^{10}Be exposure ages from southeastern Norway: Implications for the geometry of the Weichselian Scandinavian ice sheet. – Quaternary Science Reviews, 25: 1097-1109.

Liu, B., Phillips, F.M., Fabryka-Martin, J.T., Fowler, M.M. & Stone, W.D. (1994): Cosmogenic ^{36}Cl accumulation in unstable landforms, 1. Effects of the thermal neutron distribution. – Water Resources Research, 30: 3115-3125.

Marchetti, D.W. & Cerling, T.E. (2005): Cosmogenic ^{3}He exposure ages of Pleistocene debris flows and desert pavements in Capitol Reef National Park, Utah. – Geomorphology, 67: 423-435.

Marchetti D.W., Cerling, T.E. & Lips, E.W. (2005): A glacial chronology for the Fish Creek drainage of Boulder Mountain, Utah, USA. – Quaternary Research, 64: 264-271.

Marquette, G.C., Gray, J.T., Gosse, J.C., Courchesne, F., Stockli, L., Macpherson, G. & Finkel, R. (2004): Felsenmeer persistence under non-erosive ice in the Torngat and Kaumajet mountains, Quebec and Labrador, as determined by soil weathering and cosmogenic nuclide exposure dating. – Canadian Journal of Earth Sciences, 41: 19-38.

Marti, K. & Craig, H. (1987): Cosmic-ray-produced neon and helium in the summit lavas of Maui. – Nature, 325: 335-337.

Masarik, J., Frank, M., Schaefer, J.M. & Wieler, R. (2001): Correction of in-situ cosmogenic nuclide production rates for geomagnetic field intensity variations during the past 800,000 years. – Geochimica et Cosmochimica Acta, 65: 2995-3003.

Masarik, J., Kollar, D. & Vanya, S. (2000): Numerical simulation of in situ production of cosmogenic nuclides: Effect of irradiation geometry. – Nuclear Instruments & Methods in Physics Research, B 172: 786-789.

Masarik, J. & Wieler, R. (2003): Production rates of cosmogenic nuclides in boulders. – Earth and Planetary Science Letters, 216: 201-208.

Matmon, A., Crouvi, O., Enzel, Y., Bierman, P., Larsen, J., Porat, N., Amit, R. & Caffee, M. (2003): Complex exposure histories of chert clasts in the late Pleistocene shorelines of Lake Lisan, southern Israel. – Earth Surface Processes and Landforms, 28: 493-506.

Matsuoka, N., Thomachot, C.E., Oguchi, C.T., Hatta, T., Abe, M. & Matsuzaki, H. (2006): Quaternary bedrock erosion and landscape evolution in the Sør Rondane Mountains, East Antarctica: Reevaluating rates and processes. – Geomorphology, 81: 408-420.

Merchel, S., Braucher, R., Benedetti, L., Grauby, O. & Bourles, D.L. (2008): Dating carbonate rocks with in-situ produced cosmogenic ^{10}Be: Why it often fails. – Quaternary Geochronology, 3: 299-307.

Mériaux, A.-S., Ryerson, F.J., Tapponnier, P., Van der Woerd, J., Finkel, R.C., Xu, X.W., Xu, Z.Q. & Caffee, M. W. (2004): Rapid slip along the central Altyn Tagh fault: Morphochronologic evidence from Cherchen He and Sulamu Tagh. – Journal of Geophysical Research-Solid Earth, 109: B06401, 10.1029/2003JB002558.

Mériaux, A.-S., Tapponnier, P., Ryerson, F.J., Xu, X.W., King, G., Van der Woerd, J., Finkel, R.C., Li, H.B., Caffee, M.W., Xu, Z.Q. & Chen, W.B. (2005): The Aksay segment of the northern Altyn Tagh fault: Tectonic geomorphology, landscape evolution, and Holocene slip rate. – Journal of Geophysical Research-Solid Earth, 110: B04404, 10.1029/2004JB003210.

Mitchell, S.G., Matmon, A., Bierman, P.R., Enzel, Y., Caffee, M. & Rizzo, D. (2001): Displacement history of a limestone normal fault scarp, northern Israel, from cosmogenic ^{36}Cl. – Journal of Geophysical Research-Solid Earth, 106: 4247-4264.

Morris J.D., Gosse J.C., Brachfield, S. & Tera, F. (2002): Cosmogenic ^{10}Be and the solid Earth: Studies in geomagnetism, subduction zone processes, and active tectonics. – In: Grew, E.S. (ed.): Beryllium: Mineralogy, Petrology, and Geochemistry, Reviews in Mineralogy and Geochemistry, 50: 207-270.

Muzikar, P. (2005): Geomagnetic field variations and the accumulation of in-situ cosmogenic nuclides in an eroding landform. – Geochimica et Cosmochimica Acta, 69: 4127-4131.

Nelson, D.E., Korteling, R.G. & Stott, W.R. (1977): Carbon-14: Direct detection at natural

concentrations. – Science, 198: 507-508.

NICHOLS, K.K., BIERMAN, P.R., FONIRI, R., GILLESPIE, A.R., CAFFEE, M. & FINKEL, R.C. (2006): Dates and rates of arid region geomorphic processes. – Geological Society of America Today, 16: 4-11.

NIEDERMANN, S. (2002): Cosmic-ray-produced noble gases in terrestrial rocks: Dating tools for surface processes. – In: PORCELLI, D., BALLENTINE, C.J., & WIELER, R. (eds.): Noble Gases in Geochemistry and Cosmochemistry, Reviews in Mineralogy & Geochemistry, 47: 731-784.

NISHIIZUMI, K., CAFFEE, M., FINKEL, R.C., BRIMHALL, G. & MOTE, T. (2005): Remnants of a fossil alluvial fan landscape of Miocene age in the Atacama Desert of northern Chile using cosmogenic nuclide exposure age dating. – Earth and Planetary Science Letters, 237: 499-507.

NISHIIZUMI K., IMAMURA M., CAFFEE M.W., SOUTHON J.R., FINKEL R.C. & MCANINCH J. (2007): Absolute calibration of ^{10}Be AMS standards. – Nuclear Instruments & Methods in Physics Research B258: 403-413.

NISHIIZUMI K., KLEIN J., MIDDLETON R. & CRAIG H. (1990): Cosmogenic ^{10}Be, ^{26}Al and ^{3}He in olivine from Maui lavas. – Earth and Planetary Science Letters 98: 263-266.

NISHIIZUMI, K., KOHL, C.P., ARNOLD, J.R., KLEIN, J., FINK, D. & MIDDLETON, R. (1991): Cosmic-Ray Produced ^{10}Be and ^{26}Al in Antarctic Rocks - Exposure and Erosion History. – Earth and Planetary Science Letters, 104: 440-454.

NISHIIZUMI, K., KOHL, C.P., ARNOLD, J.R., KLEIN, J., DORN, R., FINK, D., MIDDLETON, R. & LAL, D. (1993): Role of in situ cosmogenic nuclides ^{10}Be and ^{26}Al in the study of diverse geomorphic processes. – Earth Surface Processes, 18: 407-425.

NISHIIZUMI, K., WINTERER, E.L., KOHL, J.R., KLEIN, J., MIDDLETON, R., LAL, D. & ARNOLD, J.R. (1989): Cosmic ray production rates of ^{10}Be and ^{26}Al in quartz from glacially polished rocks. – Journal of Geophysical Research, 94: 17907-17915.

PALUMBO, L., BENEDETTI, L., BOURLÈS, D., CINQUE, A. & FINKEL, R. (2004): Slip history of the Magnola fault (Apennines, Central Italy) from Cl-36 surface exposure dating: evidence for strong earthquakes over the Holocene. – Earth and Planetary Science Letters, 225: 163-176.

PERG, L.A., ANDERSON, R.S. & FINKEL, R.C. (2001): Use of a new ^{10}Be and ^{26}Al inventory method to date marine terraces, Santa Cruz, California, USA. – Geology, 29: 879-882.

PHILLIPS, F.M. (2003): Cosmogenic Cl-36 ages of Quaternary basalt flows in the Mojave Desert, California, USA. – Geomorphology, 53: 199-208.

PHILLIPS, F.M., AYARBE, J.P., HARRISON, J. B. J. & ELMORE, D. (2003): Dating rupture events on alluvial fault scarps using cosmogenic nuclides and scarp morphology. – Earth and Planetary Science Letters, 215: 203-218.

PHILLIPS, F.M., LEAVY, B.D., JANNIK, N.O., ELMORE, D. & KUBIK, P.W. (1986): The accumulation of cosmogenic chlorine-36 in rocks: A method for surface exposure dating. – Science, 231: 41-43.

PHILLIPS, F.M., STONE, W.D. & FABRYKA-MARTIN, J.T. (2001): An improved approach to calculating low-energy cosmic-ray neutron fluxes near the land/atmosphere interface. – Chemical Geology, 175: 689-701.

PHILLIPS, F.M., ZREDA, M., GOSSE, J.C., KLEIN, J., EVENSON, E.B., HALL, R.D., CHADWICK, O.A. & SHARMA, P. (1997): Cosmogenic ^{36}Cl and ^{10}Be ages of Quaternary glacial and fluvial deposits of the Wind River Range, Wyoming. – Geological Society of America Bulletin, 109: 1453-1463.

PHILLIPS, F.M., ZREDA, M.G., SMITH, S.S., ELMORE, D., KUBIK, P.W. & SHARMA, P. (1990): Cosmogenic chlorine-36 chronology for glacial deposits at Bloody Canyon, eastern Sierra-Nevada. – Science, 248: 1529-1532.

PHILLIPS, W.M., HALL, A.M., MOTTRAM, R., FIFIELD, L.K. & SUGDEN, D.E. (2006): Cosmogenic ^{10}Be and ^{26}Al exposure ages of tors and erratics, Cairngorm Mountains, Scotland: Timescales for the development of a classic landscape of selective linear glacial erosion. – Geomorphology, 73: 222-245.

PHILLIPS, W.M., MCDONALD, E.V., RENEAU, S.L. & POTHS, J. (1998): Dating soils and alluvium with cosmogenic ^{21}Ne depth profiles: Case studies from the Pajarito Plateau, New Mexico, USA. – Earth and Planetary Science Letters, 160: 209-223.

PIGATI, J. S. & LIFTON, N.A. (2004): Geomagnetic effects on time-integrated cosmogenic nuclide production with emphasis on in situ ^{14}C and ^{10}Be. – Earth and Planetary Science Letters, 226: 193-205.

POREDA, R.J. & CERLING, T.E. (1992): Cosmogenic neon in recent lavas from the Western United States. – Geophysical Research Letters, 18: 1863-1866.

PRAGER, C., IVY-OCHS, S., OSTERMANN, M., SYNAL, H.-A, & PATZELT, G. (2008): Geology and ra-

diometric ^{14}C-, ^{36}Cl- and Th-/U-dating of the Fernpass rockslide (Tyrol, Austria). – Geomorphology: in press.

Pratt-Sitaula, B., Burbank, D.W., Heimsath, A. & Ojha, T. (2004): Landscape disequilibrium on 1000-10,000 year scales Marsyandi River, Nepal, central Himalaya. – Geomorphology, 58: 233-241.

Putkonen J. & O'Neal M. (2006): Degradation of unconsolidated Quaternary landforms in the western North America. – Geomorphology, 75: 408-419.

Putkonen, J. & Swanson, T. (2003): Accuracy of cosmogenic ages for moraines. – Quaternary Research, 59: 255-261.

Raisbeck, G.M., Yiou, F., Fruneau, M. & Loiseaux, J.M. (1978): ^{10}Be Mass-Spectrometry with a Cyclotron. – Science, 202: 215-217.

Raisbeck, G.M., Yiou, F. & Stephan, C. (1979): ^{26}Al Measurement with a Cyclotron. – Journal de Physique Lettres, 40: L241-L244.

Repka, J.L., Anderson, R.S. & Finkel, R.C. (1997): Cosmogenic dating of fluvial terraces, Fremont River, Utah. – Earth and Planetary Science Letters, 152: 59-73.

Reusser, L.J., Bierman, P.R., Pavich, M.J., Zen, E.A., Larsen, J. & Finkel, R. (2004): Rapid late Pleistocene incision of Atlantic passive-margin river gorges. – Science, 305: 499-502.

Reuther, A.U., Herget, J., Ivy-Ochs, S., Borodavko, P., Kubik, P.W. & Heine, K. (2006a): Constraining the timing of the most recent cataclysmic flood event from ice-dammed lakes in the Russian Altai mountains, Siberia using cosmogenic in-situ ^{10}Be. – Geology, 34: 913-916.

Reuther, A.U., Ivy-Ochs, S. & Heine, K. (2006b): Application of surface exposure dating in glacial geomorphology and the interpretation of moraine ages. – Zeitschrift für Geomorphologie, Supplement 142: 335-359.

Ritz, J.F., Bourlès, D., Brown, E.T., Carretier, S., Chery, J., Enhtuvshin, B., Galsan, P., Finkel, R.C., Hanks, T.C., Kendrick, K.J., Philip, H., Raisbeck, G., Schlupp, A., Schwartz, D.P. & Yiou, F. (2003): Late Pleistocene to Holocene slip rates for the Gurvan Bulag thrust fault (Gobi-Altay, Mongolia) estimated with ^{10}Be dates. – Journal of Geophysical Research-Solid Earth, 108: B3, 2162, doi:10.1029/2001JB000553.

Ryerson, F.J., Tapponnier, P., Finkel, R.C., Mériaux, A.-S., van der Woerd, J., Lasserre, C., Chevalier, M.L., Xu, X.W., Li, H.B. & King, G.C.P. (2006): Application of morphochronology to the active tectonics of Tibet. – In: Siame, L.L., Bourles, D.L. & Brown, E.T. (eds.): In Situ–Produced Cosmogenic Nuclides and Quantification of Geological Processes, Geological Society of America Special Paper, 415: 61-86.

Schaefer, J.M., Denton, G.H., Barrell, D.J.A., Ivy-Ochs, S., Kubik, P.W., Andersen, B. G., Phillips, F.M., Lowell, T.V. & Schlüchter,Ch. (2006): Near-synchronous interhemispheric termination of the last glacial maximum in mid-latitudes. – Science, 312: 1510-1513.

Schäfer, J.M., Ivy-Ochs, S., Wieler, R., Leya, I., Baur, H., Denton, G.H. & Schlüchter, Ch. (1999): Cosmogenic noble gas studies in the oldest landscape on earth: surface exposure ages of the Dry Valleys, Antarctica. – Earth and Planetary Science Letters, 167: 215-226.

Schaller, M., Hovius, N., Willet, S.D., Ivy-Ochs, S., Synal, H.-A. & Chen, H.-C. (2005): Fluvial bedrock incision in the active mountain belt of Taiwan from in situ-produced cosmogenic nuclides. – Earth Surface Processes and Landforms, 30: 955-971.

Schaller, M., von Blanckenburg, F., Hovius, N. & Kubik, P.W. (2001): Large-scale erosion rates from in situ-produced cosmogenic nuclides in European river sediments. – Earth and Planetary Science Letters, 188: 441-458.

Schaller, M., von Blanckenburg, F., Veldkamp, A., Tebbens, L.A., Hovius, N. & Kubik, P.W. (2002): A 30000yr record of erosion rates from cosmogenic ^{10}Be in Middle Europe river terraces. – Earth and Planetary Science Letters, 204: 307-320.

Seidl, M.A., Finkel, R.C., Caffee, M.W., Hudson, G.B. & Dietrich, W.E. (1997): Cosmogenic isotope analysis applied to river longitudinal profile evolution: Problems and interpretations. – Earth Surface Processes and Landforms, 22: 195-209.

Sewell, R.J., Barrows, T.T., Campbell, S.D.G. & Fifield, L.K. (2006): Exposure dating (^{10}Be, ^{26}Al) of natural terrain landslides in Hong Kong, China. – In: Siame, L.L., Bourles, D.L. & Brown, E.T. (eds.): In Situ–Produced Cosmogenic Nuclides and Quantification of Geological Processes, Geological Society of America Special Paper, 415: 131-146.

Siame, L.L., Bourlès, D.L., Sebrier, M., Bellier, O., Castano, J.C., Araujo, M., Perez, M., Raisbeck, G.M. & Yiou, F. (1997): Cosmogenic dating ranging from 20 to 700ka of a series of alluvial fan surfaces affected by the El Tigre fault, Argentina. – Geology, 25: 975-978.

SMITH, J.A., FINKEL, R.C., FARBER, D.L., RODBELL, D.T. & SELTZER, G.O. (2005): Moraine preservation and boulder erosion in the tropical Andes: interpreting old surface exposure ages in glaciated valleys. – Journal of Quaternary Science, 20: 735-758.

SRINIVASAN, B. (1976): Barites - Anomalous xenon from spallation and neutron-induced reactions. – Earth and Planetary Science Letters, 31: 129-141.

STAIGER, J.K.W., GOSSE, J.C., JOHNSON, J.V., FASTOOK, J., GRAY, J.T., STOCKLI, D.F., STOCKLI, L. & FINKEL, R. (2005): Quaternary relief generation by polythermal glacier ice. – Earth Surface Processes and Landforms, 30: 1145-1159.

STAUDACHER, T. & ALLÈGRE, C. J. (1991): Cosmogenic neon in ultramafic nodules from Asia and in quartzite from Antarctica. - Earth and Planetary Science Letters, 106: 87-102.

STOCK, G.M., ANDERSON, R.S. & FINKEL, R.C. (2004): Pace of landscape evolution in the Sierra Nevada, California, revealed by cosmogenic dating of cave sediments. – Geology, 32: 193-196.

STONE, J.O. (2000): Air pressure and cosmogenic isotope production. – Journal of Geophysical Research, 105: 23753-23759.

STONE, J.O., ALLAN, G.L., FIFIELD, L.K. & CRESSWELL, R.G. (1996): Cosmogenic chlorine-36 from calcium spallation. – - Geochimica et Cosmochimica Acta, 60: 555-561.

STONE, J.O.H., EVANS, J.M., FIFIELD, L.K., ALLAN, G.L. & CRESSWELL, R.G. (1998): Cosmogenic chlorine-36 production in calcite by muons. – Geochimica et Cosmochimica Acta, 62: 433-454.

SUGDEN, D.E., BALCO, G., COWDERY, S.G., STONE, J.O. & SASS, L.C. (2005): Selective glacial erosion and weathering zones in the coastal mountains of Marie Byrd Land, Antarctica. – Geomorphology, 67: 317-334.

SUMMERFIELD, M.A., STUART, F.M., COCKBRUN, H.A.P., SUDGEN, D.E., DENTON, G.H., DUNAI, T. J. & MARCHANT, D. R. (1999): Long-term rates of denudation in the Dry Valleys, Transantarctic Mountains, southern Victoria Land, Antarctica based on in-situ-produced cosmogenic ^{21}Ne. – Geomorphology, 27: 113-129.

TRULL, T.W., KURZ, M.D. & JENKINS, W. J. (1991): Diffusion of cosmogenic ^{3}He in olivine and quartz: Implications for surface exposure dating. – Earth and Planetary Science Letters, 103: 241-256.

VAN DER WOERD, J., RYERSON, F.J., TAPPONNIER, P., GAUDEMER, Y., FINKEL, R., MÉRIAUX, A.-S., CAFFEE, M. & ZHAO GUOGUANG, H. (1998): Qunlu Holocene left-slip rate determined by cosmogenic surface dating on the Xidatan segment of the Kunlun fault (Qinghai, China). – Geology, 26: 695-698.

VAN HUSEN, D., IVY-OCHS, S. & ALFIMOV, V. (2007): Mechanism and age of late glacial landslides in the Calcareous Alps; The Almtal, Upper Austria. – Austrian Journal of Earth Science, 100: 114-126.

VERMEESCH, P. (2007): CosmoCalc: An Excel add-in for cosmogenic nuclide calculations. – Geochemistry Geophysics Geosystems, 8: Q08003, doi:10.1029/2006GC001530.

VON BLANCKENBURG, F. (2005): The control mechanisms of erosion and weathering at basin scale from cosmogenic nuclides in river sediment. – Earth and Planetary Science Letters, 242: 224-239.

VON BLANCKENBURG, F., BELSHAW, N.S. & O'NIONS, R.K. (1969): Separation of ^{9}Be and cosmogenic ^{10}Be from environmental materials and SIMS isotope dilution analysis. – Chemical Geology, 129: 93-99.

WARD, D.J., SPOTILA, J.A., HANCOCK, G.S. & GALBRAITH, J.M. (2005): New constraints on the late Cenozoic incision history of the New River, Virginia. – Geomorphology, 75: 54-72.

WILLIAMS, A J., STUART, F.M., DAY, S.J. & PHILLIPS, W.M. (2005): Using pyroxene microphenocrysts to determine cosmogenic ^{3}He concentrations in old volcanic rocks: an example of landscape development in central Gran Canaria. – Quaternary Science Reviews, 24: 211-222.

WOLKOWINSKY, A.J. & GRANGER, D.E. (2004): Early Pleistocene incision of the San Juan River, Utah, dated with ^{26}Al and ^{10}Be. – Geology, 32: 749-752.

YOKOYAMA, Y., CAFFEE, M.W., SOUTHON, J.R. & NISHIIZUMI, K. (2004): Measurements of in situ produced C-14 in terrestrial rocks. – Nuclear Instruments & Methods in Physics Research, B223-224: 253-258.

ZEHFUSS, P. H., BIERMAN, P. R., GILLESPIE, A. R., BURKE, R. M. & CAFFEE, M. W. (2001): Slip rates on the Fish Springs Fault, Owens Valley, California, deduced from cosmogenic ^{10}Be and ^{26}Al and soil development on fan surfaces. – Geological Society of America Bulletin, 113: 241-255.

ZREDA, M. (1994): Development and calibration of the ^{36}Cl surface expsoure dating method and its

application to the chronology of Late Quaternary glaciations. – PhD thesis. New Mexico Institute of Mining and Technology, Soccorro, USA.

Zreda, M. & Noller, J.S. (1998): Ages of prehistoric earthquakes revealed by cosmogenic chlorine-36 in a bedrock fault scarp at Hebgen Lake. – Science, 282: 1097-1099.

Zreda, M., Phillips, F.M., Kubik, P.W., Sharma, P. & Elmore, D. (1993): Cosmogenic ^{36}Cl dating of a young basaltic eruption complex, Lathrop Wells, Nevada. – Geology, 21: 57-60.

Zreda, M.G. & Phillips, F.M. (1995): Insights into alpine moraine development from cosmogenic ^{36}Cl buildup dating. – Geomorphology, 14: 149-156.

Zreda, M.G., Phillips, F.M. & Elmore, D. (1994): Cosmogenic ^{36}Cl accumulation in unstable landforms. 2. Simulations and measurements on eroding moraines. – Water Resources Research, 30: 3127-3136.

Eiszeitalter und Gegenwart Quaternary Science Journal	57/1–2	210–225	Hannover 2008

Sediment burial dating using terrestrial cosmogenic nuclides

Andreas Dehnert & Christian Schlüchter*)

Abstract: Burial dating using in situ produced terrestrial cosmogenic nuclides is a relatively new method to date sediments and quantify geomorphological processes such as erosion, accumulation and river incision. Burial dating utilises the decay of previously in situ produced cosmogenic nuclides and can be applied to sedimentary deposits such as cave fillings, alluvial fans, river terraces, delta deposits, and dunes. Using the established $^{10}Be/^{26}Al$ nuclide pair allows numerical dating of quartz bearing material from ~100 ka to 5 Ma, where other dateable material is often unavailable. To date, a number of studies have demonstrated the successful application of in situ produced cosmogenic nuclides in various scientific disciplines, such as Quaternary geology, geomorphology and palaeoanthropology. However, insufficiently defined physical properties such as nuclide half lives and complex depth dependent nuclide production rates result in relatively large uncertainties. Nevertheless, burial dating represents a promising method for determining numerical ages.

[Datierung des Überdeckungsalters mit Hilfe von terrestrischen kosmogenen Nukliden]

Kurzfassung: Die Methode der Bestimmung des Überdeckungsalters mit Hilfe von in situ produzierten terrestrischen kosmogenen Nukliden stellt ein verhältnismäßig neues Datierverfahren dar. Es ermöglicht die Altersbestimmung von Sedimenten und damit die Quantifizierung von geomorphologischen Prozessen, wie Erosion, Akkumulation und Flusseintiefung. Das Verfahren bedient sich dabei des Zerfalls von zuvor in situ produzierten kosmogenen Nukliden und kann auf sedimentäre Ablagerungen wie Höhlenfüllungen, Schwemmfächer, Flussterrassen, Deltaschüttungen und Dünen angewendet werden. Durch die Verwendung des erprobten $^{10}Be/^{26}Al$ Nuklidpaares erlaubt die Methode die Bestimmung eines numerischen Alters von quarzführendem Material über einen Zeitbereich von ~100 ka bis 5 Ma. In diesem Zeitabschnitt ist datierfähiges Material für andere Methoden oftmals nicht oder nur unzureichend vorhanden. Viele Studien konnten bereits die erfolgreiche Anwendung von in situ produzierten kosmogenen Nukliden in den verschiedensten wissenschaftlichen Bereichen, darunter zum Beispiel in der (Quartär)Geologie, Geomorphologie und Paläoanthropologie, belegen. Dennoch können die zur Zeit nur ungenügend genau bestimmten physikalischen Größen, wie zum Beispiel die Nuklidhalbwertszeiten oder die tiefenabhängigen Nuklidproduktionsraten zu vergleichsweise großen Unsicherheiten führen. Trotz dieser Nachteile stellt die Methode eine vielversprechende Möglichkeit der numerischen Altersbestimmung dar.

Keywords: cosmogenic nuclides, burial dating, numerical age determination, sediment, geochronology

*Addresses of authors: A. Dehnert, C. Schlüchter, Institut für Geologie, Universität Bern, Baltzerstrasse 1+3, 3012 Bern, Switzerland. E-Mail: andreas.dehnert@geo.unibe.ch

1 Introduction

Sedimentary archives, for example marine, terrestrial and glacial deposits, provide information regarding the climatic and environmental history as well as the tectonic development of a given area. In this context, the youngest part of the Earth' history, the Neogene and the Quaternary, are of particular interest. This time have been characterised by massive mountain forming processes, large changes in the temperature of oceans and the atmosphere as well as by important biological evolution, particularly with the appearance of early and modern hominids (Asfaw et al. 1999; Clark et al. 2003; Dèzes et al. 2004; Ravelo et al. 2004; Gibbard et al. 2005). All this information, however, is only of minor value if it can not be integrated into a global chronological framework. Only with reliable dating can such comparisons be made and the dating of sediments of the past million years is, therefore, one of the most important tasks in modern Quaternary research.

Dating of terrestrial sediments over long time periods, however, can often be highly complex, imprecise or even impossible. Available methods, for example radiocarbon and luminescence dating, cover up to 50 ka and a few 100 ka, respectively, only a relatively short part of the Quaternary (Preusser et al. 2008, Hajdas 2008). We are presenting here a brief summary on recent developments in using terrestrial cosmogenic nuclides for dating the burial age of sediments. Burial dating is based on the assumption that rocks that have been exposed to cosmic radiation for a given time are enriched with various cosmogenic radionuclides (Fig. 1). When these rocks, or their erosional products, are shielded from cosmic radiation, nuclide production ceases and the radionuclides decay according to their individual half lives (Fig. 2). Shielding may be due to transportation of sediment into a cave, by covering with overburden or by deposition in a deep water body (Fig. 3). By measuring the concentration of two nuclides (at least one radionuclide), it is possible to date the time elapsed since shielding.

Cosmogenic nuclides are produced by nuclear reactions in the Earth's atmosphere as well as in the upper parts of the Earth's crust. These nuclear reactions are initiated by high energy secondary cosmic radiation (Lal & Peters 1967). The development of accelerator mass spectrometry (AMS) over the past few decades has enabled the detection of very small amounts of cosmogenic nuclides (Finkel & Suter 1993) and is fundamental to the effective use of cosmogenic nuclides in modern geosciences.

The radionuclides ^{10}Be and ^{26}Al are good candidates for burial dating: both are produced in situ in quartz and possess relatively long half lives. Quartz is one of the most common minerals in the Earth's crust and so is present in almost all sedimentary deposits. The long half lives of both radionuclides enable dating over a time period of 5 Ma and, in addition to this, the nuclide production ratio has been quantified and is independent of latitude, altitude, depth below surface and time (Gosse & Phillips 2001). For these reasons, the method of burial dating is independent of production rate changes in time and space (Lal & Arnold 1985; Klein et al. 1986; Lal 1991), which causes most of the inaccuracies in surface exposure dating (Gosse & Phillips 2001; Ivy-Ochs & Kober 2008).

The principle of burial dating was proposed by Lal & Arnold (1985) and underwent a major revision by Lal (1991). The first application of burial dating published (Klein et al. 1986) was able to show, with the analysis of the ^{26}Al/^{10}Be-ratio, that the Libyan Desert Glass Field was occasionally covered by shifting sand dunes, although it was not possible at this time to give discrete burial ages for the sampled glass. Granger et al. (1997) were the first to date a deposition event by using the ^{26}Al/^{10}Be-ratio. They determined river down-cutting rates for the past 1.5 Ma using relocated sediments from cave fillings. Since these first applications a few studies have demonstrated the successful application of burial dating. In addition to the more application focused studies, reviews by Granger & Muzikar (2001) and more recently by Granger (2006) provide the basic knowledge needed for age calculations in various burial scenarios.

As already mentioned, the method of burial dating with cosmogenic nuclides is based on the decay of radionuclides. This requires dependable accuracy in half life determination and precision of the nuclide measurement itself. The half life of ^{26}Al of 0.702 ± 0.056 Ma (MIDDLETON et al. 1983), 0.705 ± 0.024 Ma (NORRIS et al. 1983), or 0.716 ± 0.032 Ma (RIGHTMIRE et al. 1958) is well defined and widely accepted in the cosmogenic nuclide community. However, the traditionally recognised half life of ^{10}Be of 1.51 ± 0.06 Ma (HOFMANN et al. 1987) is still undergoing discussion. Some authors (e.g. PARTRIDGE et al. 2003; HÄUSELMANN & GRANGER 2005; GRANGER et al. 2006) believe that this figure is too high and suggest a shorter ^{10}Be half life of ~1.34 Ma (MIDDLETON et al. 1993). NISHIIZUMI et al. (2007) support this, having recently re-evaluated the commonly used ICN (ICN Chemical & Radioisotope Division) and NIST (National Institute of Standards and Technology) reference material, suggesting that the ^{10}Be half life should be lowered to 1.36 ± 0.07 Ma. On the other hand, FINK & SMITH (2007) also re-evaluated the same material but hesitated to lower the ^{10}Be half life, stating that the direct and accurate specific activity measurement of the parent solution of both standards is needed to calculate the ^{10}Be half life, but this is not yet available.

2 In situ production of cosmogenic ^{10}Be and ^{26}Al

The Earth's atmosphere is undergoing permanent bombardment by primary cosmic radiation. This high energy nucleon radiation originates mainly in the Milky Way (with $E \approx 1 - 10^{10}$ GeV), with a much smaller fraction descended from beyond our galaxy ($E < 10^{20}$ eV) (GOSSE & PHILLIPS

Table 1: Constants for production rate and burial age calculations with in situ produced ^{10}Be and ^{26}Al extracted from quartz minerals. SLHL = sea level, high latitude (> 60°)

Tab. 1: Zusammenstellung der Konstanten für die Produktionsraten- und Altersbestimmung mit in situ produziertem ^{10}Be und ^{26}Al aus Quarz. SLHL (sea level, high latitude) = Meeresspiegel, hohe Breiten (> 60°)

Constant	^{10}Be	^{26}Al	reference
half life $t_{1/2}$ (Ma)	1.36 ± 0.07 * 1.51 ± 0.06 ^	0.705 ± 0.024 #	* NISHIIZUMI et al. (2007) ^ HOFMANN et al. (1987) # NORRIS et al. (1983)
total surface production rate $_{SLHL}P$ at SLHL (atoms g^{-1} a^{-1})	5.1 ± 0.3	31.1 ± 1.9	STONE (2000)
negative muonic surface production rate $_{SLHL}P_{1\mu-}$ at SLHL (atoms g^{-1} a^{-1})	0.096	0.723	GRANGER & SMITH (2000)
negative muonic surface production rate $_{SLHL}P_{2\mu-}$ at SLHL (atoms g^{-1} a^{-1})	0.021	0.156	GRANGER & SMITH (2000)
fast muonic surface production rate $_{SLHL}P_{\mu+}$ at SLHL (atoms g^{-1} a^{-1})	0.026	0.192	GRANGER & SMITH (2000)
nucleonic surface production rate $_{SLHL}P_N$ at SLHL (atoms g^{-1} a^{-1})	4.957	30.029	with $P=P_N+P_{1\mu-}+P_{2\mu-}+P_{\mu+}$
nucleon attenuation length Λ_N (g cm^{-2})	160 ± 10		GRANGER & SMITH (2000)
negative muon attenuation length $\Lambda_{1\mu-}$ (g cm^{-2})	738.6		GRANGER & SMITH (2000)
negative muon attenuation length $\Lambda_{2\mu-}$ (g cm^{-2})	2688		GRANGER & SMITH (2000)
fast muon attenuation length $\Lambda_{\mu+}$ (g cm^{-2})	4360		GRANGER & SMITH (2000)

2001). Interactions of incoming primary radiation with atoms of the Earth's atmosphere result in low-energy particles, traditionally known as "secondary cosmic radiation" (E ≈ 100 MeV). For the in situ production of ^{10}Be and ^{26}Al, both at the rock surface and subsurface level, there are two kinds of relevant particles: nucleons (neutrons and protons) and muons (fast and negative). According to strict nomenclature rules, muons belong to tertiary cosmic radiation, as they are a byproduct of decaying secondary cosmic radiation pions (π mesons) (Gosse & Phillips 2001). Cosmogenic ^{10}Be and ^{26}Al are generated in quartz (^{16}O as the main target for ^{10}Be and ^{28}Si transforms to ^{26}Al) by spallation reactions (neutrons), negative muon capture, and a cascade of reactions called Coulomb-reactions (fast muons). These processes are explained in detail in Lal & Peters (1967) and Gosse & Phillips (2001), among others. Nuclide production in near surface material is dominated by nucleons (~97.5 %)(Heisinger 1998) and changes with increasing depth, as muons display greater penetration depth as a result of their lower reactivity.
The nucleonic production as a function of depth can be shown as a simple exponential law (Lal 1991; Brown et al. 1992; Gosse & Phillips 2001):

$$P_{10N}(z) = P_{10N}(0)e^{-\rho z/\Lambda_N} \quad [1]$$

$$P_{26N}(z) = P_{26N}(0)e^{-\rho z/\Lambda_N} \quad [2]$$

with production rate in depth in atoms g^{-1} a^{-1} (P(z)), scaled surface production rate in atoms g^{-1} a^{-1} (P(0)), depth in cm (z), attenuation length in g cm^{-2} (Λ) and density of the overburden in g cm^{-3} (ρ). The index of 10 and 26 represents the nuclides ^{10}Be and ^{26}Al, respectively, and N nucleonic production. Constants for all equations are listed in Tab. 1.
The nuclide production by muons is valid within a depth range of 200 – 5000 g cm^{-2} and is well described by the sum of three exponential functions (Granger & Smith 2000). At shallower depths nuclide production by muons is negligible, as nucleonic production is predominant. Nuclide production by negative muon capture is described in the first two terms. The last one represents production by Coulomb-reactions (Granger & Smith 2000; Granger & Muzikar 2001):

$$P_{10\mu}(z) = P_{10/1\mu-}(0)e^{-\rho z/\Lambda_{1\mu-}} + P_{10/2\mu-}(0)e^{-\rho z/\Lambda_{2\mu-}} + P_{10\mu+}(0)e^{-\rho z/\Lambda_{\mu+}} \quad [3]$$

$$P_{26\mu}(0) = P_{26/1\mu-}(0)e^{-\rho z/\Lambda_{1\mu-}} + P_{26/2\mu-}(0)e^{-\rho z/\Lambda_{2\mu-}} + P_{26\mu+}(0)e^{-\rho z/\Lambda_{\mu+}} \quad [4]$$

The index μ represents muonic production, + and – show fast and negative muons respectively.
The scaled surface production rate, sometimes called local production rate, is dependent on altitude above sea level and latitude, due to the effects of the Earth's magnetic field on the se-

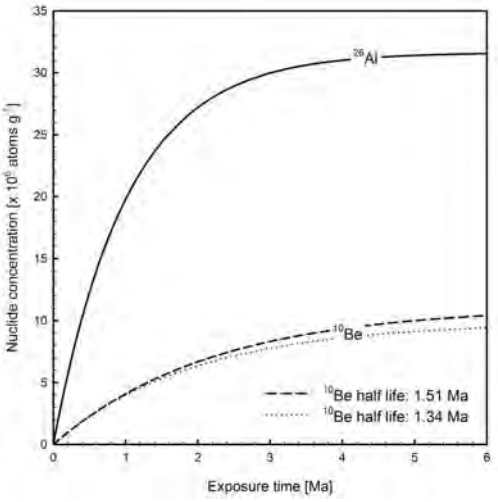

Fig. 1: Increasing nuclide concentration of ^{10}Be and ^{26}Al in quartz over time. Plotted for the ideal case for exposure at SLHL with unshielded flat surface and no erosion. Used parameters are listed in Tab. 1.

Abb. 1: Darstellung der Konzentrationsentwicklung der Nuklide ^{10}Be und ^{26}Al für den Fall der Bestrahlung unter SLHL Bedingungen einer nicht erodierenden, nicht abgeschirmten, ebenen, Quarzoberfläche. Zu Grunde liegende Parameter können Tab. 1 entnommen werden.

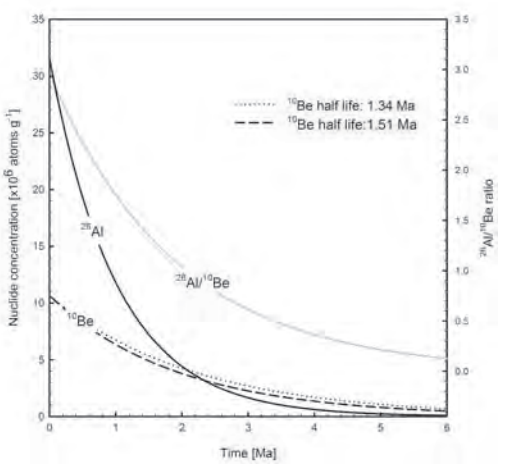

Fig. 2: Decreasing $^{26}Al/^{10}Be$ ratio (in gray) and individual nuclide concentration of ^{10}Be (dashed and dotted) and ^{26}Al (solid) in quartz over time with complete shielding from cosmic radiation after reaching individual saturation. Used parameters are listed in Tab. 1.

Abb. 2: Darstellung der Abnahme des $^{26}Al/^{10}Be$ Verhältnisses (in grau) sowie der Nuklidkonzentration von ^{10}Be (gestrichelt und gepunktet) und ^{26}Al (durchgezogen) in Quarz bei vollständiger Abschirmung der kosmischen Strahlung. Ausgangskonzentrationen entsprechen vollständiger Sättigung. Zu Grunde liegende Parameter können Tab. 1 entnommen werden.

condary cosmic rays and the attenuation effect of the atmosphere itself. Its value and scaling for the sampling position is also under debate at the moment, and is discussed in more detail in LAL (1991), DUNAI (2000), STONE (2000), WAGNER et al. (2000), DESILETS & ZREDA (2001), and references therein.

The nuclides ^{10}Be and ^{26}Al are also produced in situ by non-cosmogenic such as radiogenic reactions. SHARMA & MIDDLETON (1989) stated that only α-induced nuclear reactions could provide a significant portion of ^{10}Be and ^{26}Al. Lithium as target nuclei for production of ^{10}Be ($^{7}Li(\alpha,p)^{10}Be$) is normally present at trace levels (μg g^{-1}) but sodium, as a source of ^{26}Al ($^{23}Na(\alpha,p)^{26}Al$), is nearly always present at concentrations of one or more percent. Hence, ^{10}Be production is quite small compared to the cosmogenic compound and therefore negligible, while that of ^{26}Al may be significant. BROWN et al. (1991), however, argued that the steady-state concentrations of radiogenically produced ^{26}Al in average sandstones is ~6.0 x10^4 at g^{-1}. This low concentration, with respect to steady-state concentrations of cosmogenically produced ^{26}Al of ~3.2 x10^7 at g^{-1} (Fig. 1 & 2), will only be significant in samples with a "short" exposure history. Beside this, no relevant radiogenic ^{26}Al contamination in quartz has ever been observed and reported so far.

3 Application of burial dating

The following chapter looks at different kinds of burial situation and is designed to give an overview of the required formulas, followed by selected examples. For more detailed information see GRANGER & SMITH (2000) and GRANGER & MUZIKAR (2001).

3.1 Single stage exposure history – cave sediments

The simplest case of burial is provided by cave sediments (Fig. 4), in that shielding from cosmic rays occurs quickly and effectively to inwashed sediments. The great advantage of these deposits is that they remain almost unaffected by cosmic radiation and thus only negligible post burial production results. Assuming steady-state erosion conditions for the sediments, the burial age is directly dependent on nuclide half-lives. Thus today's $^{26}Al/^{10}Be$ ratio gives us the burial age (t in years) solving equation 5 and 6 for ^{10}Be and ^{26}Al.

$$N_{10}(t) = \frac{P_{10}}{1/\tau_{10} + \rho\varepsilon/\Lambda} e^{-t/\tau_{10}} \qquad [5]$$

$$N_{26}(t) = \frac{P_{26}}{1/\tau_{26} + \rho\varepsilon/\Lambda} e^{-t/\tau_{26}} \qquad [6]$$

Equation 5 and 6 can be combined to equation 7

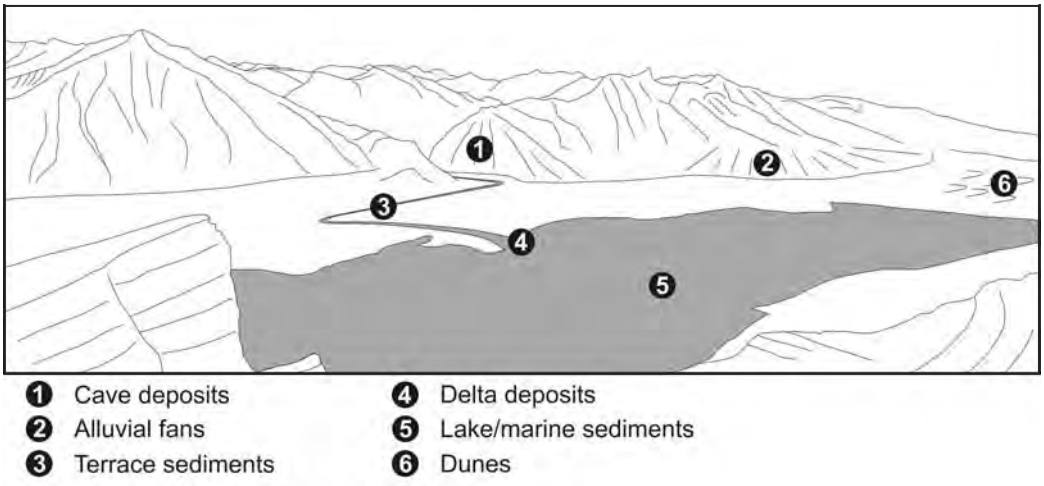

Fig. 3: Overview sketch of potential dateable sedimentary deposits with the cosmogenic burial dating technique. Quick shielding from cosmic radiation is achieved by washing into deep underground (1), covering with sediment (2, 3, 4, 6) or water (4, 5).

Abb. 3: Übersichtsdarstellung der potenziellen geologischen Archive, welche mit Hilfe des burial dating Verfahrens datiert werden können. Die notwendige rasche Abschirmung der kosmischen Strahlung kann erreicht werden durch Umlagerung in den tieferen Untergrund (1), Überdeckung durch Sediment (2, 3, 4, 6) oder Wasser (4, 5).

$$\frac{N_{26}(t)}{N_{10}(t)} = \frac{P_{26}}{P_{10}^{\tau_{10}/\tau_{26}}}\left(1/\tau_{10} + \rho\varepsilon/\Lambda\right)^{\tau_{10}/\tau_{26}}$$

$$\left(1/\tau_{26} + \rho\varepsilon/\Lambda\right)^{-1}\left(N_{10}(t)\right)^{\tau_{26}/\tau_{10}-\tau_{10}\tau_{26}} \qquad [7]$$

Granger et al. (1997) were the first to use the ^{26}Al-^{10}Be pair to date burial events of sediments. They dated quartz pebbles found in various caves within dolomites along the New River, between Eggleston and Pearisburg, Virginia, USA. The pebbles, quartz vein remnants of metamorphic host rocks in New River's headwaters, were sampled in numerous cave levels up to 35 m above the modern river. By dating the inwash events of these pebbles from 0.29 ± 0.18 Ma to 1.47 ± 0.22 Ma, Granger et al. (1997) were able to calculate river incisions rates for the New River of 30.2 ± 5.5 m Ma^{-1} at Pearisburg and 19.7 ± 3.2 m Ma^{-1} at Eggleston, with a mean rate of 27.3 ± 4.5 m Ma^{-1}.

Granger et al. (2001) conducted similar studies at the Mammoth Cave multi level system in Kentucky, USA. By analysing the ^{26}Al/^{10}Be ratio of 29 quartz gravel and sand deposits throughout the cave system and from its surface, they were able to reconstruct a water table history for the nearby Green and Ohio Rivers over the past 3.5 Ma. Furthermore, they demonstrated a glacial influence on the Ohio River behaviour with increasing incision (~1.5 Ma and ~1.2 Ma) followed by aggradation (0.7 – 0.8 Ma).

More recently, Haeuselmann et al. (2007) looked at glacially accelerated valley incision. Cave infill sediments were used to identify accelerated incision rates (up to 1.2 km Ma^{-1}) in the River Aare valley, between 0.8 to 1.0 Ma, in the Siebenhengste-Hohgant cave system, Switzerland.

Archaeological, as well as geological, questions can be solved using burial dating with ^{10}Be and ^{26}Al (see also Akçar et al. 2008). Dating of embedded bones is mostly done using U/Th dating of surrounding calcite layers (Pickering et al. 2007). In the absence of speleothems or with unsuitable U/Th con-

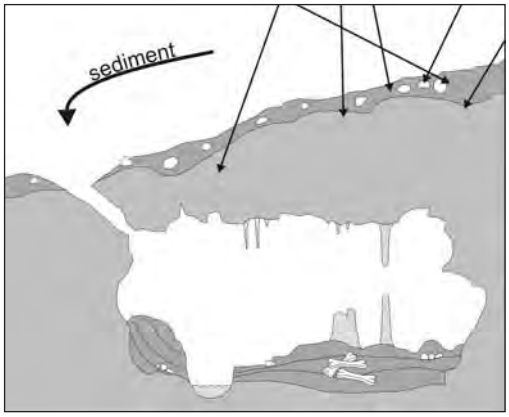

Fig. 4: Cave scenario: Exposed quartz-containing sediment or soil gets complete shielded by washing into a deep cave. Embedded fossils or artefacts can be dated by detecting the $^{26}Al/^{10}Be$ ratio of the surrounding sediment.

Abb. 4: Höhlenszenario: Bestrahltes(r) quarzführendes(r) Sediment oder Boden wird in eine Höhle umgelagert und hierdurch vollständig von der kosmischen Strahlung abgeschirmt. Die Altersbestimmung von eingebetteten Fossilien oder Artefakten kann dann durch die Bestimmung des $^{26}Al/^{10}Be$ Verhältnisses des umgebenen, zuvor eingespülten Materials erfolgen.

ditions, dating can also be done with the help of inwash sediments containing quartz. Lower Pliocene hominid remains form Sterkfontein cave, South Africa were dated indirectly by burial dating of the surrounding sediment by PARTRIDGE et al. (2003). The fossils are encased in a breccia of dolomite, chert and surface soil that accumulated as debris dropped into the cave. PARTRIDGE et al. (2003) utilised this fact to obtain burial ages from the quartz bearing material. Palaeomagnetic signals in calcitic flowstones dated the sediment layer containing hominid fossils into a timeframe ranging from 3.22 to 3.58 Ma. PARTRIDGE et al. (2003) dated this layer using the $^{26}Al/^{10}Be$ ratio to 4.17 ± 0.14 Ma in the Silberberg Grotto and the previously undated fossil layer in Jacovec Cavern to 4.02 ± 0.27 Ma. Although, these burial ages are in good agreement they are currently under debate (see WALKER et al. 2006).

3.2 Multiple stage exposure history – Nuclide profiling

Post burial nuclide production can not be ignored where sediment has only few metres of overburden, as can be done in the cave scenario described above. The post burial production is depth- and time-dependent (see chapter 2) and thus the relevant equations for both nuclides become:

$$N_{10}(z,t) = N_{10/inh}e^{-t/\tau_{10}} + \int_0^t \left[P_{10N}(z+\rho\varepsilon t') + P_{10\mu}(z+\rho\varepsilon t')\right]e^{-t'/\tau_{10}}\partial t' \quad [8]$$

$$N_{26}(z,t) = N_{26/inh}e^{-t/\tau_{26}} + \int_0^t \left[P_{26N}(z+\rho\varepsilon t') + P_{26\mu}(z+\rho\varepsilon t')\right]e^{-t'/\tau_{26}}\partial t' \quad [9]$$

Following GRANGER & SMITH (2000) the above integrals can be expressed as equation 10:

$$\begin{aligned} N_i(z,t) &= N_{i/inh}e^{-t/\tau_i} \\ &+ \left[P_{iN}e^{-\rho z/\Lambda_N}\Big/\left(1/\tau_i + \rho\varepsilon/\Lambda_N\right)\right]\left[1-e^{-t(1/\tau_i+\rho\varepsilon/\Lambda_N)}\right] \\ &+ \left[P_{i/1\mu-}e^{-\rho z/\Lambda_{1\mu-}}\Big/\left(1/\tau_i + \rho\varepsilon/\Lambda_{1\mu-}\right)\right]\left[1-e^{-t(1/\tau_i+\rho\varepsilon/\Lambda_{1\mu-})}\right] \\ &+ \left[P_{i/2\mu-}e^{-\rho z/\Lambda_{2\mu-}}\Big/\left(1/\tau_i + \rho\varepsilon/\Lambda_{2\mu-}\right)\right]\left[1-e^{-t(1/\tau_i+\rho\varepsilon/\Lambda_{2\mu-})}\right] \\ &+ \left[P_{i\mu+}e^{-\rho z/\Lambda_{\mu+}}\Big/\left(1/\tau_i + \rho\varepsilon/\Lambda_{\mu+}\right)\right]\left[1-e^{-t(1/\tau_i+\rho\varepsilon/\Lambda_{\mu+})}\right] \end{aligned} \quad [10]$$

The index i represents either the nuclide ^{10}Be or ^{26}Al. Each of equation 8 and 9 contains three unknowns (burial age, inherited nuclide concentration and erosion rate). Thus, a combination of [8] and [9] can not be solved uniquely by only analysing ^{10}Be and ^{26}Al in one sample at a specific depth. The solution for this problem lies in sampling a vertical profile within the deposit. By analysing two samples from the same profile and considering suitable constraints for the inherited nuclide concentration [8] and [9] can be solved uniquely. These assumptions are site-specific and may comprise of, for example, a constant inherited nuclide concentration

across the profile or a known inherited $^{26}Al/^{10}Be$ ratio. The model solutions from [8] and [9] need to be fitted to the field observations (measured nuclide concentrations). This can be done by least squares regression or other suitable optimisation techniques. Collecting more than two samples overconstrains the model solution, resulting in reduced random errors and yields a more robust detection of systematic deviations.

The first use of nuclide profiling to obtain sediment burial ages was done by Granger & Smith (2000). They measured the ^{10}Be and ^{26}Al concentrations of nine samples in a ~10 m profile of a river terrace of Old Kentucky River at Rice Station, Kentucky, USA. The sandy sediment was rapidly deposited, perhaps at the shores of a rising proglacial lake, and has remained exposed since deposition. By solving an equation similar to [8] and [9] and least-square-fitting of the solutions, they dated the terrace formation to $1.50\ ^{+0.32}/_{-0.25}$ Ma with a post-depositional terrace erosion rate of 6.2 ± 0.2 m Ma^{-1}. This is in good agreement with the nearby Green River incision around 1.5 Ma (Granger et al. 2001, see above).

This initial study was followed by dating of alluvial deposits above the San Juan River near Bluff and Mexican Hat, Utah, USA by Wolkowinsky & Granger (2004). Their cosmogenic ^{10}Be and ^{26}Al data suggest a deposition age of $1.36\ ^{+0.20}/_{-0.15}$ Ma and an erosion rate of 14 ± 4 m Ma^{-1} for the ~12 m thick Bluff site. Additional to t and ε, they allowed a fit within the model for bulk density and the addition of, at most, 20 cm material on top of the sampled profile. They were not able to realise dates for the Mexican Hat site due to insufficient burial depth of only 5.5 m following Granger & Muzikar (2001).

The more recent work of Häuselmann et al. (2007) utilises the nuclide profiling technique

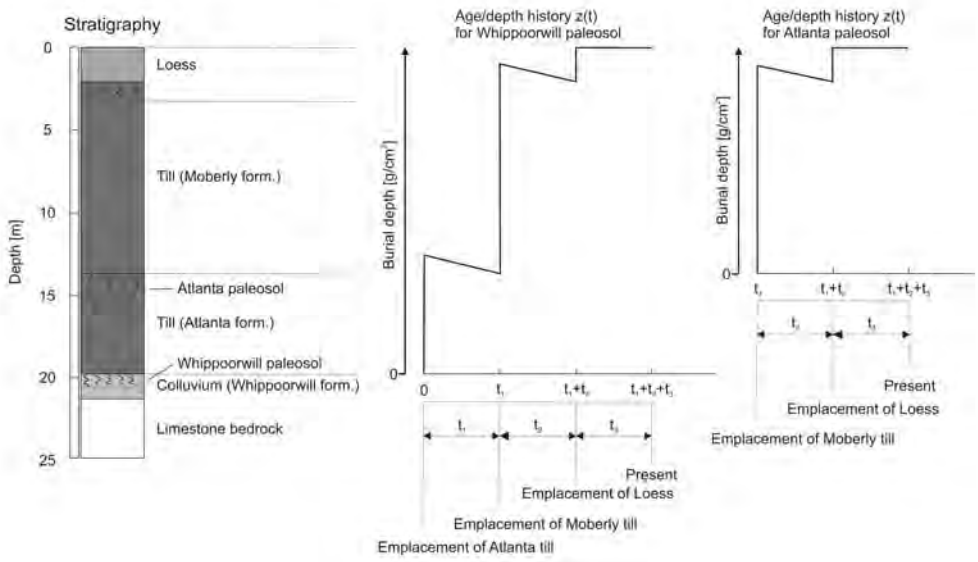

Fig. 5: Overview of the Musgrove section, Missouri, USA. Left part shows idealised stratigraphic sketch with used stratigraphic units. Right part visualise the used three-step density build-up model with rapid burial followed by moderate surface erosion. Modified after Balco et al. (2005).

Abb. 5: Schematische Darstellung des Musgrove Profils, Missouri, USA. Links: vereinfachtes stratigraphisches Profil mit Tiefenangaben. Rechts: Veranschaulichung der Entwicklung der Überlagerungsmächtigkeiten im angewendeten dreiphasigen Modell mit rascher Überdeckung und anschließender gemäßigter Oberflächenerosion. Verändert nach Balco et al. (2005).

to date glacially related gravel successions in the Bavarian foreland of the Alps, Germany, at an abandoned gravel quarry near Bad Grönenbach, and in a second site, Böhener Feld. Both sites are made up of a mixture of limestone and quartz gravels in a carbonate matrix. The pioneer work on alpine Quaternary geology by PENCK & BRÜCKNER (1909) named these gravels "Deckenschotter" (cover gravels) and placed them within the classical Mindelian (Bad Grönbach) and the Günzian (Böhner Feld) glaciation, respectively. The age and terrace erosion rate determination of HÄUSELMANN et al. (2007) follows the nuclide profiling approach of GRANGER & SMITH (2000), as described above, followed by a χ^2 minimisation. This resulted in a fitted burial age of $0.68\ ^{+0.23}/_{-0.24}$ Ma and a terrace erosion rate of $123\ ^{+139}/_{-32}$ m Ma^{-1} at Bad Grönenbach, and $2.35\ ^{+1.08}/_{-0.88}$ Ma and an erosion rate of $18\ ^{+10}/_{-4}$ m Ma^{-1} for the section at Böhener Feld. This work was the first attempt to absolutely date these gravel deposits and demonstrates the suitability of the burial dating approach using ^{10}Be and ^{26}Al within the time span of the Quaternary, although relatively high measuring uncertainties, due to the abundance of common Al impurities in the processed quartz, result in large model uncertainties and subsequently in large errors. This work also demonstrated that sample preparation and nuclide measurements are still delicate tasks.

The three examples described above, can explain the build-up of terraces in a single depositional event, which may occur over hundreds or even thousands of years. Cosmogenic burial dating of more complex deposit evolution is also possible, as long as a well constrained stratigraphy is available. In such a sedimentary sequence, each package will have its own deposition age and burial history that is determined by the deposition age of the following layer. BALCO et al. (2005) describe the age determination of such a multiple package set-up. They dated a profile containing three palaeosols buried beneath Laurentide Ice Sheet sediments and a loess cover. At the Musgrove clay pit, Missouri, USA, two tills, the Atlanta and Moberly formations, overlie deeply weathered bedrock, as well as locally derived colluvium of the Whippoorwill formation (Fig. 5). BALCO et al. (2005) developed a three step burial history for the Musgrove section with rapid burial and moderate surface erosion (Fig. 5). Using Monte Carlo simulations in MATLAB's Optimization Toolbox enables minimisation of χ^2 discrepancies between model and measurements. In doing so, they determine a burial age of 2.41 ± 0.14 Ma for the lower till section (Atlanta formation) and, one between 1.6 – 1.8 Ma for the upper till (Moberly formation).

It should be noted, however, that it was necessary to assume some initial conditions in order to complete this well-developed model. BALCO et al. (2005) chose an age of 125 ka for the deposition of the covering loess layer based on regional stratigraphy (identified by t_3 in Fig. 5). This assumption consequently affects all other age calculations in the used stepwise model (age of Atlanta till = $t_1 + t_2 + t_3$). This approach is, therefore, not an independent age determination as is normally assumed with the burial dating method, although it should be noted that a stratigraphical age of 125 ka for the loess is convincing and that BALCO et al. (2005) subsequently correlated the age of 2.41 Ma with a (global) ice sheet build up from 2.7 to 2.4 Ma, as suggested by marine oxygen isotope data (JOYCE et al. 1993).

3.3 Complex sediment burial histories

The history of sediments in the natural environment is often highly complex. The material undergoes several kinds of transportation usually involving multiple stages of exposure and burial from its source until its modern day position. It is often impossible to describe the complete transportation history with confidence.

In these situations the in situ cosmogenic nuclides ^{10}Be and ^{26}Al may provide useful information regarding, whether sediment has been buried or not. In some cases it is possible to evaluate cumulative burial and exposure durations.

The first use of the ^{10}Be/^{26}Al ratio was done by KLEIN et al. (1986). They looked at 12 Libyan

Dessert Glass samples, subdivided into three groups. Fission-track dating placed the age at 28.5 Ma, but in situ cosmogenic ^{10}Be and ^{26}Al concentrations did not agree with this estimate. Klein et al. (1986) attempted to solve this discrepancy with regard to the history of the Libyan Dessert Glass and the distribution of nuclide concentrations within the individual groups. By analysing the ratio of ^{10}Be and ^{26}Al they could clearly show that burial by sand dunes is the most plausible explanation for the obtained nuclide concentrations. Furthermore they presented the first (minimum) burial ages based on the simplification of a single exposure followed by a single burial. The article of Klein et al. (1986) marks the advent of "burial dating with in situ produced cosmogenic nuclides".

A second interesting application of the ^{10}Be/^{26}Al ratio in the early stage of burial dating development is documented by Albrecht et al. (1993), working on volcanic ash-flow tuffs at the Pajarito plateau of the Valles caldera, New Mexico, USA. These surfaces are part of the Tshirege member of the Bandelier Tuff, which was deposited during a caldera eruption at ~1.14 Ma. The Tshirege member can be subdivided into four subunits, each with its own erosive character. The analysis of nuclide concentrations of ^{10}Be and ^{26}Al identified two to five times lower concentrations than a 1.14 Ma exposure history should yield, which was mainly due to erosion and previous burial of the investigated surfaces. Albrecht et al. (1993) suggested a burial period of 0.6 ± 0.3 Ma for most of the studied samples by using the ^{26}Al/^{10}Be ratio. The former shielding of the sampled surface is explained by an eroded tuff and soil cover consisting of the overlaying subunits of the Tshirege member with an average thickness of ~6 m.

Burial by overlaying sediment is not the only explanation for a complex burial history. The shielding material does not necessarily have to be rock or sediment to result in the attenuation of secondary cosmic ray particle energy, which is dependent on the density of the overburden material. Thus any matter may shield cosmic radiation, with rock causing the most effective attenuation followed in order by sediment, water and glacial ice (Fig. 6).

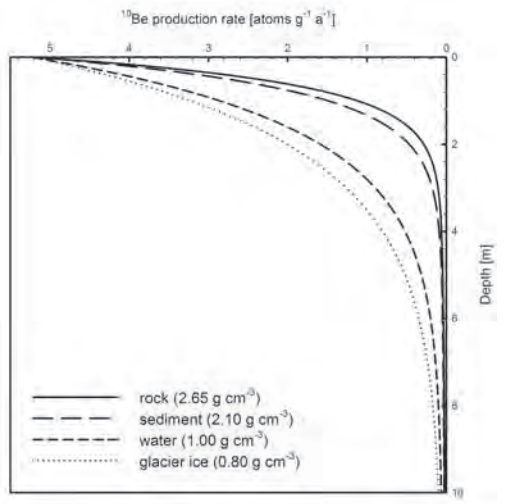

Fig. 6: Illustration of decreasing ^{10}Be production rate (at SLHL) caused by increasing shielding for typical geological overburdens with average densities at various depths. "Hard" overburdens such as rock or sediment obtain shielding rates of 90% in depth of ~1.8 m, while "soft" materials such as water or glacial ice need to be of ~4.5 m in thickness.

Abb. 6: Darstellung der ^{10}Be Produktionsratenabnahme bei zunehmender Überdeckung und damit steigender Abschirmung der kosmischen Strahlung (gültig für SLHL-Bedingungen).
Gezeigt sind ausgewählte geologisch typische Deckschichten mit ihren mittleren Dichten. „Harte" Deckschichten wie Gestein oder Sediment erreichen Abschirmungsraten von 90% bereits in Tiefen von ~1,8 m, während „weiche" Materialien, wie Wasser oder Eis, eine Mächtigkeit von ~4,5 m aufweisen müssen um die gleiche Abschirmung zu erreichen.

Any shielding history is clearly shown by the position of the sample on a two-isotope diagram, for example ^{26}Al/^{10}Be ratios vs. ^{10}Be concentrations (Fig. 7), referred to as a "steady-state erosion island plot" (Lal 1991), "simple exposure island plot" or "banana plot". The two-isotope diagram allows the detection of any shielding of a sample during its history. The "zero erosion line" and the "steady-state erosion line" frame a banana shaped area on a plot with logarithmic abscissa referred to

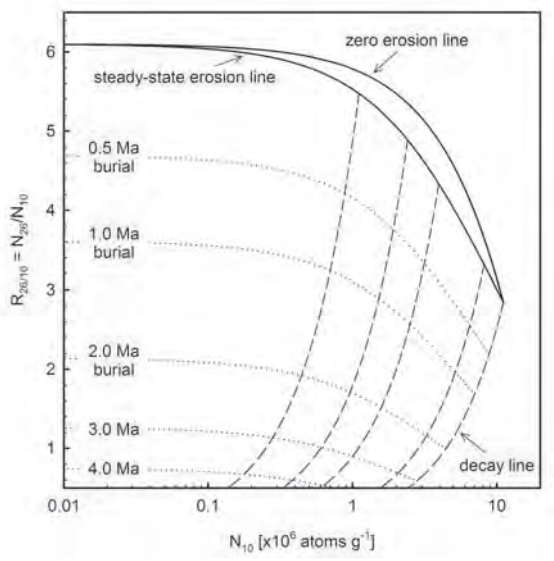

Fig. 7: Two-isotope diagram for in situ produced cosmogenic ^{10}Be and ^{26}Al in quartz as proposed by LAL (1991) with selected burial isochrones (dotted) and decay lines (dashed). Production rates are normalised to SLHL values with a ^{26}Al/^{10}Be production ratio of 6.1. Decay lines are given for complete shielding after single exposure with selected erosion rates (in mm ka^{-1}) until reaching saturation. Samples that have been shielded will plot below the steady-state erosion line in that the ^{26}Al/^{10}Be ratio will decrease resulting from the shorter half live of ^{26}Al with respect to ^{10}Be. Used parameters are listed in Table 1.

Abb. 7: Zwei-Isotopen-Diagram für in situ produziertes ^{10}Be und ^{26}Al in Quarz nach LAL (1991), mit ausgewählte Überlagerungsisochronen (gepunktet). Produktionsraten sind normalisiert auf SLHL-Bedingungen mit einem ^{26}Al/^{10}Be Produktionsverhältnis von 6,1. Zerfallsgeraden (gestrichelt) sind dargestellt für den Fall der vollständigen Abschirmung nach einmaliger, kontinuierlicher Bestrahlung für ausgewählte Erosionsraten (in mm ka^{-1}). Proben die während oder nach ihrer Bestrahlung abgeschirmt wurden, plotten unter der Gleichgewichts-Erosionsgeraden, da das ^{26}Al/^{10}Be Verhältnis abnimmt, gemäß der kürzeren Halbwertszeit des ^{26}Al Nuklids. Zu Grunde liegende Parameter können Tabelle 1 entnommen werden.

as the steady-state erosion island (LAL 1991). All samples with a nuclide inventory resulting from simple exposure will plot within this area, while samples that have also undergone some shielding will fall below that. A determination of burial duration is only possible for a single burial event. A discrete observation of multiple shielding events is not possible with the steady-state erosion island plot, as the measured nuclide inventory is a composite of all exposure and shielding periods. Nuclide concentrations and production rates have to be normalised to sea level, high latitude (> 60°; SLHL) values to avoid any affects of production rate changes resulting from scaling to sample location (for more detailed discussion of two-isotope diagrams see LAL 1991; BIERMAN et al. 1999; GOSSE & PHILLIPS 2001).

Shielding by material other than sediment or rock was studied by BIERMAN et al. (1999), who measured ^{10}Be and ^{26}Al concentrations at two locations at the northern and southern margin of the former Laurentide Ice Sheet. The northern site around Pangnirtung on Baffin Island, Canada consists of in situ deeply weathered Precambrian gneissic bedrock. In the area around these tor samples neither bedrock nor boulders display striations, grooves or chattermarks, although erratic cobbles and boulders confirm the presence of glacial ice. The southern part near Pipestone, Minnesota, USA is made up of very erosion resistant Sioux Quartzite. Its surface

preserves ice-flow indicators which have subsequently been wind polished and cross-cut by shallower grooves, and earlier studies suggested that the areas were ice-free during the last glaciation. Bierman et al. (1999), however, determined $^{26}Al/^{10}Be$ ratios that are less than the production ratio of ~6.1 within the bedrock that do not support a single exposure history, and suggest the areas must have been shielded from cosmic radiation at some point during and/or after initial exposure. On the one hand, young exposure ages (see Ivy-Ochs & Kober 2008) of the sampled erratics, lying on the modern surface, suggest deposition by ice during the Last Glacial Maximum (LGM, 14 – 30 ka). On the other hand, high nuclide concentrations within the bedrock do not support glacial cover during the LGM, due to the lack of glacial erosion and therefore the lowering of nuclide concentration. To explain these opposing observations Bierman et al. (1999) suggest cover by cold-based glaciers that would have not eroded the underlying bedrock and therefore would have not reset the "cosmogenic exposure clock". By modelling different exposure-burial scenarios they identified that the Sioux Quartzite samples have minimum total burial times that are more than twice as long as minimum exposure times, with an average minimum burial duration of 414 ± 29 ka. For the northern edge of the former Laurentide Ice Sheet on Baffin Island they conclude from ^{10}Be and ^{26}Al data, a non-erosive cold-based ice or deep snowfield cover for at least 400 ka.

A similar approach was used by Stroeven et al. (2002) and Fabel et al. (2002) who investigated ancient landscapes in Northern Sweden as relicts of the Fennoscandian Ice Sheet, to test the hypothesis of landscape preservation through multiple glacial cycles. Stroeven et al. (2002) investigated three tor samples and a bedrock outcrop in a meltwater channel in the Parkajoki area. The meltwater channel data are an exposure age of 11 ± 3 ka for both ^{10}Be and ^{26}Al, as a reliable deglaciation age. The lowered $^{26}Al/^{10}Be$ ratios of the tors, however, suggest that the sampled relict landscapes did not undergo a single exposure history, as reported in the regional literature. Fabel et al. (2002) looked at bedrock outcrops and erratics on relict surfaces in the northern Swedish mountains. These yield deglaciation ages of ~8 – 12 ka with ^{10}Be surface exposure dating of the erratics but much older surface ages of ~33 – 60 ka for the bedrock, similar to Stroeven et al. (2002). These researchers refined the approach described by Bierman et al. (1999) by using the marine benthic foraminifer oxygen isotope record of global ice volume from DSDP 607, as a proxy for the duration of periods of ice sheet cover vs. ice free conditions. They postulated 11 exposure and 10 burial events with a combined duration of 128 and 477 ka respectively for the Parkajoki area and a mean exposure-burial duration of 45 and 800 ka for the northern Swedish mountains.

4 Summary and outlook

The recent advances in terrestrial cosmogenic nuclides in geology and geomorphology have only been possible following the development of accelerator mass spectrometry in the late 1970's and early 1980's (see Finkel & Suter 1993), although the first burial and exposure histories were too complex and so difficult to interpret and provide reliable ages. A $^{26}Al/^{10}Be$ ratio significant lower than the production ratio was believed to indicate that the samples had been buried before, and only minimum burial ages could be constrained. After identifying that cave environments provide the ideal shielding scenario (instantaneous and sufficient), which prevents post burial nuclide production, it was possible to produce absolute burial ages from ^{10}Be and ^{26}Al determinations (Granger et al. 1997). This step, around 10 years ago, marked the beginning of "real" cosmogenic burial dating. In the last few years, burial dating has been applied using the nuclide profiling approach, to more complex environments such as alluvial fans (Matmon et al. 2005), fluvial terraces (Wolkowinsky & Granger 2004) or to relict surfaces beneath glacial ice that undergo partial shielding (Staiger et al. 2005; Briner et al. 2006; Davis et al. 2006). Nevertheless, this

often produces relatively large uncertainties that result in scepticism outside the cosmogenic community. As already shown, however, dating with cosmogenic nuclides offers unique advantages: application to quartz, the most common mineral on Earth's surface, and a time range of 100 ka to 5 Ma, making it very attractive to geomorphologists, (Quaternary) geologists and palaeoanthropologists.

Although fundamentals underlying its application have been recognised for almost 70 years, burial dating using cosmogenic nuclides is a relatively new technique and it is likely that in future nuclide pairs other than the $^{10}Be/^{26}Al$ one will be used. The shorter half-life of radiocarbon, 5730 ± 40 years (GODWIN 1962), would enable burial dating in the order of thousands to tens of thousands of years and allow the dating of more recent processes using the $^{10}Be/^{14}C$ pair in quartz. Additionally, slowly eroding rocks should have inherited ^{14}C concentrations close to saturation and would allow burial age determination without any other nuclides as initial nuclide concentration is reasonably well known. The $^{10}Be/^{36}Cl$ pair is also of interest, and would allow burial age determinations within carbonate rich and mafic environments. The first step towards the use of this nuclide pair has been made recently by BRAUCHER et al. (2006) who investigated the in situ ^{10}Be production rate and the chemical behaviour of ^{10}Be in carbonates as well as clinopyroxene samples. They identified a normalised ^{10}Be production rate of 37.9 ± 6.0 atoms g^{-1} a^{-1} in calcite and 3.1 ± 0.8 atoms g^{-1} a^{-1} in clinopyroxenes using the longer half life of ~1.5 Ma, and also presented laboratory protocols for the in situ ^{10}Be extraction from calcite and pyroxene samples.

New cosmogenic nuclide systems or combinations will be of interest in the coming years and the ongoing evaluation of physical constraints such as nuclide half lives (see chapter 1), nuclide production rates, muon production effects in depth and general long term production effects will also improve the precision of the general cosmogenic nuclide approach. The burial dating method stands today at a reasonably well-understood experimental level, although model evaluations and sensitivity tests are often not considered, or only partially understood, as a result of lack available data, compared to other well established dating techniques, such as radiocarbon, uranium/thorium or luminescence dating. This situation will change in the future through further research and the discovery of new applications.

Acknowledgements

We would like to thank Philipp Häuselmann, Susan Ivy-Ochs and an anonymous reviewer for their helpful reviews, Oliver Kracht for his constructive comments and Sally Lowick for improving the English of the manuscript. This work is supported by the Swiss National Science Foundation (project no. 200020-105220).

References

AKÇAR, N., IVY-OCHS, S. & SCHLÜCHTER, C. (2008): Application of in-situ produced terrestrial cosmogenic nuclides to archaeology: A schematic review. – Quaternary Science Journal (Eiszeitalter und Gegenwart): 57/1-2: 226–238.

ALBRECHT, A., HERZOG, G.F., KLEIN, J., DEZFOULY-ARJOMANDY, B. & GOFF, F. (1993): Quaternary erosion and cosmic-ray-exposure history derived from ^{10}Be and ^{26}Al produced in situ - An example from Pajarito plateau, Valles caldera region. – Geology, 21: 551-554.

ASFAW, B., WHITE, T.D., LOVEJOY, O., LATIMER, B., SIMPSON, S. & SUWA, G. (1999): *Australopithecus garhi:* A new species of early hominid from Ethiopia. – Science, 284: 629.

BALCO, G., ROVEY, C.W. & STONE, J.O.H. (2005): The first glacial maximum in North America. – Science, 307: 222-222.

BIERMAN, P.R., MARSELLA, K.A., PATTERSON, C., DAVIS, P.T. & CAFFEE, M. (1999): Mid-Pleistocene cosmogenic minimum-age limits for pre-Wisconsinan glacial surfaces in southwestern Minnesota and southern Baffin island: a multiple nuclide approach. – Geomorphology, 27: 25-39.

BRAUCHER, R., BLARD, P.-H., BENEDETTI, L. & BOURLÈS, D.L. (2006): Extending ^{10}Be applications to carbonate-rich and mafic environments. – In: L.L. SIAME, D.L. BOURLÈS & E.T. BROWN (eds.): In Situ-Produced Cosmogenic Nuclides and Quantification of Geoloigcal Processes: 17-28;

Boulder, Colorado (The Geological Society of America).

Briner, J.P., Miller, G.H., Davis, P.T. & Finkel, R.C. (2006): Cosmogenic radionuclides from fiord landscapes support differential erosion by overriding ice sheets. – Geological Society of America Bulletin, 118: 406-420.

Brown, E.T., Brook, E.J., Raisbeck, G.M., Yiou, F. & Kurz, M.D. (1992): Effective attenuation lengths of cosmic rays producing ^{10}Be and ^{26}Al in quartz: implications for exposure age dating. – Geophysical Research Letters, 19: 369-372.

Brown, E.T., Edmond, J.M., Raisbeck, G.M., Yiou, F., Kurz, M.D. & Brook, E.J. (1991): Examination of surface exposure ages of Antarctic moraines using *in situ* produced ^{10}Be and ^{26}Al. – Geochimica et Cosmochimica Acta, 55: 2269-2283.

Clark, J.D., Beyene, Y., WoldeGabriel, G., Hart, W.K., Renne, P.R., Gilbert, H., Defleur, A., Suwa, G., Katoh, S., Ludwig, K.R., Boisserie, J.-R., Asfaw, B. & White, T.D. (2003): Stratigraphic, chronological and behavioural contexts of Pleistocene *Homo sapiens* from Middle Awash, Ethiopia. – Nature, 423: 747-752.

Davis, P.T., Briner, J.P., Coulthard, R.D., Finkel, R.W. & Miller, G.H. (2006): Preservation of Arctic landscapes overridden by cold-based ice sheets. – Quaternary Research, 65: 156-163.

Desilets, D. & Zreda, M. (2001): On scaling cosmogenic nuclide production rates for altitude and latitude using cosmic-ray measurements. – Earth and Planetary Science Letters, 193: 213-225.

Dèzes, P., Schmid, S.M. & Ziegler, P.A. (2004): Evolution of the European Cenozoic Rift System: interaction of the Alpine and Pyrenean orogens with their foreland lithosphere. – Tectonophysics, 389: 1-33.

Dunai, T.J. (2000): Scaling factors for production rates of in situ produced cosmogenic nuclides: a critical reevaluation. – Earth and Planetary Science Letters, 176: 157-169.

Fabel, D., Stroeven, A.P., Harbor, J., Kleman, J., Elmore, D. & Fink, D. (2002): Landscape preservation under Fennoscandian ice sheets determined from in situ produced ^{10}Be and ^{26}Al. – Earth and Planetary Science Letters, 201: 397-406.

Fink, D. & Smith, A. (2007): An inter-comparison of ^{10}Be and ^{26}Al AMS reference standards and the ^{10}Be half-life. – Nuclear Instruments and Methods in Physics Research Section B - Beam Interactions with Materials and Atoms, 259: 600-609.

Finkel, R.C. & Suter, M. (1993): AMS in the Earth sciences: technique and applications. – In: M. Hyman & M.W. Rowe (eds.): Advances in analytical geochemnistry: 1-114; Greenwich (Jai Press Inc.).

Gibbard, P.L., Smith, A.G., Zalasiewicz, J.A., Barry, T.L., Cantrill, D., Coe, A.L., Cope, J.C.W., Gale, A.S., Gregory, F.J., Powell, J.H., Rawson, P.F., Stone, P. & Waters, C.N. (2005): What status for the Quaternary? – Boreas, 34: 1-6.

Godwin, H. (1962): Half-live of radiocarbon. – Nature, 195: 984.

Gosse, J.C. & Phillips, F.M. (2001): Terrestrial in situ cosmogenic nuclides: theory and application. – Quaternary Science Reviews, 20: 1475-1560.

Granger, D.E. (2006): A review of burial dating methods using ^{26}Al and ^{10}Be. – In: L.L. Siame, D.L. Bourlès & Brown, E.T. (eds.): In Situ-Produced Cosmogenic Nuclides and Quantification of Geological Processes: 1-16; Boulder, Colorado (The Geological Society of America).

Granger, D.E. & Smith, A.L. (2000): Dating buried sediments using radioactive decay and muogenic production of ^{26}Al and ^{10}Be. – Nuclear Instruments and Methods in Physics Research Section B – Beam Interactions with Materials and Atoms, 172: 882-826.

Granger, D.E. & Muzikar, P.F. (2001): Dating sediment burial with in situ-produced cosmogenic nuclides: theory, techniques, and limitations. – Earth and Planetary Science Letters, 188: 269-281.

Granger, D.E., Kirchner, J.W. & Finkel, R.C. (1997): Quaternary downcutting rate of the New River, Virginia, measured form differential decay of cosmogenic ^{26}Al and ^{10}Be in cave-deposited alluvium. – Geology, 25: 107-110.

Granger, D.E., Fabel, D. & Palmer, A.N. (2001): Pliocene-Pleistocene incision of the Green River, Kentucky, determined from radioactive decay of cosmogenic ^{26}Al and ^{10}Be in Mammoth Cave sediments. – GSA Bulletin, 113: 825-836.

Granger, D.E., Cyr, A.J. & Partridge, T.C. (2006): Quantitative tests of cosmogenic nuclide burial dating accuracy. – Geochimica et Cosmochimica Acta, 70, Supplement 1: A212.

Häuselmann, P., Granger, D.E., Jeannin, P.-Y. & Lauritzen, S.-E. (2007): Abrupt glacial valley incision at 0.8 Ma dated from cave deposits in Switzerland. – Geology, 35: 143-146.

HÄUSELMANN, P. & GRANGER, D.E. (2005): Dating of caves by cosmogenic nuclides: Method, possibilities, and the Siebenhengste example (Switzerland). – Acta Carsologica, 34: 43-50.

HÄUSELMANN, P., FIEBIG, M., KUBIK, P.W. & ADRIAN, H. (2007): A first attempt to date the orginal "Deckenschotter" of Penk & Brückner with cosmogenic nuclides. – Quaternary International, 164-165: 33-42.

HAJDAS, I. (2008):Radiocarbon dating and its applications in Quaternary studies – Quaternary Science Journal (Eiszeitalter und Gegenwart), 57/1-2: 2–24.

HEISINGER, B.P. (1998): Myonen-induzierte Produktion von Radionukliden. – 153 S., Ph.D. thesis; Technische Universität München, München.

HOFMANN, H.J., BEER, J., BONANI, G., VON GUNTEN, H.R., RAMAN, S., SUTER, M., WALKER, R.L., WÖLFLI, W. & ZIMMERMANN, D. (1987): 10Be: half-life and AMS-standards. – Nuclear Instruments and Methods in Physics Research Section B – Beam Interactions with Materials and Atoms, 29: 32-36.

IVY-OCHS, S. & KOBER, F. (2008): Surface exposure dating with cosmogenic nuclides. – Quaternary Science Journal (Eiszeitalter und Gegenwart, 57/1-2: 179–209.

JOYCE, J.E., TJAISMA, L.R.C. & PRUTZMAN, J.M. (1993): North American glacial meltwater history for the past 2.3 m.y.: Oxygen isotope evidence from the Gulf of Mexico. – Geology, 21: 483-486.

KLEIN, J., GIEGENGACK, R., MIDDLETON, R., SHARMA, P., UNDERWOOD, J.R. & WEEKS, R.A. (1986): Revealing histories of exposure using *in situ* produced ^{26}Al and ^{10}Be in Libyan Desert Glass. – Radiocarbon, 28: 547-555.

LAL, D. (1991): Cosmic ray labeling of erosion surfaces: in situ nuclide production rates and erosion models. – Earth and Planetary Science Letters, 104: 424-439.

LAL, D. & PETERS, B. (1967): Cosmic ray produced radioactivity on the Earth. – In: S. FLÜGGE (eds.): Handbuch der Physik = Encyclopedia of physics: 551-612; Berlin (Springer Verlag).

LAL, D. & ARNOLD, J.R. (1985): Tracing Quartz through the Environment. – Proceedings of the Indian Academy of Sciences-Earth and Planetary Sciences, 94: 1-5.

MATMON, A., SCHWARTZ, D.P., FINKEL, R., CLEMMENS, S. & HANKS, T. (2005): Dating offset fans along the Mojave section of the San Andreas fault using cosmogenic ^{26}Al and ^{10}Be. – GSA Bulletin, 117: 795-807.

MIDDLETON, R., KLEIN, J., RAISBECK, G. & YIOU, F. (1983): Accelerator mass spectrometry with ^{26}Al. – Nuclear Instruments and Methods in Physics Research, 218: 430-438.

MIDDLETON, R., BROWN, L., DEZFOULY-ARJOMANDY, B. & KLEIN, J. (1993): On ^{10}Be standards and the half-Life of ^{10}Be. – Nuclear Instruments and Methods in Physics Research Section B - Beam Interactions with Materials and Atoms, 82: 399-403.

NISHIIZUMI, K., IMAMURA, M., CAFFEE, M.W., SOUTHON, J.R., FINKEL, R.C. & MCANINCH, J. (2007): Absolute calibration of ^{10}Be AMS standards. – Nuclear Instruments and Methods in Physics Research Section B – Beam Interactions with Materials and Atoms, 258: 403-413.

NORRIS, T.L., GANCARZ, A.J., ROKOP, D.J. & THOMAS, K.W. (1983): Half-life of ^{26}Al. – Proceedings of the fourteenth Lunar and Planetary Science Conference, Part I, Journal of Geophysical Research, 88 (Supplement): B331-B333.

PARTRIDGE, T.C., GRANGER, D.E., CAFFEE, M.W. & CLARKE, R.J. (2003): Lower Pliocene hominid remains from Sterkfontein. – Science, 300: 607-612.

PENCK, A. & BRÜCKNER, E. (1909): Die Alpen im Eiszeitalter. - 1199 S.; Leipzig (Tauchnitz).

PICKERING, R., HANCOX, P.J., LEE-THORP, J.A., GRÜN, R., MORTIMER, G.E., MCCULLOCH, M. & BERGER, L.R. (2007): Stratigraphy, U-Th chronology, and paleoenvironments at Gladysvale Cave: insights into the climatic control of South African hominin bearing cave deposits. – Journal of Human Evolution, 53: 602-619.

PREUSSER, F., DEGERING, D., FUCHS, M., HILGERS, A., KADEREIT, A., KLASEN, N., KRBETSCHEK, M., RICHTER, D., SPENCER, J. 2008. Luminescence dating: Basics, methods and applications. Quaternary Science Journal (Eiszeitalter & Gegenwart), 57/1-2: 95–149.

RAVELO, A.C., ANDREASEN, D.H., LYLE, M., LYLE, A.O. & WARA, M.W. (2004): Regional climate shifts caused by gradual global cooling in the Pliocene epoch. – Nature, 429: 263-267.

RIGHTMIRE, R.A., KOHMAN, T.P. & HINTENBERGER, H. (1958): Über die Halbwertszeit des langlebigen ^{26}Al. – Zeitschrift für Naturforschung Teil A – Astrophysik, Physik, Physikalische Chemie, 13: 847-853.

SHARMA, P. & MIDDLETON, R. (1989): Radiogenic production of ^{10}Be and ^{26}Al in uranium and thorium ores: Implications for studying terrestrial samples containing low levels of ^{10}Be and

^{26}Al. – Geochimica et Cosmochimica Acta, 53: 709-716.

Staiger, J.K.W., Gosse, J.C., Johnson, J.V., Fastook, J., Gray, J.T., Stockli, D.F., Stockli, L. & Finkel, R. (2005): Quaternary relief generation by polythermal glacier ice. – Earth Surface Processes and Landforms, 30: 1145-1159.

Stone, J.O. (2000): Air pressure and cosmogenic isotope production. – Journal of Geophysical Research B, 105: 23753-23759.

Stroeven, A.P., Fabel, D., Hättestrand, C. & Harbor, J. (2002): A relict landscape in teh centre of Fennoscandian glaciation: cosmogenic radionuclide evidence of tors preserved through multiple glacial cycles. – Geomorphology, 44: 145-154.

Wagner, G., Masarik, J., Beer, J., Baumgartner, S., Imboden, D., Kubik, P.W., Synal, H.-A. & Suter, M. (2000): Reconstruction of the cosmogenic field between 20 and 60 kyr BP form cosmogenic radionuclides in the GRIP ice core. – Nuclear Instruments and Methods in Physics Research Section B – Beam Interactions with Materials and Atoms, 172: 597-604.

Walker, J., Cliff, R.A. & Latham, A.G. (2006): U-Pb isotopic age of the StW 573 hominid from Sterkfontein, South Africa. – Science, 314: 1592-1594.

Wolkowinsky, A.J. & Granger, D.E. (2004): Early Pleistocene incision of the San Juan River, Utah, dated with ^{26}Al and ^{10}Be. – Geology, 32: 749-752.

Eiszeitalter und Gegenwart Quaternary Science Journal	57/1–2	226–238	Hannover 2008

Application of in-situ produced terrestrial cosmogenic nuclides to archaeology: A schematic review

Naki Akçar, Susan Ivy-Ochs & Christian Schlüchter*)

Abstract: The wide applicability of in-situ produced Terrestrial Cosmogenic Nuclides (TCNs) to geological problems and experiences in development and testing gained over the past decade is encouraging for its application to archaeological questions, where there is a distinct need for an additional independent dating tool beyond the limits of radiocarbon (~ 40 ka). Just as TCNs are applicable to a broader time period with considerable precision in archaeology, so also are they applicable to all lithologies. Application of TCNs to archaeological problems is relatively simple: either surface exposure dating (using cosmogenic nuclide production) or burial dating (using decay of radioactive cosmogenic nuclides) can be applied. For a successful application, close collaboration between archaeologists and TCN experts is required. The total exposure from 100 a to 5 Ma of a given surface of archaeological origin can be determined by surface exposure dating. The range of burial dating is from ~0.1 to 5 Ma. TCNs have been successfully applied to many archaeological problems during the last decade and both surface exposure dating and burial dating show high potential in the solving of archaeological problems.

[Anwendung in-situ produzierter, terrestrischer kosmogener Nuklide in der Archäologie: Ein schematischer Überblick]

Kurzfassung: Die breite Anwendbarkeit von in-situ produzierten Terrestrischen Kosmogenen Nukliden (TCN) in geologischen Fragestellungen und die damit verbundenen Erfahrungen in der Entwicklung und Eignungsprüfung die im letzten Jahrzehnt erlangt wurden, ermutigen diese Methode auch für archäologische Fragestellungen anzuwenden. In diesem Zusammenhang gibt es ein konkretes Bedürfnis für eine zusätzliche unabhängige Methode der Altersbestimmung jenseits der Grenze von Radiokohlenstoff (~ 40 ka). TCN sind nicht nur in einem Grenzbereich mit einer gewissen Präzision anwendbar, sie sind auch geeignet für die unterschiedlichsten Lithologien. Die Anwendung von TCN in archäologischen Fragestellungen ist relativ einfach: entweder wird der Ansatz der Oberflächendatierung gewählt (Nutzung der Produktion von kosmogenen Nukliden) oder man verwendet den Ansatz der Begrabungsalter (Nutzung des Zerfalls von radioaktiven kosmogenen Nukliden). Für eine erfolgreiche Anwendung der Methode ist jedoch eine enge Zusammenarbeit zwischen Archäologen und TCN Spezialisten notwendig. Eine Expositionszeit zwischen 100 a bis zu 5 Ma einer archäologisch geschaffenen Fläche kann durch Oberflächendatierung bestimmt werden. Der Altersbereich der Begrabungsaltermethode liegt zwischen ~0.1 to 5 Ma. TCN wurden während des letzten Jahrzehnts erfolgreich zur Datierung vieler archäologischer Fragestellungen angewendet und sowohl die Oberflächendatierung als auch Begrabungsaltermethode zeigen ein hohes Potenzial um archäologische Fragestellungen lösen zu können.

Keywords: Terrestrial Cosmogenic Nuclides, Archaeology, Numerical Dating

*Addresses of authors: N. Akçar, Institut für Geologie, Universität Bern, Baltzerstrasse 1+3, 3012 Bern, Switzerland. E-Mail: akcar@geo.unibe.ch; S. Ivy-Ochs, Institut für Teilchenpysik, ETH Zürich, HPK/H27, Schafmattstrasse 20, 8093 Zürich, Schweiz and Geographisches Institut, Universität Zürich (Irchel), Winterthurerstrasse 190, 8057 Zürich, Switzerland; Ch. Schlüchter, Institut für Geologie, Universität Bern, Baltzerstrasse 1+3, 3012 Bern, Switzerland.

1 Introduction

Shrewder sampling, improved chemical sample preparation and analysis as well as a better understanding of the physical processes responsible for in-situ produced Terrestrial Cosmogenic Nuclides (TCNs) have significantly enhanced the reliability of the method since its conception (cf., Gosse & Phillips 2001). The best known application of TCNs is the dating of the Quaternary ice volume fluctuations from the records archived by mountain glaciers (e.g., Ivy-Ochs et al. 2006) and continental ice sheets (e.g., Briner et al. 2006). Moreover, TCN methods have been employed in dating volcanic (e.g., Licciardi et al. 1999) and palaeoseismic events (e.g., Benedetti et al. 2003) as well as to quantify surface and/or rock uplift (Ritz et al. 2006) and incision rates (e.g., Schaller et al. 2005). Due to the sensitivity of the cosmogenic nuclide concentration to surface erosion and depth below the surface, the method has led to significant breakthroughs in establishing the rates and styles of local and large-scale erosion (Schaller et al. 2001), soil development (Heimsath et al. 1997) and landscape evolution (e.g., Bierman et al. 2002). The method can also be applied to the study of surface processes over a broad range of climate settings, employing different lithologies and mineralogies (Ivy-Ochs & Kober 2008). In addition, several geologic anomalies have been dated by cosmogenic nuclides such as Libyan desert glass (Klein et al. 1986) and the Canyon Diablo meteorite impact (Nishiizumi et al. 1991; Phillips et al. 1991). Depending on the surface preservation and exposure history, this dating technique has an effective range from the Pliocene to the late Holocene (Ivy-Ochs & Kober 2008). Its rapid and wide acceptance in using ^{3}He, ^{10}Be, ^{14}C, ^{21}Ne, ^{26}Al, and ^{36}Cl is not only due to its wide applicability to problems in surface geology but also to the reproducibility of many of its early results (Gosse & Phillips 2001 and references therein).

Cosmogenic nuclides can be used to exposure date fossils, lithic artefacts or monuments directly, to exposure date rock surfaces, or to date sediments associated with fossils or stone tools, or to determine nuclide concentrations to assess tool procurement strategies. Therefore, cosmogenic nuclide methods have a largely unrealized potential in archaeology (Stuart 2001). Although several dating techniques such as radiocarbon (e.g., Gonzalez et al. 2003), U-series (e.g., Shen et al. 2001), electron spin resonance (e.g., Molodkov 2001), ^{40}Ar/^{39}Ar (e.g., Clark et al. 2003) and luminescence (e.g., Valladas et al. 2003), either directly or indirectly, can be applied to archeological problems, there is a substantial need for an additional dating tool in archaeology beyond the limits of radiocarbon and independent of the dating methods mentioned above (Fig. 1). Among several dating techniques, the TCN technique seems to be very promising due to its longer application period and efficacy without the need for any organic material (Fig. 1).

The primary focus of this review paper is on the evaluation of the application of TCNs to archaeological questions considering basically surface exposure dating and burial dating. Following the basic information on these two techniques, we discuss in detail how these techniques can be applied with assumptions, requirements, potential problems, disadvantages and advantages of each technique. This discussion is complemented with respective reviews of previous studies of TCN applications to archaeology.

2 How to apply TCNs to archaeology?

High-energy cosmic rays originating predominantly from super nova explosions within our galaxy are continuously bombarding the Earth. Interactions between these high-energy cosmic rays and the Earth's atmosphere create secondary and tertiary cosmic rays, including neutrons and muons. These high-energy particles can penetrate meters into rock and sediment when they reach the Earth's surface. Located in the upper surface of a rock, in-situ produced terrestrial cosmogenic nuclides are the product of the interaction of cosmic radiation, primarily neutrons, with a variety of target atoms within

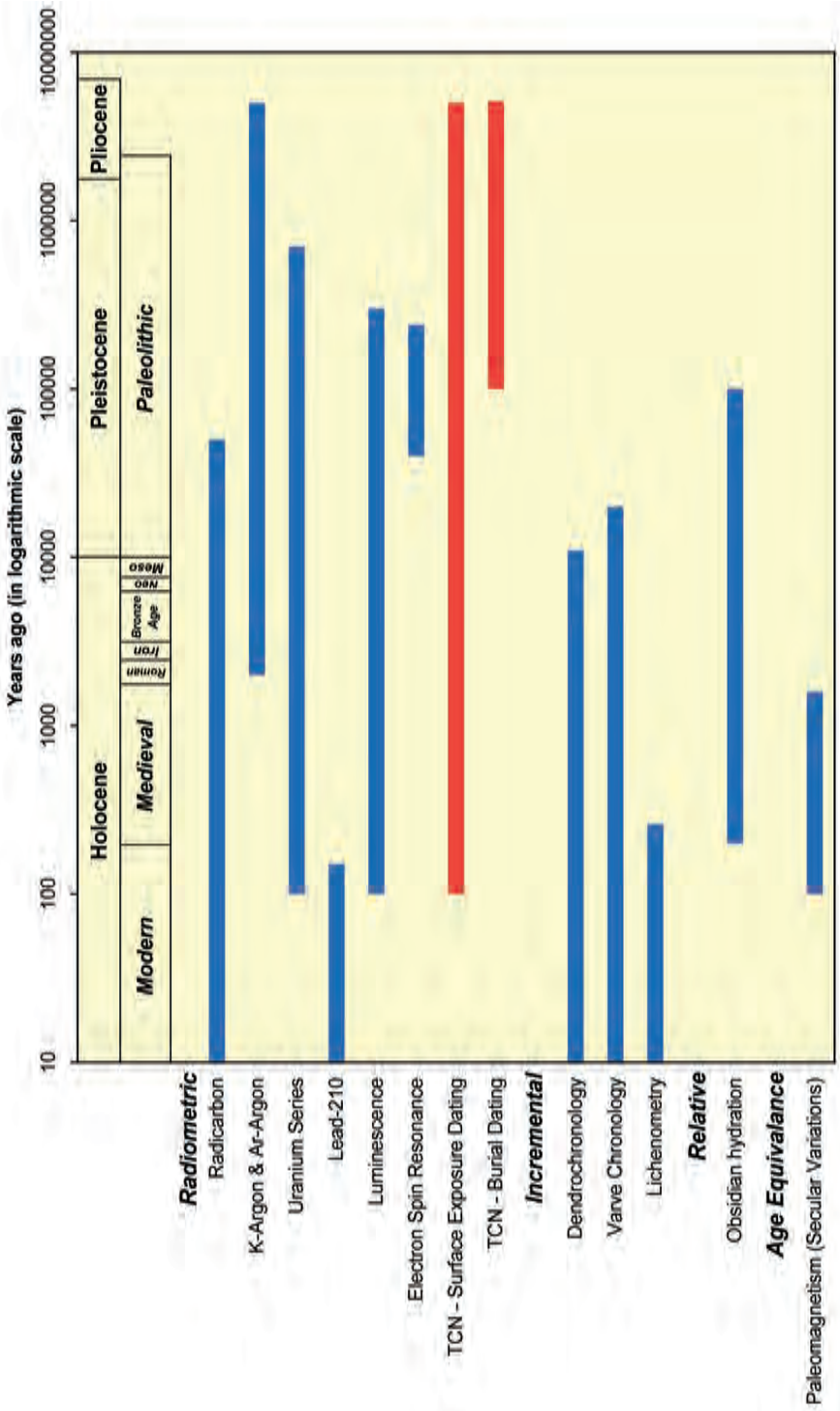

Fig. 1: The effective time ranges of the different dating methods applied (or can be applied) both in Quaternary Geology and in Archaeology (modified from ROBERTS 1998 and WALKER 2005).

Abb. 1: Effektive Zeiträume die von den verschiedenen Datierungsmethoden im Rahmen der Quartärgeologie und Archäologie abgedeckt werden oder abgedeckt werden könnten (modifiziert nach ROBERTS 1998 und WALKER 2005).

minerals (e.g., quartz, calcite, K-feldspar and olivine). This interaction results in nuclear reactions such as spallation (the splitting of nuclei), muon-induced reactions and neutron capture reactions (Lal & Peters 1967; Reedy 1987; Lal 1988). In consequence of these reactions, unstable cosmogenic nuclides such as ^{10}Be, ^{14}C, ^{26}Al, and ^{36}Cl and stable cosmogenic nuclides such as ^{3}He and ^{21}Ne are produced in respective mineral lattices (Table 1) (cf., Ivy-Ochs & Kober 2008).

Theoretically, application of TCNs to archaeological problems is relatively simple. Either the production (both stable and unstable) or decay (in the case of unstable) cosmogenic isotopes can be applied. Surface exposure dating is the most common field of the cosmogenic nuclide technique (cf., Ivy-Ochs & Kober 2008), while burial dating, based on TCN decay, is now also increasingly used (cf., Dehnert & Schlüchter 2008). Essentially, surface exposure dating can be applied over the timescales of around 100 a to 5 Ma and burial dating over around 0.1 to 5 Ma. The difference between the lower limits originates directly from the time required for a sufficient decay of unstable cosmogenic nuclides in order to detect different isotopic concentrations due to various half-lives. Both surface exposure and burial dating tools require that the archaeological sample to be dated is destroyed during the sample preparation, and this can make the application of TCNs to archaeology at first seem strange. However, a destruction of this type can be minimized with careful planning of the sampling strategy and analysis of the scientific problem. In spite of this, the number of samples required for such analysis should be in the order of five.

2.1 Surface exposure dating

The application of surface exposure dating to archaeology at first sight appears to be restricted to large archaeological structures such as buildings, monuments and standing stones (Stuart 2001). However the situation is simpler: if the concentration of the required TCN can be measured with accelerator mass spectrometry, the total exposure duration (from 100 a to 5 Ma) of a given surface can be deter-

Table 1: Characteristics of unstable cosmogenic nuclides ^{10}Be, ^{26}Al, and ^{36}Cl and stable cosmogenic nuclides ^{3}He and ^{21}Ne (modified after Ivy-Ochs & Kober 2007).

Tabelle 1: Charakteristiken der instabilen kosmogenen Nuklide ^{10}Be, ^{26}Al, und ^{36}Cl und der stabilen kosmogenen Nuklide ^{3}He und ^{21}Ne (verändert nach Ivy-Ochs & Kober 2007).

TCN	Production Rate* (atoms g^{-1} a^{-1})	Half-life (Ma)	Target Elements	Target Minerals
^{3}He	119 (Liccardi *et al.* 1999)	Stable	Many	Olivine Pyroxene
^{10}Be	5.1 (Stone 2000)	1.51 (Hofmann *et al*. 1987)	O Si	Quartz
^{21}Ne	20.33 (Niedermann 2000)	Stable	Si Mg	Quartz, Olivine Pyroxene
^{26}Al	30.1 (Stone 2000)	0.716 (Samworth *et al.* 1972)	Si	Quartz
^{36}Cl	Lithology dependent ca. 10 in granite 20 in limestone	0.301	K Ca ^{35}Cl	Whole Rock

**Nuclide production rates at sea level and high latitude (Gosse & Phillips 2001).*

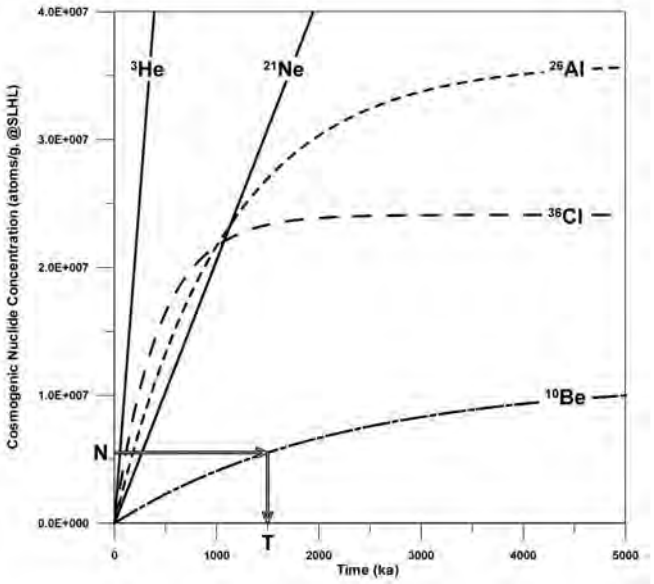

Fig. 2: Accumulation of ^{3}He, ^{10}Be, ^{21}Ne, ^{26}Al and ^{36}Cl in a rock surface as a function of exposure time at sea level high latitude (@SLHL). N is the concentration of the cosmogenic nuclide and T is the equivalent time of exposure. TCN concentrations were calculated with CosmoCalc 1.0 (VERMEESCH 2007), using STONE (2000) scaling factors and default values.

Abb. 2: Akkumulation von ^{3}He, ^{10}Be, ^{21}Ne, ^{26}Al und ^{36}Cl in Gesteinsoberflächen als Funktion der Expositionszeit im Meeresspiegelniveau (@SLHL). N ist die Konzentration des kosmogenen Nuklids und T ist die Equivalenzzeit an Exposition. TCN Konzentrationen wurden mit Hilfe von CosmoCalc 1.0 (VERMEESCH 2007) kalkuliert, unter Anwendung der Skalierungsfaktoren und Vorgaben nach STONE (2000).

mined (Fig. 2) using the local production rate of the respective isotope (Table 1) (IVY-OCHS & KOBER 2008). For this determination, three conditions must be fulfilled. The first is that the cosmogenic isotope concentration at the beginning of exposure is zero or known (i.e. inheritance). The second is that the system must have been closed with respect to either gain or loss of the respective isotope. The third assumption is that the correct production rates are known and were constant during the exposure time.

CERLING & CRAIG (1994) were the first scientists who discussed the potential application of cosmogenic nuclides to archaeology in their review publication "Geomorphology and Cosmogenic Nuclides" and suggested that the pyramids, Sphinx, Stonehenge or even the statues on Easter Island could be directly exposure dated. For instance, initial results from the analysis of ^{36}Cl in the bluestones from Stonehenge are controversial (WILLIAMS-THORPE et al. 1995). Furthermore they describe the debate on the construction age of the Sphinx (mainly "*the Final Riddle of Sphinx*") and discuss a potential solution of this debate with TCN dating suggesting that archaeologists inform their scientific progeny since the time for this study would come. In addition to this exciting review, STUART (2001) summarised the principles (mainly for archaeologists) and utility of TCN methods to address archaeological questions. In his review on in-situ cosmogenic nuclides, the controls of the production of TCN in exposed surfaces are outlined and the factors of relevance for exposure dating of archaeological

material are evaluated (Stuart 2001).

Construction of the field context in surface exposure dating of archaeological structures is the most important aspect. This context should be delineated with all available archaeological and geological data and the archaeological question discussed in detail. At this point, input from the archaeologist in the construction of the context may be determinant. Many problems which would arise later during evaluation and interpretation of the results can be omitted with careful planning during this phase. After the selection of the appropriate cosmogenic isotope to be applied (Table 1), samples are collected following the strategies defined in other surface exposure dating studies (Gosse & Phillips 2001). Not only the construction time of archaeological structures, but also collapse time can be surface exposure dated. For instance, exposure dating of blocks within the ruins of an archaeological structure can give information about the collapse event of this structure.

Several problems may arise during the building up of the field context concerning the main assumptions of surface exposure dating. Among these assumptions, the first is likely the most critical one, since the building stone (*sensu lato*) used for the construction has a possibility of being pre-exposed before quarrying and/or of having TCN concentration produced in depth and thus a significant concentration of inherited TCNs (Ivy-Ochs & Kober 2008). Although the inheritance is uncommon in practice when glacially transported erratic boulders are dated with TCNs (Putkonen & Swanson 2003), the probability for archaeological applications is more serious. This potential presence of inheriting TCN can be assessed with careful observation during sampling, particularly in the case of quarried materials. If this is not possible, the analysis of TCN concentration over a depth profile of several meters may then provide information on the inheritance and erosion rates (see Ivy-Ochs & Kober 2008 for further details). If the source quarry can be determined, the concentration of TCN on both exposed and buried surfaces from this quarry can be analysed. In the first instance, this difficulty looks discouraging; however it can after be eliminated within the field context and related sampling strategies in the field. Also, multiple TCN measurements may be helpful; for instance, measurements of unstable ^{10}Be and stable ^{21}Ne can be used to determine the exposure history of a given archaeological surface. ^{21}Ne concentration will clarify the total cosmogenic exposure history and, as the unstable ^{10}Be will decay in the case of any interruption in exposure, it will reveal the pattern of exposure history: either simple or complex. Simple exposure will result in ^{10}Be and ^{21}Ne ages, which are consistent within the error limits. However, a complex exposure will result in a younger ^{10}Be than ^{21}Ne age, due to the isotopic decay of ^{10}Be. Although complex exposure histories are successfully applied to glacially abraded bedrock and for surfaces (Bierman et al. 1999; Fabel et al. 2002; Phillips et al. 2006), the application to archaeology is more complex. In this case, the exposure episodes will be interrupted by either complete or partial (shielding by other agents such as soil, sediment etc…) burial, or a series of different burial times. In such a complicated situation, the only information that can be deduced is the total exposure time to radiation. The best solution to this complexity is the minimization of unknown parameters, i.e. the careful examination of the field context.

Another problem concerning exposure dating assumptions is inconstant local production rates of respective TCN during exposure time. In the case of archaeology, this inconsistency can occur through rebuilding, restoration, renovation of archaeological structures such as buildings, monuments and standing stones. These kinds of post-exposure displacement activities will directly affect the production rate and thus may result in meaningless exposure ages. As in the case of inheritance, the variable production rate problem can be omitted again by careful observation within a well structured context.

Although the possibility is quite low and uncommon, system closedness concerning the third assumption can also cause some problems. There are two ways this occurs: either some of the TCN is lost during the exposure time, such

as chipping out of the material through physical weathering, which will result in younger exposure ages. The prevention is simple: the surface to be sampled should be selected carefully. On the other hand, a gain of TCN through atmospheric cosmogenic isotopes (see Ivy-Ochs & Kober 2008 for further details) such as meteoric ^{10}Be and ^{36}Cl may result in higher exposure ages. Possible contamination by meteoric isotopes is unlikely and normally removed during sample preparation due to improved chemical sample preparation in the TCN technique.

In the first study to solve an archaeological problem by surface exposure dating, Phillips et al. (1997) used ^{36}Cl to address the question of whether the exposed schist surfaces of the Côa valley (northern Portugal) were available for engraving during Palaeolithic times (from around 2.5 Ma to around 10 ka ago). The age of the animal and other figures engraved on these rock surfaces is controversial and hypotheses fall into two time periods: (1) Palaeolithic, due to the stylistic indications (among others Zilhão 1995) and (2) Holocene, suggested by radiocarbon dating (Watchman 1995; 1996) and microerosion dating results (Bednarik 1995a; 1995b; 1995c). Phillips et al. (1997) revealed that the rock panels had been exposed long enough to be engraved during the Palaeolithic, and argued for a landscape stable enough to support Palaeolithic art (Stuart 2001). Although Phillips et al. (1997) had given a maximum exposure age (i.e. the real exposure age is probably younger) for the schist panels, this first application of TCNs was criticised by Watchman (1998) and Bednarik (1998), with criticisms focusing mainly on inheritance (i.e. the TCN concentration present prior to the exposure), erosion rates of the schist panels and the potential contamination of meteoric ^{36}Cl due to the high hydrological and therefore hydrochemical activity in the region, i.e. this system was not closed with respect to gain of the respective isotope.

A prime example of surface exposure dating study is by Ivy-Ochs et al. (2001) who analysed two chert artifacts (flakes made during the knapping process) of Late Acheulean or early Middle Palaeolithic age from the Thebes Mountains near Luxor, Egypt. By measuring the cosmogenic ^{10}Be concentration in the artefacts they were able to calculate 'nominal exposure ages' of 326 and 304 ka respectively.

In a later study, Farley et al. (2001) successfully measured ^{3}He in the fluorapatite of fossil teeth, opening up the possibility of dating fossil remains at archaeological sites. On the one hand the continuous exposure requirement must be satisfied. On the other, the preliminary results of Farley and coworkers imply that some of the fossils they studied comprise lag deposits and are much older than the associated sediment.

The main disadvantage of surface exposure dating of archaeological structures seems to be the inheritance as was also experienced in the earlier studies. As mentioned above, the inheritance problem can mainly be omitted during the scientific context construction phase; if not possible, this can still be excluded by applying a multiple TCN approach, but even so this will be not more than a limited approach to the problem according to the present level of experience in such situations.

Surface exposure dating is a direct, absolute dating tool which can be applied to a broader time span within and beyond the ^{14}C limit. Its independence of the organic material and lithology is a key advantage compared to the other dating techniques. Furthermore, surface exposure dating can be used as an 'event' dating tool in archaeology such as construction or destruction of archaeological structures. The precision of surface exposure dating is high enough to date such archaeological events.

In particular, lower detection limit of surface exposure dating, which is around 100 years, would for instance mean that marble statues older than 19th century can be exposure dated. This fact, in principle, would imply that TCN could be potentially used to determine whether an archaeological object is original or not. All these advantages of exposure dating are encouraging for its application to the archaeological questions. Much has been learnt from previous studies; however, there is still more to be learnt and experienced with new applications.

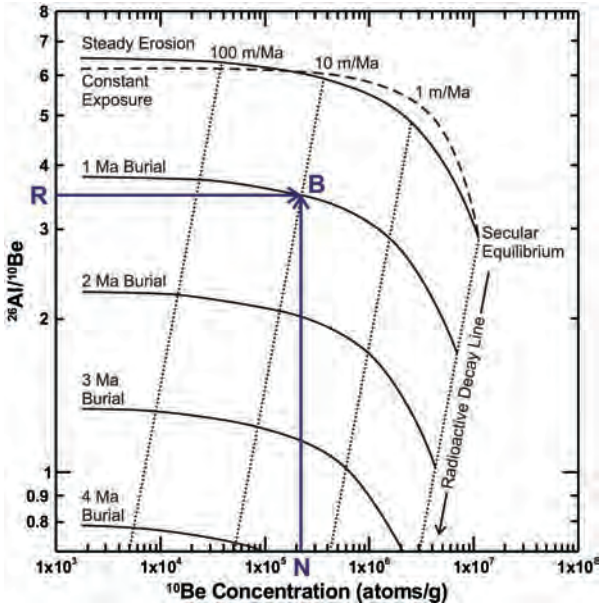

Fig. 3: Plot used in burial dating (modified from Granger & Muzikar 2001). R is showing the $^{26}Al/^{10}Be$ ratio, N the ^{10}Be concentration and B the equivalent burial time.

Abb. 3: Diagramm zu Berechnung von Begrabungsaltern (verändert nach Granger & Muzikar 2001). R ist das Verhältnis $^{26}Al/^{10}Be$, N die Konzentration an ^{210}Be und B die equivalente Begrabungszeit.

2.2 Burial dating

The application of burial dating to archaeology is a promising tool. Basically, any object of archaeological origin that has been buried can be dated with this technique (Fig. 3). Considering the period of application (from ~100 ka to 5 Ma), burial dating can be mainly applied to the Palaeolithic time (from around 2.5 Ma to around 10 ka ago). Until now, burial dating has been applied using ^{10}Be and ^{26}Al in quartz. The fundamentals are as follows: the cosmic ray cascade causes the production of TCN in quartz crystals (as sediment and/or mineral in the rock) at or near the earth's surface. When quartz grains are eroded, transported and deposited far below the surface (e.g., in a cave), the TCN production rate becomes zero due to the attenuation of the cosmic rays in the rock. The radioactive decay of ^{10}Be and ^{26}Al with time will result in a decrease in concentrations of these radionuclides in the host mineral (mainly quartz). Since ^{26}Al has a shorter half-life than ^{10}Be (Table 1), ^{26}Al vs. ^{10}Be ratio decreases with time and the time since the sediment was buried can principally be determined when the initial build-up is modelled (for details see Dehnert and Schlüchter 2008). For burial dating application, four requirements must be fulfilled. The first is that the accumulation of TCN in the quartz grains prior to burial must be sufficient enough for a successful AMS measurement. The second is that the transport and the burial of quartz should be contemporaneous with respect to timescales of radioactive decay. The third is that the prospective quartz sample must be buried deep enough to avoid significant TCN production after burial and the fourth requirement is that the TCN production should result from a simple history of exposure prior to burial.

The burial dating technique can be applied, for instance, to the settled caves of Palaeolithic times (e.g. Partridge et al. 2003). In principle,

one could burial date both the artefact and the enclosing sediment. This is a reliable way to perform a cross-control of the application of TCNs, especially when other dating techniques are not applicable. Application of burial dating to archaeology is not restricted to Palaeolithic caves. Another application can be the strata of different cultures. In this situation, an archaeological stratum can be handled as a geological unit and the deposition time of the layer can be determined within given uncertainties. Burial dating can also be applied to waste disposal in antique quarries. Here, even different phases of waste disposal can be determined in relation to the original quarry phase. Burial dating can also be applied to the special cases where archaeology and natural hazards coincide. For example, a mass movement can destroy a settlement or a part of it and the buried sediment can be dated by TCN analysis.

Again, as in surface exposure dating, construction of the field context is the most important aspect. The context should be constructed in such a way as to minimize uncertainties which can potentially cause problems during consequent phases of burial dating, using all available archaeological and geological data with close cooperation between archaeologists and TCN experts. However, some problems may still appear during archaeological applications of burial dating concerning the four requirements mentioned above. Since the accelerator mass spectrometric measurement technique is able to measure very low concentrations of TCNs, the first requirement (*Measurable TCN concentrations*) will not cause any problem. The second requirement (*Contemporaneous transport and burial*) can easily be fulfilled, since the time between the production and the burial of the archaeological artefacts is considered contemporaneous compared to the radioactive half-lives of ^{26}Al and ^{10}Be. The third requirement (*No TCN production after burial*) is likely the most critical one and affects all burial dating applications. Here, on the other hand the production of TCNs at depth cannot be neglected, since there will still be some amount of TCN concentration produced after deposition and/or burial. This potential problem can be minimized by the application of an appropriate model for production after deposition. Beside the third requirement, the fourth requirement (*Simple exposure history before burial*) is fulfilled for artefacts by approximations following appropriate models as with other burial dating applications (for details see Dehnert & Schlüchter 2008).

During the last decade, burial dating has been applied to archaeological questions. Boaretto et al. (2000) proposed the application of burial dating to archaeology with a case study from Tabun Cave, Mt. Carmel (Israel), which has a sedimentary sequence representing the type section for about the last 800 kyr in the Levant. Flint tools are also embedded within this quartz rich sequence. In this study, flint tools as well as sediments were sampled for ^{10}Be and ^{26}Al. The flints that they analyzed contained too much stable ^{27}Al and too little ^{26}Al, so that their analyses were complicated. Thus, Boaretto et al. (2000) did not calculate burial ages for these samples. The key finding of this study is that the internal environment of the flint is well sealed, so that any contamination by meteoric ^{10}Be seems to be unlikely.

Apart from the direct application of burial technique, Verri et al. (2002, 2004, 2005) studied flints that were embedded within the sedimentary sequence in the Tabun and Qesem caves in Israel. Considering the basic idea that flint mined from deeper than 2 m will have a low ^{10}Be concentration, whereas flint collected from the surface or mined from shallower than 2 m will contain a higher ^{10}Be concentration, they determined that different flint procurement strategies, including deep mining, were used at least as early as the Late Lower Palaeolithic in the Levant. For instance, ^{10}Be concentration of flints from one layer (Lower Layer E, Acheulo – Yabrudian, around 400 – 200 ka) in Tabun cave are very low and consistent compared to the layers below and above (Verri et al. 2005).

Recently, Partridge et al. (2003) applied burial dating (using ^{10}Be and ^{26}Al) to the fossiliferous breccia in the Jacovec Cavern and Silberberg Grotto at Sterkfontein, South Africa. The results of this application revealed that the ho-

minid fossils embedded within these deposits were accumulated in the Early Pliocene, and also that burial dates obtained from Jacovec Cavern and Silberberg Grotto are indistinguishable. Approximately 4 Ma of burial age for the hominid remains found in these two sites is also consistent with and similar to the findings from East Africa (Clarke et al. 2003; Partridge et al. 2003). In a subsequent study, Muzikar & Granger (2006) applied a combination of cosmogenic, stratigraphic and palaeomagnetic information using a Bayesian approach to refine the burial dating results from Sterkfontein.

The main disadvantage of burial dating of archaeological artefacts seems to be post-burial TCN production and possible complicated TCN production history prior to burial as experienced also in the earlier studies. This problem can be mainly solved –as mentioned above– just during the scientific context construction phase. Especially the complexity vs. simplicity of TCN production (complex or simple exposure) prior to burial can give information about the tool procurement as demonstrated by Verri et al. (2002, 2004, 2005). As the ^{10}Be and ^{26}Al in quartz have been used in burial dating applications until now, this can look like a disadvantage of lithology dependency, however the use of other TCNs in burial dating is still open and needs to be tested and practiced.

Much has been learnt from previous applications: burial dating is applicable to a broader time span, especially to Palaeolithic, i.e. definitely far beyond the radiocarbon dating limit; and it is also a direct, absolute dating tool which is independent of the presence of organic material. Hence, these two advantages are encouraging for its application to archaeological questions, even though there is certainly still more to be learnt and experienced with new applications.

3 Conclusions

During the last decade, TCNs have been successfully applied to a several archaeological problems, although most of these were test applications. TCN methodology has several advantages over other dating tools: as the radiocarbon technique is widely used by archaeologists, absence of organic material is generally a problem. Moreover, increasing uncertainties with time and calibration issues are sometimes problematic. At this point, TCNs seem to be an outstanding approach in solving archaeological problems. In archaeology, TCNs can be applied (1) to a larger time period beyond the radiocarbon dating limit, (2) to all lithologies, and (3) with considerable precision. Either the production or decay of cosmogenic isotopes is used for the application of TCNs: the accumulation of TCNs will be used for surface exposure dating and their decay for burial dating. The total exposure from 100 a to 5 Ma of a given surface of archaeological origin can be determined by measuring the concentration of the required TCN with accelerator mass spectrometry. Burial time from ~0.1 to 5 Ma is determined by burial dating technique. Although these two types of applications have their own problems, a selective and precise discussion of the scientific and field context before and during sampling will minimize potential complications that may arise during the interpretation phase.

TCN tools, both surface exposure dating and burial dating, have, generally speaking, high potential for applications in the field of archaeology. If we assume that the total number of archaeological sites in the Eastern Mediterranean region is around 10,000 and if < 5% of these archaeological sites are suitable and available for the application of TCN analysis, then total the number of potential study applications will still number in the hundreds.

Acknowledgements

We would like to thank Dr. Frank Preusser at the University of Bern for his motivating suggestion to write this paper. We also thank Dr. Philip Hughes at the University of Manchester and Dr. Elisabetta Boaretto at the Department of Land of Israel Studies and Archaeology for their helpful comments and suggestions. We are grateful to Heather Murray and Sally Lowick at the University of Bern for her kind help

during the preparation of this paper. This study was funded by the Swiss National Science Foundation (Project No. 200001-111878).

References

BEDRANIK, R.G. (1995a): The age of Côa valley petroglyphs in Portugal. – Rock Art Research, 12: 86-103.

BEDRANIK, R.G. (1995b): Côa Valley rock art analytical research program. Report to Portuguese government, 28 June 1995.

BEDRANIK, R.G. (1995c): Côa Valley petroglyphs: an obituary to the stylistic dating of Paleolithic rock-art. – Antiquity, 69: 877-883.

BEDRANIK, R.G. (1998): Cosmogenic radiation nuclides in archaeology: a response to Phillips et al. – Antiquity, 72: 811-815.

BENEDETTI, L., FINKEL, R., KING, G., ARMIJO, R., PAPANASTASSIOU, D., RYERSON, F., FLERIT, F.J., FABER, D. & STAVRAKAKIS, G. (2003): Motion on Kaparelli fault (Greece) prior to the 1981 earthquake sequence determined from ^{36}Cl cosmogenic dating. – Terra Nova, 15: 118-124.

BIERMAN, P.R., MARSELLA, K.A., PATTERSON, C., DAVIS P.T. & CAFFEE, M. (1999): Mid-Pleistocene cosmogenic minimum-age limits for pre-Wisconsinan glacial surfaces in southwestern Minnesota and southern Baffin island: a multiple nuclide approach. – Geomorphology, 27: 25-39.

BIERMAN, P.R., CAFFEE, M.W., DAVIS, P.T., MARSELLA, K., PAVICH, M., COLGAN, P., MICKELSON, D. & LARSEN, J. (2002): Rates and timing of earth surface processes from in-situ produced cosmogenic ^{10}Be. – Reviews in Mineralogy and Geochemistry, 50: 147-204.

BOARETTO, E., BERKOVITS, D., HASS, M., HUI, S.K., KAUFMAN, A., PAUL, M. & WEINER, S. (2000): Dating of prehistoric caves sediments and flints using ^{10}Be and ^{26}Al in quartz from Tabun Cave (Israel): Progress report. – Nuclear Instruments and Methods in Physics Research Section B: Beam Interactions with Materials and Atoms, 172: 767-771.

BRINER, J.P., GOSSE, J.C. & BIERMAN, P.R. (2006): Applications of cosmogenic nuclides to Laurentide Ice Sheet history and dynamics. – Geological Society of America Special Paper, 415: 29-42.

CERLING, T.E., CRAIG, H. (1994): Geomorphology and in-situ cosmogenic isotopes. – Annual Reviews of Earth and Planetary Sciences, 22: 273-317.

CLARK, J.D., BEYENE, Y., WOLDEGABRIEL, G., HART, W.K., RENNE, P.R., GILBERT, H., DEFLEUR, A., SUWA, G., KATOH, S., LUDWIG, K.R., BOISSERIE, J.R., ASFAW, B. & WHITE, T.D. (2003): Stratigraphic, chronological and behavioural contexts of Pleistocene Homo sapiens from Middle Awash, Ethiopia. – Nature, 423: 747-752.

CLARKE, R.J., PARTRIDGE, T.C., GRANGER, D.E. & CAFFEE, M.W. (2003): Dating the Sterkfontein fossils. – Science, 301: 596-597.

DEHNERT, A. & SCHLÜCHTER, C. (2008): Sediment burial dating using terrestrial cosmogenic nuclides. – Quaternary Science Journal (Eiszeitalter und Gegenwart), 57/1-2: 210-225.

FABEL, D., STROEVEN, A.P., HARBOR, J., KLEMAN, J., ELMORE, D. & FINK, D. (2002): Landscape preservation under Fennoscandian ice sheets determined from in situ produced Be-10 and Al-26. – Earth and Planetary Science Letters, 201: 397-406.

FARLEY, K.A, CERLING, T.E. & FITZGERALD, P.G. (2001): Cosmogenic He-3 in igneous and fossil tooth enamel fluorapatite. – Earth and Planetary Science Letters, 185: 7-14.

GONZALEZ, S., CONCEPCION, J.L., HEDGES, R., HUDDART, D., OHMAN, J.C., TURNER, A. & POMPA Y PADILLA, J.A. (2003): Earliest Humans in the Americas: new evidence from Mexico. – Journal of Human Evolution, 44: 379-387.

GOSSE, J.C. & PHILLIPS, F.M. (2001): Terrestrial in situ cosmogenic nuclides: theory and application. – Quaternary Science Reviews, 20: 1475–1560.

GRANGER, E.D. & MUZIKAR, P.F. (2001): Dating sediment burial with in situ-produced cosmogenic nuclides: theory, techniques, and limitations. – Earth and Planetary Science Letters, 188: 269-281.

HEIMSATH, A.M., DIETRICH, W.E., NISHIIZUMI, K. & FINKEL, R.C. (1997): The soil production rate function and landscape equilibrium. – Nature, 388: 358-361.

HOFMANN, H.J., BEER, J., BONANI, G., VON GUNTEN, H.R., RAMAN, S., SUTER, M., WALKER, R.L., WOÖFLI, W. & ZIMMERMANN, D. (1987): ^{10}Be: Half-life and AMS-standards. – Nuclear Instruments and Methods in Physics Research B, 29: 32-36.

IVY-OCHS, S. & KOBER, F. (2007): Cosmogenic nuclides: a versatile tool for studying landscape change during the Quaternary. – Quaternary Perspectives, 16: 134–138.

IVY-OCHS, S. & KOBER, F. (2008): Surface Exposure Dating with Cosmogenic Nuclides. – Quaternary

Science Journal (Eiszeitalter und Gegenwart), 57/1-2: 179-209.

Ivy-Ochs, S., Wüst, R., Kubik, P.W., Müller-Beck, H. & Schlüchter, C. (2001): Can we use cosmogenic isotopes to date stone artifacts? – Radiocarbon, 43: 759-764.

Ivy-Ochs, S., Kerschner, H., Reuther, A., Maisch, M., Sailer, R., Schaefer, J., Kubik, P. W., Synal, H.-A. & Schlüchter, C. (2006): The timing of glacier advances in the northern European Alps based on surface exposure dating with cosmogenic ^{10}Be, ^{26}Al, ^{36}Cl, and ^{21}Ne. – Geological Society of America Special Paper, 415: 43-60.

Klein, J., Giegengack, R., Middleton, R., Sharma, P., Underwood Jr., J.R. & Weeks, W.A. (1986): Revealing histories of exposure using in-situ produced ^{26}Al and ^{10}Be in Libyan desert glass. – Radiocarbon, 28: 547-555.

Lal, D., (1988): In situ-produced cosmogenic isotopes in terrestrial rocks. – Annual Review of Earth and Planetary Sciences, 16: 355-388.

Lal, D. & Peters, B. (1967): Cosmic ray produced radioactivity on the earth. - In: Sitte, K. (ed.): Handbuch der Physik: 551-612; Berlin (Springer).

Licciardi, J.M., Kurz, M.D., Clark, P.U. & Brook, E.J. (1999): Calibration of cosmogenic ^{3}He production rates from Holocene lava flows in Oregon, USA, and effects of the Earth's magnetic field. – Earth and Planetary Science Letters, 172: 261-271.

Molodkov, A. (2001): ESR dating evidence for early man at a Lower Palaeolithic cave-site in the Northern Caucasus as derived from terrestrial mollusc shells. – Quaternary Science Reviews, 20: 1051-1055.

Muzikar, P. & Granger, D. (2006): Combining cosmogenic, stratigraphic, and paleomagnetic information using a Bayesian approach: General results and an application to Sterkfontein. – Earth and Planetary Science Letters, 243: 400-408.

Niedermann, S. (2000): The ^{21}Ne production rate in quartz revisited. – Earth and Planetary Science Letters, 183: 361-364.

Nishiizumi, K., Kohl, C.P., Shoemaker, E.M., Arnold, J.R., Klein, J., Fink, D. & Middleton, R. (1991): In situ ^{10}Be – ^{26}Al exposure ages at Meteor Crater, Arizona. – Geochimica et Cosmochimica Acta, 55: 2699-2703.

Partridge, T.C., Granger, D.E., Caffee, M.W., Clarke, R.J. (2003): Lower Pliocene hominid remains from Sterkfontein. – Science, 300: 607-612.

Phillips, F.M., Montgomery, F., Elmore, D. & Sharma, P. (1997): Maximum ages of the Côa valley (Portugal) engravings measured with Chlorine-36. – Antiquity, 71: 100-104.

Phillips, F.M., Zreda, M.G., Smith, S.S., Elmore, D., Kubik, P.W., Dorn, R.I. & Roddy, D.J. (1991): Age and geomorphic history of Meteor Crater, Arizona, from cosmogenic ^{36}Cl and ^{14}C in rock varnish. – Geochimica et Cosmochimica Acta, 55: 2695-2698.

Phillips, W.M., Hall, A.M., Mottram, R., Fifield, L.K. & Sugden, D.E. (2006): Cosmogenic Be-10 and Al-26 exposure ages of tors and erratics, Cairngorm Mountains, Scotland: Timescales for the development of a classic landscape of selective linear glacial erosion. – Geomorphology, 73: 222-245.

Putkonen, J. & Swanson, T. (2003): Accuracy of cosmogenic ages for moraines. – Quaternary Research, 59: 255– 261.

Reedy, R.C., (1987): Nuclide production by primary cosmic-ray protons. – Journal of Geophysical Research, B, Solid Earth and Planets, 92: 697-702.

Ritz, J.-F., Vassallo, R., Braucher, R., Brown, E.T., Carretier, S. & Bourlès, D. (2006): Using in situ–produced ^{10}Be to quantify active tectonics in the Gurvan Bogd mountain range (Gobi-Altay, Mongolia). – Geological Society of America Special Paper, 415: 87-110.

Roberts, N. (1998): The Holocene. – 316 p.; Oxford (Blackwell Publishing).

Samworth, E.A., Warburto, E.K., Engelber, G.A. (1972): Beta-Decay of Al-26 Ground State. – Physical Review, C5: 138- 142.

Schaller, M., von Blanckenburg, F., Hovius, N. & Kubik, P.W. (2001): Large-scale erosion rates from in situ-produced cosmogenic nuclides in European river sediments. – Earth and Planetary Science Letters, 188: 441-458.

Schaller, M., Hovius, N., Willet, S.D., Ivy-Ochs, S., Synal, H.-A. & Chen, H.-C. (2005): Fluvial bedrock incision in the active mountain belt of Taiwan from in situ-produced cosmogenic nuclides. – Earth Surface Processes and Landforms, 30: 955-971.

Shen, G., Ku, T.L., Cheng, H., Edwards, R.L., Yuan, Z. & Wang, Q. (2001): High-precision U-series dating of Locality 1 at Zhoukoudian, China. – Journal of Human Evolution, 41: 679-688.

Stone, J.O. (2000): Air pressure and cosmogenic isotope production. – Journal of Geophysical Research – Solid Earth, 105: 23753–23759.

Stuart, F.M. (2001): In situ cosmogenic isotopes:

principles and potential for archaeology. – In: BROTHWELL, D.R. & POLLARD, A.M. (eds.): Handbook of Archaeological Sciences: 93-100; Chichester (John Wiley and Sons).

VALLADAS, H., MERCIER, N., JORON, J.L., MCPHERRON, S.P., DIBBLE, H.L. & LENOIR, M. (2003): TL dates for the Middle Paleolithic site of Combe-Capelle Bas, France. – Journal of Archaeological Science, 30: 1443-1450.

VERMEESCH, P. (2007): CosmoCalc: An Excel add-in for cosmogenic nuclide calculations. – Geochemistry Geophysics Geosystems, 8: Art. No. Q08003.

VERRI, G., BARKAI, R., BEN-DOV, Y., BOARETTO, E., BORDEANU, C., GOPHER, A., HASS, M., PAUL, M. & WEINER, S. (2002): ^{10}Be measurements on Neolithic and Paleolithic flint tools from Israel. –Geochimica et Cosmochimica Acta, 66: 805.

VERRI, G., BARKAI, R., BORDEANU, C., GOPHER, A., HASS, M., KAUFMAN, A., KUBIK, P.W., MONTANARI, E., PAUL, M., RONEN, A., WEINER, S. & BOARETTO, E. (2004): Flint mining in prehistory recorded by in situ-produced cosmogenic ^{10}Be. – PNAS, 101: 7880-7884.

VERRI, G., BARKAI, R., GOPHER, A., HASS, M., KUBIK, P.W., PAUL, M., RONEN, A., WEINER, S. & BOARETTO, E. (2005): Flint procurement strategies in the Late Lower Palaeolithic recorded by in situ produced cosmogenic ^{10}Be in Tabun and Qesem Caves (Israel). – Journal of Archaeological Science, 32: 207-213.

WALKER, M.J.C. (2005): Quaternary Dating Methods. – 286 pages; Chichester (John Wiley and Sons).

WATCHMAN, A. (1995): Recent petroglyphs, Foz Côa, Portugal. – Rock Art Research, 12: 104-108.

WATCHMAN, A. (1996): A review of the theory and assumptions in the AMS dating of the Foz Côa petroglyphs, Portugal. – Rock art Research, 13: 21-30.

WATCHMAN, A. (1998): Some observations on the radiocarbon and cosmogenic dating of petroglyphs, Foz Côa, Portugal. – Antiquity, 72: 197-200.

WILLIAMS-THORPE, O., JENKINS, G.D., JENKINS, J. & WATSON, J.S. (1995): Chlorine-36 dating and the bluestones of Stonehenge. – Antiquity, 69: 1019–1020.

ZILHÃO, J. (1995): The stylistically Paleolithic petroglyphs of the Côa valley (Portugal) are of Paleolithic age: a refutation of their 'direct dating' to recent times. – Antiquity, 69: 883-901.

Eiszeitalter und Gegenwart Quaternary Science Journal	57/1–2	239–252	Hannover 2008

The handling of numerical ages and their random uncertainties

Mebus A. Geyh*)

Abstract: The correct handling of numerical ages and their standard deviations and a proper introduction to error propagation or propagation of uncertainty and statistical evaluation are important to avoid misleading chronological conclusions and statements even though based on properly determined and reliable numerical dates. The conclusions may also be erroneous if dates were taken from databases without sufficient background information on the origin of the dated material and the applied analytical techniques. This paper is an introduction into the field of mathematical handling and testing of numerical ages. The most common and simple calculations and statistical tests that are needed are described and the steps involved are demonstrated on examples. The problems involved in the visualization of numerical dates in the form of normal histograms and dispersion histograms are discussed.

[Der Gebrauch numerischer Alter und ihre Standardabweichungen]

Kurzfassung: Die korrekte Auswertung numerischer Alter mit ihren Plus-Minus-„Fehlerangaben" oder besser Standardabweichungen und die Anwendung der damit verbundenen statistischen Auswerteverfahren sind für Geowissenschaftler und Geographen oft eine schwierige Aufgabe, weil ihnen dafür die Ausbildung fehlt. Entsprechend finden sich in der Literatur viele nur schwer nachvollziehbare geochronologische Folgerungen. Sie können allerdings auch dann falsch sein, wenn sie sich auf Ergebnisse aus Datenbanken ohne ausreichende Angaben über den Ursprung des datierten Materials und die angewandten analytischen Techniken beziehen. Diese Arbeit führt in die Beurteilung und Handhabung numerischer Altersangaben ein. Mit ihr können elementare Rechnungen und einfache statistische Tests korrekt ausgeführt werden. Entsprechende Beispiele veranschaulichen den Weg dazu. Die mit der Visualisierung von numerischen Altern in Form von einfachen und Dispersions-Histogrammen verbundenen Probleme werden diskutiert.

Keywords: numerical ages, propagation of uncertainty, histogram

1 Introduction

Owing to the growing number of databases open to the public and the increasing production of numerical ages using different dating methods and semi-automated equipment. Quaternary scientists are thus faced with the task of handling large sets of numerical ages with their random uncertainties rather than dealing with single numerical ages. Reliability checks based only on the values themselves are indispensable as in many cases information on the dated material and the analytical techniques is insufficient or not accessible.

Unqualified handling of numerical ages may result in conspicuously erroneous scientific conclusions. An example is a statistically evaluated cycle in the formation of speleothem and calcareous tufa in Europe which appeared to correlate with the 25-ka cycle of the precession of the Earth's axis (Brunnacker & Hausmann 1987; Geyh 1991). Reliable calculation of error

*Address of author: M. A. Geyh, Rübeland 12, 29308 Winsen/Aller, Germany,
E-Mail: Mebus.geyh@t-online.de

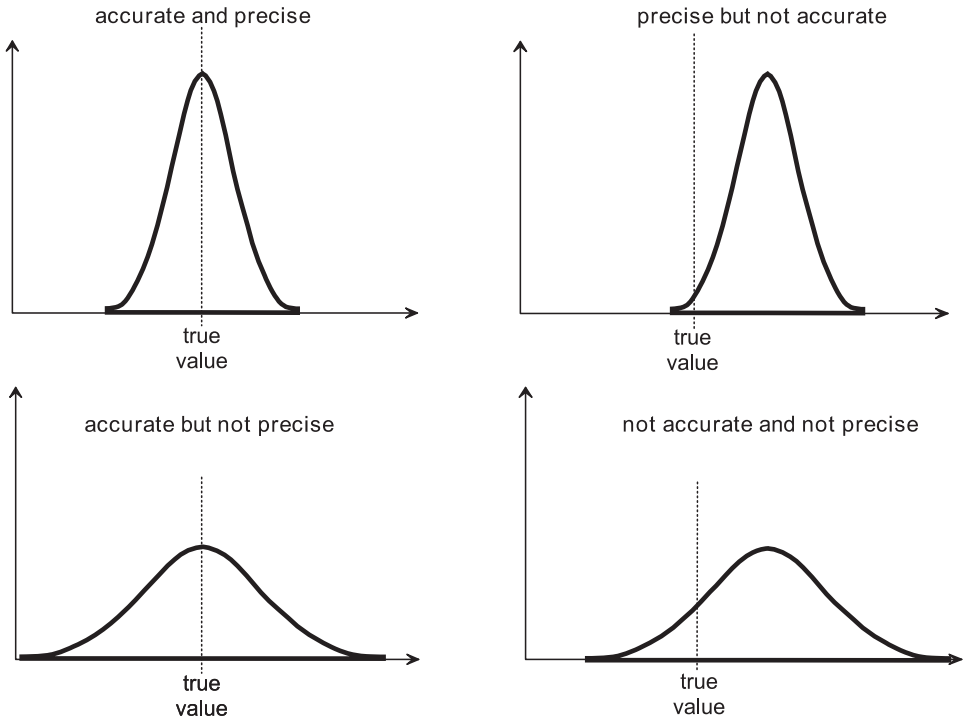

Fig. 1. The meanings of accuracy and precision: Accuracy describes the approximation of a mean to the „true" value; precision is a measure of the reproducibility of a result.

Abb. 1. Bedeutung von Genauigkeit und Präzision: Genauigkeit beschreibt die Annäherung an den „wahren" Wert. Die Präzision ist ein Maß für die Reproduzierbarkeit eines Ergebnisses.

propagation avoids such conclusions and also allows manipulated numerical ages to be identified (GEYH 1991). This paper provides the basics necessary for proper mathematical treatment of geochronological and analytical data of any origin with their random uncertainties. Complicated mathematical functions are not discussed. This paper uses the terminology of HUNTLEY (2001) in which „age" refers to a range of time something has existed, while a „date" is a particular time on a time scale. The functions given below are valid for any data, not only numerical ages.

2 Precision, accuracy and reporting of data

Precision and accuracy have distinct meanings as illustrated in Figure 1.

1) The *precision* of a result is a measure of the reproducibility of an observation and corresponds to the *uncertainty* of a result. It is expressed as random error or *random uncertainty* and is mainly determined by the analytical technique and equipment used.
2) The *accuracy* is a measure of the correctness of an observed value and its approximation to the „true" value. It depends on a large number of often unknown systematic errors, which may be eliminated by carrying out routine measurements on standard materials. Aliquots of the same set of samples of different standard materials are analyzed by laboratories throughout the world and the results compared. Reducing systematic errors increases the accuracy rather than the precision.

The expression ± σA is termed *random* or *statistical uncertainty* and has to be distinguished from *systematic errors*. A *systematic error* arises from a specific physical or chemical

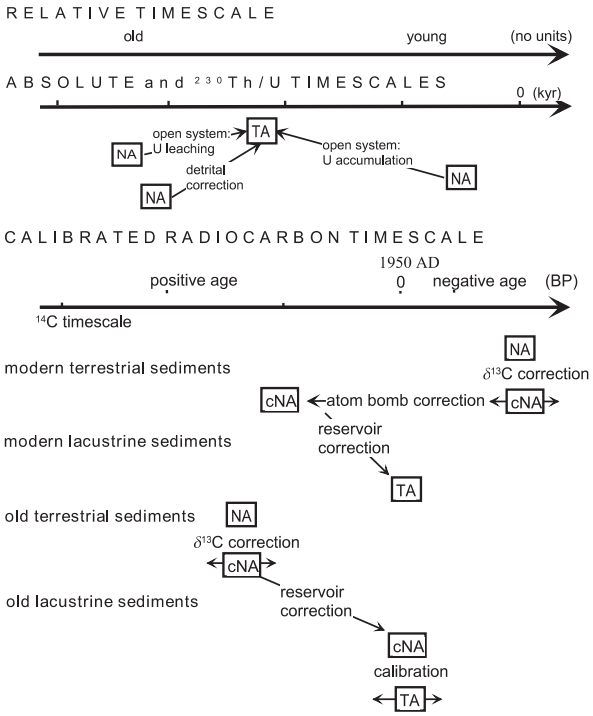

Fig. 2. Scheme for the correction and calibration of radiometric and mass spectrometric ^{14}C and $^{230}Th/U$ ages, in order to correlate them with the absolute time scale (Geyh & Grosjean 2000). TA – true age; NA – numerical age, cNA – corrected numerical age

Abb. 2. Schematische Darstellung der Korrektur und Kalibration radiometrischer und massenspektrometrischer ^{14}C- und $^{230}Th/U$-Alter zur Korrelation mit der absoluten Zeitskala (Geyh & Grosjean 2000). TA – wahres Alter; NA – numerisches Alter, cNA – korrigiertes numerisches Alter

process, only changing the measured values in one direction or the other. If the process is understood and the relevant parameters are known, the result can be corrected. As an example, the relevant processes that affect ^{14}C and $^{230}Th/U$ ages are shown in Figure 2. Contamination with material older than the sample to be dated (e.g. with coal, fossil lime or detrital thorium) increases ^{14}C and $^{230}Th/U$ ages, respectively. Five percent matter containing no radiocarbon increases the ^{14}C ages by around 400 years. The same amount of uranium of a material in which the ^{238}U series is in radioactive equilibrium will increase the $^{230}Th/U$ ages by around 5000 years. A correction of these ages is possible if the proportion of the contaminating material is known.

The conventional rules for reporting of quantitative data are often neglected. One rule is that any quantitative result should be accompanied by a statement of the intrinsic uncertainty. The *precision of the random uncertainty* (the measure of its uncertainty) is usually not better than ± 10 %. An example illustrates this rule. A random uncertainty of ± 213 a has an uncertainty of about ± 21 a. Hence, it is reasonable to report the uncertainty as ± 210 a rather than ± 213 a. This means that the uncertainty should be rounded to two digits only (Taylor & Kuyatt 1994). Another rule is that a set of values should always have the same number of places behind the decimal point. Hence, an age of 2.87 ± 0.20 ka should not be given as 2.87 ± 0.2 ka. This rule is especially important for the compilation of data in a table. Another rule is that only the final result should be rounded off rather than the values used in a calculation.

3 Numerical age, random uncertainty and frequency distribution

Any geochronological framework has to be based on numerical ages determined with suitable physical dating methods (GEYH & SCHLEICHER 1990; WAGNER 1998; GEYH 2005). The resulting ages are often inappropriately termed „absolute" ages. If an age date is obtained, for example, from stratigraphic or palynological studies it is a relative age. Physical age dating also does not yield absolute ages; the results are better called „numerical ages". The term absolute age should be reserved only for age dates related to the solar time scale.

The collected samples have to fulfill numerous criteria to be suitable for reliable dating. Different kinds of numerical ages have to be corrected for different sources of systematic error (e.g., ^{14}C ages for contamination, reservoir effect, and ^{13}C isotope fractionation; and $^{230}Th/U$ ages for detrital ^{230}Th; e.g., GEYH & GROSJEAN 2000; Fig. 2)

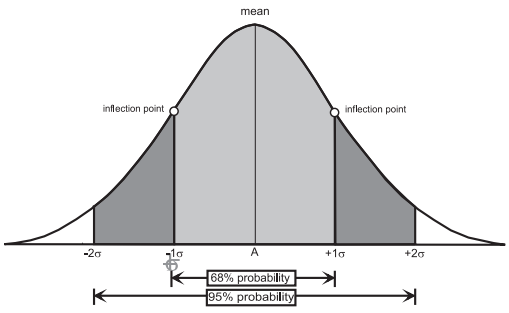

Fig. 3. Gaussian frequency distribution (also bell-shaped curve, normal distribution): The 1-sigma confidence interval lies between the two inflection points of the frequency distribution. The light gray area corresponds to nearly 68 % of the total area, the 2-sigma confidence interval represents a probability of about 95 %.

Abb. 3. Gauß'sche Häufigkeitsverteilung (auch Glockenkurve, Normalverteilung): Das 1-Sigma Vertrauensintervall liegt zwischen den beiden Wendepunkten der Glockenkurve. Die graue Fläche entspricht nahezu 68 % der Gesamtfläche, das 2-Sigma Vertrauensintervall repräsentiert eine Wahrscheinlichkeit von 95 %.

and in the case of dating with cosmogenic isotopes calibration is needed (e.g., ^{14}C dates). This is particularly important when numerical ages obtained from different materials and methods are compared with each other and/or with the absolute time scale (GEYH & SCHLEICHER 1990; WAGNER 1998; GEYH 2005).

When dealing with numerical ages, it is very important to understand the meaning of the common expression $A \pm \sigma A$, e.g., 2000 ± 50 a before present (BP). *Standard deviation*, 1-sigma interval, random uncertainty, and statistical uncertainty are used as synonyms for $\pm \sigma A$. It defines the precision of the calculated value, and represents a frequency distribution. Theoretically it is assumed that the age of the sample was determined an *infinite* number of times. In practice, however, the standard deviation is precisely determined on the basis of a *finite* number of measurements. The ages determined on the same sample deviate from each other, even under most exacting measurement conditions, and scatter around a mean value Â, which is assumed to approximate the „true" age of the sample. The frequency distribution of values is obtained by plotting all these values with the x-axis representing „age" and the y-axis representing the frequency of occurrence of each value. The resulting curve looks like a vertical cut through a bell and is know as a *Gaussian distribution*, *normal distribution* or *bell-shaped curve* (Fig. 3). It is symmetrical around the *mean* value of all values.

In reality only a finite number of results are available and the frequency distribution is not perfectly symmetrical. In this case the curve peak is given by the median rather than the mean. It divides a frequency distribution into two equal areas. This case will, however, not be discussed here as it is of minor importance in geochronological studies due to the relatively small number of ages obtained from coeval samples.

The area enclosed by the bell-shaped curve, extended to infinity in both directions, represents the total number of values or 100 % probability. The area between the two inflection points, shown in light grey, contains nearly 68 % of all values (68 % probability) (*1-sigma interval* or

1σ confidence interval). The 2-sigma confidence interval contains approximately 95 % of all values (95 % probability), corresponding to a probability of error of 5 %. Hence, one and two sigma means that 2 out of 3 or 19 out of 20 results fit the 1σ and 2σ confidence intervals, respectively, provided a sufficiently large number of ages from coeval samples are available. The 1σ confidence interval for the age A = 2000 ± 50 BP is 1950 BP to 2050 BP; one third of the values should be greater or smaller than these two values (2050 > A > 1950 BP).

The convention in science and engineering is to give the 1-sigma confidence interval for the uncertainty of a value. An exception is mass spectrometric ages in geochronology, for which the uncertainty is often given as the 2-sigma confidence interval.

The decision whether the 1-sigma or 2-sigma confidence interval is used depends on the question to be answered. An increase of the width of the confidence interval enlarges the probability that the true age is included, but it decreases the ability to distinguish two ages or to decide whether they belong to the same or different frequency distributions. Thus, it is indispensable to state in each publication whether the given uncertainty is 1σ or 2σ.

An example demonstrates this case. Two ages of 1850 ± 50 a and 2000 ± 50 a do not appear to belong to coeval samples due to the gap of 150 a between the 1σ confidence limits. In contrast, samples with the same ages but twice as large standard deviations – 1850 ± 100 a and 2000 ± 100 a – might have been considered as coeval as their confidence intervals overlap. The next chapter describes how such cases are correctly handled.

4 Arithmetic and weighted means

The *arithmetic mean* age Â (normally simply called the mean) of a set of n numerical ages (A_1 to A_n) with the same precision is given by the following equation:

$$\overline{A} = \frac{\sum_i^n A_i}{n}. \qquad (1)$$

The *standard deviation* σA *of the age values* A_i in a set of ages A is calculated as follows:

$$\sigma A = \pm\sqrt{\frac{\sum_{i=1}^{n}\left(\overline{A} - A_i\right)^2}{(n-1)}}. \qquad (2)$$

Using the three ages 2000 ± 50 a, 2050 ± 50 a and 2200 ± 100 a as an example, Equations 1 and 2 yield (for which the standard deviations of the individual ages are not used) a mean and standard deviation of 2083 ± 104 a. As explained above, this has to be reported as 2080 ± 100 a. (Contrary to the conventional rule for reporting values given in Chapter 2, the values and their uncertainties in this paper are given as calculated and not as they should be reported. This enables the reader to follow the calculations with the corresponding equations).

The larger the number of ages determined for the same sample, the higher the probability that the calculated mean approximates the „true" age. This is reflected in the standard deviation of the mean (σÂ), which decreases with $\sqrt{n}$ as follows:

$$\sigma\overline{A} = \frac{\sigma A}{\sqrt{n}} = \pm\sqrt{\frac{\sum_{i=1}^{n}(\overline{A} - A_i)^2}{n\cdot(n-1)}}. \qquad (3)$$

Our example yields ± 60 a, while that of a single measurement is ± 104 (Eq. 2).

Numerical age values usually have differing precision, requiring the introduction of a *weighting factor w*. It is calculated from the standard deviation as follows:

$$w_i = \frac{1}{\sigma A_i^{\,2}}. \qquad (4)$$

The weighting factors of our example given above are 0.0004, 0.0004 and 0.0001, respectively. This means the weighting factor for the two ^{14}C ages with a precision of ± 50 years is four times larger than the weighting factor of the ^{14}C age with a precision of ± 100 years. This is not only a mathematical artifact. The third radiometric ^{14}C measurement required four times the time needed for the first two.

x	y	sy	y-sy	y+sy
0,00	3,0	0,50	2,50	3,50
0,05	3,1	0,48	2,62	3,58
0,10	3,2	0,45	2,75	3,65
0,15	3,3	0,43	2,87	3,73
0,20	3,4	0,40	3,00	3,80
0,25	3,5	0,38	3,12	3,88
0,30	3,6	0,36	3,24	3,96
0,35	3,7	0,33	3,37	4,03
0,40	3,8	0,31	3,49	4,11
0,45	3,9	0,29	3,61	4,19
0,50	4,0	0,27	3,73	4,27
0,55	4,1	0,25	3,85	4,35
0,60	4,2	0,23	3,97	4,43
0,65	4,3	0,22	4,08	4,52
0,70	4,4	0,21	4,19	4,61
0,75	4,5	0,20	4,30	4,70
0,80	4,6	0,19	4,41	4,79
0,85	4,7	0,19	4,51	4,89
0,90	4,8	0,19	4,61	4,99
0,95	4,9	0,19	4,71	5,09
1,00	5,0	0,20	4,80	5,20

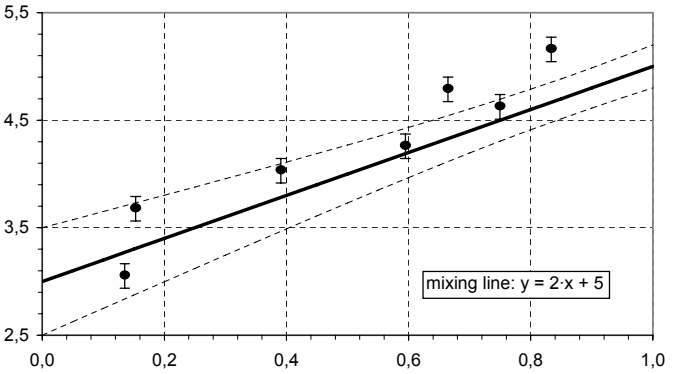

Fig. 4: Linear regression of values to obtain a binary mixing line.

Abb. 4: Lineare Regression von Werten, die einer Zweikomponenten-Mischgerade entsprechen.

The *weighted mean* $\hat{A}_w$ is obtained using the following equation:

$$(5) \qquad \overline{A}_w = \frac{\sum_{i=1}^{n} A_i \cdot w_i}{\sum_{i=1}^{n} w_i} = \frac{\sum_{i=1}^{n} A_i / \sigma A_i^2}{\sum_{i=1}^{n} 1 / \sigma A_i^2}.$$

Equation 5 reduces to Equation 1 if the measurements were done with the same precision: w_i = constant.

The *standard deviation of the weighted mean* $\sigma\hat{A}_w$ is obtained by

$$(6) \qquad \sigma \overline{A}_w = \pm \sqrt{1 / \sum_{i=1}^{n} w_i}.$$

The weighted mean of our example yields 2044 ± 33 a (to be reported as 2040 ± 30 a), deviating by 35 years from the arithmetic mean of 2083 ± 104 a (to be reported as 2080 ± 100 a) given above. The weighted mean and its standard deviation are shifted towards the more precise results.

Analogous to Equation 3 the *weighted mean standard deviation of a single value* is given by

$$(7) \qquad \sigma A_w = \sqrt{n} \cdot \sigma \overline{A}_w.$$

The example yields ± 57 years.

According to Equations 3 and 6 the precision of the mean values $\sigma\hat{A}$ and $\sigma\hat{A}_w$ theoretically approaches zero for an infinite number of ages. In reality the precision has an (often unknown) upper limit resulting from the technical limitations of the method: for example, varying contamination of coeval samples that cannot be removed and slightly deviating measurement conditions (temperature, differing calibration of the equipment in different laboratories, impure chemical reagents, etc.). Ages above the upper limit of the method are given, for example, as >40,000 a. They express the minimum age of a sample or the maximum age which can be determined by the method.

5 Chi square test

Calculation of the arithmetic or weighted means $\hat{A}$ or $\hat{A}_w$ of a set of n ages $A_i \pm \sigma A_i$ makes sense only if the σA_i values were determined for coeval samples and therefore belong to the same frequency distribution. To test for this, there are two alternative but equivalent mathematical approaches:

a) The uncertainty ± σA of the ages is calculated using Equation 2 and compared with the standard deviation σA_w of a single measure-

ment (Eq. 7). The *uncertainty of ages of different precision* is obtained (in analogy to Eq. 2) as follows:

$$(8) \qquad \sigma A_g = \pm \sqrt{\frac{\sum_{i=1}^{n} (\overline{A_w} - A_i)^2 \cdot w_i}{(1 - 1/n) \cdot \sum_{i=i}^{n} w_i}} .$$

It is permissible to calculate the mean Â only if σ*A* (Eq. 2) or σA_g (Eq. 8) is more or less equal to σA_w (Eq. 7). Our example yields ± 57 a, ± 56 a and ± 104 a, respectively. Hence, the first two standard deviations differ so much from σA_w that the samples cannot be considered to be coeval and the mean should not be calculated.

b) χ^2 test

χ^2 is obtained as follows:

$$(9) \qquad \chi^2 = \sum_{i=1}^{n} \left(\overline{A} - A_i\right)^2 \cdot w_i$$

$$\chi_w^2 = \sum_{i=1}^{n} w_i \cdot A_i^2 - \frac{\left(\sum_{i=1}^{n} w_i \cdot A_i\right)^2}{\sum_{i=1}^{n} w_i} .$$

A mean can be calculated only if χ^2 and $\chi^2_w \approx$ n-1 for n < 15. For n > 15 the χ^2 value can be taken from any textbook on statistics (e.g., SACHS 1999). Our example yields $\chi^2 = 4.4$ and $\chi^2_w = 3.2$, confirming the three ages do not belong to the same frequency distribution and thus a mean value would have no validity.

6 Error propagation: difference, rates, mathematical function

There are tasks for which more or less complicated mathematical functions are necessary, e.g., $y = f(x_i \ldots)$. Such functions have a dependent variable y and one or more independent variables $x_1, \ldots x_i, \ldots . x_n$. The most simple case is calculation of the difference between two ages which equals the duration of a process. More complicated is, for example, calculation of the sedimentation rate for a certain time interval (Eq. 11). If the uncertainties for the independent variables σx_i are known, the standard deviation of the dependent variable σy can be calculated using Equation 10.

The standard deviation σ*f* of the function $f(x_1, x_2 \ldots x_n)$ is calculated by the law of propagation of uncertainty:

$$(10) \qquad \sigma f(x_1,\ldots,x_n)^2 = \left(\frac{\partial f}{\partial x_1}\right)^2 \cdot \sigma x_1^{\,2} + \ldots + \left(\frac{\partial f}{\partial x_n}\right)^2 \cdot \sigma x_n^2 .$$

When geological sections are studied, deposition periods and sedimentation rates *r* between two levels *a* and *b* (e.g., at a depth of 100 and 150 cm and ages of 2000 ± 50 and 2200 ± 100 years) are of interest. The function is given by:

$$(11) \qquad r = \frac{b - a}{A_2 - A_1} .$$

To solve this equation, the difference *S* between two ages ($A_2 - A_1$ = 2200 ± 100 – 2000 ± 50 years) has to be calculated. Neglecting the standard deviation, this example yields a difference of 200 years and a sedimentation rate of 0.25 cm/a. The standard deviation of a *sum* $S = x_1 + x_2$ or a *difference* $\Delta = x_2 - x_1$ is obtained from Equation 12:

$$(12) \qquad \sigma S^2 = \sigma \Delta^2 = \left(\sigma x_1\right)^2 + \left(\sigma x_2\right)^2 .$$

Our example yields an age difference of 200 ± 112 years. The 1σ and 2σ confidence intervals are 88 to 312 and -24 to +424 years, respectively. The sample ages differ by at least 88 a with a 68 % probability (1σ), but they may be considered as similar with a probability of 95 % (2σ) because a negative age difference is meaningless.

Calculation of the deposition rate *r* involves a division and two subtraction steps. The corresponding formula involves both multiplication and division:

$$(13) \qquad y = \frac{x_1 \cdot x_2}{x_3} .$$

The standard deviation of y is obtained as follows:

$$(14) \quad \sigma y = \pm y \cdot \sqrt{\left(\frac{\sigma x_1}{x_1}\right)^2 + \left(\frac{\sigma x_2}{x_2}\right)^2 + \left(\frac{\sigma x_3}{x_3}\right)^2} .$$

This corresponding formula for σ*r* is derived from Equations 10 and 12. Assuming depths *a* and *b* were determined precisely (i.e., σ*a* = σ*b* = 0), the standard deviation of the deposition rate *r* is obtained by combining Equations 12 and 14 as follows:

$$\sigma r = \pm r \cdot \sqrt{\frac{\sigma A_1^2 + \sigma A_2^2}{(A_2 - A_1)^2}} \quad (15)$$

According to Equation 15, the standard deviation σ *r* decreases with increasing difference between the ages. The example yields 0.25 ± 0.14 cm/a. The result has 1σ and *2*σ confidence intervals (i.e., 68 % and 95 % probabilities) of 0.11 to 0.39 cm/a or 0 to 0.53 cm/a, respectively. Hence, the actual sedimentation rate can be smaller or greater than 0.25 cm/a by a factor of two.

It is worthwhile to note that the formulas for calculating numerical ages usually contain one or more physical parameters that are internationally agreed upon – half lives are an example. Although they were determined with a finite uncertainty, these uncertainties are not usually considered when the law of propagation of uncertainties is applied. Indeed they are not required as long as only numerical ages are compared with each other. But when the ages relate to the absolute time scale, the standard deviation has to include the uncertainties of the internationally agreed parameters and is usually larger than the standard deviation normally reported.

7 Regression analysis and least squares fit

Regression analyses are applied for prediction, testing of hypothesis, and modeling of causal relationships. Such analyses are carried out to determine correlations in numerical data consisting of values of the dependent variable y and the independent variables x_i of a function with one or more parameters, e.g., a and b in Equation (16). These parameters are adjusted to give a best fit of the function to the numerical data. This is usually done using the least squares method. Either the independent variable or the dependent variable is assumed to be a random variable with the uncertainty of the measurement. The other variable(s) is assumed to be error-free.

The simplest case is a linear function:

$$f(x) = y = b \cdot x + a \,. \quad (16)$$

Quadratic, exponential and other functions may be transformed into a linear function with a corresponding recalculation of the measured data. Both coefficients *a* and *b* are obtained by minimizing the sum of the squares of the deviation of the values y_i from a straight line (the uncertainty in *x* is assumed to be negligible). The equation is obtained by a least-squares fitting of a straight line to the data:

$$\sum \Delta y_i^2 = \sum \left[y_i - f(x_i) \right]^2 =$$

$$\sum \left[y_i - a - b \cdot x_i \right] = \min \,.$$

The values of the parameters *a* and *b* are calculated as follows:

$$\frac{\partial}{\partial a} \sum w_i \cdot \left(y_i - a - b \cdot x_i \right)^2 = 0 \quad \textit{and}$$

$$\frac{\partial}{\partial b} \sum w_i \cdot \left(y_i - a - b \cdot x_i \right)^2 = 0 \,.$$

Thus,

$$a = \left(\sum x_i^2 \cdot w_i \sum y_i \cdot w_i - \sum x_i \cdot w_i \cdot \sum x_i \cdot y_i \cdot w_i \right) / \Delta \quad (17)$$

$$b = \left(\sum w_i \cdot \sum x_i \cdot y_i \cdot w_i - \sum x_i \cdot w_i \cdot \sum y_i \cdot w_i \right) / \Delta \quad \textit{where}$$

$$\Delta = \sum w_i \cdot \sum x_i^2 \cdot w_i - \left(\sum x_i \cdot w_i \right)^2 .$$

The standard deviations of *a* and *b* are given by Equation 18 and shown in Fig. 4:

$$\sigma a = \pm \sqrt{\frac{1}{\Delta} \sum x_i^2 \cdot w_i} \quad (18)$$

$$\sigma b = \pm \sqrt{\frac{1}{\Delta} \sum w_i} \,.$$

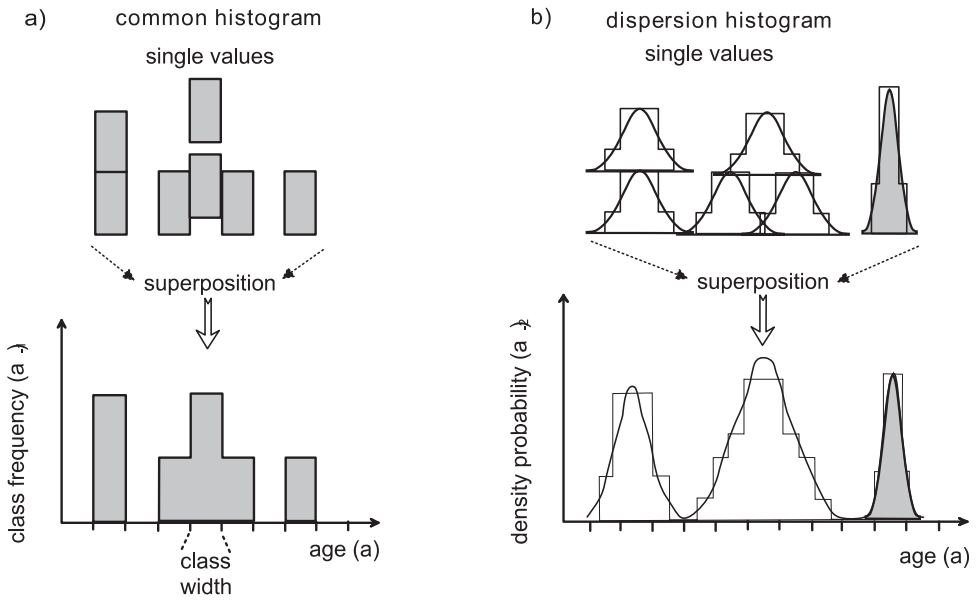

Fig. 5. a) Construction of a normal histogram of five ages based on rectangles, b) Construction of a dispersion histogram of five ages of low (white) and high (gray) precision based on polygons and bell curves, respectively.

Abb. 5. a) Konstruktion eines einfachen Histogramms mit Polygonen für fünf Alter, b) Konstruktion eines Dispersionshistogramms mit Polygonen und Glockenkurven für fünf ungenaue (weiß) und genaue (grau) Alter.

Many computer programs include a least-squares algorithm for fitting a straight line to the data. Often they can also handle composite curves consisting of the superposition of more than one function. A cubic spline can be used to fit a function to a data set. The parameter values of the function are individually chosen to obtain an optimum fit of a curve to all values or to smooth out irregularities in the curve.

8 Graphical presentation: normal and dispersion histograms

Visualization of the frequency distribution of data is often more instructive than a compilation of the data in tables. A *normal histogram* is the most simple way to present ages. The x-axis is assigned an age scale; the y-axis represents the frequency. The x-axis is divided into classes of an arbitrarily chosen width which depends on the age resolution or the average precision of the available values. Each value is represented by a rectangle with a given area and a class width as base length. All rectangles are superimposed above the x-axis (Fig. 5a). The enveloping curve represents the frequency distribution.

Ages with a mean sigma of ± 50 years (Eq. 7) may be optimally resolved with a class width of 50 years as the base length of the rectangle. If a larger class width is chosen, e.g., 200 years, the optimum age resolution is lost. The advantage of a larger class width is that the number of values per class is increased, which reduces the random scatter of the frequency distribution per class. The uncertainty in a class population is approximated by the square root of the number of values. For instance, four values per class yield $\pm\sqrt{4} = \pm 2$ or ± 50 % scatter, for nine dates we obtain $\pm\sqrt{9} = \pm 3$ or ± 33 %. As a consequence, the data density per

class governs the random fluctuation of the frequency distribution. If it is small, only minima rather than peaks provide reliable information. The random uncertainty of the histogram peaks may be larger than the actual fluctuations of the frequency of values per class. In contrast, lows always represent periods of missing values, which is why only they allow an unambiguous interpretation of a histogram. They may mirror, for example, arid periods without groundwater recharge, glacial periods without growth of trees, or periods of intensive erosion (see also Section 9.1).

A *dispersion histogram* (GEYH 1969; MICHCZYNSKA & PAZDUR 2004) provides an alternative visualization of values. A polygon or, even better, a bell-shaped curve with an area representing one value replaces the rectangle of the normal histogram. The width of the area is related to the standard deviation. As the area is constant, its height is determined by the chosen width or standard deviation. Hence, a precise value yields a polygon or bell curve with a short baseline and large height, while a less precise value is represented by a wide baseline and low height (Fig. 5b top).

In a dispersion histogram, the precision of an age represented by its weighting factor w (Eq. 4) is taken into account. Hence, the y-axis represents a density probability function with the dimension of 1/(time unit)^2 rather than the class frequency with the dimension 1/(time unit) (MICHCZYNSKA & PAZDUR 2004).

There is a special problem with histograms of ^{14}C ages. The time scale is distorted with respect to the solar or absolute time scale. In certain time periods, ^{14}C years are systematically compressed with respect to the solar time scale, in others they are stretched out. This means in the case of a uniform frequency distribution of samples along the absolute time scale that the corresponding ^{14}C histogram may show apparent peaks and lows (GEYH 1980; Fig. 6). In contrast to what is expected, the distortion of the histogram does not disappear if calibrated age intervals are used instead of the ^{14}C ages. Modern calibration programs (e.g., Cal 125 Groningen Radiocarbon Calibration Program) allow the automated construction of histograms with the calibrated ^{14}C time scale and overcomes the intrinsic problem of calibration of single values.

9 Two case studies

Two case studies are presented which may demonstrate the value of a correct statistical evaluation of ages. It is not the intention of this paper to become involved in the geological aspects of the cited papers or problems inherent in dating methods used. Here, it is mainly considered whether correct handling of the ages gives another numerical result than discussed in the papers.

In the first case study, evidence is provided that increasing the number of numerical age values may not increase the precision of the obtained values. In the second case study, it becomes ob-

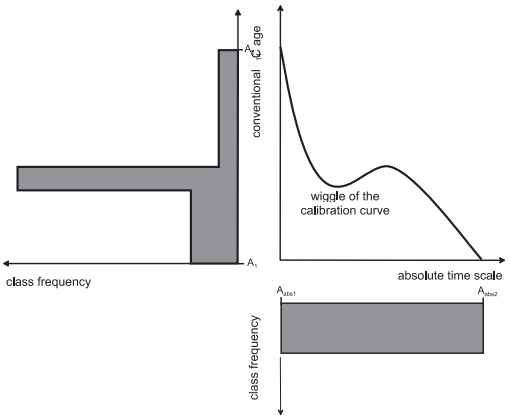

Fig. 6. The histogram between the absolute ages A_{abs1} and A_{abs2} is uniform whereas the histogram of the corresponding ^{14}C dates A_1 and A_2 is distorted. This is the consequence of the wiggles in the ^{14}C calibration curve. Peaks and lows in the ^{14}C histogram may be without actual relevance.

Abb. 6. Das Histogramm der gleich häufigen absoluten Alter A_{abs1} und A_{abs2} entspricht einem Rechteck und liefert für die entsprechenden ^{14}C-Alter ein Polygon. Die Ursache sind die Windungen der ^{14}C-Kalibrationskurve. Gipfel und Täler im ^{14}C-Histogramm zwischen den Altern A_1 und A_2 haben keine wirkliche Bedeutung.

Table 1: ^{14}C ages ordered in size from wood samples dating the beginning of the Younger Dryas in New Zealand (Denton & Hendy 1994). The standard deviation of the mean (Eq. 7) and the calibrated ^{14}C age of the 2σ confidence interval are given in parentheses.

Tab. 1: Die nach ihrer Größe geordneten ^{14}C-Alter von Holzproben, die den Beginn der Jüngeren Dryas-Zeit in Neuseeland datieren sollen. Die Standardabweichung des mittleren Alters (Gleichung 7) und das 2-Sigma-Konfidenzintervall seines kalibrierten ^{14}C-Alters sind in Klammern angegeben.

^{14}C age (BP) Group I		^{14}C age (BP) Group II	
10,650 ± 100	11,040 ± 90	11,150 ± 160	11,255 ± 95
10,750 ± 100	11,045 ± 85	11,190 ± 60	11,290 ± 150
10,800 ± 90	11,080 ± 60	11,200 ± 50	11,340 ± 110
10,830 ± 110	11,090 ± 70	11,200 ± 120	11,350 ± 90
10,920 ± 90	11,110 ± 110	11,225 ± 60	11,350 ± 60
10,950 ± 100	11,110 ± 90	11,230 ± 130	11,365 ± 60
10,980 ± 90	11,110 ± 130	11,240 ± 100	11,370 ± 190
10,980 ± 100	11,115 ± 90	11,250 ± 70	11,520 ± 170
11,040 ± 70	11,150 ± 60	11,250 ± 50	11,520 ± 140
11,150± 14 BP (± 28 a) $\chi^2 = 148$ 13,020 – 13,103 BP (12,965 – 13,117 BP)			
11,011 ± 20 BP (± 32 a) $\chi^2 = 42$ 12,899 – 12,945 BP (12,874 – 12,995 BP)		11,265 ± 19 BP (± 13 a) $\chi^2 = 17$ 13,125 – 13,193 BP (13,101 – 13,223 BP)	
10,862 ± 34 BP (±48 a) $\chi^2 = 11$ 12,835 – 12,871 BP (12,818 – 12,893 BP)	11,097 ± 27 (± 9 a) $\chi^2 = 2$ 12,960 – 13,052 BP (12,930 – 13,086 BP)		

vious that the ages were not correctly evaluated in the laboratory and the published standard deviations are meaningless.

9.1 The beginning of the Younger Dryas in New Zealand

Denton & Hendy (1994) tried to determine the beginning of the Younger Dryas in New Zealand, i.e., the age of a single event. They collected 25 pieces of wood from short-lived trees and covered by Younger Dryas moraines of the Franz-Josef Glacier in the Southern Alps of New Zealand. The holocellulose extract yielded 36 ^{14}C ages determined in three laboratories (Table 1). It was assumed that all samples were coeval and deposited at the beginning of the Younger Dryas.

The weighted mean and its standard deviation of the ^{14}C ages is 11,150 ± 14 BP (Eqs. 5 and 6) and the weighted mean standard deviation of a single ^{14}C age is ± 82 a (Eq. 7). Denton & Hendy (1994) published a mean of 11,170 ± 14 BP. The difference between these age values results from the inclusion by the authors of a ^{14}C date which they considered to be older than the target event of the Younger Dryas. The calibrated ^{14}C age interval is 13,020–13,103 BP (12,965–13,117 BP for the 2σ interval). The authors give the mean ^{14}C age as the date for the beginning of the Younger Dryas. The actual standard deviation of the weighted mean, however, is ± 28 a (Eq. 6) and the actual weighted mean standard deviation of the individual ages is ± 169 a (Eq. 8). This finding is not compatible with the assumption that the published ^{14}C

ages belong to a single frequency distribution and, therefore, to a single event. This is supported by the χ^2_w value of 148 for the 36 values.

In order to check whether the published ^{14}C ages represent more than one frequency distribution, the ages were ordered according to size and divided into two groups of 18 values each and the first group into two subgroups of nine values (Table 1). Only the weighted means of the second group and the first subgroup belong to a single frequency distribution that represents coeval samples. The other groups represent more than one frequency distribution. The too low χ^2 value for the second subgroup is an artifact of the ordering of the ^{14}C ages according to size.

The present consensus places the beginning of the Younger Dryas between 12,900 and 12,700 BP on the basis of calibrated ^{14}C ages (ALLEY 2000). The calibrated ^{14}C-age range of the weighted mean of the published ^{14}C ages of 12,965–13,117 BP (2σ confidence interval) considerably deviates from that. Only the first group and first subgroup with calibrated ^{14}C age ranges of 12,874–12,995 BP and 12,818–12,893 BP, respectively, agree with this consensus. In both cases several ^{14}C ages have to be discarded as the χ^2 values of 42 and 11 deviate from the target χ^2 values of 17 and 8, respectively.

For the purpose of this paper, it is not of interest to determine the events responsible for this. The wood samples may stem from trees in forests containing trees of different ages that were buried at different times by two or three separate glacier advances. Other causes are possible. Of importance is only that the assumption of the authors the dated samples were coeval is not valid. The precision for the beginning of the studied event was not narrowed to ± 14 years. The actual precision of the date for the beginning of this event is at least twice as large.

The reader may claim that the difference in precision between ±14 and ±26 years is small. However, one has to realize that as few as nine ^{14}C ages would have been sufficient to obtain a precision of ± 26 years. This means that up to 75 % of the dating costs could have been saved.

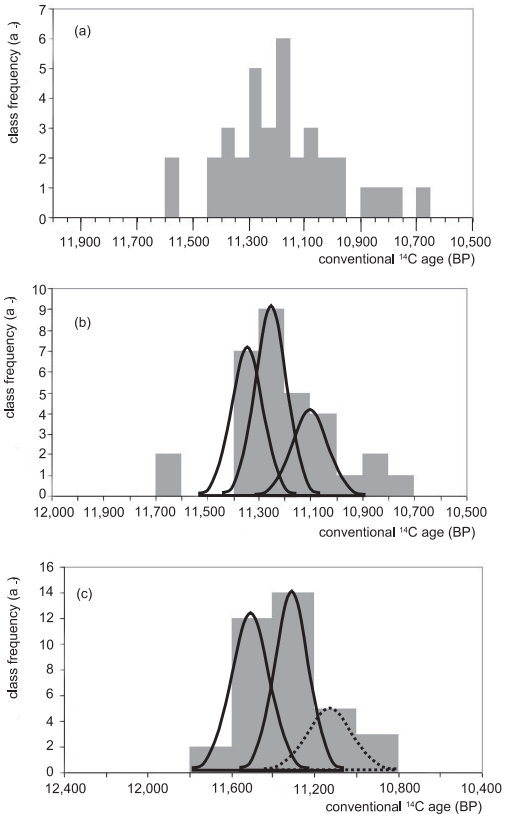

Fig. 7: Normal histogram of 36 ^{14}C ages from 25 wood samples which were assumed to represent the beginning of the Younger Dryas in southern New Zealand (DENTON & HENDY 1994). The arbitrarily chosen class widths of (a) 50, (b) 100 and (c) 200 years shows the influence on the temporal resolution and the scatter of the histogram. The optimum choice may be 100 years (b), which is close to the mean standard deviation of ± 88 years for single ages.

Abb. 7: Einfaches Histogramm von 36 ^{14}C-Altern, die von 25 Holzproben vom südlichen Neuseeland bestimmt worden sind. Sie sollen den Beginn der Jüngeren Dryas-Zeit festlegen (DENTON & HENDY 1994). Die willkürlich gewählten Klassenintervalle von (a) 50, (b) 100 und (c) 200 Jahren zeigen die Auswirkungen auf die altersmäßige Auflösung und auf die Unruhe des Verlaufs des Histogramms. Eine optimale Wahl scheint 100 Jahre zu sein (b), ein Wert, der nahe der mittleren Standardabweichung von Einzeldaten von ± 88 Jahren liegt.

Table 2: ESR ages (ka) of interglacial mollusks from Estonia (Molodkov & Raukas 1987).

Tab. 2: ESR-Alter (ka) interglazialer Mollusken von Estland (Molodkov & Raukas 1987).

	No	ESR age (ka)	standard deviation (ka)	χ^2 value
	1	95±5		0.0
	2	90±8	± 3.2	0.3
	3	92±7	± 2.5	0.0
	4	92±6	± 2.1	0.0
	5	92±9	± 2.0	0.0
	6	90±8	± 2.0	0.1
	7	82±6	± 4.7	2.5
	8	81±9	± 5.2	1.1
mean		89.9 ± 2.4 (Eqs. 5 and 6) ± 6.8 (Eq. 7)	88.6 ± 1.8 (Eqs. 3 and 8) ± 5.2 (Eq. 8)	χ^2 = 4.0 target ~ 7

A normal histogram was used for visualization of the ^{14}C ages from New Zealand (Fig. 7). As there are a large number of determined ages, the shape of the normal histogram is very similar to that of a dispersion histogram. The effect of the choice of the class width is demonstrated using 50, 100 and 200 years. The histogram with the smallest class width (Fig. 7, top) shows a large random scatter of up to ± 50 %, which may lead to incorrect statements on the temporal fluctuation of the sample population. The data density per class obviously is too small.

The histogram with a class width of 100 years seems to be the optimum solution. The class width is within the range of 82 to 169 a for the mean standard deviation of the individual ages (Eqs. 7 and 8). The asymmetry of the distribution in the middle histogram suggests the superposition of three frequency distributions with four outliers between 10,700 and 10,900 years and two outliers between 11,600–11,700 years. With the use of the largest class width of 200 years considerable temporal information is lost, but the histogram still clearly shows that the samples represented more than two events.

9.2 ESR ages from mollusks

In the majority of all case studies the scatter of the data corresponds to that expected from the size of the standard deviations or is wider. There are, however, studies in which the opposite case occurs. In these cases, the defined criteria of the expression $A \pm \sigma A$ are not fulfilled and calculations with such dates should be done without the described error algorithms.

Molodkov and Raukas (1987) published ESR ages from mollusks collected from an interglacial layer on the coast of Estonia. The results are compiled in Table 2.

The actual uncertainty of the ESR ages (Eq. 3 derived from Eq. 8) is considerably smaller than the expected one calculated from the given standard deviations (Eq. 6). Consequently, $\chi^2_w = 4.0$ (Eq. 9), which is also considerably smaller than 7 (the number of ages minus 1). This result is evidence that the propagation of uncertainty of the published ESR ages was not done properly. This is a frequent observation in published ESR, TL and OSL ages. The standard deviations are too large or too small. A discussion of the reasons for this problem would be beyond the scope of this article. One of the main problems is that the statistical uncertainty of several of the parameters involved can only be estimated or only minimum and maximum values are known for the parameters. In addition, systematic errors are often underestimated. In any case, in such cases it is not justified to use weighting factors in the statistical handling of the numerical ages determined with these methods.

10 Conclusion

It is demonstrated that the handling of numerical ages with their random uncertainties requires at least a minimum knowledge of simple statistical methods, especially the algorithms used to determine the propagation of uncertainty. A careless or unqualified use of such dates bears the risk of misleading geoscientific conclusions.

References

ALLEY, R.B. (2000): The Younger Dryas cold interval as viewed from central Greenland. – Quaternary Science Reviews, 19: 213-226.

BRUNNACKER, K. & HAUSMANN, R. (1987): Absolutes Alter klimarelevanter Gesteine im jüngeren Quartär. – Forschung in Köln. Berichte aus der Universität, 1: 67-70.

DENTON, G.H. & HENDY, C.H. (1994): Younger Dryas age advance of Franz Josef Glacier in the southern Alps of New Zealand. – Science, 264: 1434-1437.

GEYH, M.A. (1969): Versuch einer chronologische Gliederung des marinen Holozäns an der Nordseeküste mit Hilfe der statistischen Auswertung von ^{14}C-Daten. – Zeitschrift der deutschen geologischen Gesellschaft, 118: 351-360.

GEYH, M.A. (1980): Holocene sea-level history: Case study of the statistical evaluation of ^{14}C dates. – Radiocarbon, 22: 695-704.

GEYH, M.A. (1991): Determination of absolutes dates for terrestrial materials (Last Interglacial to Holocene). An appeal for careful interpretation. – In: Frenzel, B. (ed.): Klimageschichtliche Probleme der letzten 130 000 Jahre: 251-265; Stuttgart (Fischer).

GEYH, M.A. (2005): Handbuch der physikalischen und chemischen Altersbestimmung. – 211 p.; Darmstadt (Wissenschaftliche Buchgesellschaft).

GEYH, M.A. & GROSJEAN, M. (2000): Establishing a reliable chronology of lake level changes in the Chilean Altiplano: A result of close collaboration between geochronologists and geoscientists. – Zentralblatt für Geologie und Paläontologie, Teil I (7/8): 985-995.

GEYH, M.A. & SCHLEICHER, H. (1990): Absolute Age Determination. Physical and Chemical Dating Methods and Their Application. – 503 p.; Berlin (Springer).

HUNTLEY, D.J. (2001): Some notes on language. – Ancient TL, 19 (1): 27-28.

MICHCZYNSKA, D.J. & PAZDUR, A. (2004): Shape analysis of cumulative probability density function of radiocarbon dates set in the study of climate change in the late glacial and Holocene. – Radiocarbon, 46 (2): 733-744.

MOLODKOV, A. & RAUKAS, A. (1987): The age of Upper Pleistocene marine deposits of the Boreal transgression on the basis of electron-spin resonance (ESR) dating of subfossil mollusk shells. – Boreas, 17: 267-272.

SACHS, L. (1999): Angewandte Statistik. Anwendung statistischer Methoden. – 881 p.; Berlin (Springer).

STUIVER, M., REIMER, P.J., BARD, E., BECK, J.W., BURR, G.S., HUGHEN, K.A., KROMER, B., MCCORMAC, G., VAN DER PLICHT, J. & SPURK, M. (1998): INTCAL98 radiocarbon age calibration, 24,000-0 cal BP. – Radiocarbon, 40: 1041-1983.

TAYLOR, B.N. & KUYATT, C.E. (1994): Guidelines for Evaluating and Expressing the Uncertainty of NIST Measurement Results. – NIST Technical Note 1297: 20 p.; Washington D.C (National Institute of Standards and Technology).

WAGNER, G.A. (1998): Age Determinations of Young Rocks and Artifacts. – 466 p.; Stuttgart (Enke).

Hinweise für Autoren

Manuskript Übermittlung: Das Manuskript ist der Schriftleitung in dreifacher Ausfertigung zuzusenden. Manuskriptformat DIN A4, einseitig bedruckt, durchnummeriert und mit Namen und Adresse des Erstautoren versehen. Bitte benutzen Sie eine Standard-Textverarbeitung im .rtf oder .doc-Format. Als Zeichensatz verwenden Sie bitte die Standard-Fonts Times Roman, Helvetica oder Courier mit einem 1,5-fachen Zeilenabstand. Bitte das eingereichte Manuskript nicht heften.

Manuskripte, die nach der Begutachtung zum Druck angenommen sind, werden nur auf Anforderung an die Autoren zurückgesendet. Dies gilt auch für beigefügte Originale (Zeichnungen, Fotos etc.). Die überarbeitete Endversion des Manuskriptes ist abschließend auf einer CD/Diskette und als Ausdruck bei der Schriftleitung einzureichen. Eine Übermittlung via E-Mail ist ebenso möglich. Ausdruck und elektronische Fassung müssen identisch sein, etwaige notwendige Änderungen können den Autoren in Rechnung gestellt werden.

Manuskriptform: Als Publikationssprachen sind Englisch und Deutsch zugelassen. Manuskripte in deutscher Sprache müssen einen englischen Untertitel tragen sowie eine englische Kurzfassung und englische keywords beinhalten. Es gelten die Regeln der neuen Rechtschreibreform.

Die Manuskripte sollen folgendem Aufbau entsprechen: **I.** Kurze, aber prägnante Überschrift **II.** Ausgeschriebener Vor- und Nachname mit akademischem Grad, Post- und E-Mail-Adresse **III.** Bis zu fünf englische keywords, die den Inhalt des Manuskriptes widerspiegeln. **IV.** Deutsche und englische Kurzfassung des Textes mit einer Länge von bis zu 200 Wörtern. Der englische Untertitel des Manuskriptes ist der englischen Kurzfassung in eckigen Klammern voranzustellen. **V.** Klar gegliederter Text. Kapitelnummerierungen sind mit arabischen Ziffern zu versehen. **VI.** Alphabetisch geordnete Literaturliste. Die Zitierweise muss der unten angegebenen Form entsprechen.

Im fortlaufenden Text sind Literaturhinweise als Kurzzitate einzufügen, der oder die Autorennamen sind in KAPITÄLCHEN-Schrift zu setzen, das Erscheinungsjahr in Klammern, z. B. MÜLLER (2006). Werden von einem Autor mehrere Arbeiten aus einem Jahr zitiert, so sind diese durch Buchstaben zu unterscheiden: MÜLLER (2006a, 2006b). Bei mehr als drei Autoren kann et al. verwendet werden: MÜLLER et al. (2006). Arbeiten mit bis zu drei Autoren werden folgendermaßen zitiert: MÜLLER & MEYER (2006) oder MÜLLER, MEYER & SCHULZ (2006). Sind mit der Zitierung bestimmte Seiten oder Abbildungen gemeint, müssen diese genau angegeben werden: MÜLLER (2006: 14) oder MÜLLER (2006: Fig. 14).

Die wissenschaftlichen Namen von Pflanzen und Tieren (*Gattungen*, *Untergattungen*, *Arten*, *Unterarten*) sind kursiv zu schreiben. Die den biologischen Namen folgenden Autoren werden in KAPITÄLCHEN gesetzt. (*Armeria maritima* WILLD.)

Bitte keinen Blocksatz verwenden, sondern einen rechtsseitigen Flatterrand.
Bitte keine automatische Silbentrennung verwenden.
Bitte alle automatischen Formatierungen in ihrer Textarbeitung deaktivieren.
Bitte keine Seitenzählung

Abbildungen, Tabellen und Fotos nicht in den Text einbauen, sondern separat als Ausdruck beifügen. Abbildungsunterschriften am Ende des Manuskripttextes platzieren.

Abbildungen: Bitte fügen sie jede Abbildung als separaten Ausdruck bei und versehen sie den Ausdruck mit dem Namen des Autors, der Abbildungsnummer und der Ausrichtung der Abbildung. Alle Grafiken müssen eine Verkleinerung auf Spaltenbreite (= 7 cm) oder Satzspiegel (= 14,5 x 21 cm) zulassen. Die Beschriftung muss nach der Verkleinerung noch gut lesbar sein. Sollte eine Legende nötig sein, so binden sie diese in die Abbildung ein. Bitte vermeiden sie Haarlinien oder Grauwerte.
Für die Drucklegung müssen alle Abbildungen in elektronischer Form eingereicht werden. Bitte verwenden sie hoch aufgelöste Dateien im .tif- oder .eps-Format (600 dpi). Stark reduzierte .jpg oder .pdf-Dateien oder in Word-Dokumente eingebundene Abbildungen werden nicht akzeptiert.
Farbige Abbildungen sind kostenfrei möglich, wobei der Autor die Notwendigkeit farbiger Abbildung mit Einreichen des Manuskriptes begründen sollte.

Zitierweise (Beispiele):
Aufsätze:
SCHWARZBACH, M. (1968): Neue Eiszeithypothesen. – Eiszeitalter und Gegenwart, 19: 250-261.
EISSMANN, L. & MÜLLER, A. (1979): Leitlinien der Quartärentwicklung im norddeutschen Tiefland. – Zeitschrift für Geologische Wissenschaften, 7: 451-462.
ZAGWIJN, W.H. (1996): The Cromerian Complex Stage of the Netherlands and correlation with other areas in Europe. – In: TURNER, C. (ed.): The Middle Pleistocene in Europe: 145-172; Rotterdam (Balkema).
MAGNY, M. & HAAS, J.N. (2004): A major widespread climatic change around 5300 cal. yr BP at the time of the Alpine Iceman. – Journal of Quaternary Science, 19: 423-430. DOI: 10-1002/jqs.850

Monographische Werke, Bücher:
EHLERS, J. (1994): Allgemeine und historische Quartärgeologie. – 358 S.; Stuttgart (Enke).

Bitte keine Abkürzungen der Zeitschriftentitel verwenden.

Sonderdrucke: Autoren erhalten 20 Sonderdrucke kostenfrei, Weitere auf Kosten des Verfassers.

Instruction to Authors

Manuscript submission: Please send your manuscript in triplicate to the Editor, printed on one side of standard sized paper (DIN A4) with the author's permanent and temporary addresses. Microsoft Word files are preferred (.rtf or .doc-files). Use 12pt type in one of the standard fonts: Times Roman, Helvetiva, or Courier is preferred. It is not necessary to double space your manuscript. Do not use staples to fix your manuscript.

Manuscripts accepted for publication, including original artwork will not be returned to the author unless requested. The final revised and accepted manuscript should be submitted on CD/diskette along with a copy of the printout or via E-mail. The CD/diskette should be labelled with the author's name and the version of the word processing system used. The electronic files and the printout must be identical. Changes to the electronic files may be charged to the author(s).

Manuscript style: The languages of the journal are English and German. Manuscripts in German must contain an English subtitle, an abstract and English keywords.

Manuscripts should be arranged in the following order: **I.** Informative but brief title **II.** Full names, full address, E-mail and academic position of all authors. **III.** Include up to five keywords that describe your paper. **IV.** A short abstract of up to 200 words. Papers in German should additionally contain a summary in German language; the English abstract should carry the translated title of the paper in square brackets. **V.** The main text, if necessary subdivided by headings, which should be numbered with arabic numerals. **VI.** Reference list, the references should be arranged alphabetically and should be conform to the examples given below.

References should be quoted in the text as name and year within brackets and listed at the end of the text alphabetically. Use small CAPITALS for the author e.g. MÜLLER (2006). Where reference is made to more than one work by the same author published in the same year, identify each citation as follows: MÜLLER (2006a, 2006b). Where three or more authors are listed in the reference list, please cite in the text as MÜLLER et al. (2006). Papers with up to three authors should be cited as MÜLLER & MEYER (2006) or MÜLLER, MEYER & SCHULZ (2006). If a special page, figure, table etc. of a paper should be cited use following citation style: MÜLLER (2006: 14) or MÜLLER (2006: Fig. 14).

Scientific names of flora and fauna (*gender*, *sub-gender*, *species*, *sub-species*) are to be written in *italics*. Use small CAPITALS for the author (*Armeria maritima* WILLD.)

Do not justify your text, use a ragged right hand margin.
Do not break words at the end of lines.
Do not use any automatic formatting.
Do not page numbers

Graphic elements, tables and images should be kept as separate files. Figures and tables captions should be placed at the end of the manuscript.

Illustrations: Supply each figure as a separate print-out, with the author's name, the figure number and the top of the figure indicated. Illustrations should be reducible to a column width of 7 cm or a maximum size of 14,5 x 21 cm. Lettering must be of reasonable size that would be clearly readable after reduction. Where a key of symbols is required, include this in the artwork itself, not in the figure caption. Avoid fine lines and grey-shading/halftones.
For the final version all illustrations must be supplied electronically as files at a sufficient resolution (600 dpi). Please use a tiff or eps format. Pdf-files or figures in word-documents are not acceptable.
Colour illustrations are available free of charge. It is the responsibility of the author to clarify whether or not the colour figures are required in print when submitting the manuscript for review.

References (examples):
Papers:
SCHWARZBACH, M. (1968): Neue Eiszeithypothesen. – Eiszeitalter und Gegenwart, 19: 250-261; Öhringen.
EISSMANN, L. & MÜLLER, A. (1979): Leitlinien der Quartärentwicklung im norddeutschen Tiefland. – Zeitschrift für Geologische Wissenschaften, 7: 451-462.
ZAGWIJN, W.H. (1996): The Cromerian Complex Stage of the Netherlands and correlation with other areas in Europe. – In: TURNER, C. (ed.): The Middle Pleistocene in Europe: 145-172; Rotterdam (Balkema).
MAGNY, M. & HAAS, J.N. (2004): A major widespread climatic change around 5300 cal. yr BP at the time of the Alpine Iceman. – Journal of Quaternary Science, 19: 423-430. DOI: 10-1002/jqs.850

Books:
EHLERS, J. (1994): Allgemeine und historische Quartärgeologie. – 358 S.; Stuttgart (Enke).

Do not abbreviate the name of Journals.

Offprints: Authors will receive 20 offprints free of charge. Further offprints can be ordered.

Available volumes of

Eiszeitalter und Gegenwart

(status quo 8/2008)

Volume	Year	Price
6	1955	38,00 €
7	1956	38,00 €
11	1960	38,00 €
12	1962	38,00 €
13	1962	38,00 €
14	1963	38,00 €
15	1964	38,00 €
16	1965	38,00 €
17	1966	38,00 €
18	1967	vergriffen/sold out
19	1968	38,00 €
20	1969	38,00 €
21	1970	38,00 €
22	1971	38,00 €
23/24	1973	Doppelband/double feature 57,00 €
25	1974	38,00 €
26	1975	38,00 €
27	1976	38,00 €
28	1978	38,00 €
29	1979	38,00 €
30	1980	38,00 €
31	1981	38,00 €
32	1982	38,00 €
33	1983	38,00 €
34	1984	40,00 €
35	1985	40,00 €
36	1986	42,00 €
37	1987	44,00 €
38	1988	44,00 €
39	1989	44,00 €
40	1990	48,00 €
41	1991	48,00 €
42	1992	49,90 €
43	1993	49,90 €
44	1994	49,90 €
45	1995	49,90 €
46	1996	49,90 €
47	1997	49,90 €
48	1998	49,90 €
49	1999	49,90 €
50	2000	49,90 €
51	2002	49,90 €
52	2003	54,00 €
53	2003	54,00 €
54	2004	54,00 €
55	2005	54,00 €
56/1-2	2007	54,00 €
56/3	2007	27,00 €
56/4	2007	27,00 €
57/1-2	2008	54,00 €

A list of all published volumes is also shown under http://www.schweizerbart.de/j/eiszeitalter-und-gegenwart.

For members of the DEUQUA volumes 11-50 (exclusive of Vol. 17-18, 29) are available for 10,- € per volume.
The price for other volumes is 25,- € for DEUQUA-members.

Volume 6-7, 17, and 29 are exclusively offered by E. Schweizerbart'sche Verlagsbuchandlung (Nägele u. Obermiller), Johannesstr. 3A, D-70176 Stuttgart.

Also available:
Eissmann L. & Litt, T. (Hrsg.) (1994): Das Quartär Mitteldeutschlands. – Altenburger Naturwiss. Forsch., **7**; Altenburg.
The price is 43,- €

If you are interested please contact:
Deutsche Quartärvereinigung e.V., Stilleweg 2, D-30655 Hannover, deuqua@lbeg.niedersachsen.de

Volumes 1-5, 8 and 10 are available as reprints:
Firma Zwerts und Zeltinger, Heereweg 347, P.O. Box 80, NL-2160 SZ Lisse (price for DEUQUA-members is 28,- €).

Eiszeitalter und Gegenwart

Quaternary Science Journal

Published for the Deutsche Quartärvereinigung e. V.

Contents Vol. 57 No. 1/2 (2008)

ISSN 0424 -7116